THE UNIVERSITY *of* EDINBURGH

Investigating PSD-95 turnover at the synapse using the HaloTag technology

Maximilian Moritz Kratschke

Ph.D.

University of Edinburgh

Centre for Clinical Brain Sciences

2018

Declaration

I declare that this thesis, as well as the work described within, are my own unless indicated otherwise and have not been submitted for any other degree.

Maximilian Kratschke

May 2018.

Acknowledgements

I would first like to thank Professor Seth Grant, for supervising me and providing me the opportunity to conduct my PhD research in his lab. Without his support and the fantastic scientific opportunities available in his lab this project would not have been possible.

I would further like to thank Professor Andrew Jarman and Dr Paul Skehel for being on my PhD committee and supporting me with valuable insights and guidance. I would like to express particular gratitude to Professor Dies Meijer who, as my secondary supervisor, has not only given me scientific advice but also been a supportive mentor and livened up coffee breaks by joining in during our political discussion rounds.

I would also like to thank all of the members of the Grant lab, past and present, for having been there for me at critical periods, when I needed a helping hand during experiments, or simply by providing their invaluable advice. I would particularly like to thank Jess Nithianantharajah for persuading me to apply to the Grant lab for a PhD in the first place; Marcia Roy for her guidance during my early days in the lab; Kathryn Elsegood for always being there behind the scenes; Ricky Qiu for his advice and companionship while I was analysing data in the cave; and Sarah Lempriere for the help and advice she always gives generously and with a smile.

I would like to particularly thank Cathy McLaughlin who has not only grown to become an incredibly efficient and effective lab manager, but who has also helped me with countless experiments: dissecting mouse embryos alongside me; helping me plate down cells, and always being there with advice if needed.

A very special thank you goes to Matt Broadhead for welcoming me into the lab from day one, teaching me everything I now know about primary culturing, and lending a helping hand whenever I needed it. Whenever I lost confidence in my work, Matt was there to convince me otherwise, and his advice and camaraderie were essential. His incredible diligence and determination were always great motivators, and I am sure these attributes will carry him far in science.

I would also like to thank Vlad Anton for his friendship and support, and the comic relief he never failed to provide. A further big thank you to George Kanatouris and Nat O'Neill for their friendship and scientific advice. Vlad, Nat and George, it was always great fun to have a heated discussion over a coffee or a beer with you, and I really hope we will find some opportunities for this in the future!

I would further like to thank Annelies for always being there as a friend, and for being happy to discuss any bizarre topic at any time. Thank you also to Akihiro and Mosi for joining me for lunch whenever you had time.

And what would a PhD be without life outside the lab? I would first and foremost like to thank my amazing girlfriend Ioana Negulescu, for being the most supportive person anyone could ever have at their side during such a stressful period in their life. You are a lovely person, and no matter at what time I returned from the lab, I knew you would be there, waiting for me with a smile.

I would also like to thank my dear friends, who have been there with me through thick and thin. Thank you, Andrei, Greg, Veronica, Becky, Dan and all you other lovely people who have made my life in Edinburgh great over the past, what, eight years?! You have truly all become a part of me by playing such big roles in this period of my life. I wish you all the best of luck!

Finally, my family deserves all of the gratitude I can give, and I would like to dedicate this thesis to you, Sylvia, Robert and Lilly. Thank you for providing me with so many wonderful opportunities in my life, and for helping me get this far. You are truly great people, and I love you very much.

Abstract

PSD-95 is an abundant scaffolding protein found in the postsynaptic densities (PSDs) of excitatory synapses throughout the mammalian brain, and plays a critical role in innate and learned behaviours. PSD-95 assembles with numerous other proteins, including glutamate receptors, adhesion molecules and signalling proteins, into postsynaptic supercomplexes that are then organised into nanoclusters that comprise the postsynaptic density of excitatory synapses. While the subcellular localisation of PSD-95 has been widely studied, much less is known about its turnover. In this thesis, I present novel insights into PSD-95 synthesis and degradation at synapses of cultured primary neurons gained using the HaloTag technology.

The HaloTag consists of an engineered bacterial protein domain that covalently binds synthetic ligands labelled with fluorescent and affinity moieties. Hence, cells expressing proteins fused to the HaloTag can be used to study protein levels, complexes and turnover using these different ligands. This project was based upon a knock-in mouse line expressing the HaloTag fused to endogenous PSD-95 using gene targeting. After demonstrating that these mice were phenotypically normal and that PSD95-HaloTag fusion proteins normally assembled into supercomplexes in the PSD, hippocampal primary cultures were grown from this mouse line. Fluorescent HaloTag ligands were then used to label live neurons, allowing for the visualisation of PSD-95 at synapses by confocal microscopy.

Next, I established a pulse-chase labelling method, where one ligand is used to label all existing PSD-95 first, before a second ligand can then be used to label any newly synthesised PSD-95. This allows for the identification and characterisation of subpopulations of PSD-95, which can be separately analysed. I find that PSD-95 has a half-life of 36 hours at synapses, consistent with previous literature. I was also able to observe synaptic heterogeneity in PSD-95 turnover, and classify synapses into types according to their PSD-95 expression profile.

Finally, a range of chemical compounds known to modulate protein turnover and neuronal activity was applied over a 24-hour period, and their effects on PSD-95

turnover analysed. It was found that inhibiting either the proteasome or protein synthesis led to significant reductions in PSD-95 degradation as well as inhibiting PSD-95 synthesis. Thus, this project established a method offering a unique way of investigating the turnover of a specific, tagged protein, as well as gaining novel insights into the turnover of PSD-95 at individual synapses.

Lay summary

Nerve cells (neurons) communicate with each other through connections called synapses. It is thought that changes in the strength of these synaptic connections are the basis of learning and memory formation. Messages can only be passed in one direction across these synapses, and on the receiving side of each synapse there is an area densely populated by a huge variety of proteins. This area is called the postsynaptic density (PSD). It is the proteins in this area that are thought to mediate the changes in synaptic strength that underlie learning and memory formation.

The protein PSD-95 is one of the most abundant components of the PSD, and it functions as a scaffold that binds other proteins together, allowing them to interact with each other. Abnormal levels of PSD-95 have been linked to various psychiatric diseases including schizophrenia, and mice lacking this protein have severe deficits in learning certain tasks. While the localisation of PSD-95 in the brain and within neurons has been widely studied, little is known about how it is produced and how it is degraded (this cycle is termed 'turnover'). However, we know that the turnover of proteins in the PSD plays an important role in synaptic function and learning.

In this PhD project, I used a mouse in which the PSD-95 protein had been genetically fused to a protein that acts as a reporter, called HaloTag. This HaloTag reporter protein can be visualised with fluorescent labels. Only a single label can bind to a single protein, irreversibly. I grew neurons taken from the brains of embryos of these mice on glass coverslips for 2 weeks. This allowed me to take images of the neurons and their synapses using a high-magnification microscope. In these neuronal cultures, I visualised the PSD-95-HaloTag fusion proteins with fluorescent labels. I added differently-coloured labels 24 hours apart, and studied old and new PSD-95 proteins separately. Thus, I could analyse the turnover of PSD-95, as well as categorise synapses into different types based on their PSD-95 turnover. I also treated neurons with various chemicals over the 24-hour period, and analysed their effects on PSD-95 turnover. The main findings of this project were: a) that different synapses have different rates of PSD-95 turnover; and b) that chemicals known to block either protein synthesis or degradation appear to simultaneously block both synthesis and degradation of PSD-95, indicating the presence of a mechanism that aims to keep overall PSD-95 levels constant within individual synapses.

Table of contents

Table of figures

Chapter 1: Introduction

Chapter 1.1 Neurons and memories

1.1.1 The discovery of the synapse

Humanity's quest to understand the brain has been complex and full of paradigm shifts. Early on, it was believed that brains were made up of a continuous, rather than contiguous, network of cells that were seamlessly attached to each other. It was Ramon y Cajal's work, utilising Camillo Golgi's staining technique, which first allowed for the visualisation of individual nerve fibres in the late 19th century. Ultimately, it was the advent of electron microscopy which completely settled this issue. This discovery naturally led to a new controversy over the nature of the communication between these cells- was it electrical, like the propagation of activity through a single neuron, or were there chemicals involved in passing the messages across these minute gaps? It took many decades to settle this question, and only in the early 1960s did it become widely accepted that communication between neurons in the brain is predominantly chemical. This realisation kicked off a prodigious amount of research into understanding the mechanisms governing synaptic transmission; from identifying the neurotransmitters involved and their receptors, to their mechanisms of release and cessation of activity. While many of these riddles have been solved, many more have appeared. One of the most fascinating areas of synaptic research has aimed at understanding their role in learning and memory.

1.1.2 Neuronal communication

While 'messages', or action potentials, in the form of neuronal activity propagate through the neuron in waves of depolarisation caused by the influx of Na^+ following the opening of voltage-gated sodium channels, these messages need to be transmitted across the synaptic cleft that separates two neurons by chemicals called neurotransmitters. In many cases, the message will be strong enough to elicit the activation of an action potential in the receiving, postsynaptic nerve cell.

However, not every action potential that arrives at a presynaptic terminal and causes the release of neurotransmitter also causes an action potential to be evoked in the postsynaptic terminal. This is because a certain firing threshold needs to be reached

in the receiving neuron, and if this is not the case, the message fails to be transmitted. Crucially, the 'strength' of a synapse is plastic, and a 'stronger' synapse will be more likely to reach this threshold and transmit a message. This is not done by lowering the threshold, but rather by increasing the ability of the postsynaptic terminal to reach this threshold via an increased ion influx. The mechanism underlying this long-term change is referred to as long term potentiation (LTP), but the opposite effect can also occur, and this weakening of synaptic strength is called long term depression (LTD). It has been proposed that this strengthening, or potentiating, of synapses, underlies learning and memory (Nabavi et al., 2014). Both LTP and LTD are thought to be equally important, and in both cases, long term structural changes occur at the synapse, primarily on the postsynaptic, receiving side (Nicoll, 2017).

1.1.3 Long term potentiation and long term depression

As one of the first steps of activating LTP, α-amino-3-hydroxy-5-methyl-4-isoxazolepropionic acid receptors (AMPARs) are activated by the excitatory neurotransmitter glutamate, and their activation causes an influx of Na^+ and (weaker) outflow of K^+ ions resulting in depolarisation. While this may be enough to trigger an action potential in the postsynaptic neuron, this depolarisation needs to crucially be large enough to also allow N-Methyl-D-Aspartate receptors (NMDARs) to become activated, which occurs when Mg^{2+} ions, that block NMDARs, are expelled by the strong depolarisation. A depolarisation large enough to cause this effect is usually only achieved by coincident firing of several nearby synapses, or by a back-propagating action potential (Kennedy, 2000). These NMDARs, once unblocked and activated by glutamate, allow not only Na^+ but importantly also Ca^{2+} ions to enter the postsynaptic terminal. This is vital because Ca^{2+} influx triggers various protein signalling cascades, but chiefly activates Ca^{2+}-calmodulin-dependent protein kinase IIα (CaMKIIα). CaMKIIα is thought to be critical to LTP induction (Lisman et al., 2012; Nicoll, 2012), and due to its numerous interactions with other proteins, such as Kalirin-7 (Xie et al., 2007), it acts as a signalling hub. CaMKIIα has also been shown to interact with the actin cytoskeleton, causing spine enlargement (Herring and Nicoll, 2016). Linked to this activation of CaMKIIα is a concomitant increase in AMPA receptors at the postsynaptic density (PSD), an electron-dense, protein-rich area within the synapses

of postsynaptic neurons, opposite the active zone. While CaMKIIα activation has been linked to AMPA receptor enrichment at the PSD, the exact mechanism that governs this relationship has not been definitively elucidated. While the paradigm within the field for 20 years was that CaMKIIα directly modifies AMPARs and/or associated transmembrane AMPAR-regulatory proteins (TARPs), thereby causing their increased trafficking into the PSD, more recent data has begun to disprove this hypothesis (Herring & Nicoll, 2016). Two emerging theories are replacing this old paradigm. The first is the PSD-centric model, while the second is the vesicle-centric model.

In the PSD-centric model, CaMKIIα is proposed to rearrange synaptic scaffolding proteins via cytoskeletal actin polymerisation, allowing these scaffolding proteins to more effectively 'capture' AMPARs diffusion throughout the membrane and into the synapse. This increases the total number of AMPARs at the PSD (Herring & Nicoll, 2016). According to the vesicle-centric model, however, CaMKIIα promotes the fusion of AMPAR-containing vesicles within the synapse via actin polymerisation. While neither of these theories has, as of yet, come to dominate the field, it is clear overall that LTP involves a complex interplay between multiple protein actors: from glutamate receptors to signalling and scaffolding molecules. The ultimate outcome, then, is an increased number of AMPARs in the postsynaptic membrane for the neurotransmitter to bind to, 'potentiating' that synapse and making it easier for subsequent action potentials to depolarise and activate the postsynaptic cell.

Critically, neurons that are activated at the same time will potentiate their synapses in ways that will mean that the next time, when one of them is activated, the other neurons will be more easily activated as well- a process thought to be important in information recall (Kennedy, 2000). The synthesis of new proteins as a result of LTP, as well as their degradation, is also crucial. Not only can it affect the entire cell, it also affects the strengthening of the synapses themselves.

1.1.4 The role of protein synthesis and degradation in LTP and LTD

It was discovered quite early on, in the 1960's, that memory formation required the synthesis of proteins (Tai and Schuman, 2008). To date, numerous studies have shown that LTP also requires protein synthesis, and blocking protein synthesis prevents synaptic plasticity (Kang and Schuman, 1996; Krug et al., 1984). As mentioned above, the protein CaMKIIα has been identified as one of the key proteins involved in synaptic plasticity and is rapidly synthesised in response to synaptic activity (Muddashetty et al., 2007). Furthermore, it is believed that most of this activity-induced protein synthesis occurs locally, within dendritic spines, as polyribosomes and smooth endoplasmic reticulum have been documented in spines (Spacek and Harris, 1997) and it has been found that LTP induction enhances the proportion of spines containing polyribosomes (Ostroff et al., 2002). mRNAs of synaptic proteins are also found distributed along dendrites (Cajigas et al., 2010; Muddashetty et al., 2007), and in fact, local protein synthesis of CaMKIIα and other synaptic proteins such as PSD-95 has been observed occurring throughout dendrites (Dieck et al., 2015; Ifrim et al., 2015).

More recently, however, studies have shown that the degradation of proteins is just as important for synaptic plasticity as synthesis (Lopez-Salon et al., 2001; Fonseca et al., 2006; Karpova et al., 2006; Patrick et al., 2003, Lee et al., 2008). These studies have also found that the ubiquitin-proteasome system (UPS) is the main driving force behind this plasticity-driven protein degradation. Indeed, Bingol and Schuman (2006) have shown that in response to NMDAR-driven synaptic activity, the proteasome is enriched at the synapse. Both protein synthesis inhibitors and proteasome inhibitors have been demonstrated to be potent inhibitors of LTP (Karpova et al., 2006; Krug et al., 1984), unless they are applied together, in which case they alleviate each other's effects (Lee et al., 2008; Fonseca et al., 2006). Taken together, this data implies that there is a strong interplay between protein synthesis and degradation at synapses that drives synaptic plasticity. Based on the evidence, Alvarez-Castelao and Schuman (2015) have put forward a model of a highly coordinated protein synthesis and degradation system, whereby continuous crosstalk between the two ensures that protein concentrations at individual synapses are maintained within optimal ranges and adapted to the needs of each synapse.

1.1.5 The role of protein synthesis and degradation in disease

A further line of evidence for the critical role of protein turnover, the continuous process of protein synthesis and degradation (Alvarez-Castelao and Schuman, 2015), is its role in disease states. There are now many neurodegenerative diseases that are recognised to contain an element of protein degradative dysfunction. Alzheimer's (AD), Parkinson's (PD) and Huntington's (HD) diseases, as well as prion diseases, are all associated with the abnormal aggregation of proteins (Ross and Poirier, 2004; Rubinsztein, 2006). These diseases are characterised by aggregations of misfolded proteins that are resistant to degradation, such as plaques, tangles and Lewy bodies (AD, PD). The fact that many of the proteins making up these aggregates are ubiquitylated and thus tagged for degradation (Ross and Poirier, 2004), and that proteasome activity in the brain is reduced in AD, PD and normal aging (Dahlmann, 2007), implies a dysfunction of the protein degradation system in these conditions.

Fragile X syndrome, one of the most common causes of autism spectrum disorder (ASD) and inherited intellectual disability (Kazdoba et al., 2014), is a condition very strongly linked to a dysregulation of protein translation. It is characterised by the loss of the fragile X mental retardation protein (FMRP, encoded by the Fmr1 gene), a protein that binds various mRNAs, frequently repressing their translation (Ifrim et al., 2015). One of its most prominent targets is the scaffolding protein PSD-95, the most abundant protein within the PSD, thought to be a chief organizer at the synapse (Gray et al., 2006). Local PSD-95 synthesis is triggered by the activation of Group 1 metabotropic glutamate receptors (mGluRs), however, in Fmr1 knock-out mice basal translation of PSD-95 mRNA is increased while mGluR activation does not activate PSD-95 translation further (Ifrim et al., 2015). Additionally, PSD-95 degradation is reduced in Fmr1 KO mice (Muddashetty et al., 2007, 2011). The dysfunction of FMRP, which normally acts to repress PSD-95 translation, thus has profound effects on the turnover of a key synaptic protein (Muddashetty et al., 2011). Other well-known diseases whose profile is defined by aberrant protein synthesis are vanishing white matter disease (VWMD), Charcot-Marie-Tooth disease and cancer, whose oncogenesis is driven by dysregulated protein synthesis (Le Quesne et al., 2010).

Chapter 1.2 The postsynaptic density protein PSD-95

1.2.1 Introducing PSD-95

We currently believe there to be less than 20,000 protein-coding genes in humans (Ezkurdia et al., 2014), and this number is continuously being revised downwards. At the same time, ever more proteins are being identified within the postsynaptic density (PSD), the key site of synaptic plasticity. A recent study identified nearly 1500 different proteins in the PSD of the human neocortex (Bayés et al., 2011), implying that around 7.5% of the proteins encoded by the human genome are represented in the PSD. It was also found that many of the proteins that make up this PSD are absolutely crucial to the brain's normal function, as they are implicated in a variety of psychiatric disorders when dysfunctional. Indeed, Bayés et al. (2011) found that mutations in 199 human PSD genes resulted in 269 diseases, ranging from common neurodegenerative diseases such as AD, PD and HD to cognitive disorders, epilepsies and many rare diseases.

Not only is it known that the proteins making up the PSD are vital to the synapse's function and health, but it is also thought that these proteins are not simply diffusely arranged within the PSD, but rather assembled in a modular fashion into molecular machines, or complexes (Husi et al., 2000; Collins et al., 2006; Frank and Grant, 2017). A number of proteins in the PSD are known to fulfil particularly crucial roles, since they function as hubs that link receptors to their signalling cascades and facilitate the interactions of numerous other proteins in the PSD. One group of proteins has received particular attention. This is the Discs Large homolog (DLG) family. These proteins are scaffolding proteins expressed abundantly at the PSD of excitatory glutamatergic synapses, and they are part of the Membrane-Associated Guanylate Kinase (MAGUK) super-family. In humans and mice, there are four known members of the DLG family: DLG4 (also known as PSD-95), DLG3 (SAP102), DLG2 (PSD-93) and DLG1 (SAP97). Invertebrates only express a single Dlg gene. Indeed, the evolution of the Dlg-gene family can be traced back to a shared common ancestor about 550 million years ago, and the four members (paralogs) of this gene family in

vertebrates arose from two whole genome duplication events early during chordate evolution (Nithianantharajah et al., 2013).

These four paralogs all have very similar structures that contain multiple domains required for protein-protein interactions, thereby facilitating the formation of large protein networks. The conserved domains are three PSD-95/Discs large/Zona occludens-1 (PDZ) domains, a Src-homology-3 (SH3) domain and a guanylate kinase (GK) domain (Fernández et al., 2009). The members of this family do, however, have distinct N-termini (Won et al., 2017). These proteins are known to form large complexes, some of which integrate the NMDA receptor with a host of other proteins. DLG4, also known as PSD-95, is the most prominent member of this family as a major component of the PSD (Cho et al., 1992), and has been recognised as the predominant antigen in rabbit antiserum produced after immunization with isolated bovine PSD fractions (Sampedro et al., 1981). Thus, PSD-95 is now widely used as a marker for glutamatergic postsynaptic terminals. It is known to interact with the NMDA receptor, with which it forms large, 1.5MDa complexes containing not only the NMDAR tetramer but a variety of other proteins as well, such as kinases, activity-regulated proteins, and potassium channels, among others (Frank et al., 2016).

1.2.2 PSD-95 interaction with AMPA receptors and synaptic maturation

It is clear that the role of PSD-95 is central to healthy synaptic plasticity. While PSD-95 is known to directly interact with the NMDA receptor, it is also known to interact with AMPA receptors, albeit indirectly. It does this through TARPs (Transmembrane AMPA receptor Regulatory Proteins) such as Stargazin (Chen et al, 2000), thereby influencing the concentration of AMPARs at the postsynaptic membrane (Beique et al., 2006). Thus, PSD-95 also exerts a direct control over synaptic strength, and indeed PSD-95 overexpression has been shown to result in increased levels of AMPARs in the postsynaptic membrane (El-Husseini et al., 2000). Furthermore, Levy et al. (2015) have reported that the knockdown of PSD-95 reduces AMPAR endplate synaptic currents (EPSCs) as well as the number of synapses containing AMPARs. However, a synaptic program of homeostasis appears to become activated, ensuring that those synapses that retain AMPARs do so at full strength, i.e. with their full

complement of AMPARs (Levy et al., 2015). Quite recently, PSD-95 nanoclusters have been described by various groups, made up of PSD-95 sub-domains within the PSD that are between 50 and 250 nm in diameter and can thus only be resolved by super-resolution imaging (Broadhead et al., 2016; MacGillavry et al., 2013; Nair et al., 2013; Fukata et al., 2013).
These PSD-95 nanodomains have also been shown to cluster AMPARs (MacGillavry et al., 2013; Nair et al., 2013), and indeed PSD-95 and the AMPAR subunit GluA2 appear to colocalise to a far greater degree than PSD-95 and NMDARs. This clustering effect is an important determinant of synaptic strength (Nair et al., 2013), as the local AMPAR density opposite the glutamate release site on the presynaptic bouton determines the strength of the synaptic response (Lisman et al., 2007). It is through the incorporation of AMPARs into the postsynaptic membrane along with this AMPAR clustering that PSD-95 most directly and immediately enhances synaptic strength during LTP (Ehrlich and Malinow, 2004; Beique et al., 2006; Schnell et al., 2002).

The link between PSD-95 and AMPARs is also intriguing as it links PSD-95 to the process of synaptic maturation. During the first two postnatal weeks, very little PSD-95 is expressed at synapses in vivo, whereas PSD-95's paralog SAP102 is highly expressed at this time (Sans et al., 2000). Over this time period, SAP102 is responsible for the trafficking of AMPA and NMDA receptors to synapses, but PSD-95 is not (Elias et al., 2006; Elias et al., 2008). However, at a later developmental stage, around postnatal day 15 (P15), PSD-95 expression has increased dramatically and synapses have become functionally mature. Overexpressing PSD-95 at an earlier time point, around P5-P8, prematurely leads to synaptic maturation, indicating that PSD-95 is responsible for the functional maturation of synapses (Elias et al., 2008). Furthermore, the knockout of PSD-95 retained synapses in an immature state, and this effect could be rescued by restoring PSD-95 expression (Elias et al., 2008).
What are the hallmarks of functional maturation of synapses? According to Elias et al. (2008), it is the enhanced expression of AMPARs and the replacement of NR2B-NMDARs with NR2A-NMDARs. Functionally immature synapses are also called 'silent' synapses, and do not contain any AMPARs, but do still contain NMDARs (Isaac et al., 1995; Takumi et al., 1999). PSD-95 is absolutely required for the experience-dependent maturation of silent synapses, inserting AMPARs into such synapses

(Huang et al., 2015; Ashby et al., 2011). The loss of PSD-95, on the other hand, reinstates or induces a silent state (Huang et al., 2015; Elias et al., 2006). Studies by Béique et al. (2006) and Chen et al. (2015) also established that PSD-95 KO mice express a greater proportion of silent synapses; however, they were also able to find silent synapses within morphologically mature spines. This indicates that functional and morphological maturation are not one and the same. Interestingly, El-Husseini et al. (2000) also found that overexpressing PSD-95 in hippocampal primary cultures around day in vitro 10-12 (DIV10-12) not only vastly increased synaptic AMPAR labelling and mEPSC amplitude, but also enhanced the staining for presynaptic marker proteins and the presynaptic vesicle pool, indicating that PSD-95 can drive not only the maturation of postsynaptic components, but also that of the presynaptic terminal.

Taken together, then, PSD-95 is a critically important protein for the modulation of synaptic strength, and is significantly involved in the functional maturation of synapses as well as playing a role in LTP. Many of these effects appear to be mediated through PSD-95's indirect interaction with AMPARs, which allows it to regulate synaptic AMPAR number.

1.2.3 Post-translational modifications of PSD-95

While the role of PSD-95 as a synaptic scaffolding protein has been studied extensively, it is also interesting to evaluate the role that various post-translational modifications can have on a protein. Li et al (2004) used 2D-gel electrophoresis and Mass Spectrometry (MS) to discover 6 different forms of PSD-95, some of which are different isoforms and others due to post-translational modifications. While all modifications and different splice forms of PSD-95 have not been conclusively defined, it has been established that PSD-95 is subject to phosphorylation, palmitoylation and ubiquitination, all of which are critical to its function.

There is evidence that activity modulates the interaction of PSD-95 with NMDA receptors. PSD-95 directly binds to the PDZ ligand of GluN2B and stabilizes its surface expression at synapses (Lau et al., 2007). Synaptic activity activates CaMKII, which

phosphorylates the C-terminal of the NR2B subunit of NMDA receptors, disrupting their interaction with PSD-95. This results in a dramatically reduced synaptic surface expression of NMDARs, indicating that an activity-dependent phosphorylation of NMDARs may regulate NMDAR function and synaptic plasticity (Chung et al, 2004; Lau et al., 2007). Similarly, CaMKII phosphorylates stargazin, facilitating the interaction of stargazin with PSD-95 and thereby mediating AMPAR stabilisation in the PSD (Constals et al., 2015). PSD-95 has also been shown to interact in a palmitoylation-dependent manner with the tyrosine phosphatase PTPN5, a protein known to regulate surface expression of NMDARs by dephosphorylating GluN2B and causing their internalization (Won et al., 2016). Through this interaction PSD-95 causes PTPN5 degradation, preventing GluN2B internalisation. It has also been demonstrated that the binding of the inward rectifying K+ channel Kir2.3 to PSD-95 is disrupted by phosphorylation of Kir2.3 (Cohen et al., 1996). Further, PSD-95 is itself phosphorylated at serine 73 by CaMKII in an activity-dependent manner, and this phosphorylation disrupts PSD-95's interaction with the NR2A subunit of NMDARs (Gardoni et al., 2006). This phosphorylation event also triggers the trafficking of PSD-95 out of the spine, terminates spine growth, and ultimately results in the inhibition of LTP (Steiner et al., 2008). A further phosphorylation site on PSD-95 has recently been described, causing a similar destabilisation of PSD-95 at the PSD (Nelson et al., 2013).

Palmitoylation, in fact, is a critical modulator of PSD-95 localisation. Palmitoylation of the N-terminal cysteine residues is crucial for the membrane localisation of PSD-95 in the PSD, and palmitoylation-deficient PSD-95 mutant mice display PSD-95 diffusely distributed in dendrites and the cell body (Topinka and Bredt, 1998). El-Husseini et al. (2000b) found that this synaptic localisation of PSD-95 is mediated by dual palmitoylation of PSD-95 on N-terminal cysteines 3 and 5, which has the effect of associating PSD-95 with perinuclear membranous compartments that traffic with vesiculotubular structures in a microtubule-dependent manner. If this dual palmitoylation is inhibited, PSD-95 does not localise to synapses nor cluster ion channels such as the AMPAR. Indeed, the depalmitoylation of PSD-95 by activity-induced glutamate causes PSD-95 clusters to disperse, which in turns triggers AMPAR internalisation (El-Husseini et al., 2002). Inversely, blocking synaptic activity leads to the rapid induction of PSD-95 palmitoylation, and concurrent PSD-95 and

AMPAR clustering (Noritake et al., 2009). At a super-resolution level, it was found that when the palmitoylating enzyme DHHC2 was targeted to the postsynaptic plasma membrane, this resulted in the palmitoylation and hence recruitment of PSD-95 to the plasma membrane as well (Fukata et al., 2013). Enhanced synaptic activity caused the depalmitoylation of PSD-95, and the dissociation of both these proteins from the plasma membrane. Furthermore, Fukata et al. (2013) also found that this is the mechanism by which palmitoylated PSD-95 forms postsynaptic nanodomains, and these nanodomains cluster AMPAR, thereby controlling their activity-dependent surface expression. Thus, palmitoylation is essential to PSD-95's role in the synapse, controlling synaptic localisation, nanodomain formation and AMPAR clustering.

PSD-95 also interacts with proteins that are involved in dendritic spine morphology, and thus indirectly plays a role in the structural modelling of spines, as well as their morphogenesis. At synapses, PSD-95 binds directly to Kalirin-7, a GDP/GTP exchange factor for Rac1 that interacts with the cytoskeleton to control actin dynamics and thereby regulate spine morphogenesis (Penzes et al., 2001). SPAR, a Rap-specific GTPase-activating protein (RapGAP), has been found to form a complex with PSD-95 and NMDARs at synapses and also interacts with the actin cytoskeleton to effect changes in spine morphology, causing spine heads to enlarge, and enhancing PSD-95 expression at such synapses (Pak et al., 2001). Finally, PSD-95 has been found to indirectly interact with SNAP-25, a component of the SNARE complex that is involved in synaptic vesicle exocytosis, in protein complexes at the PSD (Fossati et al., 2015). A reduction in SNAP-25 levels was found to reduce dendritic spine density, impair synaptic potentiation, and reduce PSD-95 clustering at synapses. A reduction in SNAP-25 levels is associated with attention deficit hyperactivity disorder (ADHD) and schizophrenia, and may thus cause synaptic defects through its interaction with PSD-95 (Fossati et al., 2015). Overall, then, PSD-95 appears to be linked to dendritic spine morphology in an indirect fashion, interacting with proteins that directly control cytoskeletal dynamics and spine morphogenesis. The presence of PSD-95 at spines is also strongly correlated with spine stability in vivo (Cane et al., 2014). Newly formed dendritic spines that fail to recruit PSD-95 are quickly pruned, whereas PSD-95 accumulation at spines is positively correlated with an increased spine lifetime. Cane et al. (2014) also found that mature spines that were destined to be pruned reduced their PSD-95 content well in advance of the pruning event. Thus, PSD-95 not only

plays an important role in recruiting other synaptic proteins to the PSD, but its presence at synapses is also a strong indicator of spine stability. Note, however, that PSD-95 itself is not directly involved in synaptogenesis or spine maintenance, as PSD-95 knock-down does not appear to affect dendritic spine density (Levy et al., 2015).

Another posttranslational modification of PSD-95 that plays an important role is its ubiquitination, insofar as it mediates its degradation. Colledge et al. (2003) found that NMDAR activation leads to the ubiquitination of PSD-95 by the E3 ligase Mdm2, which in turn causes PSD-95 to be degraded by the 26S proteasome. Blocking this ubiquitination prevents PSD95 degradation as well as NMDA-induced endocytosis of AMPA receptors. Taken together, then, PSD-95's function is heavily dependent upon post-translational modifications. Palmitoylation is critical for the localisation of PSD-95 to the PSD, which in turn is essential for PSD-95 to be able to fulfil its function. Phosphorylation is another key modification, and one particular phosphorylation event by CaMKII appears to be critically involved in PSD-95's synaptic localisation and role in dendritic spine growth and LTP. Other phosphorylation events target interactors of PSD-95 and thus modulate its function. Other post-translational modifications of PSD-95 have also been described, such as nitrosylation, and neddylation (Vallejo et al., 2016), and while ubiquitination is thought to cause its degradation by the proteasome, one study has shown that this is not always the case (Bianchetta et al., 2011).

1.2.4 PSD-95 as a molecular organizer of supercomplexes

While PSD-95 has long been known to play important roles in AMPAR clustering, LTP, synaptic maturation and synaptic stability, its perhaps most critical role has only recently begun to be understood more fully. As mentioned above, PSD-95 localises with NMDA receptors into large multiprotein complexes, and this interaction has been known for some time (Husi et al., 2000). However, newer research has revealed that PSD-95 is in fact one of the key components of these supercomplexes, acting as one of their central organisers. Two recent studies, Frank et al. (2016) and Frank et al. (2017), have together shown that PSD-95 is not merely a component of 1.5MDa NMDAR supercomplexes, but rather acts as a critical organizer of these supercomplexes. In fact, they found that almost all PSD-95 of the forebrain is retained

within these supercomplexes. Furthermore, PSD-95 assembles a large variety of these 1.5MDa complexes, and only a minority of these contain NMDARs at all. In Frank et al. (2016), it was demonstrated that there are two discrete populations of NMDAR complexes: 0.8MDa complexes and 1.5MDa complexes. The complex at 0.8MDa is largely made up of the tetrameric NMDAR ion channel, and does not contain PSD-95. Within the 1.5MDa NMDAR supercomplex, however, 50 different proteins were identified, ranging from other ion channels over receptors and adhesion proteins to signalling enzymes. PSD-95 is essential for the formation of these 1.5MDa NMDAR complexes, and Frank et al. (2016) were able to establish a 'tripartite rule', stipulating that three proteins were absolutely mandatory for the assembly of these complexes. These three proteins are PSD-95, PSD-93 (DLG2, one of PSD-95's paralogs), and the GluN2B subunit of the NMDAR. Without the presence of these three fully functional proteins, 1.5MDa NMDAR supercomplexes are unable to form. In accordance with these rules and PSD-95's developmental expression profile, the study also showed that 0.8MDa NMDAR complexes are present at all postnatal ages, whereas 1.5MDa NMDAR supercomplexes are only found from P16 onwards, when PSD-95 expression increases. The second study (Frank et al., 2017) demonstrated that only 3% of the 1.5MDa complexes containing PSD-95 also contain NMDARs. This means that NMDAR supercomplexes are merely a subset of a much greater family of PSD-95 supercomplexes. They were further able to subdivide these PSD-95 supercomplexes, identifying complexes that were characterised by the presence of the proteins Arc/Arg3.1, Kir2.3, IQsec2/BRAG1 and Adam22. Thus, these studies concluded, there appears to be a hierarchy of PSD-95 supercomplexes, each comprising functionally distinct proteins and assembled with unique genetic prerequisites. PSD-95, however, is the key organizer of most of these 1.5MDa supercomplexes, and is on average present as a dimer in each (Frank et al., 2017). Note, however, that not all 1.5MDa supercomplexes require PSD-95 to assemble: in PSD-95 knock-out mice, PSD-93 is still able to assemble some 1.5MDa supercomplexes. However, these do not contain NMDARs, and are differ from PSD-95 1.5MDa complexes, which disappear together with PSD-95. These findings are in line with previous studies, which have shown that the loss of PSD-95 leads to a structural fragmentation of the PSD, while the simultaneous loss of the three MAGUKs PSD-95, PSD-93 and SAP102 causes the PSD to profoundly disintegrate and shrink in size (Chen et al., 2011; Chen et al., 2015).

Functionally, it is thought that these diverse supercomplexes are central to synaptic function and ultimately higher cognition and the ability to effectively process and store information. Thus, PSD-95 and the complexes it forms are thought to be key elements in the processes of learning and memory formation, as well as the normal functioning of the brain. While the NMDA receptors have been shown to function normally as an ion channel in mice lacking PSD-95 (since 0.8MDa NMDAR complexes do not contain PSD-95), these animals have impaired learning, indicating that the proteins associated with the receptors are what is crucial to the formation of memory traces. Intriguingly, Migaud et al (1998) found that when PSD-95 is knocked out, such mice display strikingly enhanced LTP, but LTD is eliminated and spatial learning severely impaired. Thus PSD-95's role in relation to NMDARs seems to be to couple these receptors to pathways that modify synaptic strength in a bidirectional manner, potentiating and depressing synaptic strength as appropriate. The lack of PSD-95 may thus result in an inappropriate strengthening of too many synapses and hence yield a degradation of information storage, manifested as a learning impairment (Migaud et al., 1998). It may be unsurprising, then, that there are a variety of diseases in which a reduction in functional PSD-95 has been observed, such as Fragile X syndrome (Ropers, 2008), bipolar disorder and schizophrenia (Toro and Deakin, 2005; Cheng et al., 2010), major depression (Feyissa et al, 2009), and autism spectrum disorder (Feyder et al, 2010; Peça and Feng, 2012).

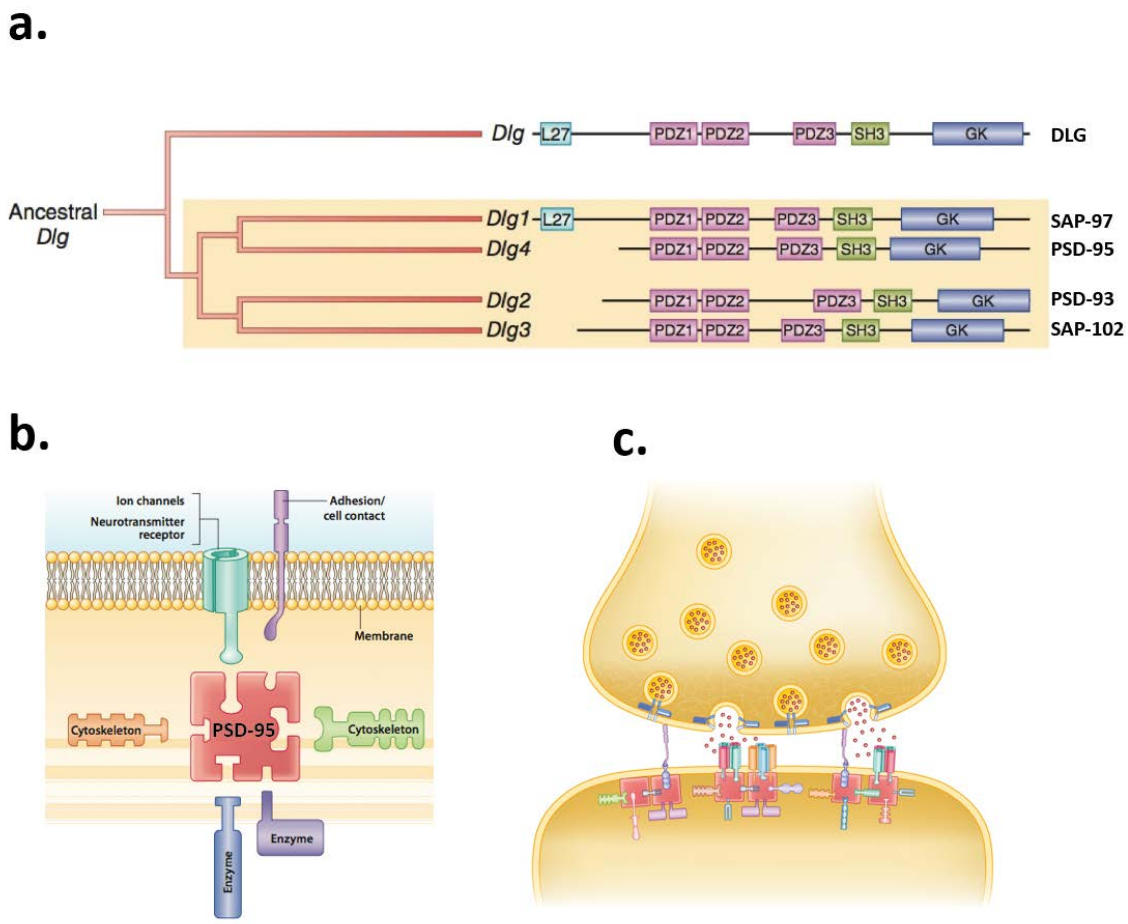

Figure 1.1. Structure and function of PSD-95.
a. Family tree and structure of the four Dlg paralog members of the MAGUK superfamily: Dlg4 (PSD-95), Dlg3 (SAP102), Dlg2 (PSD-93) and Dlg1 (SAP97). Comparison with the invertebrate Dlg protein. Adapted from Nithianantharajah et al. (2013). **b.** The scaffolding protein PSD-95 forms a core component of multiprotein supercomplexes found in the postsynaptic density (PSD) of excitatory synapses. In this way, many different synaptic proteins are brought together and assembled into a complex molecular machine. Adapted from Emes and Grant (2013). **c.** Conceptual diagram of an excitatory synapse. Diverse 1.5MDa supercomplexes are assembled to form integral components of the PSD. These complexes participate in synaptic plasticity and are thought to be important for learning and memory, and are implicated in psychiatric disease states when mutated (Frank et al., 2016). Adapted from Grant (2013).

1.2.5 PSD-95, the dynamic protein

We can gather from the recently reviewed literature that PSD-95 is central to the formation and integrity of the PSD, and acts as a hub that brings together a multitude of other proteins in large complexes that are organized into nanodomains, including NMDA and AMPA receptors. In this way, PSD-95 can help shape spine morphology, determine synaptic strength, and affect LTP and LTD. While I have discussed the importance of various factors such as palmitoylation in the synaptic localisation of PSD-95, it is important to give an insight into the dynamic properties of PSD-95 at healthy synapses, and the role that these dynamics play in PSD-95's function.

Early studies found evidence for a two-tiered population of PSD-95 within synapses and dendrites. These studies used Fluorescence-recovery after photobleaching (FRAP) to analyse the stability of PSD-95, and found that there was a small pool of 'mobile' PSD-95 molecules that rapidly moved between synapses, while the majority of PSD-95 was 'stable' and did not readily move out of synapses (e.g. Todd et al., 2003). However, these studies monitored PSD-95 mobility over short time frames (seconds to minutes), and more recent studies conducted over long time periods (hours) have found that the entire population of PSD-95 is in fact dynamic rather than immobile (Ziv and Fisher-Lavie, 2014). These newer studies indicate that the previously-observed 'mobile' PSD-95 is in fact not fully incorporated into the PSD, but only weakly associated with it and more closely connected with dynamic cytoskeletal components such as actin filaments (Zheng et al., 2010). Furthermore, these more recent studies concluded that the 'stable' fraction of PSD-95, which is fully incorporated into the PSD and associated with NMDAR and AMPAR complexes, in fact does move between PSDs. The study by Gray et al. (2006) is particularly notable, as it was conducted in vivo, within the intact cortex of mice. This study demonstrated that PSD-95 molecules do indeed move between synapses (remaining within a given synapse for less than an hour, on average), that PSD-95 mobility is greater in smaller synapses compared to larger ones, and that the mobility of PSD-95 goes down as mice mature. Finally, the study showed that the total PSD-95 content of a given synapse changes over the course of days, and this finding was more recently corroborated by Cane et al. (2014). The study by Butko et al. (2012) also demonstrated

that newly synthesised PSD-95 travels to synapses and is incorporated into PSDs within 6 hours of synthesis, rather than replenishing 'dendritic stores'. Moreover, the PSD-95 nanodomains within the PSD have also been shown to morph and appear to have lifespans shorter than one hour (MacGillavry et al., 2013; Nair et al., 2013), implying that clusters of PSD-95 within the PSD and their associated multiprotein complexes are themselves mobile. This paints a picture of a much more fluid PSD than the rigid structure initially conceptualised (Ziv and Fisher-Lavie, 2014). Within this PSD, multiprotein complexes are likely assembled and disassembled frequently, and this restructuring is mediated by the post-translational modifications of scaffolding proteins such as PSD-95 that are induced by various states of synaptic activity. One thing that is worth noting, however, is that while PSD-95 has been shown to be mobile and move between spines, it is nonetheless a lot more stable than many other synaptic proteins, such as CaMKII, Stargazin, and GluR2, which all move more rapidly between spines (Sturgill et al., 2009). As mentioned above, factors such as NMDAR activation, PSD-95 palmitoylation and PSD-95 phosphorylation all regulate the stability of PSD-95 within the synapse, and enhance or reduce its rate of removal from the PSD (Sturgill et al., 2009). One good example is the trans-synaptic organizing protein ephrin-B3, which directly interacts with PSD-95 and appears to be crucial for PSD-95's synaptic localisation and stability at the PSD (Hruska et al., 2015).

1.2.6 PSD-95 synthesis and degradation

While multiple recent studies have demonstrated that PSD-95 is a protein that is mobile and moves between synapses, there is another aspect of PSD-95's presence at the synapse, and that is its turnover rate, made up of both synthesis and degradation. As reviewed above, protein turnover has been established as being crucial to synaptic function and the induction of both LTP and LTD. The role of PSD-95 turnover, however, is much less clear. It appears that PSD-95 is synthesized in the cytosol and trafficked to synapses in vesicles (Yoshii and Constantine-Paton, 2007), however, local translation also plays a big part in PSD-95 synthesis. Thus, PSD-95 mRNA is found distributed throughout dendrites (Muddashetty et al., 2007), and local synthesis has been directly observed in dendrites and spines using single-molecule imaging of reporter-tagged PSD-95 (Ifrim et al., 2015). One explanation for these

different sites of PSD-95 synthesis may be that there is a certain amount of constitutive PSD-95 turnover, which functions to replace old proteins and hence is not urgent. It takes place in the cytosol, therefore requiring more time to deliver the synthesised proteins to their destinations. On the other hand, local synthesis of PSD-95 in dendrites and spines is induced by acute factors, necessitating a rapid increase in local PSD-95 levels. The activation of mGluRs by substances such as S-3,5-dihydrophenylglycine (DHPG) has been demonstrated to cause such a rapid, local increase in PSD-95 synthesis (Ifrim et al., 2015; Todd et al., 2003). A study by Butko et al. (2012) also demonstrated that treating neurons with chemicals enhancing or mimicking synaptic activation (bicuculline, DHPG and BDNF) increases the concentration of newly-synthesised PSD-95 both at the level of stimulated synapses and the whole neuron, although the source of this new PSD-95 was not determined. Interestingly, this study also found that immature synapses with incompletely developed PSDs tended to contain newly-synthesised PSD-95 while mature synapses are enriched in older PSD-95 molecules that are incorporated fully into the PSD.

The other determinant of PSD-95 turnover is its degradation, mediated primarily by the ubiquitin-proteasome system (Colledge et al., 2003; Tsai et al., 2012). The main measure of a protein's degradation rate is the half-life, which represents the amount of time it takes for half of a given starting amount of PSD-95 to degrade (Ziv and Fisher-Lavie, 2014). In fact, the half-life of PSD-95 has been widely studied, and has yielded a bewildering range of results. The main determinant of this diversity in results appears to be the methods utilised to obtain them. First, a study by Ehlers (2003) obtained a half-life of 8 hours, using ^{35}S-methionine metabolic labelling of isolated PSDs (12 hour pulse). Second, El-Husseini et al. (2002) derived a half-life of approximately 36 hours, also using ^{35}S-methionine metabolic labelling but in intact cultures, with a 1-hour pulse. Next, Cohen et al. (2013) found PSD-95's half-life to be about 88 hours using stable isotope labelling by amino acids in cell culture (SILAC), with a long pulse time (7 days pulse labelling). Indeed, the pulse labelling time period is critical in these metabolic labelling experiments, as its length determines what proportion of a protein's population is labelled and thus monitored. Finally, a study by Price and colleagues (2010) was conducted in which live mice were fed on a diet leading to organism-wide isotopic labelling, which could then be monitored by mass spectrometry. The results indicated a half-life of 367 hours (15.3 days) for PSD-95. The pulse period here was 32 days, but it is likely that proteins within live adult mice

simply experience greater half-lives than those within young, cultured neurons. Taken together, the results indicate that longer pulse labelling times are linked to longer half-lives, that is to say that the more accurate results indicate a longer half-life.
Intriguingly, the regulation of PSD-95 degradation appears to play an important role in synaptic plasticity. Colledge et al. (2003) found that brief NMDAR activation, inducing LTD, causes PSD-95 to be ubiquitinated and degraded by the proteasome as a result. This in turn leads to AMPAR internalisation and weakening of these synapses, and inhibition of the proteasome prevents PSD-95 degradation, AMPAR internalisation and LTD. Numerous studies have shown that blocking protein degradation by inhibiting the proteasome blocks LTP and LTD (Fonseca et al., 2006; Lopez-Salon et al., 2001; Karpova et al., 2006), and while PSD-95 is far from the only protein affected by this blockade, it may contribute significantly to the resulting effects.

1.3 The HaloTag technology

1.3.1 Introduction to the HaloTag technology

Over the past decades, many different reporter proteins have been engineered on the basis of naturally occurring proteins. The most famous example of this is the green fluorescent protein, GFP, which was derived from a jellyfish protein and is today used in a huge variety of different settings to visualise a protein of interest (Chalfie et al., 1994). The tandem affinity purification (TAP) tag is another example of a protein frequently used to affinity-purify proteins of interest and their interacting partners (Rigaut et al., 1999). There is a huge variety of such proteins nowadays, but what they have in common is that they tend to be relatively small, allowing them to be fused to a protein of interest (POI), thereby allowing us to study this POI in its natural state by a variety of methods. More recently, Promega developed another such reporter protein, called HaloTag. The HaloTag protein is a monomeric protein that has a molecular mass of 33 kDa. Like other reporters, it can be genetically fused to a POI. The original protein was derived from a haloalkane dehalogenase enzyme found in the bacterium *Rhodococcus rhodochrous*, and is thus not found in mammals, insects, yeast and even E. coli (Urh and Rosenberg, 2012). This has the great advantage of avoiding

interference by endogenous proteins or ligands if used in these systems. In its natural state, this haloalkane dehalogenase enzyme reacts with an aliphatic hydrocarbon substrate by a nucleophilic displacement reaction, forming a covalent ester bond. This intermediate is then released again by a base-catalysed hydrolysis reaction, allowing for further rounds of catalysis (Los et al., 2008). However, this *Rhodococcus* enzyme was modified, and a mutation now prevents the release of the hydrocarbon substrate. Instead, the chloroalkane substrate molecule remains tightly and covalently bound to the haloalkane dehalogenase enzyme (now called HaloTag). The chloroalkane substrate was further engineered to bear a variety of useful molecules that allow, among other things, the detection and purification of the HaloTag protein and any POI it may be fused to. These substrates are termed 'ligands'.
Los et al. (2008) then further engineered the HaloTag protein to enhance the binding rate and efficiency of these ligands to the HaloTag protein. The final binding kinetics of the HaloTag protein to its ligands display a rate similarly rapid to those of the biotin-streptavidin interactions. For instance, the HaloTag protein binding rates to a ligand bearing a fluorescent carboxytetramethylrhodamine (TMR) ligand have a second-order rate constant of 2.7×10^6 M^{-1} s^{-1}, which is comparable to the binding rate of streptavidin to TMR-biotin (Los et al., 2008).

The key aspect of this Halotag technology is the fact that the HaloTag ligands are incredibly versatile, and can be bestowed with a wide variety of functionalities, while retaining their binding affinity for the HaloTag protein. This is achieved because the ligands are designed to consist of two elements- a constant reactive group and a variable functional group. The constant group is based upon the original HaloTag enzyme's substrate and consists of a chloroalkane. This chloroalkane binds covalently to the HaloTag protein, and this covalent binding is irreversible: incubating the HaloTag protein bound by TMR ligand with GST-HaloTag protein bound by FAM ligand does not lead to cross-labelling (Los et al, 2008). This bond, which consists of an ester bond buried deep in a hydrophobic pocket (Newman et al, 1999), is stable even under conditions expected to disrupt protein structure, such as boiling in SDS for 20 minutes at 95°C. (Los et al, 2008). It is also important to note that only a single ligand binds to a single HaloTag protein in this permanent, irreversible manner.
The second element, the variable functional group, can be selected according to the desired properties. Promega supplies a number of ready-made ligands with functional

groups that are fluorescent molecules, affinity handles such as biotin, and solid support such as sepharose. Many of these are cell permeable, while some are not. All are designed to be non-toxic and to not alter cellular morphology. Cell permeable ligands have a very low molecular weight, between 439 and 702 g/Mol. Broadly, these commercially available ligands can be placed into two categories: fluorescent ligands for the visualisation of the POI, and affinity handles, for the purification of the POI and possibly interactors.

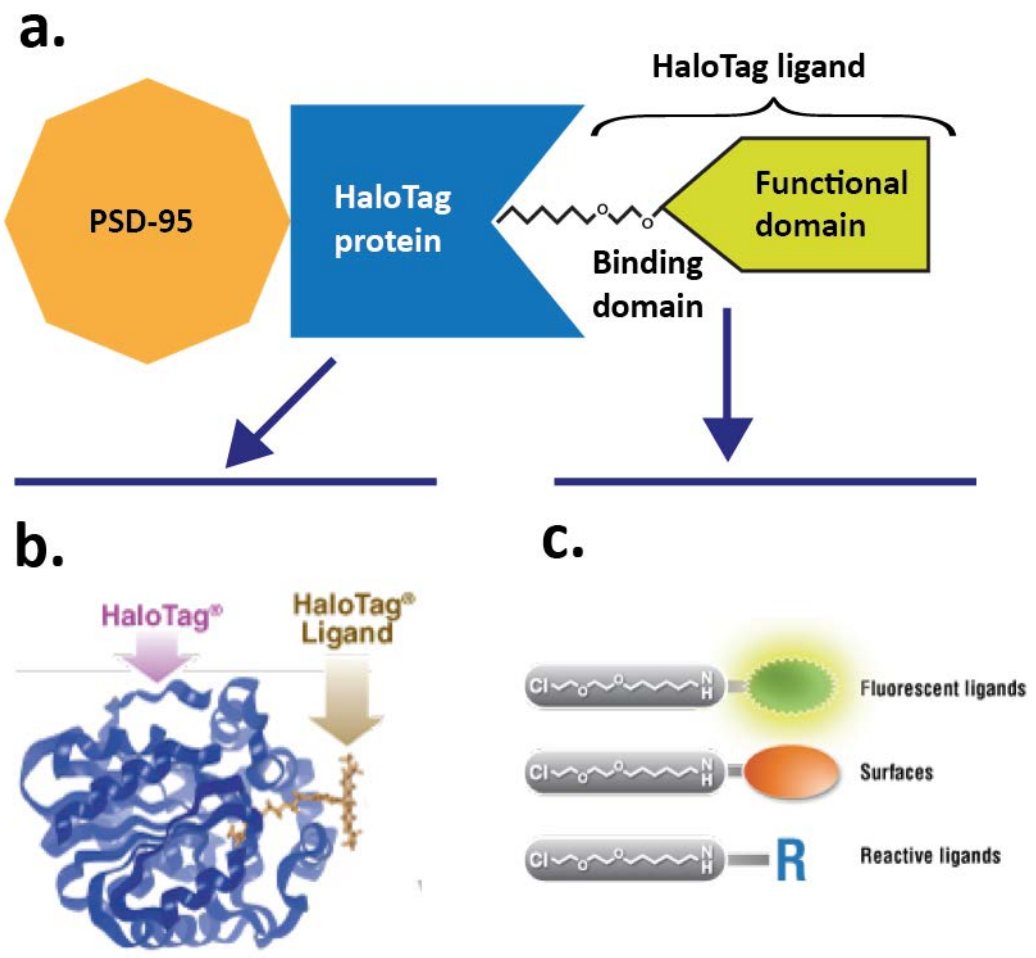

Figure 1.2. Structure of the PSD-95-HaloTag fusion protein.
a. This figure demonstrates the structural relationship between the protein of interest, in this case PSD-95, and the HaloTag protein it is fused to. A HaloTag ligand binding to the PSD-95-HaloTag fusion protein is also depicted. **b.** Model of HaloTag protein with HaloTag ligand inserted into binding pocket. HaloTag ligands bind to HaloTag proteins specifically, covalently and irreversibly. **c.** HaloTag ligands are characterised by their invariable binding domain and variable functional domain. Functional domains can be bestowed with a variety of properties, ranging from fluorescent groups and affinity surfaces such as biotin to custom-made reactive

groups, such as the degradation-inducing ligand presented in Neklesa et al. (2011). Entire figure adapted from Urh and Rosenberg (2012).

1.3.2 Imaging with HaloTag

Commercially available fluorescent ligands cover a wide range of wavelengths, from blue (Coumarin ligand, emission: 450nm) to far-red (AlexaFluor660, emission: 690nm) and everything in between. Apart from the AlexaFluor660, all of these ligands are membrane-permeating, meaning that they can penetrate live cell membranes without the need for these to be perforated beforehand. This facilitates live-cell labelling of cultured cells, allowing one to simply add the ligand to the culture media and resulting in HaloTag labelling within a short space of time (labelling protocols typically require a mere 15 minutes of incubation- see Promega's Focus on Imaging handbook). These characteristics result in the HaloTag technology being ideally suited for Pulse-Chase based experiments for the analysis of protein synthesis and degradation. In a cell culture environment, this involves labelling the entire pool of existing proteins in the cell culture with ligand A (the 'Pulse' ligand), and subsequently washing the excess unbound ligand A off. Following a stimulus or a period of time which will result in a new population of fusion proteins being synthesised, this is then followed up with a second labelling regime, this time with a different ligand, ligand B (the 'Chase' ligand). In this manner, one has labelled two discreet populations of the same fusion protein, but at different time points and with different, distinguishable ligands (Uhr & Rosenberg, 2012). This allows, for example, differences in the localisation of old and new proteins to be identified, and their half-life to be calculated (Huybrechts et al, 2009). He et al. (2011) and Okada et al. (2010) have similarly used a pulse-chase protocol with fluorescent HaloTag ligands to visualise the degradation rate of a POI, and hence calculate its half-life.

1.3.3 Purification with HaloTag

While this approach is interesting from an imaging perspective, it also creates a powerful tool for the proteomic isolation of newly synthesised proteins. If this is coupled with a stimulus protocol, it allows for the precipitation of proteins interacting with fusion proteins that were synthesised specifically in response to stimulation. Once isolated,

such multiprotein complexes could then simply be compared with complexes purified prior to stimulation, and thereby allow for a detailed analysis of different complex populations. This approach to identify protein complex members has, for instance, been used by Daniels et al. (2012). The HaloLink resin also allows newly synthesized proteins to be isolated directly, as they are captured by the chloroalkane linker attached to a resin surface. In this way, one only captures newly synthesised fusion proteins (and associated complexes) that have no ligand A bound to them, as older proteins have their binding site blocked by ligand A. Due to the very rapid and highly specific binding of this resin to the HaloTag fusion protein, this technique allows for the isolation of even a relatively small number of newly synthesised proteins. As Daniels et al. (2012) point out, this minimises the background caused by non-specific interactors when immunoprecipitating, greatly aiding Mass Spectrometry studies.
The drawback of using HaloLink resin directly is the fact that the fusion protein cannot be eluted or boiled off the resin; however, this can be circumvented by use of a TEV protease, which cleaves the HaloTag protein off the fusion partner (POI) at a specific site (Urh & Rosenberg, 2012). Since this TEV treatment will cleave the POI off the HaloLink resin, it retains all interacting proteins attached to the POI, allowing for the analysis of protein complexes.

1.3.4 Homemade tags

A further important aspect to note is that the HaloTag ligands can also be purchased from Promega in a basic form, consisting only of the chloroalkane linker region that binds to the HaloTag protein, but lacking the functional group. Instead, these ‘bare’ ligands can be bestowed with a functional group of one’s choice, and thus many groups have used this option to produce a variety of unique ligands with exceptional properties. Thus, a number of groups has created infrared and near-infrared ligands (Tseng et al., 2012; Fujita et al., 2012). Other groups have created ligands that have allowed them to target a HaloTag fusion protein with a contrast reagent for MRI (Strauch et al., 2011) as well as a reporter for positron emission tomography (PET) (Hong et al., 2011). One of the most intriguing advances in this area, however, was the discovery that a small hydrophobic tag could induce the acute degradation of a HaloTag fusion protein upon binding. In 2011, Neklesa at al. reported that a small

hydrophobic membrane permeable HaloTag ligand bearing adamantyl groups leads to the delivery of the fusion protein to the proteasome for degradation. The underlying mechanism appears to be that the hydrophobic tag mimics a partially denatured protein state. Neklesa et al. (2011) were able to degrade tumours expressing the HaloTag fusion protein in live mice by over 80% over 13 days through the intraperitoneal injection of this ligand. A truly exciting application of this ligand is that it allows the acute knock-down of a single specific POI only. Furthermore, subpopulations of this protein can be degraded if a pulse-chase protocol is used to label previously-present proteins with a non-degrading ligand (thereby keeping them safe from degradation), and labelling only newer proteins with the degradation-inducing ligand. This way, one could effectively prevent the synthesis of a specific target POI while retaining older proteins, with no off-target effects on other proteins. This allows for novel insights to be gained into protein functions and seems to be the first method to allow for such deft manipulation.

Finally, the HaloTag technology has been utilised in live animal models as well. Various studies have xenografted tumours expressing the HaloTag protein fused to a POI into live mice, and subsequently labelled these tumours using various HaloTag ligands (Tseng et al., 2012; Kosaka et al., 2009), including PET imaging of tumours (Hong et al., 2011). The study by Neklesa et al. (2011) was conducted in live mice and zebrafish, as well as cell cultures. Finally, Fujita et al. (2012) managed to label a tagged POI within the brain of a live mouse using a ligand bearing a near-infrared fluorescent dye, allowing them to visualise brain ischemia in a mouse model of stroke.

1.3.4 HaloTag conclusions

The key advantage of the HaloTag technology over most other reporter proteins, then, is its incredible versatility. This technology allows for a POI to be analysed in a huge variety of different ways, ranging from biochemistry to super-resolution microscopy (Chen et al., 2013). It even allows for the manipulation of the expression of the POI, and can be used in vivo as well as in vitro. Importantly, it also allows different subpopulations of the same target protein to be labelled with different tags. While other reporters may permit aspects of this sort of analysis as well, none are able to unite all

of these techniques within a single tag: creating a single genetically engineered mouse expressing a POI fused to the HaloTag protein allows one to utilise this entire complement of analytical techniques.

1.4 Conclusion, aims and hypotheses

Over the past decades, a lot of progress has been made in our understanding of how memories and behaviours are induced, neurons and synapses function, and molecules such as PSD-95 tie these mechanisms together. We have discovered a wide range of molecules that play important roles in the PSD, and begun to understand how they are organized within this structure in order to mediate their effects. However, there is much left for us to learn. We have also made massive strides forward in terms of scientific techniques, developing game-changing technologies such as super-resolution imaging and the CRISP-Cas9 system that constantly allow us to push the boundaries of the possible within various scientific fields.

More recently, the postsynaptic scaffolding protein PSD-95 was established as one of the major actors in structuring the PSD within excitatory neurons and mediating protein interactions and synaptic plasticity. PSD-95 has been found to undergo various modifications, such as palmitoylation and phosphorylation, and these modifications strongly affect its localisation and function. Palmitoylation appears to be critical for PSD-95's recruitment to synapses and incorporation into the PSD, and the phosphorylation of certain PSD-95 residues appears to affect its interaction with NMDA receptors as well as its removal from synapses. Its localisation and stability at the PSD are also influenced by its interactions with a variety of proteins, which can cause it to be stabilized at PSDs or removed from them. While PSD-95 is affected by a multitude of factors, it plays a role itself in recruiting and clustering AMPA receptors at the PSD, LTD, LTP, spine growth and stability, and more. It has also been found to be activity regulated, being synthesised locally in dendrites in response to mGluR activation and cycled out of synapses or degraded in response to NMDAR activation. As such, it is a dynamic protein that has been demonstrated to regularly move between synapses, while simultaneously playing an important structural role in the PSD. There, it has recently been found to be a core component of a wide variety of large,

multiprotein supercomplexes that form nanodomains and are thought to be the modular cornerstones of the PSD.

In this project, I will be utilising the novel HaloTag technology to investigate the turnover of PSD-95 at the synapses of excitatory neurons. My project is based upon a strain of genetically engineered mice expressing the HaloTag protein fused to endogenous PSD-95, allowing me to visualise the localisation of this PSD-95-HaloTag fusion protein using fluorescent HaloTag ligands. My project is principally based upon primary neuronal cultures, and in this system, I have developed a novel pulse-chase method for the differential labelling of old and new PSD-95 molecules, allowing me to localise and analyse these two subpopulations separately.

To provide a very brief overview of the structure of this thesis, I would like to highlight that there is a clear division of the results into two parts. The first part is chapter 3, which lays a foundation upon which the results of chapter 4 are built. Chapter 3 essentially characterises the PSD-95-HaloTag knock-in mouse line, probing the expression of PSD-95 using a variety of methods, from biochemistry to immunohistochemistry and more. In chapter 3, I also present my pulse-chase labelling method using the HaloTag technology, and apply it to a simple PSD-95 turnover study. In chapter 4, I use these findings to probe PSD-95 turnover at synapses in depth, categorising synapses based upon their turnover profiles and ultimately investigating the effects of various chemical agents on PSD-95 turnover in a novel manner.

Hypotheses:

- It is hypothesised that using two different HaloTag fluorescent ligands consecutively, in a Pulse-Chase labelling manner, will permit the labelling of old and new PSD-95 proteins separately and thereby allow for the calculation of PSD-95 turnover.

- It is hypothesised that using fluorescent HaloTag ligands in primary cultures and in conjunction with confocal microscopy will enable the quantitative visualisation of PSD-95 synthesis and degradation at single synapses.

- It is hypothesised that chemical modulatory drugs that affect neuronal signalling will increase or decrease synaptic PSD-95 synthesis and degradation.

- It is hypothesised that drugs that prevent protein synthesis will reduce PSD-95 turnover.

- It is hypothesised that drugs that prevent protein degradation will also reduce PSD-95 turnover.

Main aims:

- Establish a protocol, using the HaloTag technology, that allows me to measure PSD-95 turnover at the synapse in neuronal primary cultures.

- Use this protocol to analyse PSD-95 turnover at single synapses.

- Analyse the effects of a range of chemical modulators on PSD-95 turnover.

Chapter 2: Methods

2.1 Biochemistry and mouse genetics

2.1.1. Genetic engineering of PSD-95-HaloTag knock-in mice

All mouse procedures were performed in accordance with Home Office regulations. The method and targeting strategy that was used to create the PSD-95-HaloTag mice is identical to the one described by Fernandez et al., (2009). The genetic experiments were performed by Dr Fei Zhu, Dr Noboru Komiyama and David Fricker. A PSD-95 intermediate targeting vector that had been previously constructed for use in the generation of PSD-95 TAP-tag mice (Fernandez et al., 2009) was used. The HaloTag protein was fused to the C-terminal domain of PSD-95 and designed so as to not interfere with splicing, as three murine PSD-95 isoforms have been identified as containing conserved C-terminal sequences (Bence et al., 2005). The HaloTag coding sequence was obtained from Promega. The HaloTag coding sequence was inserted into the open reading frame of the PSD-95 gene on the 3' end, immediately before its stop codon (Figure 2.1), using recombination in *Escherichia coli* as described in previously published methods (Liu et al., 2004). Extraction of targeting plasmid DNAs was performed using XhoI and BglII endonuclease restriction sites, and the targeting vector was linearized with the PvuI enzyme before being electroporated into mouse embryonic stem cells. The identification of positive targeting clones was achieved by PCR, following which they were cloned, expanded and frozen down, before being injected into blastocysts from C57BL/6J mice. Chimeric male mice were then backcrossed to wildtype females, generating heterozygous mice. These animals were then crossed with transgenic CAG Cre-recombinase-expressing mice, in order to excise the neomycin cassette. Once the neomycin cassette was removed, heterozygous mice were then crossbred to produce homozygous animals.

2.1.2 Crude synaptosome preparation from mouse brains

This protocol was used on mouse brain tissue to lyse cells and enrich for the PSD protein fraction. The brain was taken out of -80 storage, placed into a tight-fitting glass homogeniser, 5ml Homogenisation buffer (320mM sucrose, 1mM HEPES (pH7.4)) was added, and the brain was homogenised with 12 strokes on ice. This was divided

up into 3 2ml Eppendorf tubes and centrifuged at 1000 xg and 2°C for 10 minutes to remove debris and vascular tissue. The supernatant (S1) was collected and saved on ice. The pellets were resuspended in a total volume of 2ml Homogenisation buffer, transferred to the glass homogeniser, and 6 strokes performed. This was transferred to Eppendorf tubes and centrifuged again at 1000 xg and 2°C for 10 minutes to remove further debris. The supernatant was collected again and pooled with the S1 supernatant in large centrifuge tubes. This was centrifuged at 18,600 xg and 2°C for 15 minutes. The supernatant was discarded, and the pellet retained. This pellet was resuspended in 2.5ml Homogenisation buffer and 2.5ml 2x Extraction buffer (0.05M Tris.HCl (pH8.0), 0.1M NaCl, 2% Na Deoxycholate (DOC)), and left on ice for 1 hour to allow for protein extraction. Following this incubation, the lysate was centrifuged at 10,000 xg for 20 minutes. The supernatant was saved and filtered with a 0.22µm filter before being aliquoted, frozen on dry ice and stored at -20°C. Note that all buffers contained protease and phosphatase inhibitors.

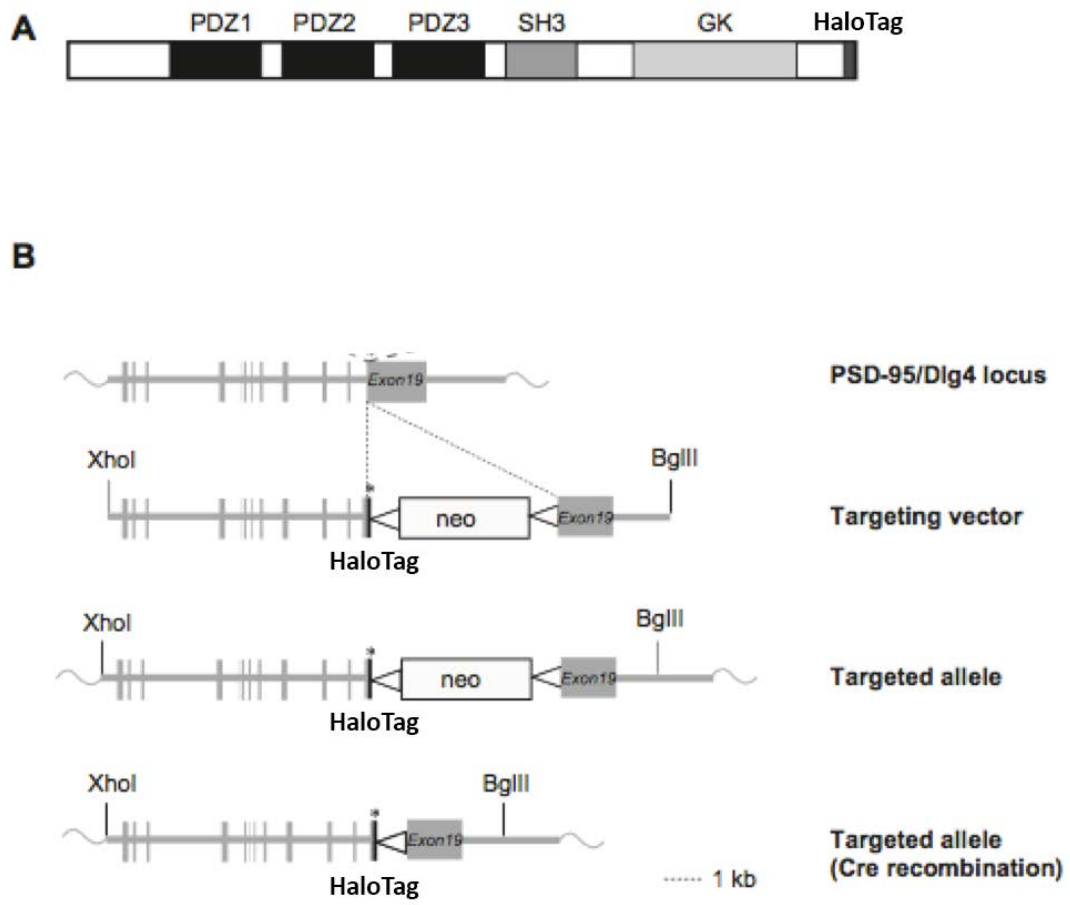

Figure 2.1. Generation of HaloTag-PSD-95 knock-in mice.
a. Domain structure of HaloTag modified PSD-95. PSD-95 domains, including three PDZ, an SH3, a GK and C-terminal HaloTag domain. **b.** Schematic diagram of the targeting strategy used for the genomic PSD-95/Dlg4 locus. The Dlg4 allele was targeted with the HaloTag sequence inserted before the stop codon (asterisk). The neomycin resistance cassette (neo) was deleted between loxP sites (triangle) by crossing the HaloTag-PSD-95 mouse line with transgenic Cre-recombinase-expressing mice (bottom diagram). Figure adapted from Fernandez et al. (2009).

2.1.3 Crude synaptosome preparation from primary cultures

This protocol used the same principles as those used for the mouse brain PSD enrichment, above. The culture dish was taken out of the incubator, the media was removed, and the dish placed on ice. The cells were gently washed in ice cold PBS, and 500µL ice cold homogenisation buffer (320mM sucrose, 1mM HEPES (pH7.4)) containing protease and phosphatase inhibitors was added to each well. Cells were

scraped free using a cell scraper or bent pipette tip, before being transferred to a tight-fitting glass homogeniser on ice. After homogenising with 12 strokes, the lysate was transferred to Eppendorf tubes and centrifuged at 18,500 xg for 15 minutes at 2°C. The supernatant was aspirated and the pellet retained. The pellet was resuspended in 0.5ml Homogenisation buffer and 0.5ml 2x Extraction buffer (0.05M Tris.HCl (pH8.0), 0.1M NaCl, 2% Na Deoxycholate (DOC)) containing inhibitors, and left on ice for 1 hour to allow for protein extraction. Following this incubation, the lysate was centrifuged at 10,000 xg for 20 minutes. The supernatant was saved and filtered with a 0.22µm filter before being aliquoted, frozen on dry ice and stored at -20°C.

2.1.4 Bradford assay for protein concentration

This assay was used to detect the total protein concentration in a given sample. The exact buffer that the sample was stored in was made up fresh, including inhibitors, and diluted down to a DOC concentration of 0.2%. This buffer was used to prepare a serial dilution using BSA to obtain the following BSA protein concentrations: 2, 1.5, 1, 0.75, 0.5, 0.25, 0.125 and 0 mg/ml. 10µL of each sample were mixed with 250µL Bradford solution. This was left to sit for 10 minutes at room temperature. Using the nanodrop, a standard curve of the absorbance at the various BSA protein concentrations was made, and the R^2 value as well as the equation of the line calculated. The R^2 value was required to be above 0.9 before being accepted. Next, a small quantity of the protein samples was diluted down to a Doc concentration of 0.2%. Then 5µL of diluted sample were taken, mixed with 125µL Bradford solution, and left to rest for 10 minutes. Then the absorbance was measured on the nanodrop, using the same blank (i.e. 0 mg/ml BSA in the same buffer) as before, with fresh Bradford solution. Using the absorbance of the samples and the equation from the standard curve, where y= absorbance and x= protein concentration, the protein concentration of each of the samples was calculated.

2.1.5 SDS polyacrylamide gel electrophoresis (SDS PAGE)

Samples were thawed on ice. Depending on the number of samples, a 10-well, 12-well or 15-well gel was used. 12- and 15-well gels could be loaded with up to 15µL

and 10-well gels with up to 30µL of sample per well. Samples were prepared in 25% LDS sample loading buffer and 10% Dithiothreitol (DTT), with the remaining 65% being made up by the sample. When loading equal protein amounts, an amount of each sample that corresponded to the same amount of total protein as could be loaded into the limiting sample was loaded. The rest of the volume was made up with sterile Mili-Q water (MQW) in the non-limiting samples. When loading equal volumes, instead the same volume of each sample was added to the LDS and DTT. The samples were then boiled at 100°C for 5 minutes.

The gels used were NuPAGE® Bis-Tris pre-cast 4-12% gradient gels. 1x NuPAGE MOPS SDS running buffer (Invitrogen), and the XCell SureLock™ Mini-Cell set-up were used. Samples were carefully loaded and a pre-stained molecular weight protein ladder using a P1000 gel-loading tip. The gel was then run at 200 volts for 50-60 minutes, or until the first protein bands reached the bottom of the gel.

Once the run was complete, the gel was removed and transferred to a membrane using a semi-dry transfer protocol. This was done by placing the gel onto a membrane, between two layers of filter paper. Both filter paper and membrane were incubated in NuPAGE transfer buffer (Invitrogen) for about 10 minutes prior. Either a nitrocellulose or PVDF membrane were used. Once the set-up for the semi-dry transfer was prepared (filter paper, membrane, gel, filter paper), bubbles were removed. The current was set to 15 volts and run for 45-90 minutes. After transferring was complete, the membrane was removed and stored in 1x PBS, and western blotting performed.

2.1.6 Blue-Native PAGE (BN-PAGE)

This is a form of polyacrylamide gel electrophoresis in which the proteins are not denatured or reduced but kept in their native conformation as well as being retained within their native complexes. This is done by a) using a Native PAGE sample loading buffer rather than LDS or SDS, and no DTT, and b) by not boiling the samples but keeping them on ice while preparing the samples.

Samples were prepared on ice as for an SDS PAGE, but in 25% Native PAGE sample loading buffer and ~3% coomassie G-250 dye. The remainder was made up with sample, and MQW when loading equal protein content. All work was performed on

ice. The XCell SureLock™ Mini-Cell set-up was used and samples loaded into the well. A Native Mark pre-stained protein standard ladder was used. Native PAGE dark blue cathode buffer was added to the centre of the set-up, and Native PAGE anode buffer to the sides. The gel was run at 150 volts. The overall running time was 90+ minutes. After 20-30 minutes, most (3/4) of the Native PAGE dark blue cathode buffer was removed from the centre, and replaced with Native PAGE light blue cathode buffer, after which the run was continued. The gels were run until the samples had migrated to the very bottom of the gels. This took a total of 90-120 minutes. When the progress was very slow, the voltage was increased to 175-200 Volts. After running was complete, the gels were transferred gels to 1x NuPAGE transfer buffer for 10 minutes so as to allow excess coomassie stain to wash off. The semi-dry transfer apparatus was set up as in chapter 2.1.5 (SDS PAGE), above. A nitrocellulose membrane was used, and once transferring was complete, the protein complexes were anchored in the membrane by incubating it for 5 minutes in acetic acid. Thereafter, wash the membrane was washed and stored in 1x PBS. Western blotting was then performed.

2.1.7 Western blotting and membrane stripping

This is a form of protein immunoblotting which utilises primary and secondary antibodies to recognise and visualise a specific epitope.

The membrane that contained the proteins and/or complexes following SDS or BN PAGE was first blocked for 1 hour in 3% milk. After blocking was complete, the membrane was washed in 1x PBS containing 1% Tween 20 detergent (PBS-T) to wash away excess milk. 3 washes of 5 minutes were performed.

Primary antibodies were then added overnight. The typical dilution used was 1:1000 for primary antibodies, and 1% milk was added to continuously coat the membrane with milk proteins and hence reduce background noise. About 3ml were required.

The next morning, the primary antibody was removed. The membrane was again washed in PBS-T three times to ensure removal of excess unbound primary antibody. Subsequently the secondary antibody was added (often conjugated to HRP for visualisation). It was usually diluted to about 1:40,000 or 1:80,000, and contained 1% milk. Incubation occured at room temperature, for 1 hour. Following this, the

membrane was stringently washed three times in PBS-T for 10-15 minutes per wash. A final wash of pure 1x PBS for 5 minutes was performed and the membrane imaged.

Blot membranes were also stripped and re-probed for a different protein in some instances. To this end, a stripping buffer such as the Restore western blot stripping buffer from Thermo Fisher was used. The membrane was incubated for 5-10 minutes (depending on the strength of the bands that needed to be stripped) in the buffer at constant rotation and RT. Thereafter, the membrane was washed 3x with PBS-T, before beginning the blocking and labelling process anew.

2.1.8 Image acquisition using LI-COR Odyssey system

Once the sample was prepared with primary and secondary antibodies, it was proceeded to the image acquisition step. If the secondary antibodies were conjugated with HRP, these steps were followed:
First, the substrate solution was prepared. A 1:1 mix of SuperSignal West Femto Stable Peroxide Buffer and Super Signal West Femto Luminol Enhancer Solution (stored at 4°C) were added to a falcon tube and vortexed. Carefully the membrane was moved out of the 1x PBS it was stored in and placed it into a plastic container that allowed the membrane to lie flat. The mixed substrate solution was added onto the membrane. Over the course of a minute, the container was tilted repeatedly and a pipette used to ensure that the entire membrane was coated.
Using forceps, the membrane was lifted up and dripped onto some tissue paper. Then the membrane was carefully placed onto plastic foil and covered while making sure that no air bubbles were trapped inside. The membrane was then placed onto a LI-COR plastic tray and insert into machine. The relevant channels and capturing time were selected. For example, 30 seconds at 700 to capture the pre-stained molecular weight ladder and 2 minutes for each other channel. Wavelengths between 500nm and 800nm can be captured. Once the correct settings were chosen, imaging was completed. After imaging was done, the membrane was carefully removed from the plastic pouch and returned to 1x PBS for storage at 4°C. When fluorescent secondary antibodies were used, the substrate labelling step was skipped, and the membrane imaged immediately, as described above.

2.2 HEK cell experiments

2.2.1 Human Embryonic Kidney cell maintenance

In order to gain insights into the HaloTag system, three lines of Human Embryonic Kidney (HEK) cells were obtained. One of these lines expressed the HaloTag protein fused to another protein, Ahrgap11a. The second line expresses only the HaloTag protein on its own, while the third line consisted of plain 293T HEK cells expressing no HaloTag protein, as controls.

All three lines were grown in the same manner. As growth media, Dulbecco's Modified Eagle Medium (DMEM) was used, containing the following supplements: 4.5g/L D-Glucose, L-glutamine and 25mM HEPES. Stock cells were grown in T75 flasks. Cells were grown to 60-90% confluence before being passaged and reseeded, at about 1-2x10^6 cells per T75 flask. Cells were passaged roughly every 3-4 days.

For proteomic analysis, cells were grown in 6-well plates until reaching 80-90% confluence before being harvested and subjected to a cell lysis protocol.

For imaging analysis, cells were grown in 24-well plates on 1.5 thickness glass coverslips that had been pre-treated with PDL for 1 hour prior to plating.

2.2.2 Labelling live HEK cells with HaloTag ligands

To test various HaloTag ligands, the HEK cells were subjected to various protocols as provided by the Promega manual. Rapid labelling:

Once cells were grown to 80-90% confluence, the medium was replaced with pre-warmed medium containing the HaloTag ligand at the desired dilution (typically at 1:1000). The cells were incubated with the ligand for a given amount of time (typically 15 minutes). Following ligand incubation, the entire medium was removed, and cells were rinsed three times with warm fresh medium. Cells were then incubated in warm fresh medium for 30 minutes to wash out unbound ligand from within the cells. Following this, cells were harvested for proteomic analysis, or coverslips were fixed and mounted on slides for later image acquisition using confocal microscopy.

2.2.3 HEK cell collection for proteomic analysis

Following the ligand addition protocol, above, the 6-well plates were taken out of the incubator and the growth medium removed. The plates were placed on ice. Each well was gently rinsed with 1ml/well (for a 6-well plate) ice cold PBS two times. 0.3ml ice cold Mammalian lysis buffer (0.05M Tris-HCl (pH8.0), 0.15M NaCl, 1% Triton X-100 and 0.1% Na deoxycholate (DOC)) containing protease and phosphatase inhibitors were added to each well. The cells were then scraped free using a cell scraper or bent pipette tip before being collected in a 2ml Eppendorf tube. Cells were then pipetted up and down repeatedly (25-30 times) to shear the cells, using a P1000. The cells were then incubated in lysis buffer on ice for 30 minutes. They were sheared occasionally. After 30 minutes and a final shearing bout, the cells werte spun down at 14,000 xg and 2-4°C for 5 minutes. The supernatant, being the cell extract, was retained and snap frozen on dry ice before being stored at -20°C.

2.3 Neuronal primary cultures

2.3.1 Reagents used during primary culturing

These are the essential stock solutions that were used for primary culturing of neurons:

500 ml working solution of Neurobasal medium (NB; Gibco, Life Technologies, UK): 484ml Neurobasal, 10 ml B27 Serum Free Supplement (Gibco, Life Technologies, UK), 5ml Penicillin / Streptomycin (Gibco, Life Technologies, UK) and 1.25 ml L-Glutamine (Gibco, Life Technologies, UK). Once ingredients were mixed, the solution was filtered using a 0.2µm diameter pore filter and stored for up to 2 weeks at 4°C.

500ml working solution of Dulbecco's Minimum Essential Medium (DMEM; Gibco, Life Technologies, UK): 445 ml of DMEM, 50ml Fetal Bovine Serum Heat-Inactivated and 5ml Penicillin / Streptomycin. Once prepared, the DMEM solution was filtered using a 0.2µm diameter pore filter and stored for up to 2 weeks at 4°C.

500 ml working solution of Hank's Buffered Salt Solution (HBSS; Gibco, Life Technologies, UK): 5ml penicillin / streptomycin was added to the solution and it was sterilised using a 0.2µm diameter pore filter. This was stored for up to 2 weeks at 4°C.

Papain solution prepared from lyophilised Papain (LS003119, Worthington Biochemical Company, Lakewood, NJ, USA): made to 10mg/ml in 1x Dulbecco's PBS (D-PBS; Gibco, Life Technologies, UK) and stored at 4°C for up to 6 months. Papain solution was sterilised using a 0.2µm diameter pore filter.

100µg/ml poly-D-lysine hydrobromide (PDL; Sigma Aldrich, P7280) stock solutions were prepared in D-PBS and stored at -20°C. Working solutions were diluted to 50µg/ml in D-PBS and sterilised using a 0.2µm diameter pore filter.

2.3.2 Preparation of coverslips and plates

The preparation of coverslips and plates for the plating down of primary neurons was performed with care and precision in a sterile environment. The following steps were performed:

1.5 thickness coverslips were prepared by first sterilising them via an autoclave and then storing them in 70% ethanol. Sterile 24-well plates were prepared by adding filtered 1ml 1xPBS to the outer 16 wells. The sterilised coverslips were prepared in 1x PBS, and after a final wash in sterilised Mili-Q water each copverslip was placed into one of the eight free central wells in the 24-well plate. This set-up ensured that cells were grown in conditions of maximum humidity, protected from evaporation and temperature fluctuations as much as possible.

Aliquoted laminin mouse tail was slowly thawed out at 4°C, to prevent aggregation from rapid thawing. Once thawed, a 10µg/ml working solution was prepared in sterile 1x PBS. Poly-D-Lysine (PDL) was also thawed. 100µg/ml PDL was diluted in sterile (0.2µm pore-filtered) 1x PBS, for a final concentration of 50µg/ml. 1ml filtered PDL solution was aqdded to each well containing a coverslip. Coverslips were incubated with PDL for 1 hour in an incubator at 37°C and 5% CO_2. After PDL-incubation was complete, PDL was aspirated and washed in 1x in PBS. Thereafter, 400µL laminin working solution was added to each well. Incubation in laminin was for a minimum of 4 hours at 37°C and 5% CO_2, ideally overnight. After incubation was complete, coverslips were washed in 1x PBS, followed by the addition of fresh NB media. Plates were placed in an incubator for at least 30 minutes to allow NB media to enrich in CO_2 and warm up to 37°C.

2.3.3 Setting up primary cultures of mouse hippocampal neurons

This involved harvesting the hippocampi of mouse embryos at the age of approximately E17.5, and growing the neurons in incubators before harvesting them and analysing them either proteomically, following PSD protein enrichment, or by confocal microscopy if grown on coverslips.

Setting up primary cultures involved sacrificing pregnant female mice when the embryos had reached an age of about E17.5, removing the heads from the embryos, and, in Hank's Buffered Saline Solution (HBSS) containing 1% Penicillin-Streptomycin, dissecting out the hippocampus. The hippocampi from embryos were pooled and incubated for 20 minutes in papain, a digestive enzyme that breaks up the brain tissue into individual cells. The cells were then washed in Dulbecco's Modified Eagle Medium (DMEM) containing 1% Pen-Strep and 10% Fetal Calf Serum (FCS). After 2 washes, the cells were re-suspended in 6ml Neurobasal media (NB), containing 1% Pen-Strep, 0.25% L-Glutamine, and 2% B27 supplement. The number of cells was estimated using a Haemocytometer, and cells were plated at the desired density. Cells in a single-cell suspension were diluted 1:1 in 0.4% Trypan Blue (Sigma Aldrich) to identify non-viable cells for count exclusion. Cells were then ready to be plated down. Wells and coverslips were prepared before plating. For details, see the protocol on preparing plates for primary neurons (chapter 2.3.2). For biochemical analysis, cells were plated at high density in 6-well plates in order to maximise protein yield ($1x10^6$ cells per well). For imaging purposes cells were grown in 24-well plates on 1.5 thickness glass coverslips at low density (100,000 cells per well). Incubation occurred at 37°C and 5% CO_2.

2.3.4 Primary culture care and maintenance

Primary cultures were grown in sterile, copper-lined and humidified cell culture incubators kept at a constant 37°C and 5% CO_2. Primary cultures intended for biochemical analysis were grown in 6-well plates in 3ml NB media per well. Following plating, after about 3 days in vitro (DIV), 1ml of media was removed, and replaced with 2ml fresh media that had been pre-warmed to 37°C and incubated in 5% CO_2.

For imaging purposes, neurons were plated in 24-well plates. Neurons were not cultured in the outer wells (due to evaporation), and these were filled with ~1ml 1x PBS to increase the humidity within each plate. On these 24-well plates, initially neurons were plated down in 500µL of NB media. After 3 days, a further 300µL of fresh NB media was added that had been pre-warmed to 37°C in 5% CO_2 for a final volume of 800µL per well.

From then on, media changes were performed roughly once per week, or when the media changed colour to orange (pH indication of a depletion of nutrients/accumulation of waste products). No more than half the media present was removed, as the neurons secrete chemicals into the media to create an ideal habitat. Furthermore, media changes were minimised (1x per week), as greater handling increases the stress on the cells. Cohen et al. (2013) remark that: 'aggressive washes and complete media exchanges are severely detrimental to neuronal viability'.

2.3.5 Fixation of cells for imaging

This work was performed protected from light to prevent bleaching of fluorescence. Following the ligand addition protocol, the 24-well plates were taken out of the incubator and placed on ice. A second plate was prepared beforehand on ice by adding chilled 1x PBS. Using a needle with a bent tip for ease of use and clean forceps, each coverslip was removed and transferred to the designated well containing PBS. The PBS was removed and the coverslips carefully rinsed 2-3 times to remove media. 0.5ml chilled 4% PFA was added to each well. The plates were then placed on a shaker at room temperature, under tin foil, and incubated for 15 minutes. After PFA incubation, they were rinsed 3x with PBS and washed in PBS for 5 minutes on shaker. They were then rinsed in autoclaved MQ water 1x to remove salt. The cells were then either stained with antibodies by following an immunocytochemistry protocol, or simply mounted on glass slides in preparation for imaging.

2.3.6 Immunocytochemistry

Once cells had been fixed in 4% PFA and washed thereafter, they were ready to be stained with antibodies if required. First, a blocking solution to reduce the background signal by diminishing the non-specific binding of antibodies to non-target proteins (BSA) and to rupture cell membranes and allow antibodies to enter the cellular compartments (detergent, e.g. Triton X-100) was prepared. The blocking solution was made up of 5% BSA + 0.1% Triton X-100 in 1x PBS. For blocking, the 1x PBS storage solution the cells are in was removed and replaced with 0.5ml blocking solution. The

plate containing the coverslips was placed onto a shaker, and incubated for 1 hour at RT, protected from light. While blocking, the primary antibody solution was prepared. This solution contained 1% BSA + 0.1% Triton X-100 and the primary antibody at the relevant concentration (usually diluted 1:1000 or 1:500). Once blocking was complete, coverslips were rinsed in 1x PBS one time before being carefully lifted out of PBS, their edge dabbed on a piece of tissue, and placed cell-side up into a wet-chamber (light-sealed petri dish containing a base of moist tissue atop which parafilm is placed as a surface). 60µL primary antibody solution was added to each coverslip, the wet-chamber closed, incubate allowed at 4°C overnight (16 hours). After primary antibody incubation was complete, antibody solution was dabbed off and coverslips immersed into 1x PBS in prepared wells in a 12-well cell culture plate. They were then washed 3x using 1x PBS. Secondary antibody solution was then prepared- this was the secondary antibody diluted to specifications in 1x PBS. Then the coverslips, after dabbing off excess liquid, were placed back into the wet-chamber. 60µL secondary antibody solution was added to each coverslip and they were incubated for 1 hour at RT. After incubation was complete, coverslips were returned to PBS-filled wells, and washed 3x 10 minutes on a shaker at RT. After a final wash in Milli-Q water to remove the salt from the PBS, coverslips were ready to be mounted or stored in 1x PBS at 4°C for a few days.

2.3.7 Mounting coverslips on slides

Once cells were ready to be mounted in preparation for imaging, about 5µL Mowiol mounting media (stored in freezer at -20) was added to a glass slide, avoiding bubbles. A needle and forceps was used to gently lift the coverslips, dab off excess water, and place the coverslip, cells down, onto the mounting media on the slide. The slide was then placed horizontally into box, and the box left outside at room temperature overnight to allow the mounting media to dry. The boxes were then moved to a freezer at -20 for long term storage and imaged as soon as possible.

2.4 Imaging and quantification

2.4.1 High magnification confocal imaging

The confocal Zeiss Laser Scanning Microscope 510 (LSM510) in our lab was equipped with multiple lenses, but during project the 63x oil immersion lens was exclusively used. The microscope was fitted with an Argon laser (458, 488, 514 nm, 25 mW), HeNe laser 543 nm, (1mW) and HeNe laser (633 nm, 5mW) for illumination. The software used was the Zeiss LSM510 META software.
In order to satisfy Nyquist sampling criteria, the optical zoom was set to provide pixel dimensions of 46 x 46 nm, and the pixel frame set to 1024 x 1024. Images were captured with a scan speed of 7 and line averaging of 4. The pinhole was set to one Airy disk unit. For each channel and data set, amplifier offset and detector gain were set manually in order to maximise capture while minimising saturation and therefore loss of information. These settings were then kept constant throughout experiments. Settings used throughout for the fluorophores were:

TMR HaloTag ligand:
The TMR HaloTag ligand has an excitation maximum at 552nm and emission maximum of 578nm. The following settings were used:
HeNe laser (543 nm, 1mW)
Excitation: 543nm
Laser power: 50%
Gain: 700
Digital offset: -0.20
Digital gain: 1.00
Filter: Bandpass 560-615

R110Direct HaloTag ligand:
The R110Direct ligand has an excitation maximum at 498nm and emission maximum of 528nm.
The following settings were used:
Argon laser (458, 488, 514 nm, 25mW)

Output: 65% (3.3A)
Excitation: 488
Laser power: 50%
Gain: 780
Digital offset: -0.20
Digital gain: 1.00
Filter: Bandpass 505-530

Anti-PSD-95 primary antibody staining with far-red (633) secondary antibody staining in neuronal primary cultures:
HeNe laser (633 nm, 5mW)
Excitation: 633nm
Laser power: 30%
Gain: 640
Digital offset: -0.60
Digital gain: 1.00
Filter: Longpass 650

2.4.2 Detection and quantification of puncta using Imaris

The commercially available Imaris software was used to detect puncta in the high-resolution images taken using the confocal LSM510 microscope. While the Imaris software was able to detect a variety of objects and shapes, such as surfaces, volumes, cells and nuclei, the 'spots' detection module was selected as this was best able to detect puncta within the synaptic size range of 200nm to 800nm (Carlin et al., 1980; Südhof, 2012). This spots module used a Mexican hat algorithm to identify structures. There are certain parameters that needed to be set by the user in the Imaris software when detecting spots. These are the seed point estimation diameter, background subtraction and spot region threshold, as well as choosing between volume or diameter from border. It was opteded for an estimated detection diameter of 300nm, as this falls within the synaptic size range and also provided the optimal detection spread. Ultimately, it was necessary to adapt the settings to each channel individually. Different fluorophores yielded different puncta intensities and antibody-

labelled puncta could differ in their staining pattern from HaloTag ligand-labelled puncta. The final settings used throughout my experiments were as follows:

R110Direct:
Estimated diameter: 0.3um
Background subtraction: Quality above 6.00
Spot region threshold: Automatic
Diameter from border.

TMR:
Estimated diameter: 0.3um
Background subtraction: Quality above 3.67
Spot region threshold: Manual: 15.32
Diameter from border.

AntiPSD95:
Estimated diameter: 0.3um
Background subtraction: Quality above 5.80
Spot region threshold: Automatic
Diameter from border.

When determining optimal settings, it was necessary to balance false positive results with false negative results, thus deriving settings that were deemed to minimise both. After synaptic puncta were detected, each image was manually inspected and any puncta that were clearly non-specific ‘blobs’ of aggregated ligand were deleted. This was only done in cases where there was no ambiguity over the identity of the puncta.

Once puncta detection was complete, puncta colocalisation was performed in images where appropriate. This colocalisation tool of the Imaris software detected which spots from different channels were within a certain distance of each other, centre to centre. Since the spot detection parameters were set to an estimated diameter of 300 nm, the spot colocalisation parameters were set to a distance of 300 nm as well. For puncta juxtaposition, the same colocalisation tool was used, but set to a distance of 600 nm.

2.4.3 Statistical analysis

Unless stated otherwise, statistical analysis was performed in Microsoft Excel for Mac, version 15.37 (2017 edition) and data was compared using Welch's t-test. Welch's t-test was selected as the default test for statistical difference as studies have indicated that this test is superior to the commonly used Student's t-test. Welch's t-test reduces Type 1 error rates when the assumption of homogeneity of variance is not met, while losing little robustness compared to Student's t-test when the assumptions are met (Delacre et al., 2017). Since many of the data sets in this project display unequal variance and unequal sample sizes, Welch's t-test is the superior choice in most instances (Ruxton, 2006). In most cases data are written as mean averages ± standard error of the mean (SEM). Single-factor analysis of variance (ANOVA) was performed using Microsoft Excel. Graphs were also made using Microsoft Excel.

2.5 HaloTag methods

2.5.1 In vitro labelling of crude synaptosome preparation with HaloTag TMR ligand

This protocol describes how PSD95-HaloTag fusion proteins were labelled with HaloTag ligands in brain lysate prepared from PSD95-HaloTag mice. For my experiments, brain lysate from heterozygous $PSD95^{HaloTag/+}$ mice was used that had been enriched for synaptosomes (see crude synaptosome preparation protocol).

The lysate was first thawed slowly on ice. HaloTag TMR ligand was then added to the brain lysate at a dilution of 1:500, for a final concentration of 5µM. This lysate was then incubated at 4°C on a rotator for 1 hour, and thereafter the SDS-PAGE protocol was performed. However, once gel electrophoresis was complete and proteins had been transferred to a membrane, no further treatment (such as blocking or western blotting) was required. Indeed, following transfer to a membrane, ligand-tagged proteins could immediately be visualised using the LiCOR Odyssey system. It was then simply proceeded with the Odyssey imaging protocol with the acquisition settings set to to

correspond to the HaloTag fluorophore. In this project, the HaloTag TMR ligand was used, yet this protocol should be applicable to other HaloTag ligands as well.

2.5.2 Post-fixation labelling of cells and brain slices using TMR ligand

Post-fixation labelling of specimens using HaloTag ligands was very simple and straight-forward when using a HaloTag ligand that is cell-membrane permeating. For both primary cultures and brain slices the labelling protocol was very similar, and only differed in the incubation time. After fixation in 4% PFA was completed, and the specimen had been washed, the coverslips or brain slices were moved to a wet-chamber and an appropriate volume of HaloTag ligand was added to each specimen (e.g. about 60µL per 24-well coverslip). The HaloTag ligand was diluted in 1x PBS to a concentration of 1µM. The primary cultured neurons were incubated on coverslips for 30 minutes at room temperature (RT) and brain slices for 1 hour at RT, protected from light. After incubation was complete, the specimen were rinsed in 1x PBS three times, before continuing with any other procedures.

2.5.3 Basic single-ligand labelling in live primary cultures

This protocol was used to label all HaloTag fusion proteins in living primary cultures with a single membrane-permeating fluorescent ligand, allowing for a quantitative visualisation of target proteins within the cell at a given time point. This gave an indication of total PSD-95 in synapses and allowed for comparisons of total PSD-95 levels per synapse with measurements at other time points.
While the Promega ‘Focus on Imaging’ manual provided a set of concentrations to use the HaloTag ligands at, it was found that some of these concentrations were needlessly high. While Promega suggest using the TMR ligand at a concentration of 1µM for 15 minutes and the R110Direct ligand at 0.1µM overnight, it was found that concentrations of 100nM for both these ligands were more than sufficient to guarantee complete labelling. For single-ligand labelling a concentration of 100nM for both the TMR ligand and the R110Direct ligand were suitable.

Neuronal primary cultures were grown in 24-well plates on 1.5 thickness glass coverslips, in a total volume of 800µL NB media. Fresh NB media that had been brought to 37°C and 5% CO_2 by pre-incubation in a cell-culture incubator was used to prepare a working solution of NB media containing the HaloTag ligand. Per well, 200µL of fresh NB media containing the HaloTag ligand at a concentration of 200nM was prepared. In single-ligand labelling experiments, 600µL of media were then removed from the well, leaving the cells in 200µL of remaining media. 200µL of ligand in working solution were then added, for a final volume of 400µL media per well and final concentration of 100nM HaloTag ligand. For most experiments in this project utilising the TMR ligand, a 30-minute incubation time was used. When using the R110Direct ligand, cells were incubated with the ligand overnight for about 16 hours. After labelling was complete, and since this protocol was a single ligand and single time point protocol, cells could immediately be further processed. For imaging, coverslips needed to be fixed as per the fixation protocol (chapter 2.3.5).

When labelling primary cultures for biochemical analysis (for instance when using the HaloTag biotin-conjugated ligand), the protocol remained essentially the same, with the only difference being the volumes used. In that case, cells were grown in 6-well plates and a final volume of 3ml. Hence, 2ml of NB media was removed and replaced with 1ml fresh NB media containing the ligand at 200nM, for a final 2ml at 100nM. After labelling was complete, cells were washed and harvested for further biochemical analysis as per the protocol outlining PSD protein extraction from primary cultures (chapter 2.1.3).

2.5.4 Titration of HaloTag ligands to establish saturation concentrations

This experiment aimed to work out what concentration of the pulse ligand was required to saturate all the available HaloTag binding sites and thereby prevent labelling by a chase ligand added subsequently. It was also designed to demonstrate that there is a direct positive correlation between pulse ligand concentration and fluorescence intensity at concentrations below the saturation point, inversely linked to the chase ligand concentration (i.e. a negative correlation between pulse ligand intensity and chase ligand intensity).

Primary neurons were grown on glass coverslips until developmental stage DIV14. On DIV14, they were labelled with the TMR ligand as a pulse ligand. This was done by following the single-ligand labelling protocol (see chapter 2.5.3), but with varying TMR ligand concentrations. The TMR ligand was titrated from a concentration of 500nM to $5x10^{-12}$nM in steps of a factor of 10, and a blank (no pulse ligand) was included. Cells were incubated with TMR pulse ligand for 30 minutes, before being washed and fixed in 4% PFA (see chapter 2.3.5). Following fixation, coverslips were then moved into a light-proof wet-chamber and incubated with diAcFAM ligand at a concentration of 1µM in PBS for 1 hour at RT. After incubation was completed, the coverslips were washed in 1x PBS three times, followed by antibody staining for PSD-95 using the immunocytochemistry protocol (chapter 2.3.6). Coverslips were then imaged using the LSM510 confocal microscope, and synaptic puncta detected using the Imaris software. The average puncta fluorescence intensity (APFI) per image for both pulse and chase ligand puncta was established. It was then possible to plot the APFI values of both pulse and chase ligand puncta over the titration steps in the pulse ligand concentration.

2.5.5 Analysis of fluorophore stability using a plate reader

This set of experiments was performed to evaluate the stability of HaloTag ligand fluorophores over longer time periods in neurobasal media in a cell culture incubator. Ligand working solution was prepared in five Eppendorf tubes by adding HaloTag ligand to PBS for a final concentration of 200nM. In a 96-well cell culture plate, 5 wells were filled from each Eppendorf, for a total of 25 wells. This gave a total of 5 technical replicates for each biological replicate (N=5). PBS and NB alone were used as controls and could be used to normalise to. This plate was then imaged using a plate reader, hence giving a fluorescence intensity read-out for each well. The 96-well plate along with the remaining working solution were then transferred into a cell culture incubator at 37°C and 5% CO_2 and stored there for 24 hours. After 24 hours, 5 new wells in the same 96-well plate were filled from the same five Eppendorf tubes containing the ligand working solution. The well was then imaged again using the plate reader. This allowed for the monitoring of the change in fluorescence intensity for the samples that

had already been imaged on the first day of the experiment (i.e. the solution remaining in the wells), as well as measuring the fluorescence intensity of the working solution that was only imaged once, after 24 hours in the incubator. The samples that were imaged twice (on day 1 and day 2 of the experiment) gave a slightly reduced fluorescence reading after 24 hours (but not significantly so), most likely due to the photo-bleaching effect of the first imaging session. The samples that were retained in the Eppendorf tubes over the 24 hours and only imaged once, on day 2, displayed the same fluorescence intensity as the samples imaged on day 1 (see chapter 3.3.6).

2.5.6 Pulse-Chase method for the study of protein turnover

Introduction

In this section, the pulse-chase method developed during this project that uses the HaloTag system to visualise the synthesis and degradation of PSD-95 will be outlined in detail. The underpinning principle is this: The pulse ligand labels all PSD95-HaloTag fusion proteins present, and thus saturates all HaloTag binding sites. After pulse labelling is complete, the pulse ligand is removed and replaced by the chase ligand. This ligand will initially be unable to bind to anything, as all existing fusion proteins will have their binding sites taken by the pulse ligand. However, over the 24 hours of chase incubation new fusion proteins will be formed, and as they are synthesised their HaloTag binding sites will be tagged by the chase ligand. Once the cells have been incubated with the chase ligand for 24 hours (or 48 hours, depending on the time-window to be studied) and have been fixed, two different subpopulations of the fusion protein will exist: proteins labelled by the pulse ligand (in essence ‘old’ proteins that were present during the pulse-labelling phase) and proteins labelled by the chase ligand (these must have been synthesised within the chase labelling period, e.g. over the last 24 hours of the experiment). After 24 hours of chase incubation it is now possible to separately analyse synaptic puncta made up of old or new fusion proteins.

Protocol

A time frame was decided over which to perform the experiment- in this project, a 24-hour time-frame of PSD-95-HaloTag turnover analysis (between DIV15 and DIV16)

was used. The R110Direct pulse ligand was prepared by making up a working solution. This working solution consisted of fresh, fully prepared NB media, to which the R110 ligand was added for a working concentration of 200nM. 100µL per well were needed. This working solution was incubated in the cell culture incubator for at least 30 minutes to raise its temperature and CO_2 levels to 37°C and 5%, respectively. On DIV 14 the cells in their plates were taken out of the incubator and into the sterile fume hood. To minimise photo-bleaching, the light inside the fume hood was turned off. 500µL of the media the cells were being cultured in was removed (leaving the remaining 300µL in the well) and this media saved in a falcon tube (all the collected media was pooled together). This solution was stored in the cell culture incubator with the lid slightly opened. Gently, 100µL of the 200nM pulse ligand working solution was added to each well, giving a final pulse ligand concentration of 50nM in 400µL in each well. Carefully, the cells were returned to their incubators, and left undisturbed overnight, for about 16 hours. The next day, on DIV15, a chase ligand working solution was first prepared. However, the preconditioned media that was saved from the day before was used as the base. 300µL of working solution was needed per well. Enough TMR HaloTag ligand was added to this media to give a TMR concentration of 666nM in this working solution. The cells were moved out of the incubator and into the fume hood. 300µL of the 400µL were removed. Quickly and gently this exact volume was replaced with 300µL of chase ligand solution. This resulted in a final volume of 400µL in each well, at a final concentration of 500nM for the chase ligand and 12.5nM for the pulse ligand. At these concentrations, the chase ligand was able to outcompete the pulse ligand for all available HaloTag binding sites (see chapter 3.4.3). The plates were returned to the incubator and incubated for as long as designed in the experimental timeframe. After incubation was complete, the coverslips were carefully removed from the wells and moved to wells in a separate plate filled with ice cold 1x PBS. Then washing and fixing of the cells according to the ‘fixation’ protocol in chapter 2.3.5 was performed. A ‘0’ time point was included, i.e. a measurement at the start of the experiment to which later time points could be compared. This time point also served as an internal control, as it permitted checking that pulse ligand labelling was saturating all HaloTag binding sites. In this protocol, a 1 hour incubation with the chase ligand was included. Since PSD-95 has a relatively long half-life (see chapter 3.4.5), this 1-hour incubation served as a ‘0’ time point, as minimal new PSD-P5 would have

formed or old PSD-95 have been degraded at this point. Thus, rates of synthesis or degradation could be calculated based upon this starting measurement.

One thing that is important to note is that whole-media changes, as advocated by Promega's 'Focus on Imaging' manual, are incompatible with primary neurons. While such protocols may be suitable for hardy cell lines such as HEK cells, primary neurons are unable to survive washing and complete media changes (Cohen et al., 2013). It is for this reason that the pulse ligand was merely diluted down from 50nM to 12.5nM during the chase ligand incubation, rather than entirely removed. However, it was demonstrated that at these experimental concentrations the TMR chase ligand is able to fully outcompete the R110Direct pulse ligand (see chapter 3.4.3).

Chapter 3: Characterising the PSD-95-HaloTag mouse model and developing a HaloTag labelling method

3.1 Chapter overview

The primary aim of this chapter is to provide a thorough narrative of the experimental approach I took to develop a set of methods with which to quantify the synthesis and degradation of endogenous PSD-95 at individual synapses. In developing these methods, I am able to provide insights into the biological functioning of PSD-95, and thus this chapter will also provide an insight into the turnover rates of this protein. Most of the work presented in this chapter was conducted so as to establish an experimental toolkit that could be used to pursue more complex and probing questions into the dynamics of PSD-95 in future experiments- these results will be presented in chapter 4. I will first outline my characterisation of the transgenic mouse model (PSD-95^{HaloTag}) that is the basis of my project, and from there move on to exploring the applications of the HaloTag system with regards to studying PSD-95 turnover.

In chapter 3.2 I will characterise different aspects of the PSD-95^{HaloTag} mouse model, including a biochemical analysis of the protein's expression level and electrophysiological analysis. In chapter 3.3 I explore different in vitro HaloTag ligand labelling techniques in the model, such as labelling live cells in primary cultures, and I investigate some of the limitations of the methods. In chapter 3.4 I focus on establishing a Pulse-Chase method with which I can quantify PSD-95 turnover, and which will form the basis of the experiments outlined in chapter 4. Chapter 3.5 will discuss my in vivo experimental efforts, and finally chapter 3.6 will summarise and discuss the overall findings of chapter 3.

3.2 Characterisation of the PSD-95-HaloTag mouse model

3.2.1 Biochemical analysis of PSD-95-HaloTag expression levels in the Knock-in mouse line

The primary objective of my project was to utilise the PSD-95^{HaloTag} mouse line to quantify the rate of turnover of PSD-95. Most previous knock-in (KI) mouse lines created in our lab using the same gene targeting technique were found to be

physiologically normal: the mice expressed the targeted protein at normal levels, they did not exhibit any aberrant behaviour and had a 'normal' electrophysiological profile (Frank et al., 2016; Fernandez et al., 2009; PhD thesis Dr. Fei Zhu); however, one KI mouse line did exhibit an abnormal profile (PSD-95-mEos2, Broadhead et al., 2016). PSD-95 deficiency is known to have a significant impact on synaptic activity and behaviour in mice (Migaud et al., 1998), and thus it is possible that a PSD-95 deficiency could also affect PSD-95 turnover. It was therefore important to confirm that PSD-95-HaloTag expression levels in the KI mouse line were similar to those in WTs.

To biochemically test the PSD-95^{HaloTag} KI mouse line for phenotypic abnormalities, whole mouse brains from wild-type (WT), heterozygous (Het, PSD-95$^{HaloTag/+}$) and homozygous (Hom, PSD-95$^{HaloTag/HaloTag}$) mice were homogenised and crude synaptosome preparations performed, as per methods chapter 2.1.2. Three preparations for each genotype were loaded into 4-12% gradient Bis-Tris gels, with equal volumes loaded into each well (20µL). The gels were then subjected to SDS PAGE and western blotting. The membrane was probed with antibodies for three different proteins, sequentially. First, western blotting for PSD-95 was performed. The membrane was then stripped using western blot stripping buffer, and this was followed up with a western blot for α-Tubulin (as a loading control). The membrane was then stripped once more, and further western blotting performed for the HaloTag protein. Bands corresponding to PSD-95, PSD-95-HaloTag and α-Tubulin were then detected using the LI-COR Odyssey imaging system.

WT PSD-95 has a molecular weight of 80kDa (Husi et al., 2000; Cai et al., 2006), while the HaloTag protein has a molecular weight of 33kDa (Los et al., 2008; Lang et al., 2006). Thus, the PSD-95-HaloTag fusion protein can be expected to have a molecular weight of about 113kDa. The resulting bands from the western blotting revealed bands corresponding to precisely these molecular weights (Figure 3.1.a). Note that faint banding can be detected just below all of the PSD-95 and PSD-95-HaloTag bands. These bands were consistently detected, and as such are unlikely to be the result of protein degradation. Furthermore, they are not the result of the antibody labelling an off-target protein, as Figure 3.4 (below) also contains this band when only the HaloTag ligand is used for labelling. While it was impossible to determine the identify of this faint band, one explanation is that a truncation event may occur as part of a post-

translational modification in a small subset of PSD-95 proteins, thereby lowering their molecular weight.

Next, the total amount of PSD-95 protein present in each sample was quantified using the LI-COR Image Studio software. In the samples from heterozygous mice, both alleles (mutant and WT) were added together to obtain the total amount of PSD-95. Variations between samples could be detected using the tubulin loading control (Figure 3.1.b). The quantity of PSD-95 was thus normalised to the tubulin loading control. Average PSD-95 expression levels were calculated for each genotype (Figure 3.1.c) (WT: 1785 ± 232; Het: 3004 ± 1299; Hom: 2407 ± 188 (Arbitrary Units, AU)), and a single-factor analysis of variance (ANOVA) performed. It was found that there is no significant difference in total PSD-95 expression at the $p<0.05$ confidence level between WT, Het and Hom samples [$F(2, 6)=0.63$, $p=0.57$]. However, it was observed that WT mice appear to express slightly less PSD-95 overall than either Het or Hom mice. Next, within heterozygous samples the amount of PSD-95 in WT and mutant alleles was compared. Again, the difference between the two was not found to be significant (Het: 492 ± 126; WT: 271 ± 64 AU), (Welch's T-Test, $p=0.22$) (Figure 3.1.d), yet heterozygous mice do appear to express slightly more of the mutant than of the WT allele.

The blot membrane was finally probed with a primary antibody against the HaloTag protein. This blot was performed by my lab colleague and fellow PhD student, Sarah Lempriere. The result reveals very strong and clear PSD-95-HaloTag bands at about 113kDa, as expected, in both Hom and Het mice, with no bands present in WT mice (Figure 3.1.e). Bands from each genotype were quantified as before, averaged, and compared. This comparison revealed that Het mice express half as much PSD-95-HaloTag as Hom mice (66.7 ± 8.1 vs 134.3 ± 6.7 AU, or 49.7%). This difference is statistically significant (Welch's t-test, $p=0.003$) (Figure 3.1.f).

a.

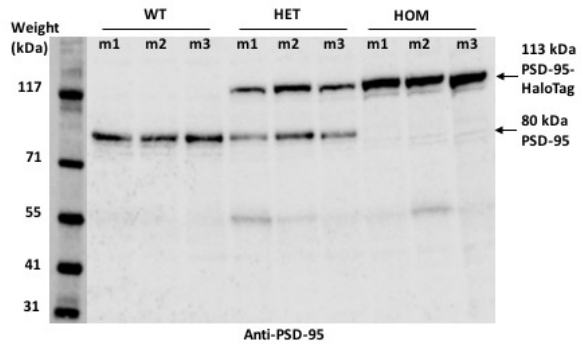
Weight (kDa)
WT
HET
HOM
m1 m2 m3 m1 m2 m3 m1 m2 m3
117
71
55
41
31
113 kDa PSD-95-HaloTag
80 kDa PSD-95
Anti-PSD-95

e.

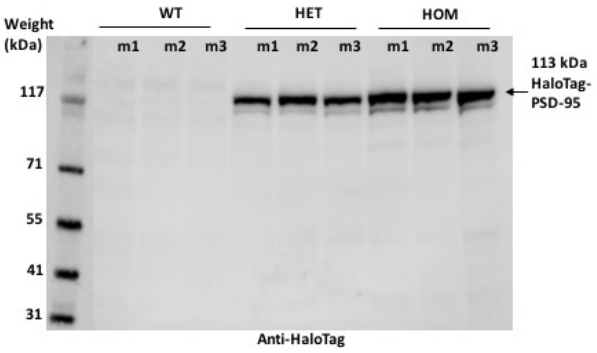
Weight (kDa)
WT
HET
HOM
m1 m2 m3 m1 m2 m3 m1 m2 m3
117
71
55
41
31
113 kDa HaloTag-PSD-95
Anti-HaloTag

b.

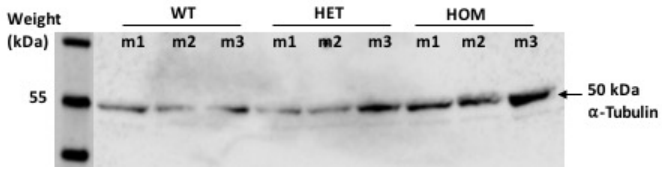
Weight (kDa)
WT
HET
HOM
m1 m2 m3 m1 m2 m3 m1 m2 m3
55
50 kDa α-Tubulin

c.

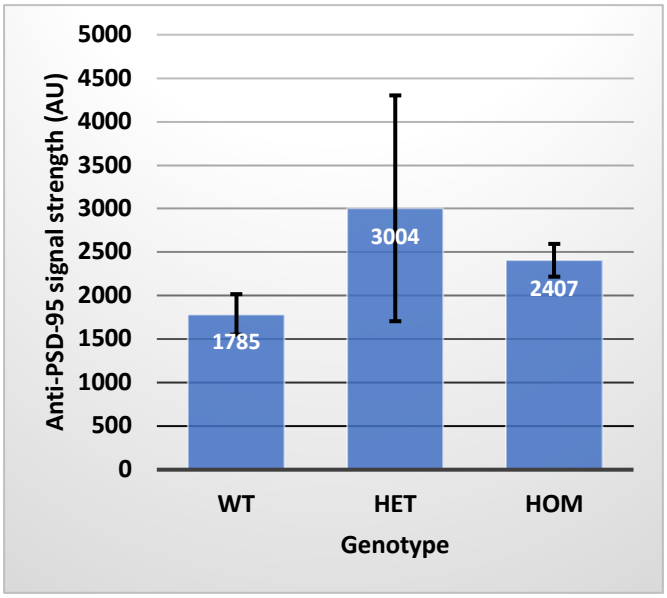
Anti-PSD-95 signal strength (AU)
5000
4500
4000
3500
3000
2500
2000
1500
1000
500
0
1785
3004
2407
WT
HET
HOM
Genotype

f.

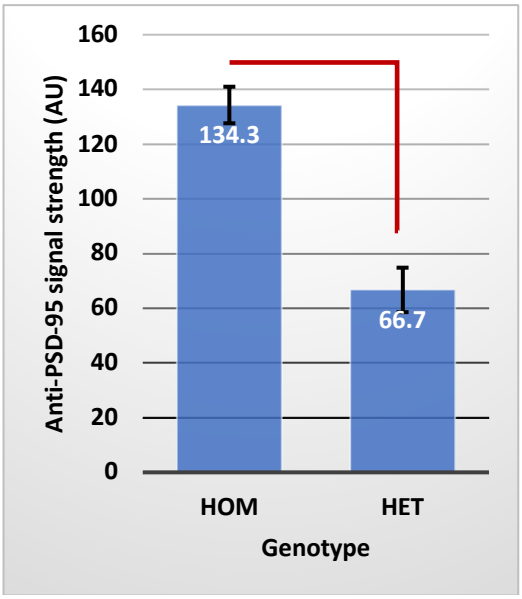
Anti-PSD-95 signal strength (AU)
160
140
120
100
80
60
40
20
0
134.3
66.7
HOM
HET
Genotype

d.

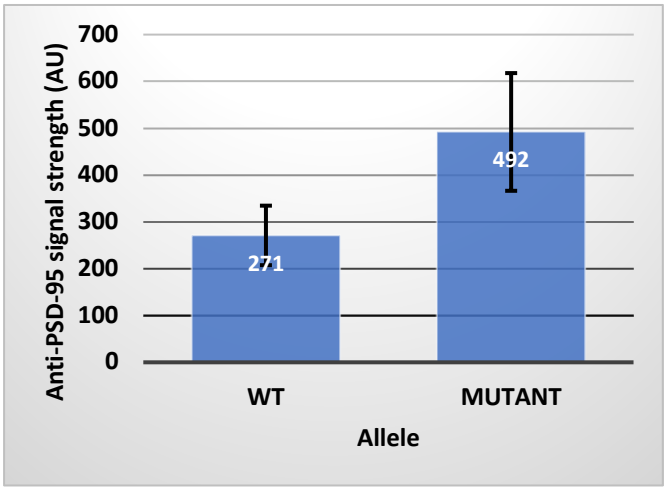
Anti-PSD-95 signal strength (AU)
700
600
500
400
300
200
100
0
271
492
WT
MUTANT
Allele

Figure 3.1. PSD-95 expression is normal in PSD-95-HaloTag knock-in mice.
a. Western blot following SDS PAGE, stained with anti-PSD-95 antibody (Mouse, BD Bioscience, 1:5000). Samples loaded were crude synaptosome preparations taken from three WT, three Het (PSD-95$^{HaloTag/+}$) and three Hom (PSD-95$^{HaloTag/HaloTag}$) mice. WT PSD-95 was found to migrate as an 80kDa band, while the PSD-95-HaloTag fusion protein migrated as a 113kDa band due to the addition of the 33kDa HaloTag protein. **b.** The membrane shown in (a.) was stripped and re-probed with an anti-α-Tubulin antibody (Rat, Serotec, 1:5000 dilution) as a loading control. **c.** Graph showing the quantification of total PSD-95 levels in the blot shown in (a.) following a normalisation to the tubulin loading control shown in (b.). The graph depicts the total amount of PSD-95 as a mean of the three samples in each group. No significant difference was found in PSD-95 levels between WT, Het and Hom mice (single-factor ANOVA, [$F(2, 6)= 0.63$, $p=0.57$]). **d.** Graph comparing mean PSD-95 expression levels of WT and mutant alleles of PSD-95 in Het mice. The difference was not found to be significant (Welch's t-test, $p=0.22$). **e.** The membrane shown in (a. and b.) was stripped and re-probed with an anti-HaloTag antibody (Mouse, Promega, 1:1000 dilution) by fellow PhD student Sarah Lempriere. Hom and Het samples display a strong HaloTag signal, which is absent in WT samples. **f.** Quantification of the anti-HaloTag signal in Hom and Het mice found in (e.). Het mice express half as much (49.7%) PSD-95-HaloTag protein as Hom mice. This difference is statistically significant (Welch's t-test, $p=0.003$). Note: in all graphs, error bars denote the standard error of the mean (SEM).

The results indicate that the expression level of the mutant allele and the WT allele of PSD-95 are not significantly different in PSD-95^{HaloTag} KI mice (N=3 mice for each of the three genotypes). However, a slightly enhanced expression level of the mutant allele was observed in both Hom and Het mice. This observation may warrant a closer examination in the future, as it could indicate an overexpression phenotype, particularly in the light of the fact that the sample size in this study was relatively small (N=3 mice for each of the three genotypes). A larger sample size may provide greater confidence in the result that the differences are not statistically significant. This study concludes that the HaloTag KI mutation does not impact upon overall PSD-95 expression levels in the brains of adult mice. The study also finds that total PSD-95-HaloTag protein expression levels are exactly proportional to the number of mutant alleles expressed.

3.2.2 Biochemical analysis of PSD-95-HaloTag fusion protein localisation to signalling complexes

Having established that the overall expression level of the PSD-95-HaloTag fusion protein is not significantly different from PSD-95 expression in WT mice, I next wanted to demonstrate that the PSD-95-HaloTag fusion protein is still incorporated into the same multiprotein signalling complexes that WT PSD-95 is a part of. PSD-95, as one of the predominant scaffolding proteins in the postsynaptic densities of glutamatergic neurons in the CNS (Fernandez et al., 2009; Husi et al., 2000; Husi and Grant, 2001; Chen at al., 2005; Cho et al., 1992), is part of large, multiprotein signalling complexes found to be approximately 1.5MDa in size (Frank et al., 2016; Frank et al., 2017). In PSD-95 KO mice, these complexes fail to form, leading to deficits in learning and behaviour (Migaud et al., 1998). Hence, I wanted to test whether PSD-95-HaloTag proteins are able to be incorporated into 1.5MDa supercomplexes in our mouse line, and thus discover whether fusing the HaloTag protein to PSD-95 impacts upon the protein's ability to assemble these complexes.

Synaptosome preparations were prepared as in chapter 3.1.2 from mice of three different genotypes: Het ($PSD\text{-}95^{HaloTag/+}$), WT ($PSD\text{-}95^{+/+}$), and complete PSD-95 Knock-out ($PSD\text{-}95^{-/-}$). I then subjected these samples to a Blue-Native (BN) PAGE, a technique that neither denatures proteins, nor breaks apart protein complexes, thereby retaining them in their natural state (Schägger, 2001). I then proceeded with a western blot for the HaloTag protein, which I identified at the expected 1.5MDa size solely in the samples from the Het mice (Figure 3.2.a). The membrane was then treated with stripping buffer as per chapter 2.1.7, and re-probed with an antibody against PSD-95. This second blot revealed a complete overlap in PSD-95 signal with the previous HaloTag signal (Figure 3.2.b). As the samples were from heterozygous mice, the results strongly indicate that both mutant and WT alleles indeed form part of the large multiprotein complexes that PSD-95 is known to assemble. However, an alternative explanation for this result is that, since these extracts were made from heterozygous mice and synaptic PSD-95 is known to frequently form dimers while part of 1.5MDa complexes (Frank et al., 2017), the anti-HaloTag signal found at 1.5MDa is due to PSD-95-HaloTag proteins that have dimerised with wild-type PSD-95, which

has in turn tethered this dimer to the 1.5MDa signalling complex. In this scenario, it is possible that mutant PSD-95-HaloTag proteins are unable to incorporate into these signalling complexes without the aid of a WT PSD-95 molecule. This question is easy to resolve, however, by repeating this experiment with brain extracts from homozygous PSD-95$^{HaloTag/HaloTag}$ mice.

An interesting study to follow up with could be to more deeply probe the composition of these 1.5MDa complexes, as was done by Husi et al. (2000) using mass spectrometry and immunoblotting. Thus one could investigate whether the mutation to the PSD-95 protein has any effect on the molecular composition of these 1.5MDa signalling complexes. Indeed, such a study would be facilitated by the HaloTag's ability to function as an affinity pull-down tag. This is possible as there exist commercially available biotin-ligands, permitting the isolation of HaloTag fusion proteins and their interactors through the biotin-streptavidin interaction. Furthermore, Promega also offers resin beads with HaloTag ligand binding groups attached, meaning that these can also be used to purify PSD-95-HaloTag fusion proteins and their associated binding partners and complexes.

In summary, the results from the BN PAGE analysis indicate that the PSD-95-HaloTag fusion protein is still capable of assembling the 1.5MDa super-complexes that are thought to play such an important role in synaptic signalling. This gives credence to the view that the PSD-95^{HaloTag} KI mouse line displays no abnormal phenotype.

a.

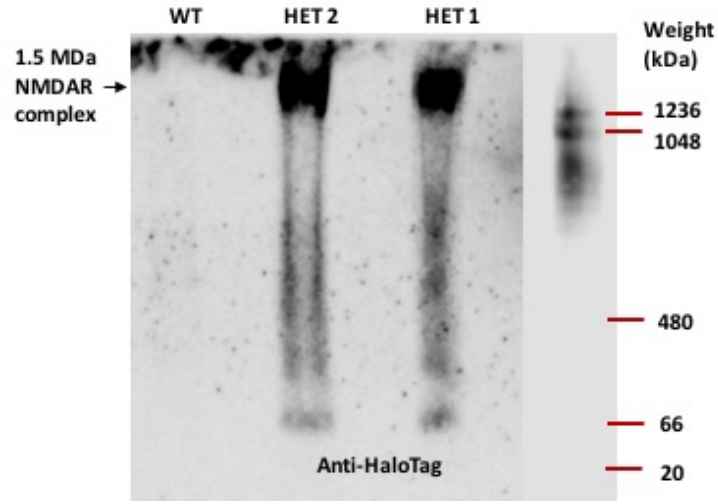

b.

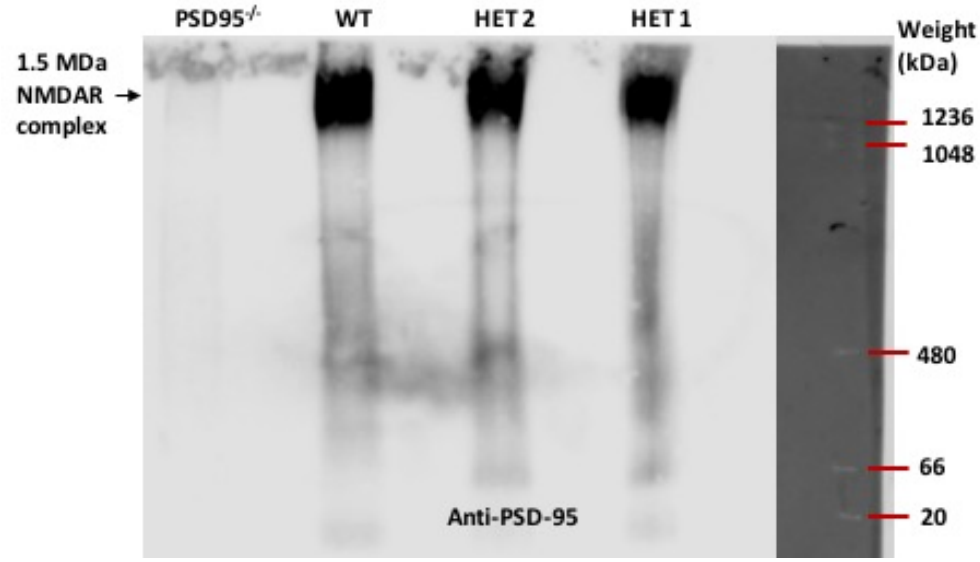

Figure 3.2. PSD-95-HaloTag fusion proteins continue to incorporate into multiprotein signalling complexes.

a. Synaptosome preparations from a PSD-95$^{HaloTag/+}$ (Het) mouse, a WT mouse and a PSD-95$^{-/-}$ KO mouse where subjected to Blue-Native PAGE, and western blotting was performed using an antibody against the HaloTag protein (Mouse, Promega, 1:1000). Clear bands are visible at ~1.5MDa in each of the two Het lanes, but not in any other lane.

b. The membrane in (a.) was stripped and probed with an anti-PSD-95 antibody (Rb, BD Bioscience, 1:1000). Clear bands are visible at ~1.5MDa in the WT and both Het lanes, but not the PSD-95 KO lane. PSD-95-HaloTag appears to be normally incorporated into 1.5MDa multiprotein signalling complexes.

3.2.3 Electrophysiological analysis of the PSD-95-HaloTag Knock-in mouse line

It has previously been found that knocking out PSD-95 results in a distinct electrophysiological and behavioural phenotype (Migaud et al., 1998). Thus, we wanted to assess whether the PSD-95^{HaloTag} mouse line displays significantly altered electrophysiological characteristics that might indicate altered synaptic function. This electrophysiological analysis was performed by Thomas O'Dell, and the results are displayed in Figure 3.3. It was found that for both heterozygous and homozygous PSD-95^{HaloTag} mice, none of the results differed significantly from wild-types ($p>0.05$; N= 5 (WT); 5 (het); 4 (hom)). Properties analysed were: Fiber volley/fEPSP input/output curves generated by eliciting fEPSPs (Figure 3.3.a); Paired-pulse facilitation (Figure 3.3.b); Excitatory postsynaptic currents (EPSCs) (Figure 3.3.c); Ratio of NMDAR to AMPAR-mediated currents (Figure 3.3.d); Weighted decay time constants for currents (Figure 3.3.e); Examples of sEPSCs (Figure 3.3.f); Cumulative probability plots of sEPSC amplitudes (Figure 3.3.g) and of inter-event intervals (Figure 3.3.h); analysis of fEPSP profiles in brain slices after LTP induction (Figure 3.3.i). It can thus be concluded that PSD-95^{HaloTag} KI mice are electrophysiologically normal.

It is important to note that no behavioural experiments were performed alongside the electrophysiological expoeriments. In 1998, Migaud et al. found that mice lacking PSD-95 also had an abnormal electrophysiological profile, as they displayed a dramatic propensity for LTP induction at very low frequency stimulation (1Hz). This included paired-pulse facilitation, which was significantly greater in mutant than WT mice. PSD-95-KO mice also displayed aberrant behaviour, as they failed to reveal spatial learning capabilities in the open-field watermaze.
Our mouse line did not display aberrant paired-pulse facilitation. However, no behaviour experiments were conducted, and it is possible that the knocking-in of the HaloTag protein into the PSD-95 sequence could have had different effects than those found when PSD-95 was knocked out. As such, while behavioural deficits may be accompanied by electrophysiological phenotypes in some instances, the link between the two has been insufficiently explored to be able to rule out a behavioural phenotype on the basis of a normal electrophysiological profile.

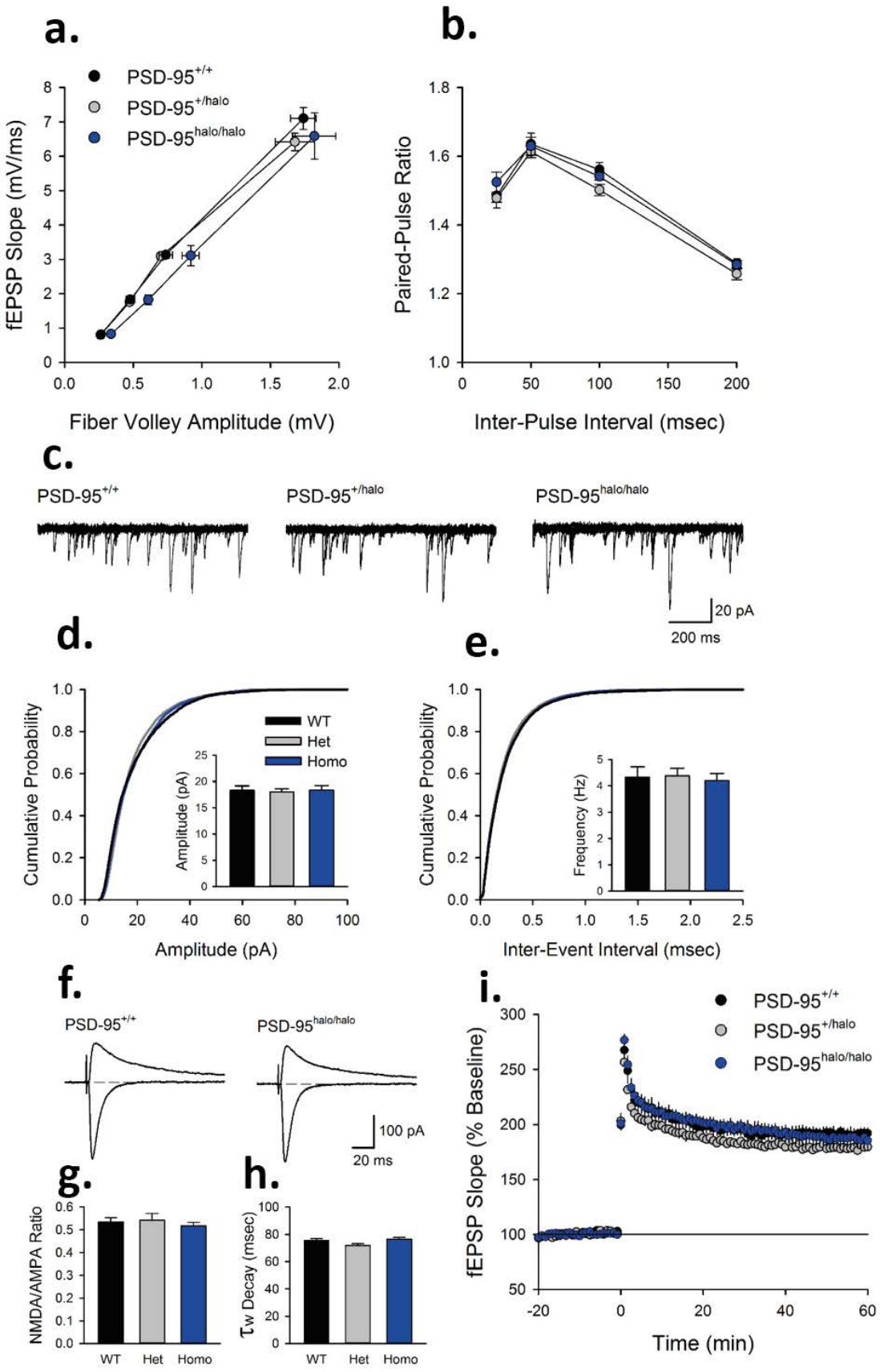
a.
PSD-95+/+
PSD-95+/halo
PSD-95halo/halo
fEPSP Slope (mV/ms)
Fiber Volley Amplitude (mV)
b.
Paired-Pulse Ratio
Inter-Pulse Interval (msec)
c.
PSD-95+/+
PSD-95+/halo
PSD-95halo/halo
20 pA
200 ms
d.
Cumulative Probability
Amplitude (pA)
WT
Het
Homo
e.
Cumulative Probability
Inter-Event Interval (msec)
Frequency (Hz)
f.
PSD-95+/+
PSD-95halo/halo
100 pA
20 ms
g.
NMDA/AMPA Ratio
WT
Het
Homo
h.
τw Decay (msec)
WT
Het
Homo
i.
PSD-95+/+
PSD-95+/halo
PSD-95halo/halo
fEPSP Slope (% Baseline)
Time (min)

Figure 3.3. PSD-95-HaloTag knock-in mice are electrophysiologically normal.
a. Fiber volley/fEPSP input/output curves generated by eliciting fEPSPs with intensities of presynaptic stimulation corresponding to 100, 75, 50, and 25% of max. Results are from 5 wild type mice, 5 hets, and 4 homozygous mutants. **b.** Paired-pulse facilitation is normal in PSD-95 halo mutants. Results are from 5 wild type mice (20 slices), 5 hets (21 slices), and 4 homozygous mutants (18 slices). **c.** Example excitatory postsynaptic currents (EPSCs) recorded at membrane potential of -80 and +40 mV in wild type and homozygous mutants. **d.** Ratio of NMDAR to AMPAR-mediated currents recorded at V_m = +40 mV. No difference with one-way ANOVA, $F_{(2,11)}$ = 0.345, *P* = 0.717. **e.** Weighted decay time constants for currents elicited at V_m = +40 mV. No difference in decay times $F_{(2,11)}$ = 3.602, *P* = 0.071. Results in B and C are from 5 wild type mice (19 cells), 3 heterozygous mutants (12 cells), and 4 homozygous mutants (16 cells). **f.** Examples of sEPSCs (5 superimposed, 1 second-long recordings for each). **g.-h.** Cumulative probability plots of sEPSC amplitudes (**g.**) and inter-event intervals (**h.**). Results are from 4 wild type mice (11 cells), 3 hets (11 cells) and 4 homozygous mutants (15 cells). Histograms show mean (± SEM) values. One-way ANOVAs for the results shown in the histograms: $F_{(2,8)}$ = 0.049, *P* = 0.952 for sEPSC amplitude and $F_{(2,8)}$ = 0.836, *P* = 0.921 for sEPSC frequency. **i.** LTP induced by two, 1-second-long, trains of 100 Hz stimulation (delivered at time = 0, inter-train interval = 10 sec). Sixty minutes post-100 Hz stimulation fEPSPs were potentiated to 191 ± 4.5% of baseline in wild type slices (n = 10 slices from 5 mice), 179 ± 1.3% of baseline in het slices (n = 10 slices from 5 mice), and 186 ± 8.2% of baseline in slices from homozygous mutants (n = 9 slices from 4 mice). One-way ANOVA gives $F_{(2,11)}$ = 1.706, *P* = 0.226.

3.3 Using the HaloTag system to label PSD-95-HaloTag fusion proteins with ligands

3.3.1 In vitro labelling of crude synaptosomes with HaloTag ligands

One of the key aims early on in the project was to demonstrate that it is possible to label the PSD-95-HaloTag fusion protein with HaloTag ligands in a variety of experimental scenarios, thereby laying a foundation upon which to design future experiments. One early pilot study in this area involved adding a commercially available HaloTag ligand (carboxytetramethyrhodamine (TMR) ligand) to a crude mouse brain synaptosome preparation (brain lysate enriched for synaptic proteins), subjecting this to SDS PAGE and then imaging the membrane using the LI-COR imaging system. This technique functions similarly to a western blot in that it allows the visualisation of a protein on a membrane, but does not require the use of antibodies.

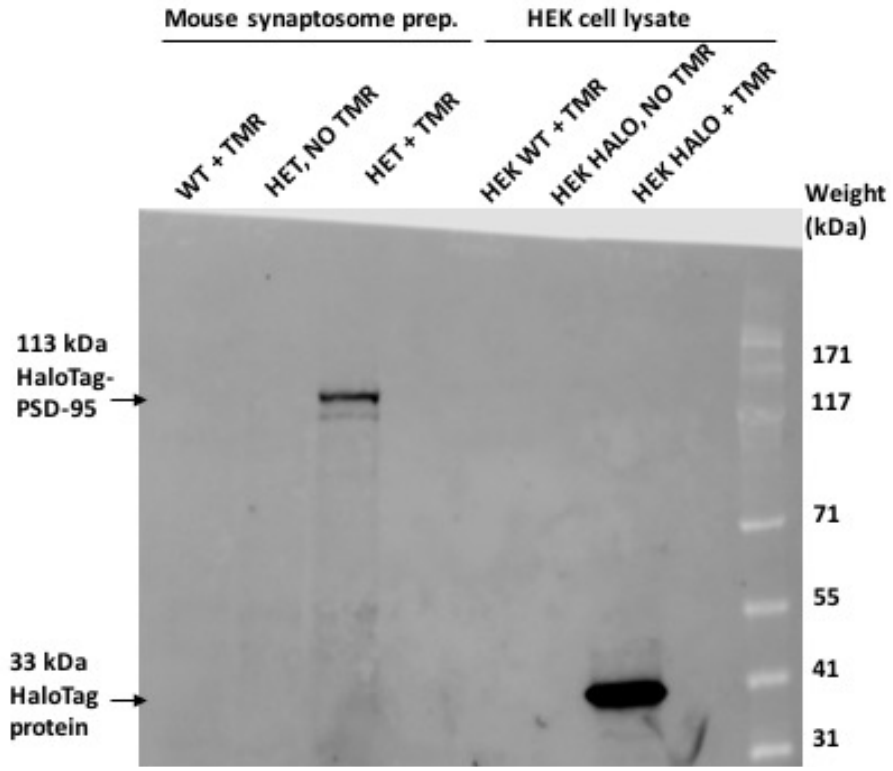

Figure 3.4. In crude synaptosome preparations the PSD-95-HaloTag fusion protein can be labelled with the HaloTag TMR ligand and be visualised by SDS PAGE

Crude synaptosome preparations from a heterozygous PSD-95$^{HaloTag/+}$ mouse (Het + TMR) and a wild-type mouse (WT + TMR) were incubated with carboxytetramethylrhodamine (TMR) ligand (1µM) for 1h at 4°C (negative control: Het, NO TMR). As further controls, HEK293 cells expressing the HaloTag protein, alongside WT HEK293 control cells, were lysed and also incubated with the HaloTag TMR ligand for 1h at 4°C (negative control: Halo-HEK cells not incubated with TMR). The gel was then subjected to SDS PAGE, and imaged using the LiCOR imaging system. A strong, distinct band is visible at 113kDa in the Het + TMR lane for the mouse synaptosome preparations, corresponding to the expected molecular weight of the fusion protein combining PSD-95 (80kDa) with the HaloTag protein (33kDa). There is an even stronger band at 33kDa in the Halo-HEK cell lane treated with TMR. Thus, both samples expressing the HaloTag protein and exposed to TMR ligand display very strong and specific labelling that is absent in all of the negative control lanes. This demonstrates the viability of using the HaloTag system to visualise proteins of interest using SDS PAGE without the requirement for antibodies. Note the lack of non-specific banding that is often associated with western blotting, and lack of signal in the negative control lanes.

Crude synaptosomes were prepared from the brains of a heterozygous PSD-95$^{HaloTag/+}$ mouse and a WT mouse, as per methods chapter 2.1.2. TMR ligand was then added to 100 µL of lysate at a final concentration of 5 µM, and incubated at 4°C with constant rotation for 1 hour.

Human Embryonic Kidney (HEK293) cells expressing the HaloTag protein on its own (not fused to a second protein) were kindly provided by Dr. Masaru Ishii's lab in Japan and used as positive controls in this experiment. These Halo-HEK cells were lysed in mammalian lysis buffer (see chapter 2.2.3) and incubated with TMR ligand in the same manner as the mouse synaptosome preparations had been treated, i.e. incubated at 4°C with constant rotation for 1 hour. For both HEK cells and synaptosome preparations, negative controls were either HaloTag-containing samples that did not receive any TMR ligand treatment (untreated controls), or WT samples (synaptosomes and HEK cells) not expressing the HaloTag protein that were treated with the TMR ligand (WT controls).

These samples were subjected to SDS PAGE and transferred to a nitrocellulose membrane as per the protocol in chapter 2.1.5. The membrane was then imaged using the LI-COR Odyssey imaging system, without requiring the addition of antibodies.

The results showed a distinct and highly specific band corresponding to PSD-95-HaloTag at the expected molecular weight of 113kDa (Figure 3.4), with an emission range of 500-600nm (The TMR ligand emits maximally at 578 nM). Note that this experiment was performed on a synaptosome preparation from the brain of a heterozygous knock-in mouse, and thus in a homozygous sample an even stronger signal would be expected. The positive control lane, containing TMR-treated Halo-HEK cell lysate, also displayed a very strong band at about 33kDa, thus corresponding to the molecular weight of the HaloTag protein. This band is markedly more intense than the band in the synaptosome sample, presumably because the HEK cell line is expressing the HaloTag protein at a very high level, driven by the human cytomegalovirus (CMV) intermediate early enhancer/promoter (see Promega website for product details). Furthermore, equal volumes were loaded into the gel wells, and the HEK cell culture had been grown to a very high density (About 90% confluence at the time of harvesting). Wild-type lanes and untreated control lanes did not exhibit any signal (not even non-specific background bands).

This result reveals that in vitro labelling of homogenised brain tissue from PSD-95-HaloTag mice is feasible and can be used in place of western blotting. This has great implications, as western blotting can frequently yield ambiguous results, arising due to

the experimental process producing 'dirty' blots from the blocking solution or nonspecific adherence of the antibody to the membrane, non-specific labelling of non-target proteins, epitope similarities leading to other proteins being labelled, and potentially species cross-reactivity of the antibodies. Using a HaloTag ligand instead not only provides a much cleaner result, but also gives much greater confidence in the result since specificity is so high, and the potential cross-reactivity with native proteins in most systems is greatly reduced due to the HaloTag's bacterial source (Los et al., 2008).

This experiment's results also serves to underline the strength of the covalent ester bond formed between the chloroalkane linker of the HaloTag ligand and the deep hydrophobic pocket of the HaloTag protein. This bond was not broken by the boiling of the sample at 100°C for 5 minutes, nor by the subjection to the denaturing SDS detergent during SDS PAGE, in agreement with results by Los et al. (2008).

3.3.2 Labelling of fixed mouse brain slices with HaloTag ligands

A further important experiment that was performed was the attempt to stain fixed brain slices from PSD-95^{HaloTag} KI mice using HaloTag ligands. According to Los et al. (2008), HaloTag ligands can be used to label HaloTag proteins in fixed tissue. Nevertheless, it was important to demonstrate that HaloTag ligands are capable of penetrating the protein-rich postsynaptic density after cross-linking by PFA fixation has taken place. Furthermore, this would reveal whether the expression pattern of the PSD-95-HaloTag fusion protein in the KI mouse line matches that of PSD-95 in control samples.

Coronal brain sections were prepared from adult heterozygous PSD-95$^{HaloTag/+}$ mouse brains that had been prepared by cardiac perfusion. Sections were cut to a thickness of 18µm using a cryostat. Perfusions and sectioning were kindly performed by technician Jamie Rose. TMR ligand was diluted in PBS to a 1µM concentration (1:1000), and brain sections incubated for 1 hour at room temperature. Immunohistochemistry was performed using a mouse anti-PSD-95 antibody (Neuromab, 1:1000). Sections were then imaged, first using the Zeiss Axio Scan.Z1 slide scanner, at 20x magnification, followed by higher magnification imaging using

a.

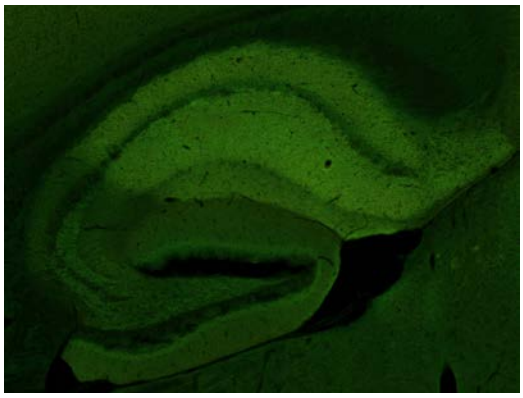

b.

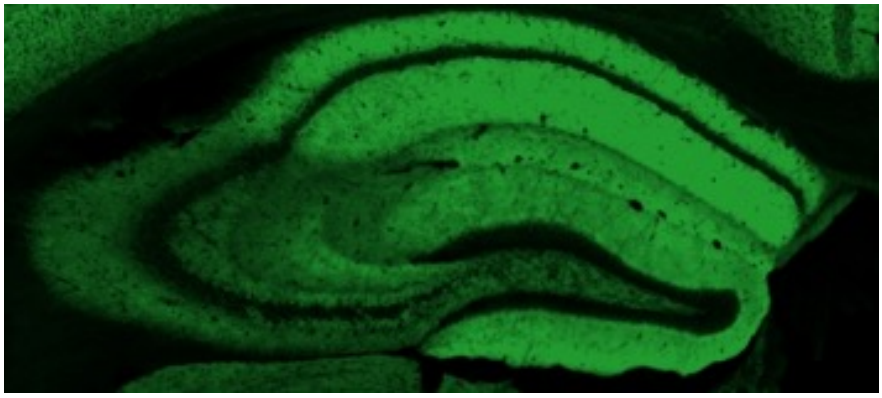

c.

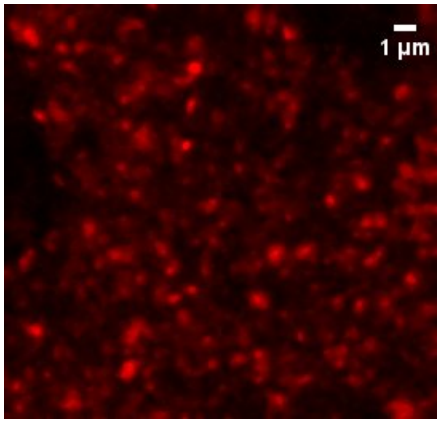

d.

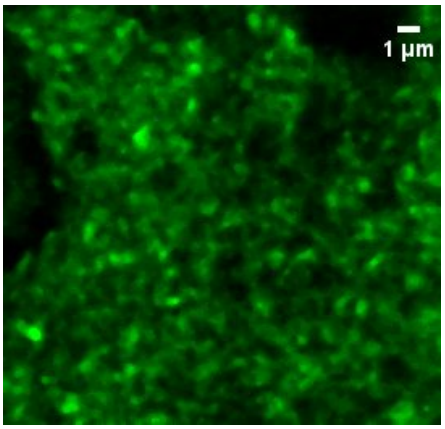

e.

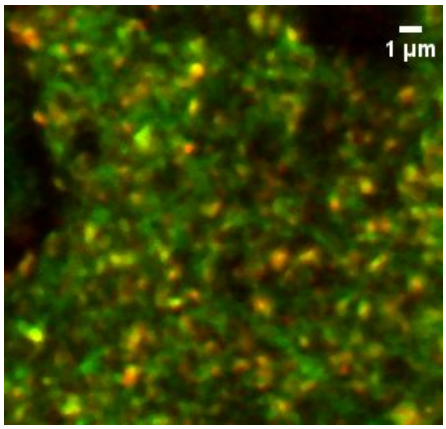

f.

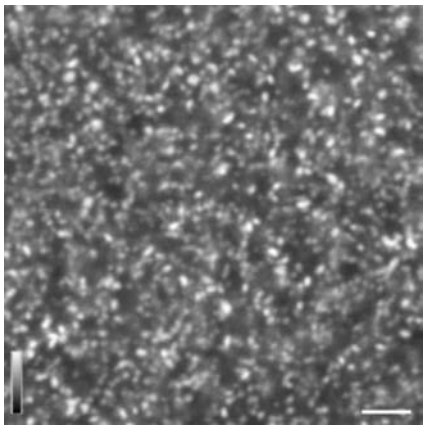

Figure 3.5. Imaging of coronal brain sections of PSD-95-HaloTag mice treated with TMR ligand post fixation.

a.-b. Fixed brain sections were imaged at low-magnification (20x) using the Axio Scan slide scanner. Hippocampal areas are displayed. **a.** Section taken from het PSD-95$^{HaloTag/+}$ mouse and treated with TMR ligand (1µM, 1h at RT). **b.** Section taken from hom PSD-95-eGFP mouse, untreated. The PSD-95 expression profile for both mouse lines appears to be very similar. **c-e.** Fixed brain section of het PSD-95$^{HaloTag/+}$ mouse treated with TMR ligand (1µM, 1h at RT) and stained with anti-PSD-95 antibody (Neuromab, 1:250). TMR ligand channel displayed in (c.) and antibody staining displayed in (d.), with overlay in (e.). Images taken in the CA1 region of the hippocampus. **f.** Brain slice of PSD-95-eGFP KI homozygous mouse line, imaged in the CA1 region of the hippocampus. Images in (c.-f.) acquired at high magnification (63x) using a Zeiss LSM510 confocal microscope. The synaptic expression pattern again looks very similar in the two genotypes (c. and f.), while the ligand signal overlaps strongly with the antibody staining (e.). Note that the scale bar in (f.) is 2µm in length. Both PSD-95-eGFP images (b. and f.) were taken and kindly provided by Dr. Matthew Broadhead.

the confocal LSM 510 at 63x magnification. Imaging using the Axio Scan slide scanner was again kindly performed by Jamie Rose.

Low magnification (20x) imaging of brain slices using the slide scanner and qualitative analysis revealed an expression profile very similar to that of eGFP-tagged PSD-95 (Figure 3.5.a and 3.5.b). Based upon qualitative fluorescence intensity, PSD-95 expression levels appear to be high in the CA1 area of the hippocampus in both mouse lines. More specifically, it appears that PSD-95 expression is particularly high in the CA1 Stratum Oriens (CA1 S.O.) and CA1 Stratum Radiatum (CA1 S.R.), whereas cell body layers such as the granule cell layer of the dentate gyrus and the pyramidal cell body layers of the CA1 – CA3 layers do not appear to express PSD-95 at all, as is to be expected (Yan et al., 2013).

At higher magnification (63x), images taken in the CA1 region of the hippocampus reveal a dense pattern of bright PSD-95 puncta in the PSD-95^{HaloTag} mouse brain slices treated with TMR ligand (Figure 3.5.c). The anti-PSD-95 staining with an antibody (Neuromab Mu anti-PSD-95, 1:1000) reveals a similar staining pattern (figure 3.5.d), with a high degree of colocalisation between the ligand and the antibody (figure 3.5.e). Note that the antibody staining appears to be less specific than the TMR ligand labelling, with the ligand displaying less background signal. Finally, this punctate staining pattern is very similar to that found in the PSD-95-eGFP mouse brain section (Figure 3.5.f).

Note that all images of the PSD-95-eGFP mouse line were kindly provided by Dr. Matthew Broadhead.

There are two conclusions that can be drawn from the high and low magnification analysis of PSD-95^{HaloTag} mouse brain sections treated with a HaloTag ligand (TMR). Firstly, it is possible to effectively label PSD-95-HaloTag fusion proteins within fixed brain tissue simply by using ligands briefly applied to mounted sections. Secondly, the staining pattern revealed by ligand-labelling of PSD-95-HaloTag fusion proteins in the hippocampus follows the expected expression pattern of PSD-95, and is similar to the PSD-95-eGFP expression pattern in another line of KI mice. Together, the biochemical and microscopic analysis indicates that the overall expression levels and expression pattern of PSD-95 in the adult mouse brain are unperturbed by the HaloTag protein fused to PSD-95. It therefore stands to reason that this mouse model is not only technically suitable for the study of PSD-95 using the HaloTag technology, but is also phenotypically normal in all measured criteria, and thus the legitimate claim can be made that results from experiments performed on this mouse line can be expected to be biologically representative of PSD-95 in all mice.

3.3.3 Labelling living neurons grown in primary culture with HaloTag ligands

The next step was to grow neuronal primary cultures to demonstrate that the HaloTag system could be used to reliably label PSD-95-HaloTag fusion proteins in the synapses of living neurons. To this end, primary cultures were grown as per the methodology detailed in chapter 2.3. Briefly, the brains of embryos at developmental stage E17.5 were dissected such that the forebrain portion was retained, and pooled together from the entire litter. These brain dissections were then turned into a single-cell suspension, and plated onto PDL- and laminin-coated glass coverslips. These neuronal primary cultures were then grown for two weeks, and at developmental stage DIV14 (Day In Vitro 14) experiments were performed. This age was decided upon as this is the time when cultured mouse primary neurons are not yet fully mature, and undergoing high levels of synaptogenesis (Lesuisse and Martin, 2002; Cohen et al.,

2013). At this stage, glutamate receptors are already being expressed strongly (Li et al., 1998), and PSD-95 levels are also high, making this a commonly used time point when studying this protein (Fernandez et al., 2009; El-Husseini et al., 2002).

First experiments involved simply adding HaloTag ligands to the live PSD-95-HaloTag and WT control neurons, fixing them, and performing immunocytochemistry to stain for PSD-95. In early experiments, HaloTag ligands were diluted in the media 1:1000, as per instructions, for a final concentration of 1 μM. Cells were incubated for 15 minutes, before being fixed in 4% paraformaldehyde (PFA), and immunocytochemistry being performed, as per protocols in chapter 2.3. Imaging of coverslips was performed using the laser scanning confocal as per chapter 2.4.1, and synapses detected using the IMARIS software as per chapter 2.4.2.

A qualitative inspection of the images revealed a very strong and specific labelling of synapses when the R110Direct ligand was applied at 0.1 μM overnight (16h) (Figure 3.6.a-c), but no labelling at all in WT neurons (Figure 3.6.d-f). The same effect was observed when using the TMR ligand, applied at a concentration of 1 μM for 30 minutes (Figure 3.6.g-l). See Figure 3.7.a (page 76) for a lower-magnification view of the labelling of synaptic puncta along dendrites in neuronal primary cultures. Background labelling in both cultures was similarly low, with the exception being occasional large ‘blobs’ of very high intensity. These are much greater in diameter than synaptic puncta that are expected to range in size from 200 nm to 800 nm (Carlin et al., 1980; Südhof, 2012). These non-specific ‘blobs’, often many microns in size, were easily identified, and where not excluded automatically by the Imaris detection thresholds they were manually removed from any further analysis.

I then calculated the percentage colocalisation of synaptic puncta with the PSD-95 antibody label separately for each channel. Briefly, synaptic puncta were detected using a seed point estimation diameter of 300 nm, and puncta were considered as colocalised if within 300 nm of each other (centre to centre). The results indicated an average of 67.75 ± 2.0 % colocalisation of R110 ligand with the antibody staining, and a 73.88 ± 2.7 % colocalisation of the antibody staining with the R110 ligand (Figure 3.6.m). For the TMR ligand, colocalisation of the ligand with the antibody staining was 67.25 ± 3.4 %, while colocalisation of the antibody staining

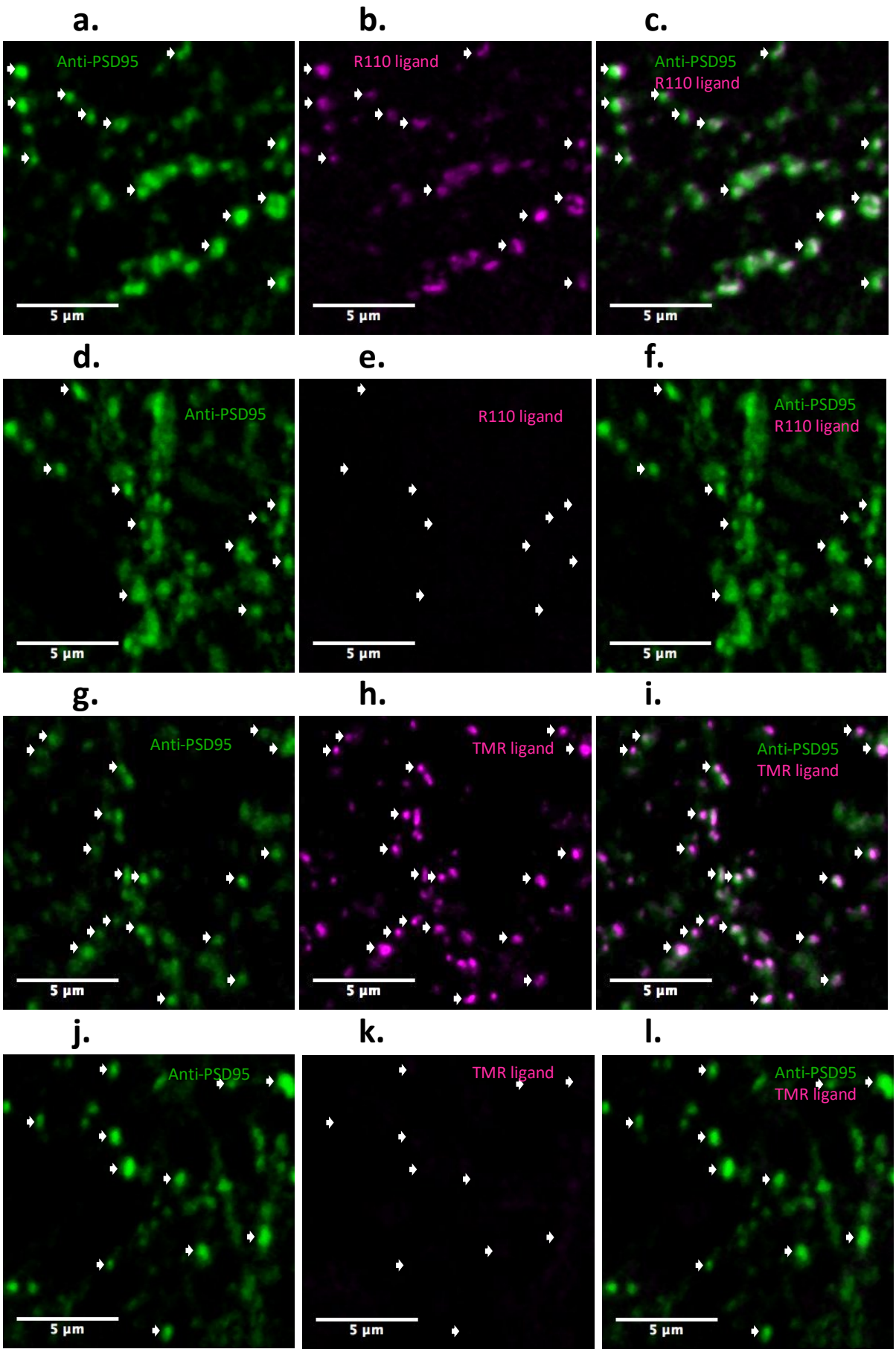
a.
Anti-PSD95
5 µm
b.
R110 ligand
5 µm
c.
Anti-PSD95
R110 ligand
5 µm
d.
Anti-PSD95
5 µm
e.
R110 ligand
5 µm
f.
Anti-PSD95
R110 ligand
5 µm
g.
Anti-PSD95
5 µm
h.
TMR ligand
5 µm
i.
Anti-PSD95
TMR ligand
5 µm
j.
Anti-PSD95
5 µm
k.
TMR ligand
5 µm
l.
Anti-PSD95
TMR ligand
5 µm

m.

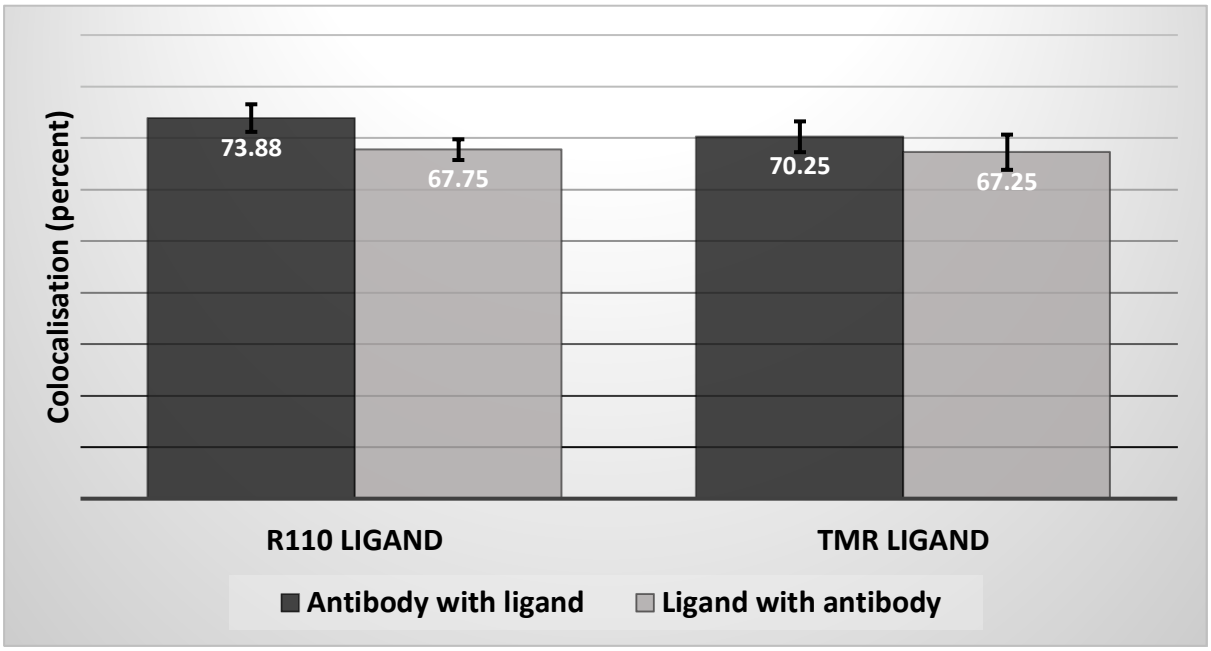

Figure 3.6. The fluorescent HaloTag ligands R110Direct and TMR can be used to label PSD-95-HaloTag fusion proteins in the postsynaptic densities of primary neuronal cultures

a.-f. Heterozygous PSD-95$^{HaloTag/+}$ (Het) primary cultures alongside WT control cultures were labelled with R110Direct ligand (100nM, 16h) at DIV14, fixed on DIV15, and stained with anti-PSD-95 antibody (Mouse, Neuromab 1:1000). Images taken with confocal LSM510 at 63x zoom3.1. **a.** Anti-PSD-95 antibody labelling in Het neurons. **b.** R110 ligand labelling in Het neurons. **c.** Overlay of anti-PSD-95 channel and R110 ligand channel in Het neurons (a. and b.). **d.** Anti-PSD-95 antibody labelling in WT neurons. **e.** R110 ligand labelling in WT neurons. **f.** Overlay of anti-PSD-95 channel and R110 ligand channel in WT neurons (d. and e.). A high degree of overlap of R110 signal with antibody staining is visible in Het cultures (a-c). In WT cultures (d-f), no ligand signal is detectable at all. **(g.-l.)** As in (a.-f.), primary neurons were cultured from WT or Het KI mice, and labelled with carboxytetramethylrhodamine (TMR) HaloTag ligand (1µM, 15 mins) on DIV14. **g.** Anti-PSD-95 antibody labelling in Het neurons. **h.** TMR ligand labelling in Het neurons. **i.** Overlay of anti-PSD-95 channel and TMR ligand channel in Het neurons (g. and h.). **j.** Anti-PSD-95 antibody labelling in WT neurons. **k.** TMR ligand labelling in WT neurons. **l.** Overlay of anti-PSD-95 channel and TMR ligand channel in WT neurons (j. and k.). As before, a high degree of overlap is visible between the TMR ligand signal and the anti-PSD-95 signal in Het cultures, whereas no ligand signal at all is visible in WT cultures. Note that for the whole panel, white arrows denote synaptic puncta. **m.** Graph showing analysis of colocalisation between anti-PSD-95 antibody labelling and PSD-95-HaloTag labelled with R110 ligand (100nM, 16h) or TMR ligand (1µM, 15 mins) in Het PSD-95$^{HaloTag/+}$ cultures. Puncta were deemed colocalised if their centre points were within 0.3um. Error bars denote SEM.

with the TMR ligand was 70.25 ± 3.0 % (Figure 3.6.m). WT cultures did not exhibit any detectable synaptic puncta in the TMR or R110 ligand channels.

As a control, one of the image channels was rotated 90° in order to evaluate the probability of puncta overlapping by chance (Figure 3.7.a-b). The actual observed colocalisation rate (as opposed to after rotation) was found to be very significantly higher both when looking at the overlap of antibody with R110 ligand (non-rotated: 73.88 ± 2.69; rotated: 6.43 ± 0.84; Paired T-test: $p=6.71x10^{-8}$) and R110 ligand with antibody (non-rotated: 67.75 ± 2.01; rotated: 6.76 ± 1.11; Paired T-test: $p=4.88x10^{-8}$) (Figure 3.7.c). In TMR ligand-labelled cultures the actual observed colocalisation rate was also found to be significantly higher in both instances: antibody with TMR ligand: non-rotated: 70.25 ± 2.99; rotated: 8.51 ± 2.34; Paired T-Test $p=8.54x10^{-7}$; and TMR ligand with antibody: non-rotated: 67.25 ± 3.42; rotated: 6.94 ± 1.74; Paired T-test $p=1.31x10^{-8}$; (Figure 3.7.d).

It should be noted that these results were gained from cultures that were grown from heterozygous embryos, thereby expressing both mutant and WT alleles of PSD-95. It is unlikely that this would affect the results, since the presumption is that all synapses would incorporate a mixture of mutant and WT PSD-95 proteins. Therefore, all postsynaptic densities would be labelled by HaloTag ligands. Nevertheless, it would be of value to repeat these colocalisation experiments using Homozygous PSD-$95^{HaloTag/HaloTag}$ mice.

As a further control experiment, PSD-95-HaloTag mice were crossed with PSD-95-eGFP mice, and embryos from these PSD-$95^{HaloTag/eFP}$ (Het/Het) mice used as the basis for another set of primary cultures. This stably PSD-95-eGFP expressing KI mouse line has previously been used for a lot of imaging work in our lab, and is known to display no aberrant phenotype, with PSD-95 localising to synapses normally (Broadhead et al., 2016).

As above, DIV14 cultured primary forebrain neurons were treated with TMR ligand and stained with anti-PSD-95 antibodies (Figure 3.8.a-d). Colocalisation analysis between the TMR ligand puncta and the eGFP puncta revealed a colocalisation of 71.20 ± 2.5 % between TMR ligand puncta and eGFP puncta, and a colocalisation of

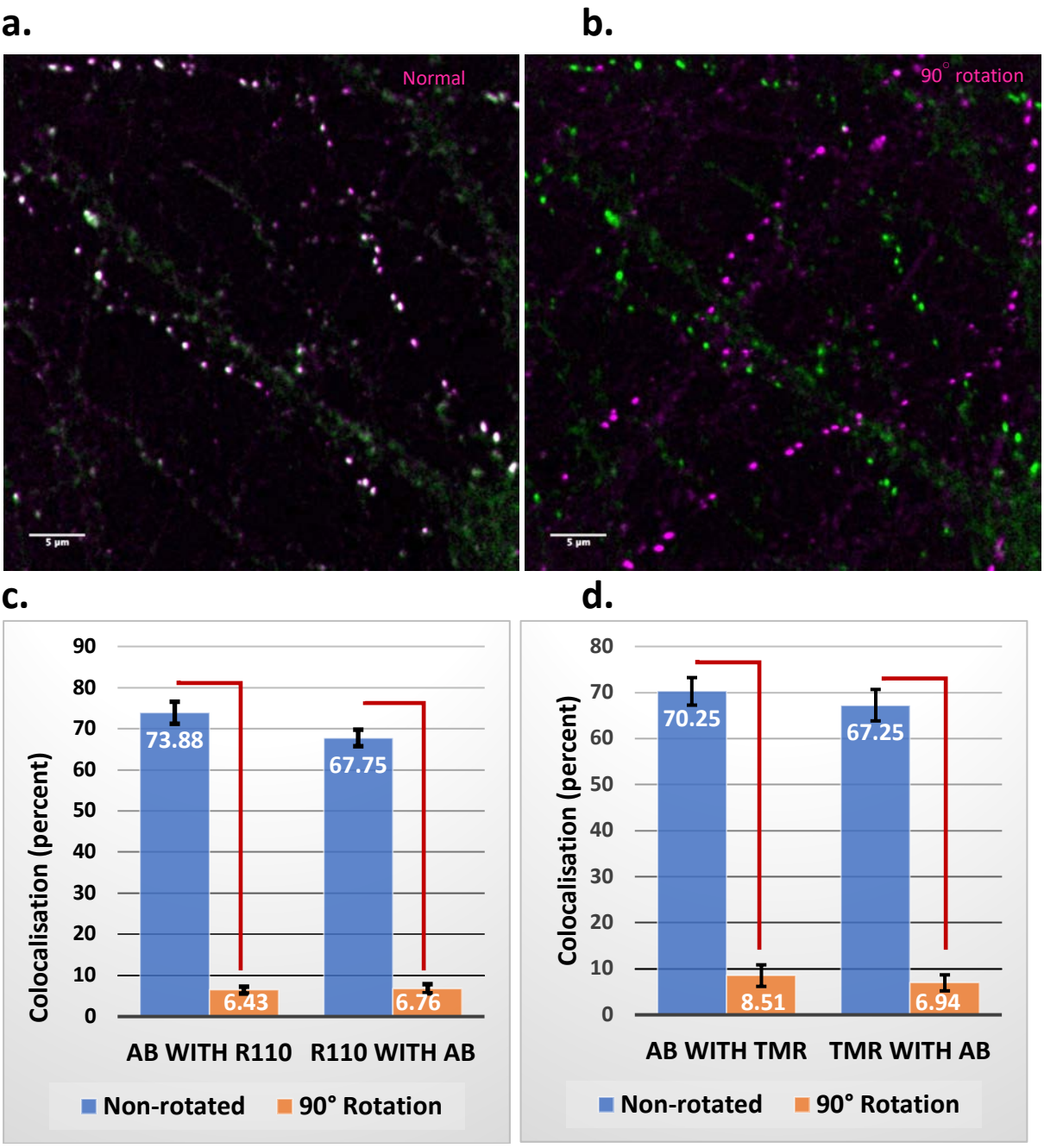

Figure 3.7. The colocalisation of antibody staining with ligand signal is not due to chance. **a.** Image of Het PSD-95$^{HaloTag/+}$ hippocampal primary neurons labelled with R110Direct ligand overnight (100nM, 16h), fixed DIV15 and stained with anti-PSD-95 antibody (Mouse, Neuromab 1:1000). Note the strong puncta overlap (white spots). **b.** The same image as in (a.), but the ligand channel of the image was rotated 90° using the ImageJ software. Note the lack of puncta overlap. **c.** Graph showing the percentage colocalisation between antibody and R110 ligand signal, before and after 90° rotation. **d.** Graph showing the percentage colocalisation between antibody and TMR ligand signal, before and after 90° rotation.

63.31 ± 1.8 % between eGFP puncta and TMR ligand puncta (Figure 3.8.e). In this experiment, too, 90° rotations of the images were performed, to evaluate the probability of chance puncta overlap. The actual observed colocalisation rate in both

cases is very significantly higher than would be expected by chance (Paired T-test: $p=8.95x10^{-9}$ (eGFP with ligand) and $p=3.47x10^{-9}$ (ligand with eGFP)).

Finally, it was of interest to discover whether HaloTag ligands are able to label Halo-PSD-95 in primary neurons after these have been fixed in 4% PFA for 15 minutes. As per the protocol given in chapter 2.3.5, primary neurons aged DIV14 were fixed and washed. Following the final washing step, the 24-well glass coverslips with the primary neurons attached were incubated for 30 minutes at room temperature with PBS containing TMR ligand at a concentration of 1µM. Coverslips were then stained with anti-PSD95 antibody, imaged using the LSM510 confocal and puncta detected with the Imaris software, as usual. When comparing antibody and ligand colocalisation in live-treated cells with post-fixation-treated cells, no statistically significant difference between the two groups was found (Welch's t-test, antibody colocalisation with TMR ligand p= 0.07; TMR colocalisation with antibody p=0.81) (Figure 3.9.a).

Overall, it was found that there is a high level of overlap between HaloTag ligand-labelled synapses and both anti-PSD-95 antibodies as well as eGFP-tagged synaptic puncta. WT cultures, displayed no ligand-labelling whatsoever. It may be expected that both HaloTag ligands and anti-PSD-95 antibodies would label all existing PSD-95-HaloTag proteins, and thus one should expect a 100% colocalisation between the two. The same holds true in PSD-95$^{HaloTag/eGFP}$ (Het/Het) cultures, where one might expect PSD-95 molecules of both alleles to be present in every postsynaptic density, and therefore likewise expect a 100% colocalisation rate. Nevertheless, colocalisation falls between 65% and 75% in both cases. One explanation for this discrepancy is incomplete labelling by the HaloTag ligands. However, this is highly unlikely, also because of numerous later results that imply complete saturation of all HaloTag binding sites by ligands (see chapters 3.4.3 and 3.4.4 as examples). It is more likely that the results are due to a combination of factors such as incomplete and irregular staining by the anti-PSD-95 antibody and imperfect detection and/or colocalisation measurements. This is because antibody staining can be varyingly effective (depending on the degree of cell membrane permeabilisation for example), and the settings used for the taking and analysing of images are optimised, but nonetheless never perfect. It was found that primary neurons grown on glass coverslips can indeed be successfully labelled with HaloTag ligands after fixation. This adds a useful

dimension to the HaloTag toolkit, as in some scenarios, it may be advantageous to fix cells and label them with ligands subsequently (see chapter 3.4.2).

A further point of discussion is that the results in chapter 3.3.3 indicate that there are marked differences in synaptic puncta size (diaqmeter and area). While puncta size was not used during the analysis, this could indeed have been an interesting aspect to investigate. Thus, correlating puncta size with intensity could have provided an interesting perspective on understanding the link between the size of synapses with the concentration of PSD-95 molecules within. Indeed, the normalisation of puncta intensity to size could have been an important aspect of analysis. This would have allowed for puncta size to be factored into the calculation of PSD-95 expression levels at synapses. Further, normalising ligand puncta intensity to antibody puncta intensity could have allowed for more direct comparisons between different ligand labels. However, the slight variability in labelling efficiency between samples when antibody staining could have caused difficulties in such an approach.

In the experiments conducted throughout this project, only single z-stacks were used when acquiring images. This means that the results represent information gathered at a single focal plane, with no information about planes above and below. This prevents conclusions from being drawn regarding the 3-dimensional structure of the puncta, as we do not know if individual puncta stretch across multiple focal planes, and thus what shape they take. Incorporating images taken across multiple z-stacks, while undoubtedly vastly more time consuming, would have allowed for interesting insights into PSD-95 expression levels at synapses of different shapes and sizes. Using multiple z-stacks would also have permitted a greater analysis of puncta colocalization, as it would facilitate our understanding of the spatial relationship between individual synapses and dendritic spines.

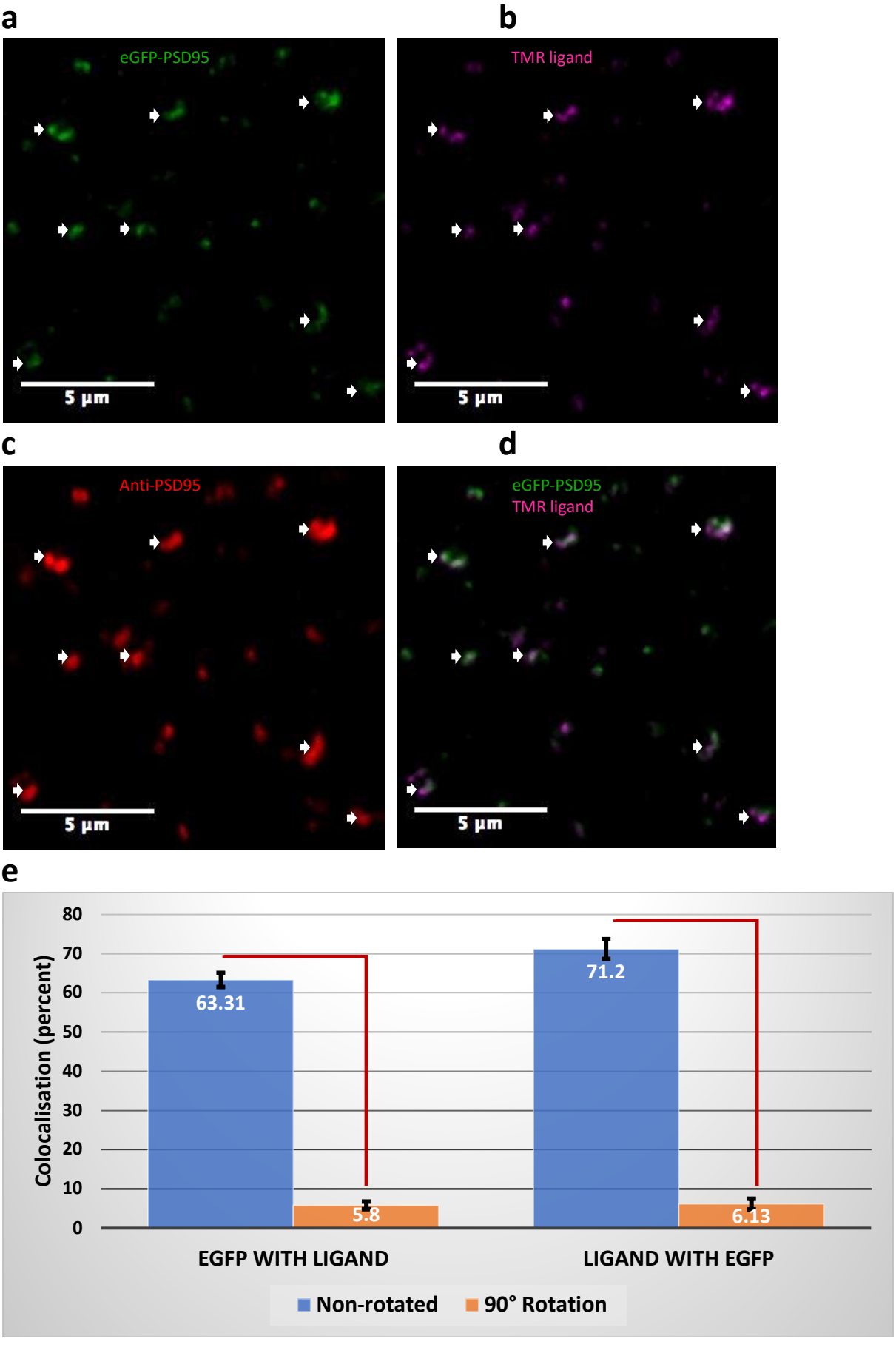
a
eGFP-PSD95
5 µm
b
TMR ligand
5 µm
c
Anti-PSD95
5 µm
d
eGFP-PSD95
TMR ligand
5 µm
e
Colocalisation (percent)
80
70
60
50
40
30
20
10
0
63.31
5.8
71.2
6.13
EGFP WITH LIGAND
LIGAND WITH EGFP
Non-rotated
90° Rotation

Figure 3.8. PSD-95-eGFP puncta overlap strongly with HaloTag ligand puncta in PSD-95$^{HaloTag/eGFP}$ (Het/Het) mice.

a.-d. Primary neuronal cultures from mice expressing PSD-95 tagged with eGFP and HaloTag (Het/Het, PSD-95$^{HaloTag/eGFP}$). LSM510 images of PSD-95$^{HaloTag/eGFP}$ cultures at DIV14, treated with TMR ligand (1µM, 15 mins) and anti-PSD-95 antibody. **a.** LSM510 green channel (excitation: 488nm) revealing synaptic puncta labelled by eGFP-PSD-95. **b.** LSM510 red channel (excitation: 543nm) revealing synaptic PSD-95-HaloTag puncta labelled by TMR ligand. **c.** LSM510 far red channel (excitation: 633nm) revealing synaptic puncta labelled by anti-PSD-95 antibody. **d.** Composite image of (a.) and (b.) showing both eGFP-tagged PSD-95 and PSD-95-HaloTag labelled with TMR ligand. A strong overlap between the eGFP signal and the TMR signal is evident. White arrows point out some overlapping puncta. **e.** Graph of colocalisation analysis between synaptic puncta labelled with TMR ligand and eGFP puncta. As controls, images were rotated 90° to be able to evaluate random puncta overlap. Error bars denote SEM.

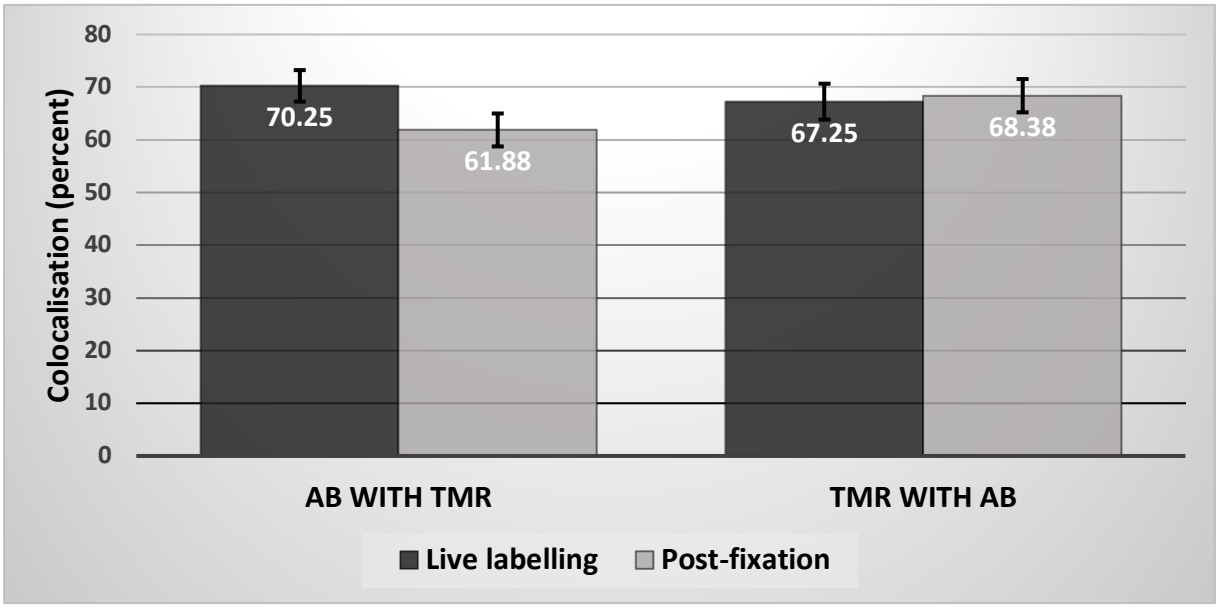

Figure 3.9. The TMR ligand is able to label Halo-PSD-95 fusion proteins in fixed primary cultures to the same extent as in live cells.

Hippocampal primary neurons were fixed in 4% PFA for 15 minutes on DIV14, and immediately after fixation and subsequent washing was completed, cells were incubated with TMR ligand diluted in PBS at 1µM for 30 minutes at room temperature. Thereafter they were stained with anti-PSD-95 (Mouse, Neuromab, 1:1000). Subsequent colocalisation analysis revealed a high degree of puncta colocalisation between TMR ligand and antibody. This was indistinguishable from live-cell labelling results (Welch's t-test, antibody colocalisation with TMR ligand p= 0.07; TMR colocalisation with antibody p=0.81).

3.3.4 Analysis of postsynaptic density puncta juxtaposition with presynaptic markers

As a further validation that observed puncta indeed represent the postsynaptic density of glutamatergic synapses, I decided to perform antibody staining for presynaptic markers, and quantify the juxtaposition of pre- and postsynaptic puncta. VGlut1 is the predominant vesicular glutamate transporter in the mammalian brain, accounting for the uptake of about 80% of glutamate (Fremeau et al, 2004). Synapsin1 is another presynaptic marker protein that is widely expressed in the mammalian forebrain (Schiebler et al, 1986). It is associated with the cytoplasmic surface of synaptic vesicles, and makes up about 6% of the total protein amount in synaptic vesicles (Huttner et el, 1983). As such, it stands to be expected that the majority of excitatory glutamatergic synapses would express VGlut1 and Synapsin1a at synaptic vesicles in the presynaptic bouton. However, the distance between these areas of presynaptic VGlut1 density and the PSD is great enough to be visible when viewing merged images of PSD-95 and VGult1 staining. Hence, unlike when quantifying colocalisation, the 'colocalisation' distance was extended to 600 nm (centre to centre) when quantifying pre- and postsynaptic puncta juxtaposition.

Hippocampal primary cultures were grown as per my standard protocol (chapter 2.3), again using embryos from the PSD-95$^{HaloTag/eGFP}$ (Het/Het) cross, as detailed above in chapter 3.3.3. At DIV14, cells from these cultures were treated with the TMR ligand (500nM) for 1h, before being fixed and immunocytochemistry performed as per the standard protocol (chapter 2.3.6). Immunocytochemical staining was performed for either VGlut1, or Synapsin1a. Coverslips were then imaged using the Leica 510 laser scanning confocal microscope, and synaptic puncta identified and colocalisation determined as per protocols in chapter 2.4.2. As before, synaptic puncta were detected using a seed point estimation diameter of 300 nm.

A qualitative analysis revealed that postsynaptic puncta labelled with the HaloTag TMR ligand appeared to be frequently juxtaposed with presynaptic marker puncta, in the case of both VGlut1 (Figure 3.10) and Synapsin1a (Figure 3.11) staining. Quantitative analysis revealed that 50.4 ± 6.4 % of Vglut1 puncta were juxtaposed with

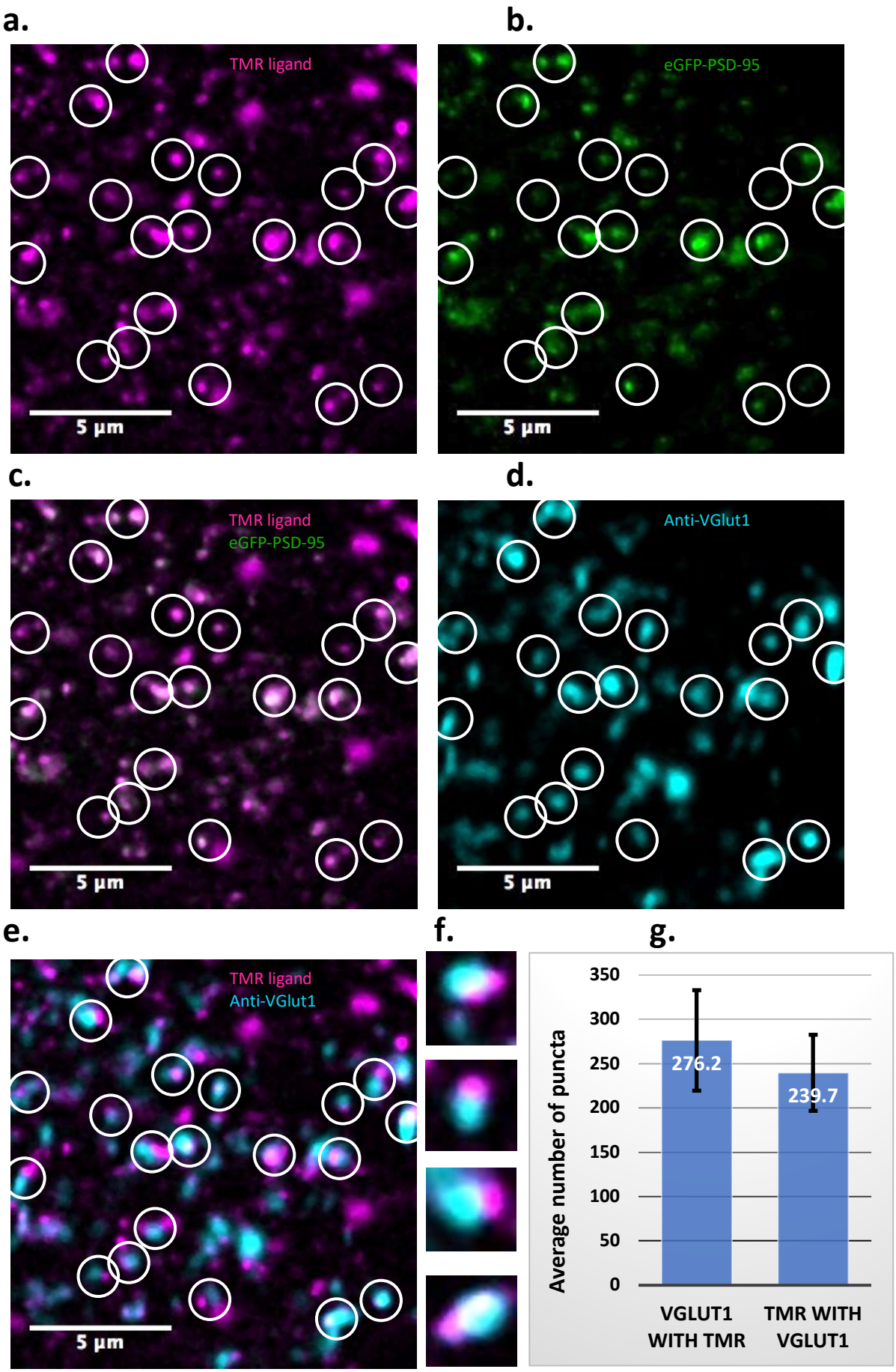
a.
TMR ligand
5 µm
b.
eGFP-PSD-95
5 µm
c.
TMR ligand
eGFP-PSD-95
5 µm
d.
Anti-VGlut1
5 µm
e.
TMR ligand
Anti-VGlut1
5 µm
f.
g.
Average number of puncta
350
300
250
200
150
100
50
0
276.2
239.7
VGLUT1 WITH TMR
TMR WITH VGLUT1

h.

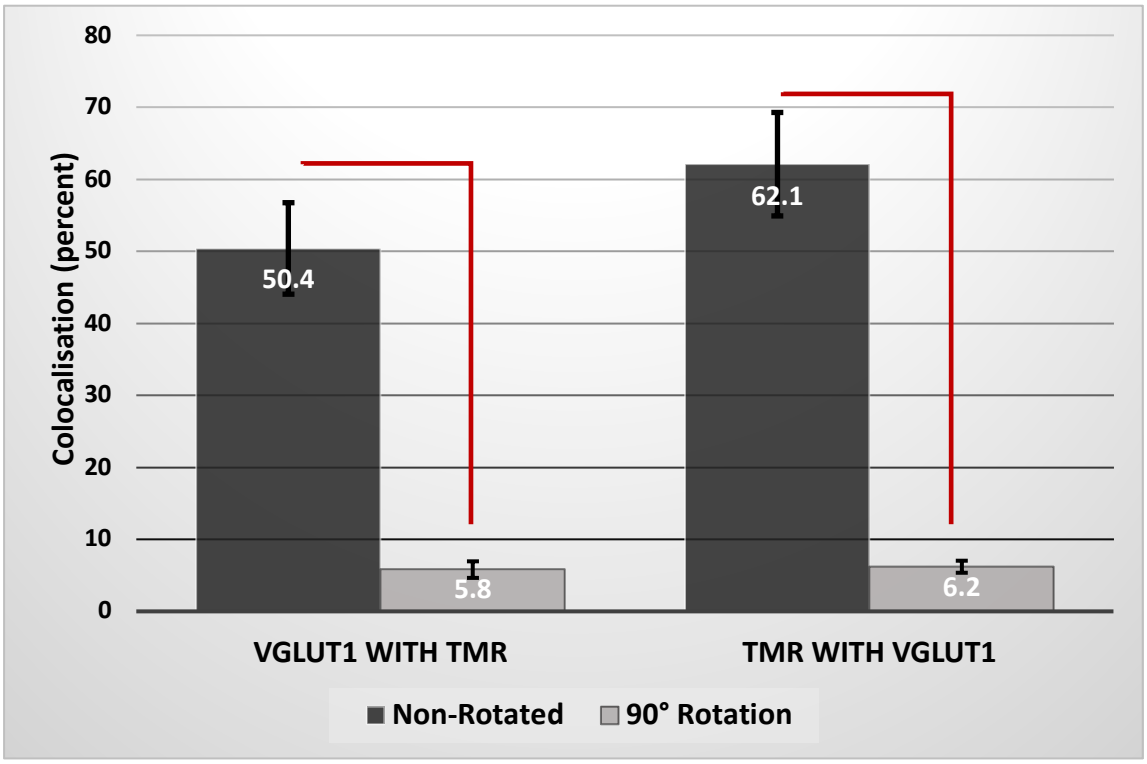

Figure 3.10. Postsynaptic puncta labelled by HaloTag ligands are juxtaposed with VGlut1 presynaptic marker puncta.

Primary neuronal cultures from mice expressing PSD-95 tagged with eGFP and HaloTag (Het/Het, PSD-95$^{HaloTag/eGFP}$) were treated with TMR ligands at DIV14 and stained for the presynaptic marker VGlut1. **a.** Red channel of LSM510 image showing postsynaptic puncta visualised by TMR ligand bound to PSD-95-HaloTag proteins. **b.** Green channel of image showing postsynaptic puncta visualised by eGFP-tagged PSD-95. **c.** Overlay of red and green channels, revealing colocalisation of PSD-95 tagged with HaloTag-TMR and eGFP. Note the very high degree of colocalisation. **d.** Far-red channel of image showing VGlut1 antibody staining of presynaptic puncta. **e.** Overlay of far-red and red channels, revealing juxtaposition of presynaptic puncta visualised by anti-VGlut1 staining with postsynaptic puncta labelled by TMR ligands bound to PSD-95-HaloTag proteins. **f.** Panel of close-up images of individual synapses displaying presynaptic VGlut1 staining and postsynaptic TMR labelling of PSD-95-HaloTag. **g.** Graphs showing the average number of TMR-ligand labelled postsynaptic puncta juxtaposed with presynaptic VGlut1 puncta, and vice versa. **h.** Graph showing the percentage of TMR-ligand labelled postsynaptic puncta juxtaposed with presynaptic VGlut1 puncta and vice versa, alongside the colocalisation analysis of the same images when the TMR ligand channel is rotated by 90°.

TMR ligand puncta, and 62.1 ± 7.2 % of TMR ligand puncta were juxtaposed with VGlut1 puncta (Figure 3.10.h). The average number of juxtaposed puncta in each of these groups was 276.2 ± 56.7 and 239.7 ± 43.0 puncta respectively, per image analysed (Figure 3.10.g). Images used were also rotated 90° as a control as before, to evaluate chance puncta juxtaposition. As before, the observed colocalisation rate

is significantly higher than would be expected by chance (Paired T-test: $p=7.92x10^{-6}$ (eGFP with ligand) and $p=5.69x10^{-7}$ (ligand with eGFP)).

Quantitative analysis of Synapsin1a juxtaposition revealed that 68.02 ± 3.1 % of Synapsin1a puncta were juxtaposed with TMR ligand puncta, while 74.21 ± 1.2 % of TMR ligand puncta were juxtaposed with Synapsin1a puncta (Figure 3.11.e). The average number of juxtaposed puncta in each of these groups was 389 ± 47.1 and 379 ± 61.5 puncta respectively, per image analysed (Figure 3.11.d). 90° rotation once again revealed a very low level of juxtaposition by chance, which was significantly different from observed puncta juxtaposition (Synapsin1a with TMR: 7.50 ± 1.8 %, paired T-test: $p= 4.67x10^{-8}$) (TMR with Synapsin1a: 8.36 ± 0.8 %, paired T-test: $p= 1.39x10^{-9}$).

These results indicate that the majority of puncta analysed by my method are indeed excitatory synapses that are made up of pre- and postsynaptic components. As in chapter 3.3.3, it is possible that the observed colocalisation level is lower due to inaccuracies in the staining by the presynaptic antibody, detection and/or colocalisation measurements. However, there are alternative explanations for the reduced level of colocalisation, particularly in the case of VGlut1, which had an even lower level of colocalisation (between 50% and 62% (Figure 3.10.h)). There are in fact two different major subtypes of the vesicular glutamate transporter: VGlut1 and VGlut2. While in adult mice, VGlut1 is the dominant isoform, in neonatal mouse brains VGlut2 predominates (Herzog et al, 2006; Miyazaki et al, 2003). The transition from one isoform to the other occurs at around 2 weeks of age, which corresponds roughly to DIV14 in primary cultures, and this maturation process is indeed recapitulated in vitro (Wojcik et al, 2004). It is therefore very possible that the lower level of colocalisation between postsynaptic PSD-95 puncta and presynaptic VGlut1 puncta is partially due to a lower expression level of VGlut1 at this developmental stage.

Synapsin1 similarly undergoes a shift in its expression level throughout postnatal development. While in mature neurons synapsin1 is localised to the majority of nerve terminals, synapsin1 expression correlates with synapse formation in the CNS and is implicated in their functional maturation (Di Liegro et al, 1995). Thus, synapsin1 levels have been shown to become detectable immunocytochemically around DIV14 in

a.

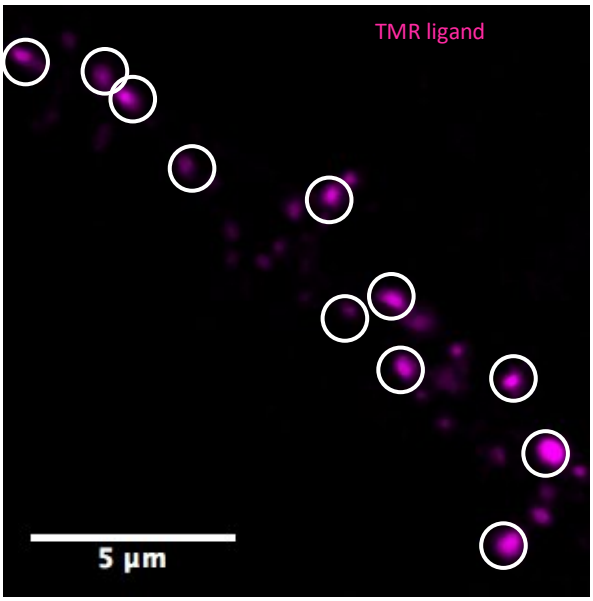
TMR ligand
5 µm

b.

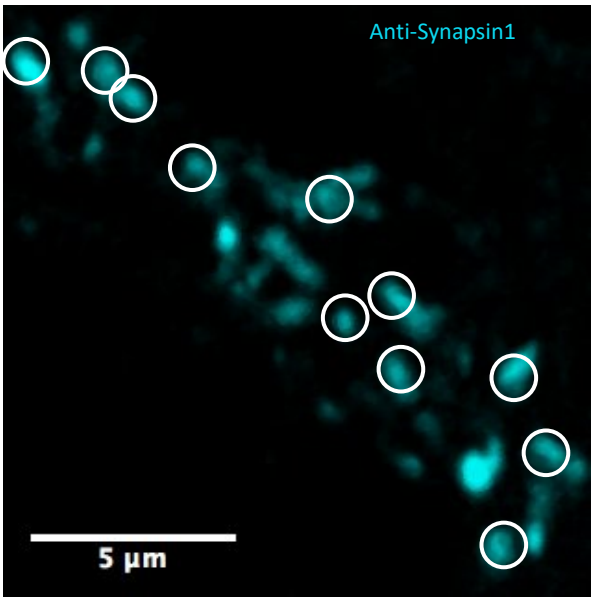
Anti-Synapsin1
5 µm

c.

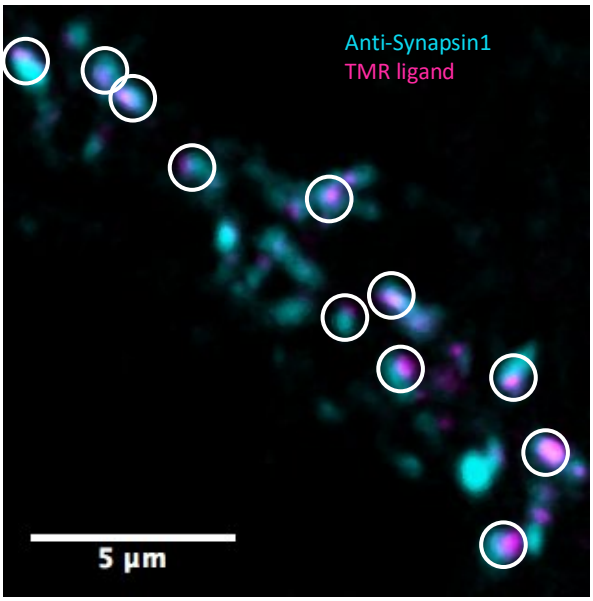
Anti-Synapsin1
TMR ligand
5 µm

d.

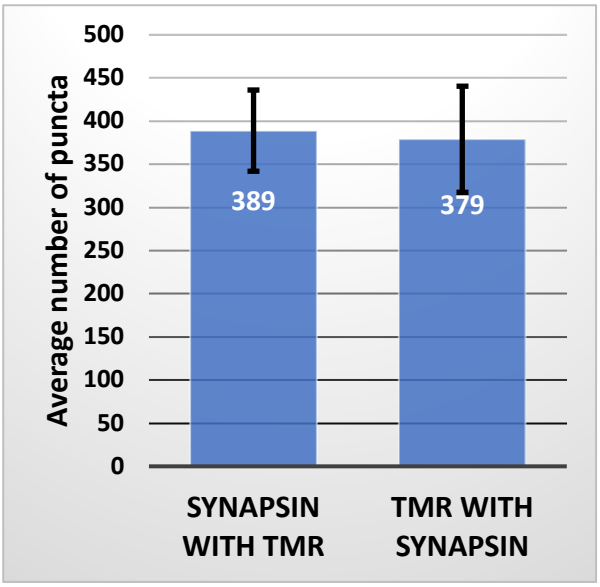
Average number of puncta
500
450
400
350
300
250
200
150
100
50
0
389
379
SYNAPSIN WITH TMR
TMR WITH SYNAPSIN

e.

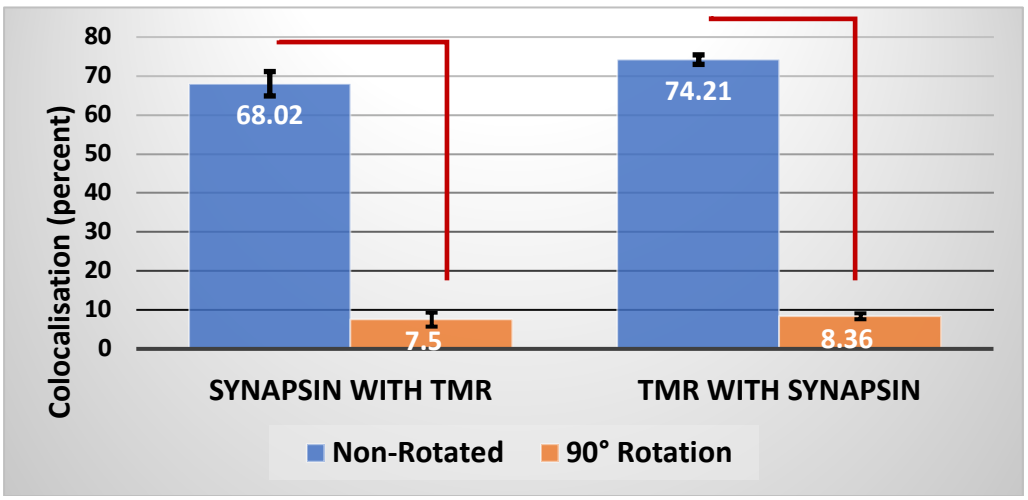
Colocalisation (percent)
80
70
60
50
40
30
20
10
0
68.02
7.5
74.21
8.36
SYNAPSIN WITH TMR
TMR WITH SYNAPSIN
Non-Rotated
90° Rotation

Figure 3.11. Postsynaptic puncta labelled by HaloTag ligands are juxtaposed with Synapsin1a presynaptic marker puncta.
Primary neuronal cultures from Homozygous PSD-95$^{HaloTag/HaloTag}$ mice were treated with TMR ligands at DIV14 and stained for the presynaptic marker Synapsin1a.
a. Red channel of LSM510 image showing postsynaptic puncta visualised by TMR ligand bound to PSD-95-HaloTag proteins. **b.** Far-red channel of image showing VGlut1 antibody staining of presynaptic puncta. **c.** Overlay of far-red and red channels, revealing juxtaposition of postsynaptic puncta visualised by anti-Synapsin1a staining with postsynaptic puncta labelled by TMR ligands bound to PSD-95-HaloTag proteins. **d.** Graphs showing the average number of TMR-ligand labelled postsynaptic puncta juxtaposed with presynaptic Synapsin1a puncta, and vice versa. **e.** Graph showing the percentage of TMR-ligand labelled postsynaptic puncta juxtaposed with presynaptic Synapsin1a puncta and vice versa, alongside the colocalisation analysis of the same images when the TMR ligand channel is rotated by 90°.

neuronal primary cultures, at which point they begin to rapidly increase (Salemi et al, 1990). Since the age of my cultures again falls directly into this period of increasing level of expression, this may account for the colocalisation rate being lower than anticipated.

3.3.5 MAP2 staining analysis

As a further validation of the primary culture model I used as the basis of my study, I decided to visualise dendrites and thereby evaluate the localisation of PSD-95 puncta relative to the dendrites. To this end, I used an antibody against microtubule-associated protein 2 (MAP2) as a dendritic marker. MAP2 is one of the major microtubule-associated proteins in the brain, critical for microtubule assembly and stability and, within neurons, confined to dendrites (Goedert et al, 1991).

Primary cultures at DIV14 were treated with R110 ligand as before, fixed, and stained with MAP2 antibodies. A qualitative analysis revealed that synaptic puncta were indeed distributed along dendrites positive for MAP2 (Figure 3.12). One observation one makes when viewing these images is that there appears to be significant heterogeneity in the synaptic morphology along a single dendrite. PSD-95 puncta vary in shape, diameter and fluorescence intensity (e.g. Figure 3.10.b). While such heterogeneity of synapses along single dendrites is not surprising (Craig & Boudin, 2001), it does raise the possibility of utilising the HaloTag technology to observe PSD-95 turnover at individual synapses along the same dendritic branch. This would allow

for novel insights into the turnover of a postsynaptic protein. However, while certainly interesting, I was unable to address this particular aspect of PSD-95 turnover during my project due to time constraints.

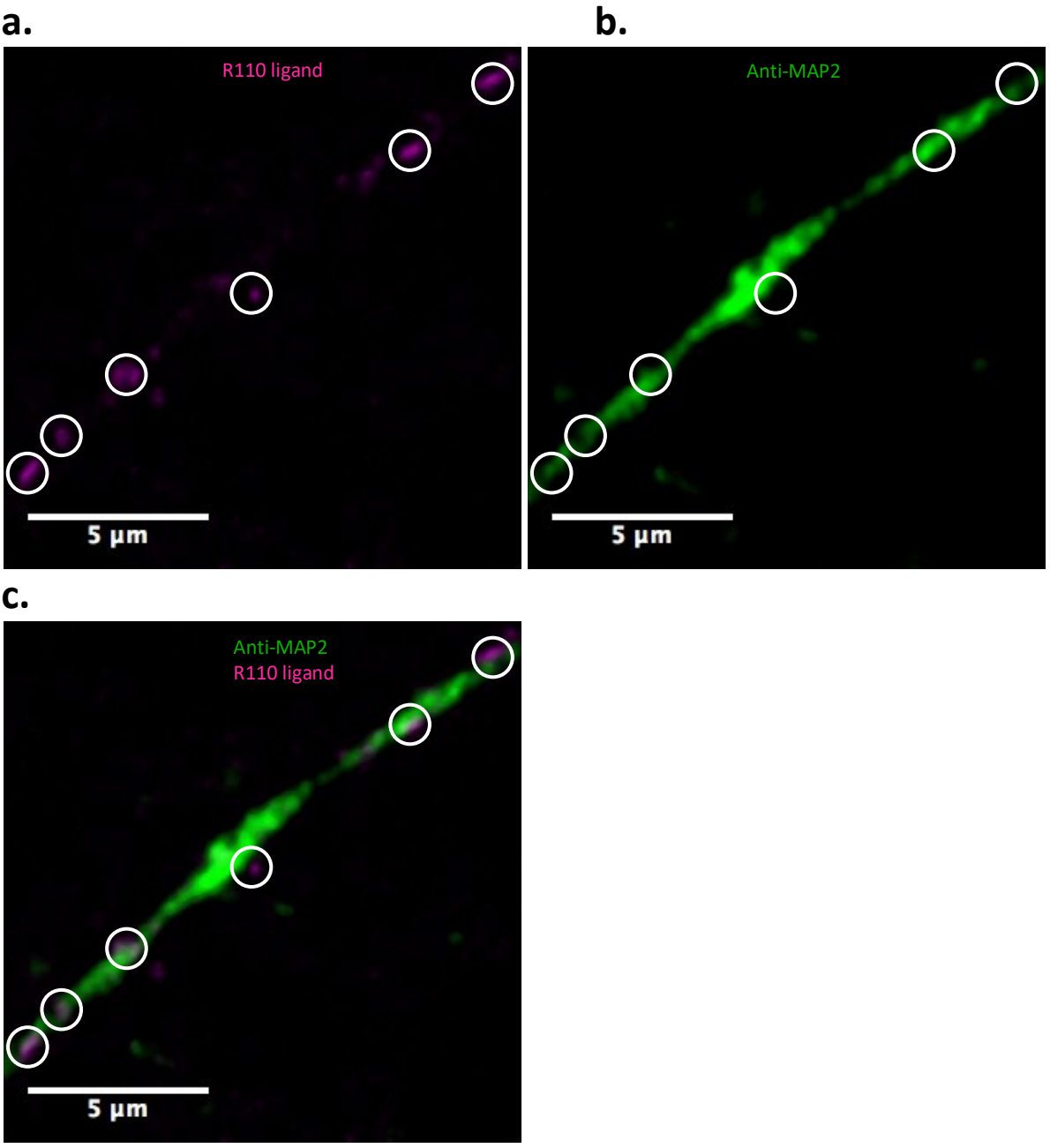

Figure 3.12. Postsynaptic puncta labelled by HaloTag ligands are located along dendrites. Hippocampal primary cultures were treated with R110Direct ligand (100nM 16h) before being fixed and stained with a MAP2 antibody (Chicken, Abcam, 1:1000). **a.** R110 ligand visualising PSD puncta. **b.** Anti-MAP2 antibody marking a dendritic branch. **c.** Overlay of (a.) and (b.) revealing that synaptic puncta tagged by the R110 HaloTag ligand lie along a dendritic branch stained with MAP2. White circles mark out synaptic puncta labelled by R110 HaloTag ligand.

3.3.4 Using single-ligand labelling to compare puncta intensities on DIV15 with DIV16.

Once I had established that the HaloTag ligands could be used to highly specifically label Halo-PSD-95 fusion proteins in the postsynaptic densities of excitatory primary neurons, I decided to apply this technique to explore the change in absolute PSD-95 expression as well as synapse number over the time-frame I intended to investigate PSD-95 turnover over (i.e. DIV15-DIV16). As explained in chapter 3.3.3, this is a good time period for the investigation of PSD-95 turnover in primary cultures.

To this end, I added the TMR ligand to hippocampal primary cultures at DIV15 or DIV16 for 30 minutes at a 1μM final concentration. After labelling was completed, cells were fixed, imaged and puncta detected and analysed with the standard protocol using the Imaris software (see chapter 2.4.2). This analysis was performed for five different cultures (N=5) and four images were used per culture (taken from a single coverslip).

In each of the five distinct cultures analysed, the average puncta intensity was slightly greater at DIV16 than at DIV15 (figure 3.13.a). However, this difference was only statistically significant at the $p<0.05$ confidence level in a single case, culture 21 E2 (using Welch's t-test). I then calculated the mean puncta fluorescence intensity for all groups at DIV15 and DIV16 to give a more complete picture (figure 3.13.c). While the mean puncta intensity was overall greater at DIV16 (89.84 ± 3.79) than DIV15 (80.86 ± 2.03), this difference was not statistically significant ($p=0.08$, Welch's t-test).

Using the same images, the number of puncta per image at these two time points was explored. When analysing each culture separately, the picture that emerged was similar to the evaluation of puncta intensity: for three out of five cultures, more synaptic puncta were detected on DIV16 than DIV15 (figure 3.13.b). The difference between these results was only significant at the $p<0.05$ confidence level in two cases: culture 21 E1 and culture 21 E2 (in both cases, there were more puncta at DIV16 than DIV15). When the mean puncta number for all groups was calculated, the result was the same as when evaluating puncta intensity: there was an overall greater number of synaptic

puncta per image at DIV16 (445.32 ± 86.64) than DIV15 (351.36 ± 67.17) (figure 3.13.d). This difference was, again, not statistically significant (p=0.42, Welch's t-test).

Interestingly, no significant increase in puncta intensity or number was detected from DIV15 to DIV16, a time period that falls precisely into the developmental stage when primary neurons undergo high levels of synaptogenesis (Lesuisse and Martin, 2002).

However, when analysing puncta numbers, there is a much greater range of puncta per image than when analysing puncta intensity. This is due to the variability of the images taken- while it was attempted to take images at similar locations (i.e. along dendrites and without including cell bodies), there is nevertheless a lot of heterogeneity in the way primary cultures grow and neurons connect with each other. This large variability may explain the lack of statistical significance of the difference in puncta number between DIV15 and DIV16.

Puncta intensity, on the other hand, is directly proportional to the number of PSD-95 molecules present in the postsynaptic density that makes up each punctum. The number of PSD-95 molecules in a synapse is thought to be approximately 300 (Chen et al., 2005; MacGillavry et el., 2013), restricting the possible variability of synaptic puncta intensity. Furthermore, the puncta detection parameters used when analysing images with the Imaris software have a lower intensity detection threshold to reduce the incidence of false positives. Thus, any synapses containing a very small number of PSD-95 molecules will likely fall under this threshold, and not be detected as puncta. This limits the variability in detected puncta intensity.

It appears from these results that while the overall synaptic population at this stage may be undergoing both synaptogenesis and synaptic pruning (Tang et al., 2014), the mean puncta intensity across this large population did not significantly change within the 24-hour time window. However, it might be expected that if this synaptic population at DIV15 were compared with a synaptic population at a later developmental stage, say DIV28, the ratios of mature to immature synapses and thus PSD-95 content would be significantly different. At DIV28 more synapses might have matured, with fewer immature synapses present that express lower PSD-95 levels and reduce the mean puncta intensity value.

a.

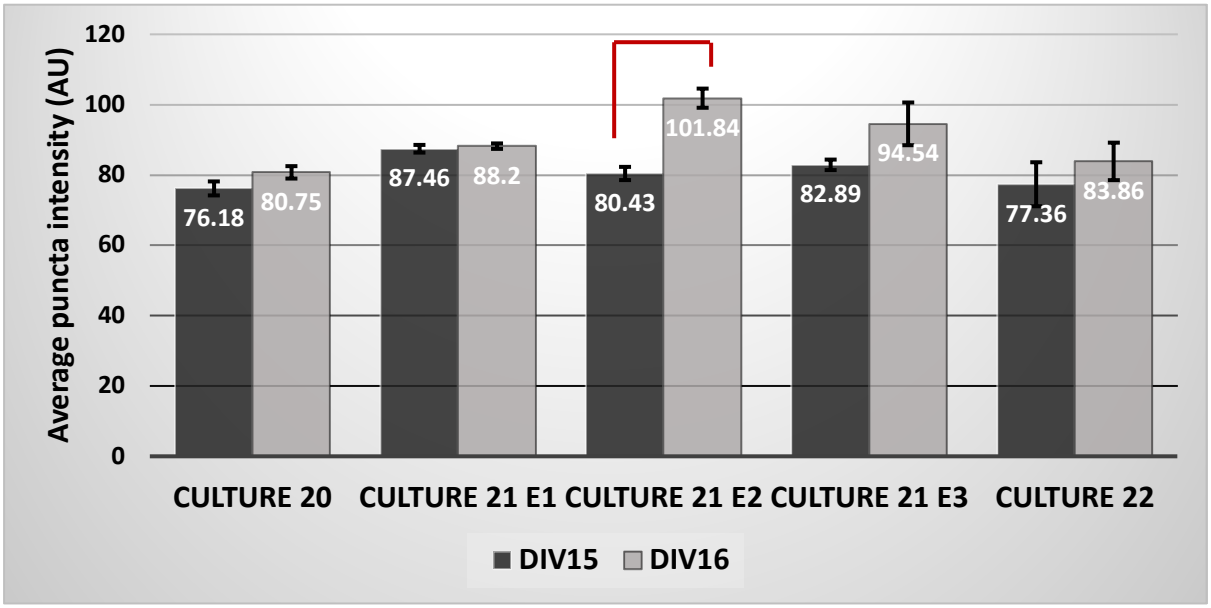
Average puncta intensity (AU)
120
100
80
60
40
20
0
76.18
80.75
87.46
88.2
80.43
101.84
82.89
94.54
77.36
83.86
CULTURE 20
CULTURE 21 E1
CULTURE 21 E2
CULTURE 21 E3
CULTURE 22
DIV15
DIV16

b.

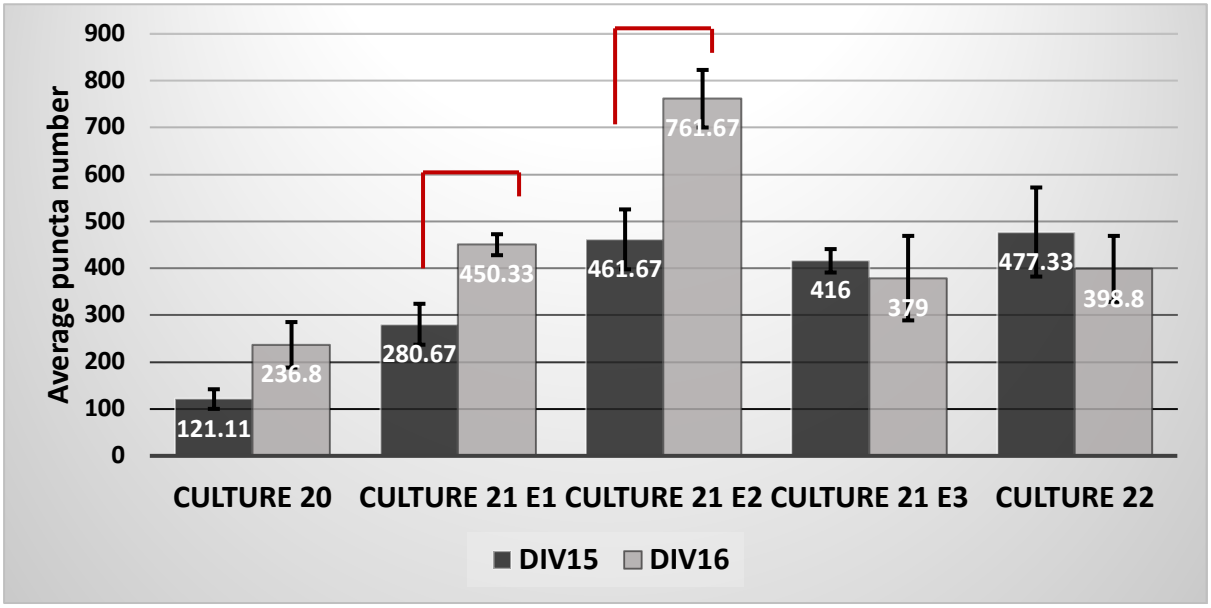
Average puncta number
900
800
700
600
500
400
300
200
100
0
121.11
236.8
280.67
450.33
461.67
761.67
416
379
477.33
398.8
CULTURE 20
CULTURE 21 E1
CULTURE 21 E2
CULTURE 21 E3
CULTURE 22
DIV15
DIV16

c.

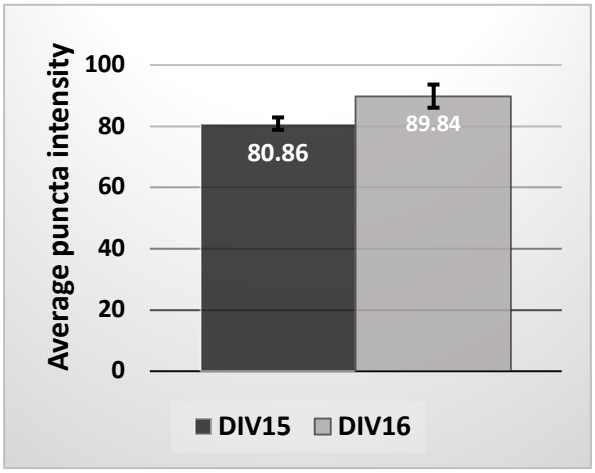
Average puncta intensity
100
80
60
40
20
0
80.86
89.84
DIV15
DIV16

d.

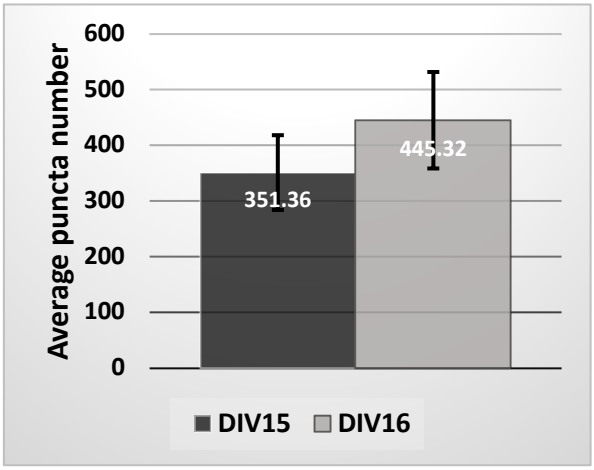
Average puncta number
600
500
400
300
200
100
0
351.36
445.32
DIV15
DIV16

Figure 3.13. There is no difference in average puncta fluorescence intensity and number between DIV15 and DIV16.

a. Graph depicting the average fluorescence intensities of PSD puncta labelled with the HaloTag TMR ligand in five different Het (PSD-95$^{HaloTag/+}$) cultures (N=5), on DIV15 and DIV16. **b.** Graph depicting the average number of PSD puncta labelled with the HaloTag TMR ligand in five different Het (PSD-95$^{HaloTag/+}$) cultures (N=5), on DIV15 and DIV16. **c.** The mean puncta intensity was calculated over the five cultures depicted in (a.). The graph thus depicts a 'mean of means' regarding TMR ligand puncta intensity at DIV15 and DIV16. **d.** As in (c.), the mean puncta number was calculated over the five cultures depicted in (b.). The resulting graph depicts a 'mean of means' regarding TMR ligand puncta number at DIV15 and DIV16.

3.3.6 Evaluating HaloTag ligand fluorophore stability

Having established that the HaloTag ligands can be used to reliably and specifically label the Halo-PSD-95 fusion protein in live primary cultures, and thereby accurately visualise glutamatergic synapses, I next wanted to investigate the stability of the R110 and TMR HaloTag ligands' fluorophores. This step is crucial to allow for the accurate quantification of PSD-95 turnover, as it is essential to take into consideration any loss of fluorescence intensity of fluorophores when monitoring the degradation of ligand-labelled Halo-PSD-95 proteins. I decided upon two separate tests to probe fluorophore stability. The first involved using a plate reader to record fluorescence intensities of HaloTag ligands diluted in NB media at representative concentrations with or without incubation in a cell culture incubator for 24 hours (see chapter 2.5.5 for the full protocol). The labelled live primary neurons as per the standard protocol and measured puncta intensity with or without incubation in a cell culture incubator for 24 hours following fixation (details below).

Both sets of experiments should allow for the evaluation of the effect of incubating HaloTag ligands with fluorophores attached in in a cell culture incubator for 24 hours, thereby replicating the conditions the live cells experience over the duration of a Pulse-Chase experiment.

The advantage of analysing fluorescence intensities of entire wells of HaloTag ligands in a 96-well plate is that, apart from being fairly quick to perform, there is much less variability involved than is the case when comparing the average intensities of synaptic puncta. Nevertheless, there is the caveat that if wells that have already been imaged

are reimaged, photobleaching will have to be taken into consideration. Analysing the difference in R110 ligand fluorescence intensity between wells that were not incubated (16.99 ± 1.7 at the '0-hour' time point) and wells that were incubated for 24 hours (18.76 ± 1.8 after 24-h incubation), I find there to be no difference in the average fluorescence intensity of the wells (Welch's t-test, p=0.32) (Figure 3.14.a). However, when comparing the exact same wells that were imaged at the 0-hour time point with their fluorescence intensity reading after 24 hours of incubation, I find that photobleaching has indeed occurred, and the intensity has gone down from 16.99 ± 1.7 to 14.38 ± 1.6 (Figure 3.14.b). Note that this difference is still statistically insignificant (Welch's t-test, p=0.10).

Finally, I placed all of the imaged wells in the incubator for a further 4 days, and reimaged them at the 120-hour time point. This time point consisted of well that had been imaged a variable amount of times, making it the least reliable comparison, but I decided to include it nevertheless, as it still provides some valuable information. The results indicate that while there is a slight loss in fluorescence intensity, most likely solely due to the photobleaching induced by multiple imaging sessions in the plate reader, the R110 HaloTag ligand fluorophore is remarkably stable and there is no significant change in its intensity, even over 120 hours in neurobasal media in a cell culture incubator (single-factor ANOVA, $F(2,122)=0.62$, $p=0.54$).
Note that the R110 ligand was selected for this experiment over the TMR ligand, as the R110 ligand is used as the Pulse ligand in later Pulse-Chase experiments. This means that this fluorophore is exclusively used to provide information about the degradation of PSD-95, whereas the TMR ligand labels newly-formed PSD-95 and therefore does not provide information about PSD-95 degradation. Nevertheless, future studies may wish to repeat this experiment with the TMR ligand.

Having established that the R110 ligand's fluorophore is unaffected by incubation while diluted in neurobasal media, it was necessary to investigate whether the same held true for ligands bound to Halo-PSD-95 fusion proteins within the PSD's of primary

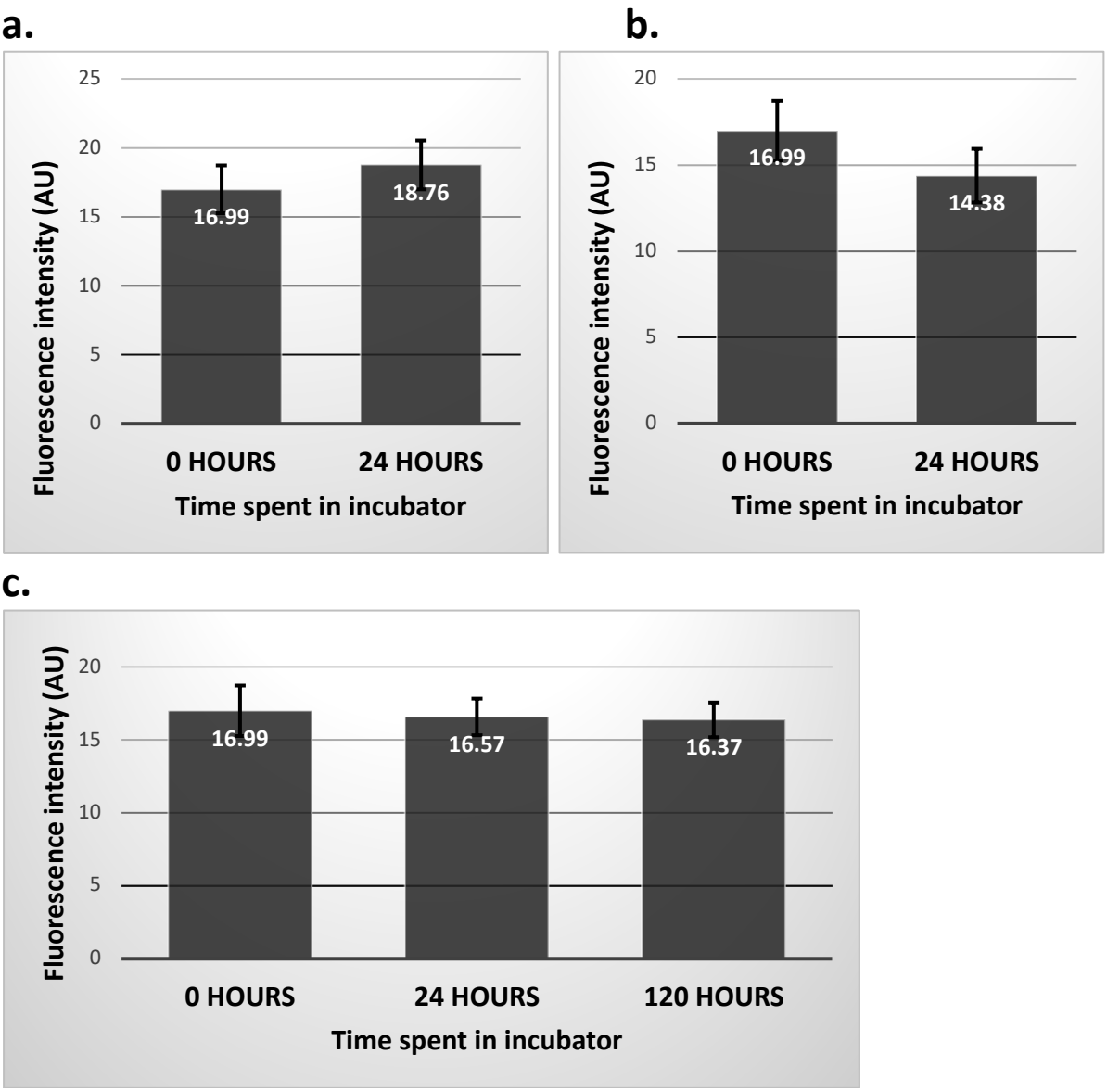

Figure 3.14. The HaloTag R110Direct ligand fluorophore does not decay in intensity while kept in a cell culture incubator.

a. For 5 separately prepared stock vials (N=5), R110Direct ligand was diluted to a concentration of 200nM in NB media. From each stock vial 5 different wells in a 96-well plate were filled (5 technical replicates), and fluorescence intensity measured using a plate reader in on day 1 (0 hours). Stock vials were then incubated for 24 hours in a cell culture incubator at 37°C and 5% CO_2, and thereafter 5 new samples were taken from each vial and fluorescence intensity measured on day 2 (24 hours). Fluorescence intensity was not statistically significantly different (Welch's t-test, p=0.32). **b.** For the experiment in (a.), the samples imaged at the 0-hour time point were incubated at 37°C and 5% CO_2 for 24 hours, and then the same samples reimaged. Fluorescence intensity has gone down due to photobleaching, but not significantly (Welch's t-test, p=0.1). **c.** For the same experiment, the samples were imaged after 0 hours, 24 hours and 120 hours of incubation at 37°C and 5% CO_2. Note that at the 24-hour time point, half of the samples had been previously imaged at the start of the experiment, and at the 120-hour time point all of the samples had been imaged at least once, and in some cases twice before. Nevertheless, a single-factor ANOVA did not reveal a significant difference between the samples ($F(2,122)=0.62$, $p=0.54$).

neurons. This set of experiments involves treating live cells with both pulse and chase HaloTag ligands as per the single-ligand labelling standard protocol (see chapter 2.5.3). The cells are fixed in 4% PFA immediately after labelling is complete (see chapter 2.3.5). Coverslips are then split into two groups: coverslips in one group are submerged in standard cell culture NB media, and returned to the cell culture incubators. There, they are incubated at 37°C and 5% CO_2 for 24 hours. Coverslips in the second group are stored for 24 hours, protected from light, at 4°C in 1x PBS. After the 24 hours, coverslips in both groups are washed and mounted on glass slides, before being imaged and puncta detected and quantified with the Imaris software. It is then possible to compare average puncta intensities and numbers as usual between the two groups. This process was performed for both R110 and TMR ligands.

Qualitatively, the images taken from the two treatment groups are indistinguishable for both ligands (Figures 3.15.a-b and Figures 3.16.a-b). Quantitative analysis revealed that there was no statistically significant difference between the two treatment groups in terms of average puncta intensity (R110 ligand: Welch's t-test p=0.67 (Figure 3.15.c); TMR ligand: Welch's t-test p=0.58 (Figure 3.16.c)) and average puncta number (R110 ligand: Welch's t-test p=0.68 (Figure 3.15.d); TMR ligand: Welch's t-test p=0.45 (Figure 3.16.d)), for both ligands. It was noted that the puncta number in these experiments displayed a very high degree of variance, ranging between 350-650 (R110Rirect, Figure 3.15) and 130-330 (TMR, Figure 3.16) puncta per image. A possible explanation for this is that the images, which were taken along the dendrites of neurons grown on glass coverslips, varied in the number of dendrites that were captured (in some cases including larger numbers of dendrites, in others only few). Within these images, the Imaris software was then used to detect the synaptic puncta as outlined in chapter 2.4.2. Briefly, the 'spots' detection module was used to identify areas that displayed a signal above a certain intensity threshold (manually set) and at an estimated diameter from the seedpoint (set to 300nm). The software then utilises the Mexican Hat algorithm to identify structures based on these parameters.

The results from this set of experiments clearly indicate that the fluorophores used in the R110 and TMR HaloTag ligands are highly stable in, and unaffected by, the incubation conditions they are exposed to during all of my experiments conducted on

neuronal primary cultures. This allows me to make the assumption that any loss of fluorescence intensity over time during an experiment is due to cellular processes such as the degradation of the Halo-PSD-95 proteins that have been tagged by these ligands. It allows me to rule out the possibility that reduced fluorescence intensity may be caused by fluorophore instability while being incubated in cell culture conditions, and as such provides a crucial baseline for subsequent Pulse-Chase experiments.

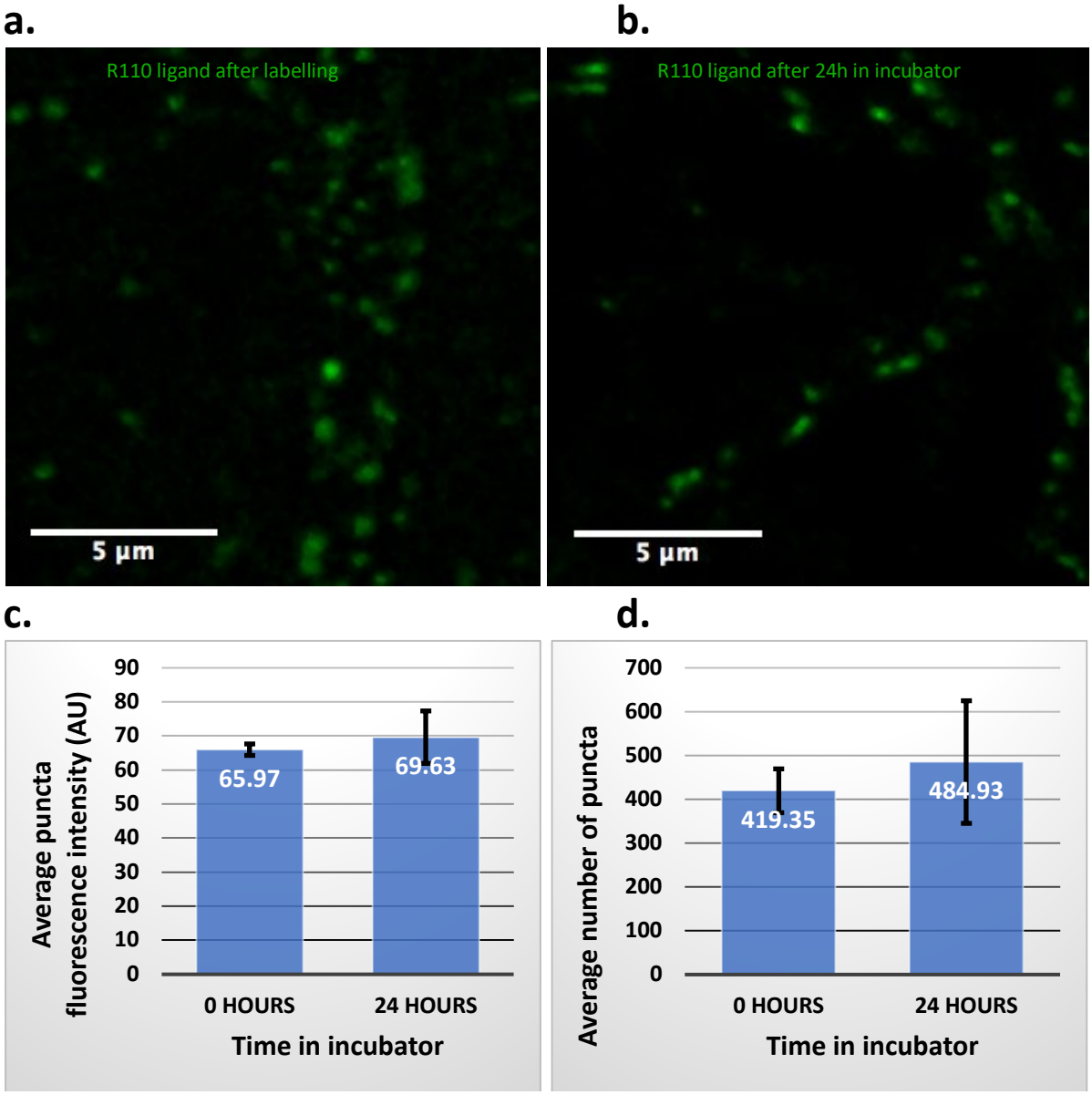

Figure 3.15. Synaptic puncta labelled by the R110Direct ligand do not lose their fluorescence intensity after being kept in a cell culture incubator.

a. Hippocampal primary neurons were labelled with R110 ligand at DIV14 (50nM, 16h), fixed on DIV15, and stored at 4°C in PBS for 24 hours before being mounted and imaged.

b. As in (a.), hippocampal primary neurons were labelled with R110 ligand at DIV14 (50nM, 16h), fixed on DIV15, but stored at 37°C and 5% CO_2 in Neurobasal medium for 24 hours before being mounted and imaged. **c.** Graph of average puncta fluorescence intensity for coverslips stored at 4°C in PBS for 24 hours (0 hours in incubator) or at 37°C and 5% CO_2 in

Neurobasal medium for 24 hours (24 hours in incubator). The difference is not significant (Welch's t-test, p=0.67). **d.** Graph as in (c.), but analysing puncta number instead. The difference is not significant (Welch's t-test, p=0.68). N=5 cultures.

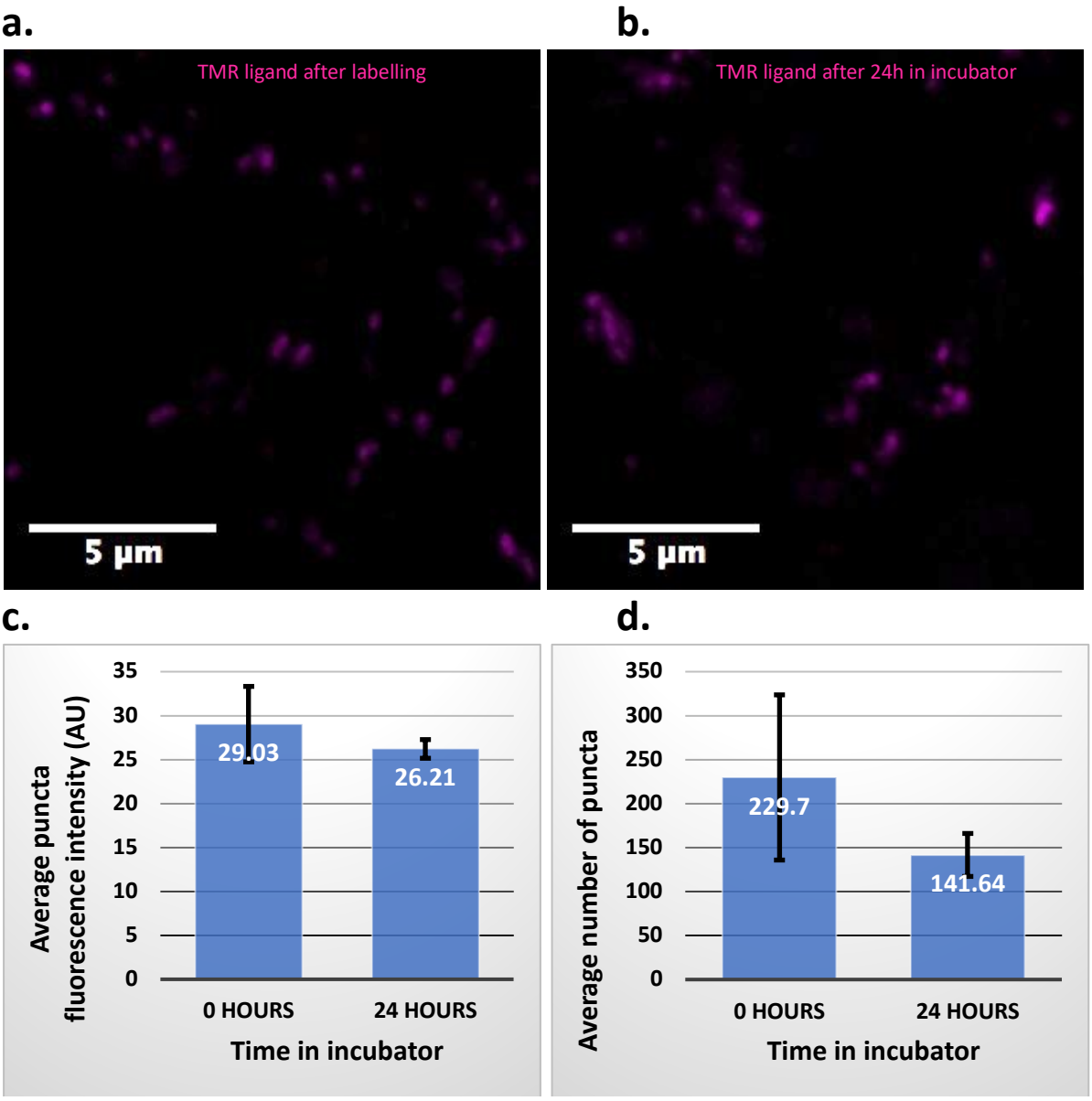

Figure 3.16. Synaptic puncta labelled by the TMR ligand do not lose their fluorescence intensity after being kept in a cell culture incubator.

a. Hippocampal primary neurons were labelled with TMR ligand at DIV15 (500nM, 1h), fixed, and stored at 4°C in PBS for 24 hours before being mounted and imaged.

b. As in (a.), hippocampal primary neurons were labelled with TMR ligand at DIV15 (500nM, 1h), fixed, but stored at 37°C and 5% CO_2 in Neurobasal medium for 24 hours before being mounted and imaged. **c.** Graph of average puncta fluorescence intensity for coverslips stored at 4°C in PBS for 24 hours (0 hours in incubator) or at 37°C and 5% CO_2 in Neurobasal medium for 24 hours (24 hours in incubator). The difference is not significant (Welch's t-test, p=0.58). **d.** Graph as in (c.), but analysing puncta number instead. The difference is not significant (Welch's t-test, p=0.45). N=3 cultures.

3.4 Developing a Pulse-Chase method for the accurate measurement of PSD-95 synthesis and degradation

3.4.1 Developing a Pulse-Chase method for the study of PSD-95 turnover

One of the main aims of this project was to develop a method of studying the turnover of PSD-95. The first steps were to perform the basic experiments of characterising our KI mouse model (chapter 3.2) and establishing the viability of the in vitro model of using neuronal primary cultures in conjunction with the HaloTag system (chapter 3.3). Once these hurdles had been cleared, the next step was to develop a methodology that would allow me to use the available tools to probe the turnover of PSD-95 and ask biologically pertinent questions. As outlined in the introduction (chapter 1), there is a wide variety of ways of probing a protein's turnover rate, and indeed multiple interpretations of what constitutes 'turnover'. As mentioned before, my project focuses upon protein turnover in the context of degradation and synthesis, rather than protein mobility. As such, turnover measurements such as FRAP were eschewed in favour of focussing on methods that permit the isolated analysis of protein degradation and synthesis. The HaloTag system allows for many different applications, as outlined in chapter 1, and it is this versatility that makes it such a unique technology. However, after performing the various experiments outlined thus far, utilising the fluorophore-bearing HaloTag ligands in a Pulse-Chase approach was deemed the most promising avenue.

In chapter 3.2, I established that labelling live primary neurons could be accomplished successfully while retaining the stability of the HaloTag ligand's fluorophores, as well as ensuring that these ligands were indeed labelling PSD-95-HaloTag fusion proteins at glutamatergic postsynaptic densities. The next step was working out ideal concentrations for these ligands to be used at, as well as deriving a working protocol to investigate PSD-95 turnover. Chapter 3.4 is therefore dedicated to working out the concentrations at which the R110 and TMR ligands are able to successfully saturate HaloTag binding sites and outcompete each other, as well as exploring whether there is a significant change in overall PSD-95 levels over the time course of

experimentation (DIV15-DIV16). Finally, I apply all of the results from the previous experiments to design a Pulse-Chase experiment allowing me to work out the rate of degradation of PSD-95 (half-life).

3.4.2 Titration of ligand concentrations to establish Pulse-Chase protocol

This experiment was designed to work out what concentration of the pulse ligand is required to saturate all the available HaloTag binding sites and thereby prevent labelling by a chase ligand added subsequently. This concept was also used in one of the original HaloTag papers by Los et al. (2008) to prove saturation of binding sites by a HaloTag ligand.
My experiment also aimed to act as a proof of concept and demonstrate a theoretical model in practice: that reducing the concentration of the pulse ligand from the point of saturation in a step-by-step titration series would increase labelling with the chase ligand (kept at a constant, high concentration) concomitantly.

The exact protocol used is outlined in chapter 2.5.4. Briefly, the TMR ligand (pulse) is added to live primary neurons at DIV14 at concentrations titrated down by a factor of 10, from 500nM to $5x10^{-12}$nM, for 30 minutes. Cells are then fixed in 4% PFA and thereafter labelled with a second ligand, the diAcFAM ligand, at a constant concentration of 1µM for 1 hour. Cells are then imaged, synaptic puncta detected as usual (see methods chapter 2.4), and average puncta fluorescence intensity recorded.

There are some key aspects that differ in this experiment from later pulse-chase experiments: Firstly, later experiments use the R110Direct HaloTag ligand as the pulse and the TMR ligand as the chase. In this experiment, I used the TMR ligand as the pulse ligand, and then a different ligand, the diAcFAM ligand, as the chase. The reason for this disparity is that this experiment was performed early on during the study, when the final ligand combination had not yet been decided upon, and thus it was not clear which ligands were ideally suitable for certain roles.
Furthermore, the chase ligand was applied post-fixation, i.e. once the cells had been fixed, whereas pulse-chase experiments have both ligands added to live cells. This difference is due to the experiments fundamentally having the opposite objectives. In

the later pulse-chase experiments aimed at studying PSD-95 turnover, it is crucial for the cells to continue their production and degradation of proteins after pulse ligand labelling. In this experiment, however, it is essential that there is no further protein turnover after labelling with the pulse ligand is complete, since the objective is to evaluate the ability of the pulse ligand to saturate all available binding sites. Had protein turnover been allowed to continue, new, unlabelled proteins would have been synthesised for the chase ligand to bind, confounding the results. Fixation of the cells after pulse labelling is therefore required. The efficacy of post-fixation labelling of cells with ligands had previously been tested, and found to be indistinguishable from live cell labelling (see chapter 3.3.3).

The graphs in figure 3.17 reveal a number of things. The graph in figure 3.17.a, depicting average TMR ligand intensity of synaptic puncta over the range of titrated TMR concentrations, shows that TMR intensity starts off at a maximum intensity plateau between 75-80 arbitrary units (AU) of fluorescence intensity, at TMR concentrations of 500nM and 50nM. At a TMR concentration of 5nM, the fluorescence intensity begins to drop, and continues to do so until the TMR concentration is reduced to $5x10^{-8}$ nM. At this point, average fluorescence intensity appears to level off between 15-30 AU, and does not dip below this range of signal strength. Finally, in the blank group, when no TMR ligand at all is added, no TMR puncta are detectable. Thus there is a direct (positive) correlation between TMR ligand concentration and TMR puncta intensity.

The graph in figure 3.17.b shows the chase ligand (diAcFAM) average puncta fluorescence intensity over the range of titrated TMR concentrations. When TMR ligand concentration is at 500nM and 50nM, no diAcFAM signal could be detected. At a TMR concentration of 5nM, diAcFAM puncta start being detectable, at a low intensity around 30 AU. From this point onwards, average diAcFAM puncta intensity gradually increases, and appears to level off around 70-80 AU, when TMR concentration has been titrated to between $5x10^{-10}$ nM and $5x10^{-12}$ nM. When no TMR ligand is added at all (blank), diAcFAM signal is at its highest, at about 95 AU. It is noteworthy that the gradient of the curve (isignifiying the rise in average puncta fluorescence intensity) appears to be greatest between a TMR concentration of 50nM and $5x10^{-4}$ nM. At a TMR concentration of $5x10^{-4}$ nM, diAcFAM puncta intensity levels off around 60 AU,

and further increases in intensity are modest. Again, there appears to be a direct (negative) correlation between TMR ligand concentration and diAcFAM puncta intensity.

From the graphs in figures 3.17.a and 3.17.b, it is evident that there is a direct correlation between pulse ligand concentration, and the degree to which pulse and chase ligands are able to bind the Halo-PSD-95 fusion protein binding sites. At high TMR (pulse) concentrations all the binding sites are saturated by it, and as the TMR concentration goes down, more and more binding sites remain unbound and thus available for the chase (diAcFAM) ligand to bind. This becomes particularly clear when looking at the graph in figure 3.17.c. Here, the overlay of the two previous graphs nicely demonstrates the inverse relationship between the two ligands. Indeed, the small periods over which both ligands experience some of the greatest amount of change overlap strongly (TMR ligand: 5nM to $5x10^{-3}$ nM, -31.8%; diAcFAM ligand: 50nM to $5x10^{-4}$ nM, +66.4%).

Based on these results, we can therefore conclude that it is possible for the pulse ligand (in this case the TMR ligand) to saturate all of the binding sites on the Halo-PSD-95 fusion proteins, thereby preventing binding by the chase ligand. In this experiment, the saturating concentration of pulse ligand was found to be 50nM, incubated with the live cells for 30 minutes. At this pulse ligand concentration, no chase ligand (diAcFAM) labelling could be detected. We can also conclude that indeed, titrating down the pulse ligand concentration reduces the proportion of Halo-PSD-95 proteins that are labelled by the pulse ligand, and increases the proportion labelled by the chase ligand. This early experiment was thus an important step in designing a pulse-chase protocol for the study of PSD-95 turnover.

a.

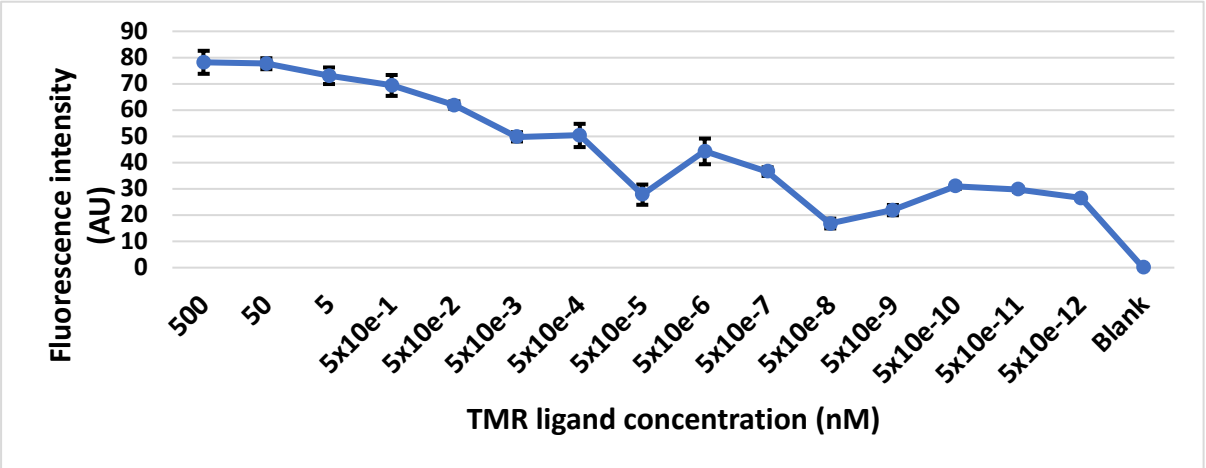
Fluorescence intensity (AU)
90
80
70
60
50
40
30
20
10
0
500
50
5
5x10e-1
5x10e-2
5x10e-3
5x10e-4
5x10e-5
5x10e-6
5x10e-7
5x10e-8
5x10e-9
5x10e-10
5x10e-11
5x10e-12
Blank
TMR ligand concentration (nM)

b.

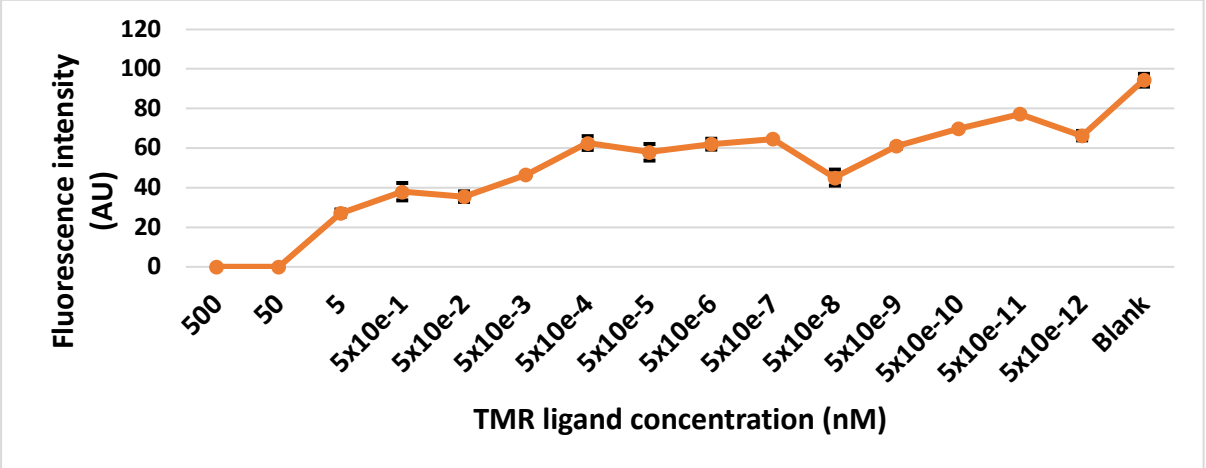
Fluorescence intensity (AU)
120
100
80
60
40
20
0
500
50
5
5x10e-1
5x10e-2
5x10e-3
5x10e-4
5x10e-5
5x10e-6
5x10e-7
5x10e-8
5x10e-9
5x10e-10
5x10e-11
5x10e-12
Blank
TMR ligand concentration (nM)

c.

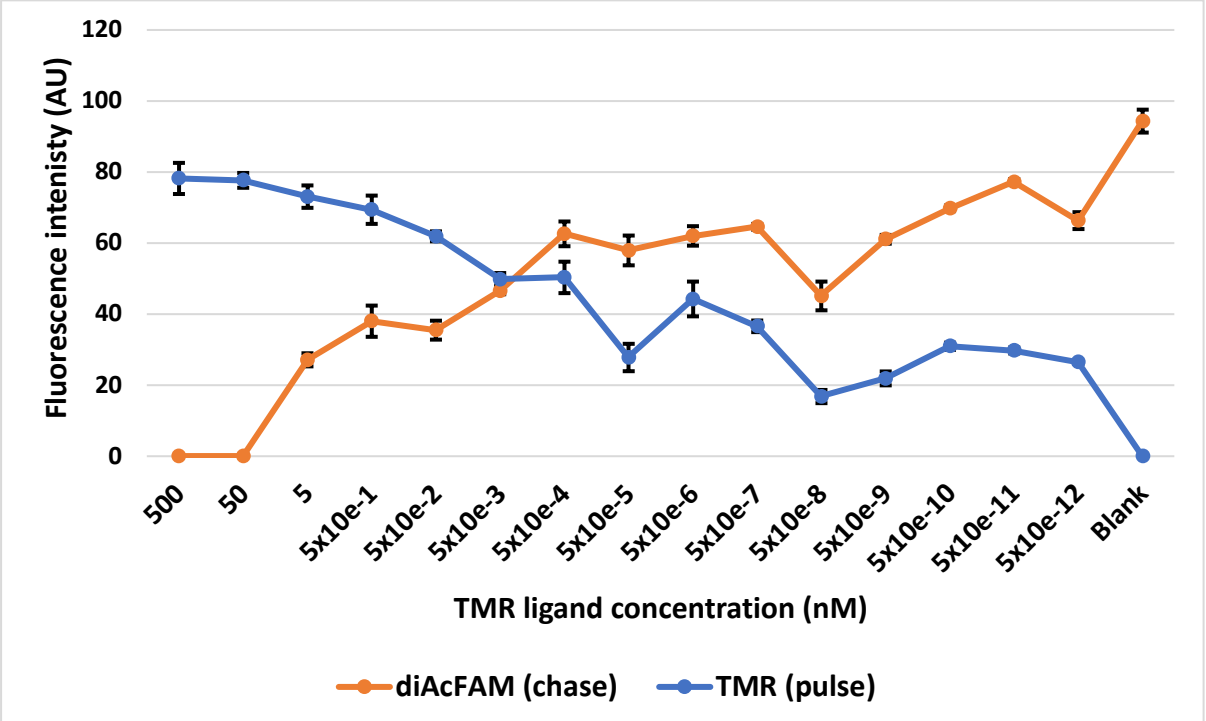
Fluorescence intensity (AU)
120
100
80
60
40
20
0
500
50
5
5x10e-1
5x10e-2
5x10e-3
5x10e-4
5x10e-5
5x10e-6
5x10e-7
5x10e-8
5x10e-9
5x10e-10
5x10e-11
5x10e-12
Blank
TMR ligand concentration (nM)
diAcFAM (chase)
TMR (pulse)

Figure 3.17. Titrating a pulsed HaloTag ligand (TMR) followed by a chase HaloTag ligand (diAcFAM) demonstrates the ability of ligands to saturate and compete for binding sites.

Neuronal primary cultures at DIV14 were treated for 30 minutes with a pulse ligand (TMR) at a titrated concentration, ranging from 500nM to $5x10^{-12}$nM. Cells were then fixed and treated with the diAcFAM ligand at a concentration of 1µM for 1 hour. They were then imaged using the LSM510 and puncta detected for each ligand channel separately using the Imaris software. **a.** Graph plotting the average intensity of TMR (pulse) ligand puncta at titrated TMR ligand concentrations. As TMR concentration goes down, so too does TMR ligand puncta intensity. **b.** Graph plotting the average intensity of diAcFAM (chase) ligand puncta at titrated TMR ligand concentrations. As TMR concentration goes down, diAcFAM puncta intensity goes up. **c.** Combination of the graphs in (a.) and (b.). This clearly illustrates that there is an inverse relationship between pulse and chase ligand puncta intensity. At high TMR (pulse) concentrations, HaloTag binding sites are saturated, preventing diAcFAM (chase) ligand binding. As TMR concentrations are titrated below the saturation point, an increasing amount of HaloTag binding sites remain unbound and available for the diAcFAM ligand.

3.4.3 'Competition experiment'- applying Pulse and Chase ligand simultaneously

Having established that it was possible to saturate HaloTag binding sites on Halo-PSD-95 fusion proteins in live primary neurons with a first ligand (pulse), and thereby block any binding by a second ligand (chase) if added immediately afterwards, the next step was to develop an actual protocol that would allow for the measurement of PSD-95 turnover.

The objective, then, was to determine what combination of ligands and ligand concentrations would allow not only for all existing HaloTag binding sites to be occupied by the pulse ligand, but also for newly synthesised Halo-PSD-95 proteins to exclusively be bound by the chase ligand. In this manner, previously-present ('old') and newly synthesised ('new') Halo-PSD-95 proteins would be labelled with different ligands. This differential labelling is the key to separating these two subpopulations of the same protein, and thus being able to monitor each of them independently. In addition to such exclusive labelling of old and new protein populations by pulse and chase ligands respectively, the protocol would have to ensure that neuronal health remained intact and protein turnover continued throughout the experiment.

Initial experiments roughly followed Promega's 'Focus on imaging' manual. Primary neurons were incubated with 500nM TMR ligand as the pulse for 30 minutes (as this

concentration had been shown to saturate HaloTag binding sites, see chapter 3.4.3). Following Promega's manual, the culture media that the neurons were submerged in was then entirely removed, and the cells washed using warm complete medium in order to remove the pulse ligand. However, it was noted, as Cohen et al (2013) did as well, that: 'aggressive washes and complete media exchanges are severely detrimental to neuronal viability.' Indeed, very few of the neurons survived this treatment. This meant that incomplete media changes were the only viable option going forward, if the cells were to remain healthy and continue to turnover proteins. Incomplete media exchanges brought a different problem with them, however: the TMR ligand proved to be extremely effective at labelling Halo-PSD-95 proteins, so much so that even an extremely low concentration was enough to visibly label synaptic puncta. As can be seen in figure 3.17, even the lowest concentration of TMR ligand ($5x10^{-12}$ nM or 5 zeptomolar) still yielded detectable puncta labelling.

This labelling is also extremely rapid. At one point, it was attempted to titrate down the incubation time required for successful labelling of Halo-PSD-95 using the TMR ligand. The first time point used was 1 second- the ligand-containing media was added to the cells, and media immediately removed, followed by the rinsing of the cells in PBS and fixing them. Even at this time point, synaptic puncta were clearly labelled, prompting that experiment to be abandoned. Having gained experience with the diAcFAM ligand (see chapter 3.4.2), it was known that this ligand required a much higher concentration to be effective, and its labelling ability was in fact inconsistent. It was thus surmised that the TMR ligand had to be used as the chase ligand, as it was likely that it would be able to outcompete other ligands for the HaloTag binding pocket.

This raised an interesting point of discussion: different ligands displayed seemingly different levels of affinity for the HaloTag binding site. However, since the binding domain of HaloTag ligands is identical, there are two alternative explanations for these differences in binding kinetics, both linked to the variable functional group: firstly, that the different functional groups interact varyingly with other molecules, particularly the area around the binding pocket; and secondly, that these different functional groups allow the ligand molecules to penetrate through cells, membranes, and protein-dense areas such as the PSD at varying rates. These differences in properties may explain why some ligands are able to bind to PSD-95-HaloTag fusion proteins more rapidly

than others. Further on from this point, it was noted that there are differences in relative brightness between the different fluorophores attached to the HaloTag ligands. This meant that acquisition settings when taking images using the LSM510 microscope differed substantially between ligands, including laser power and gain settings. Even with optimised settings, it was noted that some ligands yielded a stronger signal than others. Imaris analysis settings were optimised separately for each fluorophore and no direct comparisons were made in terms of absolute fluorescence intensity between different ligands, meaning that this should not directly affect the results in this study. Nevertheless, these are points worth bearing in mind, particularly when designing future projects that may aim to quantify absolute PSD-95 molecule numbers or compare the intensities of different fluorophores with each other.

A variety of different ligands were tested for the pulse role, and ultimately the R110Direct ligand (R110) was selected. This ligand is sold as a 'direct' ligand by Promega, meaning that it needs to be applied to live cells over a much longer time period (overnight) at a lower concentration. The upside of this is that it is unnecessary to wash out the ligand, presumably because the lower concentration reduces the background. This R110Direct ligand proved to be highly effective at labelling Halo-PSD-95 proteins, and capable of saturating all HaloTag binding sites when cells were incubated overnight. However, it is also slower to bind to HaloTag proteins than the TMR ligand, meaning that even if it is not entirely removed from the media, the TMR ligand should still be able to bind to the vast majority of HaloTag binding sites if added in excess. This did, however, mean that it was required to add the chase ligand (TMR) immediately after the pulse labelling was complete rather than at the end of the experiment, thereby labelling newly synthesised Halo-PSD-95 proteins as soon as they were being produced.

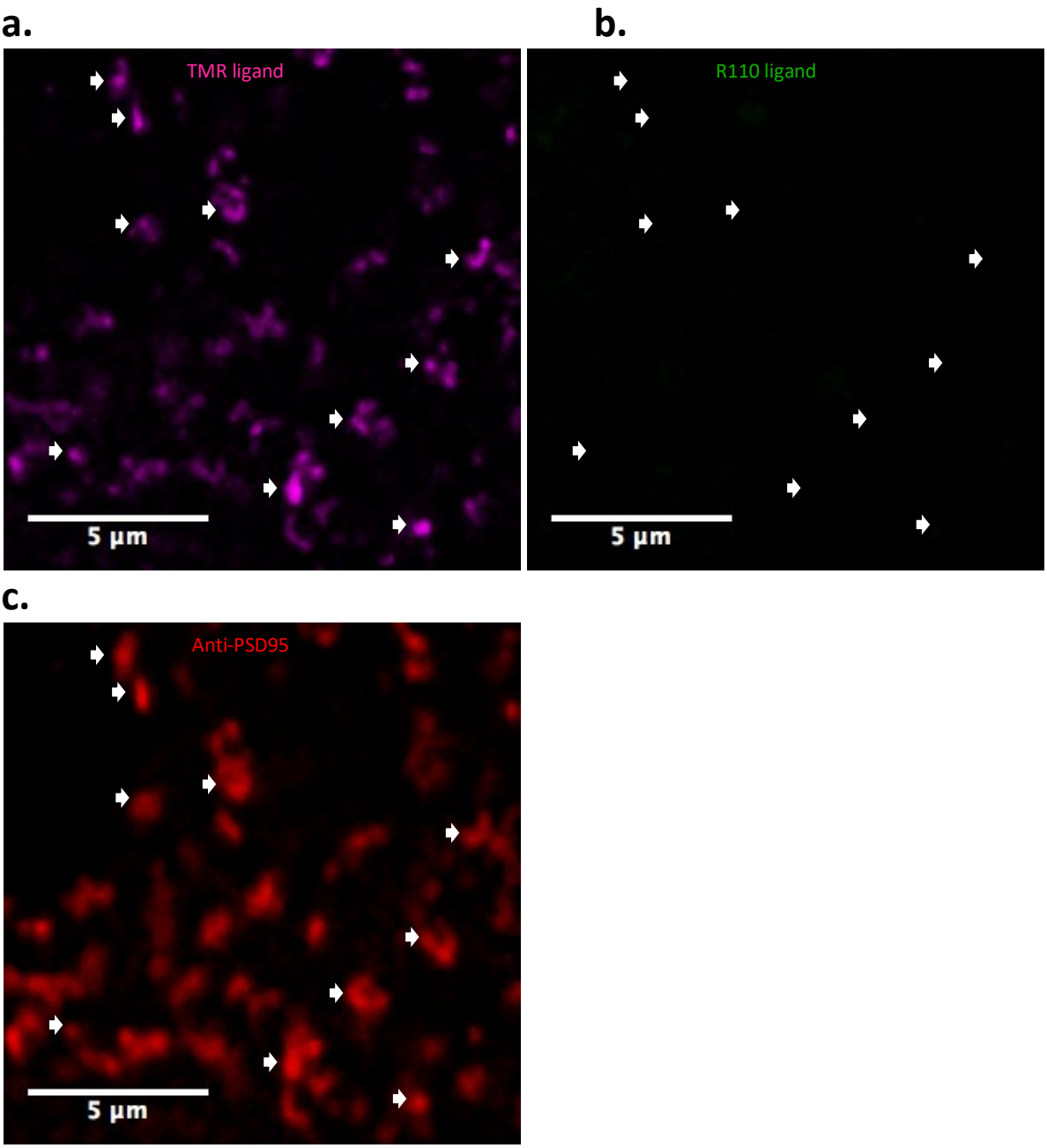

Figure 3.18. The TMR ligand outcompetes the R110Direct ligand when simultaneously applied at experimentally representative concentrations.

a. Heterozygous PSD-95$^{HaloTag/+}$ hippocampal primary cultures at DIV15 had the R110Direct ligand (12.5nM) and the TMR ligand (500nM) added to them. After 24 hours of incubation, the cells were fixed, stained with anti-PSD-95, mounted and imaged using the LSM510. Qualitative analysis reveals very strong TMR labelling (white arrows). **b.** In the R110 ligand channel (green channel), so ligand-staining is visible at all. **c.** Strong anti-PSD-95 antibody staining is visible in the far-red channel. Antibody puncta overlap with TMR ligand puncta (see white arrows). White arrows denote some strong TMR ligand puncta for reference purposes. The results clearly demonstrate that at the experimentally representative conditions, the TMR ligand is able to outcompete the R110Direct ligand, binding to the vast majority of HaloTag binding sites.

Combining the experience gained with various ligands and primary neurons, a final protocol was derived that allowed for the successful labelling of Halo-PSD-95 fusion proteins at different time points with different ligands, thereby permitting the study of PSD-95 turnover. The full detailed protocol is given in chapter 2.5.6. In brief:

1. R110Direct ligand is added to the primary neurons for a final ligand concentration of 50nM.
2. The neurons are incubated with the R110 ligand overnight (16 hours), saturating all of the binding sites on Halo-PSD-95 proteins.
3. After pulse incubation is complete, 75% of the media is removed from the cultures, and replaced with preconditioned media containing the TMR ligand, for a final TMR concentration of 500nM (final R110 concentration: 12.5nM).
4. The cultures are then incubated for as long as the time period over which turnover is to be measured- 1 hour, 24 hours, or 48 hours.
5. After this time period, cultures are washed in PBS, fixed in 4% PFA, stained with an antibody if appropriate, mounted, imaged and analysed.

This protocol has an internal control in that the 1-hour incubation time point ensures that R110 (pulse) ligand labelling has indeed saturated all of the binding sites, as the 1-hour time window was deemed insignificant in terms of PSD-95 turnover. This permitted confirmation that there is no TMR (chase) signal present after 1 hour of incubation. The remaining uncertainty in this protocol was, then, whether or not the TMR ligand was indeed capable of fully outcompeting the remaining R110 ligand.

To test this, both R110 (12.5nM) and TMR (500nm) ligands were simultaneously added to primary neurons at these representative concentrations and incubated for 24 hours. These are the final concentrations that neurons are exposed to once the chase ligand has been added in a pulse-chase experiment. Figure 3.18 reveals that no R110 signal could be detected at all, while robust TMR labelling is present. This experiment was performed on 6 different coverslips, with identical results- strong TMR labelling with no detectable R110 signal. The Imaris software was used with the usual puncta detection parameters for the R110 ligand (seed point estimation diameter of 300 nm, Background subtraction quality above 6.00, automatic spot region threshold, diameter from border). None of the images contained any detectable puncta (Figure 3.18.b).

3.4.4 Performing a basic Pulse-Chase experiment

Once a working pulse-chase protocol had been established, I wanted to utilise it to perform a full set of 48-hour experiments, and work out the half-life of PSD-95. Using the final pulse-chase protocol detailed in chapter 2.5.6, I incubated the cells with the chase ligand for 1 hour, 24 hours and 48 hours after pulse labelling was complete. This experiment was performed on hippocampal primary neurons taken from PSD-95-Halo$^{-/-}$ (homozygous) mouse embryos at E17.5, starting at neuronal age DIV14 (time of pulse ligand addition). It was performed on a single culture, i.e. all the neurons were derived from the same embryonic litter. Each time point (1h, 24h, 48h) was made up of 3 coverslips, and three images from each coverslip were used (for a total of 9 images per time point). Mean puncta intensity and number was derived for each image separately, and then these means per image were averaged together to give the final mean puncta intensity and number per group (i.e. time point).

Figure 3.19 depicts the qualitative results of these experiments. Figures 3.19.a-d represent the 1-hour incubation time point. From these four images, it is clear that the R110 ligand has labelled all HaloTag binding sites on the fusion proteins, and the TMR ligand has been unable to bind to any Halo-PSD-95 proteins. The 24-hour incubation time point is shown in figures 3.19.e-h, revealing that, qualitatively, R110 ligand intensity has gone down, while synaptic puncta labelled with the TMR ligand have now clearly appeared. The overlay (Figure 3.19.h) reveals that most of the puncta labelled with either ligand overlap with those labelled by the other ligand, indicating that these are synapses in which PSD-95 is actively being turned over. It is also interesting to note that there appears to be a lot of heterogeneity in terms of the ratio of R110 to TMR signal intensity in these synaptic puncta. Some of the puncta appear to contain a lot more ‘old’ than ‘new’ PSD-95, whereas others are dominated by ‘new’ proteins. This observation was of great interest and will be further examined in chapter 4.

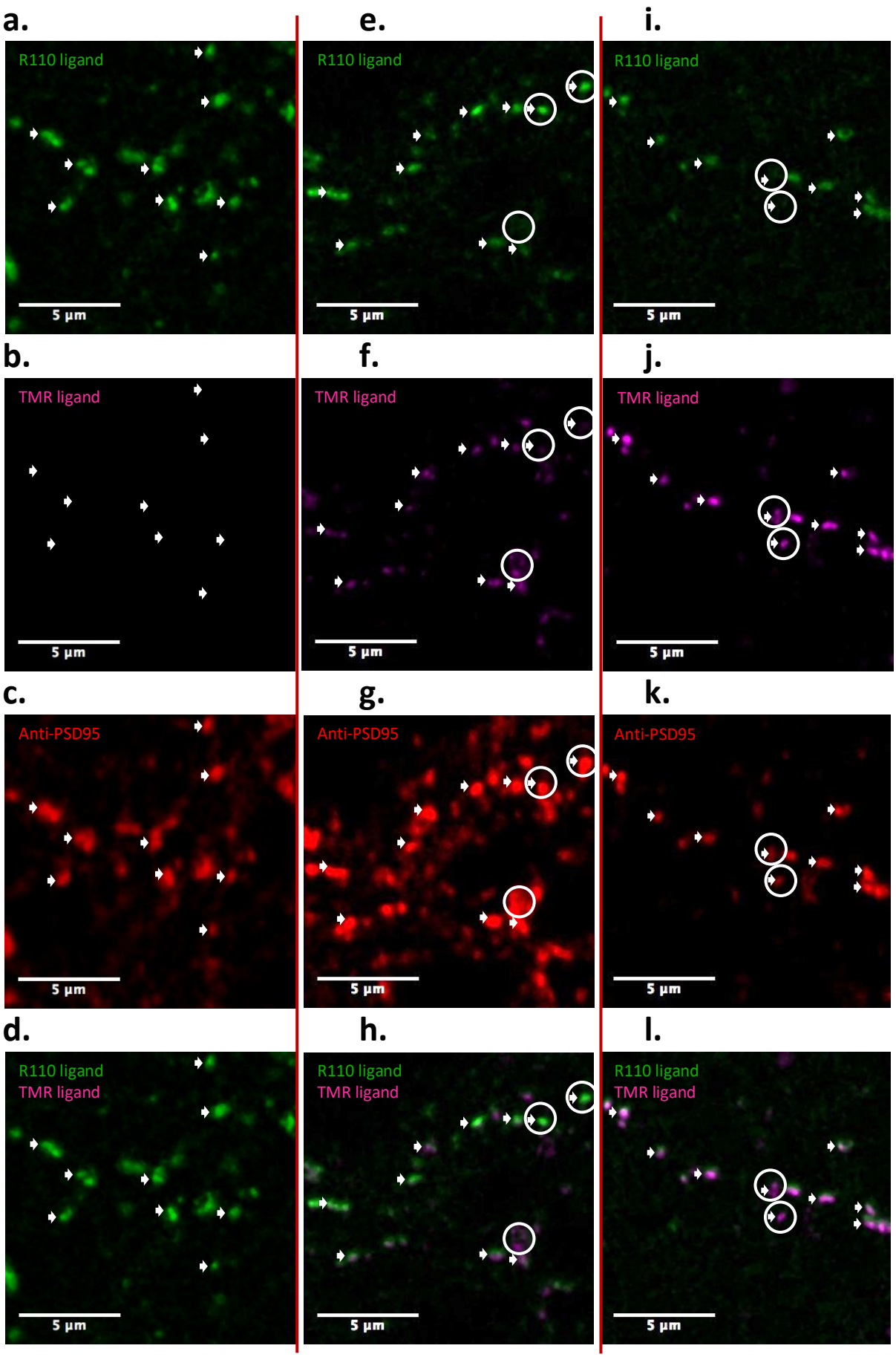
a.
R110 ligand
5 µm
e.
R110 ligand
5 µm
i.
R110 ligand
5 µm
b.
TMR ligand
5 µm
f.
TMR ligand
5 µm
j.
TMR ligand
5 µm
c.
Anti-PSD95
5 µm
g.
Anti-PSD95
5 µm
k.
Anti-PSD95
5 µm
d.
R110 ligand
TMR ligand
5 µm
h.
R110 ligand
TMR ligand
5 µm
l.
R110 ligand
TMR ligand
5 µm

Figure 3.19. A 48-hour Pulse-Chase experiment.
Hippocampal primary cultures derived from homozygous PSD-95$^{HaloTag/Halotag}$ mice were cultured to DIV14, when they were labelled with the R110Direct HaloTag ligand (50nM, 16h). On DIV15, the TMR ligand was added to the cultures at 500nM and the concentration of the R110 ligand reduced to 12.5nM. Cells were fixed after either 1 hour, 24 hours, or 48 hours of incubation thereafter. Coverslips were then stained for PSD-95 (Mouse, Neuromab 1:1000), imaged on the LSM510, and puncta detected using the Imaris software.
a.-d. Images taken from the 1-hour incubation time point. **a.** R110 pulse ligand signal. **b.** TMR chase ligand signal. **c.** Anti-PSD-95 staining signal. **d.** Overlay of pulse and chase ligand signals in (a.) and (b.). Note that a strong pulse but no chase signal are visible.
e.-h. Images taken from the 24-hour incubation time point. **e.** R110 pulse ligand signal. **f.** TMR chase ligand signal. **g.** Anti-PSD-95 staining signal. **h.** Overlay of pulse and chase ligand signals in (e.) and (f.). Note that both pulse and chase signals are clearly visible.
i.-l. Images taken from the 24-hour incubation time point. **i.** R110 pulse ligand signal. **j.** TMR chase ligand signal. **k.** Anti-PSD-95 staining signal. **l.** Overlay of pulse and chase ligand signals in (i.) and (j.). Note that both pulse and chase signals are clearly visible, but the pulse signal has weakened and the chase signal become stronger.

Finally, figures 3.19.i-l represent the 48-hour time point. Here it has become evident that those Halo-PSD-95 proteins labelled by the pulse ligand are slowly being degraded, with their signal intensity markedly reduced. On the other hand, many more PSD-95 proteins have been synthesised over this time period, leading to an enhanced TMR signal. Indeed, there appear to be some synaptic puncta entirely devoid of old proteins, containing only new PSD-95 (rings, figure 3.19.l). In fact, such chase-only synapses can also be observed at the 24-hour time point (rings, figure 3.19.h). It is possible that such synapses have only appeared in this 24- or 48-hour time window through the process of synaptogenesis, and thus don't contain any older PSD-95. An alternative explanation would be that such synapses have a higher turnover rate of PSD-95 and may simply have degraded all of their older PSD-95 proteins.

Note that for both the 24-hour and 48-hour time points, the white rings highlight synaptic puncta that are exclusively labelled by one or the other ligand. The white arrows point to synapses tagged by both ligands. Note further that all synapses tagged by either ligand display a strong overlap with the anti-PSD-95 antibody label.

The quantitative analysis of these results reflects what is visualised in figure 3.19. Pulse ligand fluorescence intensity is highest at the first time point (1h, figure 3.20.a), right after pulse labelling is complete (67.11 ± 2.76 Arbitrary Units). At this time point, no chase label is detectable at all (figure 3.20.b), since all of the binding sites are

saturated with pulse ligand. As mentioned before, this result acts as an internal control by demonstrating that the pulse ligand does in fact saturate all of the HaloTag binding sites. After 24 hours of chase ligand incubation, some of the pulse labelled proteins have been degraded, leading to a loss of pulse fluorescence intensity, with average puncta intensity significantly reduced to 43.53 ± 1.9 AU (Welch's t-test: $p=9.99x10^{-7}$). Conversely, chase ligand intensity has massively increased over these 24 hours as new Halo-PSD-95 proteins are being synthesised, giving an average puncta intensity of 30.50 ± 1.59 AU (figure 3.20.b). This trend continues after 48 hours, with pulse ligand intensity falling significantly to 29.71 ± 1.99 AU (Welch's t-test, $p=2.4x10^{-4}$), and chase ligand intensity rising to 35.23 ± 2.63 AU (not statistically significant at $p<0.05$). This increase is a lot smaller than in the first 24 hours; however, one explanation for this is that a significant portion of the proteins synthesised within the first 24-hour incubation phase were degraded again during the subsequent 24 hours.

Note that the absolute puncta fluorescence intensities cannot be directly compared between pulse (R110) and chase (TMR) ligands, as each is a different fluorophore with different properties. We can, however, directly compare the intensities within each ligand, as each HaloTag protein is only labelled by a single ligand molecule in a highly quantitative manner.

The second aspect of the pulse-chase experiment that I wanted to evaluate is the change in synaptic puncta number. While not a direct measurement of PSD-95 synthesis or degradation the way puncta intensity is, looking at puncta number can nevertheless provide valuable insights into PSD-95 turnover. An estimation of the number of pulse-labelled puncta that disappear over 24 hours can give an indication of the proportion of puncta that turn over all of their copies of PSD-95 in that time period (although synaptic pruning is an alternate explanation). I found that on average, each image contained 598.67 ± 69.1 synaptic puncta when labelled with the pulse ligand at the start of the experiment, and this number goes down to 329.55 ± 49.3 puncta after 24 hours. After 48 hours, only an average of 69.67 ± 11 puncta per image

a.

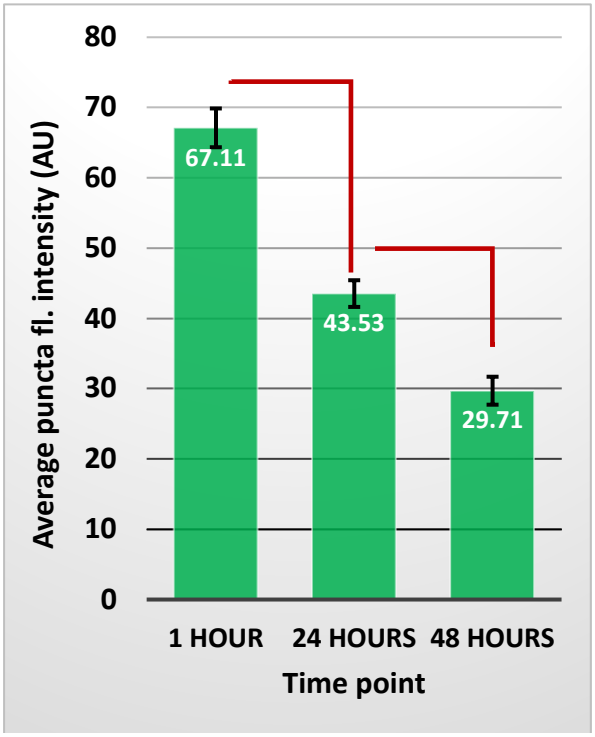
Average puncta fl. intensity (AU)
80
70
60
50
40
30
20
10
0
67.11
43.53
29.71
1 HOUR
24 HOURS
48 HOURS
Time point

b.

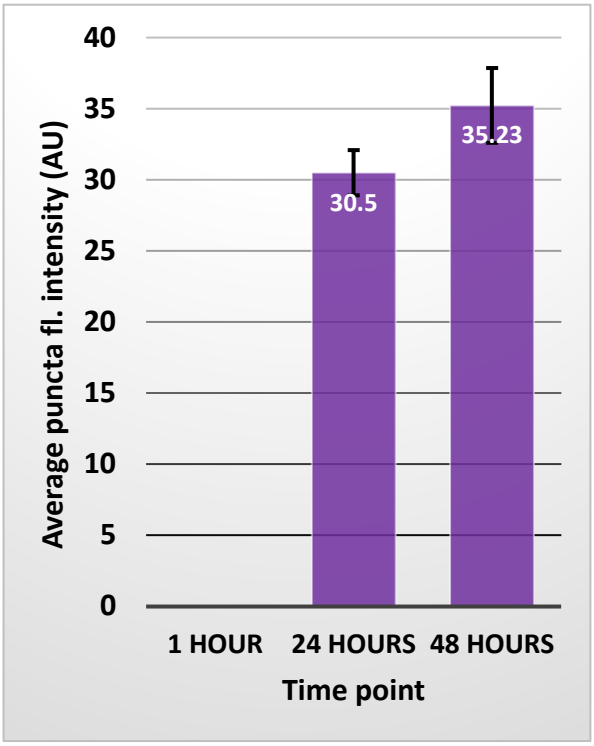
Average puncta fl. intensity (AU)
40
35
30
25
20
15
10
5
0
30.5
35.23
1 HOUR
24 HOURS
48 HOURS
Time point

c.

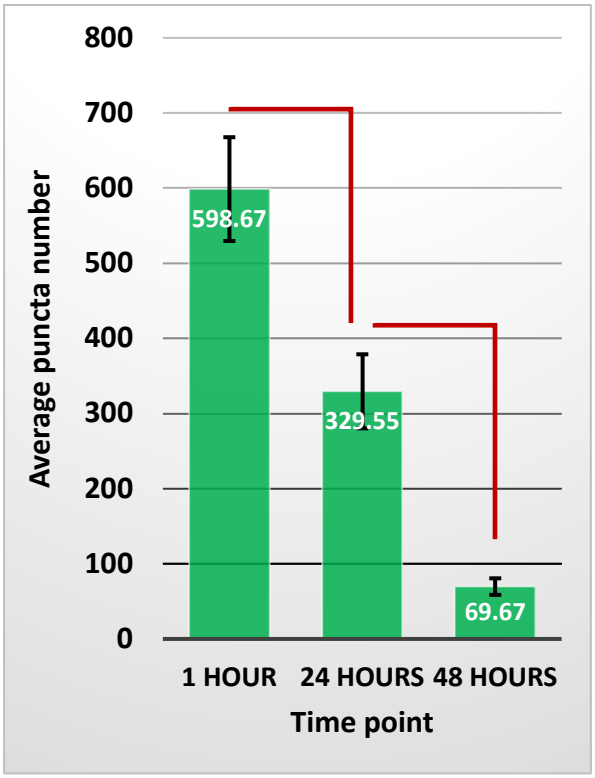
Average puncta number
800
700
600
500
400
300
200
100
0
598.67
329.55
69.67
1 HOUR
24 HOURS
48 HOURS
Time point

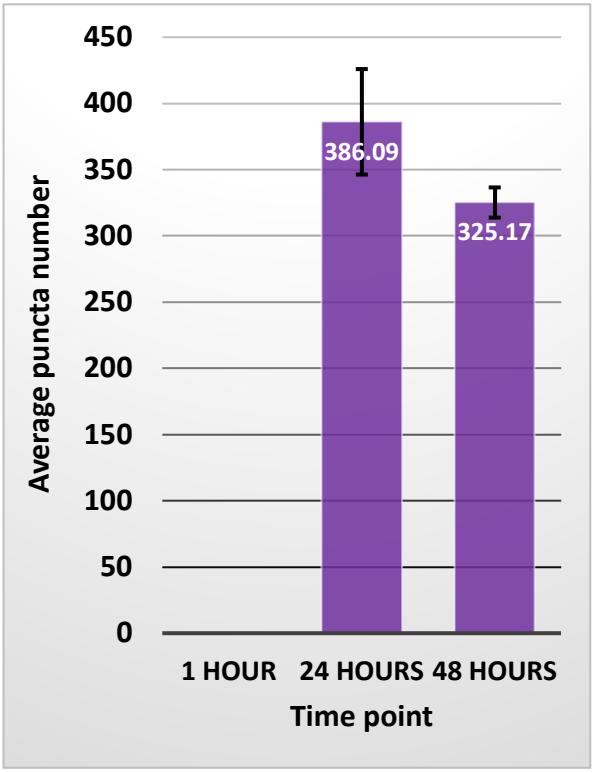
Average puncta number
450
400
350
300
250
200
150
100
50
0
386.09
325.17
1 HOUR
24 HOURS
48 HOURS
Time point

Figure 3.20. Quantification of a 48-hour pulse-chase experiment.
Using the Imaris software, I detected synaptic puncta labelled by the R110 pulse ligand and the TMR chase ligand for cells fixed after 1 hour, 24 hours or 48 hours of chase ligand labelling. This allowed me to quantify the average fluorescence intensity of synaptic puncta per image at the experimental time points as well as the average puncta number per image. **a.** Graph of the average R110 pulse ligand puncta intensity. Note the gradual reduction in puncta intensity as pulse-labelled 'old' PSD-95 proteins are degraded over time. **b.** Graph of the average TMR chase ligand puncta intensity. Note the lack of signal after 1 hour of incubation due to the complete HaloTag binding-site saturation by the pulse ligand at this time point. **c.** Graph of the average R110 pulse ligand puncta number. The decrease in puncta number mirrors the decrease in fluorescence intensity seen in (a.). **d.** Graph of the average TMR chase ligand puncta number. As in (b.), no puncta are detected at the 1 hour incubation time point due to saturation by the pulse ligand.

remain (figure 3.20.c). The difference in between each time point is statistically significant in each case: P= 0.005 and 0.0003 between the 1 and 24, and 24 and 48 hour time points, respectively (Welch's t-test). From these changes in puncta numbers, we can infer that roughly 45% of synapses that are labelled by the pulse ligand at the 1h time point no longer express pulse-labelled 'old' PSD-95 proteins after 24 hours, and over 48 hours this number rises to 88%. One explanation for this is that these synapses have completely degraded all of their 'old' PSD-95 in order to replace it with 'new' PSD-95 that is labelled by the chase ligand. A second explanation is that these synapses have been pruned away and have thereby completely disappeared, potentially being replaced by new synapses through the process of synaptogenesis. Most likely, both of these factors combine to cause this drop in pulse ligand puncta number.

Chase ligand puncta number, meanwhile, goes up dramatically within the first 24 hours of the experiment, from no puncta at all being detectable after 1 hour of labelling, to an average number of 386.09 ± 39.84 of puncta being detected after 24 hours. This amount also appears to be the maximum total number of puncta labelled with the chase ligand, as average puncta number actually decreases over the next 24 hours down to 325.17 ± 11.40 puncta, at the 48-hour time point. This difference is, however, not statistically significant at the $p<0.05$ confidence interval. The majority of these puncta are most likely made up of synapses that are stable and thus were present at the start of the experiment, thereby containing both 'old' and 'new' PSD-95. Over time, these synapses are likely to lose all of their 'old' PSD-95, and only contain PSD-95 molecules that are labelled by the chase ligand. However, at this early developmental

stage that experiences a lot of synaptogenesis, many of these chase-labelled synapses may also have newly formed over the past 24 or 48 hours. This is a topic of considerable interest and complexity, and I will further address it in more depth in chapter 4.

It does appear strange that the maximal number of puncta labelled with pulse ligand is nearly 600 at the 1h time point, yet only about 400 with the TMR ligand at the 24-hour time point. It is possible that this discrepancy is linked to the lower intensity detection threshold in the Imaris software, which was set at 3.67 AU for the TMR ligand. 3.67 makes up 10.42% of the maximal average puncta intensity of 35.23 AU, whereas the intensity threshold of the R110 pulse ligand was set at 6.00, thereby only making up 8.94% of the average maximal intensity of 67.11 AU. It is further possible that, since the chase ligand labels 'new' PSD-95 proteins only, it may label many newly formed synapses that only express low levels of PSD-95 at this immature stage, thereby falling below the detection threshold.

Overall, then, the results reveal a clear pattern that follows the trajectory one would predict for a protein being turned over continuously. Synapses lose their populations of 'old', pulse labelled PSD-95 molecules, and replace them with 'new', chase-labelled PSD-95 molecules. This, alongside synaptic pruning and synaptogenesis, contributes to the declining number of pulse-labelled synapses and the increasing number of chase-labelled synapses. It appears that the HaloTag system is well-suited to analysing the turnover of a fusion protein, Halo-PSD-95, by using two different fluorescent HaloTag ligands in a pulse-chase approach.

3.4.5 Calculating the half-life of PSD-95

Once I had established a working pulse-chase method for the study of PSD-95 turnover, I wanted to use these results to work out the half-life of PSD-95. The half-life of a protein represents the amount of time it takes for a given protein quantity to degrade to half of its original value (Ziv and Fisher-Lavie, 2014), thereby quantifying the stability of that protein. This value can be calculated from the change in a protein's concentration over a known time period.

In this case, I can calculate the half-life of PSD-95 using the change in fluorescence intensity of the pulse ligand over a known time period (representing the change in the concentration of pulse-labelled Halo-PSD-95 over that time period).

Using the change in pulse ligand intensity over the space of 24 hours, I calculated that the half-life of PSD-95 is 38.43 hours:

$$t_{\frac{1}{2}} = \frac{24\ hours}{Log2(\frac{67.11}{43.53})} = 38.43$$

This calculation matches closely with the greater-than-36-hour half-life estimation published in El-Husseini et al. (2002). However, when using the change in pulse ligand intensity over the space of 48 hours, I derive a slightly longer half-life of 40.83 hours:

$$t_{\frac{1}{2}} = \frac{48\ hours}{Log2(\frac{67.11}{29.71})} = 40.83$$

While the difference between these two results above is not massive, if we calculate the half-life from the average intensity at the 24h and 48h time points, we get an even greater half-life measure of 43.55 hours. There is a possible biological explanation for this difference in results, apart from the conceivable experimental variability that may have had an effect. It is possible that synapses are heterogeneous in their rate of PSD-95 turnover, with some synapses perhaps degrading and synthesizing PSD-95 more rapidly than other synapses. If this is the case, then we might expect a shorter half-life estimation (i.e. more rapid degradation rate) over the first 24 hours than over the following 24 hours. This is because synapses turning over PSD-95 more rapidly would contribute to the puncta intensity calculation over the first 24 hours (lowering the mean intensity), but might have completely degraded all of their pulse-labelled PSD-95 proteins after 48 hours, thereby no longer contributing to the mean puncta intensity at that time point. It would therefore seem that overall PSD-95 degradation has slowed down over the second 24 hours, when in reality we are now restricted to measuring the turnover rate of PSD-95 in the subpopulation of synapses that are turning over PSD-95 more slowly, as we are no longer taking into account synapses that contain

no pulse ligand. If one wanted to correct for this, one could look at the number of synapses expressing pulse-labelled PSD-95 on all three days of measurement (i.e. DIV15/1h, DIV16/24h and DIV17/48h), and calculate the difference in each group from the starting number (DIV15/1h). This difference could be taken to represent synapses that degraded all of their PSD-95, and thus each of these would represent a pulse ligand intensity of '0'. If all of these '0' puncta values were added to the calculation, the mean puncta intensity would drop for the 24 hour and 48 hour time points. An additional point to consider in this context is that we are not actually losing synapses from the calculation at an intensity of '0', but rather at an intensity of 6.00 AU, as this is the detection threshold applied to the Imaris software for this pulse ligand channel. Finally, it is certainly possible that the half-life of PSD-95 increases with the age of the primary neurons, as in the case of some proteins, more mature neurons contain proteins with greater half-lives (Mammen et al., 1997). This is a question I will address further in chapter 4. Holistically, then, it would seem that the best method of analysing the results from this set of pulse-chase experiments is to calculate the half-life of PSD-95 over the first 24 hours only, since we want to calculate the half-life of the average PSD-95 molecule in any synapse between DIV15 and DIV16, as well as mitigating the other factors as much as possible. This experiment thus concludes with a half-life measurement of 38.43 hours for PSD-95 between DIV15 and DIV16.

Regarding PSD-95 synthesis, it is not truly possible to calculate an absolute 'rate' of synthesis in terms of number of PSD-95 molecules synthesised per hour using my pulse-chase method, as we do not know what the specific number of PSD-95 proteins is that a certain ligand fluorescence intensity correlates with. We could attempt to calculate a rough synthesis rate for PSD-95 based on certain assumptions, but the primary presumption would have to be that all the synapses have a total average PSD-95 number of 300 copies (Chen et al., 2005; MacGillavry et el., 2013). With that presumption, we would be able to make a rough calculation of the rate of synthesis, based on the starting intensity of pulse ligand being equal to 300 copies, thereby deducing the amount of pulse-labelled PSD-95 molecules remaining in each synapse after 24 hours, which in turn gives us an idea of the number of PSD-95 molecules that are represented by the chase ligand signal in these colocalising synapses (as the total number would still be 300). However, if we have to consider that many of these synapses may not be mature at DIV15, due to the high rate of synaptogenesis

between DIV14 and DIV21 (Lesuisse and Martin, 2002; Cohen et al., 2013), our core premise is not valid, thus preventing the calculation from having much validity at all. A further issue is that I am using a measurement of average puncta intensity, which provides an indication of PSD-95 concentration at a given synapse. However, it does not give an indication of total PSD-95 present at a synapse, as this would have required the measurement of integrated puncta intensity (i.e. aggregate intensity) to be used. Thus, I cannot work with the presumption that the maximal average puncta intensity is equal to 300 copies of PSD-95 in a synapse. For this reason, I will not attempt to calculate PSD-95 synthesis in this study, but rather evaluate relative synthesis rates by comparing the average chase puncta intensities. This will still give ample information about changes in synthesis, but not permit absolute synthesis rates to be calculated.

In conclusion, I find that PSD-95 half-life in primary neurons between DIV15 and DIV16 to be around 38 hours, which matches previously reported results (>36 hours, El-Husseini et al., 2002; >24 hours, Todd et al., 2003). Nevertheless, one must take into consideration that this result is limited to this specific time window in the development of primary hippocampal neurons, and as this is still a period of great flux in terms of synaptic stability and synaptogenesis, the results may not be transposable onto neurons of other developmental ages. As such, this topic will be addressed again in chapter 4.

3.5 Chapter conclusion

This chapter has aimed to provide a detailed explanation of all of the experiments that act as the foundation of this project, and allowed me to proceed to ask the biologically intriguing questions presented in the subsequent chapter. I started off by probing the validity of the mouse model that is central to nearly every single experiment performed throughout the project, using biochemical, electrophysiological and microscopy-based techniques. I then went on to evaluate the functionality of using the HaloTag technology in a primary culture setting, and finally established a working method to analyse the turnover of PSD-95. These experiments, taken together, firmly establish that the KI mouse model is phenotypically normal, displaying no aberrant profile with

regards to fusion protein expression or localisation, or its electrophysiology. However, one point that must be noted is that no behavioural tests were performed. While unlikely given the other results, it cannot be ruled out that the mouse line used in this project may display some abnormal behavioural phenotype. A deeper analysis of this aspect may thus be warranted in future experiments. Furthermore, additional replicates of the biochemical analysis may be required in order to definitively confirm that PSD-95-HaloTag expression levels are not significantly different from PSD-95 levels in WT mice.

A further aspect that was noted was that while a reduction in the number of puncta labelled with the pulse ligand over a 24-hour time period does give some indication of a loss of 'old' PSD-95 proteins that are degraded and replaced by new, chase-labelled PSD-95 proteins, synaptic pruning is a viable alternative explanation for this, particularly at this early developmental stage. Future studies may wish to employ live cell imaging techniques in order to resolve such questions. Live imaging would allow for the observation of pruning of individual dendritic spines, as well as the visualisation of the degradation of PSD-95 molecules represented by a gradual dimming of pulse ligand signal at individual synaptic puncta. Such experiments were not within the scope of this project, but would provide valuable insights for future studies.

The results presented in this chapter confirm that the HaloTag technology provides a fantastic tool for the study of PSD-95 turnover at the postsynaptic densities of live primary neurons. I then went on to use this HaloTag technology to work out the half-life of PSD-95 between DIV15 and DIV16, which was found to be about 38 hours. The fact that this result matches those previously reported in the literature adds further confidence in the validity of the results. Overall, the result presented in chapter 3 provide the bedrock for the remaining experiments to be presented in chapter 4.

Chapter 4: Using the PSD-95-HaloTag mouse model to evaluate PSD-95 turnover at synapses

4.1 Chapter overview

The experiments that will be presented in this chapter are based upon the methods that I firmly established in chapter 3. All of the experiments utilise the HaloTag technology and our KI mouse line, and the majority of these experiments use the pulse-chase method in neuronal primary cultures established in chapter 3.4. This chapter will have two focal points: First, I will analyse PSD-95 turnover at single synapses rather than in bulk as I have done in chapter 3.4. Second, I will analyse PSD-95 turnover following the treatment of neurons with a chemical reagent.

After I had successfully managed to establish a working protocol for performing pulse-chase experiments, and had been able to use this protocol to observe and quantify PSD-95 turnover, I decided to apply various chemical modulators to the neuronal primary cultures and quantify their effect upon PSD-95 turnover. This decision was driven by my desire to a) observe the effect of known modulators of PSD-95 turnover using my method, and b) ask biologically pertinent questions in a cell culture system using the tools at my disposal. In order to do this, I designed a study that allowed me to gather a huge quantity of data simultaneously within a relatively small number of experiments. I will give a detailed description of this study in chapter 4.2.

I decided to break up the data gathered during this study into two main parts- chapter 4.3 will focus on the untreated control group and analyse normal PSD-95 turnover at a single-synapse level. I will also attempt to classify synapses into different types according to the data gathered in this section. In chapter 4.4 I will evaluate the effects that a range of modulatory chemical reagents known or thought to affect neuronal activity and/or PSD-95 regulation in CNS neurons has on PSD-95 turnover, both at the bulk and single-synapse level.

In chapter 4.5 I will investigate PSD-95 turnover in mature neurons at a later developmental stage, DIV29+ (rather than DIV15+ for the other studies). Finally, I will discuss and summarise the chapter's findings in the conclusion.

4.2 Overview of large-scale study

In order to gather as many data sets as possible and concurrently maximising the comparability of these data sets by minimising the variation, I set up a total of eight identical experimental rounds. Each round of experiments was made up of a single set of hippocampal neuronal primary cultures, prepared from a single litter of PSD-95$^{HaloTag/HaloTag}$ (homozygous) embryos taken at day E17.5. The hippocampi from all of the embryos in the litter were pooled together and, once in a single-cell suspension, plated out on 24-well glass coverslips according to the standard protocol (see chapter 2.3.3). These primary cultures were grown until they had reached developmental stage DIV14, at which point the pulse ligand (R110Direct, 50nM) was added for 16 hours. After pulse ligand incubation was complete on DIV15, coverslips were split up into groups according to their treatment. Each experiment contained 10 groups:

1. Control group 1h: This group was only treated with the chase (TMR, 500nM) ligand for 1 hour before being fixed at DIV15. No other treatment was administered.

2. Control group 24 hours: This group was treated with the chase ligand for 24 hours before being fixed at DIV16. No other treatment was administered.

3. Tetrodotoxin: This group was treated with tetrodotoxin at 1µM alongside the chase ligand for 24 hours before being fixed at DIV16.

4. Bicuculline: This group was treated with bicuculline at 40µM alongside the chase ligand for 24 hours before being fixed at DIV16.

5. Lactacystin: This group was treated with lactacystin at 1µM alongside the chase ligand for 24 hours before being fixed at DIV16.

6. MG132: This group was treated with MG132 at 10µM alongside the chase ligand for 24 hours before being fixed at DIV16.

7. Anisomycin: This group was treated with anisomycin at 1μM alongside the chase ligand for 24 hours before being fixed at DIV16.

8. Cycloheximide: This group was treated with cycloheximide at 3μM alongside the chase ligand for 24 hours before being fixed at DIV16.

9. BDNF: This group was treated with BDNF at 3.7nM alongside the chase ligand for 24 hours before being fixed at DIV16.

10. Ketamine: This group was treated with ketamine at 10nM alongside the chase ligand for 24 hours before being fixed at DIV16.

Each group contained two coverslips per experimental round. The pulse-chase protocol was the standard protocol I had established in chapter 3.4, that is outlined in chapter 2.5.6. After cells had been fixed, the coverslips were individually mounted on glass slides in preparation for imaging. At this stage the experiment was blinded, such that I did not know which slide was part of which experimental group. This was done by asking another member of our lab to assign each slide a number, and record the treatment group that this number correlated with. Unblinding only occurred in the final stage of the experiment, once all of the data had been acquired and analysed (i.e. once all of the quantitative data such as average puncta intensity, number and colocalisation had been gathered). The slides were then imaged using the LSM510 confocal microscope (63x magnification, zoom3.1) at previously established standard settings (see chapter 2.4.1).

For each slide, six images were taken with attempts made to keep image locations as similar between slides as possible (along dendrites, excluding cell bodies). The Imaris software was then used to detect synaptic puncta as detailed in chapter 2.4.2. A colocalisation analysis was performed and as before, puncta were detected using a seed point estimation diameter of 300nm, with puncta considered colocalised if within 300nm of each other (centre to centre). When using the puncta colocalisation tool, the Imaris software automatically sorts the entire population of puncta in each channel according to whether they do or do not colocalise with puncta in the other channel.

After puncta had been detected and colocalisation analysis performed for each image, the mean was calculated for each parameter (e.g. mean puncta intensity per image, mean puncta number per image). It was only at this stage that unblinding took place. After the identity of each coverslip in each experimental round had been revealed, the results of coverslips in the same treatment groups were merged (that is to say that the average value was calculated across all 12 data points, 6 data points from each coverslip). This means that for every experimental set, the results from 12 images were averaged together (6 images per coverslip and 2 coverslips per experimental group). Finally, after all eight rounds of experiments had been completed, the final mean value for each parameter was calculated across the eight sets of experiments. In this way, each set of experiments was values as an N of 1, having been derived from a genetically distinct embryonic litter.

This experimental design allows me to compare the results from these experiments with a high degree of confidence that differences are due to treatment, particularly as all data sets were collected from the exact same cultures derived from the same pool of embryos, meaning genetic variability and differences in culture conditions could be discounted. Furthermore, while the nominal N is eight, the results are the end-product of analysing tens of thousands of synaptic puncta for each treatment group. Indeed, each treatment group is made up of 96 images (8 experiments, 2 coverslips per experiment, 6 images per coverslip). If we estimate about 500 synaptic puncta per image (given that according to figure 3.19.c about 600 puncta were labelled with the pulse ligand at the start of the experiment), we arrive at 48,000 synaptic puncta being analysed for each treatment group.

Nevertheless, some sources of variability remain. For one, the fact remains that neurons were grown on different coverslips in separate wells, and it can frequently be observed that neurons on one coverslip grow differently to neurons on another coverslip. Thus, neuronal cell density and the extent of dendritic outgrowth can differe from well to well. This can have an impact on the data, for example if this affects the number of synapses per image. Likewise, there can be significant differences in neuronal growth between separate cultures. Another point to consider is that while cultures were derived from the embryonic hippocampus, cells within the hippocampus can be diverse, and thus some coverslips or imaged regions may contain a

preponderance of cells of one type over another. Furthermore, hippocampal dissections are technically challenging, and thus some amount of surrounding cortical tissue is inevitable included. This, again, can vary in its extent from culture to culture, potentially introducing a source of variability. While large sample sizes and pooling helps to mitigate these variabilities to some extent, a power calculation could have been a useful tool in order to work out the statistically required sample sizes to limit the impact.

In the following section, chapter 4.3, I will only focus on the control groups in this study, and analyse PSD-95 turnover at a single-synapse level across these eight experiments. Thereafter, in chapter 4.4, I will turn my attention to the different treatment groups and evaluate the effect of these chemical reagents on PSD-95 turnover at both a bulk as well as a single-synapse level.

4.3 Analysing PSD-95 turnover in bulk and at a single-synapse level over 24 hours in untreated controls

4.3.1 Introducing the concept of single-synapse analysis of PSD-95 turnover

The concept of protein turnover can be understood in different ways, and protein turnover can be studied using a variety of techniques. Some studies have used time-lapse confocal microscopy to observe the appearance and disappearance of individual GFP-tagged PSD-95 puncta in transfected neuronal cell cultures (Marrs et al., 2001; Okabe et al., 1999; Okabe et al., 2001), but this does not give an indication of PSD-95 degradation and synthesis and only allows for the study of synapse dynamics. Other studies have used photoactivatable GFP tagged to PSD-95 to visualise the degradation of PSD-95 at individual synapses over time (Sturgill et al., 2009). However, this technique does not allow for the observation of PSD-95 synthesis, only degradation. Fluorescence recovery after photobleaching (FRAP) is another technique that has been applied to the study of PSD-95 turnover at single-synapses (Zheng et al., 2010). This technique allows for an estimation of the size of the stable pool of the POI thereby giving an indication of the dynamism of a protein at synaptic locations, but it does not permit for synthesis or degradation to be evaluated.

Furthermore, the vast majority of these studies are performed using transfected neuronal cultures, meaning that PSD-95 is being overexpressed, which can lead to enhanced basal synaptic transmission and spine size (El-Husseini et al., 2000; Stein et al., 2003; Choe and Ehrlich, 2006), as well as decreased dendritic branching (Charych et al., 2006). In addition, fusion protein expression is not under the control of the endogenous promoter, and fluorescent proteins require a certain amount of time (four hours in the case of GFP) to become fluorescent by oxidation (Okabe et al., 1999). All of these factors can potentially have an effect on the experimental outcome.

Those studies that wish to specifically study protein synthesis and degradation tend to use metabolic labelling techniques such as SILAC (Stable Isotope Labelling with

Amino acids in Cell culture). This method has been used to work out the half-lives of synaptic proteins, including PSD-95 (Cohen et al., 2013; El-Husseini et al., 2002). However, while this technique is undoubtedly well-suited for establishing the half-life of a protein, it can only be used to study proteins in bulk, never at individual synapses.

Finally, there is a newer set of techniques involving non-canonical amino acid tagging that can be used to study protein turnover. FUNCAT (Fluorescent non-canonical amino acid tagging) involves the tagging of proteins with non-canonical amino acids followed by their detection using fluorescent labelling *in situ,* and can be used to visualise protein turnover at single-synapses in live primary neuronal cultures (Dieck et al., 2015). Quantitative non-canonical amino acid tagging (QuaNCAT) combines biorthogonal non-canonical amino acid tagging (BONCAT) with SILAC, allowing for the study of bulk protein turnover using mass spectrometry (Alvarez-Castelao et al., 2015). Taken together, these techniques are able to cover most aspects of protein turnover, yet none of them allows for the simultaneous study of protein turnover at the bulk and single-synapse level. Furthermore, FUNCAT, while able to visualise the turnover of a POI at single synapses, is unable to differentially label older and newer subpopulations of the same protein, and can thus not give an insight into the abundance ratio of these two groups at individual synapses.

The pulse-chase technique I established in chapter 3.4 using the HaloTag technology and the PSD-95^{HaloTag} KI mouse line combines many of the strengths of the aforementioned approaches to studying PSD-95 turnover, and even allows for the simultaneous analysis of PSD-95 turnover in bulk and at single synapses. This versatility is one of the greatest strengths of the HaloTag technology. In chapter 3.4 I outlined how the pulse-chase application of different fluorescent HaloTag ligands can be used to measure the turnover of a tagged POI (PSD-95) in bulk. By measuring the fluorescence intensity of pulse or chase ligands at individual synaptic puncta, calculating the mean puncta intensity per image taken, and ultimately calculating the mean puncta intensity over a number of images that make up a time point, the average puncta intensity is calculated across a huge number of synaptic puncta. This gives a very reliable estimate of the amount of ‘old’ or ‘new’ PSD-95 present at PSDs in a culture at a certain time point. However, because we detect puncta intensity for each synapse separately, we are also able to use this method to analyse PSD-95 turnover

at individual synapses, and identity different synaptic types according to their PSD-95 turnover profile.

The first and simplest manner of analysing single-synapse data is to subdivide the bulk data according to whether the puncta labelled by one ligand colocalise with the puncta labelled by the other ligand. This results in the formation of three synaptic subgroups: synapses containing both pulse- and chase-labelled PSD-95, and synapses containing only pulse- or only chase-labelled PSD-95. This analysis can be performed in varying situations, such as after 24 hours of chase ligand incubation and after 48 hours of chase incubation. Shifts in the abundance as well as the mean intensity of puncta in these groups can then be analysed and interpreted.

The fact that each synaptic punctum is a separate data point also allows for an analysis of the frequency of puncta intensities, i.e. how puncta are distributed across the range of fluorescence intensities. Such frequency distribution histograms may be skewed in different ways, which can indicate variations in population dynamics.

Finally, because each synaptic punctum can be analysed for both its pulse and chase ligand intensity separately, it is possible to work out the ratio of pulse:chase ligand intensity for each synapse. These ratios can then be analysed further, such as by comparing changes in the average ratios at different time points, or by examining the frequency distributions of these ratios. One important point to bear in mind when comparing the relative intensities of pulse and chase ligands, however, is that pulse and chase ligands carry different fluorophores with different fluorescent properties, as well as having been acquired with different microscope parameters and detected with different detection parameters in the Imaris software. Thus fluorescence intensity ratios cannot give any information about the absolute abundance of one ligand relative to the other (for example, a 1:1 intensity ratio does not mean that pulse and chase ligands are equally abundant in a given synapse). Instead, it is the differences in the pulse:chase intensity ratios that are of significance- a decrease in the average pulse:chase ratio means that the chase ligand has become relatively more abundant than the pulse ligand. For example, if a synapse were to go from a pulse:chase ratio of 2:1 to a ratio of 1:1, then we can presume that relative to the pulse ligand, there is now twice as much chase ligand present.

Nevertheless, because only a single HaloTag ligand binds to a single HaloTag protein (fused to PSD-95), the fluorescence intensity of a synaptic punctum is directly proportional to the number of PSD-95 molecules present in that synapse. This means that if the average puncta intensity across all synapses doubles over the course of 24 hours, we can presume that the average amount of PSD-95 labelled by that ligand has also doubled.

In the following sections of chapter 4.2 I will expand the bulk analysis of PSD-95 turnover performed in chapter 3.4 to the analysis at a single-synapse level. This will not only give interesting insights into the turnover of PSD-95, but also provide a reference point for the future analysis of data sets coming from primary neurons treated with various chemical modulatory agents in chapter 4.3.

4.3.2 Analysing PSD-95 turnover over 24 hours

In this section I will present the parts of the data from the large-scale study outlined in chapter 4.2 that pertain to the untreated control groups (1 hour of chase incubation and 24 hours of chase incubation). The details of the experiment design have been outlined in chapter 4.2, but briefly hippocampal primary cultures were derived from eight different litters of PSD-95$^{HaloTag/HaloTag}$ (homozygous) embryos. These cultures were grown until DIV14, at which point the pulse ligand (R110Direct, 50nM) was added for 16 hours. Following pulse ligand incubation, the majority of the media containing the pulse ligand was removed and replaced with media containing an excess of chase ligand (TMR, 500nM) at DIV15. Incubation with the chase ligand occurred for 1 hour and 24 hours, depending on the control group. Thereafter cells were fixed in 4% PFA, mounted on glass slides, imaged on an LSM510 confocal microscope and analysed using the Imaris software.

4.3.2.1 Bulk analysis

Briefly looking back at the single 48-hour pulse-chase experiment presented in chapter 3.4.4 and figure 3.19, we see that the mean fluorescence intensity and number of synaptic puncta labelled by the pulse (R110) ligand diminished rapidly (intensity decreases statistically significantly from 67.11 ± 2.76 Arbitrary Units (AU) to 43.53 ± 1.9 AU over the first 24 hours (Welch's t-test: $p=9.99x10^{-7}$). Concomitantly, the mean fluorescence intensity and number of synaptic puncta labelled by the chase (TMR) ligand went up over the first 24 hours, and then remained constant over the following 24 hours (from no signal at all at the 1-hour time point to 30.50 ± 1.59 AU). The results from the new, large data set are very similar to these.

Figure 4.1.a shows that the mean intensity of puncta labelled by the pulse (R110) ligand is 65.97 ± 1.69 AU at the 1-hour time point. After 24 hours of chase-labelling, the mean pulse ligand puncta intensity has decreased markedly down to 41.44 ± 0.85 AU (statistically significant, Welch's t-test $p=9.51x10^{-8}$). Over the same 24-hour time period, the average puncta intensity of the chase (TMR) ligand shoots up to

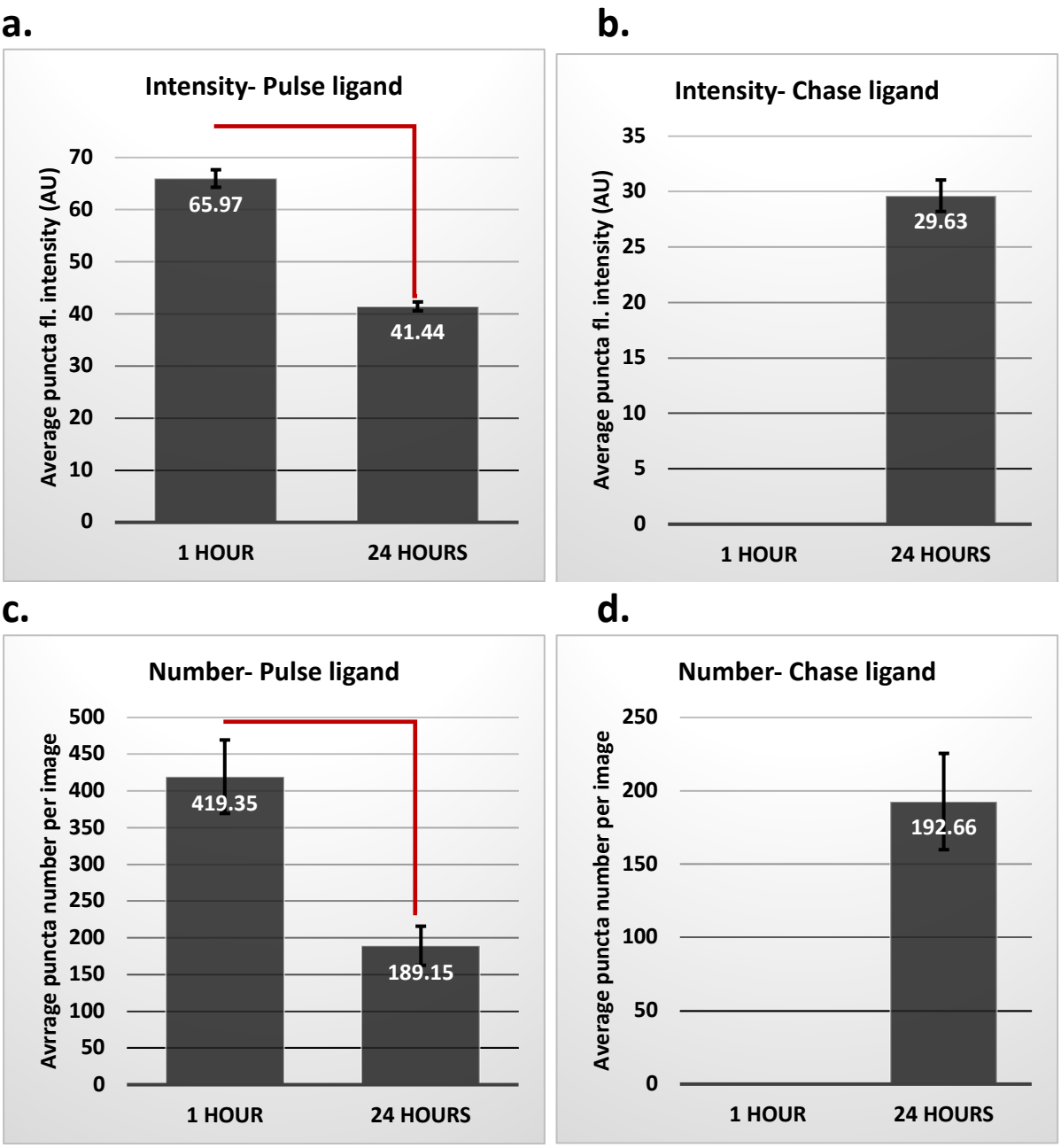

Figure 4.1. Measuring mean PSD-95 puncta intensity and number per image in bulk. Neuronal primary cultures from pooled homozygous PSD-95$^{HaloTag/HaloTag}$ mouse hippocampi taken at embronal stage E17.5 were grown on glass coverslips until DIV14. At DIV14 they were labelled with the R110Direct HaloTag ligand (50nM, 16h), and on DIV15, the TMR ligand was added to the cultures at 500nM and the concentration of the R110 ligand reduced to 12.5nM. Cells were fixed in 4% PFA after either 1 hour or 24 hours of incubation. Coverslips were imaged on the LSM510, and puncta detected using the Imaris software. Average puncta fluorescence intensity per image as well as average puncta number per image were then calculated. This was performed across 8 different cultures (N=8), with the graphs here presenting the mean values across these eight cultures. **a.** Graph of the average R110 pulse ligand puncta intensity. Note the significant reduction in puncta intensity as pulse-labelled 'old' PSD-95 proteins are degraded over time (Welch's t-test, $p=9.51x10^{-8}$). **b.** Graph of the average TMR chase ligand puncta intensity. Note the lack of signal after 1 hour of incubation due to the complete HaloTag binding-site saturation by the pulse ligand at this time point.

c. Graph of the average R110 pulse ligand puncta number. The significant decrease in puncta number mirrors the decrease in fluorescence intensity seen in (a.) (Welch's t-test, p=0.0020). **d.** Graph of the average TMR chase ligand puncta number. As in (b.), no puncta are detected at the 1 hour incubation time point due to saturation by the pulse ligand.

29.63 ± 1.42 AU (figure 4.1.b). When comparing these numbers to those of the single experiment from chapter 3.4.4, as mentioned above, it is striking how similar they are.

When looking at puncta number, we see a similar pattern. From the earlier experiment we see in figure 3.19.c, pulse ligand puncta number decreases from a peak of 598.67 ± 69.1 puncta down to 329.55 ± 49.3 puncta over 24 hours (significant, p=0.005). Chase ligand puncta number goes up from no puncta detected at all to 386.09 ± 39.84 puncta over the same time period. In the new data set (figure 4.1.c-d), the number of synaptic puncta labelled by the pulse ligand goes down significantly from 419.35 ± 50.05 to 189.15 ± 26.64 (Welch's t-test, p=0.002). The number of puncta labelled by the chase ligand goes up from no puncta detected to 192.66 ± 32.83 over 24 hours. While the results from the larger data set (figure 4.1) are lower than those observed in the single data set (figure 3.19), they clearly follow the same pattern.

To complete this bulk analysis of PSD-95 turnover in untreated controls, I repeated the protein half-life calculation. With the single data set, the half-life of PSD-95 was found to be 38.43 hours (chapter 3.4.5). With the new numbers, this half-life is slightly decreased, to 35.78 hours. While this is a slight downwards revision, it is nonetheless very similar and consistent with the literature ('approximately 36 hours', El-Husseini et al., 2002).

4.3.2.2 Single-synapse analysis A: Colocalised vs Non-Colocalised

Following the bulk analysis, we move to the results of the single-synapse analysis by looking at differences in average puncta intensity between puncta of one ligand that colocalise with puncta of the other ligand, and those that do not colocalise. Figure 4.2.a. shows that after 24 hours of chase ligand incubation, pulse-labelled puncta that are colocalised with chase-labelled puncta have a greater average intensity than those that are not colocalised. At this time point, colocalised pulse-labelled puncta had an average intensity of 45.13 ± 0.93 AU while non-colocalised puncta had an average

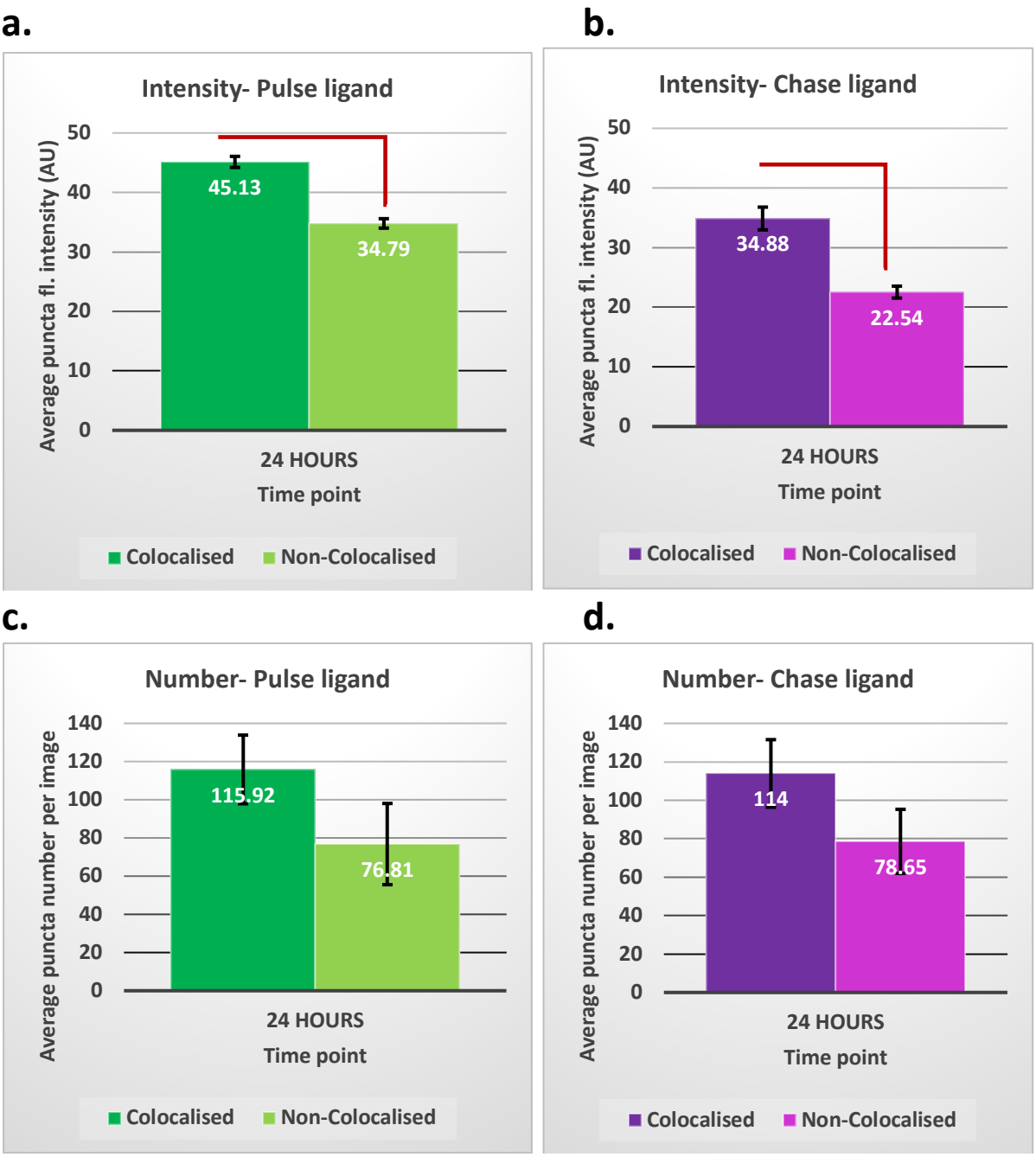

Figure 4.2. Colocalised and non-colocalised puncta differ in their average puncta intensity and number.

Average puncta fluorescence intensity (APFI) and number per image were calculated for pulse and chase ligand labelled synaptic puncta that are colocalised with puncta of the other ligand, and those that are not. **a.** Graph comparing pulse ligand (R110Direct) APFI of colocalised with non-colocalised puncta (difference is significant: Welch's t-test, $p=9.01x10^{-7}$). **b.** Graph comparing chase ligand (TMR) APFI of colocalised with non-colocalised puncta (difference is significant: Welch's t-test, p=0.00016). **c.** Graph comparing average pulse ligand (R110Direct) puncta number per image of colocalised with non-colocalised puncta (difference is not significant: Welch's t-test, p=0.18). **d.** Graph comparing average chase ligand (TMR) puncta number per image of colocalised with non-colocalised puncta (difference is not significant: Welch's t-test, p=0.17).

intensity of 34.79 ± 0.80 AU. This difference is highly statistically significant (Welch's t-test, $p=9.01x10^{-7}$).

Figure 4.2.b. shows the results of the same analysis for the chase ligand at the same 24-hour time point. Just like with the pulse ligand, average chase ligand puncta intensity is greater in those puncta that are colocalised (34.88 ± 1.91 AU) with the pulse ligand than those that are not (22.54 ± 1.00 AU). Again, the difference is statistically significant (Welch's t-test, p=0.00016).

When looking at puncta number, the exact same picture emerges: Colocalised puncta are more numerous than non-colocalised puncta (figure 4.2.c). For the pulse ligand, there are on average 115.92 ± 17.98 colocalised puncta per image and 76.81 ± 21.29 non-colocalised puncta per image (not significant, Welch's t-test, p=0.18). For the chase ligand (figure 4.2.d), there are on average 114.00 ± 17.58 colocalised puncta per image and 78.65 ± 16.67 non-colocalised puncta per image (not significant, Welch's t-test, p=0.17). In neither case is the difference statistically significant, however, which can be explained by the high degree of variance when it comes to puncta number per image.

Next, I wanted to find out what percentage of synapses in the whole synaptic population expressed either both ligands (colocalised) or only one of the ligands but not the other. Figure 4.3. shows the results visualised as a pie chart. From this graph we can see that 28% of synapses contain only pulse ligands (i.e. 'old' PSD-95), 29% contain only chase ligands ('new' PSD-95) and in 43% of synapses pulse and chase ligands are colocalised.

Taken together all of these results allow some very interesting insights into the whole synaptic population in hippocampal primary neurons at DIV15. Firstly, we can clearly observe that there are three distinct synaptic populations- those containing only 'old' PSD-95, those containing only 'new' PSD-95, and those containing a mixture of the two. The other interesting observation is that there is a clear link between puncta colocalisation and synapse fluorescence intensity (which directly correlates with PSD-95 expression). For both ligands, pulse and chase, colocalised synapses display a greater fluorescence intensity. Since these synapses were likely present over the

course of the entire 24-hour pulse-chase experiment (and longer, due to the 16-hour pulse ligand incubation period), as they contain 'old' PSD-95 proteins, a possible explanation is that these are large, well-established and mature stable synapses that steadily turn over PSD-95. On the other hand, synapses containing only chase ligand ('new' PSD-95) may be young synapses that have only appeared over the final 24 hours and were not present during pulse labelling. This may explain why they tend to express less PSD-95- they may simply still be immature. Synapses containing only the pulse ligand ('old' PSD-95) may on the other hand express less PSD-95 for other reasons- perhaps they are in the process of being pruned, or else they may have been silenced. I will discuss the implications of these observations further in chapter 4.3.3, but for now, we can clearly observe differences in PSD-95 expression over what appears to be a very heterogeneous synaptic population.

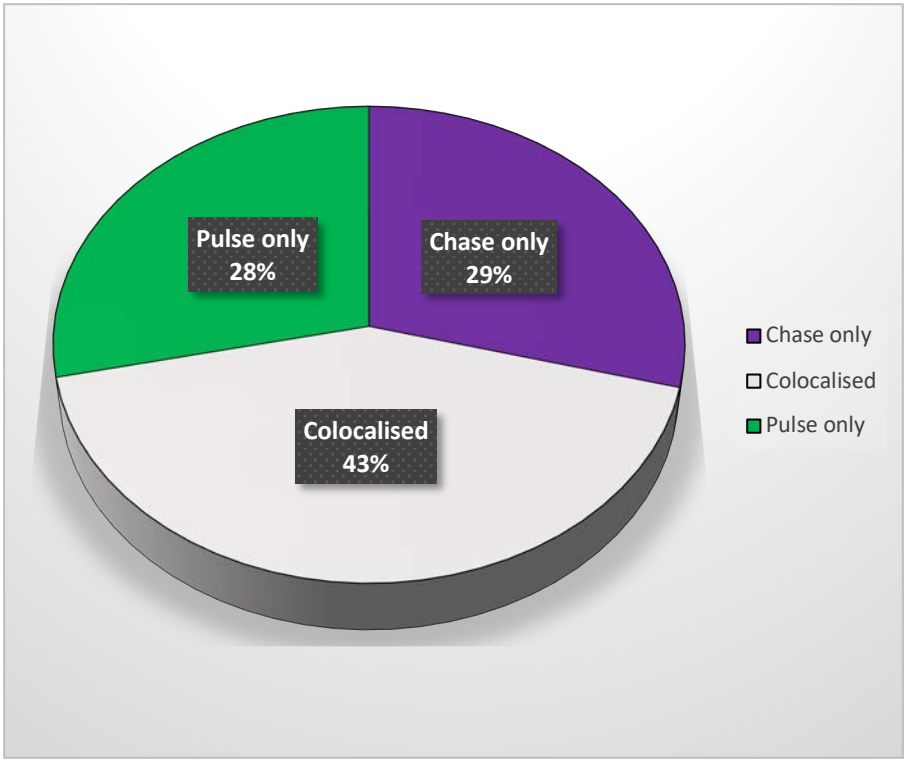

Figure 4.3. Proportional representation of synaptic population by HaloTag ligand-labelling. Synaptic puncta were categorised according to whether they colocalised with puncta labelled by the other ligand or not. This pie chart depicts the proportional representation of the three types of synaptic puncta observed.

4.3.2.3 Single-synapse analysis B- Frequency histograms

Another interesting analytical perspective that is possible when analysing single-synapses is to look at frequency histograms. As my data consists primarily of values for individual puncta, it is easy to plot such frequency histograms for entire populations of synaptic puncta. These graphs can then give valuable information about a population by their shape and skewness, allowing for reasonable deductions about the dynamic state of the population.

Figure 4.4 shows a frequency distribution histogram of pulse ligand puncta at the 1-hour time point, as well as a cumulative distribution function plot. Since there are no chase ligand puncta detectable at this stage, the data at this time point represents the entire population of synaptic puncta. Mean intensity is 65.97 ± 1.69 AU (as revealed in the bulk analysis above), with median intensity being 54.94 AU and the mode being 42 AU (3.79% of puncta). Observing the shape of the histogram (Figure 4.4.a), we can immediately see that the histogram is asymmetric- there is a distinct positive skewness, i.e. low-intensity synaptic puncta are more common than high-intensity puncta. Indeed, 61% of puncta have an intensity that is lower than the mean intensity. We can also observe that the range of puncta intensities is quite large- puncta range in intensity from 18 to more than 220 arbitrary units. One possible explanation for this distribution is that at this developmental stage (DIV16), there are many immature synapses that are still growing in size and hence number of PSD-95 molecules expressed, and therefore the majority of synapses are small and low in PSD-95 count. If this is the case, we can expect the peak of the histogram (and therefore average puncta intensity) to shift upwards in older, mature neuronal cultures. An alternative explanation is that the overall synaptic population is simply very diverse in size and degree of PSD-95 expression, and that this population histogram accurately reflects the distribution of PSD-95 that is expressed by each synapse. If this is the case, we must deduce that the synaptic population, while heterogeneous, tends to have a preponderance of smaller synaptic puncta expressing relatively less PSD-95 and only few synapses that lie at the maximal end of the PSD-95 expression spectrum.

a.

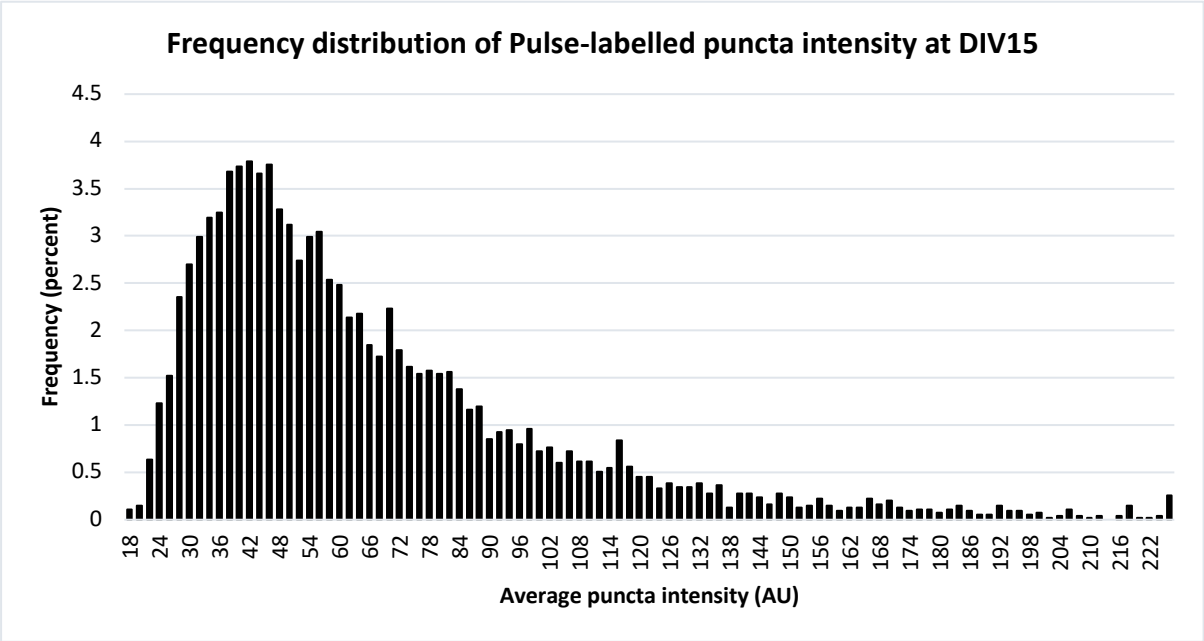

b.

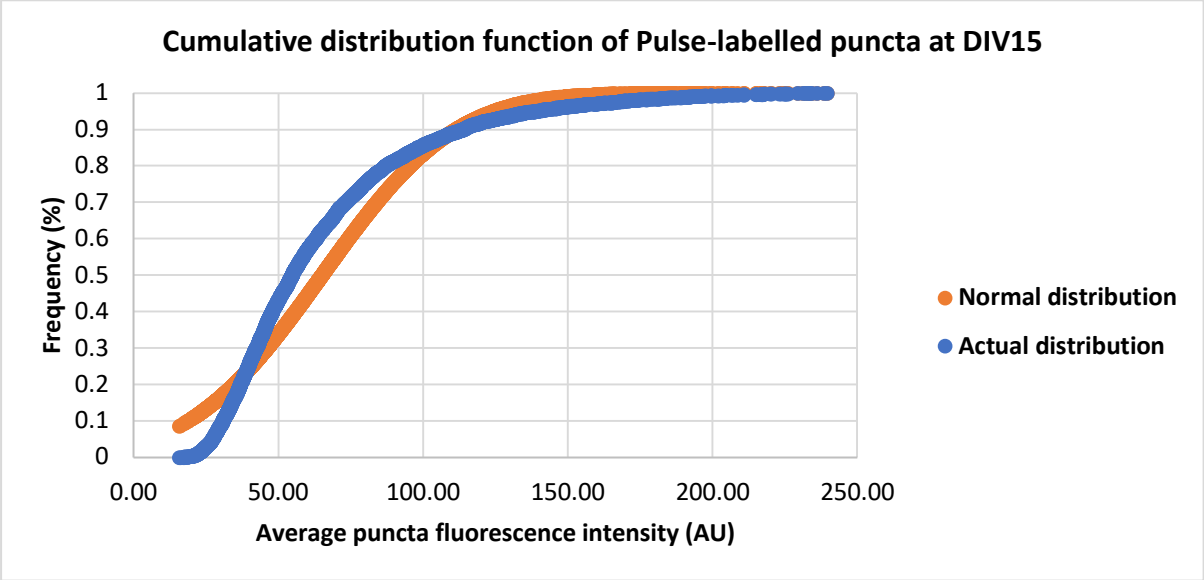

Figure 4.4. Frequency distribution histogram and cumulative distribution function of synaptic puncta labelled with the pulse ligand at DIV15.

a. The frequency distribution histogram depicts the full range of average puncta fluorescence intensities of pulse ligand puncta after 16 hours of incubation with the pulse ligand (R110Direct, 50nM), and 1 hour of incubation with the chase ligand (TMR, 500nM). The histograms reveals a positive skew and heterogenous synaptic population in terms of PSD-95 expression levels. Mean intensity is 65.97 ± 1.69 arbitrary units (AU), with median intensity being 54.94 AU and the mode being 42 AU (3.79% of puncta). **b.** The cumulative distribution function shows the actual distribution of the data alongside the theoretical distribution if it were perfectly normally distributed.

Looking at figure 4.4.b, we can see that the cumulative distribution function reveals that the actual data points are, for the most part, quite similar to the hypothetical points if the data points followed a perfectly normal distribution. This indicates that while the data does have a slight skew towards lower-intensity puncta, overall the data is nevertheless normally distributed.

Next, we look at puncta intensity frequency distribution histograms for the 24-hour time point. Figure 4.5 shows four histograms representing the three distinct groups of synapses that make up the synaptic population at this point- pulse ligand puncta colocalised, pulse ligand puncta non-colocalised, chase ligand puncta colocalised and chase ligand puncta non-colocalised. Pulse ligand puncta that are colocalised with chase ligand puncta (figure 4.5.a) unsurprisingly display a very similar distribution curve to chase ligand puncta that are colocalised with pulse ligand puncta (figure 4.5.c). Both graphs are slightly positively skewed, and taper out very gradually towards the higher puncta intensity. Both populations appear to be very heterogenous, with mildly sloping curves and relatively low peaks (pulse mode: 34 AU, 3.47%; chase mode: 19 AU, 3.96%). While this similarity may not be surprising given that both graphs represent the same population of synapses, viewed from the perspective of the two different ligands, it does nevertheless mean that over the course of the 24-hour experiment PSD-95 expression levels in these synapses appear to remain constant. Thus, we can postulate that in these colocalising synapses, PSD-95 that is degraded is being replaced by newly synthesised PSD-95 at the same rate, keeping the overall PSD-95 expression level constant over this subpopulation of synapses.

However, the picture we see in the other two synaptic populations is very different. Looking at figure 4.5.b, we see that the population of pulse ligand puncta that are not colocalised with chase ligand puncta appears to be much less diverse. The slopes are much steeper than in figure 4.5.a, and the mode has a much higher frequency value (mode 24 AU at 5.59%). The graph representing the population of chase ligand puncta that are not colocalised (figure 4.5.d) is similar but even more extreme. The shape of the graph displays a very pronounced peak at a low puncta intensity (bimodal, mode is 14 and 15 AU, at 8.53%), and very steep slopes with few outliers. The vast majority of the puncta frequencies are grouped around the modal values, i.e. a great proportion of these puncta are of low intensity compared to colocalising puncta (figure 4.5.c).

a.

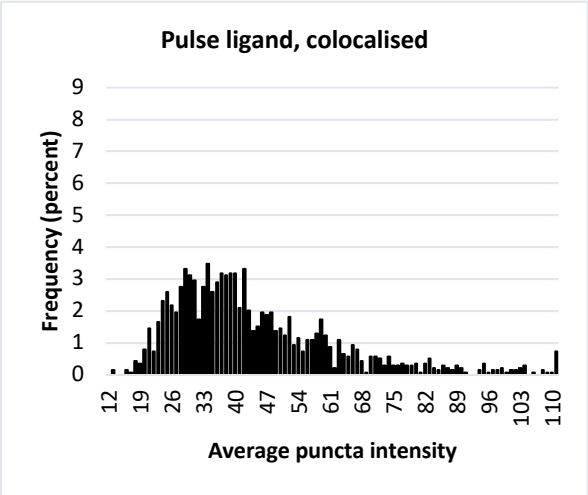
Pulse ligand, colocalised
Frequency (percent)
0 1 2 3 4 5 6 7 8 9
12 19 26 33 40 47 54 61 68 75 82 89 96 103 110
Average puncta intensity

b.

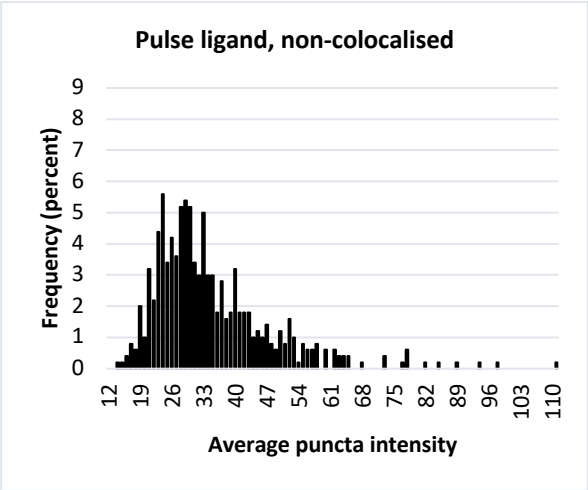
Pulse ligand, non-colocalised
Frequency (percent)
0 1 2 3 4 5 6 7 8 9
12 19 26 33 40 47 54 61 68 75 82 89 96 103 110
Average puncta intensity

c.

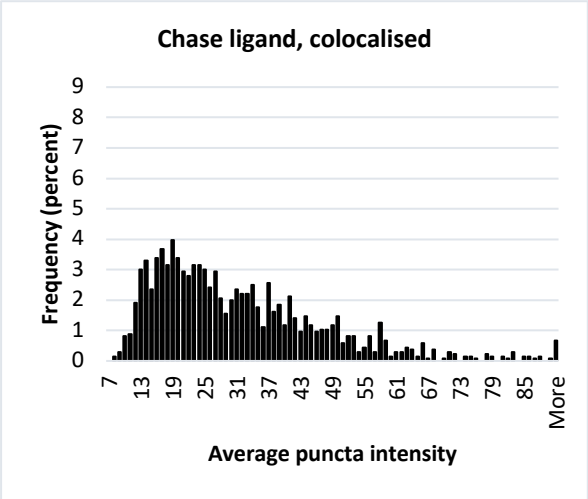
Chase ligand, colocalised
Frequency (percent)
0 1 2 3 4 5 6 7 8 9
7 13 19 25 31 37 43 49 55 61 67 73 79 85 More
Average puncta intensity

d.

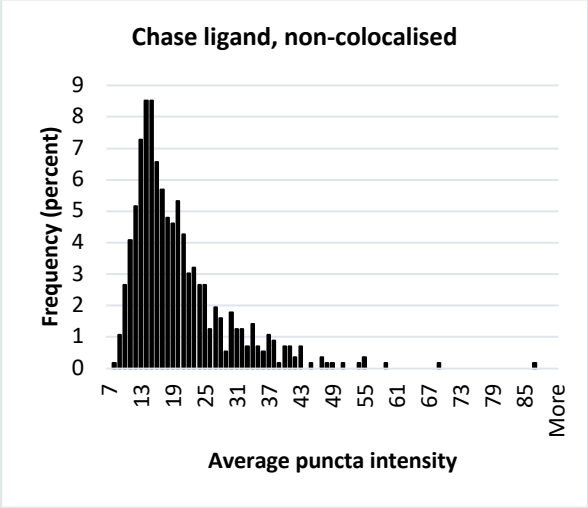
Chase ligand, non-colocalised
Frequency (percent)
0 1 2 3 4 5 6 7 8 9
7 13 19 25 31 37 43 49 55 61 67 73 79 85 More
Average puncta intensity

e.

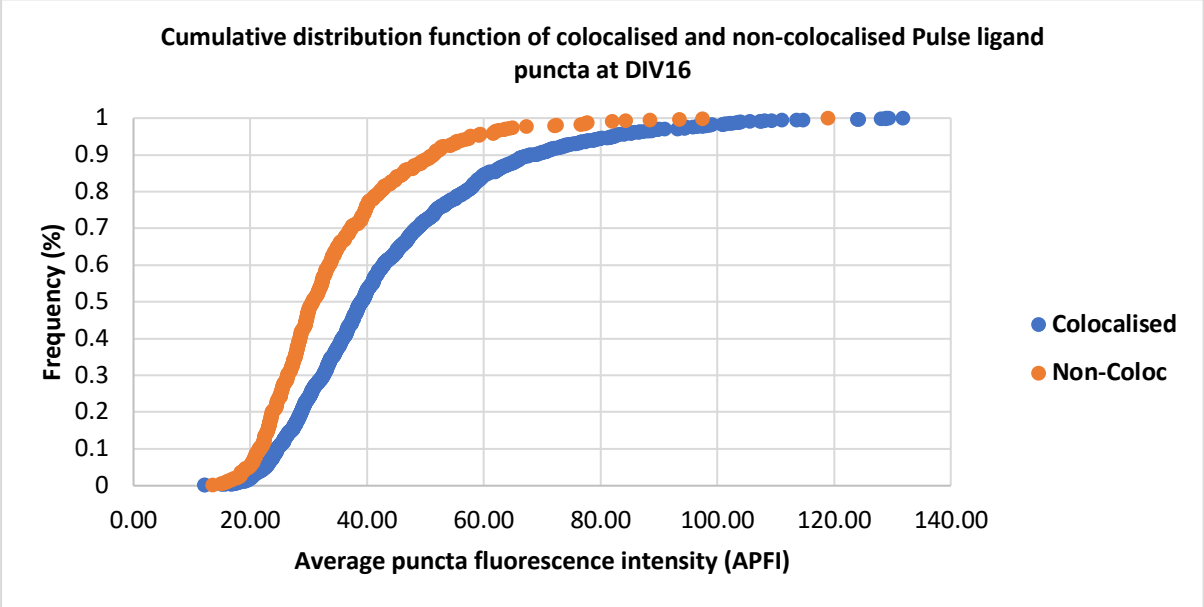
Cumulative distribution function of colocalised and non-colocalised Pulse ligand puncta at DIV16
Frequency (%)
0 0.1 0.2 0.3 0.4 0.5 0.6 0.7 0.8 0.9 1
0.00 20.00 40.00 60.00 80.00 100.00 120.00 140.00
Average puncta fluorescence intensity (APFI)
Colocalised
Non-Coloc

Figure 4.5. Frequency distribution histograms of colocalised and non-colocalised pulse and chase ligand labelled synaptic populations.

After 24 hours of chase-ligand labelling, synaptic populations labelled by both pulse and chase ligand were categorised according to whether they colocalised with puncta of the other ligand. A frequency distribution histogram for APFI was then plotted from each of these four populations. **a.** Graph represents pulse ligand puncta that are colocalised with chase ligand puncta. **b.** Graph represents pulse ligand puncta that are not colocalised with chase ligand puncta. **c.** Graph represents chase ligand puncta that are colocalised with pulse ligand puncta. **d.** Graph represents chase ligand puncta that are not colocalised with pulse ligand puncta. **e.** Cumulative distribution function of colocalised and non-colocalised Pulse-ligand labelled puncta at the 24-hour time point. The two populations are significantly different from each other (Kolmogorov-Smirnov test, two-tailed, $p<0.0001$).

Next, the frequency distributions of pulse ligand puncta in figures 4.5.a and 4.5.b were compared using a cumulative distribution function (figure 4.5.e). This distribution indicates that low-intensity puncta are indeed more frequent in non-colocalising synapses than in colocalising synapses, which are more likely to display a greater intensity. This was probed using a two-tailed Kolmogorov-Smirnov test for difference, and the result conclusively indicated that the two populations are indeed distinct ($p<0.0001$).

While the two graphs of non-colocalising puncta populations (4.5.b and 4.5.d) are similar in some ways, they also display differences: 4.5.d has a much higher frequency peak, and much steeper slopes, while 4.5.b is more evenly spread. It is likely that these two graphs capture two separate populations of puncta undergoing different transformations. Figure 4.5.b represents a population of synapses containing solely 'old' PSD-95, and these synapses appear to be undergoing either pruning or stagnation as PSD-95 proteins that are being degraded are not being replaced with newly synthesised proteins. Indeed, a study by Cane et al. (2014) has shown that dendritic spines significantly reduce their PSD-95 content well before the actual pruning event. In this case, it could be expected that in preparation for pruning such synapses would cease to incorporate new PSD-95. These synapses could also be undergoing a transition into becoming 'silent' synapses, characterised by their lack of AMPA receptor expression and most likely lacking PSD-95 (Huang et al., 2015; Béı̈que et al., 2006), and are therefore reducing their protein content and slowing down protein turnover.

Figure 4.5.d, on the other hand, most likely represents ongoing synaptogenesis, as these synapses do not contain ‘old’ PSD-95 and are low in intensity. It is thus likely that these synapses have formed over the past 24 hours, and are in the process of enlarging their pool of PSD-95 (and other) proteins in the PSD. This would interestingly imply that newly formed synapses gradually build up PSD-95 levels as they mature, rather than importing the complete and final amount of PSD-95 allocated to that specific synapse by some predetermined mechanism. And alternative explanation is that these synapses have a much quicker turnover rate, and have simply broken down their entire contingent of ‘old’ PSD-95 and replaced it with ‘new’ PSD-95 over these 24 hours. In that case, one could argue that synapses could be split into two groups- those that have a slower rate of turnover of PSD-95 and also contain much more PSD-95 in total, and perhaps smaller synapses containing much fewer PSD-95 molecules that are turned over rapidly. To resolve this question one would have to use live imaging of neuronal cultures and observe protein turnover as it happens. However, with my method I am unable to rule out either one of these explanations, and perhaps both are correct to some extent. Nevertheless, my inclination is to attribute these result to synaptogenesis and conclude that chase-ligand labelled puncta that do not colocalise with the pulse ligand are most likely synapses that have been newly formed and therefore contain less PSD-95 at this stage. Indeed, Butko et al. (2012) found that newly-synthesised PSD-95 tends to be found preferentially at immature synapses, while mature synapses tend to contain older PSD-95 molecules.

4.3.2.4 Single-synapse analysis C- Ratios

In this section of the single-puncta analysis, I will focus solely on those synapses that contain both old and new PSD-95 molecules, i.e. synapses in which pulse and chase ligands colocalise. In the previous sections I have looked at the puncta labelled by on or the other ligand separately, but now I will investigate the relationship between the two ligands within these synapses.

Figure 4.6 is a frequency histogram of the ratio of pulse:chase ligand intensity. I obtained this data by working out the ratio of pulse to chase ligand intensity at individual synapses, and plotting the frequencies of these ratios. I find that the mean pulse:chase ligand ratio is 2.55 ± 0.051 (SEM), with a median ratio of 2.06. The mode is a ratio of 1.7, with 5.14%. The range of ratios is quite large, from 0.6 to more than 10, indicating a diverse synaptic population. Note that very few synapses have a pulse:chase ratio below 1, but since these are different fluorophores this does not necessarily mean that most of these synapses contain more old than new PSD-95. This graph may indicate that there is a high degree of heterogeneity with regards to PSD-95 turnover, as some synapses retain varying amounts of old PSD-95 and/or obtain newly synthesised PSD-95 at varying rates. However, such conclusions need to be treated with caution, since we do not know what the starting amount of old PSD-95 in these synapses was. While we can presume that these synapses were already present during the pulse incubation time period and are therefore at least ~30 hours old, they may at that point have been well-established and mature synapses with a full contingent of PSD-95 molecules in their PSD, or have been in the early stages of synaptogenesis and thus still have been recruiting additional PSD-95 molecules while establishing their PSDs. Indeed, this graph looks strikingly similar in its shape to the intensity frequency histogram of synapses at the 1-hour time point displayed in figure 4.4. This might imply that the PSD-95 turnover rate is the same in all synapses, but it is the starting amount of pulse-labelled PSD-95 that varies and thus causes the vast differences in ratios we see in figure 4.6.

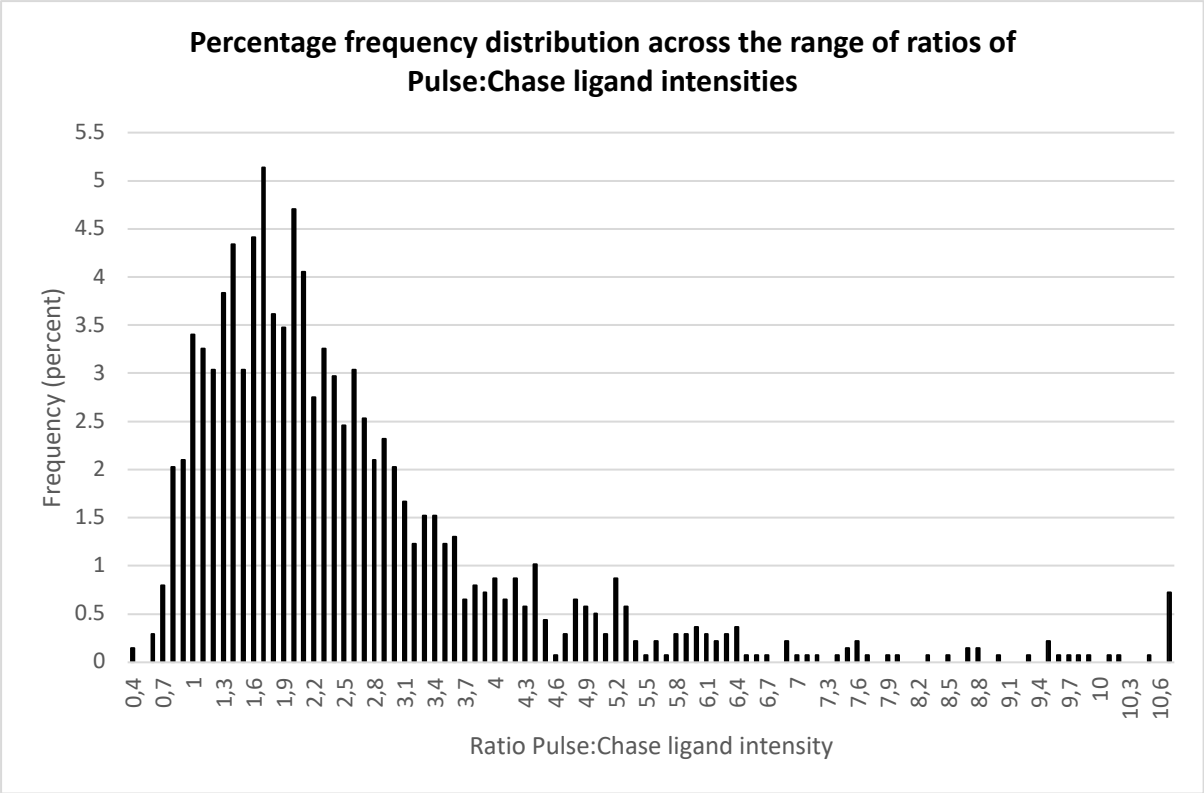

Figure 4.6. Frequency distribution histogram for pulse to chase ligand APFI ratios at colocalised synapses.

In the synaptic population in which pulse and chase ligand-labelled PSD-95-HaloTag molecules were colocalised, the ratio of pulse ligand fluorescence intensity to chase ligand fluorescence intensity was calculated for each individual synapse. This histogram represents the frequencies of all the pulse:chase ratios. Note that pulse and chase ligands carry different fluorophores, such that their intensities cannot be compared. This means that a 1:1 ratio of pulse to chase ligand (i.e. a ratio of 1) does not mean that the number of pulse-labelled PSD-95-HaloTag molecules is equal to the number of chase-labelled PSD-95-HaloTag molecules in that synapse. However, a punctum with a ratio of 2 contains twice as many pulse-labelled molecules relative to chase labelled molecules than a punctum with a ratio of 1. Note also the diverse spread of ratios, ranging from a ratio of 0.4 to above a ratio of 10. Mean ratio: 2.55 ± 0.051 (SEM), Median ratio: 2.06, Mode: 1.7 (5.14%).

However, there are differences between the two graphs- the modal puncta intensity in figure 4.4 having a frequency of 3.79% while the modal ratio in figure 4.6 has a frequency of 5.14% (note that the number of x-axis values is equal in the two graphs). This means that there are fewer low-intensity puncta at the start of the experiment than there are puncta with a low pulse:chase ligand ratio after 24 hours. There also appears to be a greater spread in the average pulse ligand puncta intensity at the 1-hour time point than spread of ratios. However, type 3 synapses do not contribute to the graph of ratios of type 2 synapses, while these synapses were present at the 1-hour time point and thus did contribute to the intensity distribution in figure 4.4. Thus,

we cannot make definitive statements about PSD-95 turnover rates from this data alone, but there does seem to be an indication that PSD-95 turnover differs between type 2 synapses. Over the entire synaptic population, however, we can definitively say that PSD-95 turnover does indeed differ. This is simply because out of the synaptic population that was present throughout the entire experiment (type 2 and type 3 synapses), type 3 synapses clearly experience no new PSD-95 synthesis, while type 2 synapses do.

I next decided to correlate pulse with chase ligand puncta intensity. I used a sample of twelve images to create the scatter plot depicted in figure 4.7.a. While there does appear to be a slight positive correlation, the R^2 value is quite low (0.16). To expand this analysis a further, I sorted puncta by pulse ligand intensity into percentiles, and then measured average chase ligand intensity in each of these percentiles. The results in figure 4.7.b show that there is a very strong positive correlation (R^2=0.96) between pulse ligand intensity percentile and average chase ligand intensity. When doing the opposite (plotting average pulse ligand intensity over the range of chase ligand percentiles, figure 4.7.c), the same strong correlation is observed (R^2=0.92). Overall, then, it appears that among synapses that contain both pulse and chase ligand-tagged PSD-95 molecules there is a very strong positive correlation between pulse and chase ligand intensity. In other words, the more of one ligand a synapse contains, the more of the other ligand it will contain as well.

While this does not sound surprising at first, it is actually not at all intuitive. Take a synapse with a low level of pulse ligand fluorescence intensity for instance. We might assume that such a synapse is immature, perhaps, as it may have had a small amount of PSD-95 within it while being pulse labelled. In this case, we would expect this synapse to recruit a large amount of new PSD-95 over the 24 hours of chase incubation, in order to bring its PSD up to a ‘regular’ level of PSD-95. In that case, we would expect synapses will little pulse ligand to express more chase ligand. Yet it is not what we see.

a.

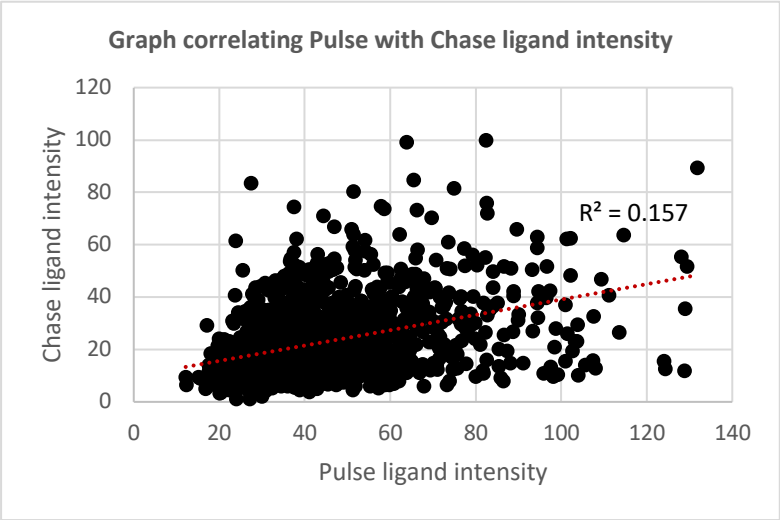

b.

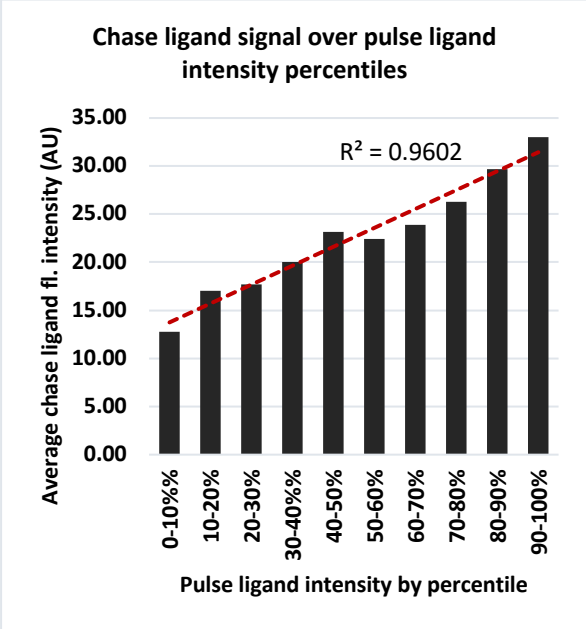

c.

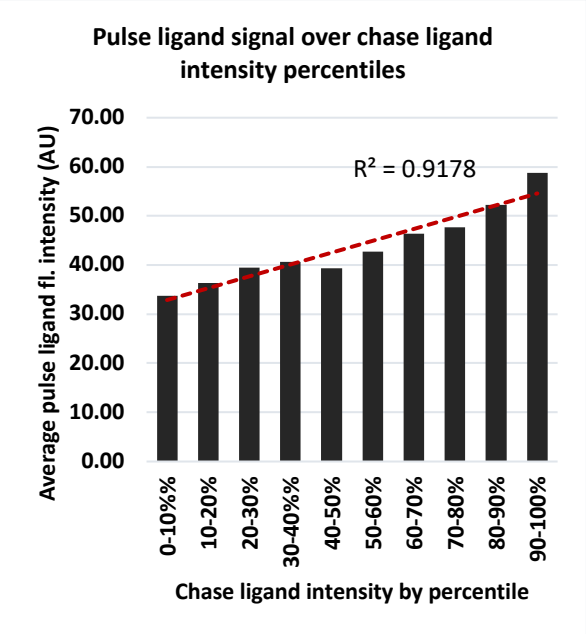

Figure 4.7 Correlation of pulse ligand intensity with chase ligand intensity at colocalised synaptic puncta.

a. The APFI of the pulse ligand was plotted against the APFI of the chase ligand at individual synapses in which the two ligands colocalise. There is a weak positive correlation, R^2=0.16. **b.** Colocalising synapses were sorted by their pulse ligand APFI (lowest to highest). For each ten percentile steps, average chase ligand APFI was calculated. There is a strong positive correlation, R^2=0.96. **c.** Colocalising synapses were sorted by their chase ligand APFI (lowest to highest). For each ten percentile steps, average pulse ligand APFI was calculated. There is a strong positive correlation, R^2=0.92.

The other scenario is the opposite, where a synapse expresses a high level of pulse ligand. In that case we might presume that this synapse was large and mature at the start of the experiment during pulse labelling, and thus a large proportion of that pulse-labelled old PSD-95 is still left after 24 hours of chase labelling. However, if this synapse already had a full complement of PSD-95 in its PSD, and was at this stage merely turning PSD-95 over at a 'normal' pace, why does it also recruit a high level of new PSD-95?

While the results do not give an answer to these riddles, we can try to explain these phenomena nonetheless. One possible explanation is that synapses vary vastly both in the size of their overall PSD-95 pool as well as their rate of PSD-95 turnover. Smaller synapses may thus express a smaller overall amount of PSD-95, and only turn over a small part of these proteins. Larger synapses may express a lot of PSD-95 and have high rates of turnover.

Indeed, a study by Gray et al. (2006) has shown that PSD-95 stability at synapses is activity- and size-dependent, with more active and larger synapses recruiting more PSD-95 molecules and inactive synapses losing them. Thus, PSD-95 levels in a given synapse may determine synaptic strength and size (Ehrlich and Malinow, 2004). There appears to be a causal link between synaptic size and PSD-95 turnover rates- highly active synapses may require a large amount of molecular machinery and therefore have large, dense PSDs.

Large synapses have also been shown to retain PSD-95 for longer time periods than smaller synapses (Gray et al., 2006), which would explain the greater amount of old PSD-95 in colocalised synapses. Among type 2 synapses, then, greater amounts of PSD-95 appear to correlate with greater rates of PSD-95 turnover, likely linked to greater activity levels.

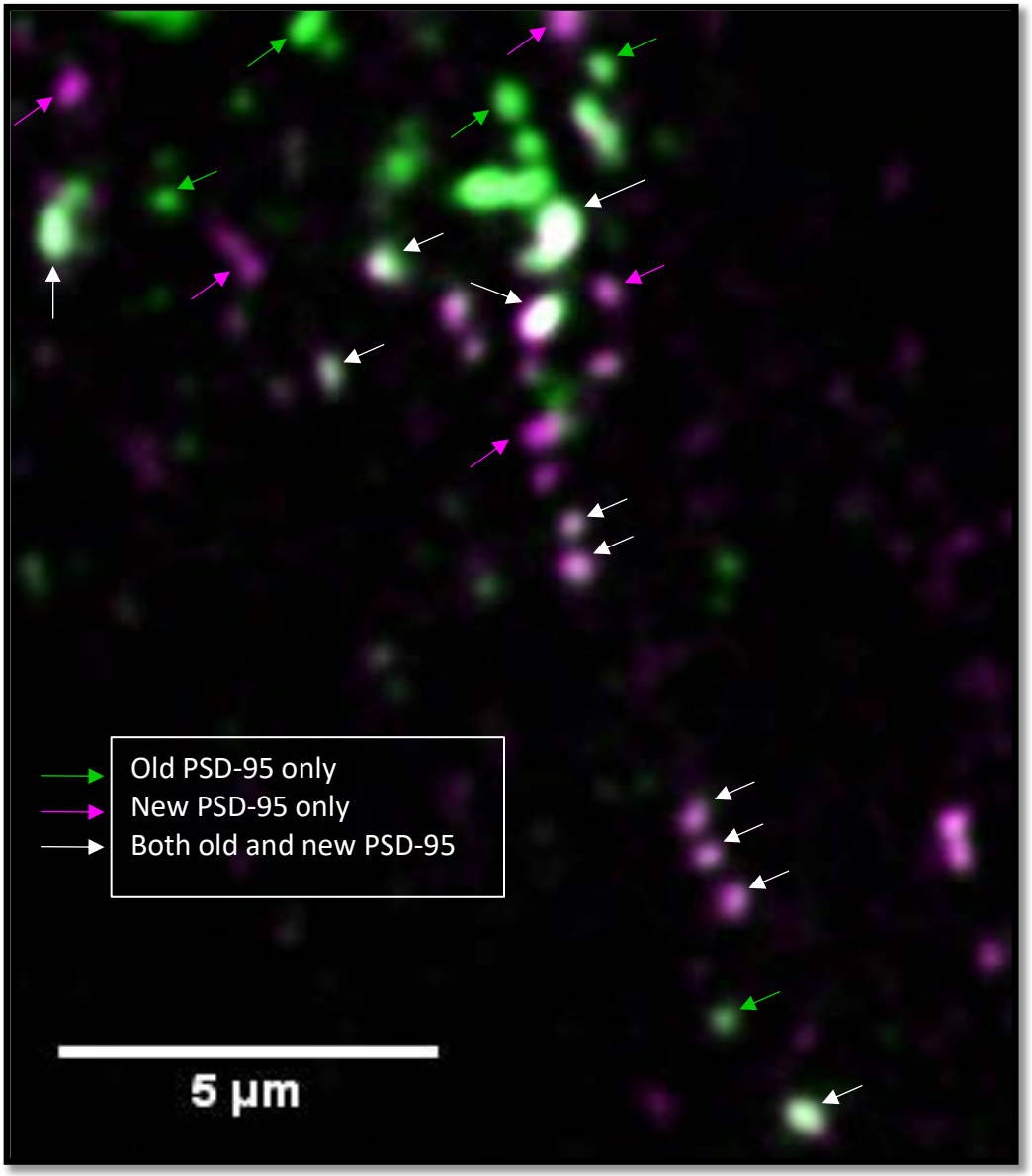

Figure 4.8. Synapses are very heterogeneous in their expression level of old and new PSD-95 molecules.

An example image from a hippocampal primary culture on DIV16, taken after 16 hours of pulse ligand (R110Direct, 50nM) incubation followed by 24 hours of chase-ligand (TMR, 500nM) incubation. The pulse ligand thus labels 'old' PSD-95 proteins and the chase ligand labels newly-synthesised PSD-95 proteins. The pulse ligand is marked in green and the chase ligand in magenta, with white indicating areas of overlap. Puncta can be categorised by the presence of one or both ligands. Note the high degree of variability in puncta labelling, particularly among puncta labelled by both ligands.

4.3.3 Classifying synaptic types and summary

From the single-synapse analysis performed in 4.3.2, it is evident that the synaptic population is very diverse. While this diversity itself pertains to multiple different synaptic properties, such as old to new PSD-95 expression ratios and PSD-95 turnover, it is very difficult to pin down these properties and their driving factors. Nevertheless, I will attempt to categorise synapses at least rudimentarily according to some of these traits.

Figure 4.8 is a showcased example of what many confocal images taken after 24 hours of pulse-chase labelling look like. The first thing that jumps out is the sheer diversity of the synaptic puncta. These synaptic puncta vary greatly in terms of size, shape, fluorescence intensity and, last but not least, the degree to which they express both ‘old’ and/or ‘new’ PSD-95. Simply by qualitatively appraising this image we can see many examples of synapses that express only old PSD-95 (pulse label only, green), only new PSD-95 (chase label only, magenta), and synapses in which both old and new PSD-95 are found (colocalisation, white). The other aspect, which I discussed in the previous section (chapter 4.3.2.4), is that we can clearly see that colocalised synapses vary greatly in the extent to which they contain old or new PSD-95, i.e. the ratio of the two labels. While categorising these colocalising synapses by their ratio of pulse to chase ligand content is complicated by the lack of prerequisite data such as starting intensity, we can certainly attempt to categorise synapses according to the aforementioned binary factors: the presence or absence of one or the other ligand.

In the table in figure 4.9 I give an overview of the three types of synapses I have observed. Type 1 synapses are made up of puncta containing only new PSD-95, i.e. PSD-95 labelled by the chase (TMR) ligand. Type 2 synapses contain a mixture of both old and new PSD-95, meaning both ligands colocalise in these synapses. Finally, type 3 synapses contain solely old PSD-95, labelled by the pulse (R110) ligand. In my further analysis I will be referring to synapses according to their type when I discuss the presence or absence of ligands and the category they thus fall into.

According to my results, type 1 synapses synthesise less new PSD-95 over the 24-hour time period between DIV15 and DIV16 than type 2 (colocalised) synapses, and there are overall fewer type 1 synapses than type 2 synapses. The population of type 1 synapses also yields a frequency histogram that is heavily skewed towards a low puncta intensity (figure 4.5.d), making this the most homogenous of the synapse populations in terms of PSD-95 expression level. There are two possible explanations

	Type 1	Type 2	Type 3
Pulse signal	Absent	Present	Present
Chase signal	Present	Present	Absent
Synaptic phenotype		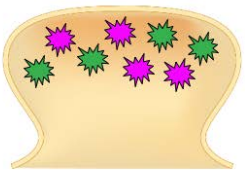	

Figure 4.9. Synapses can be categorised according to the presence of one or both HaloTag ligands.

This table gives an overview of the three proposed types of synapses. **Type 1** synapses contain only newly-synthesised PSD-95 molecules that are labelled with the chase (TMR) ligand. These synapses are proposed to be immature and newly formed by synaptogenesis. **Type 3** synapses contain only previously-present, 'old' PSD-95 molecules that are labelled with the pulse (R110) ligand. These synapses are proposed to be inactive or stagnant, and are therefore not incorporating any newly-synthesised PSD-95 molecules into their PSD. **Type 2** synapses contain both pulse and chase ligand-labelled PSD-95 molecules. These synapses are proposed to be mature, active synapses that are continuously turning over PSD-95 molecules.

for type 1 synapse: first, they come about when synaptogenesis results in new synapses forming, and these synapses exclusively contain newly synthesised PSD-95. Second, these synapses could have been present before the chase incubation phase and therefore contained old, pulse-labelled PSD-95, but all of this PSD-95 was degraded or cycled out of the synapse and replaced with newly-synthesised PSD-95. Using my HaloTag methodology without live-cell imaging it is impossible to rule out either of these explanations (and indeed both explanations may be partially correct). However, that fact that type 1 synapses have lower levels of PSD-95 expression and are fairly homogenous in this respect does make the first explanation more likely- that

these are predominantly immature synapses in the process of recruiting new PSD-95 and establishing their PSD. Furthermore, a study by Butko et al. (2012) has demonstrated that new PSD-95 molecules tend to be found in immature synapses, whereas older PSD-95 molecules are preferentially found at mature spines. It seems that the most likely explanation, then, is that type 1 synapses are predominantly made up of immature synapses that have recently been formed.

Type 3 synapses are very similar to type 1 synapses in multiple ways, but do have their differences. Like type 1 synapses, type 3 synapses contain less PSD-95 than type 2 (colocalised) synapses overall and also less 'old' PSD-95 more specifically. This histogram is also skewed towards a lower puncta intensity, but to a less extreme degree than is the case in type 1 synapses (the slopes are less steep and the frequency peak is lower- see figure 4.5.b). There is really only a single explanation for the presence of type 3 synapses, and that is that these are synapses that were present during the pulse labelling phase, but that did not synthesise any new PSD-95 during the subsequent 24-hour chase incubation phase. The question, rather, is why did these synapses not synthesise any new PSD-95? The answer will be hard to pin down, but and again there are two possibilities. As mentioned above in chapter 4.3.2.3, the first possibility is that these synapses are in the process of being degraded (pruned), and hence their pool of PSD-95 is not being replenished but rather broken down (see Cane et al., 2014). The other explanation is that these synapses are not very active, and thus not recruiting new PSD-95 but rather losing PSD-95 molecules. It is possible that synapses in such a state might not only reduce the total amount of PSD-95 (and probably also other proteins) they express, but also lower the rate of turnover of the proteins that they do retain.

It is of interest to note that between DIV15 and DIV16 type 1 and type 3 synapses are equally common, both groups making up just under 30% of the total synaptic population (figure 4.3). Interestingly, therefore, the majority of synapses contains only a single type of ligand and not both.

Finally, the largest single group of synapses is made up of type 2 synapses- those containing both old and new PSD-95. Synapses in this group contain the greatest quantity of PSD-95 overall and also of each ligand separately. This means that these

are also the synapses with the greatest rate of PSD-95 synthesis. This group makes up 43% of the entire synaptic population, and the frequency histograms of these puncta indicate that this is a very heterogeneous collection of synapses with regards to PSD-95 expression levels. Both pulse and chase histograms of type 2 synapses look very similar, with a wide intensity spread and a very low frequency peak below 4% (figure 4.5). It is likely that type 2 synapses are relatively stable synapses, not too immature nor in decline, as they have been present for more than 24 hours and have a regular turnover of PSD-95. However, as revealed in chapter 4.3.2, type 2 synapses can be further broken down according to their pulse:chase ligand intensity ratios. When this analysis is performed, it reveals a very diverse population of synapses indeed. Nevertheless, the general trend appears to be that the more of one ligand is present, the more of the other will be present as well. It thus appears that overall, the synapses with the greatest rate of turnover of PSD-95 (as far as can be determined) are also those synapses that contain the largest amount of total PSD-95. One explanation of this phenomena is that these synapses are the most active and have therefore established a strong synaptic connection, which in turn results in a high rate of PSD-95 turnover. As we know that NMDAR activity enhances the recruitment of components of the protein synthesis and degradation machinery to individual dendritic spines (Bingol and Schuman, 2006; Ostroff et al., 2002), it could be postulated that this may lead to an enhanced protein turnover at these synapses. Indeed, Hruska et al. (2015) found that synaptic activity enhances PSD-95 turnover. The fact that these synapses also contain the greatest amount of both old and new PSD-95 supports the assumption that these synapses are particularly strong and stable (see Cane et al., 2014). Thus, type 2 synapses are likely to be experiencing the greatest amount of NMDAR activation, which may in turn lead to enhanced rates of PSD-95 turnover as well as greater synaptic stability.

4.4 Drug treatment groups

4.4.1 Introduction to drug treatment groups

In this section I will provide the data collected over the course of this study that pertains to PSD-95 turnover in primary neurons treated with a variety of chemical agents. Here, I will briefly explain the rationale behind the inclusion of each of the chemicals used.

The first chemical modulators I wanted to include in this study were tetrodotoxin (TTX) and bicuculline (BCC), due to their opposing effects on neuronal activity and the conflicting reports in the literature regarding their effect on PSD-95 expression levels and turnover. Both of these drugs have frequently been used to modulate the activity of excitatory neurons, either by directly blocking it (TTX) or by indirectly enhancing it via a blockade of inhibitory GABA-ergic neurons (BCC). TTX is a highly potent antagonist of voltage-gated sodium channels in excitatory neurons (Bane et al., 2014). BCC acts as an antagonist of $GABA_A$ receptors, thereby blocking inhibitory GABAergic transmission and increasing the activity of excitatory neurons (Ehlers, 2003). While the mechanisms of action of these two drugs are well known, the effects of enhanced or blocked neuronal activity on PSD-95 expression at synapses and on PSD-95 turnover are less clearly defined. A study by Ehlers (2003) concluded that enhanced activity results in an increase in PSD-95 levels at synapses, while blocking activity reduces PSD-95 levels at synapses. The study by Ehlers also concluded that PSD-95 turnover at a whole-cell level was unaffected by either treatment. In contrast, a number of studies demonstrated the opposite effect, namely that activity blockade increases PSD-95 levels at synapses and that enhancing neuronal activity reduces synaptic PSD-95 (Kim et al., 2007; Noritake et al., 2009; El-Husseini et al., 2002; Colledge et al., 2003). In contrast to the studies by Ehlers (2003) and Kim et al. (2007), who found no change, Colledge et al. (2003) found that enhanced neuronal activity led to a loss of PSD-95 at a whole-cell level. Butko et al. (2012) instead found that enhanced neuronal activity by bicuculline treatment caused an increase in PSD-95 synthesis. Likewise, while the studies by Ehlers (2003) and Noritake et al. (2009) found PSD-95 synthesis to be unaffected by TTX treatment, a study by Okabe et al. (1999) revealed reduced dynamic turnover of PSD-95 clusters. The overall picture that emerges of the

effect of activity modulation on PSD-95 expression at synapses and PSD-95 turnover, then, is not very clear and warrants further investigation.

Brain-derived neurotrophic factor (BDNF) is a chemical agent linked to many different neuronal functions, ranging from neuronal survival and maturation to dendritic and axonal growth and synaptogenesis. Furthermore, it is also linked to neuronal activity, but rather than affecting neuronal activation it is released at glutamatergic synapses in response to activity, affecting AMPA receptor currents and NMDAR-dependent long-term potentiation (Yoshii and Constantine-Paton, 2007). TrkB is the receptor to which BDNF binds, and NMDAR activation can lead to BDNF-TrkB signalling that in turn recruits PSD-95 to synapses, neuron-wide, in a synthesis-independent manner (Yoshii and Constantine-Paton, 2007). Other studies, too, have shown that BDNF causes PSD-95 to be trafficked to synapses, markedly enhancing synaptic PSD-95 level (Hu et al., 2011). Finally, a study by Butko et al. (2012) appeared to indicate that 3-hour BDNF treatment of DIV14 cultured neurons enhanced PSD-95 synthesis. Together, these results made BDNF an interesting treatment candidate to evaluate the effect on synaptic PSD-95 turnover using my HaloTag method.

Ketamine is a chemical agent that has only fairly recently risen to prominence in neuroscience, when it was discovered that, if administered at low concentrations, it is extremely quick and effective at treating patients with otherwise treatment-resistant major depressive disorder (MDD) (Zarate et al., 2006). Interestingly, it has been established that patients with MDD display reduced levels of PSD-95 protein in certain brain regions (Feyissa et al., 2009). Furthermore, a number of studies have shown that low-dose (but not high-dose) ketamine treatment of rodents causes synaptic PSD-95 levels to rise (Li et al., 2010; Choi et al., 2015; Browne & Lucki, 2013). I was thus intrigued to determine whether I would be able to discover a similar effect on synaptic PSD-95 levels and turnover in primary cultures of hippocampal neurons.

Having chosen the above chemicals for my study due to their roles in modulating synapses and PSD-95 levels at synapses, but with questionable effect on the turnover of PSD-95, I decided to include two classes of drugs that would surely affect the synthesis and degradation of PSD-95. These two drugs groups were protein synthesis inhibitors and protein degradation inhibitors. Even if these drugs were perhaps less

exciting from a biological perspective since their effect and mode of action are well known, I nonetheless felt compelled to include them since it would give me the opportunity to use my method to measure assured changes in PSD-95 synthesis and degradation. I decided to include two drugs from each of these two classes, as these drugs are frequently used and well established, and also to act as controls for each other and allow for comparisons between results. For the inhibitors of protein degradation I decided to use the drugs lactacystin and MG132, whereas I opted for anisomycin and cycloheximide as the protein synthesis blockers.

Lactacystin and MG132 are both known to block protein degradation, with lactacystin being a highly potent and selective proteasome inhibitor, while MG132 is known to inhibit both the proteasome and calpains (Hakim et al., 2016). The ubiquitin-proteasome system (UPS) has been widely shown to be the major route by which PSD-95 is degraded, and blocking the proteasome with lactacystin or MG132 prevents PSD-95 degradation (Tsai et al., 2012; Colledge et al., 2003). Interestingly, lactacystin injections into the hippocampus of live mice have been demonstrated to cause full retrograde amnesia (Lopez-Salon et al., 2001), implicating the UPS and protein degradation as playing a role in memory formation. While lactacystin and MG132 are commonly used in studies that wish to modulate synaptic protein turnover (e.g. Ehlers, 2003), a recent study by Hakim et al. (2016) is of particular interest as it found that blocking the proteasome with lactacystin did not lead to an increase in synaptic PSD-95 levels, but rather, caused a profound suppression of PSD-95 synthesis. My goal in this study was to separately apply both lactacystin and MG132, measure the effects of these agents on synaptic PSD-95 turnover and investigate the phenomenon observed by Hakim et al. (2016).

The final set of chemicals used in my study consists of the protein synthesis inhibitors anisomycin and cycloheximide. Cycloheximide inhibits the elongation step during the translation of proteins (Ennis and Lubin, 1964), whereas anisomycin acts on peptidyl transferase and prevents the release of nascent peptides from polyribosomes (Grollman, 1967). Both substances have been very widely employed in the study of synaptic protein synthesis (Todd et al., 2003; Noritake et al., 2009; Yoshii and Constantine-Paton, 2007), and have profound effects on memory retention in mammals (Tai and Schuman, 2008). Anisomycin, particularly, has been widely used

to study memory loss, as injecting it into hippocampal brain regions can disrupt the expression of fear memories (Frankland et al., 2006). Interestingly, lactacystin co-injection can rescue anisomycin-induced fear learning (Lee et al., 2008). I thus decided to utilise the protein synthesis inhibitors anisomycin and cycloheximide as mechanistic opposites to the proteasome inhibitors lactacystin and MG132, and measure the effects on PSD-95 turnover that these drugs would have.

Overall, I selected the chemical modulators that I wished to use for this study based upon two criteria: first, whether their effect was likely to affect the turnover of PSD-95, allowing me to apply my method to a scenario in which turnover is altered compared to untreated controls; and second, whether their effect was likely to address a biologically interesting question. In the next section, I will reveal the results from these experiments and discuss their implications.

4.4.2.1 TTX and BCC: bulk analysis

The first set of results that I will evaluate for the TTX- and BCC-treated cultures is the bulk data, and thereafter I will move on to the single-synapse data. In this first section, I will take the entire population of pulse or chase ligand labelled synapses together, and compare their results to the untreated control group.

Figure 4.10.a shows the average intensity of pulse-ligand (R110) puncta in hippocampal primary neurons at DIV16 after having been treated with TTX (1μM) for 24 hours, compared with untreated controls. Figure 4.10.b depicts the same results for neurons treated with BCC (40μM). Average pulse ligand intensity at the 1-hour time point is 65.97 ± 1.69 AU, and this goes down over the 24-hour chase period to 41.44 ± 0.85 AU in untreated controls. In TTX treated neurons, the pulse ligand intensity decreases to 46.36 ± 1.76 AU over 24 hours, and in BCC treated neurons to 48.92 ± 3.51 AU. While the difference in pulse ligand intensity at the 24-hour time point compare to untreated controls is statistically significant in the TTX-treated group (Welch's t-test, $p=0.034$), the difference between BCC-treated neurons and controls is not significant ($p=0.087$).

Figure 4.10.c and figure 4.10.d represent the bulk chase ligand (TMR) intensity after 24 hours of chase incubation. From figure 4.10.c we can see that TTX treatment causes average chase puncta intensity to be only very slightly and insignificantly (Welch's t-test, p=0.46) higher (31.61 ± 2.18 AU) than in untreated controls (29.63 ± 1.42 AU). In figure 4.10.d, we see that BCC similarly has no significant (p=0.099) effect on average chase ligand puncta intensity (32.41 ± 0.49 AU).

When looking at synaptic puncta number, a very similar result is obtained. In the untreated control group, pulse ligand puncta number decreases over the 24-hour chase period from 419.35 ± 50.05 to 189.15 ± 26.64 puncta per image. In the TTX treatment group, pulse ligand puncta number decreases to 284.00 ± 65.53 puncta over 24 hours (figure 4.11.a), and in the BCC treatment group it decreases to 243.85 ± 33.09 puncta over 24 hours (figure 4.11.b). Neither result was significantly different to the control group (Welch's t-test, TTX: p=0.22, BCC: p=0.23).

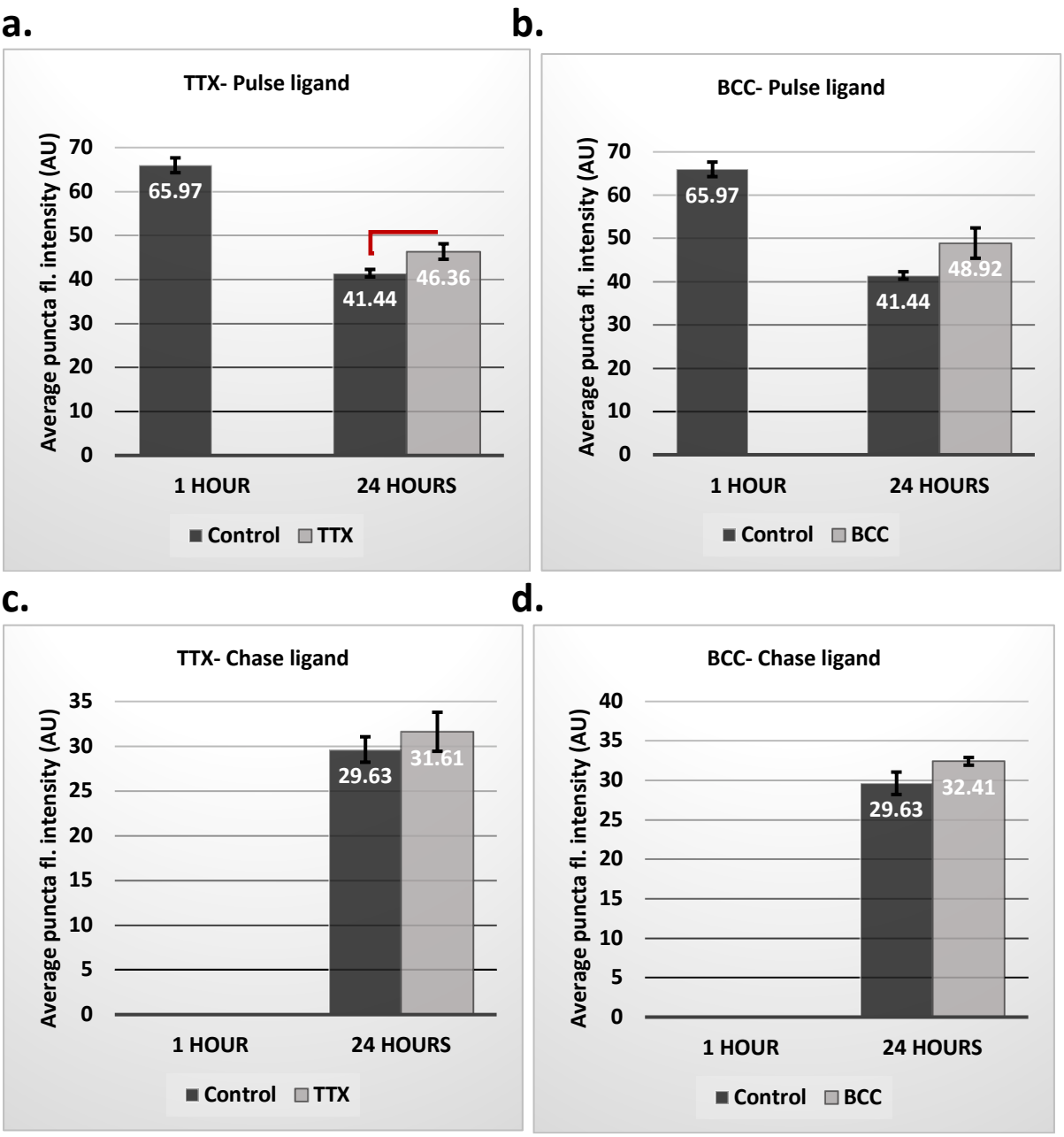

Figure 4.10. The effects of Tetrodotoxin and Bicuculline on PSD-95 puncta intensities. Hippocampal neuronal primary cultures from PSD-95$^{HaloTag/HaloTag}$ mice were grown on glass coverslips and on DIV14 they were labelled with the R110Direct HaloTag ligand (50nM, 16h). On DIV15 the TMR ligand was added to the cultures at 500nM for 1 hour and 24 hours, alongside either tetrodotoxin (TTX) at 1µM or bicuculline (BCC) at 40µM. Coverslips were imaged on the LSM510, and puncta detected using the Imaris software. Average puncta fluorescence intensity per image (APFI) was then calculated. This was performed across 8 different cultures (N=8), with the graphs here presenting the mean values across these eight cultures. **a.** Graph of the average R110 pulse ligand puncta fluorescence intensity following TTX treatment. APFI is significantly higher after 24 hours in the TTX group than in untreated controls (Welch's t-test, p=0.034). **b.** Graph of the average R110 pulse ligand puncta intensity following BCC treatment. APFI is not significantly higher after 24 hours in the BCC group than in untreated controls (Welch's t-test, p=0.087). **c.** Graph of the average TMR chase ligand puncta fluorescence intensity following TTX treatment. The difference between the TTX group

and untreated controls is not significant (Welch's t-test, p=0.46). **d.** Graph of the average TMR chase ligand puncta fluorescence intensity following BCC treatment. The difference between the BCC group and untreated controls is not significant (Welch's t-test, p=0.099).

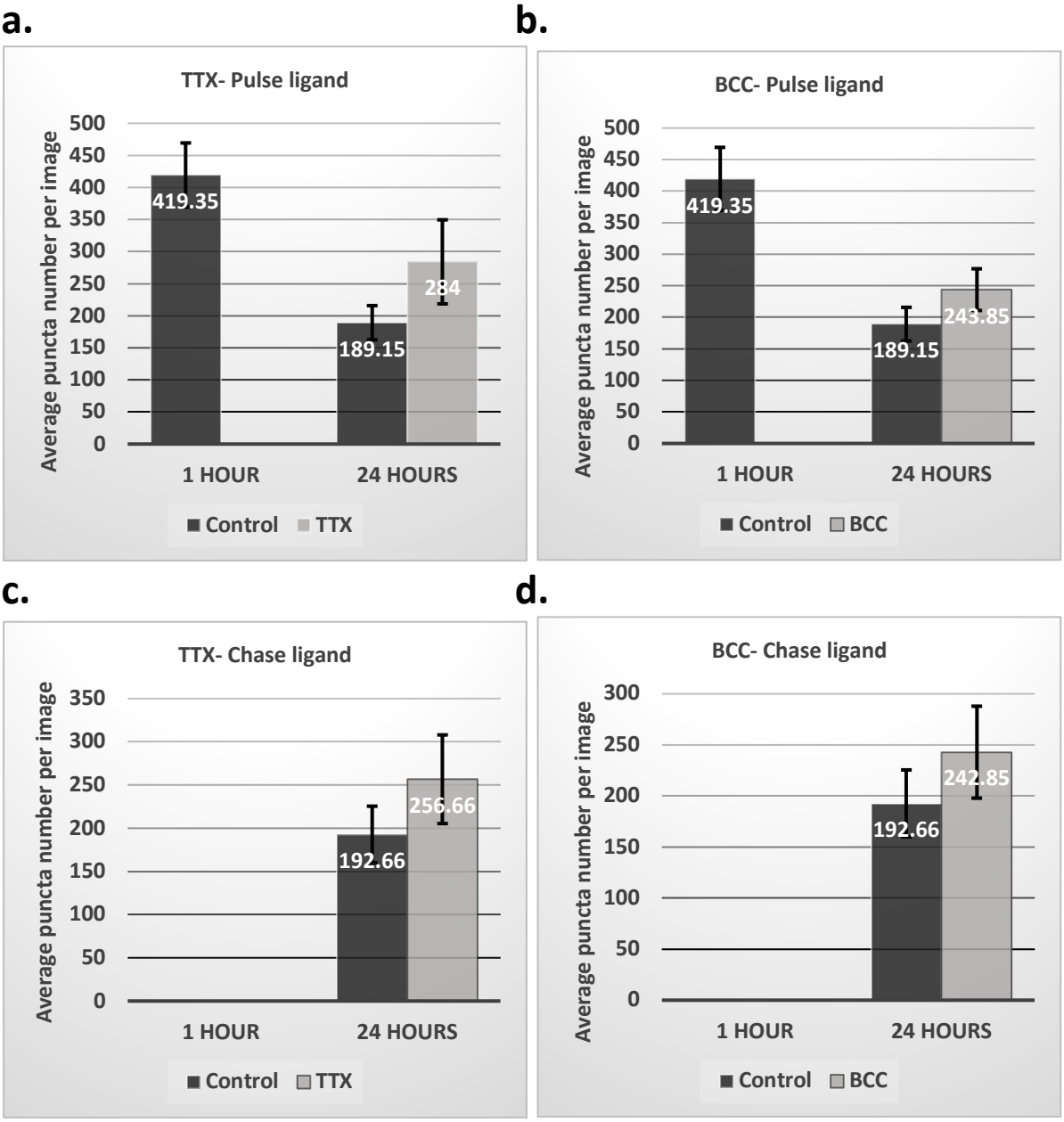

Figure 4.11. The effects of Tetrodotoxin and Bicuculline on PSD-95 puncta numbers.
As in figure 4.10, hippocampal neuronal primary cultures from PSD-95$^{HaloTag/HaloTag}$ mice were grown for 14 days in vitro, and thereafter pulse-chase experiments performed using the R110Direct and TMR HaloTag ligands. Tetrodotoxin (TTX) at 1µM or bicuculline (BCC) at 40µM were added alongside the chase ligand for 1 or 24 hours. The graphs here present the mean values across eight cultures (N=8). **a.** Graph of the average R110 pulse ligand puncta number following TTX treatment. The number is not significantly higher after 24 hours in the TTX group than in untreated controls (Welch's t-test, p=0.22). **b.** Graph of the average R110 pulse ligand puncta number following BCC treatment. The number is not significantly higher after 24 hours in the BCC group than in untreated controls (Welch's t-test, p=0.23). **c.** Graph of the

average TMR chase ligand puncta number following TTX treatment. The difference between the TTX group and untreated controls is not significant (Welch's t-test, p=0.32). **d.** Graph of the average TMR chase ligand puncta number following BCC treatment. The difference between the BCC group and untreated controls is not significant (Welch's t-test, p=0.39).

Similarly, chase ligand puncta number per image is only insignificantly different in both TTX- and BCC-treated groups when compared to untreated controls (Welch's t-test, TTX: p=0.32, BCC: p=0.39). While untreated controls had on average 192.66 ± 32.83 chase-ligand puncta per image, images from the TTX-treated group contained an average of 256.66 ± 51.32 puncta (figure 4.11.c) and images from the BCC-treated group contained an average of 242.85 ± 45.04 puncta (figure 4.11.d).

It is therefore difficult to tell from the results whether TTX treatment has an effect on bulk PSD-95 turnover. The only result that was significantly different from untreated controls was the average synapse intensity of the pulse ligand after 24 hours of TTX treatment (figure 4.10.a), with all other results being insignificantly different from controls. While it is difficult to interpret this lone significant result, it is possible that this indicates that a blockade of synaptic signalling may reduce the degradation rate of synaptic PSD-95, which would indicate an overall increase in PSD-95 levels at synapses in the light of the result that synthesis rates remain unchanged. This result would match some of the aforementioned results in the literature that indicate that activity blockade causes an enrichment of PSD-95 at the synapse. It is possible, then, that in response to reduced neuronal firing the degradation of PSD-95 is lowered while synthesis is retained constant, thereby increasing synaptic PSD-95 levels and thus potentially increasing the clustering of signalling receptor complexes at the postsynaptic membrane. Future studies could explore this result further by investigating the surface expression levels of AMPA and NMDA receptor complexes following TTX application, for instance.

On the other hand, bicuculline treatment did not have a measurable impact upon PSD-95 expression levels at synapses, and synaptic puncta numbers were unaffected by both drugs.

4.4.2.2 TTX and BCC: single-synapse analysis

As in chapter 4.3.2.2, I will first analyse the single-synapse results by splitting synapses up into colocalised and non-colocalised groups. However, having categorised synapses into three types in chapter 4.3.3, I will be using these categories during my analysis here. Type 1 synapses are made up of puncta containing only new (chase-labelled) PSD-95. Type 2 synapses contain a mixture of both old and new PSD-95. Type 3 synapses contain only old (pulse-labelled) PSD-95.

Looking at figure 4.12.a we see that in type 2 synapses, the average puncta fluorescence intensity after 24 hours of chase-ligand incubation is 45.13 ± 0.93 AU in untreated controls, while it is 50.35 ± 2.41 AU in TTX-treated cultures. This difference is not statistically significant (Welch's t-test, p=0.079). In type 3 synapses (figure 4.12.b), the average puncta fluorescence intensity at the same time point is markedly lower, 34.79 ± 0.80 AU for controls and 38.64 ± 1.56 AU following TTX treatment. Again, the difference is not significant (p=0.055). Next, I compare the average puncta fluorescence intensity (APFI) of type 2 with type 3 synapses within the TTX-treated group only (figure 4.12.c). Type 2 synapses (50.35 ± 2.41 AU) have a significantly greater APFI than type 3 synapses (38.64 ± 1.56 AU) (p=0.0021). The results are, therefore, very similar to untreated controls. Neither type 2 nor type 3 synapses differ in their APFI from controls, and as in the control group (figure 4.2.a), type 2 synapses are significantly more fluorescent than type 3 synapses.

We next look at the chase ligand, and evaluate the effect of TTX treatment on the chase ligand APFI in type 2 and type 1 synapses. In figure 4.12.d we see that the chase ligand APFI is essentially the same in the TTX-treated group as in the control group for type 2 synapses (35.17 ± 2.56 AU in the TTX group, 34.88 ± 1.91 AU in the control group) (Welch's t-test, p=0.93). Similarly, the chase ligand APFI in type 1 synapses treated with TTX does not differ from untreated controls (about 22 AU, figure 4.12.e) (p=0.71). Finally, the APFI of type 2 (35.17 ± 2.56 AU) and type 1 (21.87 ± 1.44 AU) synapses treated with TTX differs significantly (p=0.0013) (figure 4.12.f), like in the control group.

a.

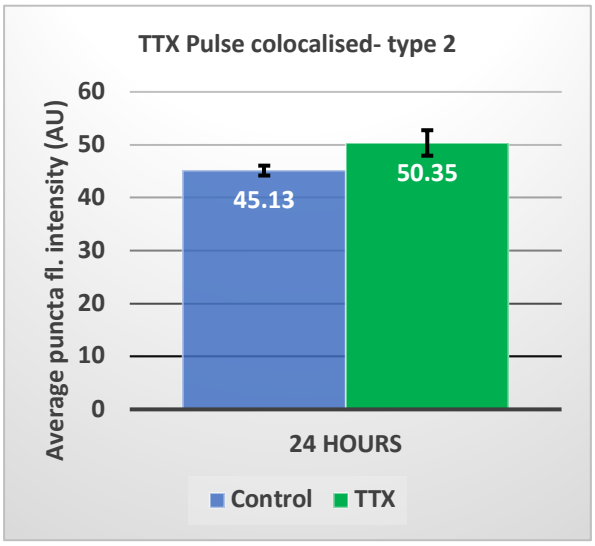
TTX Pulse colocalised- type 2
Average puncta fl. intensity (AU)
60
50
40
30
20
10
0
45.13
50.35
24 HOURS
Control
TTX

b.

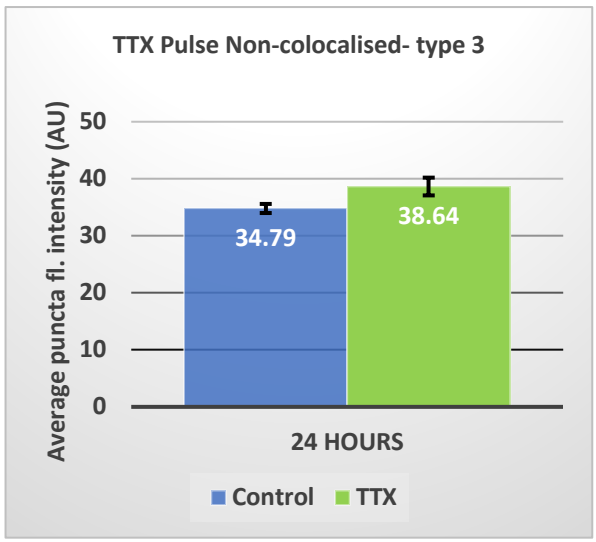
TTX Pulse Non-colocalised- type 3
Average puncta fl. intensity (AU)
50
40
30
20
10
0
34.79
38.64
24 HOURS
Control
TTX

c.

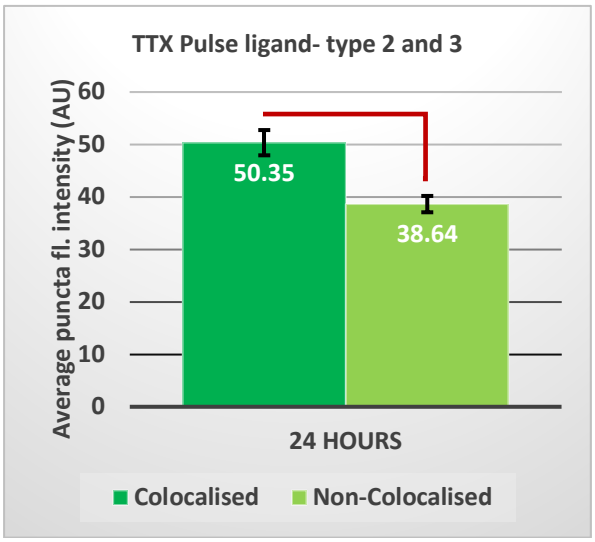
TTX Pulse ligand- type 2 and 3
Average puncta fl. intensity (AU)
60
50
40
30
20
10
0
50.35
38.64
24 HOURS
Colocalised
Non-Colocalised

d.

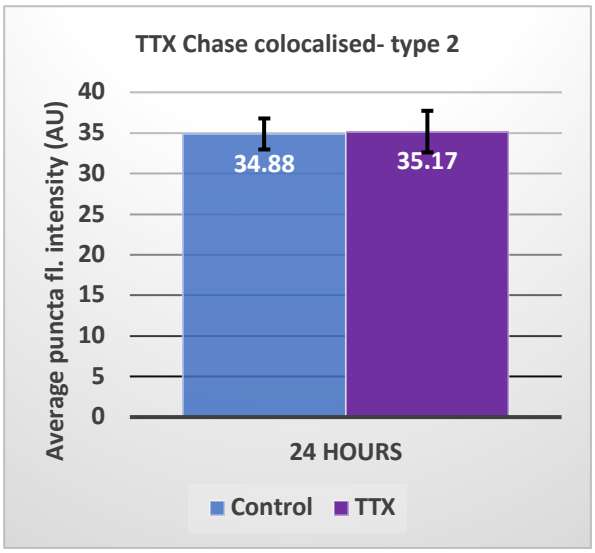
TTX Chase colocalised- type 2
Average puncta fl. intensity (AU)
40
35
30
25
20
15
10
5
0
34.88
35.17
24 HOURS
Control
TTX

e.

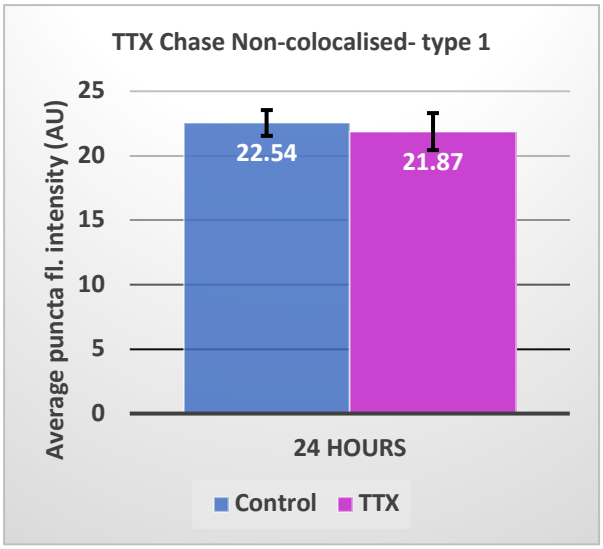
TTX Chase Non-colocalised- type 1
Average puncta fl. intensity (AU)
25
20
15
10
5
0
22.54
21.87
24 HOURS
Control
TTX

f.

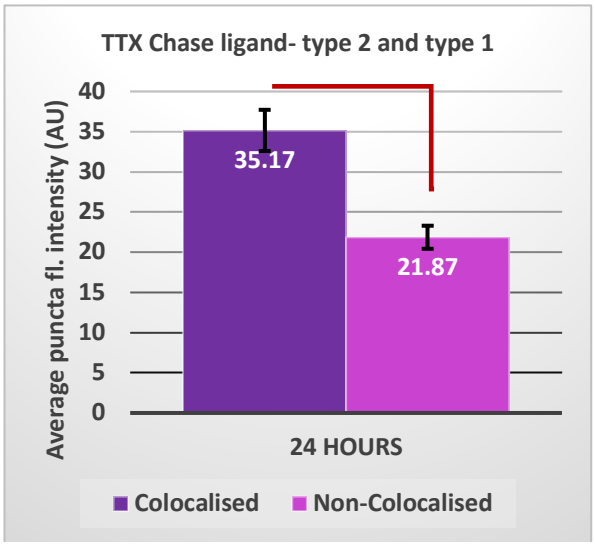
TTX Chase ligand- type 2 and type 1
Average puncta fl. intensity (AU)
40
35
30
25
20
15
10
5
0
35.17
21.87
24 HOURS
Colocalised
Non-Colocalised

Figure 4.12. The effect of tetrodotoxin on PSD-95 average puncta intensity at synaptic types. Average puncta fluorescence intensity (APFI) per image was calculated for pulse and chase ligand labelled synaptic puncta in type 1, type 2 and type 3 synapses separately. Images were taken after 24 hours of pulse-chase treatment with 50nM R110Direct ligand (pulse) and 500nM TMR ligand (chase) in hippocampal primary cultures from PSD-95$^{HaloTag/HaloTag}$ mice on DIV16. TTX (1µM) was applied for 24 hours together with the chase ligand between DIV15 and DIV16. The graphs here present the mean values across eight cultures (N=8). **a.** Pulse ligand (R110Direct) APFI per image in synapses where pulse and chase ligands colocalise (type 2). The difference between the TTX group and untreated controls is not statistically significant (Welch's t-test, p=0.079). **b.** Pulse ligand (R110Direct) APFI per image in synapses where pulse and chase ligands do not colocalise (type 3). The difference between the TTX group and untreated controls is not statistically significant (Welch's t-test, p=0.055). **c.** Comparison of pulse ligand APFI per image in type 2 synapses and type 3 synapses following TTX treatment. The difference between the two groups is statistically significant (Welch's t-test, p=0.0021). **d.** Chase ligand (TMR) APFI per image in synapses where pulse and chase ligands colocalise (type 2). The difference between the TTX group and untreated controls is not statistically significant (Welch's t-test, p=0.93). **e.** Chase ligand (TMR) APFI per image in synapses where pulse and chase ligands do not colocalise (type 1). The difference between the TTX group and untreated controls is not statistically significant (Welch's t-test, p=0.71). **f.** Comparison of chase ligand APFI per image in type 2 synapses and type 1 synapses following TTX treatment. The difference between the two groups is statistically significant (Welch's t-test, p=0.0013).

Figure 4.13 now looks at the effect of BCC treatment on the APFI of type 2 and type 3 synapses. Essentially, the results are the same as for the TTX-treated group, in that the results mirror untreated controls. In type 2 synapses, BCC treatment results in an APFI of 54.49 ± 3.76 AU (compared to 45.13 ± 0.93 AU in controls) (p=0.055). In type 3 synapses, BCC treatment yields an APFI of 39.44 ± 3.27 AU (compared to 34.79 ± 0.80 AU in controls) (p=0.22). Within the BCC-treated group, type 2 synapses are significantly more fluorescent than type 3 synapses (p=0.013) (figure 4.13.c).

Within the BCC group, the results for the chase ligand are again very similar to those of the TTX group. Type 2 synapses do not differ significantly in their APFI (around 37 AU, figure 4.13.d) from controls (p=0.17), and type 1 synapses are even closer to the control group in their APFI (about 22 AU, p=0.63, figure 4.13.e). As in controls, type 2 (38.83 ± 1.94 AU) and type 1 (21.97 ± 0.53 AU) synapses are very significantly different in their APFI (p=0.00020) (figure 4.13.f).

a.

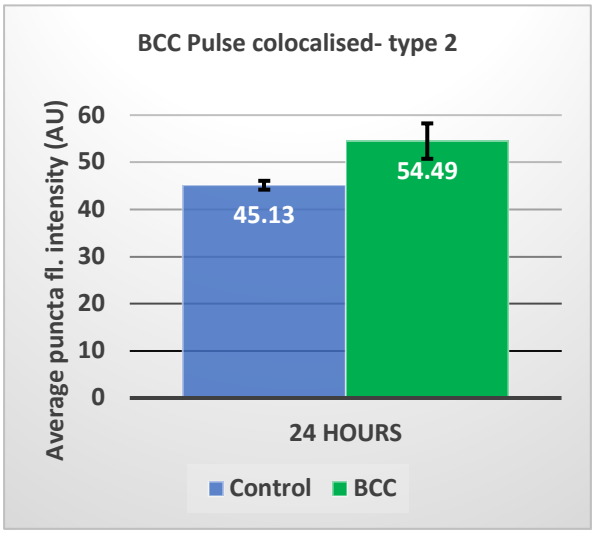
BCC Pulse colocalised- type 2
Average puncta fl. intensity (AU)
60
50
40
30
20
10
0
45.13
54.49
24 HOURS
Control
BCC

b.

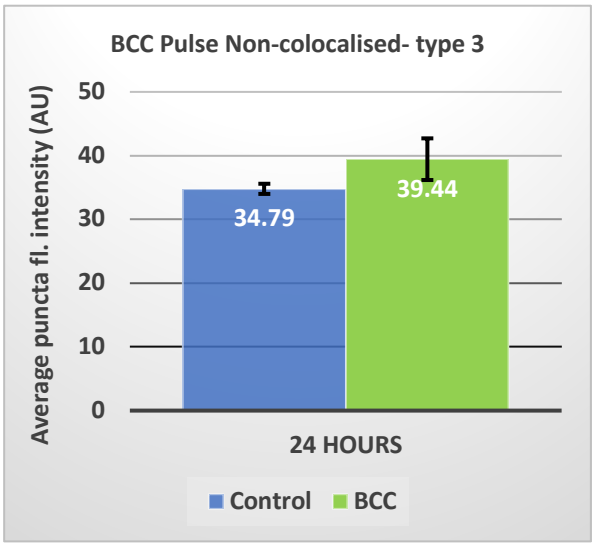
BCC Pulse Non-colocalised- type 3
Average puncta fl. intensity (AU)
50
40
30
20
10
0
34.79
39.44
24 HOURS
Control
BCC

c.

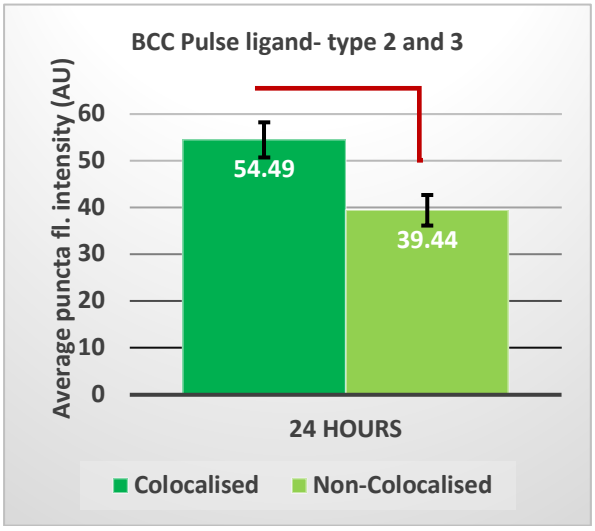
BCC Pulse ligand- type 2 and 3
Average puncta fl. intensity (AU)
60
50
40
30
20
10
0
54.49
39.44
24 HOURS
Colocalised
Non-Colocalised

d.

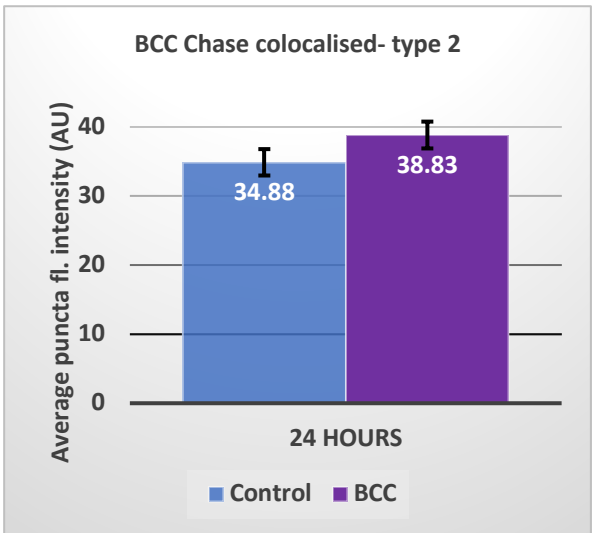
BCC Chase colocalised- type 2
Average puncta fl. intensity (AU)
40
30
20
10
0
34.88
38.83
24 HOURS
Control
BCC

e.

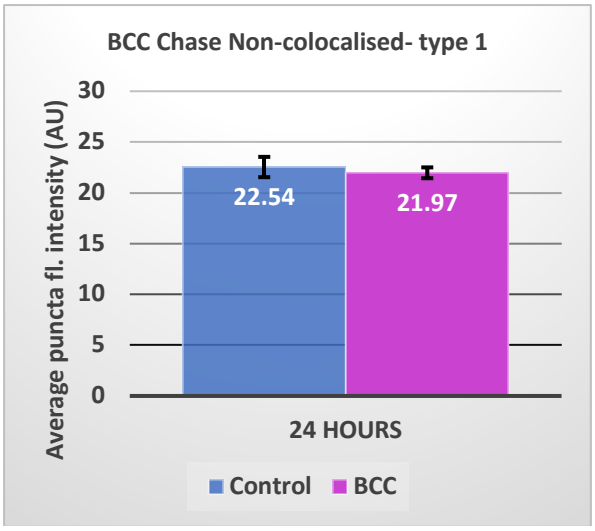
BCC Chase Non-colocalised- type 1
Average puncta fl. intensity (AU)
30
25
20
15
10
5
0
22.54
21.97
24 HOURS
Control
BCC

f.

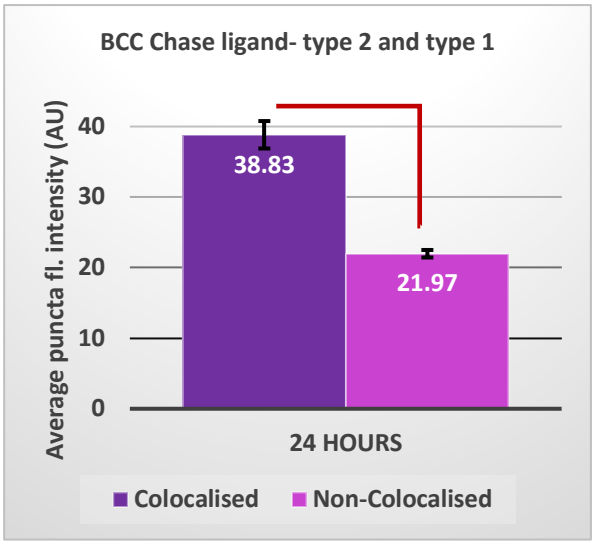
BCC Chase ligand- type 2 and type 1
Average puncta fl. intensity (AU)
40
30
20
10
0
38.83
21.97
24 HOURS
Colocalised
Non-Colocalised

Figure 4.13. The effect of bicuculline on PSD-95 average puncta intensity at synaptic types. Average puncta fluorescence intensity (APFI) per image was calculated for pulse and chase ligand labelled synaptic puncta in type 1, type 2 and type 3 synapses separately. Images were taken after 24 hours of pulse-chase treatment with 50nM R110Direct ligand (pulse) and 500nM TMR ligand (chase) in hippocampal primary cultures from PSD-95$^{HaloTag/HaloTag}$ mice on DIV16. BCC (40µM) was applied for 24 hours together with the chase ligand between DIV15 and DIV16. The graphs here present the mean values across eight cultures (N=8). **a.** Pulse ligand (R110Direct) APFI per image in synapses where pulse and chase ligands colocalise (type 2). The difference between the BCC group and untreated controls is not statistically significant (Welch's t-test, p=0.055). **b.** Pulse ligand (R110Direct) APFI per image in synapses where pulse and chase ligands do not colocalise (type 3). The difference between the BCC group and untreated controls is not statistically significant (Welch's t-test, p=0.22). **c.** Comparison of pulse ligand APFI per image in type 2 synapses and type 3 synapses following BCC treatment. The difference between the two groups is statistically significant (Welch's t-test, p=0.013). **d.** Chase ligand (TMR) APFI per image in synapses where pulse and chase ligands colocalise (type 2). The difference between the BCC group and untreated controls is not statistically significant (Welch's t-test, p=0.17). **e.** Chase ligand (TMR) APFI per image in synapses where pulse and chase ligands do not colocalise (type 1). The difference between the BCC group and untreated controls is not statistically significant (Welch's t-test, p=0.63). **f.** Comparison of chase ligand APFI per image in type 2 synapses and type 1 synapses following BCC treatment. The difference between the two groups is statistically significant (Welch's t-test, p=0.00020).

Looking at puncta numbers, the results are essentially the same for both the TTX and BCC groups. Type 1, type 2 and type 3 synapses all have a very similar number of synaptic puncta per image as the untreated control group. No group of synapses, be they colocalised or not, differs in puncta number from untreated controls. Figure 4.14 shows the synaptic puncta numbers for the both pulse and chase ligands in the TTX treated group, and figure 4.15 does the same for the BCC treated group. The only point of difference between the treatment groups and the control group was that in controls, there was no statistically significant difference between colocalised and non-colocalised pulse and chase puncta (figure 4.2.c and figure 4.2.d). However, in the TTX treatment group, non-colocalised (type 1) chase ligand puncta were significantly lower in number than colocalised (type 2) chase ligand puncta (figure 4.14.f) (Welch's t-test, p=0.027). This was not the case for the pulse ligand (figure 4.14.c) (p=0.089).

a.

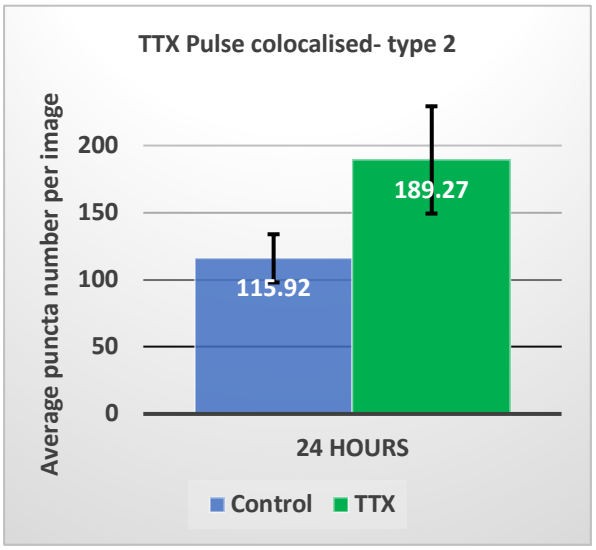
TTX Pulse colocalised- type 2
Average puncta number per image
200
150
100
50
0
115.92
189.27
24 HOURS
Control
TTX

b.

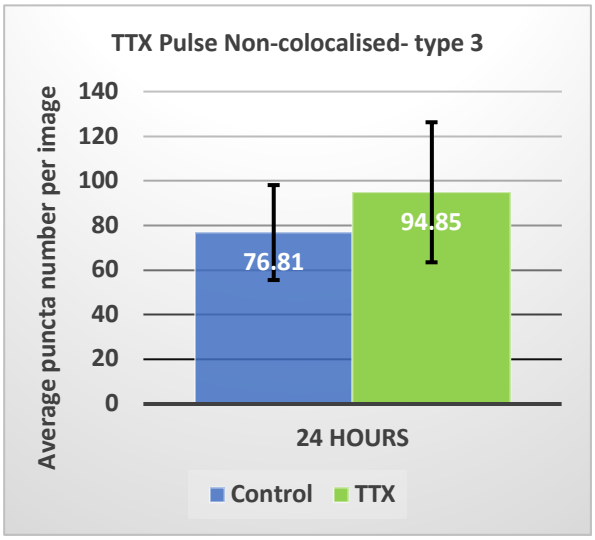
TTX Pulse Non-colocalised- type 3
Average puncta number per image
140
120
100
80
60
40
20
0
76.81
94.85
24 HOURS
Control
TTX

c.

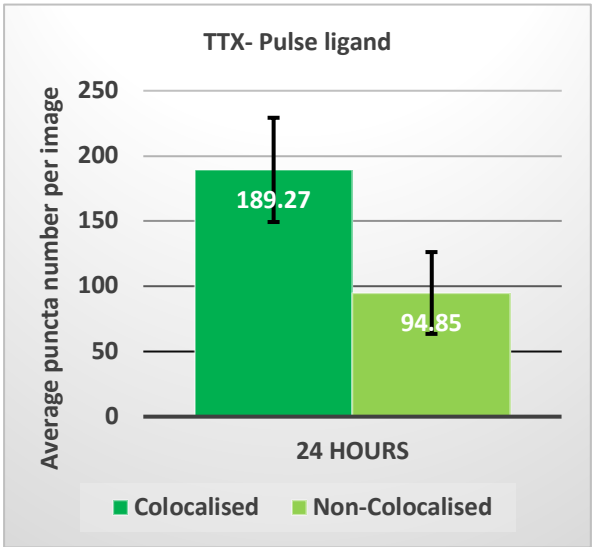
TTX- Pulse ligand
Average puncta number per image
250
200
150
100
50
0
189.27
94.85
24 HOURS
Colocalised
Non-Colocalised

d.

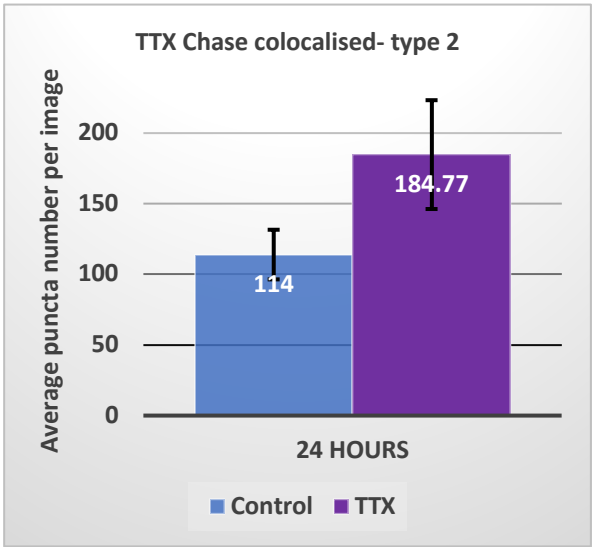
TTX Chase colocalised- type 2
Average puncta number per image
200
150
100
50
0
114
184.77
24 HOURS
Control
TTX

e.

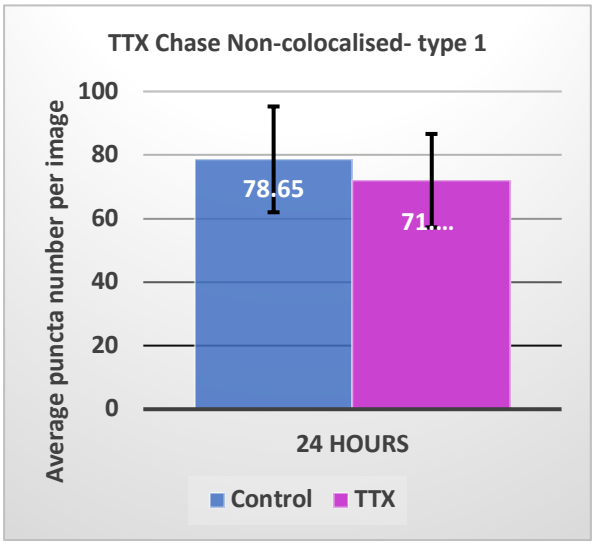
TTX Chase Non-colocalised- type 1
Average puncta number per image
100
80
60
40
20
0
78.65
71....
24 HOURS
Control
TTX

f.

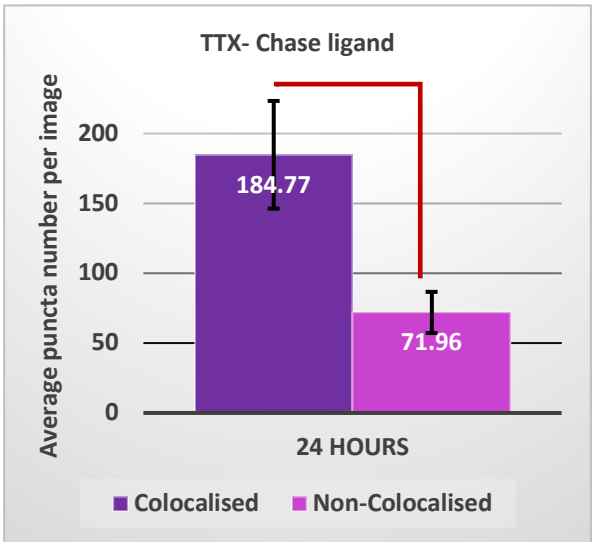
TTX- Chase ligand
Average puncta number per image
200
150
100
50
0
184.77
71.96
24 HOURS
Colocalised
Non-Colocalised

Figure 4.14. The effect of tetrodotoxin on PSD-95 average puncta number at synaptic types. Average puncta number per image was calculated for pulse and chase ligand labelled synaptic puncta in type 1, type 2 and type 3 synapses separately. Images were taken after 24 hours of pulse-chase treatment with 50nM R110Direct ligand (pulse) and 500nM TMR ligand (chase) in hippocampal primary cultures from PSD-95$^{HaloTag/HaloTag}$ mice on DIV16. TTX (1µM) was applied for 24 hours together with the chase ligand between DIV15 and DIV16. The graphs here present the mean values across eight cultures (N=8). **a.** Pulse ligand (R110Direct) average puncta number per image in synapses where pulse and chase ligands colocalise (type 2). The difference between the TTX group and untreated controls is not statistically significant (Welch's t-test, p=0.13). **b.** Pulse ligand (R110Direct) average puncta number per image in synapses where pulse and chase ligands do not colocalise (type 3). The difference between the TTX group and untreated controls is not statistically significant (Welch's t-test, p=0.64). **c.** Comparison of pulse ligand average puncta number per image in type 2 synapses and type 3 synapses following TTX treatment. The difference between the two groups is not statistically significant (Welch's t-test, p=0.089). **d.** Chase ligand (TMR) average puncta number per image in synapses where pulse and chase ligands colocalise (type 2). The difference between the TTX group and untreated controls is not statistically significant (Welch's t-test, p=0.13). **e.** Chase ligand (TMR) average puncta number per image in synapses where pulse and chase ligands do not colocalise (type 1). The difference between the TTX group and untreated controls is not statistically significant (Welch's t-test, p=0.77). **f.** Comparison of chase ligand average puncta number per image in type 2 synapses and type 1 synapses following TTX treatment. The difference between the two groups is statistically significant (Welch's t-test, p=0.027).

In the BCC group, I found the opposite to be the case, with type 3 (non-colocalised) pulse ligand puncta being significantly lower in number than type 2 (colocalised) pulse ligand puncta (figure 4.15.c) (p=0.038). This was not the case for the chase ligand (figure 4.15.f) (p=0.079). While these results do differ from the untreated control group (figure 4.2.c and 4.2.d), the same trend can be seen in these control group graphs, and it is likely that these results were simply caused by a higher degree of variation among the control group.

Next, we look at the overall synaptic population as per its distribution into type 1 (only new, chase labelled PSD-95), type 2 (mixed population of old and new PSD-95) and type 3 (only old, pulse labelled PSD-95) synapses (figure 4.16). Figure 4.16.a shows the synaptic population of untreated controls, while figure 4.16.b shows the TTX-treated synaptic population and 4.16.c shows the BCC-treated synaptic population.

a.

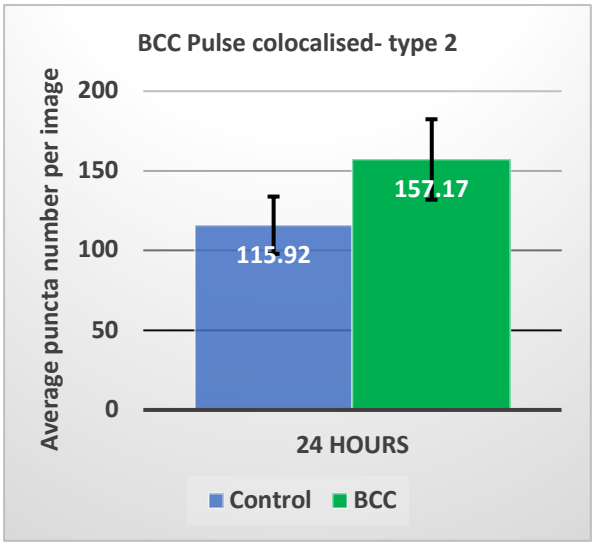
BCC Pulse colocalised- type 2
Average puncta number per image
200
150
100
50
0
115.92
157.17
24 HOURS
Control
BCC

b.

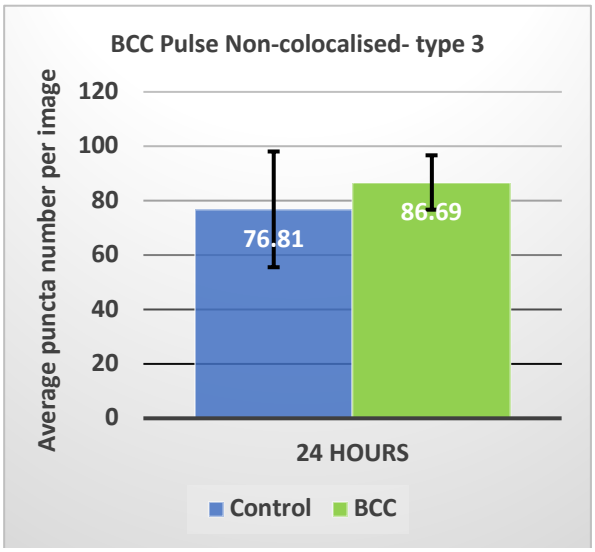
BCC Pulse Non-colocalised- type 3
Average puncta number per image
120
100
80
60
40
20
0
76.81
86.69
24 HOURS
Control
BCC

c.

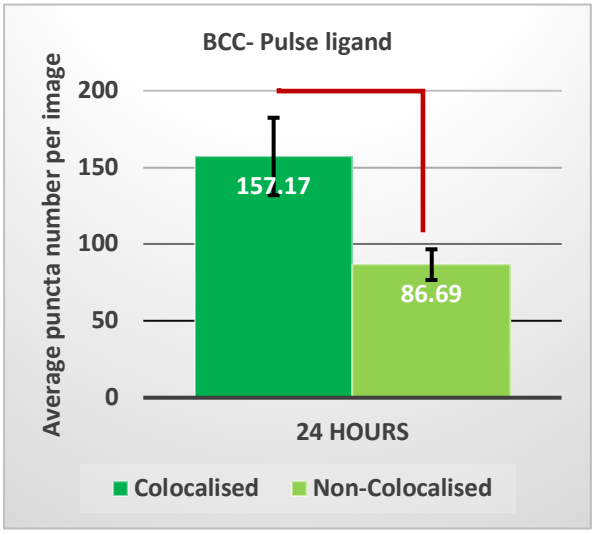
BCC- Pulse ligand
Average puncta number per image
200
150
100
50
0
157.17
86.69
24 HOURS
Colocalised
Non-Colocalised

d.

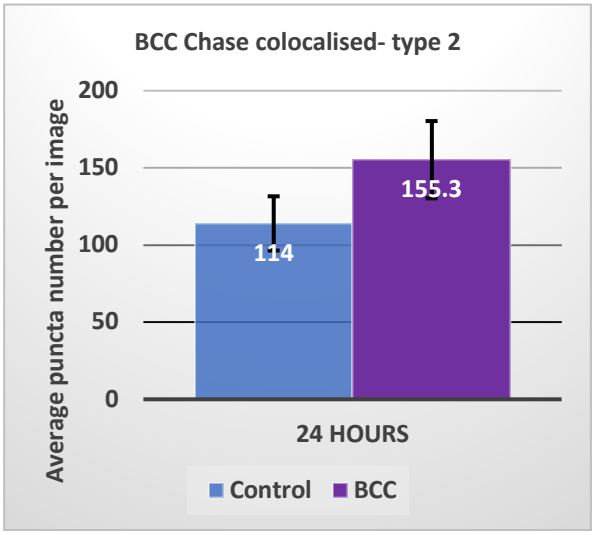
BCC Chase colocalised- type 2
Average puncta number per image
200
150
100
50
0
114
155.3
24 HOURS
Control
BCC

e.

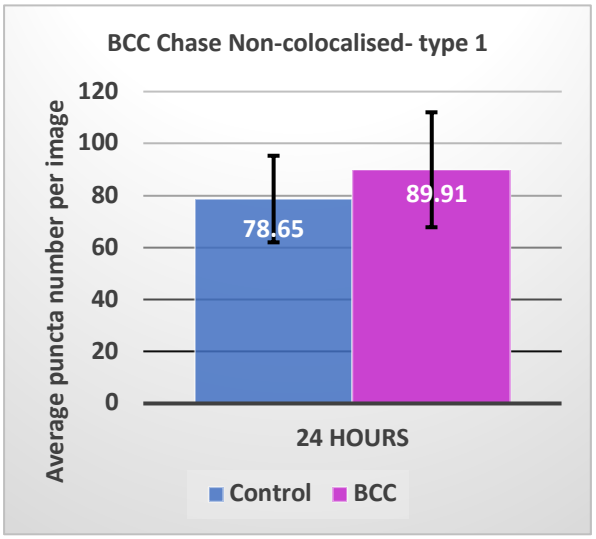
BCC Chase Non-colocalised- type 1
Average puncta number per image
120
100
80
60
40
20
0
78.65
89.91
24 HOURS
Control
BCC

f.

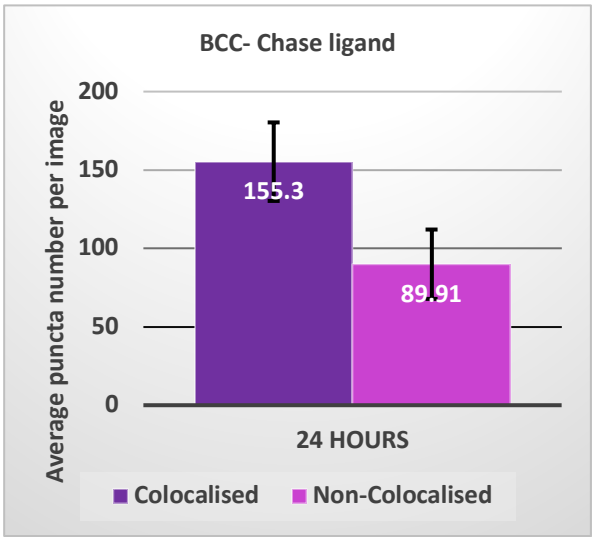
BCC- Chase ligand
Average puncta number per image
200
150
100
50
0
155.3
89.91
24 HOURS
Colocalised
Non-Colocalised

Figure 4.15. The effect of bicuculline on PSD-95 average puncta number at synaptic types. Average puncta number per image was calculated for pulse and chase ligand labelled synaptic puncta in type 1, type 2 and type 3 synapses separately. Images were taken after 24 hours of pulse-chase treatment with 50nM R110Direct ligand (pulse) and 500nM TMR ligand (chase) in hippocampal primary cultures from PSD-95$^{HaloTag/HaloTag}$ mice on DIV16. BCC (40µM) was applied for 24 hours together with the chase ligand between DIV15 and DIV16. The graphs here present the mean values across eight cultures (N=8). **a.** Pulse ligand (R110Direct) average puncta number per image in synapses where pulse and chase ligands colocalise (type 2). The difference between the BCC group and untreated controls is not statistically significant (Welch's t-test, p=0.21). **b.** Pulse ligand (R110Direct) average puncta number per image in synapses where pulse and chase ligands do not colocalise (type 3). The difference between the BCC group and untreated controls is not statistically significant (Welch's t-test, p=0.68). **c.** Comparison of pulse ligand average puncta number per image in type 2 synapses and type 3 synapses following BCC treatment. The difference between the two groups is statistically significant (Welch's t-test, p=0.038). **d.** Chase ligand (TMR) average puncta number per image in synapses where pulse and chase ligands colocalise (type 2). The difference between the BCC group and untreated controls is not statistically significant (Welch's t-test, p=0.21). **e.** Chase ligand (TMR) average puncta number per image in synapses where pulse and chase ligands do not colocalise (type 1). The difference between the BCC group and untreated controls is not statistically significant (Welch's t-test, p=0.69). **f.** Comparison of chase ligand average puncta number per image in type 2 synapses and type 1 synapses following BCC treatment. The difference between the two groups is not statistically significant (Welch's t-test, p=0.079).

We immediately observe that the three pie charts look very similar. In all three graphs, roughly 26% of synapses contain only one of the two ligands (i.e. are type 1 or type 3 synapses), and thus about 48% of synapses contain both ligands (type 2 synapses). Only in the TTX-treated group is the percentage of type 1 synapses slightly lower (20%), even here the difference compared to the number of type 3 synapses (27%) is not significant (Welch's t-test, p=0.53). It therefore appears that in all three groups, about half of the synaptic population consists of mixed old and new PSD-95 and a quarter of synapses contains either old or new PSD-95. Blocking or enhancing synaptic activity with TTX or BCC respectively appears to have no impact on this distribution of synaptic types. Similarly, in all three treatment groups colocalised type 2 synapses express both more old and more new PSD-95 than the total amount of PSD-95 expressed by non-colocalised type 1 or type 3 synapses.

a.

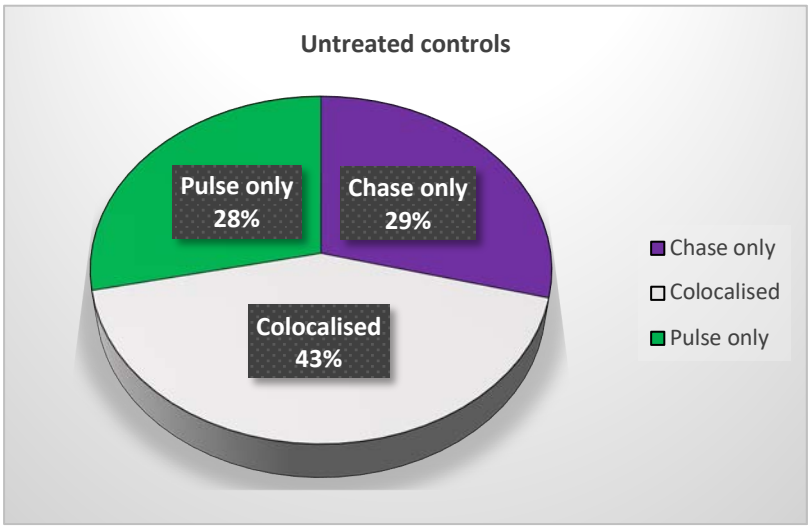
Untreated controls
Pulse only 28%
Chase only 29%
Colocalised 43%
Chase only
Colocalised
Pulse only

b.

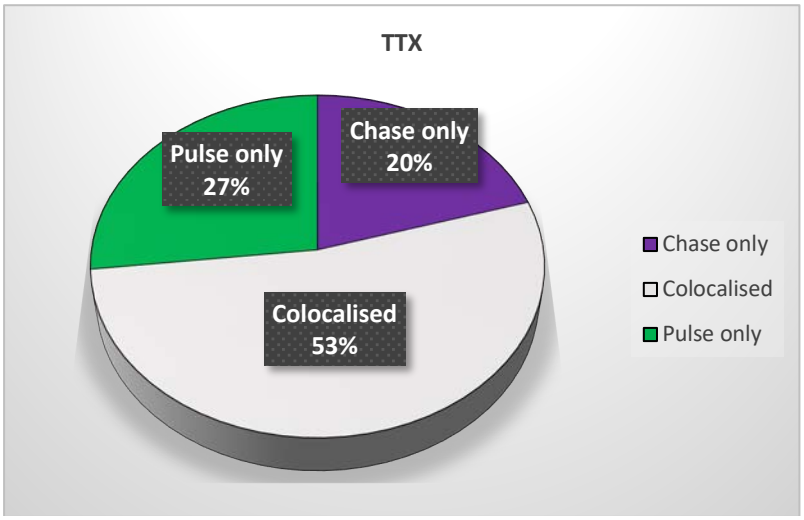
TTX
Pulse only 27%
Chase only 20%
Colocalised 53%
Chase only
Colocalised
Pulse only

c.

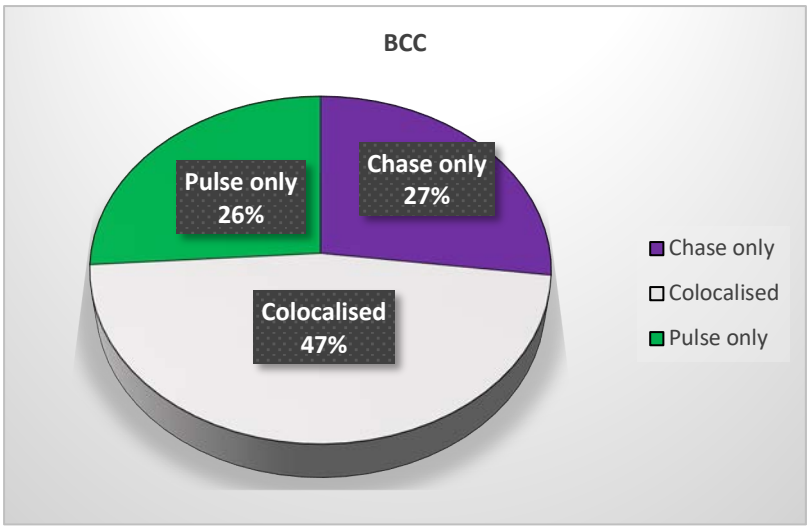
BCC
Pulse only 26%
Chase only 27%
Colocalised 47%
Chase only
Colocalised
Pulse only

Figure 4.16. Proportional representation of synaptic population by HaloTag ligand-labelling following activity modulation.

Synaptic puncta were categorised according to whether they colocalised with puncta labelled by the other ligand or not. This pie chart depicts the proportional representation of the three types of synaptic puncta observed.

Images were taken after 24 hours of pulse-chase treatment with 50nM R110Direct ligand (pulse) and 500nM TMR ligand (chase) in hippocampal primary cultures from PSD-$95^{HaloTag/HaloTag}$ mice on DIV16. **a.** In untreated controls, 28% of puncta contain only the pulse (R110Direct) ligand (type 3), 43% of puncta contain both pulse and chase (TMR) ligands (type 2), and 29% contain only the chase ligand (type 1). **b.** Following 24 hours of TTX treatment (1µM), 27% of puncta contain only the pulse (R110Direct) ligand (type 3), 53% of puncta contain both pulse and chase (TMR) ligands (type 2), and 20% contain only the chase ligand (type 1). **c.** Following 24 hours of BCC treatment (40µM), 26% of puncta contain only the pulse (R110Direct) ligand (type 3), 47% of puncta contain both pulse and chase (TMR) ligands (type 2), and 27% contain only the chase ligand (type 1).

Finally, I will look into the data pertaining to the ratio of pulse to chase ligand average puncta fluorescence intensity within type 2 (colocalised) synapses. As in figure 4.6 when I looked into the ratios for the control group only, I graphed a frequency histogram to depict the frequencies of different pulse:chase ligand ratios in TTX and BCC treated groups. In figure 4.19 I compare these histograms, with figure 4.19.a representing the untreated control group, figure 4.19.b the TTX-treated group, and figure 4.19.c the BCC-treated group.

When looking at the shapes of these three histograms, it is quite evident that there is no marked difference in these results. As I discussed in chapter 4.3.2.4, this large spread in ratios and great heterogeneity indicates a heterogenous synapse population with likely differing rates of PSD-95 turnover. In figure 4.19.d I compare the mean ratios of pulse to chase ligand APFI. For the control group, the mean ratio is 2.55 ± 0.051 (SEM), with a median ratio of 2.06. The mode is a ratio of 1.8, with 8.76%. For the TTX-treated group, the mean ratio is 2.31 ± 0.039 (SEM), with a median ratio of 2.05. The mode is a ratio of 1.6, with 8.83%. For the BCC-treated group, the mean ratio is 2.84 ± 0.071 (SEM), with a median ratio of 2.34. The mode is a ratio of 1.8,

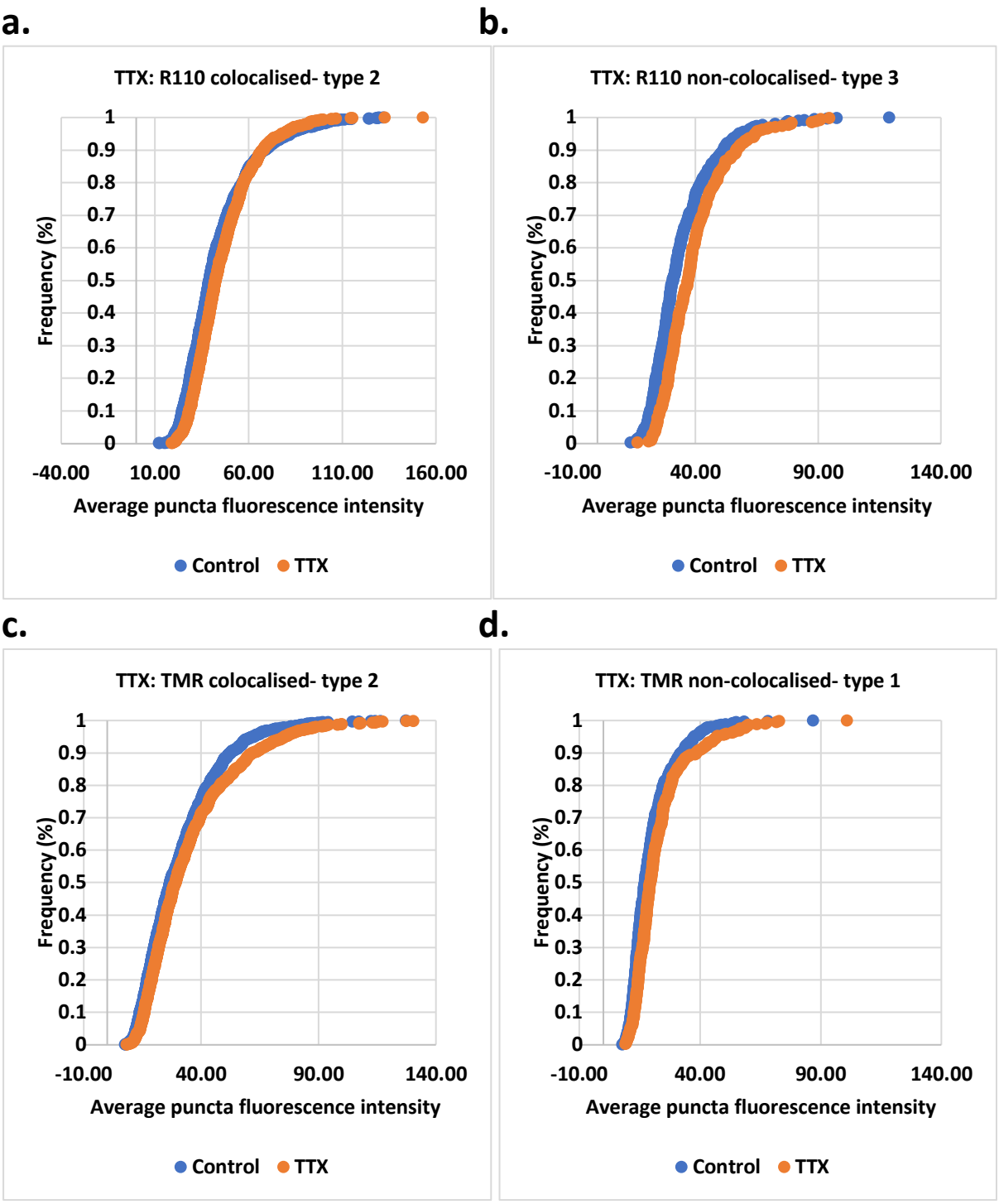

Figure 4.17. Cumulative distribution functions of average puncta fluorescence intensity following TTX treatment.

CDFs were constructed using the single-synapse data following TTX treatment, and compared with the untreated control group. Whether the difference was statistically significant or not was tested using the Kolmogorov-Smirnov test for difference. **a.** Comparison between R110 ligand puncta in colocalised type 2 synapses of TTX-treated neurons with those in untreated controls. The difference is significant (Kolmogorov-Smirnov, $p<0.0001$). **b.** Comparison between R110 ligand puncta in non-colocalised type 3 synapses of TTX-treated neurons with those in untreated controls. The difference is significant (Kolmogorov-Smirnov, $p<0.0001$). **c.**

Comparison between TMR ligand puncta in colocalised type 2 synapses of TTX-treated neurons with those in untreated controls. The difference is significant (Kolmogorov-Smirnov, p=0.004). **d.** Comparison between TMR ligand puncta in non-colocalised type 1 synapses of TTX-treated neurons with those in untreated controls. The difference is significant (Kolmogorov-Smirnov, p<0.0001).

a.

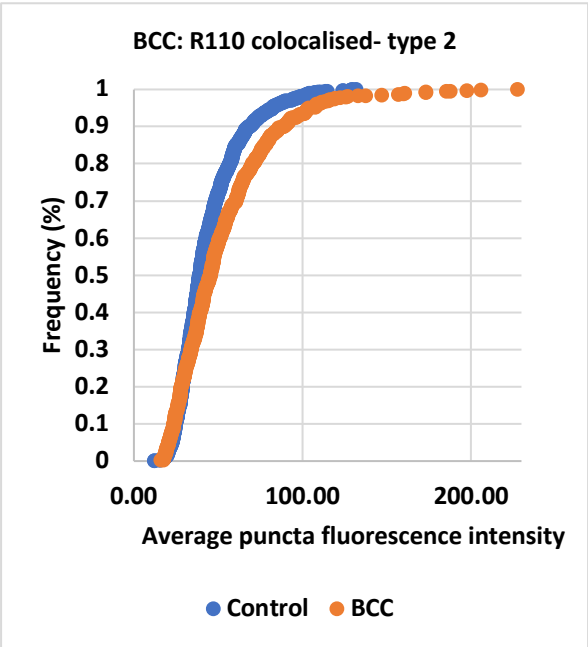

b.

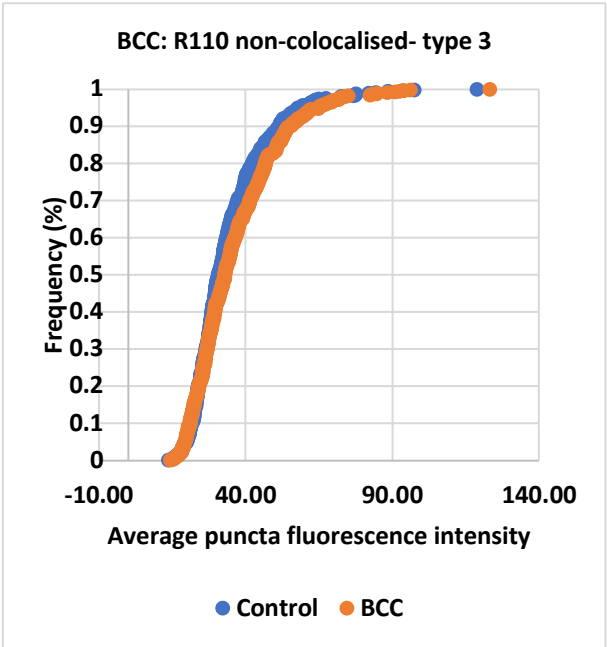

c.

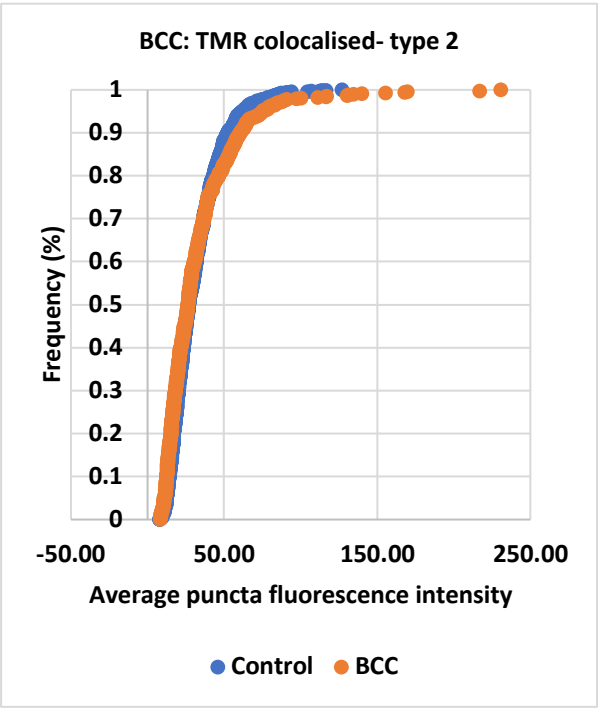

d.

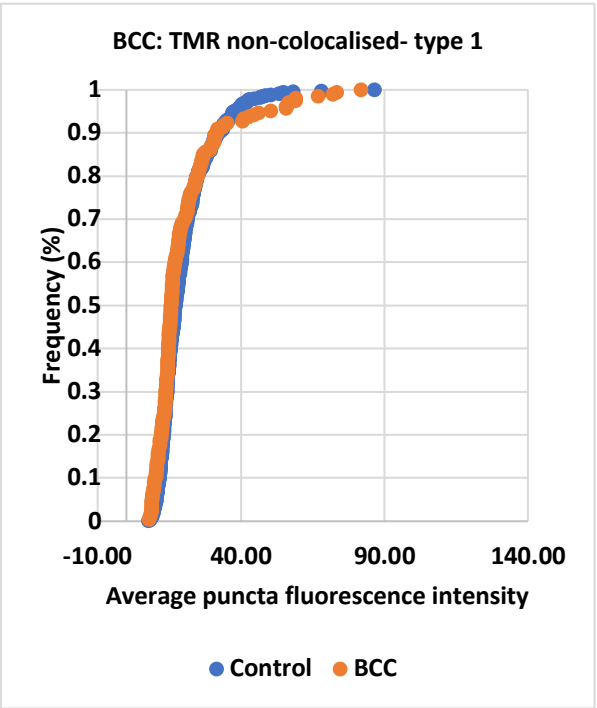

Figure 4.18. Cumulative distribution functions of average puncta fluorescence intensity following BCC treatment.

CDFs were constructed using the single-synapse data following BCC treatment, and compared with the untreated control group. Whether the difference was statistically significant or not was tested using the Kolmogorov-Smirnov test for difference. **a.** Comparison between R110 ligand puncta in colocalised type 2 synapses of BCC-treated neurons with those in untreated controls. The difference is significant (Kolmogorov-Smirnov, $p<0.0001$). **b.** Comparison between R110 ligand puncta in non-colocalised type 3 synapses of BCC-treated neurons with those in untreated controls. The difference is significant (Kolmogorov-Smirnov, $p=0.016$). **c.** Comparison between TMR ligand puncta in colocalised type 2 synapses of BCC-treated neurons with those in untreated controls. The difference is significant (Kolmogorov-Smirnov, $p=0.011$). **d.** Comparison between TMR ligand puncta in non-colocalised type 1 synapses of BCC-treated neurons with those in untreated controls. The difference is significant (Kolmogorov-Smirnov, $p=0.013$).

with 9.04%. It appears, therefore, that the differences in pulse to chase ligand APFI in these three treatment groups do not differ by much, with very similar frequency distribution histograms and similar mean, median and modal ratio values.

Next, I sorted puncta by pulse ligand intensity into percentiles, and then measured chase ligand APFI in each of these percentiles the way I had also done it in figure 4.7.b for the control group only. The results indicate that both TTX- and BCC-treated groups have very strong positive correlations between pulse and chase ligand APFI, similar to the control group. For the control group $R^2=0.96$ (figure 4.20.a), while for the TTX group $R^2=0.92$ (figure 4.20.b) and for the BCC group $R^2=0.81$ (figure 4.20.c).

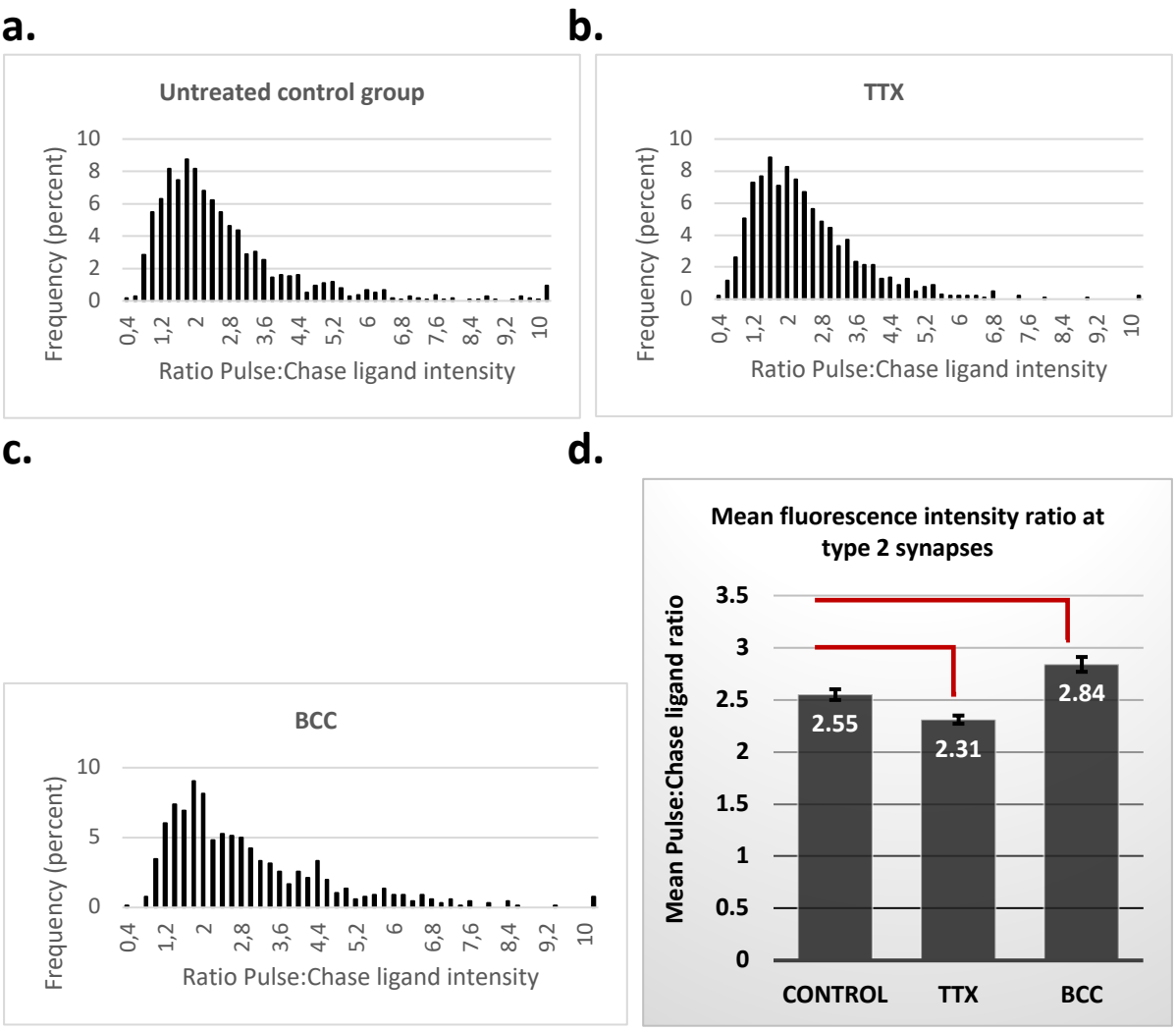

Figure 4.19. Graphs showing the ratio of pulse to chase ligands at individual type 2 synapses following activity modulation.

In the synaptic population in which pulse and chase ligand-labelled PSD-95-HaloTag molecules were colocalised (type 2), the ratio of pulse ligand fluorescence intensity to chase ligand fluorescence intensity was calculated for each individual synapse. The frequency histograms represent the frequencies of all the pulse:chase ratios. **a.** Frequency distribution in untreated controls. Mean ratio: 2.55 ± 0.051 (SEM), Median ratio: 2.06, Mode: 1.8 (8.76%). **b.** Frequency distribution following 24 hours of TTX (1µM) treatment. Mean ratio: 2.31 ± 0.039 (SEM), Median ratio: 2.05, Mode: 1.6 (8.83%). **c.** Frequency distribution following 24 hours of BCC (40µM) treatment. Mean ratio: 2.84 ± 0.071 (SEM), Median ratio: 2.34, Mode: 1.8 (9.04%). **d.** Comparison of mean pulse:chase ligand ratio in untreated controls with TTX and BCC treated cultures. Differences are statistically significant in the TTX group (Welch's t-test, p=0.00016) and the BCC group (Welch's t-test, p=0.0011).

Lastly, cumulative distribution functions (CDF's) were calculated for each of the eight groups (Figure 4.17 and 4.18). Visually, the CDF curves of the treated groups look very similar to those of untreated controls, displaying a very similar S-shaped curve

that indicates a normal distribution. However, a statistical test for difference between the curves, the Kolmogorov-Smirnov test for difference, revealed that in each of the eight graphs the curves differ just significantly from the control group. This, then, implies that treatment with these drugs does appear to affect the distribution of puncta intensities to a statistically significant extent.

4.4.2.3 TTX and BCC: Discussion

This fairly expansive investigation into the effect of activity modulation on PSD-95 turnover has resulted in some interesting insights. The main conclusion from this study, however, seems to be that over a 24-hour time window, blocking or enhancing excitatory neuronal activity has a negligible impact upon PSD-95 synthesis and degradation.

Interestingly, the only statistically significant results following activity modulation was that TTX appears to have reduced the loss of PSD-95 at synapses. Previous studies have found PSD-95 to be elevated following TTX treatment (Kim et al., 2007; Noritake et al., 2009; El-Husseini et al., 2002), but only at synaptic locations. These same studies, as well as a study by Colledge et al. (2003) found that enhancing activity reduces synaptic PSD-95 levels. Indeed, these studies described that NMDAR activity specifically caused increased destabilisation and degradation of PSD-95 at synapses. It stands to reason, then, that blocking such activity will reduce the loss of synaptic PSD-95. Thus, my observation of reduced PSD-95 loss matches that of other studies. However, along the same vein one might expect BCC, which increases excitatory neuronal activity by reducing GABAergic inhibition, to enhance turnover of PSD-95, but this was not observed. Another study, by Butko et al. (2012), found BCC to increase new PSD-95 synthesis. Such an effect could also not be observed.

Frequency histograms of pulse:chase ligand ratios at mixed-ligand (type 2) synapses have the same shape in treated and untreated groups, and mean ratios are very similar. The proportion of the total synaptic population that is made up of type 1, type 2 and type 3 synapses is also nearly identical in all three groups.

a.

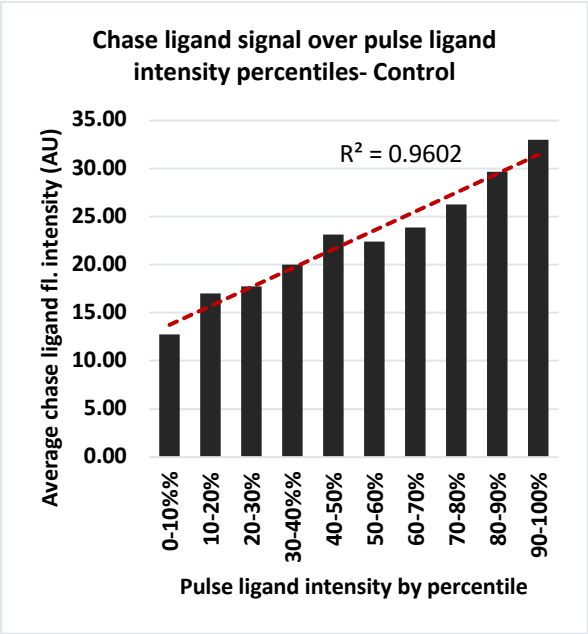

b.

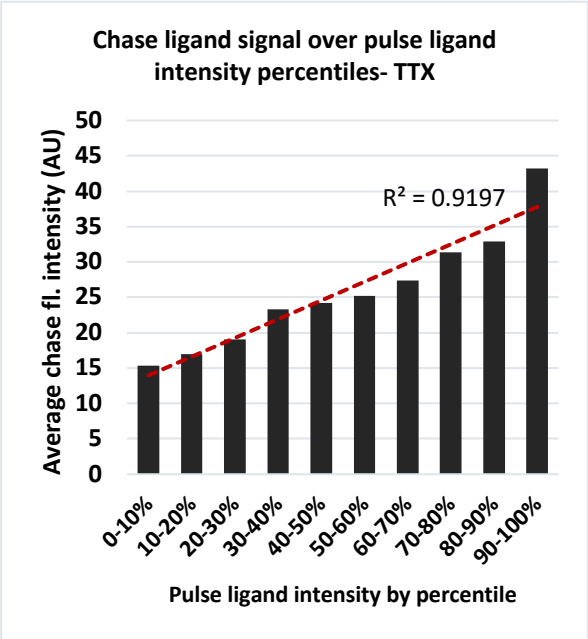

c.

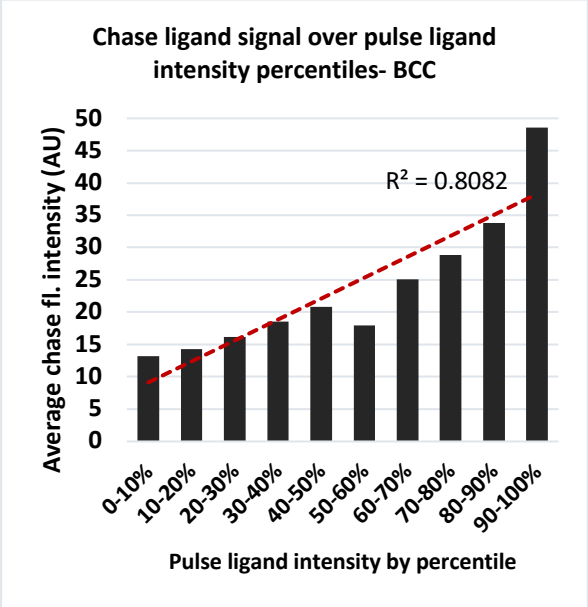

Figure 4.20 Correlation of pulse ligand intensity with chase ligand intensity at colocalised synaptic puncta following activity modulation.

Colocalising (type 2) synapses were sorted by their pulse ligand APFI (lowest to highest). For each ten percentile steps, average chase ligand APFI was calculated. **a.** In untreated controls, there is a strong positive correlation, R^2=0.96. **b.** In the TTX-treated cultures, there is also a strong positive correlation, R^2=0.92. **c.** In the BCC-treated cultures, the correlation is slightly weaker, but still high, R^2=0.81.

4.4.3.1 BDNF: bulk analysis

The next set of data I will look at is the BDNF results set. Again, I will first cover the bulk data, and then move on to a single-puncta analysis.

Figure 4.21.a shows the average intensity of pulse-ligand (R110) puncta in hippocampal primary neurons at DIV16 after having been treated with BDNF (3.7nM) for 24 hours, compared with untreated controls. Compared to controls, where APFI drops down to 41.44 ± 0.85 AU over 24 hours, APFI only drops down to 45.44 ± 1.30 AU in BDNF-treated cultures.
This difference, while fairly small, is statistically significant (Welch's t-test, p=0.024).

Similarly, we see that 24 hours of BDNF treatment results in a small but significant increase in chase ligand APFI (figure 4.21.b). Untreated controls display an APFI of 29.63 ± 1.42 AU, while BDNF-treated cultures have a significantly higher APFI of 34.85 ± 1.55 AU (p=0.026).

When looking at synapse number (figure 4.21.c-d), the results are similar to those of puncta intensity. For both the pulse and the chase ligand, puncta number is increased in BDNF-treated cultures compared with untreated controls, particularly for the chase ligand (control: mean 192.66 ± 32.83 synapses per image; BDNF: mean 296.87 ± 42.15 synapses per image) (figure 4.21.d). However, due to the high variation these results are not statistically significant (pulse ligand: p=0.25; chase ligand: p=0.073).

4.4.3.2 BDNF: single-synapse analysis

While at a bulk level BDNF causes significantly more pulse-labelled, old PSD-95 to be found at synapses than in untreated controls, at the single-synapse level (figure 4.22) I find that in type 2 synapses (old and new PSD-95 colocalised) this increase is not significant (p=0.098, figure 4.22.a). However, in non-colocalised type 3 synapses the difference is indeed significant (p=0.036, figure 4.22.b), with BDNF-treated neurons displaying an APFI of 38.45 ± 1.32 AU compared to that of untreated controls at

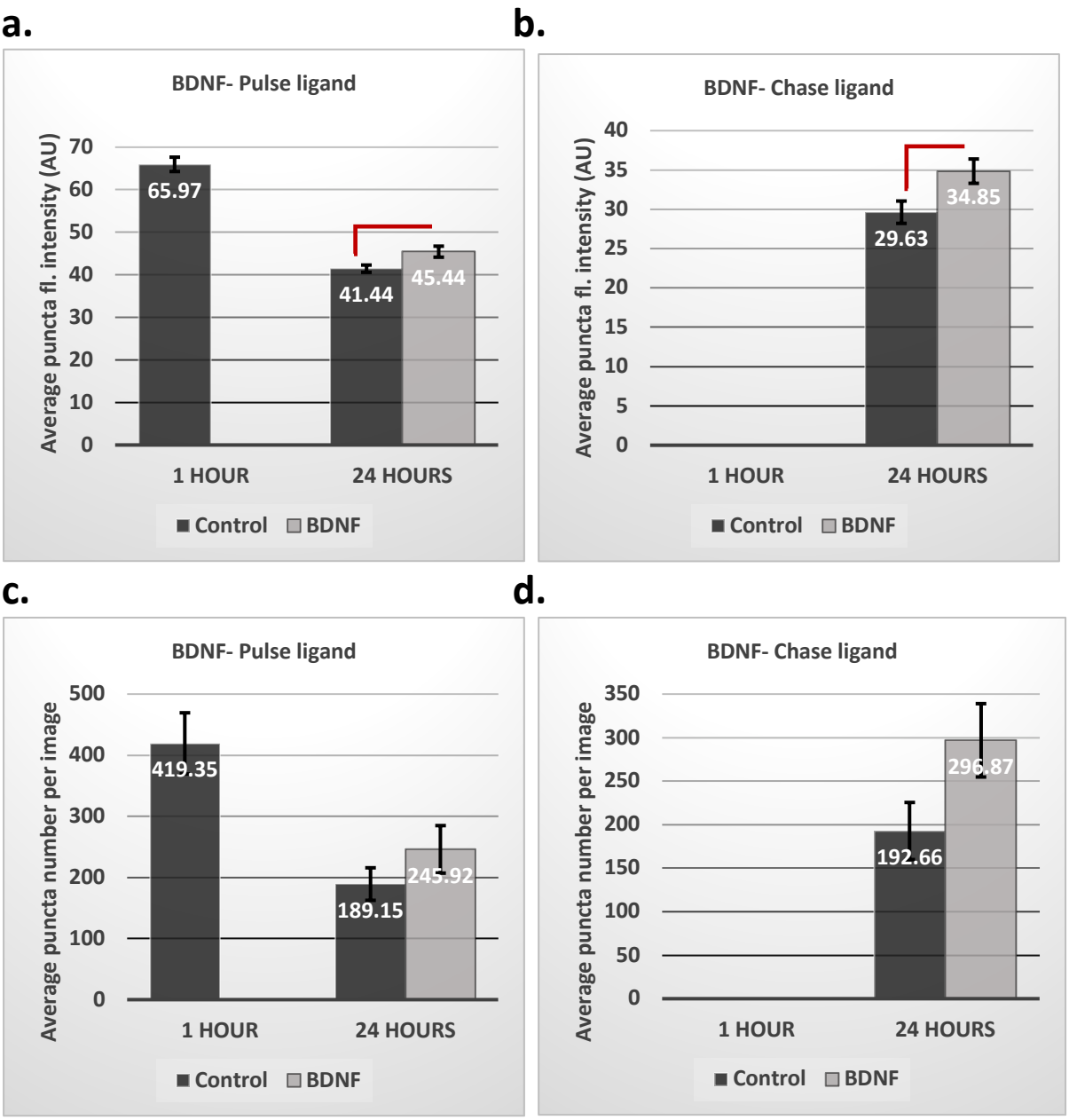

Figure 4.21. The effect of BDNF on PSD-95 puncta intensities and numbers.
Hippocampal neuronal primary cultures from PSD-95$^{HaloTag/HaloTag}$ mice were grown on glass coverslips and on DIV14 they were labelled with the R110Direct HaloTag ligand (50nM, 16h). On DIV15 the TMR ligand was added to the cultures at 500nM for 1 hour and 24 hours, alongside BDNF (3.7nM). Average puncta fluorescence intensity (APFI) and number per image were then calculated. This was performed across 8 different cultures (N=8), with the graphs here presenting the mean values across these eight cultures. **a.** Graph of the R110 pulse ligand APFI following BDNF treatment. APFI is significantly higher after 24 hours in the BDNF group than in untreated controls (Welch's t-test, p=0.024). **b.** Graph of the average TMR chase ligand APFI following BDNF treatment. APFI is significantly higher in the BDNF group than in untreated controls (Welch's t-test, p=0.026). **c.** Graph of the average pulse ligand puncta number following BDNF treatment. The difference between the BDNF group and untreated controls after 24 hours is not significant (Welch's t-test, p=0.25). **d.** Graph of the average chase ligand puncta number following BDNF treatment. The difference between the BDNF group and untreated controls is not significant (Welch's t-test, p=0.073).

a.

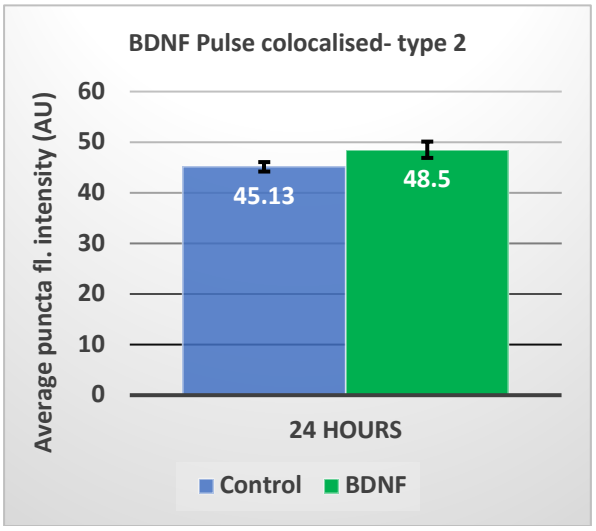
BDNF Pulse colocalised- type 2
Average puncta fl. intensity (AU)
60
50
40
30
20
10
0
45.13
48.5
24 HOURS
Control
BDNF

b.

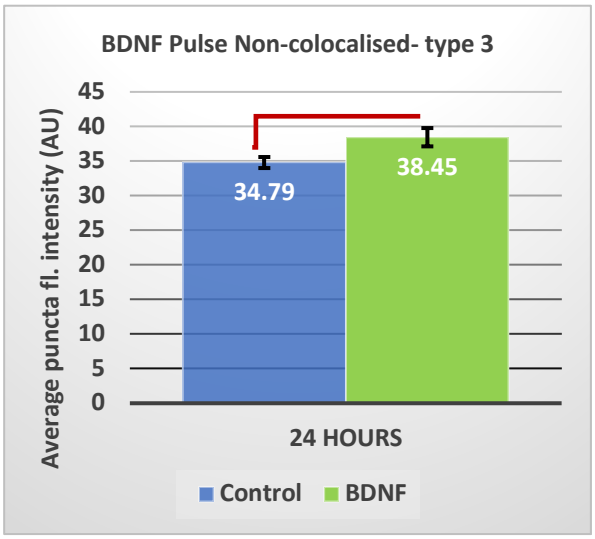
BDNF Pulse Non-colocalised- type 3
Average puncta fl. intensity (AU)
45
40
35
30
25
20
15
10
5
0
34.79
38.45
24 HOURS
Control
BDNF

c.

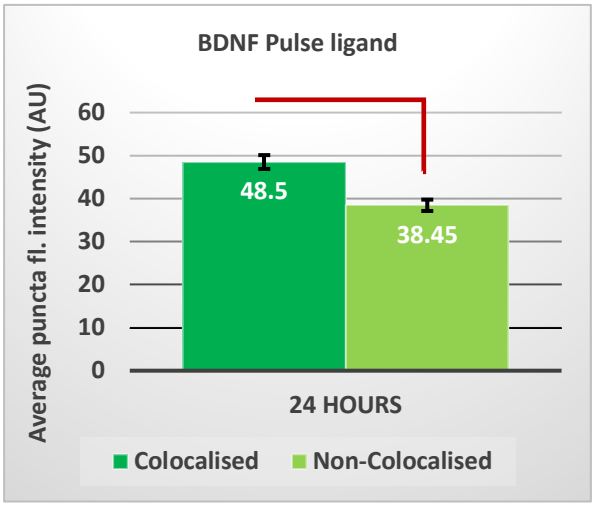
BDNF Pulse ligand
Average puncta fl. intensity (AU)
60
50
40
30
20
10
0
48.5
38.45
24 HOURS
Colocalised
Non-Colocalised

d.

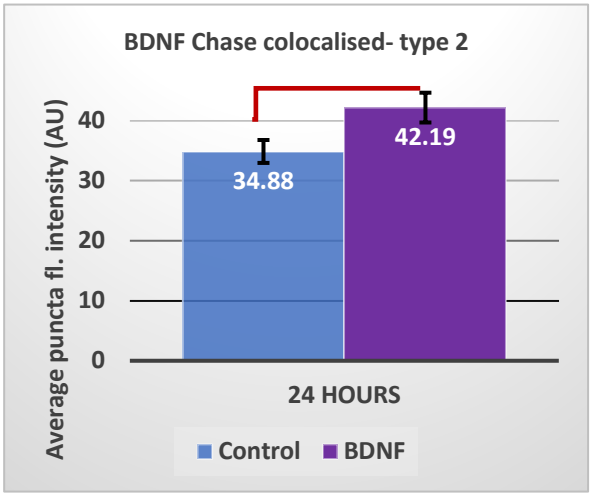
BDNF Chase colocalised- type 2
Average puncta fl. intensity (AU)
40
30
20
10
0
34.88
42.19
24 HOURS
Control
BDNF

e.

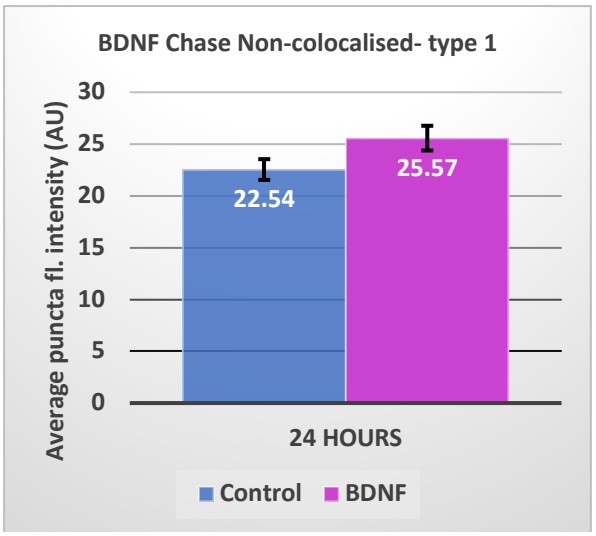
BDNF Chase Non-colocalised- type 1
Average puncta fl. intensity (AU)
30
25
20
15
10
5
0
22.54
25.57
24 HOURS
Control
BDNF

f.

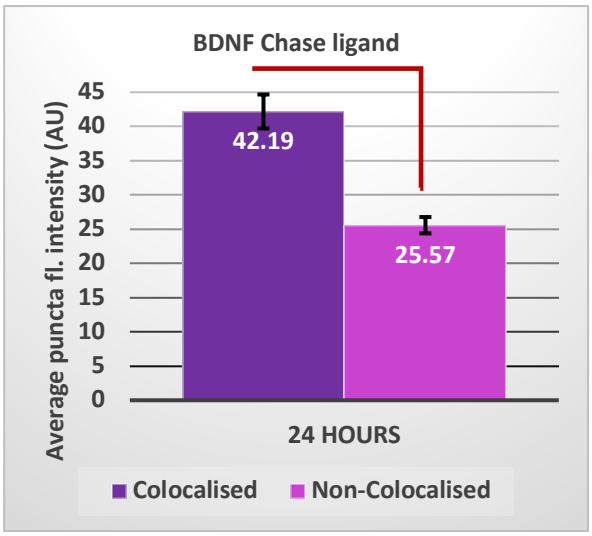
BDNF Chase ligand
Average puncta fl. intensity (AU)
45
40
35
30
25
20
15
10
5
0
42.19
25.57
24 HOURS
Colocalised
Non-Colocalised

Figure 4.22. The effect of BDNF on PSD-95 average puncta intensity at synaptic types.
Average puncta fluorescence intensity (APFI) per image was calculated for pulse and chase ligand labelled synaptic puncta in type 1, type 2 and type 3 synapses separately. Images were taken after 24 hours of pulse-chase treatment with 50nM R110Direct ligand (pulse) and 500nM TMR ligand (chase) in hippocampal primary cultures from PSD-95$^{HaloTag/HaloTag}$ mice on DIV16. BDNF (3.7nM) was applied for 24 hours together with the chase ligand between DIV15 and DIV16. The graphs here present the mean values across eight cultures (N=8). **a.** Pulse ligand (R110Direct) APFI per image in synapses where pulse and chase ligands colocalise (type 2). The difference between the BDNF group and untreated controls is not statistically significant (Welch's t-test, p=0.098). **b.** Pulse ligand APFI per image in synapses where pulse and chase ligands do not colocalise (type 3). The difference between the BDNF group and untreated controls is statistically significant (Welch's t-test, p=0.036). **c.** Comparison of pulse ligand APFI per image in type 2 synapses and type 3 synapses following BDNF treatment. The difference between the two groups is statistically significant (Welch's t-test, p=0.00031).
d. Chase ligand (TMR) APFI per image in synapses where pulse and chase ligands colocalise (type 2). The difference between the BDNF group and untreated controls is statistically significant (Welch's t-test, p=0.036). **e.** Chase ligand APFI per image in synapses where pulse and chase ligands do not colocalise (type 1). The difference between the BDNF group and untreated controls is not statistically significant (Welch's t-test, p=0.073). **f.** Comparison of chase ligand APFI per image in type 2 synapses and type 1 synapses following BDNF treatment. The difference between the two groups is statistically significant (Welch's t-test, p=0.00012).

34.79 ± 0.80 AU. When looking at the chase ligand results (figure 4.22.d-f), we can observe the opposite effect: APFI is significantly greater than controls in type 2 (colocalised) synapses (p=0.036, figure 4.22.d), but this is not the case in type 1 synapses (p=0.073, figure 4.22.e).

Looking at puncta numbers (figure 4.23), the results match up with the bulk number data in figure 4.21: None of the results are significantly different to the control group, yet the pattern still indicates that puncta numbers are increased by BDNF, particularly for the chase ligand (figure 4.23.d-e).

Looking at the proportion of the total synaptic population that the three synaptic types make up, the pie chart in figure 4.24 reveals that the number of type 1 synapses (only new, chase-labelled PSD-95) has gone up relative to the other two types. Type 1 synapses now make up a total of 35% of synapses (figure 4.24.b), compared to 29% in the control group (4.24.a), and this appears to be at the expense of type 3 synapses (down to 21% from 28% in controls). However, the difference between type 1 and type 3 synapses is just barely not statistically significant (Welch's t-test, p=0.060).

a.

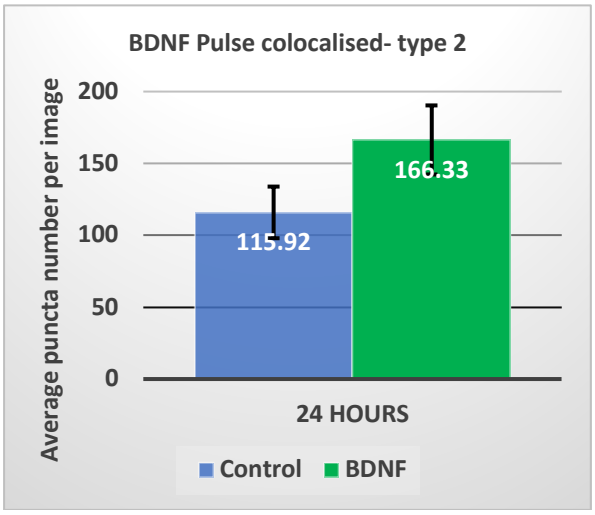
BDNF Pulse colocalised- type 2
Average puncta number per image
200
150
100
50
0
115.92
166.33
24 HOURS
Control
BDNF

b.

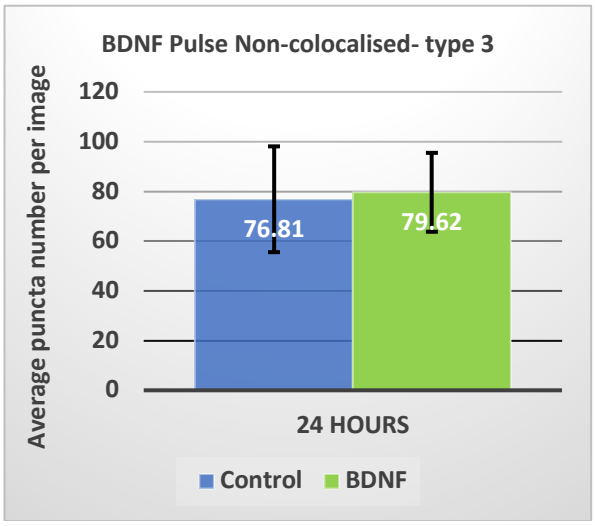
BDNF Pulse Non-colocalised- type 3
Average puncta number per image
120
100
80
60
40
20
0
76.81
79.62
24 HOURS
Control
BDNF

c.

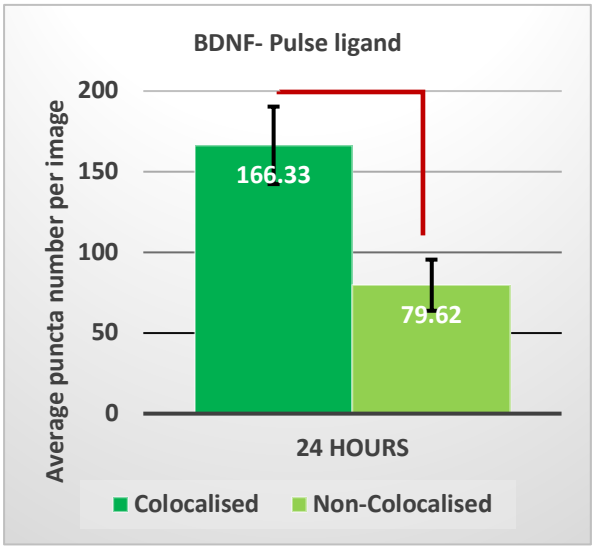
BDNF- Pulse ligand
Average puncta number per image
200
150
100
50
0
166.33
79.62
24 HOURS
Colocalised
Non-Colocalised

d.

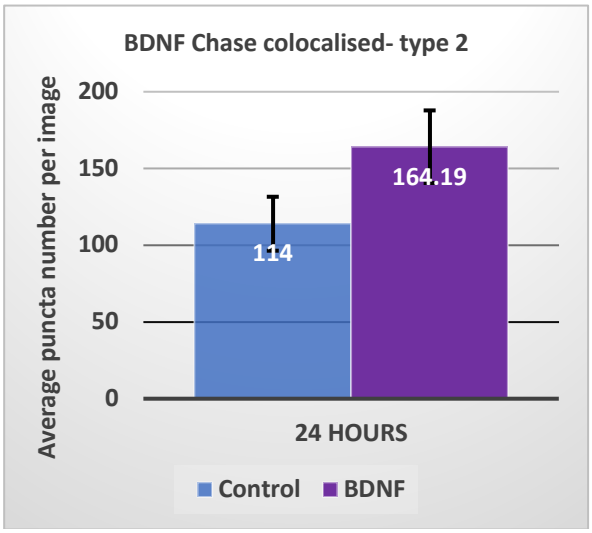
BDNF Chase colocalised- type 2
Average puncta number per image
200
150
100
50
0
114
164.19
24 HOURS
Control
BDNF

e.

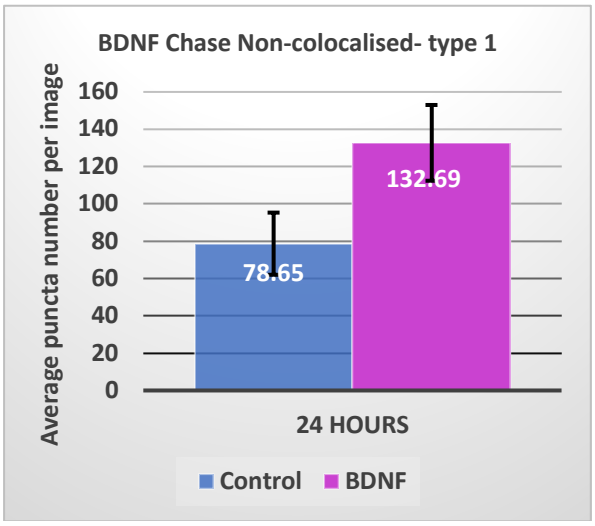
BDNF Chase Non-colocalised- type 1
Average puncta number per image
160
140
120
100
80
60
40
20
0
78.65
132.69
24 HOURS
Control
BDNF

f.

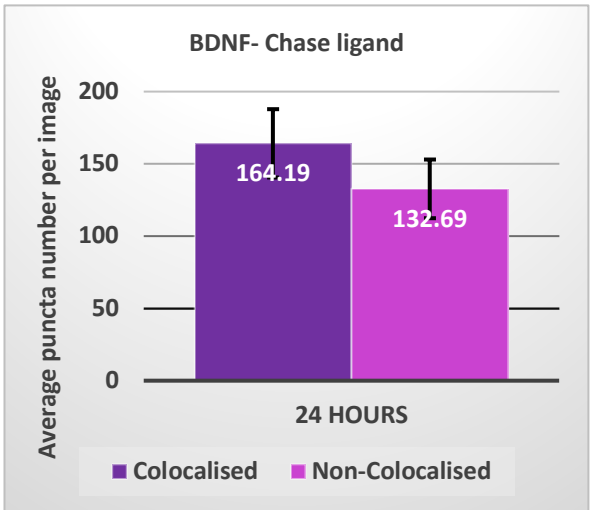
BDNF- Chase ligand
Average puncta number per image
200
150
100
50
0
164.19
132.69
24 HOURS
Colocalised
Non-Colocalised

Figure 4.23. The effect of BDNF on PSD-95 average puncta number at synaptic types.
Average puncta number per image was calculated for pulse and chase ligand labelled synaptic puncta in type 1, type 2 and type 3 synapses separately. Images were taken after 24 hours of pulse-chase treatment with 50nM R110Direct ligand (pulse) and 500nM TMR ligand (chase) in hippocampal primary cultures from PSD-95$^{HaloTag/HaloTag}$ mice on DIV16. BDNF (3.7nM) was applied for 24 hours together with the chase ligand between DIV15 and DIV16. The graphs here present the mean values across eight cultures (N=8). **a.** Pulse ligand (R110Direct) average puncta number per image in synapses where pulse and chase ligands colocalise (type 2). The difference between the BDNF group and untreated controls is not statistically significant (Welch's t-test, p=0.12). **b.** Pulse ligand average puncta number per image in synapses where pulse and chase ligands do not colocalise (type 3). The difference between the BDNF group and untreated controls is not statistically significant (Welch's t-test, p=0.92). **c.** Comparison of pulse ligand average puncta number per image in type 2 synapses and type 3 synapses following BDNF treatment. The difference between the two groups is statistically significant (Welch's t-test, p=0.012). **d.** Chase ligand (TMR) average puncta number per image in synapses where pulse and chase ligands colocalise (type 2). The difference between the BDNF group and untreated controls is not statistically significant (Welch's t-test, p=0.11). **e.** Chase ligand average puncta number per image in synapses where pulse and chase ligands do not colocalise (type 1). The difference between the BDNF group and untreated controls is not statistically significant (Welch's t-test, p=0.060). **f.** Comparison of chase ligand average puncta number per image in type 2 synapses and type 1 synapses following BDNF treatment. The difference between the two groups is not statistically significant (Welch's t-test, p=0.33).

Moving to the analysis of pulse to chase ligand ratios at single synapses, we can see that there is no clear difference in the frequency distribution histograms between controls and BDNF-treated cultures (figures 4.25.a-b). The shapes of the histograms are very similar, covering the same range of ratios with very similar peaks. In the BDNF group, the mean ratio is 2.39 ± 0.064 (SEM), with the median ratio being 1.99 and the mode being a ratio of 1.2, at 9.18%. (For the control group the values are: mean ratio: 2.55 ± 0.051 (SEM); median ratio: 2.06; mode: 1.8 (8.76%)). It therefore does not appear as though BDNF affects pulse to chase ligand ratios at individual synapses.

Next, figure 4.25.c shows the APFI for the chase ligand at the different percentiles of the pulse ligand intensity. While the trend is the same as for the control group (a positive correlation between puncta intensities), the R^2 value is lower than the very high R^2=0.96 for the control group (figure 4.7.b), with R^2=0.68.

a.

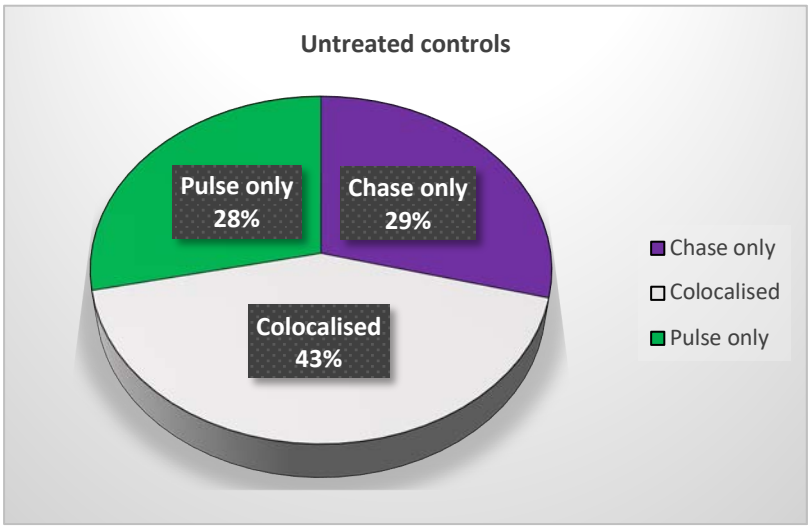

b.

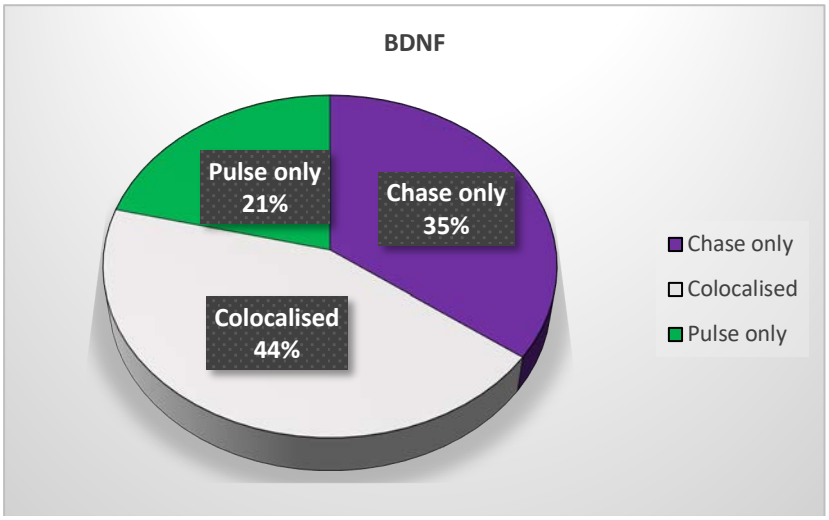

Figure 4.24. Proportional representation of synaptic population by HaloTag ligand-labelling following BDNF treatment.

Synaptic puncta were categorised according to whether they colocalised with puncta labelled by the other ligand or not. This pie chart depicts the proportional representation of the three types of synaptic puncta observed.

Images were taken after 24 hours of pulse-chase treatment with 50nM R110Direct ligand (pulse) and 500nM TMR ligand (chase) in hippocampal primary cultures from PSD-95$^{HaloTag/HaloTag}$ mice on DIV16. **a.** In untreated controls, 28% of puncta contain only the pulse (R110Direct) ligand (type 3), 43% of puncta contain both pulse and chase (TMR) ligands (type 2), and 29% contain only the chase ligand (type 1). **b.** Following 24 hours of BDNF treatment (3.7nM), 21% of puncta contain only the pulse (R110Direct) ligand (type 3), 44% of puncta contain both pulse and chase (TMR) ligands (type 2), and 35% contain only the chase ligand (type 1).

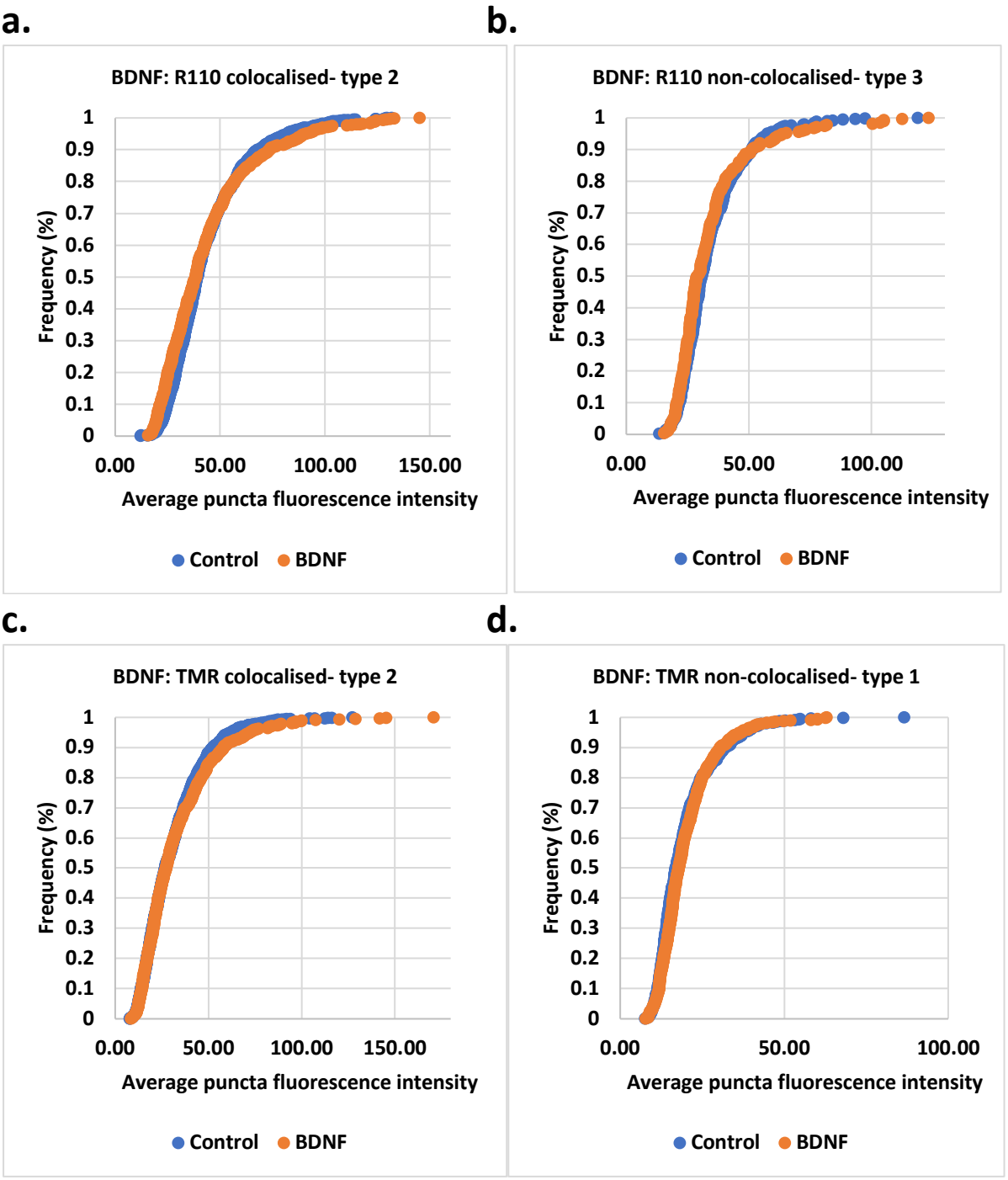

Figure 4.25. Cumulative distribution functions of average puncta fluorescence intensity following BDNF treatment.

CDFs were constructed using the single-synapse data following BDNF treatment, and compared with the untreated control group. Whether the difference was statistically significant or not was tested using the Kolmogorov-Smirnov test for difference. **a.** Comparison between R110 ligand puncta in colocalised type 2 synapses of BDNF-treated neurons with those in untreated controls. The difference is significant (Kolmogorov-Smirnov, $p<0.0001$). **b.** Comparison between R110 ligand puncta in non-colocalised type 3 synapses of BDNF-treated neurons with those in untreated controls. The difference is not significant (Kolmogorov-Smirnov, $p=0.061$). **c.** Comparison between TMR ligand puncta in colocalised type 2 synapses

of BDNF-treated neurons with those in untreated controls. The difference is not significant (Kolmogorov-Smirnov, p=0.313). **d.** Comparison between TMR ligand puncta in non-colocalised type 1 synapses of BDNF-treated neurons with those in untreated controls. The difference is not significant (Kolmogorov-Smirnov, p=0.063).

Lastly, cumulative distribution functions (CDF's) were calculated for each of the four groups (Figure 4.25). As before, a visual inspection indicates that the CDF curves of the treated groups look highly similar to those of untreated controls, displaying a very similar S-shaped curve that indicates a normal distribution. In this group, only a single test indicated statistically significant difference: the comparison between treated and untreated puncta within colocalising pulse (R110) puncta, i.e. type 2 synapses (Kolmogorov-Smirnov, $p<0.0001$). The other three groups were not statistically different from untreated controls: type 3 synapses ($p=0.061$), type 2 synapses chase ligand ($p=0.313$) and type 1 synapses ($p=0.063$). This indicates that the two synaptic populations are identical in terms of their average puncta fluorescence intensity distributions, meaning that the probability of a punctum having a specific intensity is equal in both populations.

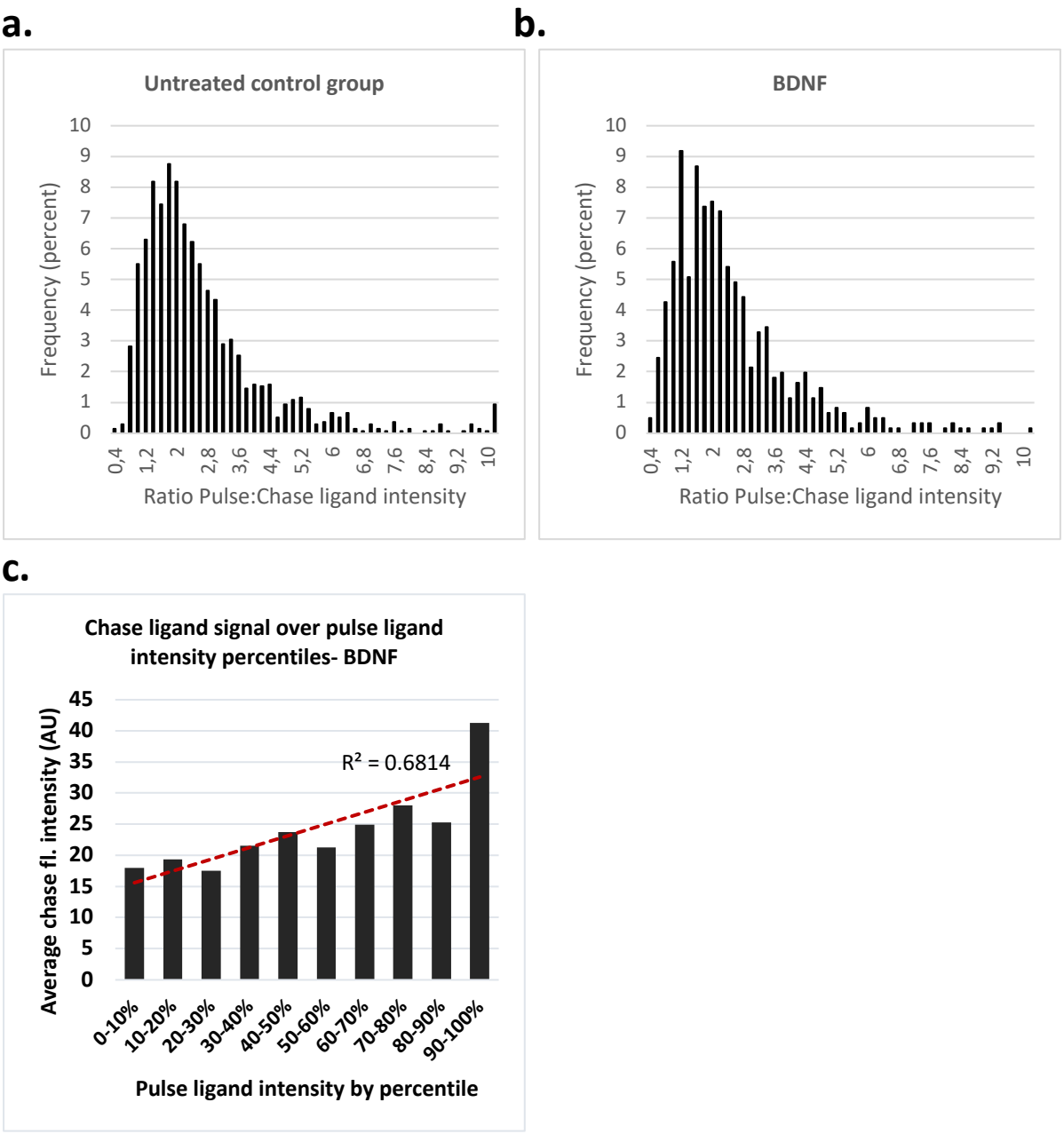

Figure 4.26. Graphs showing the ratio of pulse to chase ligands and correlation of pulse ligand intensity with chase ligand intensity at individual type 2 synapses following BDNF treatment.

In the synaptic population in which pulse and chase ligand-labelled PSD-95-HaloTag molecules were colocalised (type 2), the ratio of pulse ligand fluorescence intensity to chase ligand fluorescence intensity was calculated for each individual synapse. The frequency histograms represent the frequencies of all the pulse:chase ratios. **a.** Frequency distribution in untreated controls. Mean ratio: 2.55 ± 0.051 (SEM), Median ratio: 2.06, Mode: 1.8 (8.76%). **b.** Frequency distribution following 24 hours of BDNF (3.7nM) treatment. Mean ratio: 2.39 ± 0.064 (SEM), Median ratio: 1.99, Mode: 1.2 (9.18%). **c.** Type 2 synapses were sorted by their pulse ligand APFI (lowest to highest). For each ten percentile steps, average chase ligand APFI was calculated. Following BDNF treatment, there is a positive correlation (R^2=0.68).

4.4.3.3 BDNF: Discussion

It seems from these results, then, that BDNF does have an effect on total PSD-95 at synapses. Both pulse and chase ligand APFI are significantly higher (albeit not by a lot) than in untreated controls. This necessarily implies that total PSD-95 numbers at synapses are increased, too. Taken at face value, these results imply that BDNF causes an increase in PSD-95 synthesis (chase ligand), but also causes more old PSD-95 (pulse ligand) to be found at synapses. While the increased amount of new PSD-95 can only be explained by enhanced synthesis, the increased amount of old PSD-95 has two explanations- a reduced degradation of old PSD-95, or the cycling of old PSD-95 into synapses from dendrites and adjacent synapses. While my method does not allow me to distinguish between these two explanations, it does support the studies by Hu et al (2011) and Yoshii and Constantine-Paton (2007) that found BDNF to cause the trafficking of PSD-95 to synapses. On the other hand, my results are based on the analysis of thousands of synapses averaged together, meaning that if a synapse recruits old PSD-95 at the expense of an adjacent synapse (see Gray et al., 2006), then overall levels of old PSD-95 should not, on average, be higher. The indication, then, is that PSD-95 degradation is reduced following BDNF treatment.
My finding that PSD-95 synthesis is enhanced stands in contrast to the study by Yoshii and Constantine-Paton, who did not observe this effect, but supports the findings of Butko et al. (2012). While I found the increase in synaptic chase puncta number to be statistically insignificantly (figure 4.19.d, $p=0.073$), the difference was nevertheless marked, and quite close to becoming statistically significant. Furthermore, figure 4.22 shows that the proportion of type 1 synapses has increased as well. These results seem to support the positive role that BDNF plays in dendritic outgrowth and synaptogenesis, although a greater time window would perhaps have been required to make such large structural changes manifest themselves more noticeably. Out of all of my results, puncta numbers are the most variable, making these results the least likely to be statistically significant. A larger sample size would thus also have been useful.

Looking at the single-synapse level, compared to controls I found an increase in old PSD-95 at type 3 synapses and an increase in new PSD-95 at type 2 synapses. One

possible explanation for this is that type 2 synapses, which are presumably steadily turning over PSD-95, synthesise or recruit more new PSD-95 in response to BDNF (i.e. their rate of PSD-95 turnover changes to allow an increase in new PSD-95 in these synapses). This is supported by findings by Butko et al. (2012). Type 3 synapses, on the other hand, that only contain old PSD-95, respond to the BDNF stimulus by reducing their rate of PSD-95 degradation. This appears strange if assuming that type 3 synapses are undergoing pruning. However, as mentioned before they may also be in a state of low activity, tending towards becoming quiet synapses, and if that is the case they may not contain much protein synthesis machinery such as polyribosomes anymore. Instead, they may need to respond to the BDNF signal by reducing degradation, and thus enhancing their PSD-95 levels. Nevertheless, their responsiveness to BDNF does create a lot of uncertainty about the nature of type 3 synapses. Type 1 synapses, however, are probably newly formed synapses, and are therefore already recruiting new PSD-95 to rapidly establish their PSDs. In these synapses, BDNF does not cause an increased rate of PSD-95 recruitment, as they are already at the limit of their synthesis and recruitment capabilities. While this is only one possible scenario to explain the results obtained in this study, ultimately BDNF does cause synaptic PSD-95 levels to be enhanced.

4.4.4.1 Ketamine: bulk analysis

Moving to the group treated with ketamine, I initially set up experiments with two doses of ketamine- one high, and the other low. Since previous studies (Zarate et al., 2006; Li et al., 2010; Choi et al., 2015) had shown that ketamine only exhibits its effect of treating major depressive disorder and enhancing PSD-95 levels at low doses, but not high doses, I decided to test both in order to observe this difference. For the first two cultures, I therefore exposed neurons to ketamine at both high (10μM) and low (10nM) doses. However, after 24 hours of incubation, neurons exposed to 10μM ketamine all died. While the mechanism of action of ketamine that causes the anti-depressive effect has not yet been fully established (Gould et al., 2017), it is thought to exert its effect through a variety of different routes. These include the disinhibition of pyramidal neurons by blocking NMDA receptors on inhibitory GABA-ergic interneurons, which induces a glutamate surge and AMPA receptor activation, thereby stimulating BDNF release and increased protein synthesis (Abdallah et al., 2016). This mechanism of action would explain the increased PSD-95 levels that have been reported previously, and the glutamate surge could explain the toxic effect on neurons at high concentrations over 24 hours of exposure. Since this neurotoxic effect prevented me from gaining any data from the high-dose treatment group, I decided to cease this treatment, and focus solely on low ketamine doses (10nM).

The first noticeable result was that pulse ligand APFI was significantly higher after 24 hours of chase incubation with ketamine than in untreated controls (figure 4.27.a). While in controls APFI went down to 41.44 ± 0.85 AU over 24 hours, the APFI only went down to 50.95 ± 2.20 AU in the ketamine-treated group. This difference was statistically very significant (Welch's t-test, $p=0.0091$). Chase ligand APFI, on the other hand, was unaffected by ketamine treatment (figure 4.27.b, $p=0.31$). Likewise, synaptic puncta number appeared to be unchanged in ketamine-treated cultures compared to controls, for both pulse-ligand puncta (figure 4.27.c, $p=0.46$) and chase-ligand puncta (figure 4.27.d, $p=0.78$).

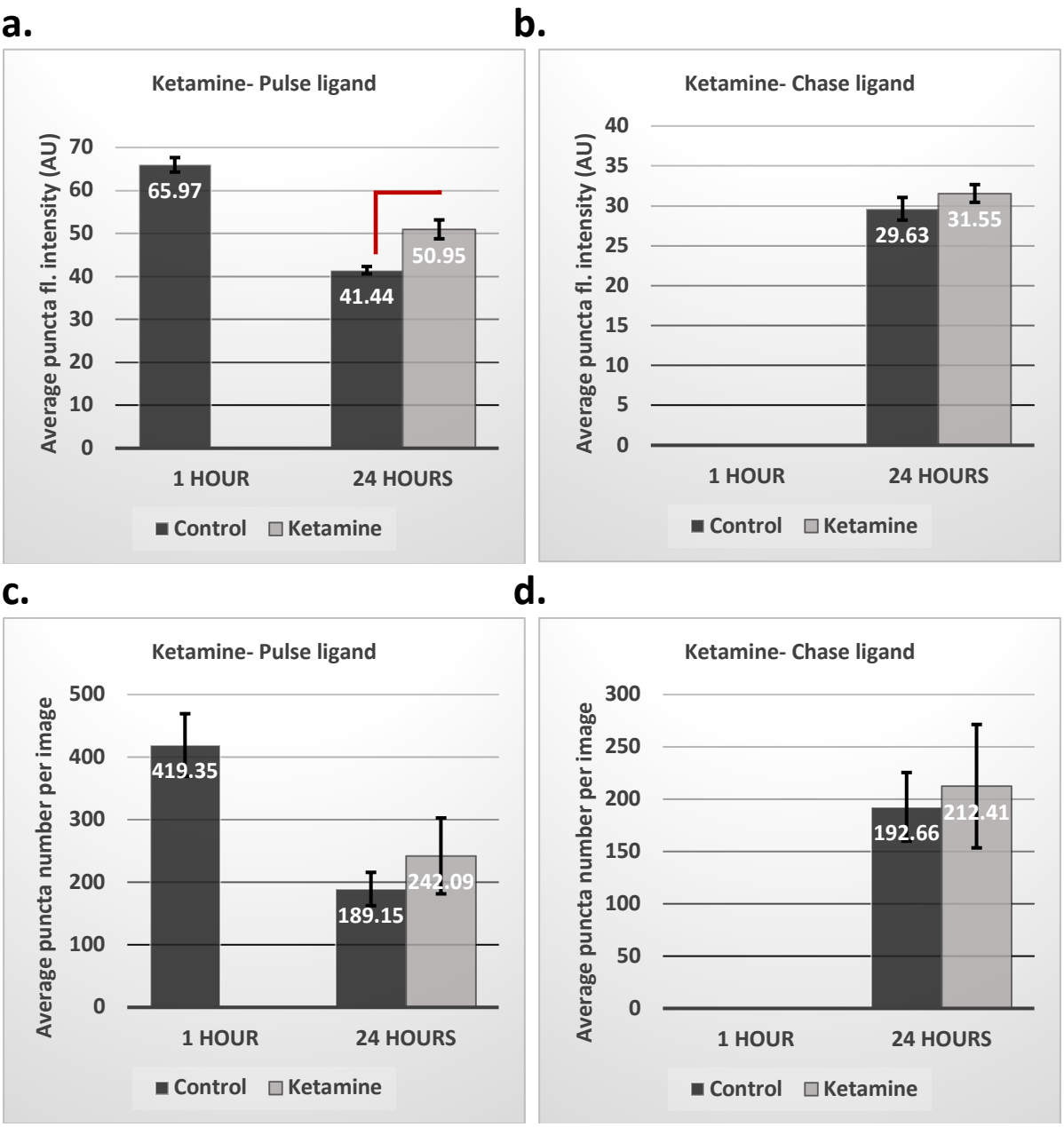

Figure 4.27. The effect of ketamine on PSD-95 puncta intensities and numbers.
Hippocampal neuronal primary cultures from PSD-95$^{HaloTag/HaloTag}$ mice were cultured until DIV14, when they were labelled with the R110Direct HaloTag ligand (50nM, 16h). On DIV15 the TMR ligand was added to the cultures at 500nM for 1 hour and 24 hours, alongside ketamine (10nM). APFI and number per image were then calculated. This was performed across 8 different cultures (N=8), with the graphs here presenting the mean values across these eight cultures. **a.** Graph of the R110 pulse ligand APFI following ketamine treatment. APFI is significantly higher after 24 hours in the ketamine group than in untreated controls (Welch's t-test, p=0.0091). **b.** Graph of the average TMR chase ligand APFI following ketamine treatment. APFI is not significantly higher in the ketamine group than in untreated controls (Welch's t-test, p=0.31). **c.** Graph of the average pulse ligand puncta number following ketamine treatment. The difference between the ketamine group and untreated controls after 24 hours is not significant (Welch's t-test, p=0.46). **d.** Graph of the average chase ligand puncta number following ketamine treatment. The difference between the ketamine group and untreated controls is not significant (Welch's t-test, p=0.78).

4.4.4.2 Ketamine: single-synapse analysis

At a single-synapse level, I was only able to observe statistically significant differences compared to controls in the APFI of the pulse ligand for both type 2 and type 3 synapses. In type 2 synapses (colocalised), pulse ligand APFI was significantly higher at 56.49 ± 2.80 AU than in controls, with 45.13 ± 0.93 AU (figure 4.28.a, p=0.013). In type 3 synapses (non-colocalised), the APFI was 41.94 ± 1.66 AU compared to 34.79 ± 0.80 AU for controls (figure 4.28.b, p=0.0084). For the chase ligand (figure 4.25.d-f), no differences in APFI were observed in type 2 and type 1 synapses. Similarly, synaptic puncta numbers did not differ from controls for any synaptic type (figure 4.29).

When looking at the overall synaptic population and proportion of synaptic types (figure 4.30), we see that there are in fact fewer type 1 (chase ligand only) synapses than synapses of other types. While this finding runs counter to the proposed mechanism of ketamine action, which postulates that ketamine enhances synaptogenesis (Abdallah et al., 2016), and average puncta number for type 1 synapses following ketamine treatment is lower than in controls (figure 4.29.e), this difference is not statistically significant (p=0.31).

At individual type 2 synapses, the ratios of pulse to chase ligands appears to be very similar to untreated controls (figure 4.32). The frequency histograms have a very similar shape and distribution, with the ketamine-treated group having an average ratio of 3.09 ± 0.050 (SEM), with the median ratio being 2.57 and the mode being a ratio of 2, at 7.23%. (For the control group the values are: mean ratio: 2.55 ± 0.051 (SEM); median ratio: 2.06; mode: 1.8 (8.76%)). It therefore does not appear as though ketamine affects pulse to chase ligand ratios at individual synapses.

Next, when puncta were sorted by pulse ligand intensity into percentiles (figure 4.32.c), and the correlating average chase ligand intensities for these puncta calculated, the graph showed a strong positive correlation (R^2=0.79), although not as strong as for the control group (R^2=0.96, figure 4.7.b). Nevertheless, it is clear that as with TTX, BCC and BDNF treated cultures, ketamine treatment does not affect the

a.

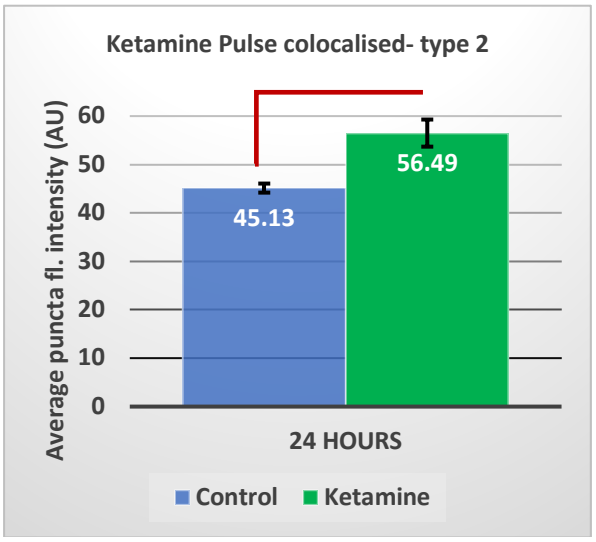
Ketamine Pulse colocalised- type 2
Average puncta fl. intensity (AU)
60
50
40
30
20
10
0
45.13
56.49
24 HOURS
Control
Ketamine

b.

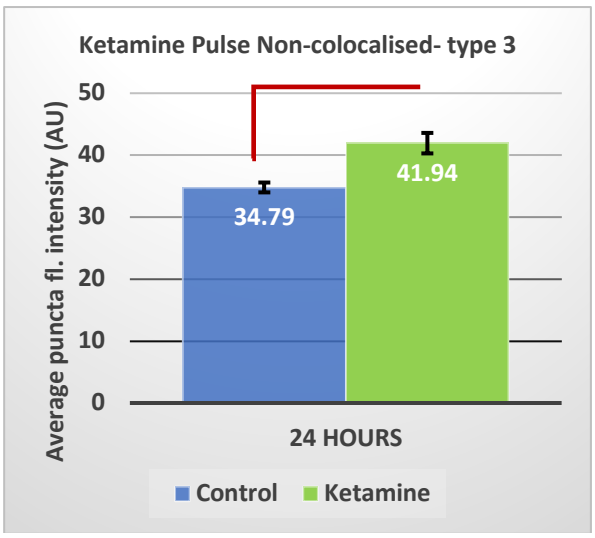
Ketamine Pulse Non-colocalised- type 3
Average puncta fl. intensity (AU)
50
40
30
20
10
0
34.79
41.94
24 HOURS
Control
Ketamine

c.

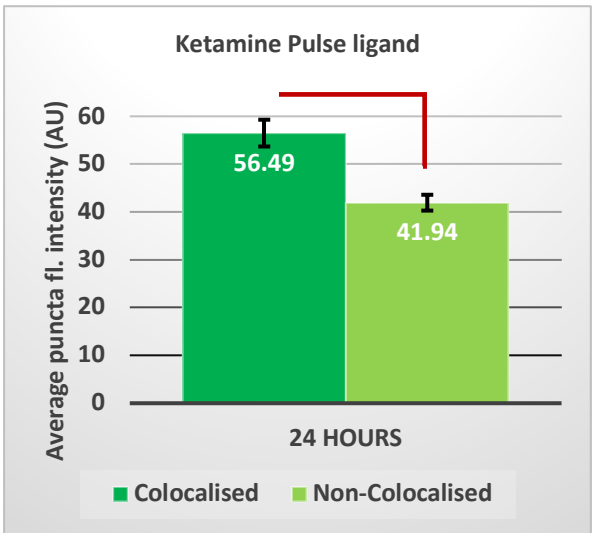
Ketamine Pulse ligand
Average puncta fl. intensity (AU)
60
50
40
30
20
10
0
56.49
41.94
24 HOURS
Colocalised
Non-Colocalised

d.

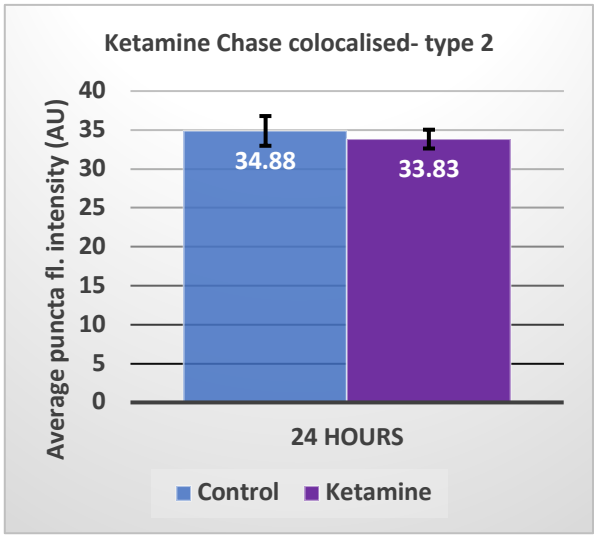
Ketamine Chase colocalised- type 2
Average puncta fl. intensity (AU)
40
35
30
25
20
15
10
5
0
34.88
33.83
24 HOURS
Control
Ketamine

e.

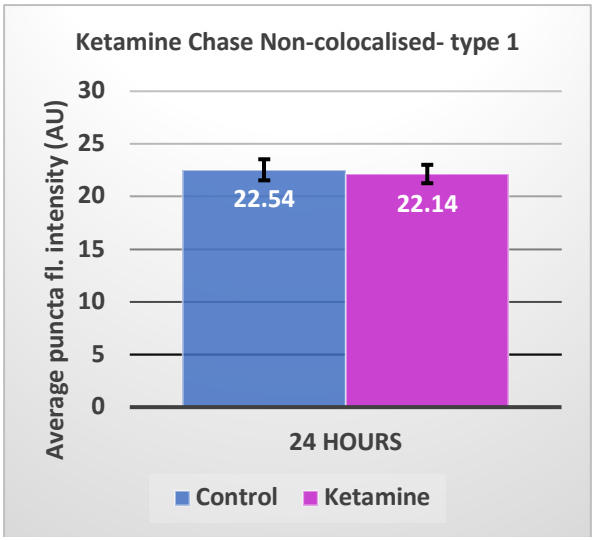
Ketamine Chase Non-colocalised- type 1
Average puncta fl. intensity (AU)
30
25
20
15
10
5
0
22.54
22.14
24 HOURS
Control
Ketamine

f.

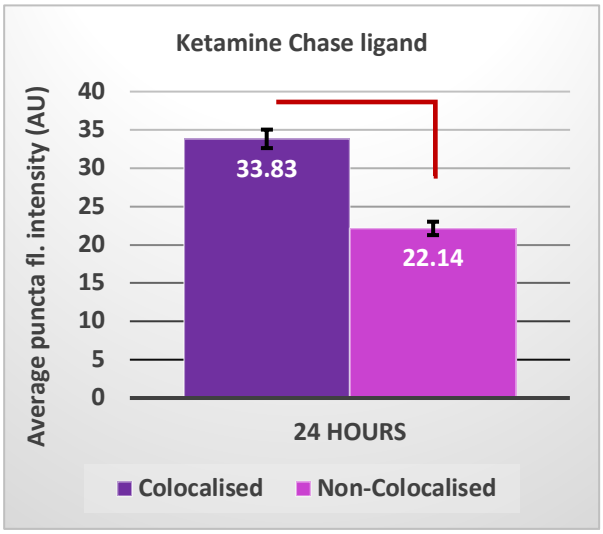
Ketamine Chase ligand
Average puncta fl. intensity (AU)
40
35
30
25
20
15
10
5
0
33.83
22.14
24 HOURS
Colocalised
Non-Colocalised

Figure 4.28. The effect of ketamine on PSD-95 average puncta intensity at synaptic types. Average puncta fluorescence intensity (APFI) per image was calculated for pulse and chase ligand labelled synaptic puncta in type 1, type 2 and type 3 synapses separately. Images were taken after 24 hours of pulse-chase treatment with 50nM R110Direct ligand (pulse) and 500nM TMR ligand (chase) in hippocampal primary cultures from PSD-95$^{HaloTag/HaloTag}$ mice on DIV16. Ketamine (10nM) was applied for 24 hours together with the chase ligand between DIV15 and DIV16. The graphs here present the mean values across eight cultures (N=8). **a.** Pulse ligand (R110Direct) APFI per image in synapses where pulse and chase ligands colocalise (type 2). The difference between the ketamine group and untreated controls is statistically significant (Welch's t-test, p=0.013). **b.** Pulse ligand APFI per image in synapses where pulse and chase ligands do not colocalise (type 3). The difference between the ketamine group and untreated controls is statistically significant (Welch's t-test, p=0.0084). **c.** Comparison of pulse ligand APFI per image in type 2 synapses and type 3 synapses following ketamine treatment. The difference between the two groups is statistically significant (Welch's t-test, p=0.0035). **d.** Chase ligand (TMR) APFI per image in synapses where pulse and chase ligands colocalise (type 2). The difference between the ketamine group and untreated controls is not statistically significant (Welch's t-test, p=0.65). **e.** Chase ligand APFI per image in synapses where pulse and chase ligands do not colocalise (type 1). The difference between the ketamine group and untreated controls is not statistically significant (Welch's t-test, p=0.77). **f.** Comparison of chase ligand APFI per image in type 2 synapses and type 1 synapses following ketamine treatment. The difference between the two groups is highly statistically significant (Welch's t-test, p=3.35x10^{-5}).

strong pattern that synapses with a stronger pulse ligand APFI also display a stronger chase ligand APFI.

Lastly, CDF's were calculated for each of the four groups (figure 4.31). Again, a view of the CDF curves of the treated groups indicates a shape similar to those of untreated controls. However, one can observe that in each of the four graphs the treated group's curve is shifted slightly to the right relative to untreated controls. This indicates that the expected fluorescence intensity of a given punctum is slightly higher in the ketamine-treated group than the control group. In this treatment group, all of the synaptic types were found to be statistically significant different: In each case, the Kolmogorov-Smirnov test for difference indicated that the treated groups were different to controls by a high margin (p=0.0004 or lower). Overall, then, this data indicates qualitatively and quantitatively that ketamine may enhance PSD-95 expression levels at individual synapses.

4.4.4.3 Ketamine: Discussion

The main finding from this study regarding the effect of ketamine on PSD-95 is that the bulk APFI value for the pulse ligand is significantly higher following 24 hours of ketamine treatment than in controls (figure 4.27.a). This higher intensity could be detected at the level of type 2 and type 3 synapses. Chase ligand intensity, however, was unaffected. While this result does not allow me to definitively state that total PSD-95 levels at synapses increased, since it only represents old, pulse-labelled PSD-95, this does appear to be the implication. It appears that this result is the effect of reduced PSD-95 degradation, but not increased synthesis. Interestingly, this occurs at both type 2 and type 3 synapses, unlike with BDNF, which only affects type 3 synapses. Contrary to BDNF treatment, however, ketamine does not enhance the synthesis of new PSD-95. Thus, ketamine may activate different cellular pathways and responses than BDNF, which is somewhat surprising given that ketamine has been proposed to cause BDNF release at synapses (Browne & Lucki, 2013). Nevertheless, ketamine's complete effect on neurons is still not fully understood, and is thought to be complex, making it difficult to say why it appears to significantly reduce the degradation of PSD-95 at synapses while not affecting its synthesis. Indeed, it is possible that ketamine exerts part of its effect through the stabilisation of PSD-95 at the PSD, thus effecting the increased glutamate transmission observed (Duman et al., 2012).

As mentioned above, my results did not support the finding that ketamine causes increased synaptogenesis (Abdallah et al., 2016), with the number of observed type 1 synapses slightly lower than in the control group, albeit not statistically significantly. The results do warrant a further investigation of the effect of ketamine on PSD-95 turnover, however, and one next step would be to perform western blots of cultures treated with ketamine in conjunction with my pulse-chase method, in order discover whether ketamine enhances total PSD-95 levels. Also, using a single ligand as opposed to pulse-chase labelling, in the presence of ketamine, would give valuable information about changes in total PSD-95 levels at synapses.

a.

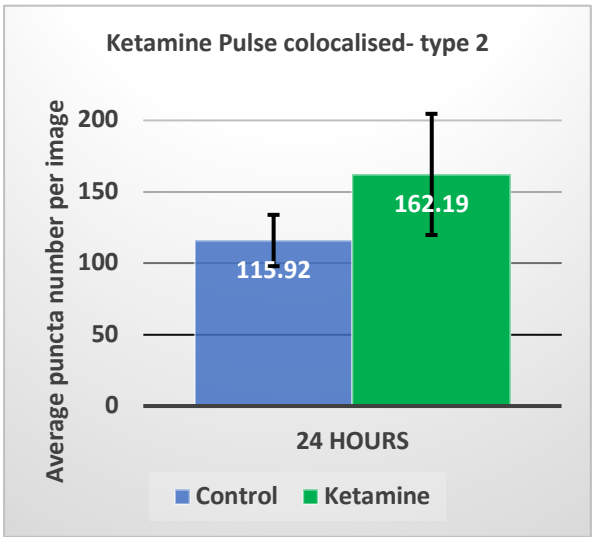
Ketamine Pulse colocalised- type 2
Average puncta number per image
200
150
100
50
0
115.92
162.19
24 HOURS
Control
Ketamine

b.

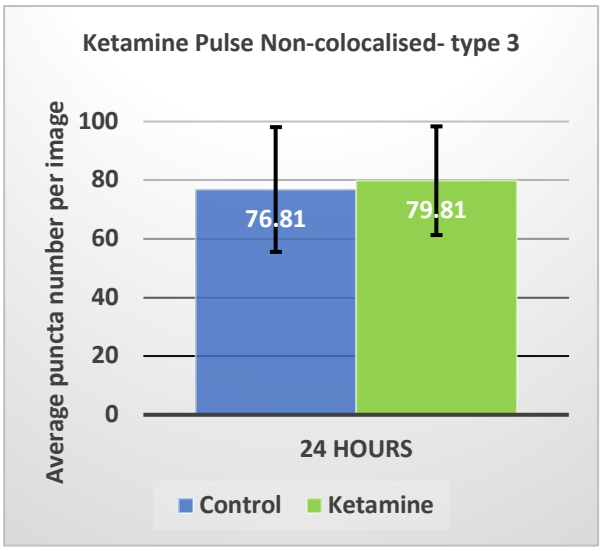
Ketamine Pulse Non-colocalised- type 3
Average puncta number per image
100
80
60
40
20
0
76.81
79.81
24 HOURS
Control
Ketamine

c.

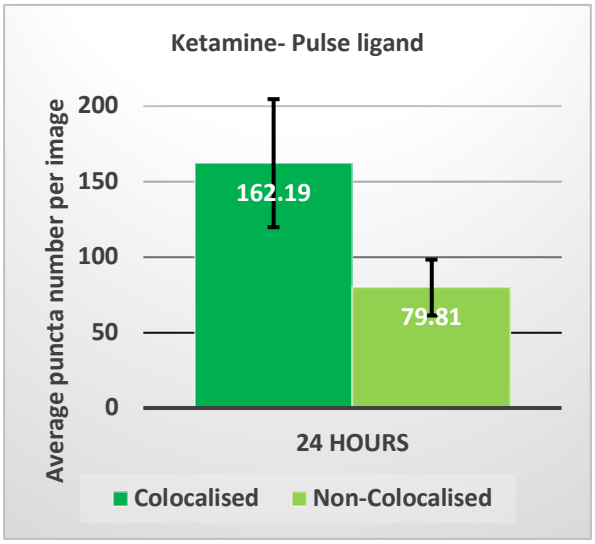
Ketamine- Pulse ligand
Average puncta number per image
200
150
100
50
0
162.19
79.81
24 HOURS
Colocalised
Non-Colocalised

d.

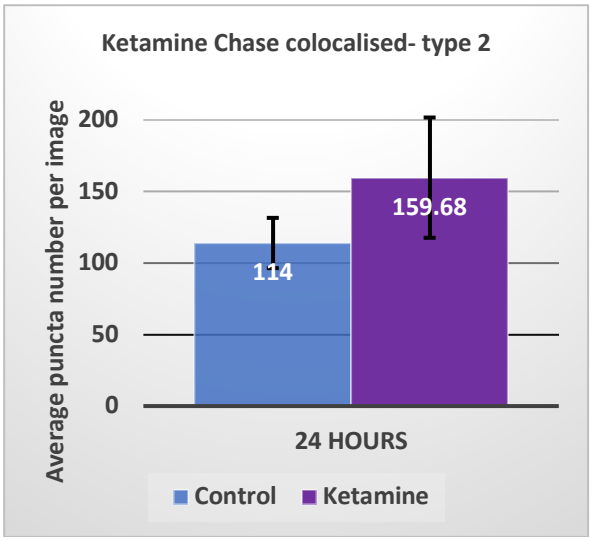
Ketamine Chase colocalised- type 2
Average puncta number per image
200
150
100
50
0
114
159.68
24 HOURS
Control
Ketamine

e.

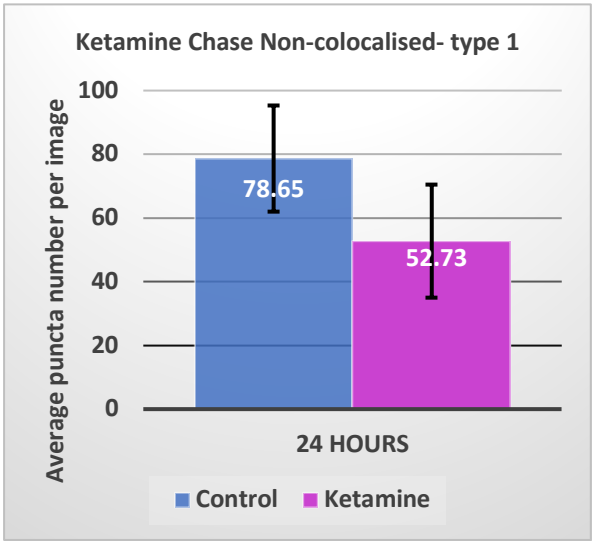
Ketamine Chase Non-colocalised- type 1
Average puncta number per image
100
80
60
40
20
0
78.65
52.73
24 HOURS
Control
Ketamine

f.

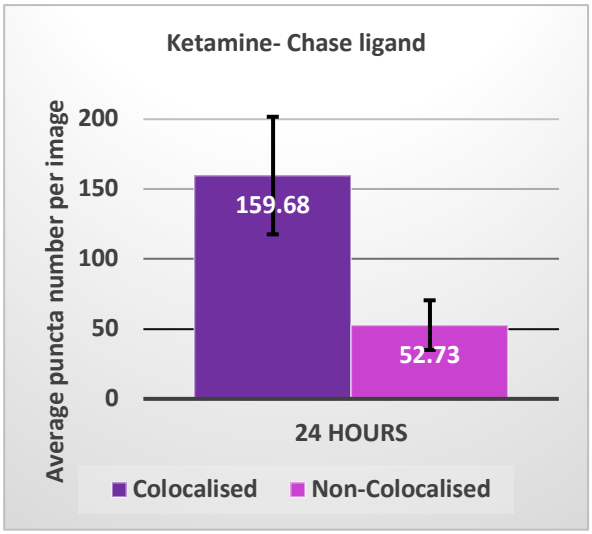
Ketamine- Chase ligand
Average puncta number per image
200
150
100
50
0
159.68
52.73
24 HOURS
Colocalised
Non-Colocalised

Figure 4.29. The effect of ketamine on PSD-95 average puncta number at synaptic types. Average puncta number per image was calculated for pulse and chase ligand labelled synaptic puncta in type 1, type 2 and type 3 synapses separately. Images were taken after 24 hours of pulse-chase treatment with 50nM R110Direct ligand (pulse) and 500nM TMR ligand (chase) in hippocampal primary cultures from PSD-95$^{HaloTag/HaloTag}$ mice on DIV16. Ketamine (10nM) was applied for 24 hours together with the chase ligand between DIV15 and DIV16. The graphs here present the mean values across eight cultures (N=8). **a.** Pulse ligand (R110Direct) average puncta number per image in synapses where pulse and chase ligands colocalise (type 2). The difference between the ketamine group and untreated controls is not statistically significant (Welch's t-test, p=0.36). **b.** Pulse ligand average puncta number per image in synapses where pulse and chase ligands do not colocalise (type 3). The difference between the ketamine group and untreated controls is not statistically significant (Welch's t-test, p=0.92). **c.** Comparison of pulse ligand average puncta number per image in type 2 synapses and type 3 synapses following ketamine treatment. The difference between the two groups is not statistically significant (Welch's t-test, p=0.13). **d.** Chase ligand (TMR) average puncta number per image in synapses where pulse and chase ligands colocalise (type 2). The difference between the ketamine group and untreated controls is not statistically significant (Welch's t-test, p=0.36). **e.** Chase ligand average puncta number per image in synapses where pulse and chase ligands do not colocalise (type 1). The difference between the ketamine group and untreated controls is not statistically significant (Welch's t-test, p=0.31). **f.** Comparison of chase ligand average puncta number per image in type 2 synapses and type 1 synapses following ketamine treatment. The difference between the two groups is not statistically significant (Welch's t-test, p=0.063).

a.

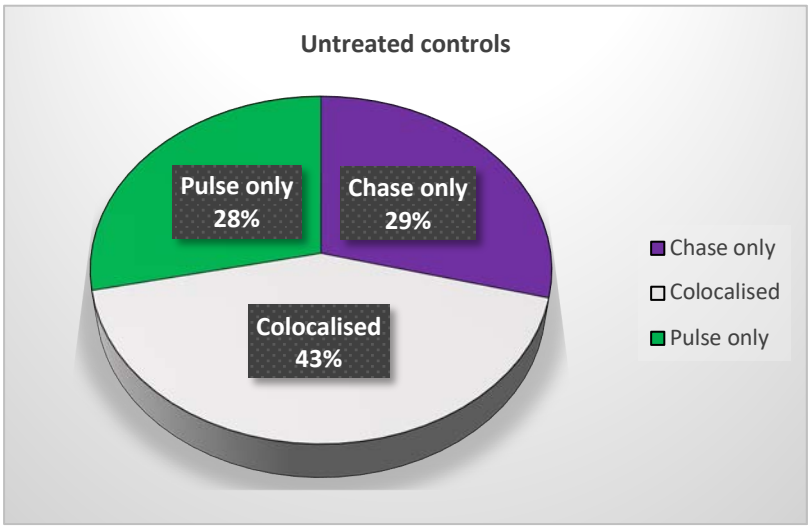

b.

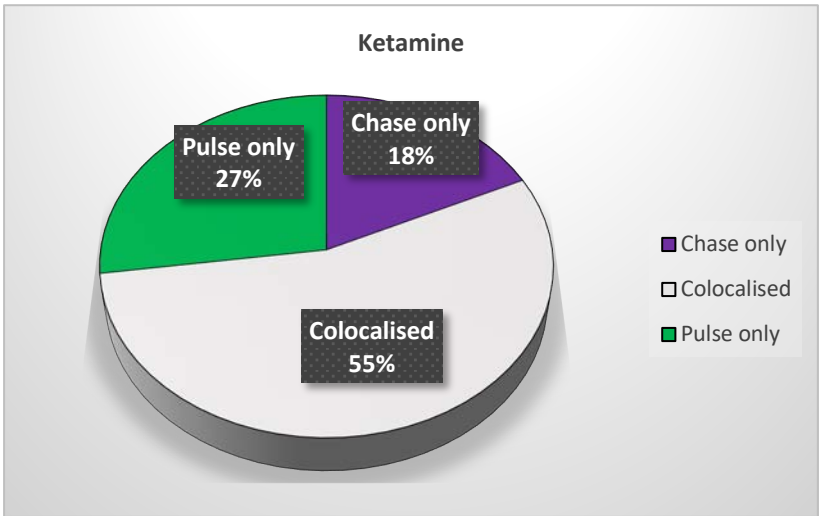

Figure 4.30. Proportional representation of synaptic population by HaloTag ligand-labelling following ketamine treatment.

Synaptic puncta were categorised according to whether they colocalised with puncta labelled by the other ligand or not. This pie chart depicts the proportional representation of the three types of synaptic puncta observed.

Images were taken after 24 hours of pulse-chase treatment with 50nM R110Direct ligand (pulse) and 500nM TMR ligand (chase) in hippocampal primary cultures from PSD-95$^{HaloTag/HaloTag}$ mice on DIV16. **a.** In untreated controls, 28% of puncta contain only the pulse (R110Direct) ligand (type 3), 43% of puncta contain both pulse and chase (TMR) ligands (type 2), and 29% contain only the chase ligand (type 1). **b.** Following 24 hours of ketamine treatment (10nM), 27% of puncta contain only the pulse (R110Direct) ligand (type 3), 55% of puncta contain both pulse and chase (TMR) ligands (type 2), and 18% contain only the chase ligand (type 1).

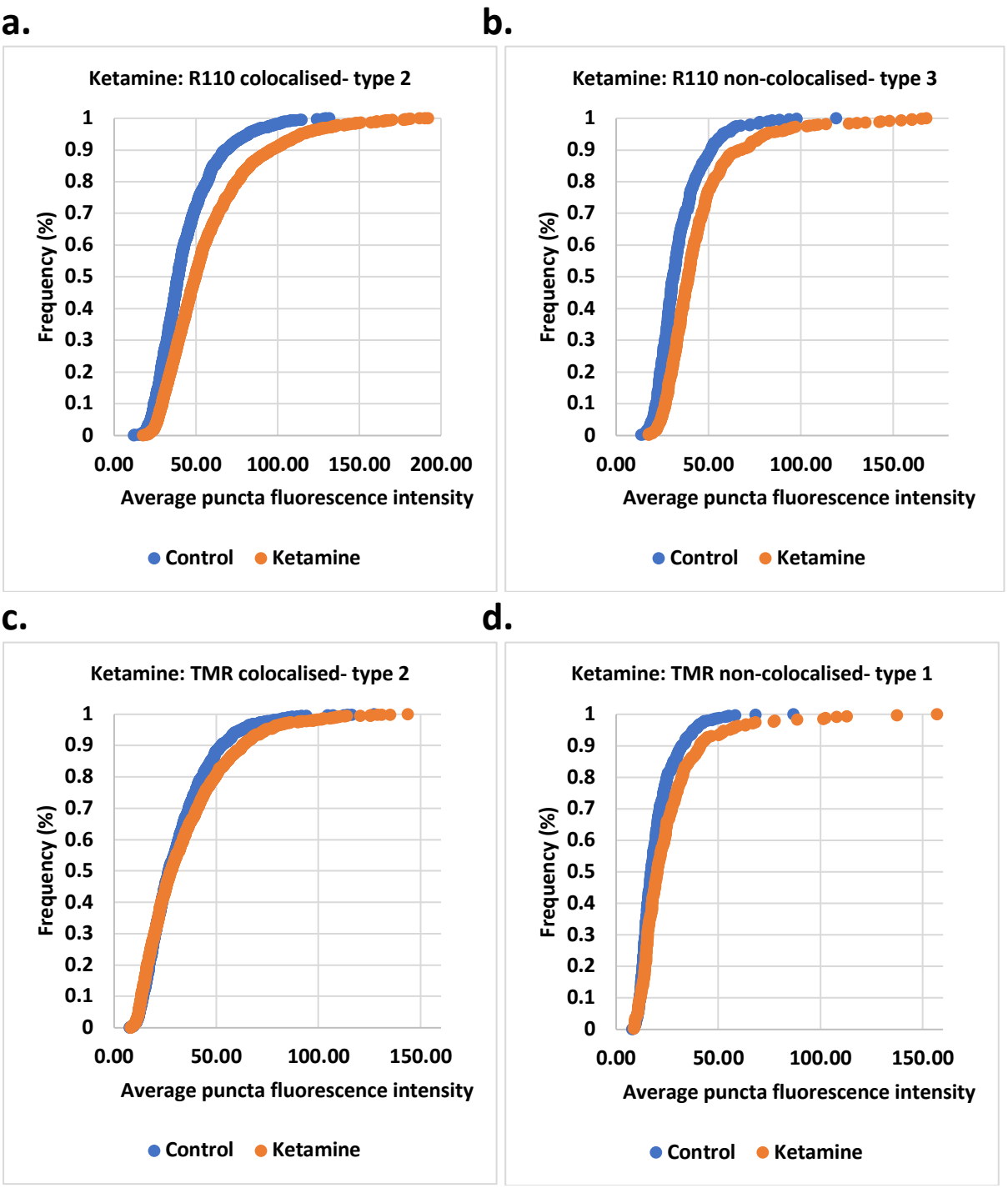

Figure 4.31. Cumulative distribution functions of average puncta fluorescence intensity following ketamine treatment.

CDFs were constructed using the single-synapse data following ketamine treatment, and compared with the untreated control group. Whether the difference was statistically significant or not was tested using the Kolmogorov-Smirnov test for difference. **a.** Comparison between R110 ligand puncta in colocalised type 2 synapses of ketamine-treated neurons with those in untreated controls. The difference is significant (Kolmogorov-Smirnov, $p<0.0001$). **b.** Comparison between R110 ligand puncta in non-colocalised type 3 synapses of ketamine-treated neurons with those in untreated controls. The difference is significant (Kolmogorov-Smirnov, $p<0.0001$). **c.** Comparison between TMR ligand puncta in colocalised type 2 synapses of ketamine-treated neurons with those in untreated controls. The difference is significant

(Kolmogorov-Smirnov, p=0.0004). **d.** Comparison between TMR ligand puncta in non-colocalised type 1 synapses of ketamine-treated neurons with those in untreated controls. The difference is significant (Kolmogorov-Smirnov, p<0.0001).

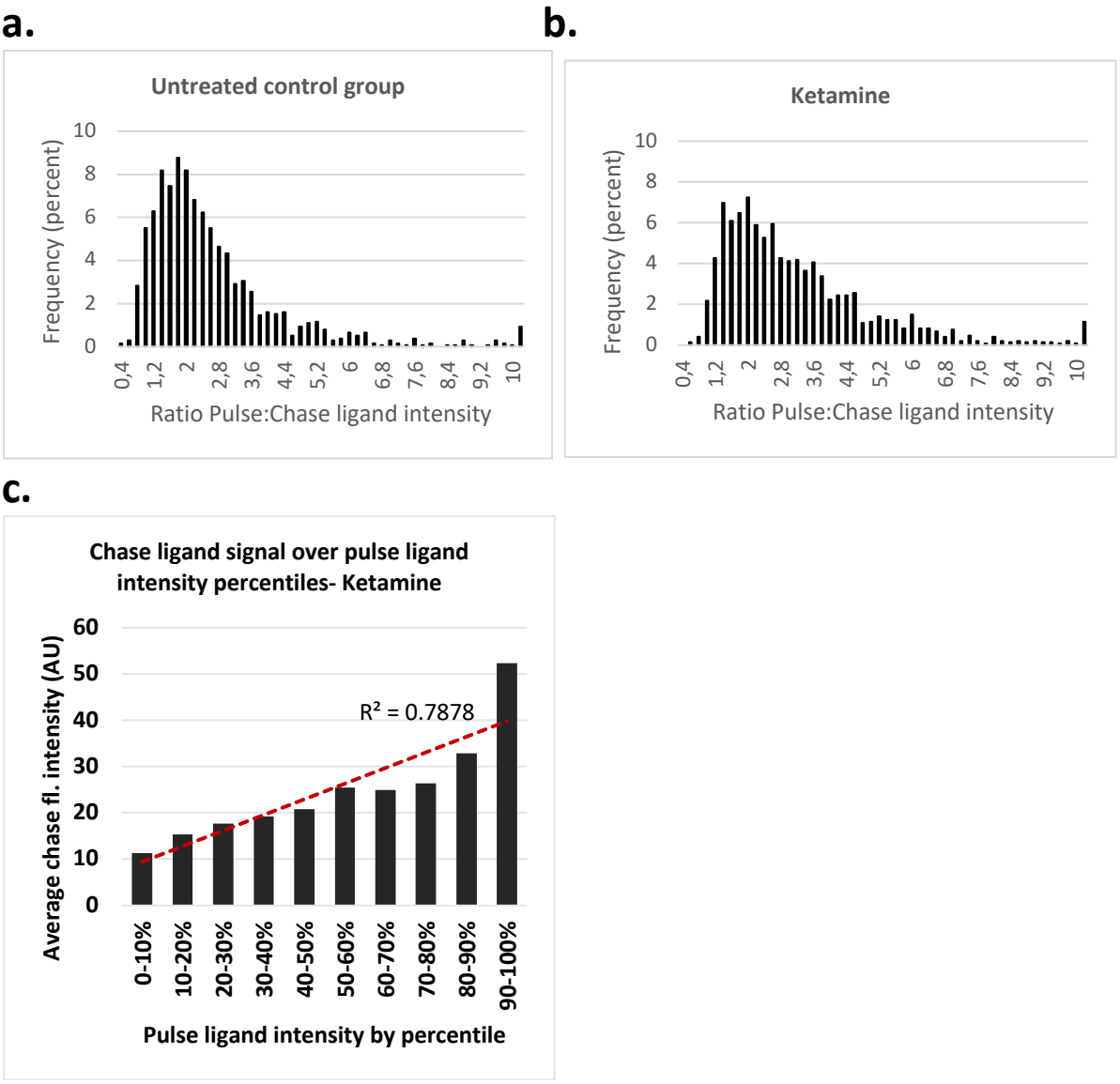

Figure 4.32. Graphs showing the ratio of pulse to chase ligands and correlation of pulse ligand intensity with chase ligand intensity at individual type 2 synapses following ketamine treatment.

In the synaptic population in which pulse and chase ligand-labelled PSD-95-HaloTag molecules were colocalised (type 2), the ratio of pulse ligand fluorescence intensity to chase ligand fluorescence intensity was calculated for each individual synapse. The frequency histograms represent the frequencies of all the pulse:chase ratios.

a. Frequency distribution in untreated controls. Mean ratio: 2.55 ± 0.051 (SEM), Median ratio: 2.06, Mode: 1.8 (8.76%). **b.** Frequency distribution following 24 hours of ketamine (10nM) treatment. Mean ratio: 3.09 ± 0.050 (SEM), Median ratio: 2.57, Mode: 2 (7.23%).

c. Type 2 synapses were sorted by their pulse ligand APFI (lowest to highest). For each ten percentile steps, average chase ligand APFI was calculated. Following ketamine treatment, there is a positive correlation (R^2=0.79).

4.4.5.1 Proteasome inhibitors- Lactacystin and MG132: bulk analysis

As mentioned before, Lactacystin and MG132 are both commonly used to block protein degradation by inhibiting the proteasome, the organelle known to be the main agent of PSD-95 degradation. From figure 4.33, we can immediately observe that both of these drugs have a strong, and similar, effect on PSD-95. Unlike in the study by Hakim et al. (2016), I do indeed find that lactacystin, as well as MG132, have what appears to be a severe effect upon PSD-95 degradation. There is a massive difference in the APFI of the pulse ligand after 24 hours of incubation with either of the proteasome inhibitors. In figure 4.33.a we see that pulse ligand APFI drops from 65.97 ± 1.69 AU at the 1-hour time point to 55.12 ± 2.33 AU after being incubated with lactacystin for 24 hours. In contrast, pulse ligand APFI in the untreated control group is reduced to 41.44 ± 0.85 AU at the same time point. The difference between these two values is highly statistically significant (Welch's t-test, p=0.00068). Following MG132 treatment for 24 hours, we see a similar effect as pulse ligand APFI falls to 56.10 ± 3.03 AU (p=0.0024) (figure 4.33.b).

Intriguingly, and matching the results reported by Hakim et al. (2016), I was also able to observe a marked effect upon PSD-95 synthesis. Figures 4.33.c and 4.33.d show that lactacystin and MG132 treatment both lead to a reduced synthesis of PSD-95, since chase ligand APFI is significantly lower for both groups. Lactacystin treatment (figure 4.33.c) results in a chase ligand APFI of 22.32 ± 1.45 AU, compared to 29.63 ± 1.42 AU for untreated controls (Welch's t-test, p=0.0033). In the MG132-treated group (figure 4.33.d), PSD-95 synthesis is affected even more strongly, with chase ligand APFI reduced to 16.88 ± 0.72 AU ($p=1.01x10^{-5}$).

Moving to the puncta number analysis, the results mirror those obtained for the puncta fluorescence intensity in figure 4.33. All of the results except for those pertaining to pulse ligand puncta number following lactacystin (figure 4.34.a) were significantly different from untreated controls. In the MG132-treated group, pulse ligand puncta number (mean 316.60 ± 43.36 puncta per image) was significantly higher than the mean 189.15 ± 26.64 puncta per image for controls (figure 4.34.b, p=0.031). In the lactacystin group, the mean puncta number per image was also higher than in controls

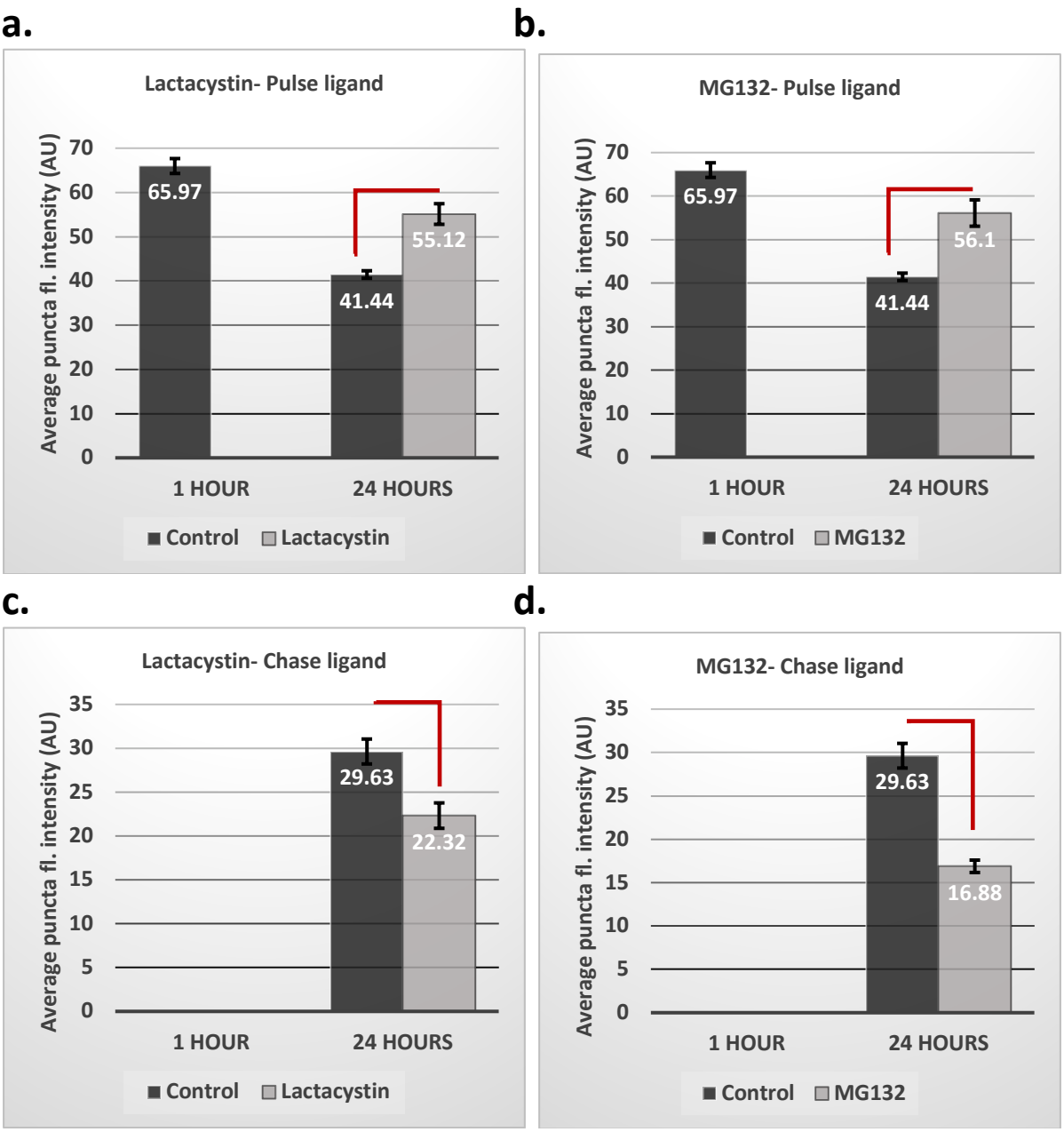

Figure 4.33. The effects of Lactacystin and MG132 on PSD-95 puncta intensities.
Hippocampal neuronal primary cultures from PSD-95$^{HaloTag/HaloTag}$ mice were grown for 14 days in vitro, and thereafter pulse-chase experiments performed using the R110Direct and TMR HaloTag ligands. Lactacystin at 1µM or MG132 at 10µM were added alongside the chase ligand for 1 or 24 hours. The graphs here present the mean values across eight cultures (N=8). **a.** Graph of the average R110 pulse ligand puncta fluorescence intensity following lactacystin treatment. APFI is significantly higher after 24 hours in the lactacystin group than in untreated controls (Welch's t-test, p=0.00068). **b.** Graph of the average R110 pulse ligand puncta intensity following MG132 treatment. APFI is significantly higher after 24 hours in the MG132 group than in untreated controls (Welch's t-test, p=0.0024). **c.** Graph of the average TMR chase ligand puncta fluorescence intensity following lactacystin treatment. The difference between the lactacystin group and untreated controls is significant (Welch's t-test, p=0.0033). **d.** Graph of the average TMR chase ligand puncta fluorescence intensity following MG132 treatment. The difference between the MG132 group and untreated controls is highly significant (Welch's t-test, $p=1.01x10^{-5}$).

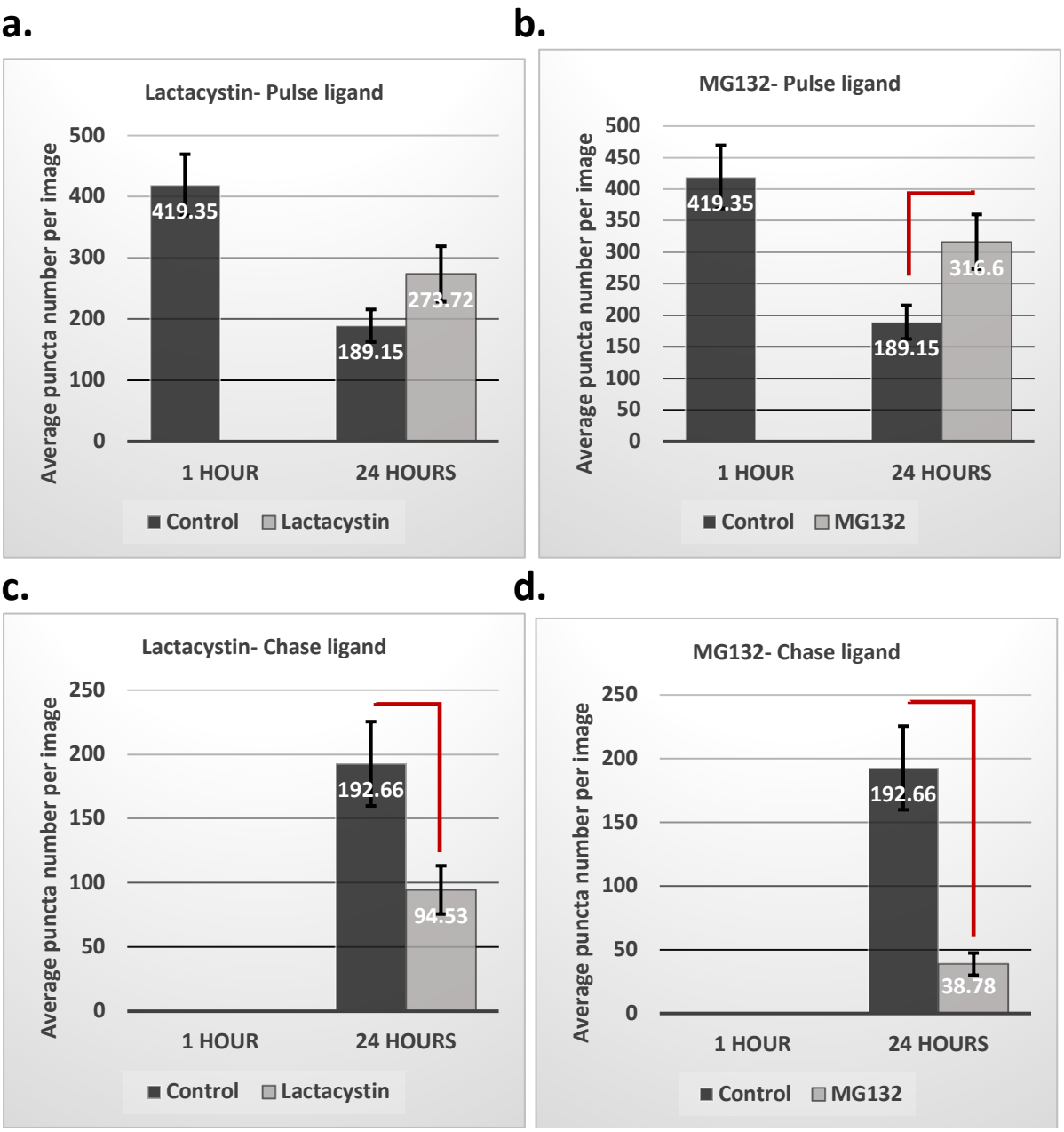

Figure 4.34. The effects of Lactacystin and MG132 on PSD-95 puncta numbers.
Hippocampal neuronal primary cultures from PSD-95$^{HaloTag/HaloTag}$ mice were grown for 14 days in vitro, and thereafter pulse-chase experiments performed using the R110Direct and TMR HaloTag ligands. Lactacystin at 1µM or MG132 at 10µM were added alongside the chase ligand for 1 or 24 hours. The graphs here present the mean values across eight cultures (N=8). **a.** Graph of the average R110 pulse ligand puncta number following lactacystin treatment. The number is not significantly higher after 24 hours in the lactacystin group than in untreated controls (Welch's t-test, p=0.14). **b.** Graph of the average R110 pulse ligand puncta number following MG132 treatment. The number is significantly higher after 24 hours in the MG132 group than in untreated controls (Welch's t-test, p=0.031). **c.** Graph of the average TMR chase ligand puncta number following lactacystin treatment. The difference between the lactacystin group and untreated controls is significant (Welch's t-test, p=0.025). **d.** Graph of the average TMR chase ligand puncta number following MG132 treatment. The difference between the MG132 group and untreated controls is significant (Welch's t-test, p=0.0019).

with 273.72 ± 45.38 puncta, but the difference in this case wasn't statistically significant (figure 4.34.a, p=0.14). Chase ligand puncta number was much lower compared to the 192.66 ± 32.83 puncta per image value for the control group in the lactacystin group (mean 94.53 ± 18.82 puncta per image, p=0.025, figure 4.34.c) and in the MG132 group as well (mean 38.78 ± 8.75 puncta per image, p=0.0019, figure 4.34.d).

Overall, then, I find bulk puncta number to be dramatically affected by both lactacystin and MG132 treatment. In terms of both average puncta fluorescence intensity (APFI) and average puncta number per image both drugs cause the pulse ligand numbers to remain higher than in the control group (implying a lower PSD-95 degradation rate), while chase ligand numbers are lower than in the control group (implying a lower PSD-95 synthesis rate).

4.4.5.2 Proteasome inhibitors- Lactacystin and MG132: single-synapse analysis

Once the results are sorted by synaptic types, it is interesting to see that the great differences in the fluorescence intensity values between the control group and the drug-treated groups are primarily being driven by type 2 (colocalised) synapses. For both lactacystin (figure 4.35.a) and MG132 (figure 4.36.a) the pulse ligand intensity differs most significantly from controls in type 2 synapses (control: 45.13 ± 0.93 AU; lactacystin: 77.33 ± 2.92 AU, $p=1.22x10^{-5}$; MG132: 103.49 ± 4.86 AU, $p=1.33x10^{-5}$). At type 3 synapses (pulse-ligand only), the values are still statistically significantly different from controls, but less so (lactacystin: p=0.0017, figure 4.35.b; MG132: $p=9.66x10^{-5}$, figure 4.36.b).

The same is true of the chase ligand- colocalised type 2 synapses exhibit a much greater degree of difference from controls than type 1 synapses. In figure 4.35.d we see that in type 2 synapses chase ligand APFI following lactacystin treatment is significantly lower with 22.38 ± 1.44 AU than the control group's value of 34.88 ± 1.91 AU (p=0.00019). This holds true for the MG132-treated group, with a value of 16.57 ± 0.73 AU ($p=9.22x10^{-6}$, figure 4.36.d). At type 1 synapses, the differences are not

a.

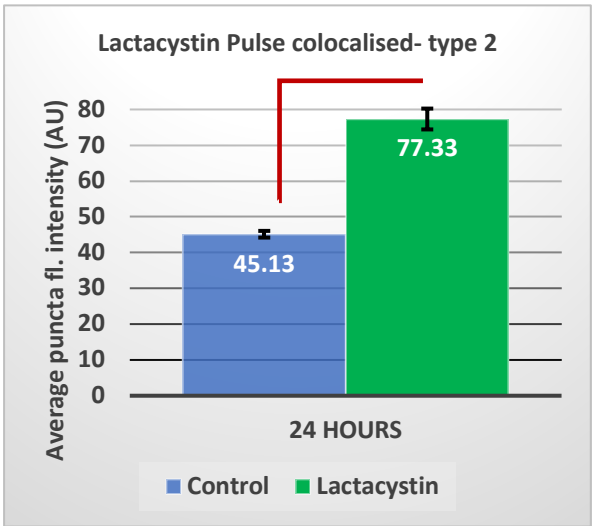
Lactacystin Pulse colocalised- type 2
Average puncta fl. intensity (AU)
80
70
60
50
40
30
20
10
0
45.13
77.33
24 HOURS
Control
Lactacystin

b.

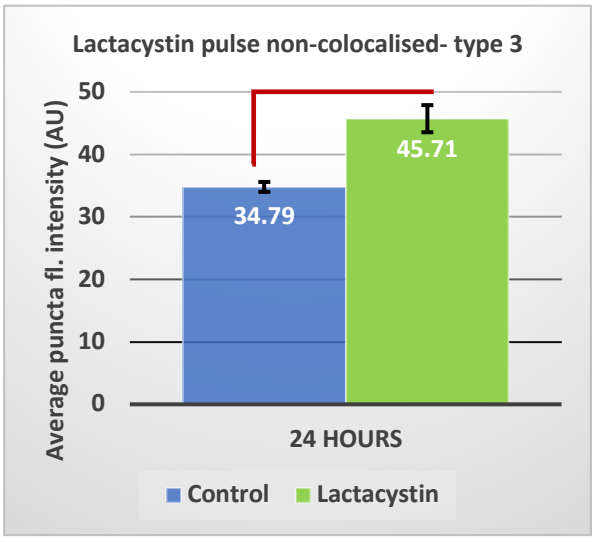
Lactacystin pulse non-colocalised- type 3
Average puncta fl. intensity (AU)
50
40
30
20
10
0
34.79
45.71
24 HOURS
Control
Lactacystin

c.

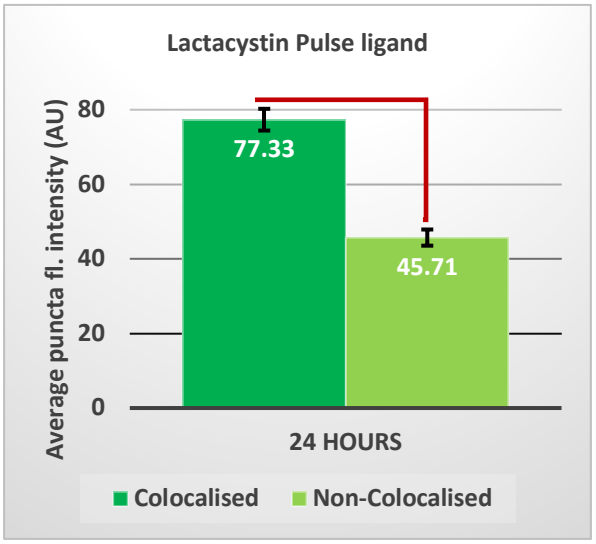
Lactacystin Pulse ligand
Average puncta fl. intensity (AU)
80
60
40
20
0
77.33
45.71
24 HOURS
Colocalised
Non-Colocalised

d.

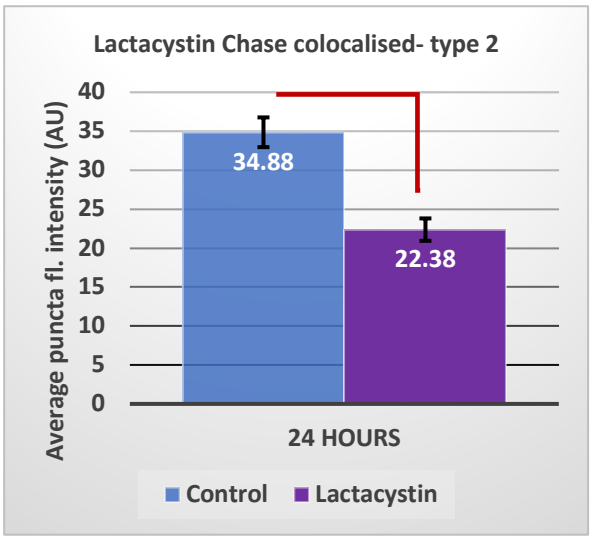
Lactacystin Chase colocalised- type 2
Average puncta fl. intensity (AU)
40
35
30
25
20
15
10
5
0
34.88
22.38
24 HOURS
Control
Lactacystin

e.

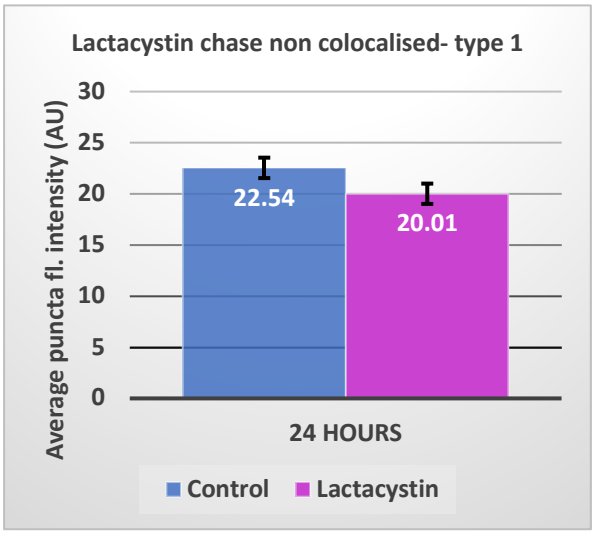
Lactacystin chase non colocalised- type 1
Average puncta fl. intensity (AU)
30
25
20
15
10
5
0
22.54
20.01
24 HOURS
Control
Lactacystin

f.

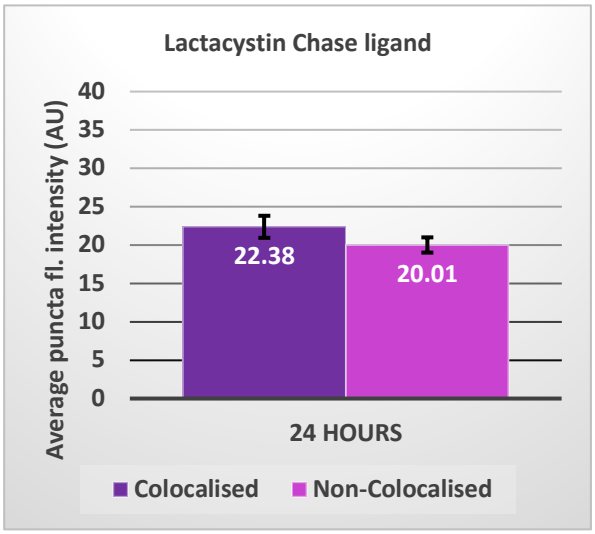
Lactacystin Chase ligand
Average puncta fl. intensity (AU)
40
35
30
25
20
15
10
5
0
22.38
20.01
24 HOURS
Colocalised
Non-Colocalised

Figure 4.35. The effect of lactacystin on PSD-95 average puncta intensity at synaptic types. Average puncta fluorescence intensity (APFI) per image was calculated for pulse and chase ligand labelled synaptic puncta in type 1, type 2 and type 3 synapses separately. Images were taken after 24 hours of pulse-chase treatment with 50nM R110Direct ligand (pulse) and 500nM TMR ligand (chase) in hippocampal primary cultures from PSD-95$^{HaloTag/HaloTag}$ mice on DIV16. Lactacystin (1µM) was applied for 24 hours together with the chase ligand between DIV15 and DIV16. The graphs here present the mean values across eight cultures (N=8). **a.** Pulse ligand (R110Direct) APFI per image in synapses where pulse and chase ligands colocalise (type 2). The difference between the lactacystin group and untreated controls is statistically significant (Welch's t-test, $p=1.22x10^{-5}$). **b.** Pulse ligand APFI per image in synapses where pulse and chase ligands do not colocalise (type 3). The difference between the lactacystin group and untreated controls is statistically significant (Welch's t-test, p=0.0017). **c.** Comparison of pulse ligand APFI per image in type 2 synapses and type 3 synapses following lactacystin treatment. The difference between the two groups is statistically significant (Welch's t-test, $p=2.76x10^{-6}$). **d.** Chase ligand (TMR) APFI per image in synapses where pulse and chase ligands colocalise (type 2). The difference between the lactacystin group and untreated controls is statistically significant (Welch's t-test, p=0.00019). **e.** Chase ligand APFI per image in synapses where pulse and chase ligands do not colocalise (type 1). The difference between the lactacystin group and untreated controls is not statistically significant (Welch's t-test, p=0.097). **f.** Comparison of chase ligand APFI per image in type 2 synapses and type 1 synapses following lactacystin treatment. The difference between the two groups is not statistically significant (Welch's t-test, p=0.20).

a.

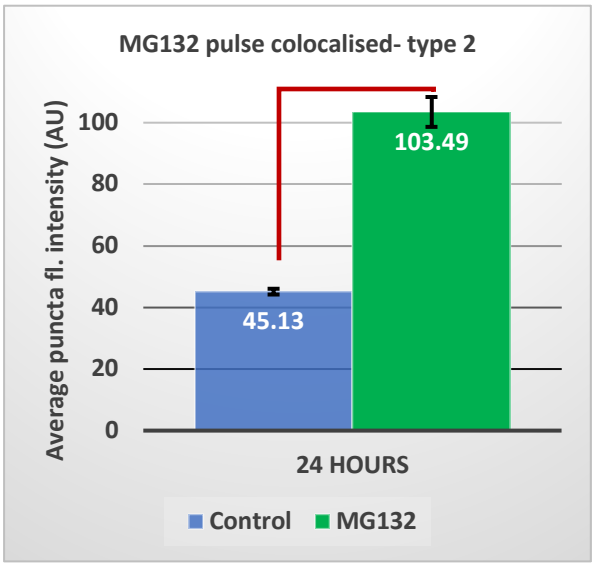
MG132 pulse colocalised- type 2
Average puncta fl. intensity (AU)
100
80
60
40
20
0
45.13
103.49
24 HOURS
Control
MG132

b.

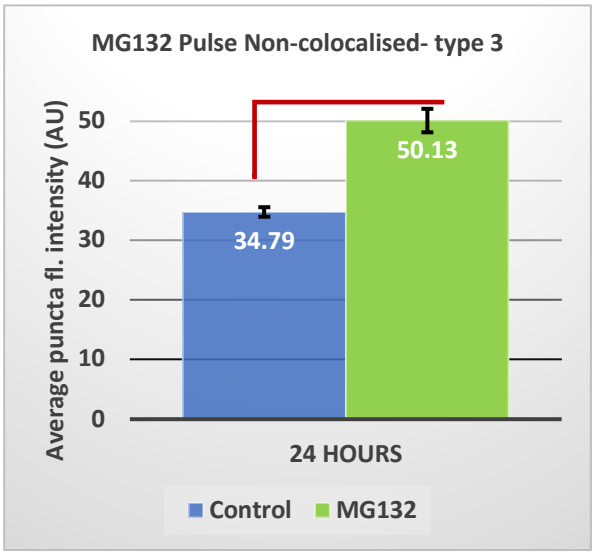
MG132 Pulse Non-colocalised- type 3
Average puncta fl. intensity (AU)
50
40
30
20
10
0
34.79
50.13
24 HOURS
Control
MG132

c.

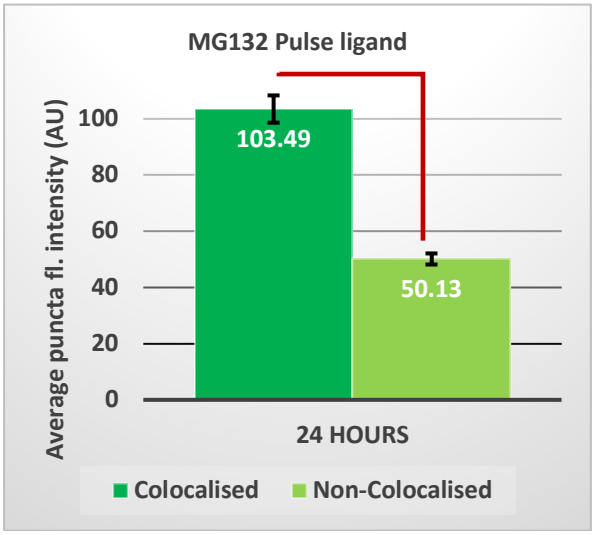
MG132 Pulse ligand
Average puncta fl. intensity (AU)
100
80
60
40
20
0
103.49
50.13
24 HOURS
Colocalised
Non-Colocalised

d.

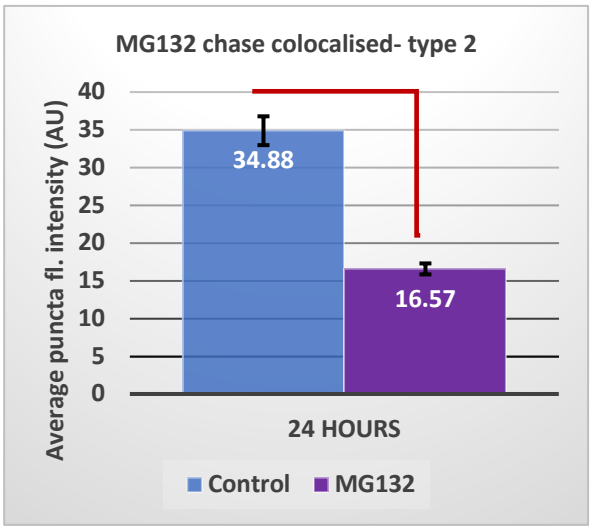
MG132 chase colocalised- type 2
Average puncta fl. intensity (AU)
40
35
30
25
20
15
10
5
0
34.88
16.57
24 HOURS
Control
MG132

e.

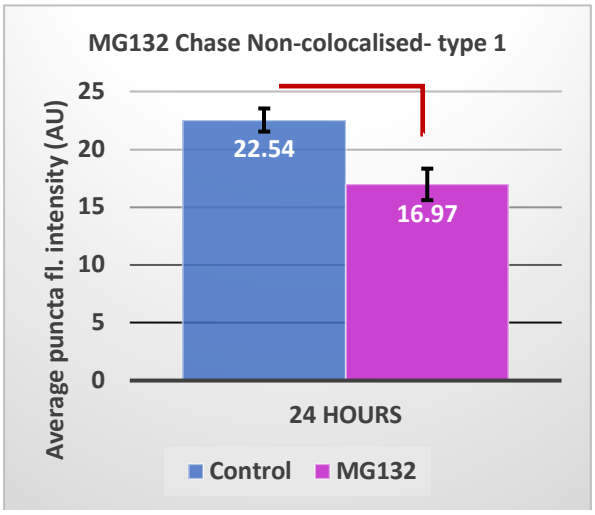
MG132 Chase Non-colocalised- type 1
Average puncta fl. intensity (AU)
25
20
15
10
5
0
22.54
16.97
24 HOURS
Control
MG132

f.

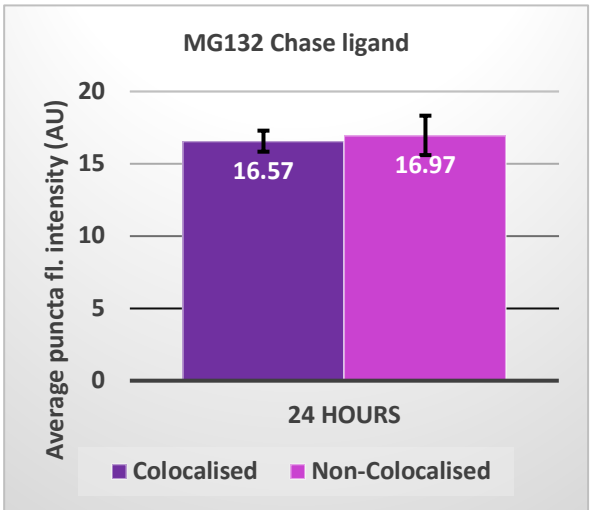
MG132 Chase ligand
Average puncta fl. intensity (AU)
20
15
10
5
0
16.57
16.97
24 HOURS
Colocalised
Non-Colocalised

Figure 4.36. The effect of MG132 on PSD-95 average puncta intensity at synaptic types. Average puncta fluorescence intensity (APFI) per image was calculated for pulse and chase ligand labelled synaptic puncta in type 1, type 2 and type 3 synapses separately. Images were taken after 24 hours of pulse-chase treatment with 50nM R110Direct ligand (pulse) and 500nM TMR ligand (chase) in hippocampal primary cultures from PSD-95$^{HaloTag/HaloTag}$ mice on DIV16. MG132 (10µM) was applied for 24 hours together with the chase ligand between DIV15 and DIV16. The graphs here present the mean values across eight cultures (N=8). **a.** Pulse ligand (R110Direct) APFI per image in synapses where pulse and chase ligands colocalise (type 2). The difference between the MG132 group and untreated controls is statistically significant (Welch's t-test, $p=1.33x10^{-5}$). **b.** Pulse ligand APFI per image in synapses where pulse and chase ligands do not colocalise (type 3). The difference between the MG132 group and untreated controls is statistically significant (Welch's t-test, $9.66x10^{-5}$). **c.** Comparison of pulse ligand APFI per image in type 2 synapses and type 3 synapses following MG132 treatment. The difference between the two groups is statistically significant (Welch's t-test, $p=7.90x10^{-6}$). **d.** Chase ligand (TMR) APFI per image in synapses where pulse and chase ligands colocalise (type 2). The difference between the MG132 group and untreated controls is statistically significant (Welch's t-test, $p=9.22x10^{-6}$). **e.** Chase ligand APFI per image in synapses where pulse and chase ligands do not colocalise (type 1). The difference between the MG132 group and untreated controls is statistically significant (Welch's t-test, p=0.0069). **f.** Comparison of chase ligand APFI per image in type 2 synapses and type 1 synapses following MG132 treatment. The difference between the two groups is not statistically significant (Welch's t-test, p=0.81).

statistically significant in the lactacystin group (p=0.10, figure 4.35.e). In the MG132 group the differences are still very statistically significant (p=0.0069, figure 4.36.e), but much less so than in type 2 synapses.

Interestingly, for both treatment groups the chase ligand is not different in its APFI when comparing type 2 with type 1 synapses (figure 4.35.f and figure 4.36.f), in contrast with the control group (figure 4.2.b). For the pulse ligand, the difference between type 2 and type 3 synapses is still very significant (lactacystin: figure 4.35.c, $p=2.76x10^{-6}$; MG132: figure 4.36.c, $p=7.90x10^{-6}$).

Looking at puncta number, we see the results actually diverge from the puncta intensity results for the first time. In both the lactacystin and the MG132 groups, APFI in type 2 synapses is much higher than in controls (figure 4.35.a and figure 4.36.a), while average puncta number in type 2 synapses is lower than in controls (figure 4.37.a and figure 4.38.a). While mean pulse ligand puncta number per image for the untreated control group is 115.92 ± 17.98, the value for the lactacystin group is 85.10 ± 15.90 (p=0.22) and the value for the MG132 group is 34.00 ± 8.15 (p=0.0021). At

type 3 synapses, the opposite is the case (figure 4.37.b and figure 4.38.b). Interestingly, the majority of pulse-labelled puncta are found to be type 3 synapses (figure 4.37.c and figure 4.38.c). The explanation for this is that many synapses that have not synthesised any new PSD-95 at all following drug treatment and therefore become type 3 synapses would have been type 2 synapses under control conditions.

Looking at chase ligand puncta numbers, the main observation is that puncta numbers are strongly reduced compared to controls. This effect is particularly pronounced in non-colocalised type 1 synapses, with images from lactacystin-treated cultures having an average of 10.92 ± 3.70 synaptic puncta (figure 3.37.e) and from MG132-treated cultures 6.17 ± 1.49 puncta (figure 3.38.e). These values differ very significantly from the average 78.65 ± 16.67 puncta per image in controls (lactacystin: $p=0.0045$; MG132: $p=0.0033$). The reduction in type 2 synapses labelled by the chase ligand is much less pronounced, and thus there are significantly fewer type 1 synapses labelled by the chase ligand than type 2 synapses (lactacystin: figure 4.37.f, $p=0.0031$; MG132: figure 4.38.f, $p=0.014$).

This skewed distribution of synaptic types becomes very clear when looking at the pie chart in figure 4.39. Here we can clearly see that the vast majority of synapses is made up of type 3, pulse-only synapses. Type 2 synapses are drastically reduced in number, and there are barely any type 1 synapses. Following lactacystin treatment (figure 4.39.b), the numbers are type 3: 66%, type 2: 30% and type 1: 4%. Following MG132 treatment (figure 4.39.c), the numbers are even more skewed- type 3: 88%, type 2: 10% and type 1: 2%. Compare this to untreated controls (figure 4.39.a), and the shift becomes very evident. From these numbers, there is one conclusion we can come to: a large number of type 3 synapses would, in untreated control conditions, have been classified as type 2 synapses instead. However, following proteasome inhibition, they have not incorporated any newly-synthesised PSD-95 into their PSDs, thereby leading to their classification as type 3 synapses.

We then turn to looking at the ratios between pulse and chase ligands at type 2 synapses (Figure 4.42). From the shapes of the frequency histograms, we can see that a transformation of the synaptic population has taken place. Compared to the curves for lactacystin (figure 4.42.b) and MG132 (figure 4.42.c), the control group's

a.

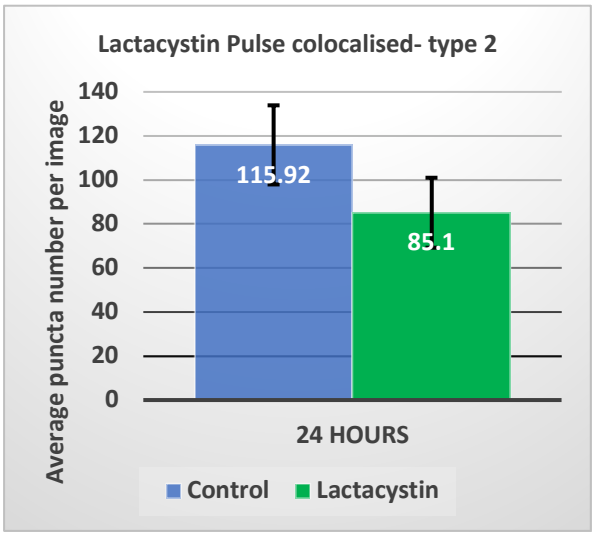
Lactacystin Pulse colocalised- type 2
Average puncta number per image
140
120
100
80
60
40
20
0
115.92
85.1
24 HOURS
Control
Lactacystin

b.

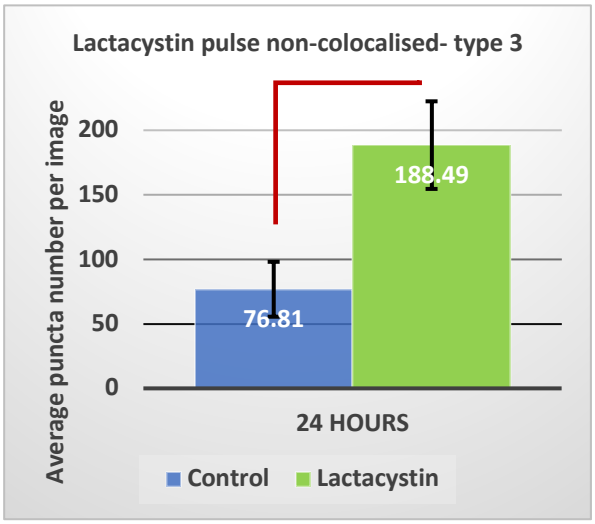
Lactacystin pulse non-colocalised- type 3
Average puncta number per image
200
150
100
50
0
76.81
188.49
24 HOURS
Control
Lactacystin

c.

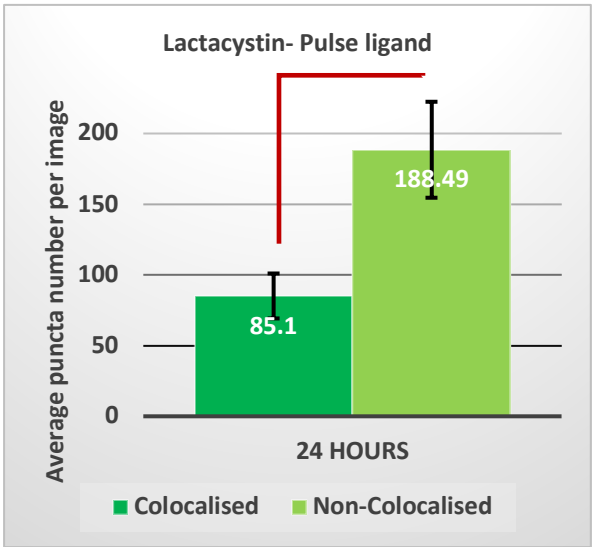
Lactacystin- Pulse ligand
Average puncta number per image
200
150
100
50
0
85.1
188.49
24 HOURS
Colocalised
Non-Colocalised

d.

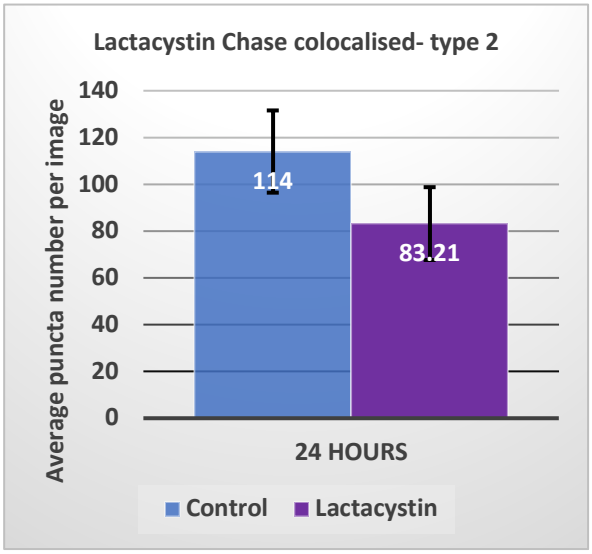
Lactacystin Chase colocalised- type 2
Average puncta number per image
140
120
100
80
60
40
20
0
114
83.21
24 HOURS
Control
Lactacystin

e.

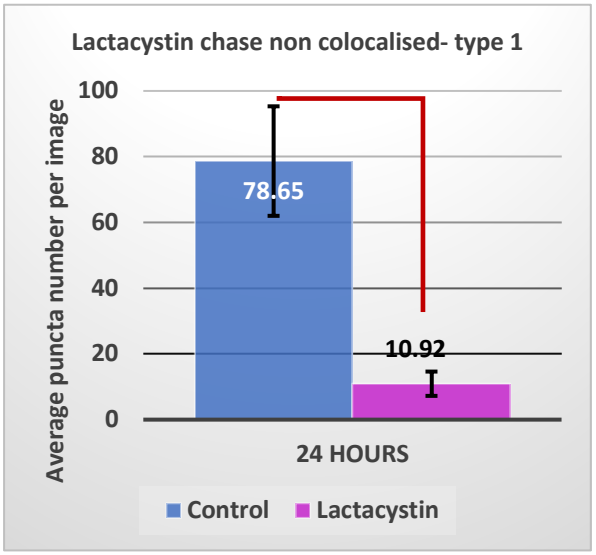
Lactacystin chase non colocalised- type 1
Average puncta number per image
100
80
60
40
20
0
78.65
10.92
24 HOURS
Control
Lactacystin

f.

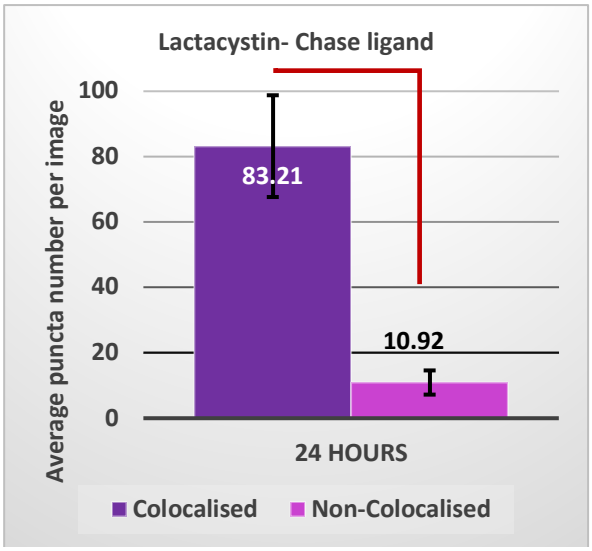
Lactacystin- Chase ligand
Average puncta number per image
100
80
60
40
20
0
83.21
10.92
24 HOURS
Colocalised
Non-Colocalised

Figure 4.37. The effect of lactacystin on PSD-95 average puncta number at synaptic types.
Average puncta number per image was calculated for pulse and chase ligand labelled synaptic puncta in type 1, type 2 and type 3 synapses separately. Images were taken after 24 hours of pulse-chase treatment with 50nM R110Direct ligand (pulse) and 500nM TMR ligand (chase) in hippocampal primary cultures from PSD-95$^{HaloTag/HaloTag}$ mice on DIV16. Lactacystin (1µM) was applied for 24 hours together with the chase ligand between DIV15 and DIV16. The graphs here present the mean values across eight cultures (N=8).
a. Pulse ligand average puncta number per image in synapses where pulse and chase ligands colocalise (type 2). The difference between the lactacystin group and untreated controls is not statistically significant (Welch's t-test, p=0.22). **b.** Pulse ligand average puncta number per image in synapses where pulse and chase ligands do not colocalise (type 3). The difference between the lactacystin group and untreated controls is statistically significant (Welch's t-test, p=0.019). **c.** Comparison of pulse ligand average puncta number per image in type 2 synapses and type 3 synapses following lactacystin treatment. The difference between the two groups is statistically significant (Welch's t-test, p=0.023). **d.** Chase ligand (TMR) average puncta number per image in synapses where pulse and chase ligands colocalise (type 2). The difference between the lactacystin group and untreated controls is not statistically significant (Welch's t-test, p=0.21). **e.** Chase ligand average puncta number per image in synapses where pulse and chase ligands do not colocalise (type 1). The difference between the lactacystin group and untreated controls is statistically significant (Welch's t-test, p=0.0045). **f.** Comparison of chase ligand average puncta number per image in type 2 synapses and type 1 synapses following lactacystin treatment. The difference between the two groups is statistically significant (Welch's t-test, p=0.0031).

a.

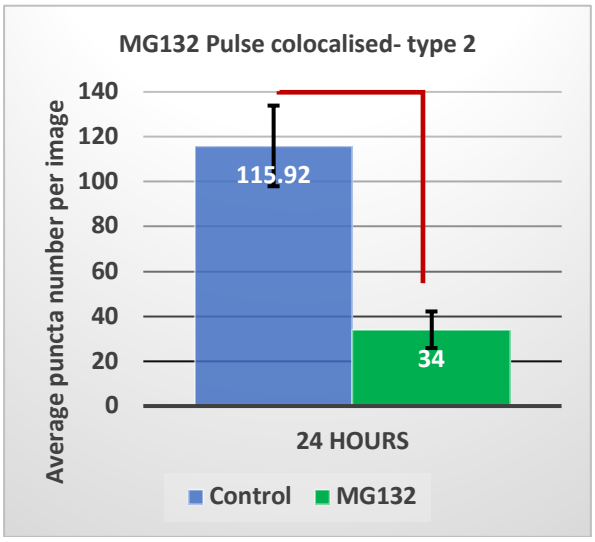
MG132 Pulse colocalised- type 2
Average puncta number per image
140
120
100
80
60
40
20
0
115.92
34
24 HOURS
Control
MG132

b.

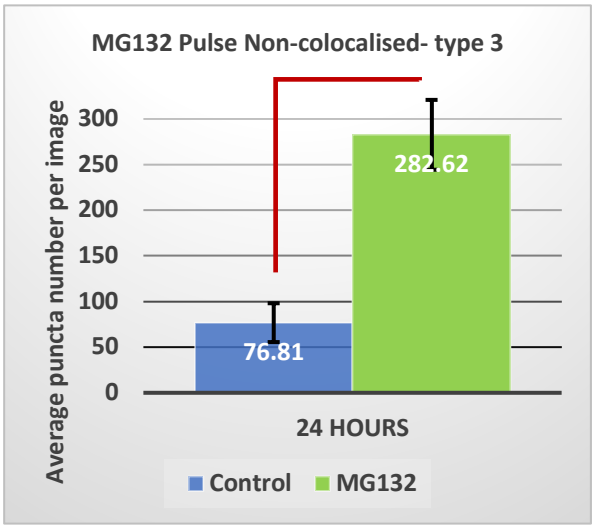
MG132 Pulse Non-colocalised- type 3
Average puncta number per image
300
250
200
150
100
50
0
76.81
282.62
24 HOURS
Control
MG132

c.

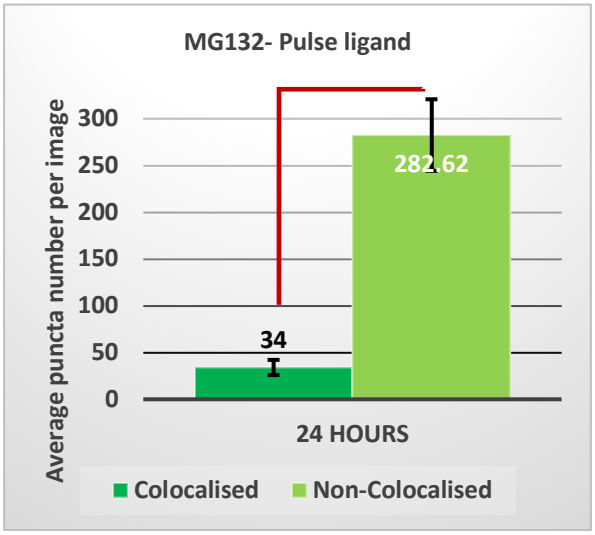
MG132- Pulse ligand
Average puncta number per image
300
250
200
150
100
50
0
34
282.62
24 HOURS
Colocalised
Non-Colocalised

d.

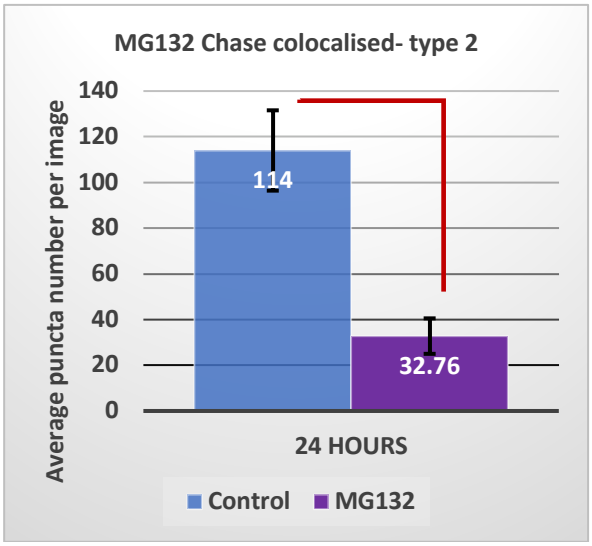
MG132 Chase colocalised- type 2
Average puncta number per image
140
120
100
80
60
40
20
0
114
32.76
24 HOURS
Control
MG132

e.

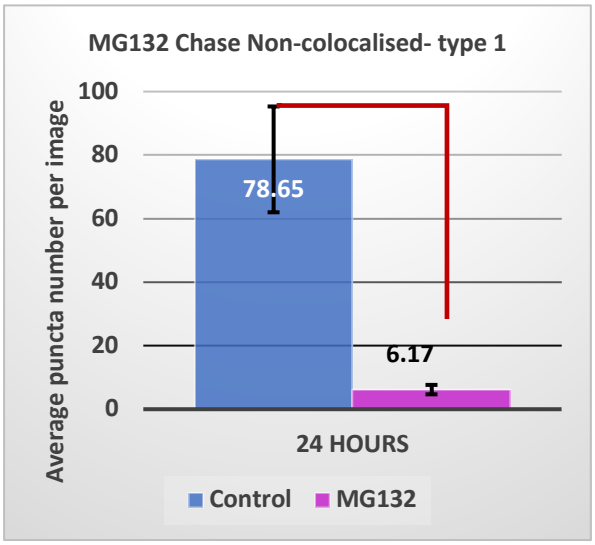
MG132 Chase Non-colocalised- type 1
Average puncta number per image
100
80
60
40
20
0
78.65
6.17
24 HOURS
Control
MG132

f.

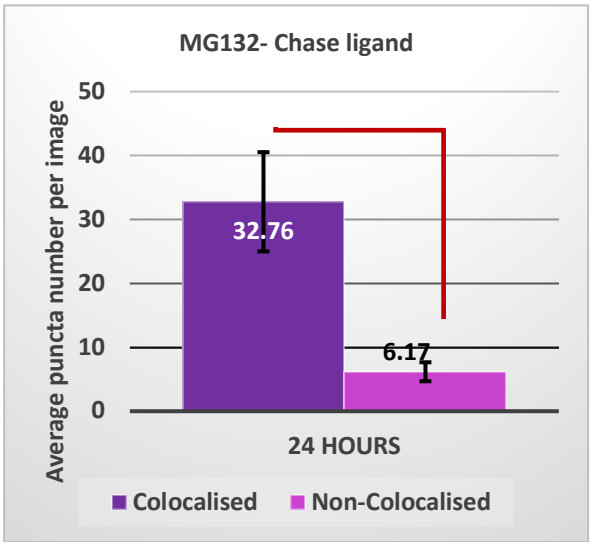
MG132- Chase ligand
Average puncta number per image
50
40
30
20
10
0
32.76
6.17
24 HOURS
Colocalised
Non-Colocalised

Figure 4.38. The effect of MG132 on PSD-95 average puncta number at synaptic types.
Average puncta number per image was calculated for pulse and chase ligand labelled synaptic puncta in type 1, type 2 and type 3 synapses separately. Images were taken after 24 hours of pulse-chase treatment with 50nM R110Direct ligand (pulse) and 500nM TMR ligand (chase) in hippocampal primary cultures from PSD-95$^{HaloTag/HaloTag}$ mice on DIV16. MG132 (10µM) was applied for 24 hours together with the chase ligand between DIV15 and DIV16. The graphs here present the mean values across eight cultures (N=8). **a.** Pulse ligand average puncta number per image in synapses where pulse and chase ligands colocalise (type 2). The difference between the MG132 group and untreated controls is statistically significant (Welch's t-test, p=0.0021). **b.** Pulse ligand average puncta number per image in synapses where pulse and chase ligands do not colocalise (type 3). The difference between the MG132 group and untreated controls is statistically significant (Welch's t-test, p=0.00097). **c.** Comparison of pulse ligand average puncta number per image in type 2 synapses and type 3 synapses following MG132 treatment. The difference between the two groups is statistically significant (Welch's t-test, p=0.00050). **d.** Chase ligand (TMR) average puncta number per image in synapses where pulse and chase ligands colocalise (type 2). The difference between the MG132 group and untreated controls is statistically significant (Welch's t-test, p=0.0019). **e.** Chase ligand average puncta number per image in synapses where pulse and chase ligands do not colocalise (type 1). The difference between the MG132 group and untreated controls is statistically significant (Welch's t-test, p=0.0033).
f. Comparison of chase ligand average puncta number per image in type 2 synapses and type 1 synapses following MG132 treatment. The difference between the two groups is statistically significant (Welch's t-test, p=0.014).

histogram (figure 4.42.a) is strongly positively skewed. The control group's histogram has a fairly well-defined peak (mode 1.8 at 8.76%), and the slopes are relatively steep compared to the histograms in the drug-treated groups. The mean ratio for the control group is 2.55 ± 0.051 (SEM), with the median ratio being 2.06. For both treatment groups the histograms display much more gradually sloping curves, with no well-defined peak. The ratios are also evidently much greater than in the control group. In the lactacystin group, the mean ratio is 7.19 ± 0.18 (SEM) (figure 4.42.d), with a median ratio of 6.03. The mode is a ratio of 6, with 3.78%. In the MG132 group, the mean ratio is 10.25 ± 0.21 (SEM) (figure 4.42.d), with a median ratio of 9.56. The mode is a ratio of 8.6, with 4.92%. Apart from the very wide spread of values, we can also observe that in the treatment groups the mode is less clearly defined, and much less pronounced (around 4% as opposed to around 8%). Next, figure 4.43 reveals that the correlation between pulse and chase ligand intensity in type 2 synapses remains unchanged following lactacystin or MG132 treatment. For both drugs we see that as pulse ligand intensity goes up by percentiles, chase ligand intensity goes up as well (lactacystin R^2=0.86, MG132 R^2=0.74).

a.

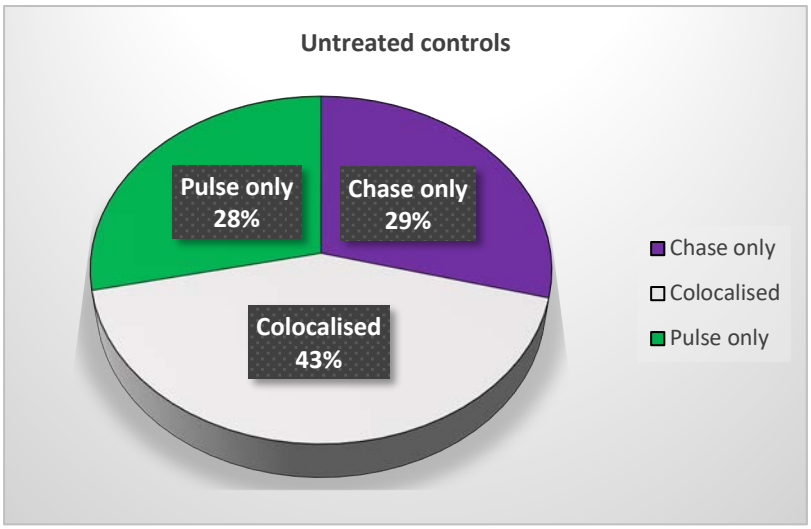
Untreated controls
Pulse only 28%
Chase only 29%
Colocalised 43%
Chase only
Colocalised
Pulse only

b.

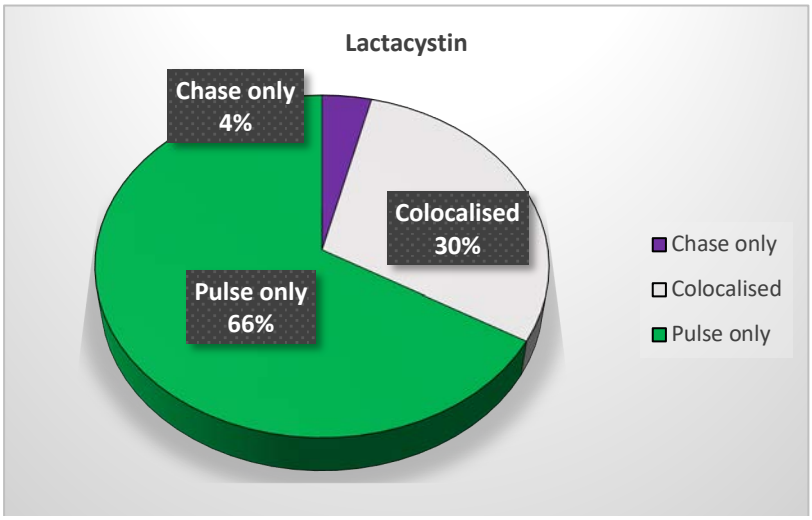
Lactacystin
Chase only 4%
Colocalised 30%
Pulse only 66%
Chase only
Colocalised
Pulse only

c.

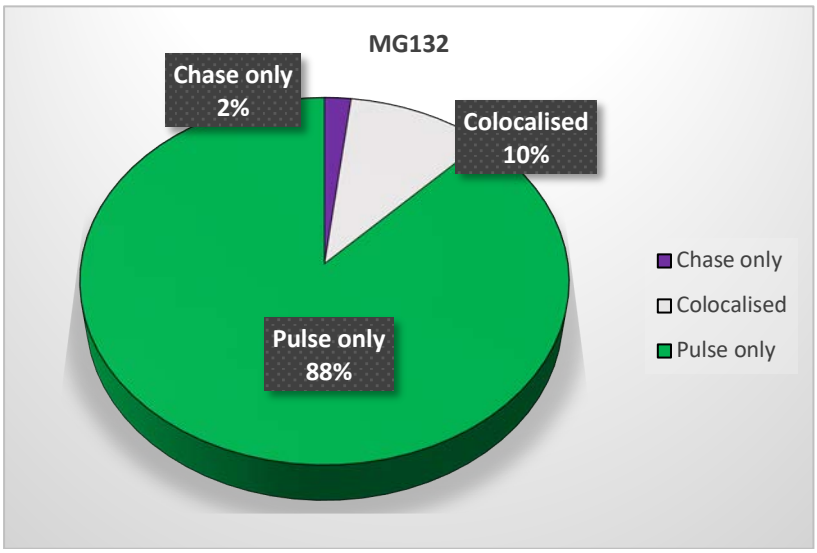
MG132
Chase only 2%
Colocalised 10%
Pulse only 88%
Chase only
Colocalised
Pulse only

Figure 4.39. Proportional representation of synaptic population by HaloTag ligand-labelling following proteasome inhibition.

Synaptic puncta were categorised according to whether they colocalised with puncta labelled by the other ligand or not. This pie chart depicts the proportional representation of the three types of synaptic puncta observed.

Images were taken after 24 hours of pulse-chase treatment with 50nM R110Direct ligand (pulse) and 500nM TMR ligand (chase) in hippocampal primary cultures from PSD-95$^{HaloTag/HaloTag}$ mice on DIV16. **a.** In untreated controls, 28% of puncta contain only the pulse (R110Direct) ligand (type 3), 43% of puncta contain both pulse and chase (TMR) ligands (type 2), and 29% contain only the chase ligand (type 1). **b.** Following 24 hours of lactacystin treatment (1µM), 66% of puncta contain only the pulse (R110Direct) ligand (type 3), 30% of puncta contain both pulse and chase (TMR) ligands (type 2), and 4% contain only the chase ligand (type 1). **c.** Following 24 hours of MG132 treatment (10µM), 88% of puncta contain only the pulse (R110Direct) ligand (type 3), 10% of puncta contain both pulse and chase (TMR) ligands (type 2), and 2% contain only the chase ligand (type 1).

a.

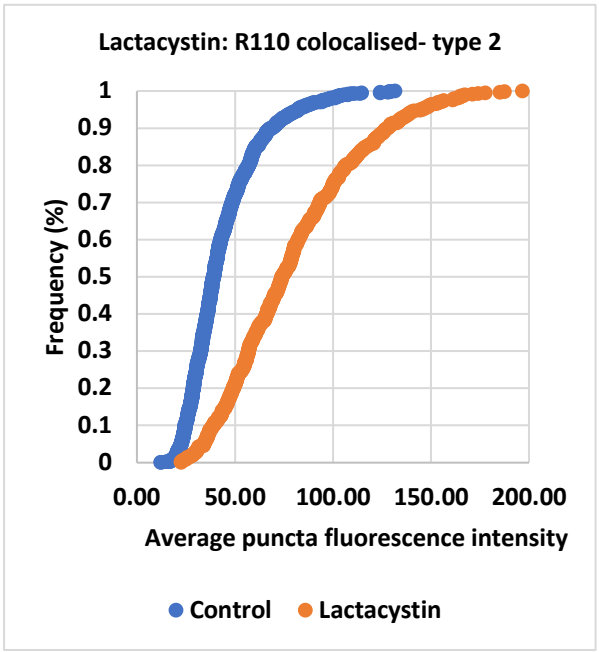

b.

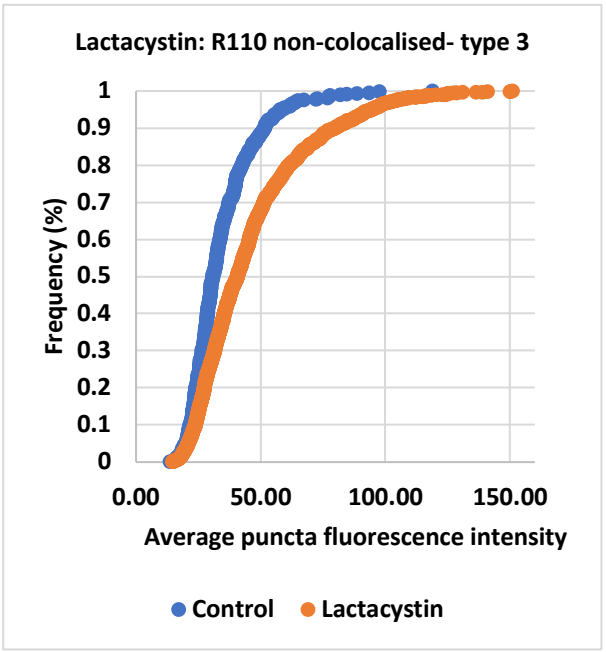

c. d.

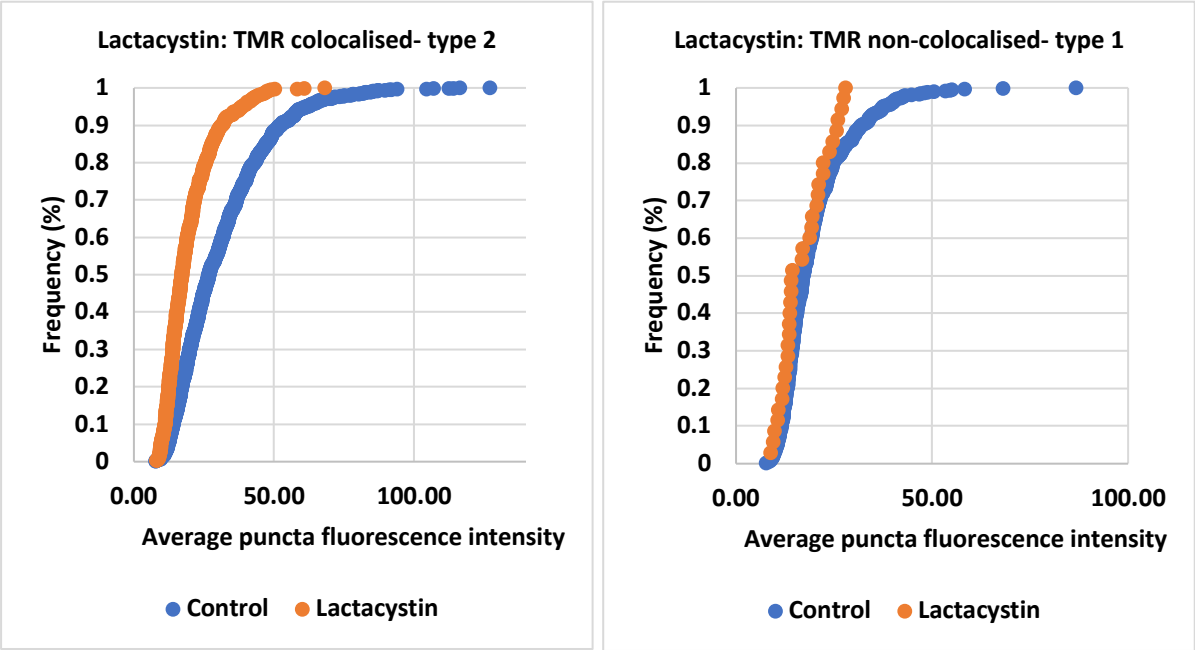

Figure 4.40. Cumulative distribution functions of average puncta fluorescence intensity following lactacystin treatment.

CDFs were constructed using the single-synapse data following lactacystin treatment, and compared with the untreated control group. Whether the difference was statistically significant or not was tested using the Kolmogorov-Smirnov test for difference. **a.** Comparison between R110 ligand puncta in colocalised type 2 synapses of lactacystin-treated neurons with those in untreated controls. The difference is significant (Kolmogorov-Smirnov, $p<0.0001$). **b.** Comparison between R110 ligand puncta in non-colocalised type 3 synapses of lactacystin-treated neurons with those in untreated controls. The difference is significant (Kolmogorov-Smirnov, $p<0.0001$). **c.** Comparison between TMR ligand puncta in colocalised type 2 synapses of lactacystin-treated neurons with those in untreated controls. The difference is significant (Kolmogorov-Smirnov, $p<0.0001$). **d.** Comparison between TMR ligand puncta in non-colocalised type 1 synapses of lactacystin-treated neurons with those in untreated controls. The difference is not significant (Kolmogorov-Smirnov, $p=0.137$).

Lastly, CDF's were calculated for each of the eight groups (Figures 4.40 and 4.41). In these two treatment groups (lactacystin and MG132), the CDF curves of the treated groups have similar shapes to untreated controls, except for type 1 synapses. For both treatments, type 1 synapses are so low in frequency that the curves are in fact lines. It is of interest to note that the results reflect what previous graphs have also shown- that pulse ligand (R110) puncta following treatment are more likely than controls to have a higher APFI. This is evident by the shift of the curve to the right. Conversely, for chase ligand (TMR) puncta, drug treatment results in a lower expected APFI, as the curve is shifted to the left relative to controls.

The only curve found to not be significantly different from the untreated control group when tested using the Kolmogorov-Smirnov test for difference was that belonging to type 1 synapses when treated with lactacystin (p=0.137). All other groups were found to be significantly different from the control group. This difference is due to the high percentage of puncta overlap between the lactacystin-treated group and the untreated control group, which can be seen when viewing the two curves (figure 4.40.d).

a.

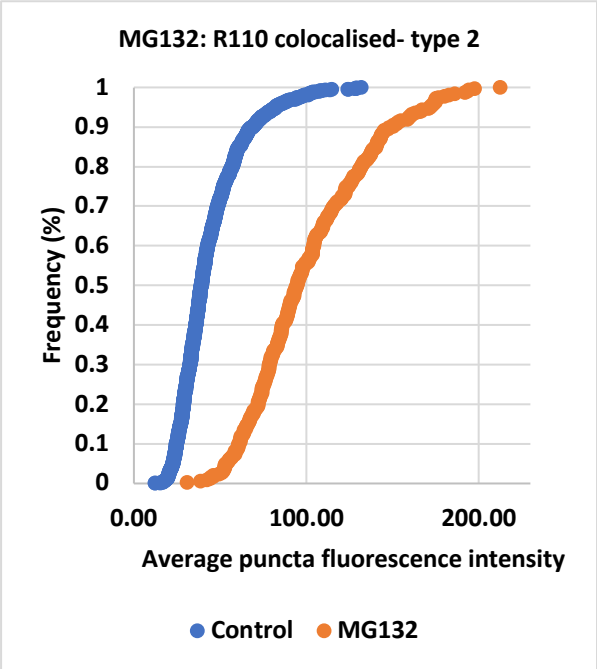

b.

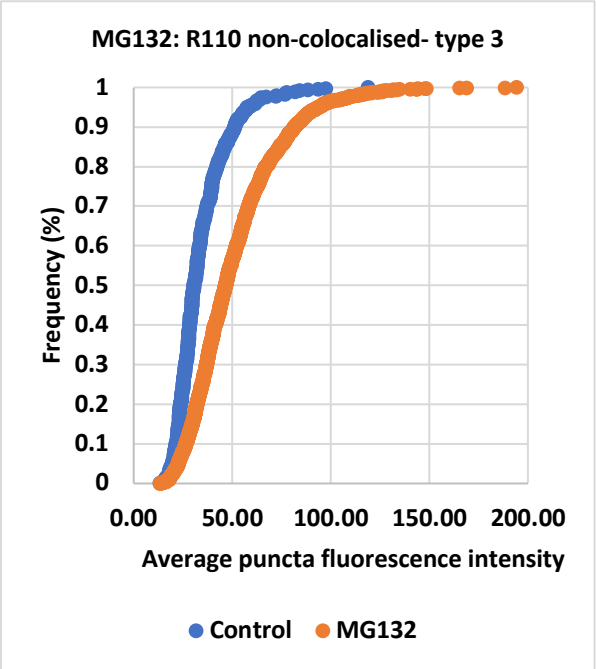

c.

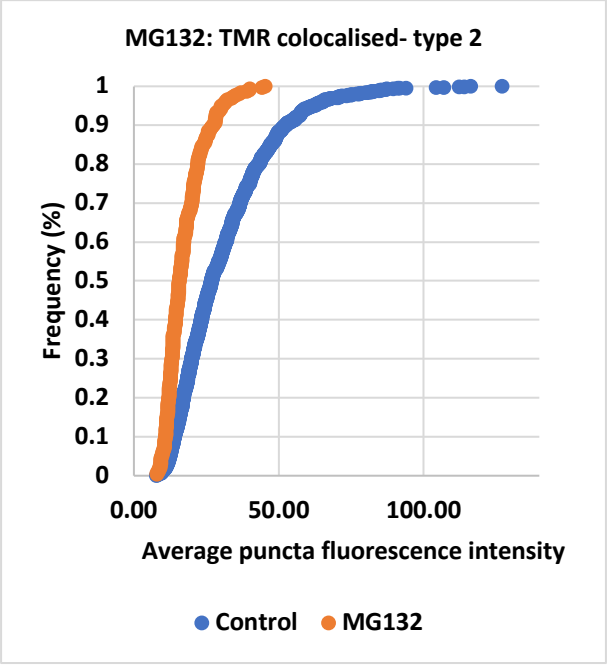

d.

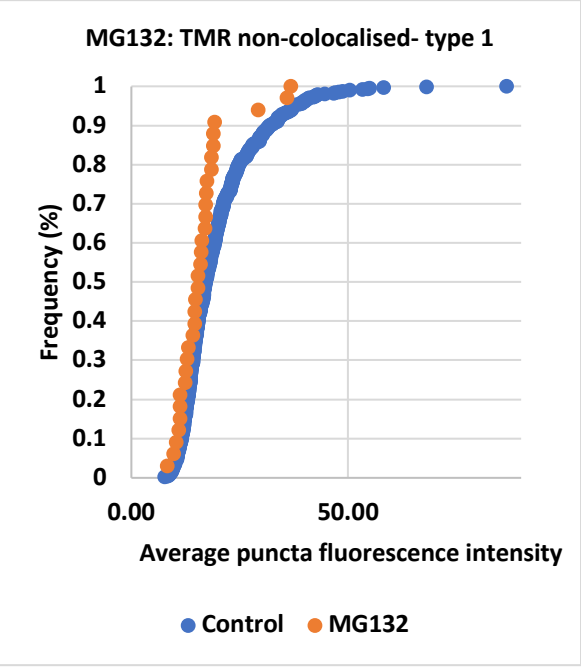

Figure 4.41. Cumulative distribution functions of average puncta fluorescence intensity following MG132 treatment.

CDFs were constructed using the single-synapse data following MG132 treatment, and compared with the untreated control group. Whether the difference was statistically significant or not was tested using the Kolmogorov-Smirnov test for difference. **a.** Comparison between R110 ligand puncta in colocalised type 2 synapses of MG132-treated neurons with those in untreated controls. The difference is significant (Kolmogorov-Smirnov, $p<0.0001$). **b.** Comparison between R110 ligand puncta in non-colocalised type 3 synapses of MG132-treated neurons with those in untreated controls. The difference is significant (Kolmogorov-Smirnov, $p<0.0001$). **c.** Comparison between TMR ligand puncta in colocalised type 2 synapses of MG132-treated neurons with those in untreated controls. The difference is significant (Kolmogorov-Smirnov, $p<0.0001$). **d.** Comparison between TMR ligand puncta in non-colocalised type 1 synapses of MG132-treated neurons with those in untreated controls. The difference is significant (Kolmogorov-Smirnov, $p=0.006$).

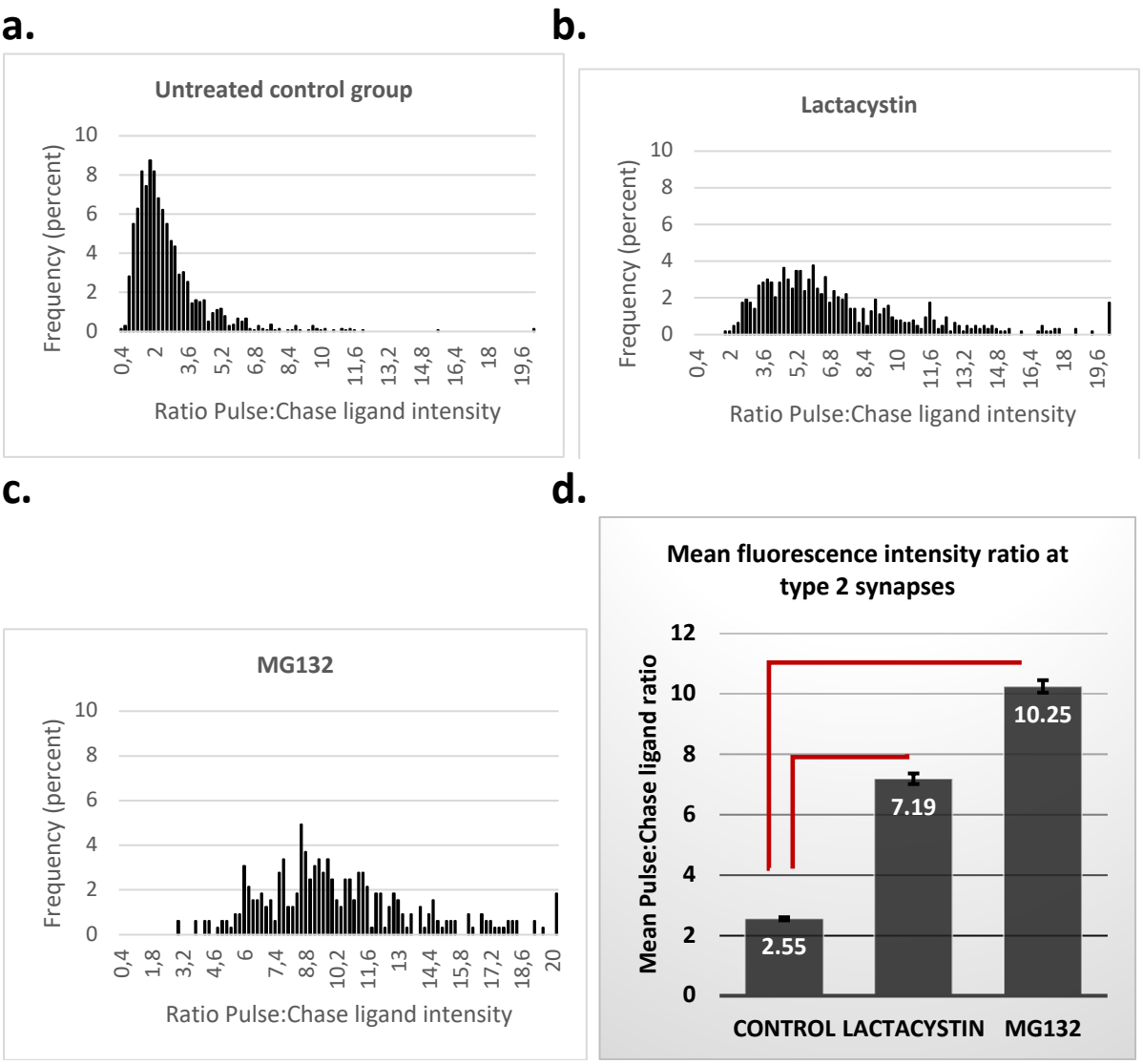

Figure 4.42. Graphs showing the ratio of pulse to chase ligands at individual type 2 synapses following proteasome inhibition.

In the synaptic population in which pulse and chase ligand-labelled PSD-95-HaloTag molecules were colocalised (type 2), the ratio of pulse ligand fluorescence intensity to chase ligand fluorescence intensity was calculated for each individual synapse. The frequency histograms represent the frequencies of all the pulse:chase ratios. **a.** Frequency distribution in untreated controls. Mean ratio: 2.55 ± 0.051 (SEM), Median ratio: 2.06, Mode: 1.8 (8.76%). **b.** Frequency distribution following 24 hours of lactacystin (1µM) treatment. Mean ratio: 7.19 ± 0.18 (SEM), Median ratio: 6.03, Mode: 6 (3.78%). **c.** Frequency distribution following 24 hours of MG132 (10µM) treatment. Mean ratio: 10.25 ± 0.21 (SEM), Median ratio: 9.56, Mode: 8.6 (4.92%). **d.** Comparison of mean pulse:chase ligand ratio in untreated controls with lactacystin and MG132 treated cultures. Differences are statistically significant for both the lactacystin (Welch's t-test, $p=9.10x10^{-103}$) and MG132 group (Welch's t-test, $p=5.39x10^{-123}$).

a.

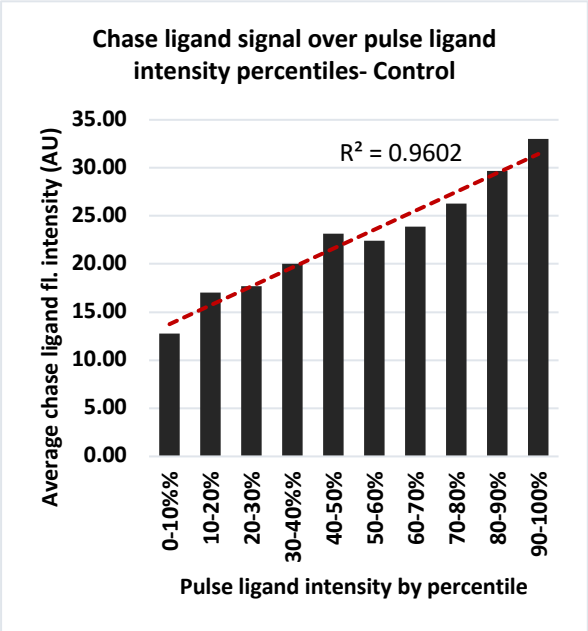

b.

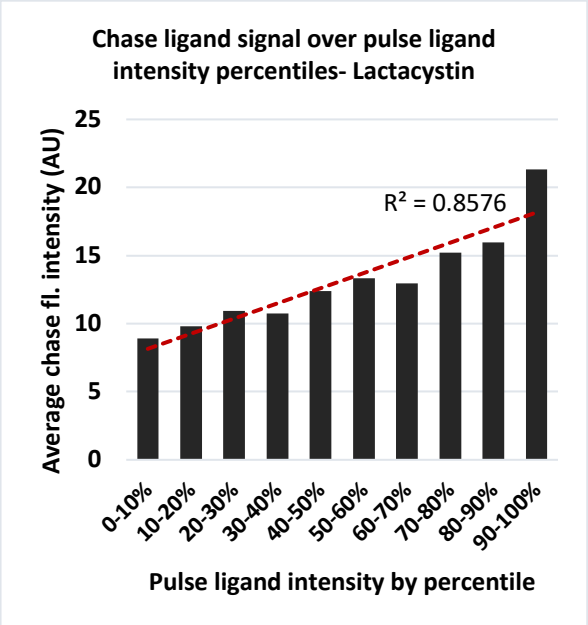

c.

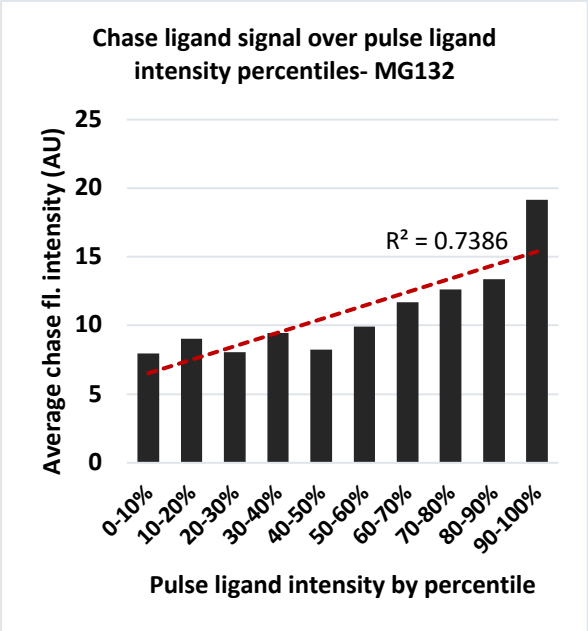

Figure 4.43 Correlation of pulse ligand intensity with chase ligand intensity at colocalised synaptic puncta following proteasome inhibition.

Colocalising (type 2) synapses were sorted by their pulse ligand APFI (lowest to highest). For each ten percentile steps, average chase ligand APFI was calculated. **a.** In untreated controls, there is a strong positive correlation, R^2=0.96. **b.** In the lactacystin-treated cultures, there is also a strong positive correlation, R^2=0.86. **c.** In the MG132-treated cultures, the correlation is slightly weaker, but still high, R^2=0.74.

4.4.5.2 Proteasome inhibitors- Lactacystin and MG132: discussion

The results presented in the previous sections strongly indicate that the proteasome inhibitors lactacystin and MG132 have a profound effect upon the expression and turnover of PSD-95 at the synapse. Nearly all characteristics that I am monitoring over this study, such as pulse and chase ligand puncta intensity and number, synaptic types, frequencies and ratios, appear to be affected by the treatment with these chemicals. Overall, the main findings in the treatment groups compared to untreated controls are:

1. Overall (bulk) pulse ligand APFI remains significantly higher over 24 hours. This effect could also be observed at both type 2 and type 3 synapses.
2. Overall (bulk) chase ligand APFI rises to a much lower level over these 24 hours. This appears to be mediated chiefly through type 2 and much less so type 1 synapses.
3. Type 1 and type 2 synapses contain equal amounts of new PSD-95, unlike untreated controls.
4. There are significantly fewer type 1 synapses.
5. There are significantly fewer type 2 synapses.
6. There are significantly more type 3 synapses.
7. Within type 2 synapses, the ratio of pulse:chase ligand APFI is skewed strongly towards the pulse ligand.

Let us take a closer look at the study by Hakim et al. (2016). This study used multiplexed and pulsed SILAC, in addition to immunocytochemistry, in primary cultures of rat hippocampal neurons to measure synthesis and degradation rates of synaptic proteins following suppression of proteasomal activity by 10μM lactacystin, applied for 10 hours (immunocytochemistry) and 24 hours (SILAC). Immunocytochemically the study found no change in total synaptic PSD-95 levels at all after the 10 hours of incubation. Following the 24-hour incubation and analysis by SILAC, the study found no reduction in PSD-95 degradation, but were able to measure a significant reduction in PSD-95 synthesis.

In my study, which in fact used lactacystin at a ten-fold lower concentration (1μM), had I been able to measure total synaptic PSD-95 levels it is possible that I, too, would have seen no significant change. This is because pulse ligand intensity remained high, even though chase ligand intensity was significantly lower than in controls. The overall amount of PSD-95 present at synapses, then, may have remained unchanged.

It became clear once the results were analysed that a measurement of total PSD-95 levels would have proved highly useful and would have helped some of the questions that remain unanswered at this stage. There are various techniques that could have been employed in order to gain information on this. Firstly, western blotting could have been performed, allowing for a quantitative read-out of total PSD-95 levels in neuronal cultures. Secondly, single-ligand labelling using the HaloTag system could have been used, using one ligand to label treated and untreated cultures and comparing relative fluorescence intensities. This would have accomplished much the same as an antibody staining approach for PSD-95, which is a conventional method frequently used to measure total protein levels, including at synaptic locations.

As mentioned in previous experiments, there are two possible explanations for the pulse ligand APFI remaining high: reduced degradation of PSD-95, or degraded PSD-95 being replaced by extra-synaptic PSD-95, potentially cycled in from other synapses. However, I am looking at the entire population of synapses, such that PSD-95 molecules moving between synapses should overall be accounted for. There is also other evidence that points in the direction of degradation being affected. Firstly, type 3 (pulse-only) synapses contain greater amounts of old PSD-95 than controls, which further implies a reduced degree of PSD-95 degradation. Indeed, there are significantly greater numbers of type 3 synapses. It is possible that blocking proteasomal activity inhibits the pruning of synapses, and there is some evidence supporting a role for the proteasome in synaptic pruning (DiAntonio et al., 2004; Riccomagno et al., 2015). Secondly, type 2 (mixed) synapses display pulse-to-chase ligand ratios that are heavily skewed towards the pulse ligand. This is the effect of reduced degradation of old PSD-95 (which remains much higher than in controls), but also because less new PSD-95 is recruited (chase ligand intensity is much lower than in controls). Indeed, these results imply that many type 2 synapses effectively turned into type 3 synapses by virtue of not incorporating new PSD-95. While some amount

of cycling of dendritic PSD-95 into synapses may occur, it is very likely that old PSD-95 levels at synapses remain high due to reduced degradation brought on by the proteasome blockade of lactacystin or MG132.

The other interesting finding is that there is reduced synthesis of PSD-95, matching the finding by Hakim et al. (2016). While this result cannot be interpreted in any other way, there is a second aspect to it that is more intriguing. Not only is PSD-95 synthesis reduced at existing type 2 and type 3 synapses, but there are also fewer type 1 synapses. As discussed in chapter 4.3.3, type 1 synapses are most likely newly formed, immature synapses that are recruiting new PSD-95 in order to establish their PSDs. Reduced numbers of these type 1 synapses, then, may imply that synaptogenesis is reduced in these cultures. As Hakim et al. (2016) propose, blocking proteasomal activity may have deep-reaching consequences for the cell as a whole, and trigger such reactions as the unfolded protein response (UPR) and integrated stress response. These responses are further implicated in causing synaptic loss in various disease states, and thus the first stage of this in immature primary neurons may be an immediate and significant reduction in synaptogenesis. Alternatively, synaptogenesis may still be going on unhindered, but new synapses may simply not be incorporating PSD-95. However, since PSD-95 is known to be critical for the structural maturation of synaptic spines (El-Husseini et al., 2000), healthy synaptogenesis may become impossible, or this could lead to the handicapping of the synaptic maturation process. Indeed, the lack of PSD-95 may cause more silent synapses to be formed, if synaptogenesis is indeed still ongoing at the usual rate, since this appears to be the effect of knocking down or knocking out PSD-95 in mouse models (Huang et al., 2015; Béı ̈que et al., 2006). What is also intriguing about type 1 synapses is that while their numbers have gone down significantly, their rate of incorporation of new PSD-95 has not been affected to the same extent. Following lactacystin treatment, type 1 synapses still contained the same amount of new PSD-95 as untreated controls, while MG132 only had a slight (albeit significant) effect. What this implies is that while there are fewer new synapses being formed, those that are formed still recruit new PSD-95 at similar, only slightly reduced, rates. This gives further credence to the concept that immature synapses, newly formed, are recruiting PSD-95 in order to fill their PSD to a predetermined quota and thus allow them to stabilise. Even if PSD-95 synthesis is dramatically depressed across the neuron, then,

these new synapses still continue to synthesise and/or recruit specifically new PSD-95 at a nearly unaffected rate. This is reminiscent of the all-or-nothing incorporation of AMPARs. In this phenomenon, the loss of PSD-95 increases the number of silent synapses containing no AMPARs at all, while those synapses that retain an AMPAR presence do so at a normal level: they still contain the full complement of receptors (Elias et al., 2006; Ehrlich et al., 2007). The result of this effect is that unlike in untreated cultures, which display significantly more new PSD-95 in type 2 synapses than type 1 synapses, cultures treated with proteasome inhibitors have equal amounts of new PSD-95 in type 2 and type 1 synapses.

Finally, another interesting observation is that there is a drastic effect by these chemicals on the frequency histogram of pulse:chase ratios in type 2 synapses. This is particularly evident when this histogram is compared to the frequency histogram of pulse ligand intensities at the 1-hour time point (figure 4.4). Although not definitive, this result seems to imply that blocking proteasomal activity affects different synapses to differing extents, as otherwise one might expect a histogram that is similar in shape to that of the control group after 24 hours (figure 4.42.a), and merely shifted towards a greater ratio value. However, the actual result displays not only a shift, but also a wholesale alteration of the histogram's shape.

I do want to reiterate at this point that I used lactacystin at a 10-fold lower concentration (1μM) than the standard 10μM used throughout the literature (Hakim et al., 2016; Colledge et al., 2003; Ehlers, 2003). This most likely explains the slightly lower effect of lactacystin treatment than MG132 treatment. Nevertheless, it drives home the strong effect that this drug has, even at a lower concentration.

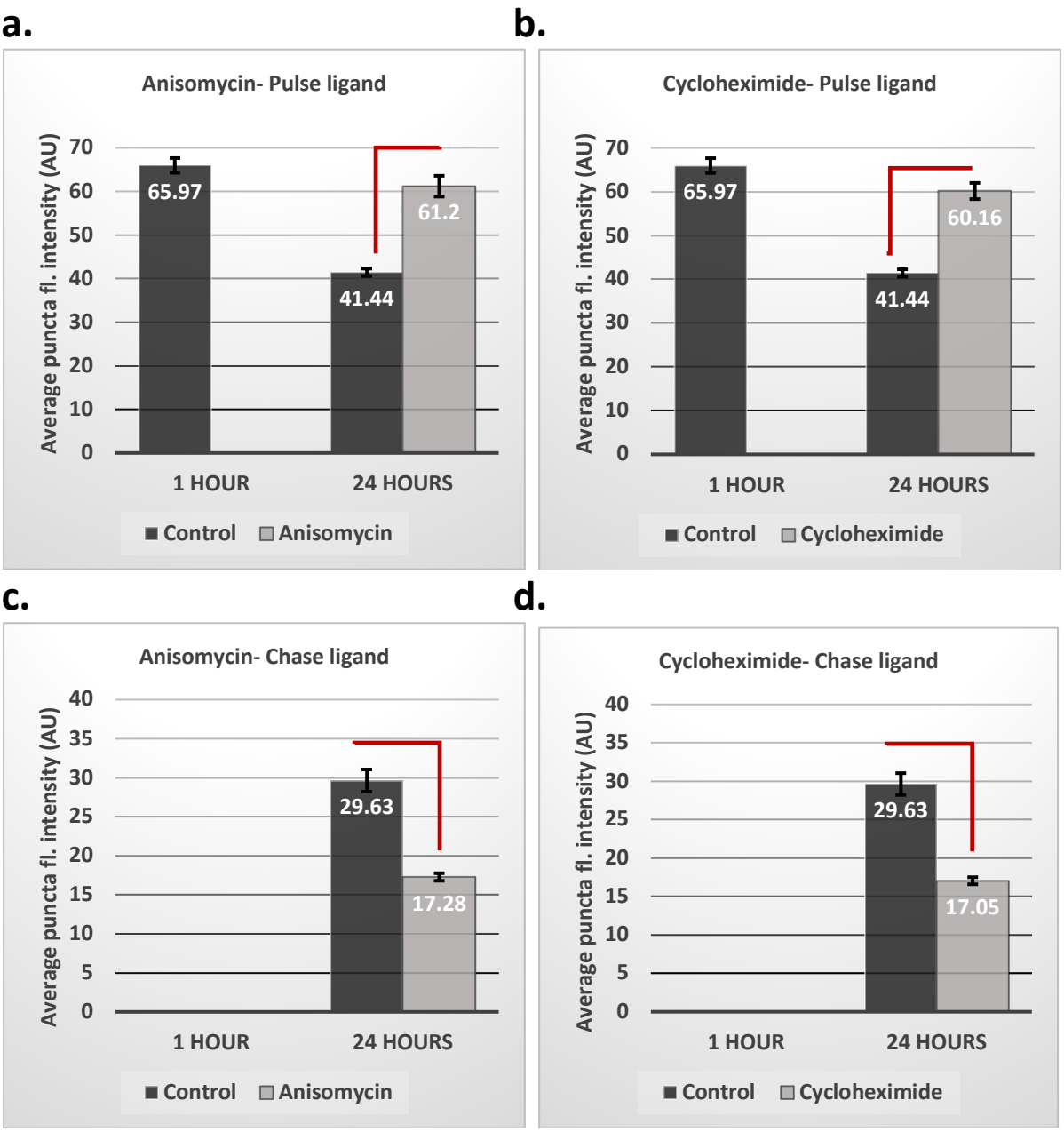

Figure 4.44. The effects of Anisomycin and Cycloheximide on PSD-95 puncta intensities. Hippocampal neuronal primary cultures from PSD-95$^{HaloTag/HaloTag}$ mice were grown for 14 days in vitro, and thereafter pulse-chase experiments performed using the R110Direct and TMR HaloTag ligands. Anisomycin at 1µM or cycloheximide at 3µM were added alongside the chase ligand for 1 or 24 hours. The graphs here present the mean values across eight cultures (N=8). **a.** Graph of the average R110 pulse ligand puncta fluorescence intensity following anisomycin treatment. APFI is significantly higher after 24 hours in the anisomycin group than in untreated controls (Welch's t-test, p=0.00019). **b.** Graph of the R110 pulse ligand APFI following cycloheximide treatment. APFI is significantly higher after 24 hours in the cycloheximide group than in untreated controls (Welch's t-test, $p=3.39x10^{-5}$). **c.** Graph of the average TMR chase ligand puncta fluorescence intensity following anisomycin treatment. The difference between the anisomycin group and untreated controls is highly significant (Welch's t-test, $p=2.41x10^{-5}$). **d.** Graph of the TMR chase ligand APFI following cycloheximide treatment. The difference between the cycloheximide group and untreated controls is highly significant (Welch's t-test, $p=2.22x10^{-5}$).

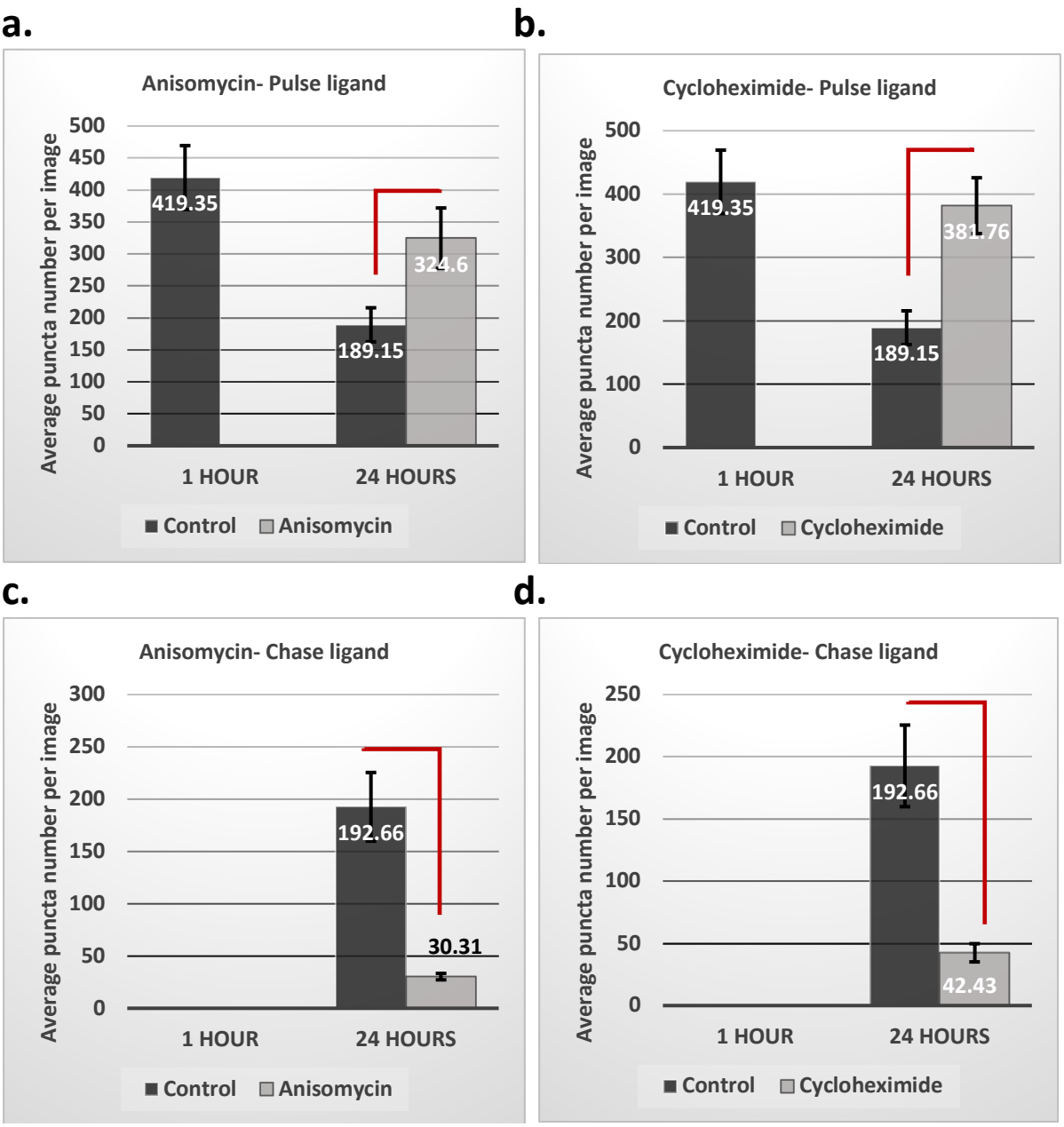

Figure 4.45. The effects of Anisomycin and Cycloheximide on PSD-95 puncta numbers. Hippocampal neuronal primary cultures from PSD-95$^{HaloTag/HaloTag}$ mice were grown for 14 days in vitro, and thereafter pulse-chase experiments performed using the R110Direct and TMR HaloTag ligands. Anisomycin at 1µM or cycloheximide at 3µM were added alongside the chase ligand for 1 or 24 hours. The graphs here present the mean values across eight cultures (N=8). **a.** Graph of the average R110 pulse ligand puncta number following anisomycin treatment. The number is significantly higher after 24 hours in the anisomycin group than in untreated controls (Welch's t-test, p=0.037). **b.** Graph of the average R110 pulse ligand puncta number following cycloheximide treatment. The number is significantly higher after 24 hours in the cycloheximide group than in untreated controls (Welch's t-test, p=0.0051). **c.** Graph of the average TMR chase ligand puncta number following anisomycin treatment. The difference between the anisomycin group and untreated controls is significant (Welch's t-test, p=0.0016). **d.** Graph of the average TMR chase ligand puncta number following cycloheximide treatment. The difference between the cycloheximide group and untreated controls is significant (Welch's t-test, p=0.0023).

4.4.6.1 Protein synthesis inhibitors- Anisomycin and Cycloheximide: bulk analysis

The final set of chemicals I used in my study were the protein synthesis inhibitors anisomycin and cycloheximide. Both are widely used, and have been shown to affect memory retention in live mammals. I decided to use these drugs for a similar reason as the proteasome inhibitors: I reasoned that blocking protein synthesis would surely have a noticeable effect on PSD-95 turnover, and thus provide interesting insights while also allowing me to test my HaloTag pulse-chase method in a state of cellular perturbation.

One thing to note at this point is that I decided to use anisomycin at a concentration of 1μM and cycloheximide at 3μM because I discovered that higher concentrations of these two drugs (anisomycin: 10μM; cycloheximide: 72μM) for 24 hours cause drastic cell death in primary cultures. My initial thought was to use these drugs to completely block all protein synthesis and thus prevent any chase ligand signal from being detectable, however, after my first pilot experiments I had to settle on reducing protein synthesis with lower doses of these two chemicals.

When first looking at the results of the bulk analysis of average puncta fluorescence intensity (APFI) for both anisomycin and cycloheximide treated cultures (figure 4.44), the first observation is that the graphs look strikingly similar to those of the proteasome inhibitor-treated cultures in the previous section (figure 4.33). The APFI of the pulse ligand after 24 hours is much higher than in untreated controls (anisomycin: figure 4.44.a, 61.2 ± 2.39 AU, p=0.00019; cycloheximide: figure 4.44.b, 60.16 ± 1.85 AU, $p=3.39x10^{-5}$; untreated control: 65.97 ± 1.69 AU). Likewise, the APFI of the chase ligand after 24 hours is much lower than in untreated controls (anisomycin: figure 4.44.c, 17.28 ± 0.48 AU, $p=2.41x10^{-5}$; cycloheximide: figure 4.44.d, 17.05 ± 0.46 AU, $p=2.22x10^{-5}$; untreated control: 29.63 ± 1.42 AU). Somewhat surprisingly, then, these two protein synthesis inhibitors appear to not only block the synthesis of new PSD-95, but also reduce PSD-95 degradation.

The results for bulk puncta numbers (figure 4.45) are, likewise, very similar to those obtained from the proteasome inhibitors (figure 4.34). Average pulse ligand puncta number per image is higher than in controls for both drugs, while chase ligand puncta number is much lower than in controls (figure 4.45, $p<0.05$).

4.4.6.2 Protein synthesis inhibitors- Anisomycin and Cycloheximide: single-synapse analysis

At the next stage of analysis, the similarities to the results obtained from the proteasome-inhibitor treatment continue. In figures 4.46 and 4.47 we see that the discrepancy between the control group and treatment group is greater in type 2 synapses than in type 3 synapses in terms of APFI of the pulse ligand. For both synaptic types, pulse ligand intensity is a lot higher than in controls. This is the case for both anisomycin (figure 4.46.a-b) and cycloheximide (figure 4.47.a-b) treatment. The difference between control and treatment fluorescence intensity is highly significant in each case ($p<5x10^{-5}$). For the chase ligand, the results are again incredibly similar to those obtained following proteasome inhibition. Figures 4.46 and 4.47 show that type 2 synapses contain much less new PSD-95 (chase ligand APFI is far below controls), while in type 1 synapses the APFI is significantly lower than in controls ($p<0.05$), but much less so. Following anisomycin treatment, for instance, type 2 synapses exhibit an APFI of 17.10 ± 0.45 AU compared to 34.88 ± 1.91 AU for controls ($p=2.14x10^{-5}$; figure 4.46.d), while type 1 synapses have an APFI of 18.95 ± 1.26 AU compared to 22.54 ± 1.00 AU for controls ($p=0.049$, figure 4.46.e). The results are nearly identical following cycloheximide treatment (figure 4.47.d-e). Again, type 1 and type 2 synapses are no different in their chase ligand APFI (figures 4.46.f and figure 4.47.f), unlike in controls (figure 4.2.b).

Puncta numbers are again very similar to those under the influence of proteasome inhibitors- very many type 3 (pulse ligand-only) synapses are found (figures 4.48.b and 4.49.b), with only very few type 2 synapses and barely any type 1 synapses (chase-ligand only). These results are made particularly clear by the pie chart in figure 4.50, as we can see that about 90% of synapses in anisomycin and cycloheximide treated groups contain only pulse ligands (old PSD-95), 9% contain both ligands and

a.

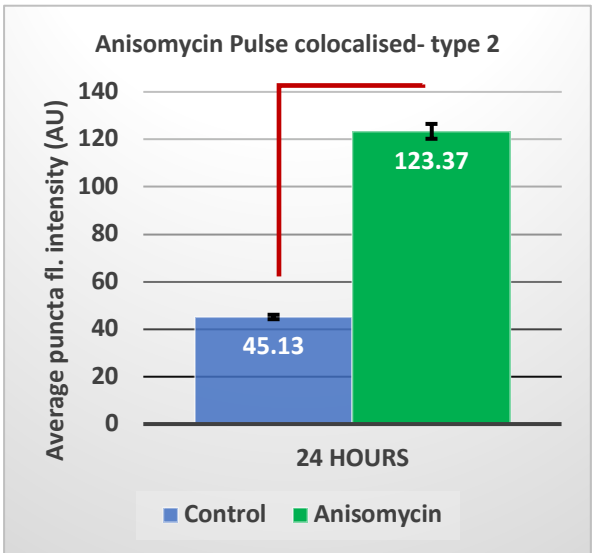
Anisomycin Pulse colocalised- type 2
Average puncta fl. intensity (AU)
140
120
100
80
60
40
20
0
45.13
123.37
24 HOURS
Control
Anisomycin

b.

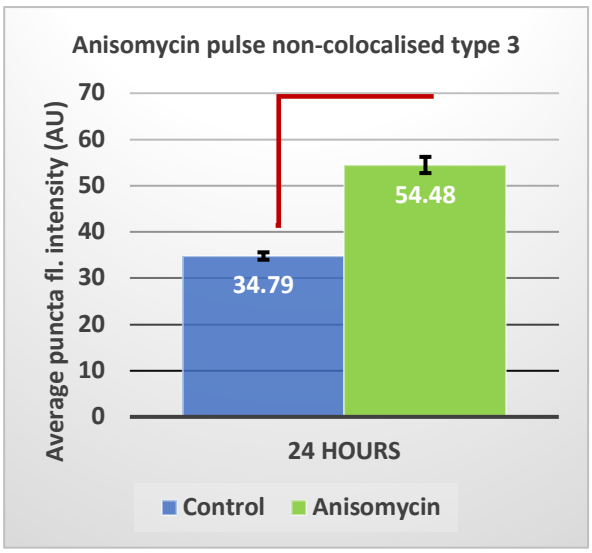
Anisomycin pulse non-colocalised type 3
Average puncta fl. intensity (AU)
70
60
50
40
30
20
10
0
34.79
54.48
24 HOURS
Control
Anisomycin

c.

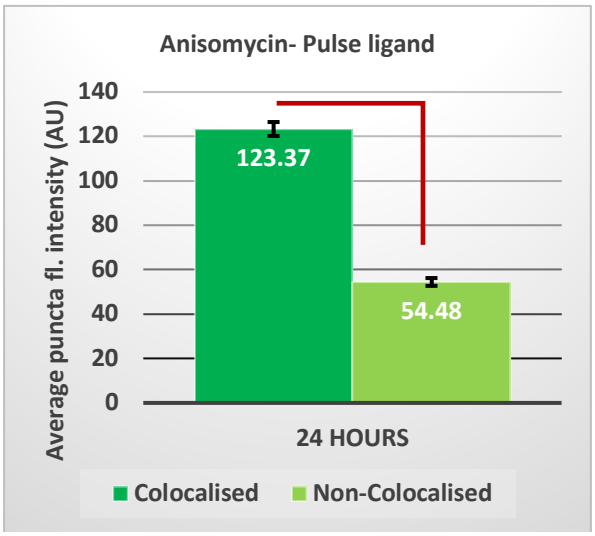
Anisomycin- Pulse ligand
Average puncta fl. intensity (AU)
140
120
100
80
60
40
20
0
123.37
54.48
24 HOURS
Colocalised
Non-Colocalised

d.

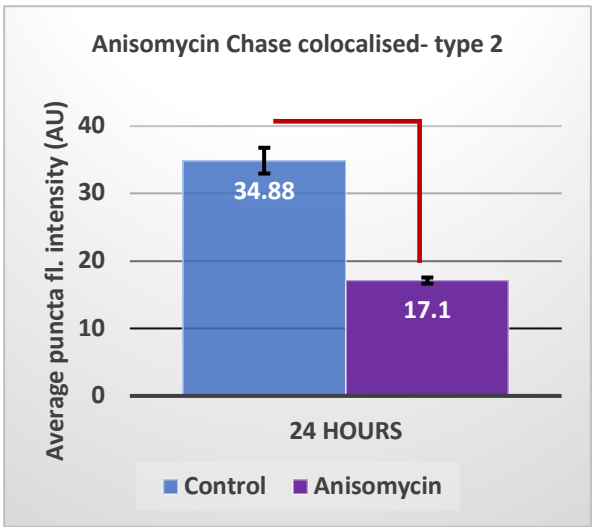
Anisomycin Chase colocalised- type 2
Average puncta fl. intensity (AU)
40
30
20
10
0
34.88
17.1
24 HOURS
Control
Anisomycin

e.

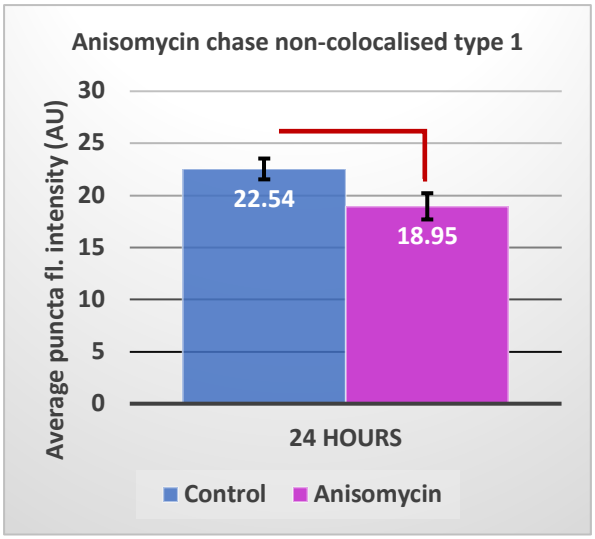
Anisomycin chase non-colocalised type 1
Average puncta fl. intensity (AU)
30
25
20
15
10
5
0
22.54
18.95
24 HOURS
Control
Anisomycin

f.

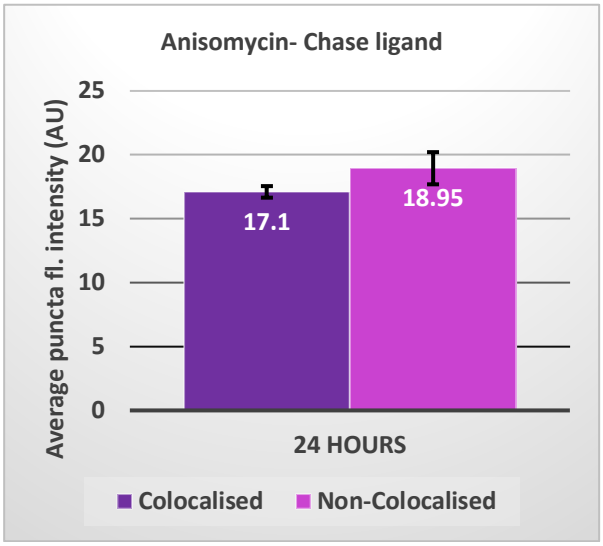
Anisomycin- Chase ligand
Average puncta fl. intensity (AU)
25
20
15
10
5
0
17.1
18.95
24 HOURS
Colocalised
Non-Colocalised

Figure 4.46. The effect of anisomycin on PSD-95 average puncta intensity at synaptic types. Average puncta fluorescence intensity (APFI) per image was calculated for pulse and chase ligand labelled synaptic puncta in type 1, type 2 and type 3 synapses separately. Images were taken after 24 hours of pulse-chase treatment with 50nM R110Direct ligand (pulse) and 500nM TMR ligand (chase) in hippocampal primary cultures from PSD-95$^{HaloTag/HaloTag}$ mice on DIV16. Anisomycin (1µM) was applied for 24 hours together with the chase ligand between DIV15 and DIV16. The graphs here present the mean values across eight cultures (N=8). **a.** Pulse ligand (R110Direct) APFI per image in synapses where pulse and chase ligands colocalise (type 2). The difference between the anisomycin group and untreated controls is statistically significant (Welch's t-test, $p=4.31x10^{-7}$). **b.** Pulse ligand APFI per image in synapses where pulse and chase ligands do not colocalise (type 3). The difference between the anisomycin group and untreated controls is statistically significant (Welch's t-test, $1.76x10^{-5}$). **c.** Comparison of pulse ligand APFI per image in type 2 synapses and type 3 synapses following anisomycin treatment. The difference between the two groups is statistically significant (Welch's t-test, $p=7.15x10^{-8}$). **d.** Chase ligand (TMR) APFI per image in synapses where pulse and chase ligands colocalise (type 2). The difference between the anisomycin group and untreated controls is statistically significant (Welch's t-test, $p=2.14x10^{-5}$). **e.** Chase ligand APFI per image in synapses where pulse and chase ligands do not colocalise (type 1). The difference between the anisomycin group and untreated controls is statistically significant (Welch's t-test, p=0.049). **f.** Comparison of chase ligand APFI per image in type 2 synapses and type 1 synapses following anisomycin treatment. The difference between the two groups is not statistically significant (Welch's t-test, p=0.21).

1% contain only the chase ligand. The conclusions are the same as those arrived at for the proteasome inhibitors: both of these classes of drugs massively reduce PSD-95 synthesis, while appearing to (most likely but not certainly) diminish PSD-95 degradation. This appears to have the effect of reducing synaptogenesis (fewer type 1 synapses), and moving synapses that would otherwise have become type 2 synapses through continuous PSD-95 turnover to become type 3 synapses by not incorporating newly synthesised PSD-95.

The graphs depicting the pulse:chase ratio at type 2 synapses appear alike in anisomycin and cycloheximide treatment groups (figure 4.53). In both graphs, the shape differs greatly from the control group, and is shifted massively towards higher ratios. For the anisomycin treatment group, the mean ratio is 12.99 ± 0.32 (SEM) (figure 4.53.d), with a median ratio of 13.00 and a mode of 13.2 with 4.12%. For the cycloheximide treatment group, the mean ratio is 14.12 ± 0.34 (SEM) (figure 4.53.d), with a median ratio of 13.89. The cycloheximide frequency histogram (figure 4.53.c) is trimodal, with modes of 11.2, 13.8 and 15.5, all at 3.61%. These graphs have no clear

a.

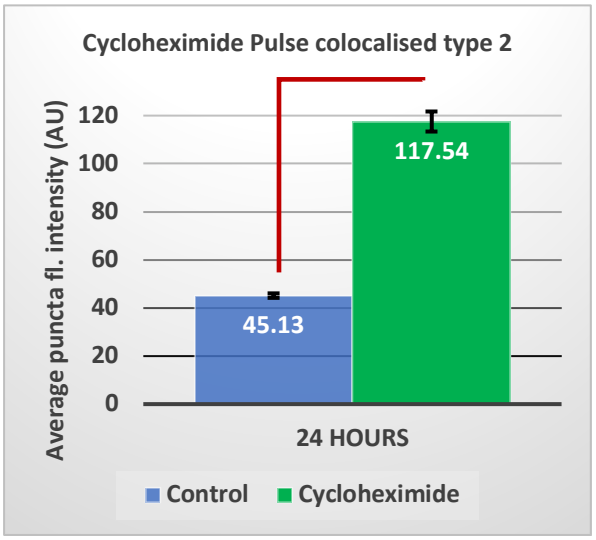
Cycloheximide Pulse colocalised type 2
Average puncta fl. intensity (AU)
120
100
80
60
40
20
0
45.13
117.54
24 HOURS
Control
Cycloheximide

b.

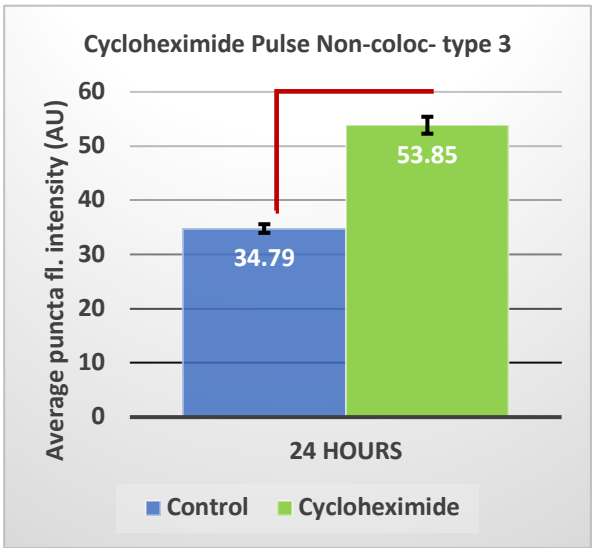
Cycloheximide Pulse Non-coloc- type 3
Average puncta fl. intensity (AU)
60
50
40
30
20
10
0
34.79
53.85
24 HOURS
Control
Cycloheximide

c.

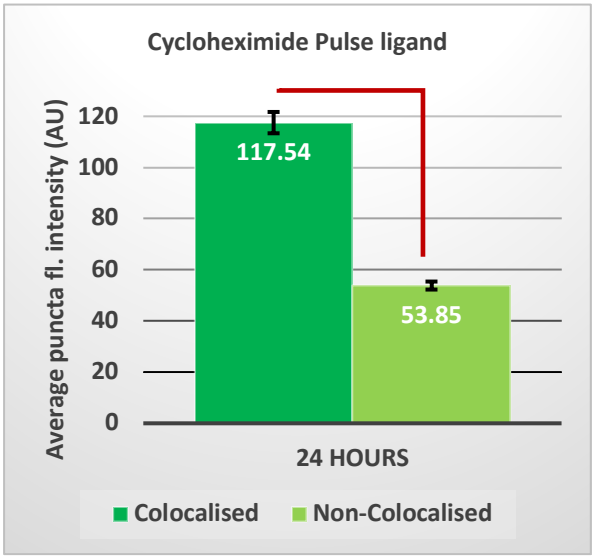
Cycloheximide Pulse ligand
Average puncta fl. intensity (AU)
120
100
80
60
40
20
0
117.54
53.85
24 HOURS
Colocalised
Non-Colocalised

d.

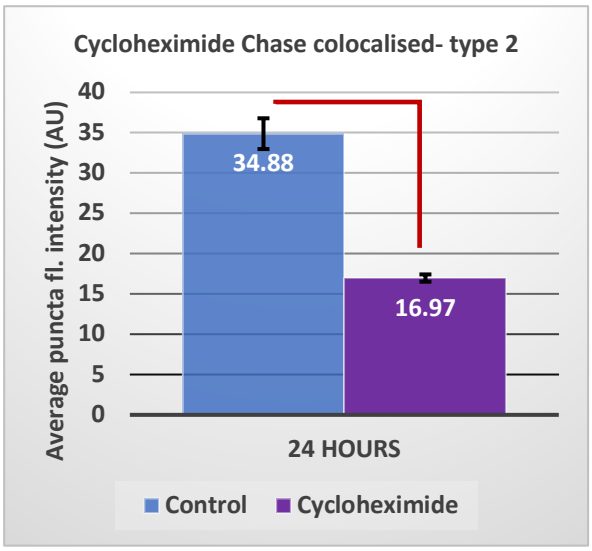
Cycloheximide Chase colocalised- type 2
Average puncta fl. intensity (AU)
40
35
30
25
20
15
10
5
0
34.88
16.97
24 HOURS
Control
Cycloheximide

e.

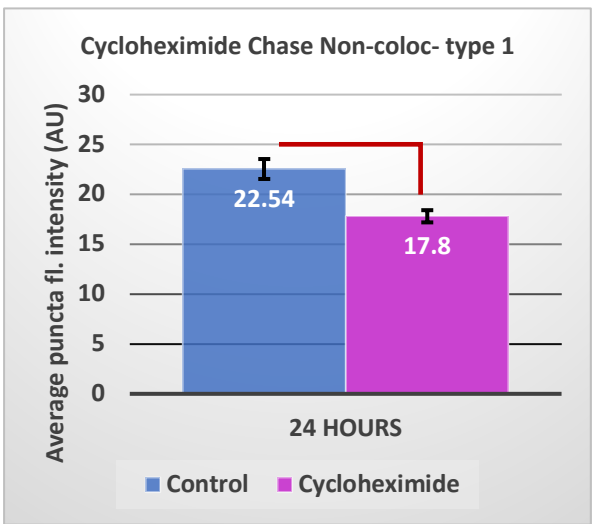
Cycloheximide Chase Non-coloc- type 1
Average puncta fl. intensity (AU)
30
25
20
15
10
5
0
22.54
17.8
24 HOURS
Control
Cycloheximide

f.

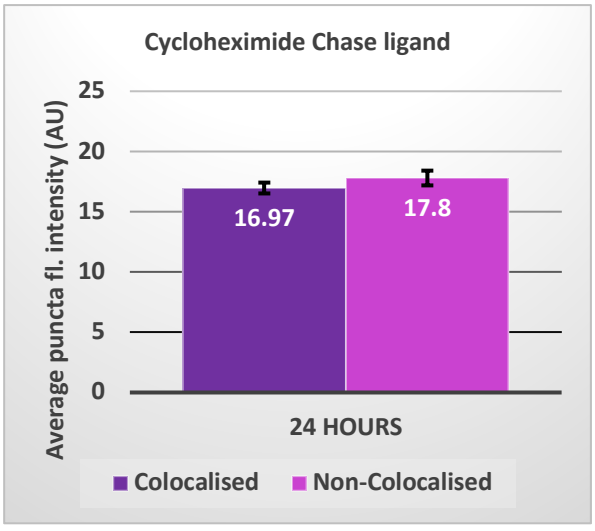
Cycloheximide Chase ligand
Average puncta fl. intensity (AU)
25
20
15
10
5
0
16.97
17.8
24 HOURS
Colocalised
Non-Colocalised

Figure 4.47. The effect of cycloheximid on PSD-95 average puncta intensity at synaptic types
Average puncta fluorescence intensity (APFI) per image was calculated for pulse and chase ligand labelled synaptic puncta in type 1, type 2 and type 3 synapses separately. Images were taken after 24 hours of pulse-chase treatment with 50nM R110Direct ligand (pulse) and 500nM TMR ligand (chase) in hippocampal primary cultures from PSD-95$^{HaloTag/HaloTag}$ mice on DIV16. Cycloheximide (3µM) was applied for 24 hours together with the chase ligand between DIV15 and DIV16. The graphs here present the mean values across eight cultures (N=8). **a.** Pulse ligand (R110Direct) APFI per image in synapses where pulse and chase ligands colocalise (type 2). The difference between the cycloheximide group and untreated controls is statistically significant (Welch's t-test, $p=5.82x10^{-6}$). **b.** Pulse ligand APFI per image in synapses where pulse and chase ligands do not colocalise (type 3). The difference between the cycloheximide group and untreated controls is statistically significant (Welch's t-test, $7.00x10^{-6}$). **c.** Comparison of pulse ligand APFI per image in type 2 synapses and type 3 synapses following cycloheximide treatment. The difference between the two groups is statistically significant (Welch's t-test, $p=4.37x10^{-6}$). **d.** Chase ligand (TMR) APFI per image in synapses where pulse and chase ligands colocalise (type 2). The difference between the cycloheximide group and untreated controls is statistically significant (Welch's t-test, $p=2.04x10^{-5}$). **e.** Chase ligand APFI per image in synapses where pulse and chase ligands do not colocalise (type 1). The difference between the cycloheximide group and untreated controls is statistically significant (Welch's t-test, p=0.0019). **f.** Comparison of chase ligand APFI per image in type 2 synapses and type 1 synapses following cycloheximide treatment. The difference between the two groups is not statistically significant (Welch's t-test, p=0.31).

peak, and experience a wide range of ratios, ranging from 1.2 to more than 27. Note that these protein synthesis inhibitors do appear to have an even more pronounced effect than the proteasome inhibitors, as the ratio range has shifted from about 1.8 – 20 (proteasome inhibitors) to about 1.6 – 27 (synthesis inhibitors).

Next, type 2 synapses still exhibit a positive correlation between pulse and chase ligand average puncta intensity (figure 4.54) (anisomycin: $R^2=0.50$; cycloheximide: $R^2=0.62$). However, the correlations are less pronounced than in the untreated control group ($R^2=0.96$).

a.

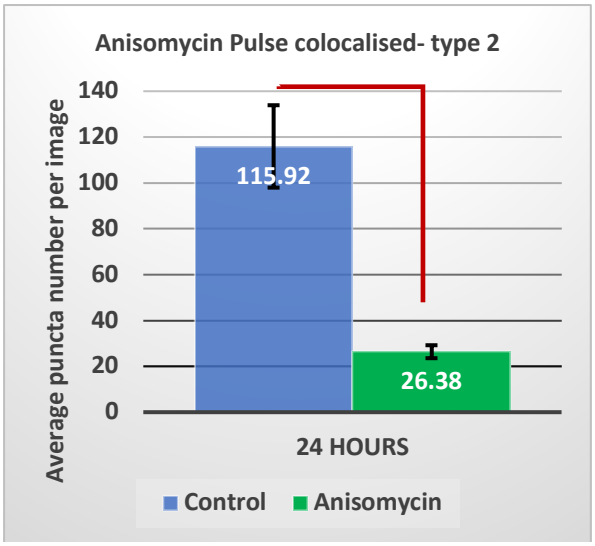
Anisomycin Pulse colocalised- type 2
Average puncta number per image
140
120
100
80
60
40
20
0
115.92
26.38
24 HOURS
Control
Anisomycin

b.

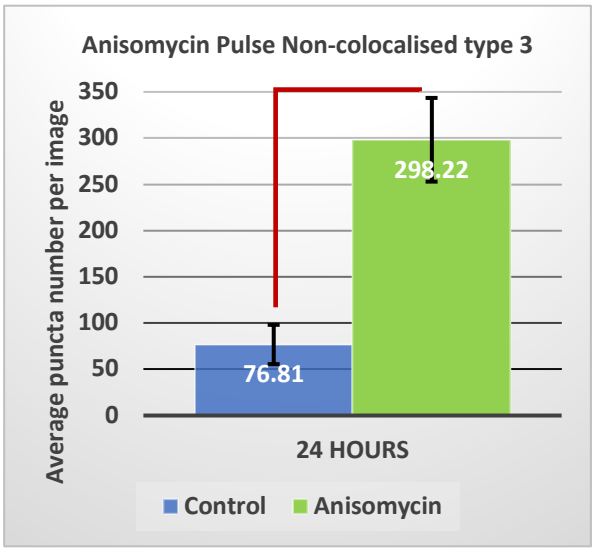
Anisomycin Pulse Non-colocalised type 3
Average puncta number per image
350
300
250
200
150
100
50
0
298.22
76.81
24 HOURS
Control
Anisomycin

c.

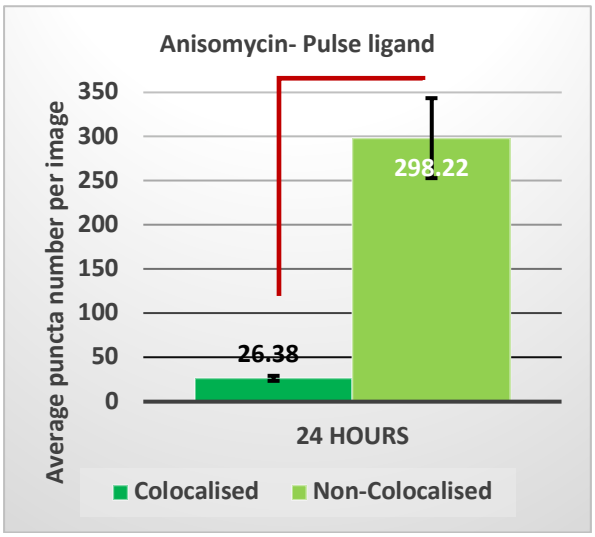
Anisomycin- Pulse ligand
Average puncta number per image
350
300
250
200
150
100
50
0
298.22
26.38
24 HOURS
Colocalised
Non-Colocalised

d.

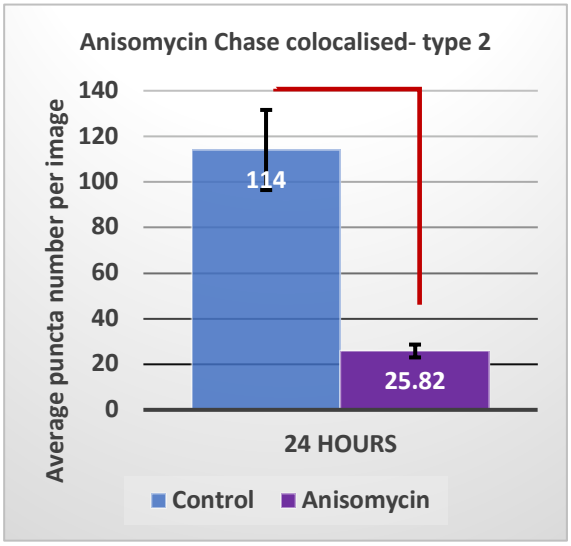
Anisomycin Chase colocalised- type 2
Average puncta number per image
140
120
100
80
60
40
20
0
114
25.82
24 HOURS
Control
Anisomycin

e.

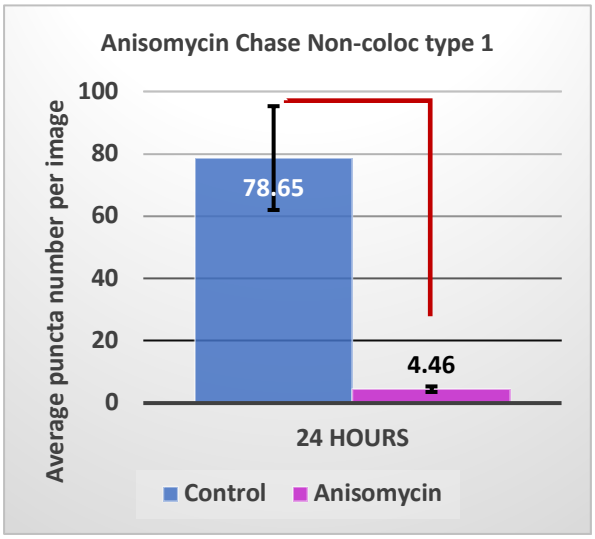
Anisomycin Chase Non-coloc type 1
Average puncta number per image
100
80
60
40
20
0
78.65
4.46
24 HOURS
Control
Anisomycin

f.

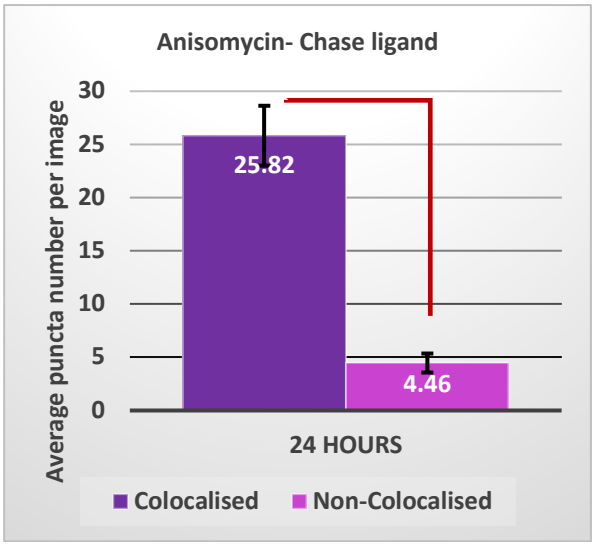
Anisomycin- Chase ligand
Average puncta number per image
30
25
20
15
10
5
0
25.82
4.46
24 HOURS
Colocalised
Non-Colocalised

Figure 4.48. The effect of anisomycin on PSD-95 average puncta number at synaptic types. Average puncta number per image was calculated for pulse and chase ligand labelled synaptic puncta in type 1, type 2 and type 3 synapses separately. Images were taken after 24 hours of pulse-chase treatment with 50nM R110Direct ligand (pulse) and 500nM TMR ligand (chase) in hippocampal primary cultures from PSD-95$^{HaloTag/HaloTag}$ mice on DIV16. Anisomycin (1µM) was applied for 24 hours together with the chase ligand between DIV15 and DIV16. The graphs here present the mean values across eight cultures (N=8).
a. Pulse ligand average puncta number per image in synapses where pulse and chase ligands colocalise (type 2). The difference between the anisomycin group and untreated controls is statistically significant (Welch's t-test, p=0.0015). **b.** Pulse ligand average puncta number per image in synapses where pulse and chase ligands do not colocalise (type 3). The difference between the anisomycin group and untreated controls is statistically significant (Welch's t-test, p=0.0029). **c.** Comparison of pulse ligand average puncta number per image in type 2 synapses and type 3 synapses following anisomycin treatment. The difference between the two groups is statistically significant (Welch's t-test, p=0.0018). **d.** Chase ligand (TMR) average puncta number per image in synapses where pulse and chase ligands colocalise (type 2). The difference between the anisomycin group and untreated controls is statistically significant (Welch's t-test, p=0.0014). **e.** Chase ligand average puncta number per image in synapses where pulse and chase ligands do not colocalise (type 1). The difference between the anisomycin group and untreated controls is statistically significant (Welch's t-test, p=0.0030). **f.** Comparison of chase ligand average puncta number per image in type 2 synapses and type 1 synapses following anisomycin treatment. The difference between the two groups is statistically significant (Welch's t-test, p=0.00036).

Finally, CDF's were calculated for each of the eight groups (Figures 4.51 and 4.52). The resulting curves look similar to those for the previous set of drugs, lactacystin and MG132. In these two treatment groups (anisomycin and cycloheximide), type 1 synapses are very low in frequency, such that the curves look very different to the control group. As before, the curves of type 2 and type 3 synapses are shifted- to the right for the pulse ligand and the left for the chase ligand. This indicates a greater probability of pulse ligand puncta having a higher APFI and reduced probability of chase ligand puncta having a high APFI, relative to controls. It is also noteworthy that the curves in figure 4.51.a and 4.52.a are steeper for the controls and shallower for the treated group. This indicates that the vast majority of the control group puncta are of a lower intensity, with very few having a high intensity, but in the case of the drug treatment groups the puncta intensities are much more spread, with a substantial percentage of puncta found at high intensities. For example, from figure 4.51.a, 90% of control puncta have an APFI below 68 AU, while 90% of anisomycin-treated puncta have an APFI below 172 AU.

The only curve found to not be significantly different from the untreated control group when tested using the Kolmogorov-Smirnov test for difference was that belonging to type 1 synapses when treated with cycloheximide ($p=0.606$). All other groups were found to be significantly different from the control group. This difference is due to the high degree of puncta overlap between the treated group and the control group, which is also visually discernible.

a.

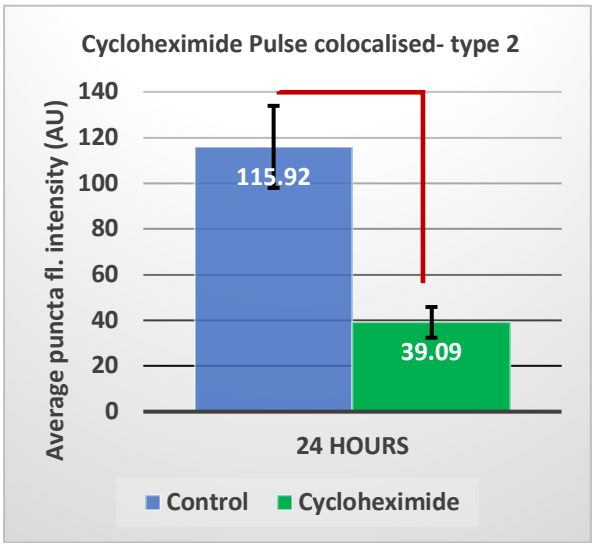
Cycloheximide Pulse colocalised- type 2
Average puncta fl. intensity (AU)
140
120
100
80
60
40
20
0
115.92
39.09
24 HOURS
Control
Cycloheximide

b.

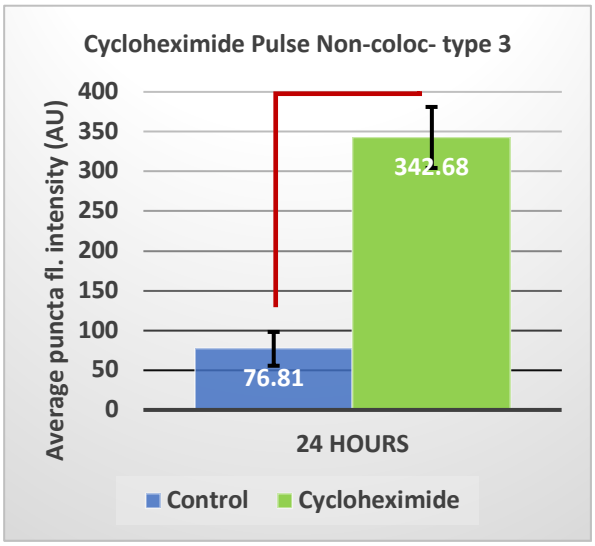
Cycloheximide Pulse Non-coloc- type 3
Average puncta fl. intensity (AU)
400
350
300
250
200
150
100
50
0
342.68
76.81
24 HOURS
Control
Cycloheximide

c.

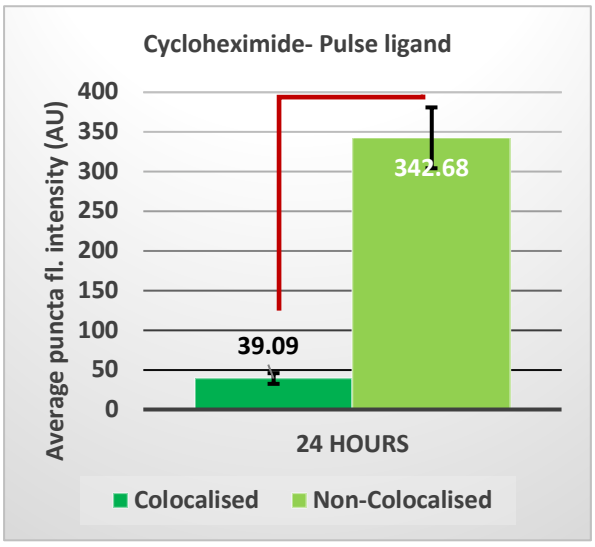
Cycloheximide- Pulse ligand
Average puncta fl. intensity (AU)
400
350
300
250
200
150
100
50
0
342.68
39.09
24 HOURS
Colocalised
Non-Colocalised

d.

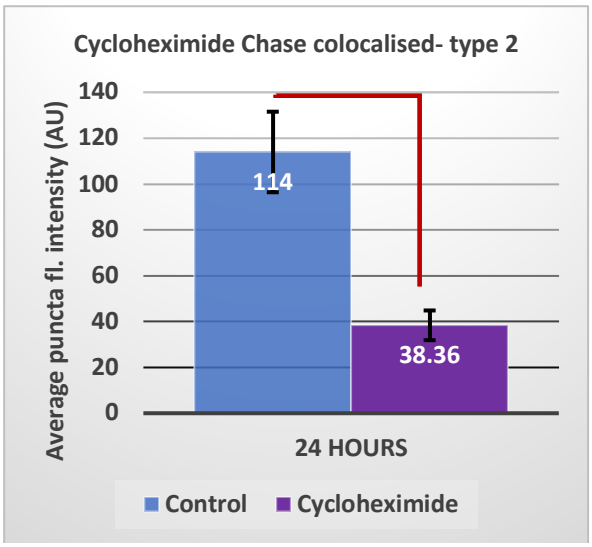
Cycloheximide Chase colocalised- type 2
Average puncta fl. intensity (AU)
140
120
100
80
60
40
20
0
114
38.36
24 HOURS
Control
Cycloheximide

e.

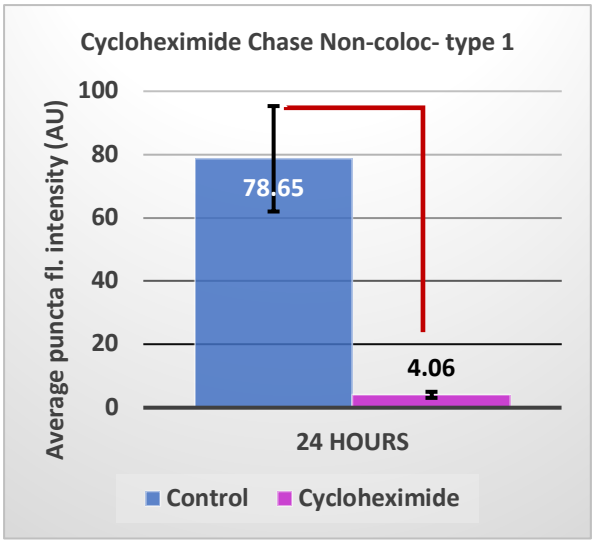
Cycloheximide Chase Non-coloc- type 1
Average puncta fl. intensity (AU)
100
80
60
40
20
0
78.65
4.06
24 HOURS
Control
Cycloheximide

f.

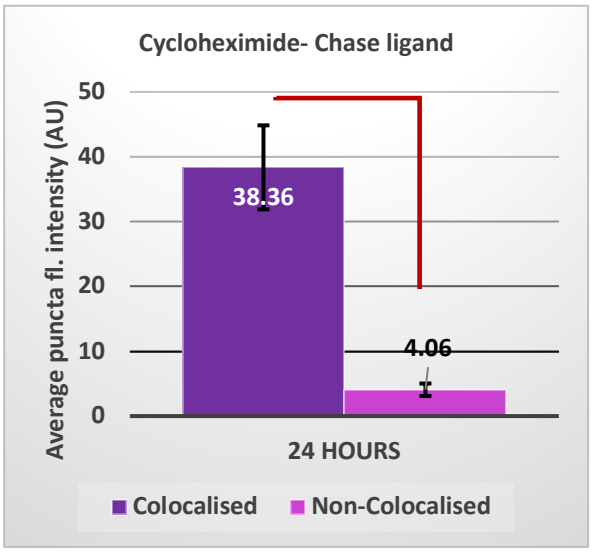
Cycloheximide- Chase ligand
Average puncta fl. intensity (AU)
50
40
30
20
10
0
38.36
4.06
24 HOURS
Colocalised
Non-Colocalised

Figure 4.49. The effect of cycloheximide on PSD-95 average puncta number at synaptic types.

Average puncta number per image was calculated for pulse and chase ligand labelled synaptic puncta in type 1, type 2 and type 3 synapses separately. Images were taken after 24 hours of pulse-chase treatment with 50nM R110Direct ligand (pulse) and 500nM TMR ligand (chase) in hippocampal primary cultures from PSD-95$^{HaloTag/HaloTag}$ mice on DIV16. Cycloheximide (3µM) was applied for 24 hours together with the chase ligand between DIV15 and DIV16. The graphs here present the mean values across eight cultures (N=8). **a.** Pulse ligand average puncta number per image in synapses where pulse and chase ligands colocalise (type 2). The difference between the cycloheximide group and untreated controls is statistically significant (Welch's t-test, p=0.0032). **b.** Pulse ligand average puncta number per image in synapses where pulse and chase ligands do not colocalise (type 3). The difference between the cycloheximide group and untreated controls is statistically significant (Welch's t-test, p=0.00030). **c.** Comparison of pulse ligand average puncta number per image in type 2 synapses and type 3 synapses following cycloheximide treatment. The difference between the two groups is statistically significant (Welch's t-test, p=0.00043). **d.** Chase ligand (TMR) average puncta number per image in synapses where pulse and chase ligands colocalise (type 2). The difference between the cycloheximide group and untreated controls is statistically significant (Welch's t-test, p=0.0031). **e.** Chase ligand average puncta number per image in synapses where pulse and chase ligands do not colocalise (type 1). The difference between the cycloheximide group and untreated controls is statistically significant (Welch's t-test, p=0.0029). **f.** Comparison of chase ligand average puncta number per image in type 2 synapses and type 1 synapses following cycloheximide treatment. The difference between the two groups is statistically significant (Welch's t-test, p=0.0030).

a.

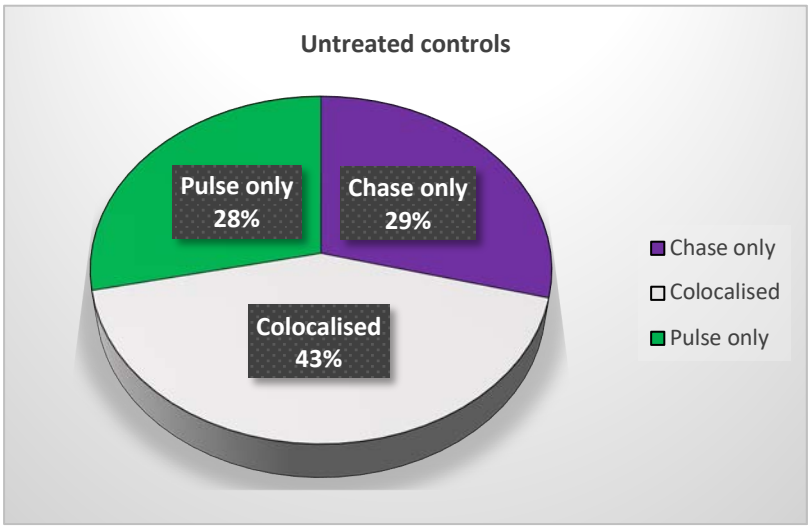
Untreated controls
Pulse only 28%
Chase only 29%
Colocalised 43%
Chase only
Colocalised
Pulse only

b.

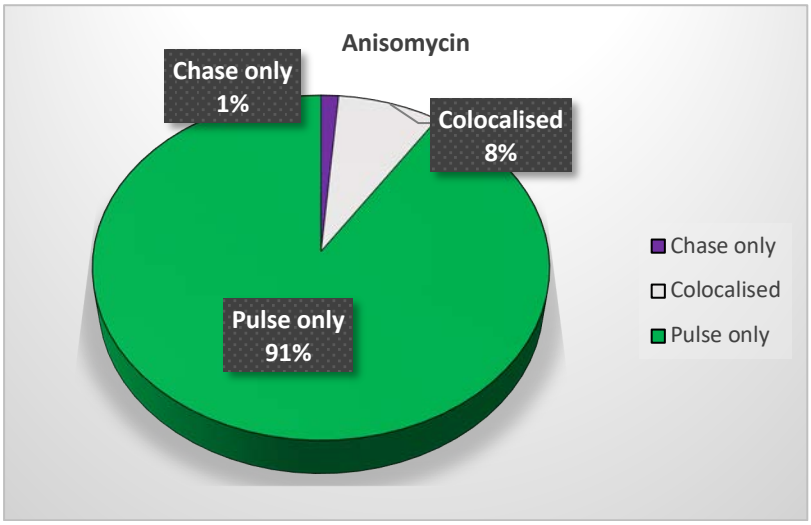
Anisomycin
Chase only 1%
Colocalised 8%
Pulse only 91%
Chase only
Colocalised
Pulse only

c.

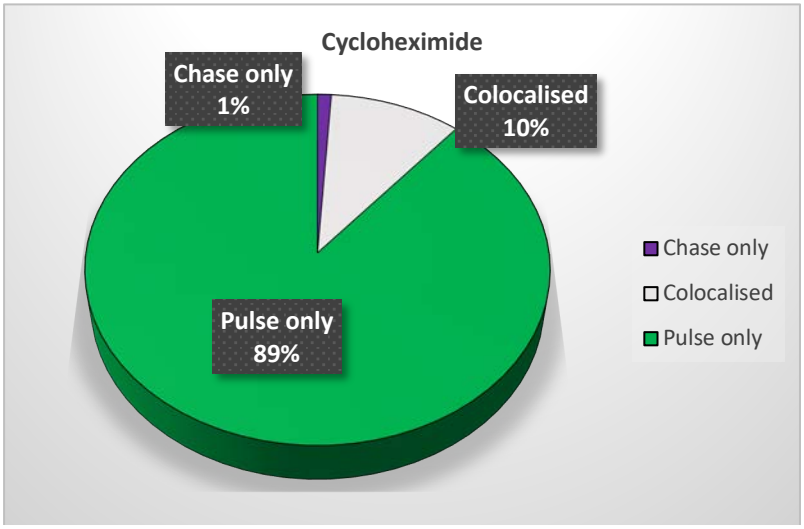
Cycloheximide
Chase only 1%
Colocalised 10%
Pulse only 89%
Chase only
Colocalised
Pulse only

Figure 4.50. Proportional representation of synaptic population by HaloTag ligand-labelling following the inhibition of protein synthesis.

Synaptic puncta were categorised according to whether they colocalised with puncta labelled by the other ligand or not. This pie chart depicts the proportional representation of the three types of synaptic puncta observed. Images were taken after 24 hours of pulse-chase treatment with 50nM R110Direct ligand (pulse) and 500nM TMR ligand (chase) in hippocampal primary cultures from PSD-95$^{HaloTag/HaloTag}$ mice on DIV16. **a.** In untreated controls, 28% of puncta contain only the pulse (R110Direct) ligand (type 3), 43% of puncta contain both pulse and chase (TMR) ligands (type 2), and 29% contain only the chase ligand (type 1). **b.** Following 24 hours of anisomycin treatment (1µM), 91% of puncta contain only the pulse (R110Direct) ligand (type 3), 8% of puncta contain both pulse and chase (TMR) ligands (type 2), and 1% contain only the chase ligand (type 1). **c.** Following 24 hours of cycloheximide treatment (3µM), 89% of puncta contain only the pulse (R110Direct) ligand (type 3), 10% of puncta contain both pulse and chase (TMR) ligands (type 2), and 1% contain only the chase ligand (type 1).

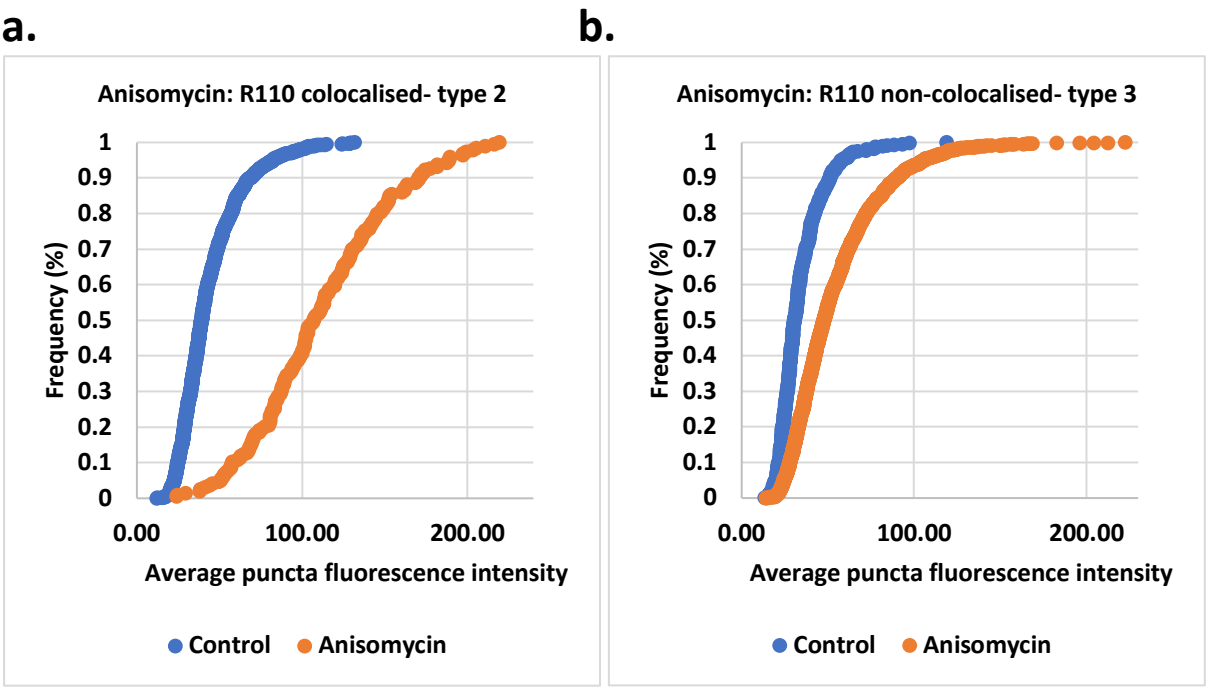

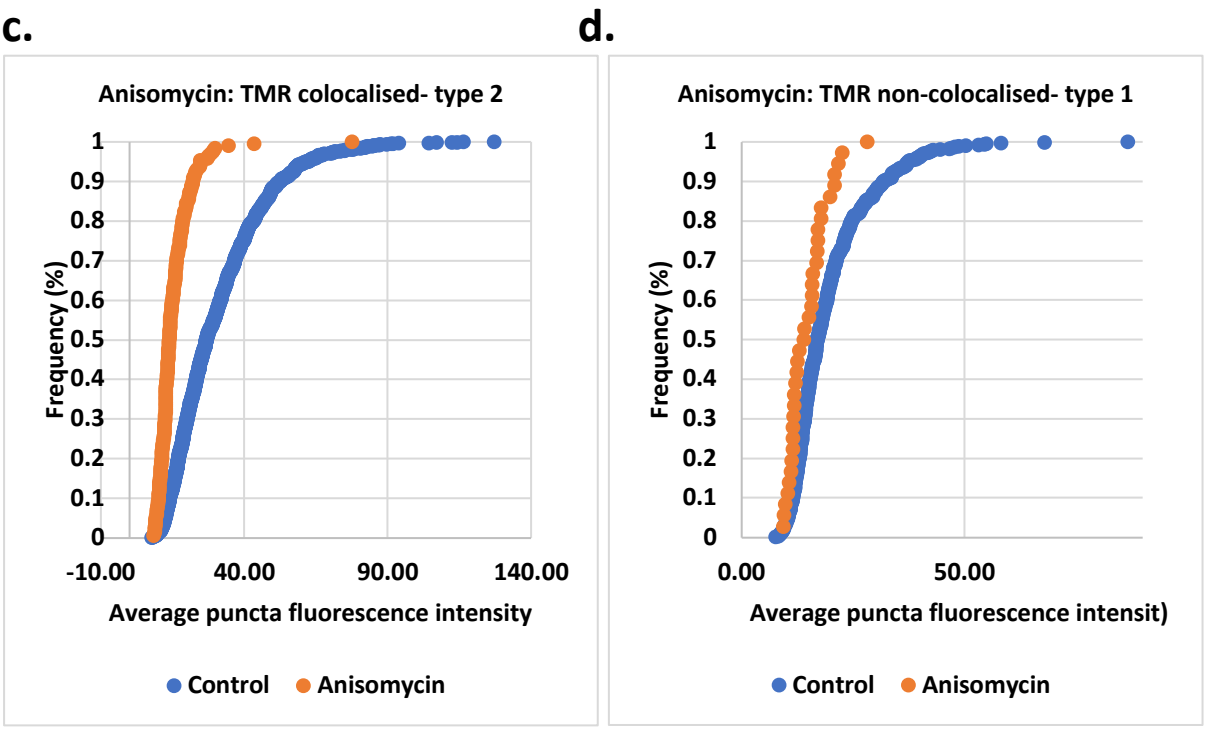

Figure 4.51. Cumulative distribution functions of average puncta fluorescence intensity following anisomycin treatment.

CDFs were constructed using the single-synapse data following anisomycin treatment, and compared with the untreated control group. Whether the difference was statistically significant or not was tested using the Kolmogorov-Smirnov test for difference. **a.** Comparison between R110 ligand puncta in colocalised type 2 synapses of anisomycin-treated neurons with those in untreated controls. The difference is significant (Kolmogorov-Smirnov, $p<0.0001$). **b.** Comparison between R110 ligand puncta in non-colocalised type 3 synapses of anisomycin-treated neurons with those in untreated controls. The difference is significant (Kolmogorov-Smirnov, $p<0.0001$). **c.** Comparison between TMR ligand puncta in colocalised type 2 synapses of anisomycin-treated neurons with those in untreated controls. The difference is significant (Kolmogorov-Smirnov, $p<0.0001$). **d.** Comparison between TMR ligand puncta in non-colocalised type 1 synapses of anisomycin-treated neurons with those in untreated controls. The difference is significant (Kolmogorov-Smirnov, $p=0.006$).

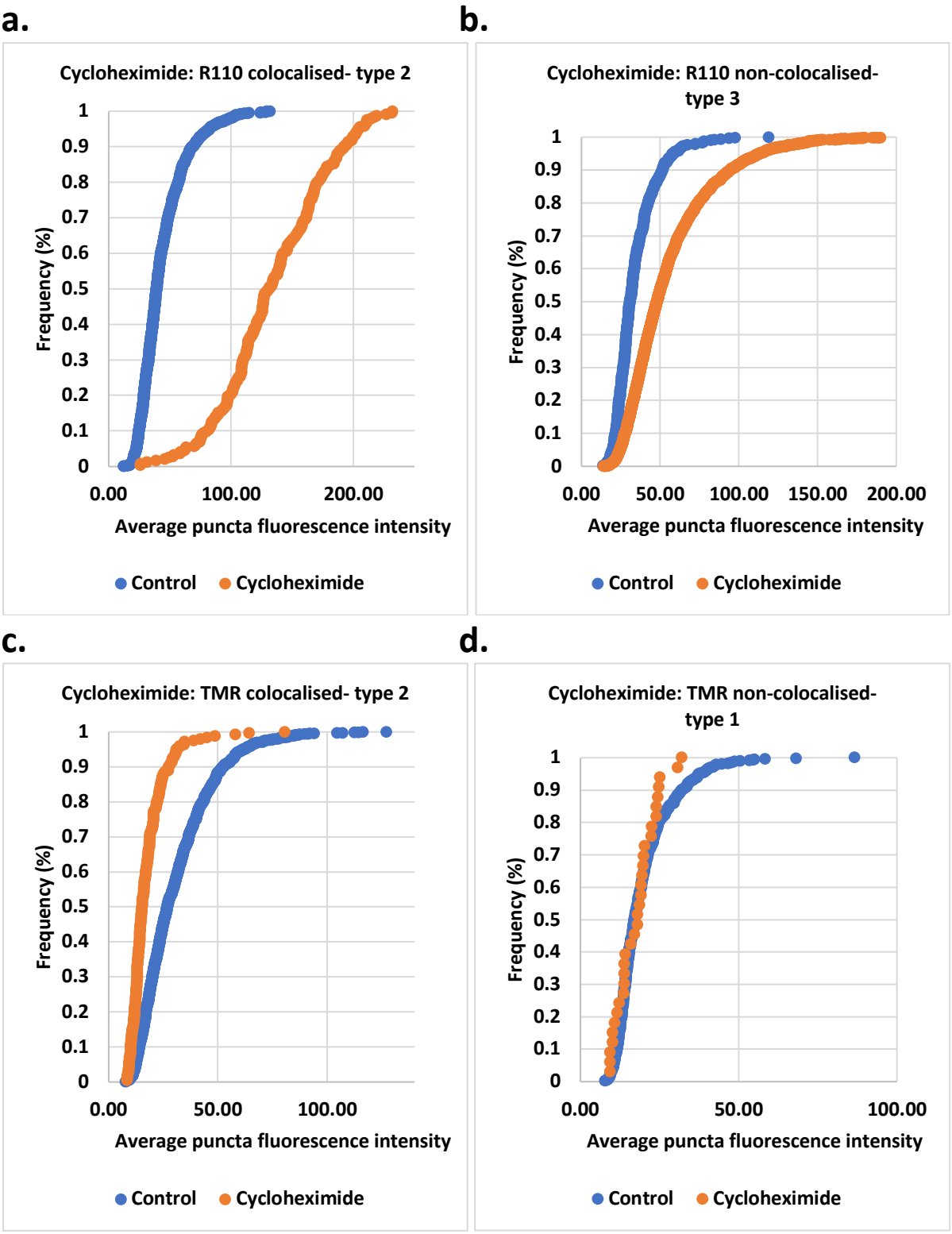

Figure 4.52. Cumulative distribution functions of average puncta fluorescence intensity following cycloheximide treatment.

CDFs were constructed using the single-synapse data following cycloheximide treatment, and compared with the untreated control group. Whether the difference was statistically significant or not was tested using the Kolmogorov-Smirnov test for difference. **a.** Comparison

between R110 ligand puncta in colocalised type 2 synapses of cycloheximide-treated neurons with those in untreated controls. The difference is significant (Kolmogorov-Smirnov, $p<0.0001$). **b.** Comparison between R110 ligand puncta in non-colocalised type 3 synapses of cycloheximide-treated neurons with those in untreated controls. The difference is significant (Kolmogorov-Smirnov, $p<0.0001$). **c.** Comparison between TMR ligand puncta in colocalised type 2 synapses of cycloheximide-treated neurons with those in untreated controls. The difference is significant (Kolmogorov-Smirnov, $p<0.0001$). **d.** Comparison between TMR ligand puncta in non-colocalised type 1 synapses of cycloheximide-treated neurons with those in untreated controls. The difference is not significant (Kolmogorov-Smirnov, $p=0.606$).

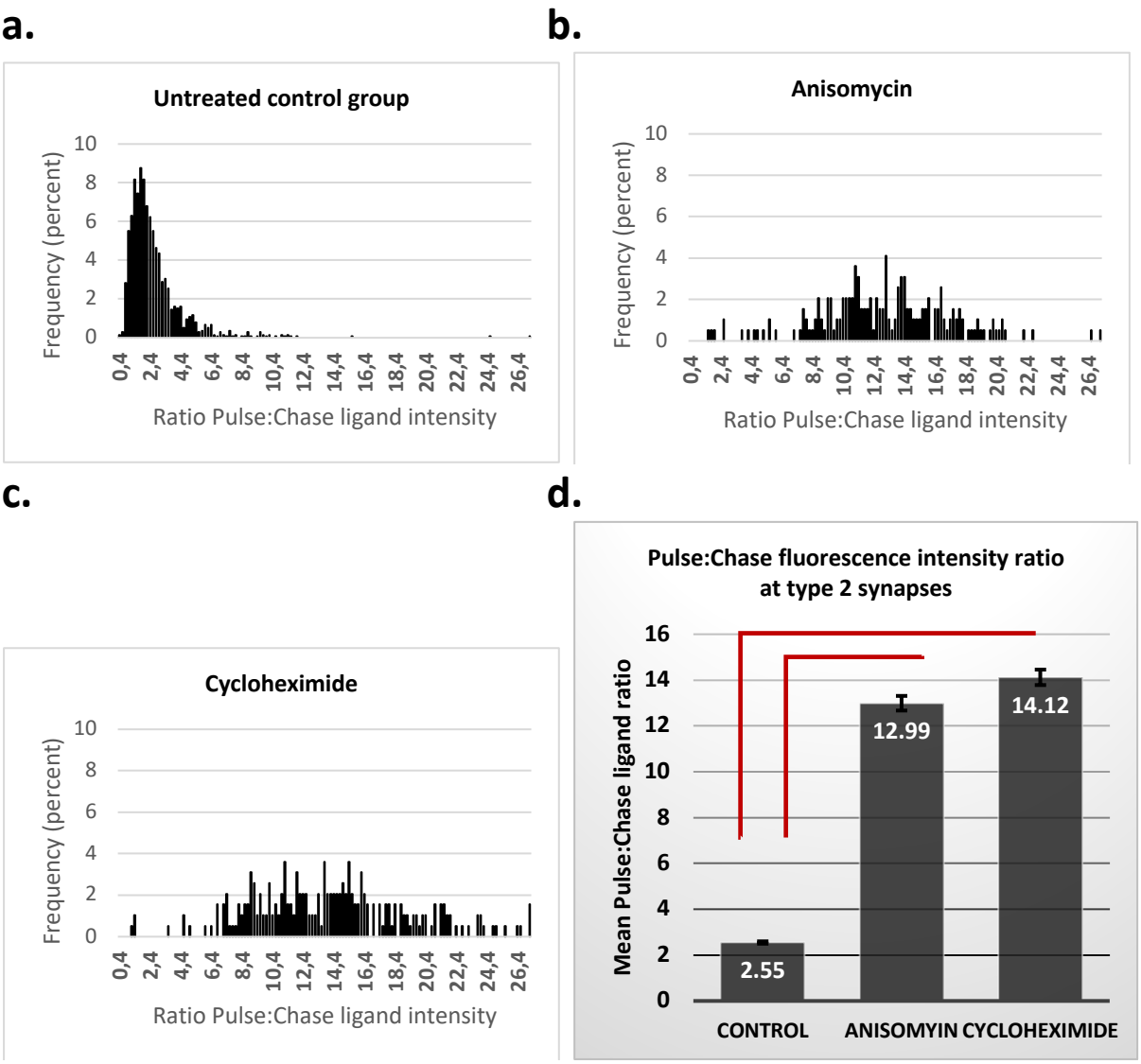

Figure 4.53. Graphs showing the ratio of pulse to chase ligands at individual type 2 synapses following protein synthesis inhibition.

In the synaptic population in which pulse and chase ligand-labelled PSD-95-HaloTag molecules were colocalised (type 2), the ratio of pulse ligand fluorescence intensity to chase ligand fluorescence intensity was calculated for each individual synapse. The frequency histograms represent the frequencies of all the pulse:chase ratios. **a.** Frequency distribution in untreated controls. Mean ratio: 2.55 ± 0.051 (SEM), Median ratio: 2.06, Mode: 1.8 (8.76%). **b.** Frequency distribution following 24 hours of anisomycin (1µM) treatment. Mean ratio: 12.99 ± 0.32 (SEM), Median ratio: 13.00, Mode: 13.2 (4.12%). **c.** Frequency distribution following 24 hours of cycloheximide (3µM) treatment. Mean ratio: 14.12 ± 0.34 (SEM), Median ratio: 13.89, Modes: 11.2, 13.8, 15.4 (all 3.61%). Note that the graph s trimodal. **d.** Comparison of mean pulse:chase ligand ratio in untreated controls with anisomycin and cycloheximide treated cultures. Differences are statistically significant in for both the anisomycin (Welch's t-test, $p=7.24x10^{-82}$) and the cycloheximide group (Welch's t-test, $p=2.46x10^{-96}$).

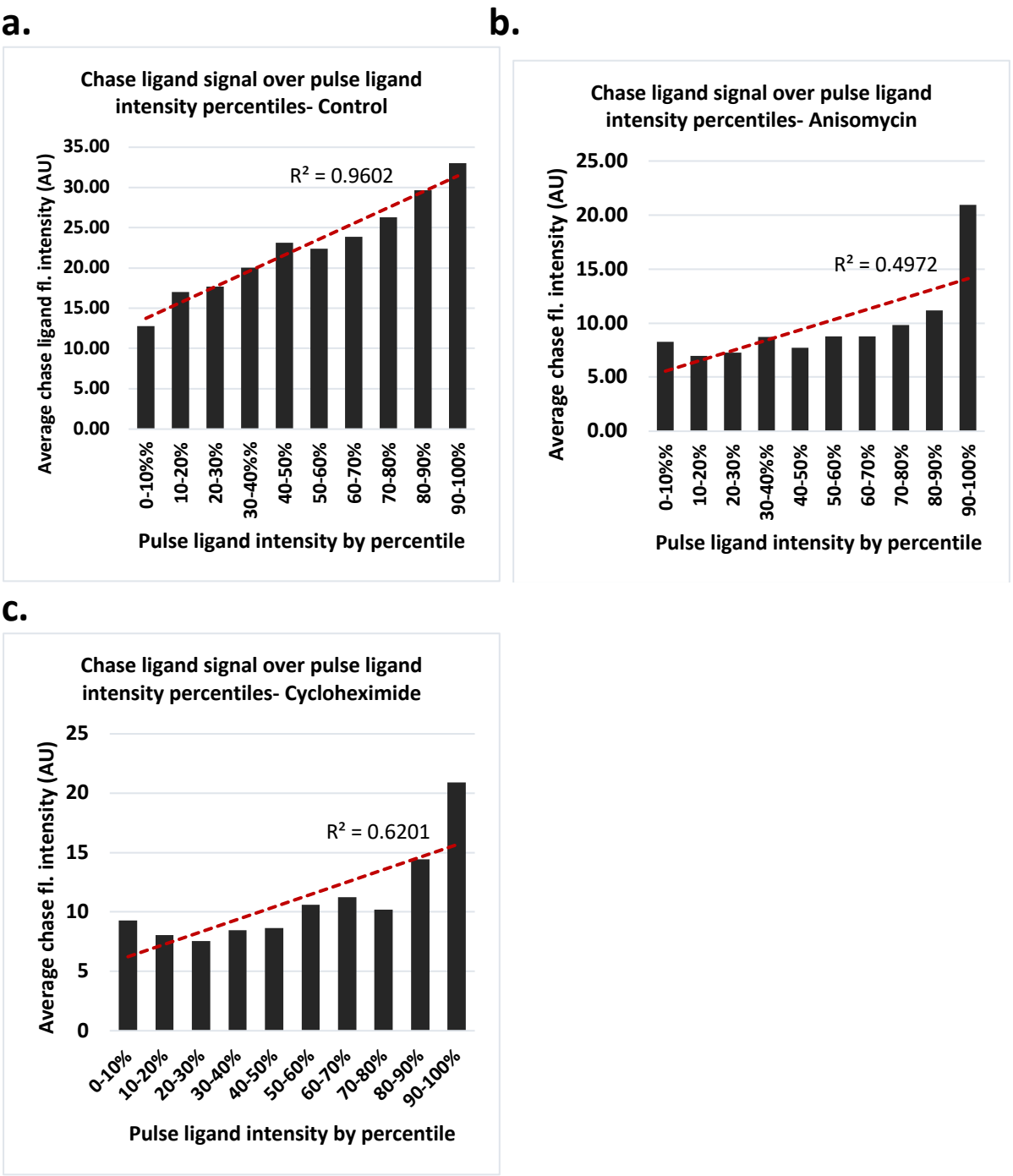

Figure 4.54 Correlation of pulse ligand intensity with chase ligand intensity at colocalised synaptic puncta following protein synthesis inhibition.

Colocalising (type 2) synapses were sorted by their pulse ligand APFI (lowest to highest). For each ten percentile steps, average chase ligand APFI was calculated. **a.** In untreated controls, there is a strong positive correlation, R^2=0.96. **b.** In the lactacystin-treated cultures, there is a weak positive correlation, R^2=0.50. **c.** In the MG132-treated cultures, the correlation is also weak at R^2=0.62.

4.4.6.3 Protein synthesis inhibitors- Anisomycin and Cycloheximide: discussion

I will limit my discussion of the effects of anisomycin and cycloheximide on PSD-95 turnover in this section, as the results in this section, chapter 4.4.6, are incredibly similar to those obtained using the proteasome inhibitors in chapter 4.4.5. Instead, I will focus on trying to explain the phenomena observed in these subchapters based upon the evidence and the literature as well as I can in the next subchapter, 4.4.7.

Nevertheless, I will summarise my findings here in order to provide an overview of the results obtained. As with proteasome inhibitors, the main observations are:

1. Overall (bulk) pulse ligand APFI remains significantly higher over 24 hours. This effect could also be observed at both type 2 and type 3 synapses.
2. Overall (bulk) chase ligand APFI rises to a much lower level over these 24 hours. This appears to be mediated chiefly through type 2 and much less so type 1 synapses.
3. Type 1 and type 2 synapses contain equal amounts of new PSD-95, unlike untreated controls.
4. There are significantly fewer type 1 synapses.
5. There are significantly fewer type 2 synapses.
6. There are significantly more type 3 synapses.
7. Within type 2 synapses, the ratio of pulse:chase ligand APFI is skewed strongly towards the pulse ligand.

As with proteasome inhibitors, this class of drugs appears to have two effects on PSD-95: Firstly, more old PSD-95 is retained at synapses. This is most likely due to decreased PSD-95 degradation, although replenishment from freely diffusing dendritic PSD-95 cannot be ruled out completely. Secondly, less newly-synthesised PSD-95 is incorporated into synapses, the obvious explanation being that less PSD-95 is being synthesised in the cell. We can therefore conclude that these drugs have two effects: one is linked directly to the action of the drug; in this case the inhibition of protein synthesis preventing new PSD-95 from being formed. The other is a knock-on effect,

here reducing the loss of old PSD-95. All of the other observations, such as changes in the balance between synaptic types and in the ratio of pulse to chase ligands in mixed-ligand synapses are merely by-products of these two effects. In order to underline the significance of the effect of these two classes of drugs on the ratios of pulse to chase ligands at type 2 synapses, I have directly compared all of the drug-treatment groups with each other in terms of these ratios. Figure 4.55 shows just how strongly PSD-95 ratios are affected compared to the other treatment groups.

The fact that two groups of drugs with opposing mechanisms of actions have such similar outcomes in terms of their effect on both PSD-95 synthesis and degradation is something that is very much worth noting, and something that warrants further investigation. It implies that both of these drugs have far reaching consequences in their use, as they appear to affect not only the target mechanism, but other neuronal mechanism as well. Given that both these classes of drugs are very widely used, and their apparent secondary effects are not widely reported (particularly those pertaining to the protein synthesis inhibitors), it may become necessary to take the knock-on effects reported here into account when designing any future experiments involving these chemicals.

In section 4.4.8 I will discuss one possible interpretation of these results.

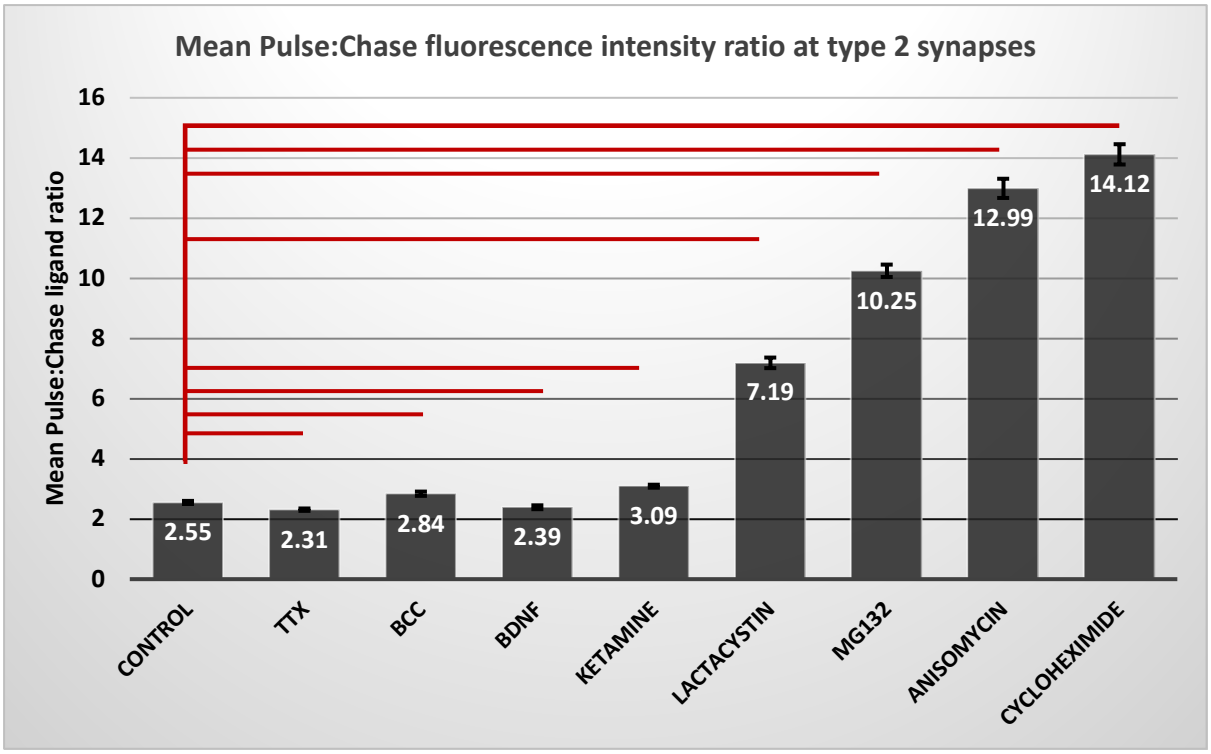

Figure 4.55. The ratio of pulse:chase ligands in type 2 synapses is perturbed most strongly following treatment with proteasome inhibitors and protein synthesis inhibitors.

The mean pulse to chase ligand ratio at individual colocalised type 2 synapses was calculated for cultures treated with one of a list of drugs (detailed below). Note that ratios were calculated for each synapse, and the mean ratio across all synapses calculated. All of these treatment groups differed in their mean ratio statistically significantly from untreated controls (Welch's t-test): tetrodotoxin (1µM, p=0.00016), bicuculline (40µM, p=0.0011), BDNF (3.7nM, p=0.047), ketamine (10nM, $p=7.11\times10^{-14}$), lactacystin (1µM, $p=9.10\times10^{-103}$), MG132 (10µM, $p=5.39\times10^{-123}$), anisomycin (1µM, $p=7.24\times10^{-82}$), cycloheximide (3µM, $p=2.46\times10^{-96}$).

4.4.7 Correction for multiple testing

Throughout this study, statistical significance of the difference between two sets of data was evaluated using Welch's T-test, as outlined in the methods section in chapter 2. While this does provide an accurate indication, it must be noted that the samples from which the results in this drugs-treatment chapter were derived were part of the same batch of cells, with the same control group used for each treatment group. This means that while all of the treatment groups were not compared with each other, but only with the control group, a correction for multiple testing should be considered. In this instance, the Bonferroni correction for multiple testing was used. The Bonferroni correction divides the required value of *P* to attain statistical significance (usually *P*=0.05) by the number of times the null hypothesis is tested within a sample. In this case, we had one control group and 8 treatment groups. Each treatment group was compared once with the control group, making it a total of 8 times that the null hypothesis was tested. Thus, the *P* value that was tested against was 0.05/8 = 0.00625. Therefore, if P<0.00625 the difference was deemed statistically significant.

When testing all of the results in this chapter with the Bonferroni correction, i.e. when using P=0.00625 as the bar for significance, the following five results are affected:

- Ketamine treatment, bulk analysis, pulse ligand (P=0.0091).
- Ketamine treatment, single-synapse analysis, pulse ligand colocalised (P=0.0125).
- Ketamine treatment, single-synapse analysis, pulse ligand non-colocalised (P=0.0084).
- BDNF treatment, bulk analysis, pulse ligand (P=0.0241).
- BDNF treatment, bulk analysis, chase ligand (P=0.0263).

In all five of the above cases, the difference between the treatment group and the untreated control group is only statistically significant at a level of $P<0.05$ but not at the level of $P<0.00625$.

This indicates that in these instances, the chance that the difference between the two groups occurred by chance is greater than 5%, due to multiple testing. It is interesting to see that all five of the above instances are allocated to two treatment groups: ketamine treatment and BDNF treatment. Furthermore, in the case of ketamine treatment the bulk analysis of the pulse ligand is in fact made up of the combined results of the single-synapse analysis of the pulse ligand that is colocalised and the one that is not colocalised. It thus makes sense that if the single-synapse analysis is affected by the Bonferroni correction, the associated bulk analysis would too. Similarly, the single synapses analysis for both colocalised and non-colocalised puncta in the BDNF group (pulse and chase) is not statistically significant, making it unsurprising that the associated bulk analysis results are affected by the Bonferroni correction.

This correction for multiple testing does call into question some of the conclusions derived earlier in the chapter and may indicate that both ketamine and BDNF treatment have no significant impact on synaptic PSD-95 turnover. Nevertheless, since treatment groups were not actually compared with each other, but rather each separate treatment group with the same control group, in effect making them separate experiments, there is a reduced need for a correction for multiple testing. However, it is worth bearing these results in mind when interpreting the results from the two affected treatment groups.

4.4.8 Subchapter discussion

Overall, the results from this study that analysed the effects of various chemical agents upon PSD-95 turnover at synapses were very varied, in some cases yielding startling results. Treatment of hippocampal neurons with the activity modulators tetrodotoxin or bicuculline for 24 hours was found to only result in a single significant outcome: blocking neuronal firing with TTX causes an enhanced retention of old PSD-95 at synapses. This does not correlate with some literature that has found TTX to reduce synaptic PSD-95 levels (Colledge et al., 2003; Noritake et al., 2009; Kim et al., 2007; El-Husseini et al., 2002). However, it does match other literature that indicates that higher rates of synaptic activity, particularly NMDAR activation, cause an enhanced loss of PSD-95 at synapses by degradation (Colledge et al., 2003) or trafficking out of the spine (Sturgill et al., 2009). If neuronal activity is reduced by TTX, then, PSD-95 may be stabilised at PSDs instead. On the flip side, Ehlers (2003) and Butko et al. (2012) found that enhancing excitatory neuronal activity by reducing GABAergic inhibition with BCC increased synaptic PSD-95 levels, which Butko and colleagues found to be down to enhanced synthesis, while Ehlers did not. My lack of significant results following BCC treatment, then, are not unexpected given that there is no clear consensus in the field on the effect of enhanced neuronal activity by BCC on PSD-95 turnover.

BDNF has long been recognised as causing enhanced PSD-95 levels at synapses (Hu et al., (2011); Yoshii and Constantine-Paton (2007)), making my result unsurprising but matching with previous literature. I find that both old and new PSD-95 molecules are enriched at synapses following BDNF treatment for 24 hours, implying that PSD-95 synthesis is enhanced and old PSD-95 either experiences reduced degradation, or enhanced recruitment to synapses. Increased PSD-95 synthesis has also been observed by Butko et al. (2012), and together these results mean that overall synaptic PSD-95 levels are increased by BDNF treatment.

The effect of low-dose ketamine treatment on PSD-95 has so far not been studied extensively, but some studies have suggested that it causes enhanced PSD-95 levels at synapses in live rodents (Li et al., 2010; Choi et al., 2015; Browne & Lucki, 2013).

While I was unable to observe any enhanced synaptogenesis, as has been reported by Abdallah et al. (2016), I did measure increased levels of old PSD-95 at synapses. This results was found both at type 2 and type 3 synapses. As with BDNF treatment, this implies that ketamine may enhance the localisation of PSD-95 at synapses. It may further signify that PSD-95 is stabilised at synapses rather than degraded, for instance by increasing palmitoylation and thereby preventing its cycling out of the PSD. Since ketamine is linked to an enhanced BDNF-release at synapses (Browne & Lucki, 2013), it is not unexpected for the two drugs to have a similar effects. Nevertheless, ketamine's effect is restricted to old PSD-95 molecules being enriched at synapses, while BDNF also increases new PSD-95 synthesis. Moreover, ketamine's effect on old PSD-95 retention compared to controls is markedly more significant ($p=0.0091$) than that of BDNF ($p=0.024$). Interestingly, patients with major depressive disorder are reported as displaying lower levels of NR2A and NR2B subunits of NMDARs (Feyissa et al., 2009), as well as PSD-95, which is required for the formation of 1.5MDa NMDAR supercomplexes (Frank et al., 2016). Furthermore, major depression appears to result in the internalisation of the GluA1 subunit of AMPARs, and ketamine rapidly increases glutamate transmission (Duman et al., 2012). Thus, it is conceivable that ketamine exerts its influence to some extent by causing PSD-95 to be enriched at synapses and therefore also enhancing glutamate receptor clustering at the PSD. What is particularly interesting about these results is that while previous studies have used western blots to measure total PSD-95 levels, and were able to observe moderate increases thereof, this is the first study to look at PSD-95 expression at the level of synapses of cultured hippocampal neurons, and specifically to look at new and old PSD-95 molecules separately. This result is certainly of great interest, and worth pursuing further.

The proteasome inhibitors lactacystin and MG132 certainly delivered one of the most fascinating sets of results in this study. The literature is somewhat divided on the effects of these drugs, in that Hakim et al. (2016) reported no effect at all on PSD-95 degradation but a strong synthesis blockade following lactacystin treatment. Other studies (Tsai et al., 2012; Colledge et al., 2003) have related a reduced level of PSD-95 degradation by lactacystin and MG132. My study appears to support both of these findings: following 24 hours of either lactacystin or MG132 treatment, I find PSD-95 degradation to be reduced and as well as PSD-95 synthesis to be down-regulated. The second set of results that was perhaps even more unexpected came from the

protein synthesis inhibitors. Along the same vein as the proteasome inhibitors, the protein synthesis blockers anisomycin and cycloheximide not only prevent new PSD-95 from being synthesised, as one would expect and has been demonstrated in the literature (Ennis and Lubin, 1964; Grollman, 1967), but also reduce PSD-95 degradation. Hakim et al. (2016) propose that the explanation for the reduced synthesis following lactacystin application is that blocking the proteasome prevents the degradation of misfolded proteins, leading to their accumulation, and thereby triggering various stress responses such as the unfolded protein response (UPR). In their paper, they explain the fact that they were not able to observe a reduced degradation of PSD-95 by postulating that other degradation pathways become active when the proteasome is blocked. However, this partially contradicts their theory that the cells activate various stress responses (as other proteins would then most likely also be degraded by similar alternative pathways), and furthermore, my study was able to clearly measure a reduction in PSD-95 degradation since old PSD-95 was retained at synapses to a significant extent. I would like to, therefore, propose a different explanation for these results and the results obtained using the protein synthesis inhibitors anisomycin and cycloheximide.

My proposition would be a mechanisms of proteostasis, wherein synapses attempt to keep the levels of certain proteins such as PSD-95 within a certain concentration range. In order to attain this goal, the rates of synthesis and degradation of these proteins are aligned with these needs. Thus, if there is a surplus of PSD-95 because the proteasome has been inhibited and PSD-95 degradation slowed down, PSD-95 synthesis is also reduced. If a drug blocks protein synthesis and there is a shortage in PSD-95, the response causes a reduction in PSD-95 degradation, to prevent depletion. We know that both protein synthesis and degradation are strongly regulated in neurons, with a coordinated crosstalk between the two systems ensuring that a balance is maintained (Alvarez-Castelao and Schuman, 2015). Indeed, this balance of protein synthesis and degradation is required for long term memories to form (Fonseca et al., 2006). Furthermore, individual proteins can display different half-lives in different cellular compartments (Boisvert et al., 2012), implying that turnover of individual proteins can be tightly regulated depending on cellular needs and regional differences. It seems logical, then, that a neuron would be able to down- or up-regulate both the synthesis and degradation rate of a protein such as PSD-95. This mechanism

would not necessarily mean that synthesis and degradation are controlled at a single-synapse level, since it has been well-established that PSD-95 molecules move between synapses (Marrs et al., 2001; Sturgill et al., 2009; Zheng et al., 2010; Okabe et al., 2001), and synapses can rapidly and directly recruit PSD-95 without relying on new synthesis (Gray et al., 2006). Thus, individual synapses may enhance their PSD-95 levels by trafficking in dendritic PSD-95. However, various post-translational modifications of PSD-95 have been described as enhancing its stability at the PSD, such as palmitoylation (Fukata et al., 2013) and phosphorylation (Nelson et al., 2013). It is thus certainly conceivable that individual synapses are able to control the level of PSD-95 palmitoylation and phosphorylation in order to stabilise it at the synapse, or conversely to destabilise it if required. My proposed model, then, involves a dynamic interplay of tightly controlled PSD-95 synthesis, degradation and cycling in and out of the synapse, depending on each synapse's need. This is mediated through various protein-protein interactions, and post-translational modifications, as well as local synthesis and degradation at dendritic spines. This model describes a form of proteostasis, whereby individual synapses can keep their concentrations of PSD-95 within a certain range.

Under normal conditions, synapses may increase or decrease their need for PSD-95 depending upon the synapse's level of activity and state of potentiation. A synapse undergoing high levels of activity and LTP may recruit new PSD-95 to bolster the PSD-95 levels in its PSD and meet enhanced structural needs. Indeed, Butko et al. (2012) showed that synapses experiencing enhanced activity preferentially incorporate newly-synthesised PSD-95. A synapse undergoing long periods of inactivity or LTD may destabilise PSD-95 in its PSD and thus cycle some of its PSD-95 out and back into the dendrite, to become available for neighbouring synapses, or enhance degradation. The majority of the time, this system would most likely be in equilibrium, with a further slow background rate of PSD-95 turnover as older proteins are degraded and need to be replaced by newly synthesised ones. However, a whole-system perturbation such as the application of a protein synthesis inhibitor or proteasome blocker may cause a drastic unbalancing. Suddenly, the cell is confronted by a widespread shortage or surplus of PSD-95, and needs to meet the changed demands. The cell conceivably responds by altering its synthesis or degradation rates, depending on the situation. It may be this mechanism that explains the dual effects of the synthesis inhibitors and proteasome inhibitors. This model has also already been

put forward in the review by Hanus and Schuman (2015) to explain the rapid and more long-term changes in synaptic protein turnover that have been observed in various studies, and may satisfactorily explain some of the observed phenomena in this study. Furthermore, this model has important implications for any studies planning on using either of these groups of drugs. The underlying message is clear: altering protein synthesis or degradation has strong effects on the proteostatic equilibrium that binds these two processes together, and the resulting crosstalk needs to be considered when designing experiments.

4.5 Developmental study

4.5.1 PSD-95 turnover in cultures aged DIV28+

The vast bulk of the work throughout my project was performed on primary cultures aged between DIV14 and DIV16. This is a relatively immature stage in neuronal development, during which a high level of synaptogenesis is still ongoing (Lesuisse and Martin, 2002; Cohen et al., 2013). I therefore wished to compare my results to older cultures as well, at a stage when neurons have developmentally matured. For this reason, I decided to perform the same analysis as I have done so far, on both bulk and single-synapse data, in cultures aged between DIV28 and DIV30. I set up three separate hippocampal primary cultures, derived from three different litters of PSD-95$^{HaloTag/HaloTag}$ (homozygous) embryos aged E17.5 as in previous studies, and allowed the neurons to develop normally for 28 days (N=3). On DIV28, I applied the pulse ligand (R110Direct, 50nM) as per the standard protocol (see chapter 2.5.6) for 16 hours. On DIV29, when pulse ligand incubation was complete, most of the neurobasal (NB) media was replaced with preconditioned NB media containing the chase ligand (TMR), and incubated with this chase ligand (final concentration 500nM). For the 1-hour time point, chase incubation was kept to 1 hour, after which cells were fixed in 4% PFA. For all other cells, chase-incubation lasted for 24 hours, and thereafter cells were fixed, mounted, imaged and analysed as usual.

In figure 4.48 I show some example images taken from cultures aged DIV29+. Figure 4.56.a shows pulse-labelled puncta after the 16-hour pulse incubation and subsequent

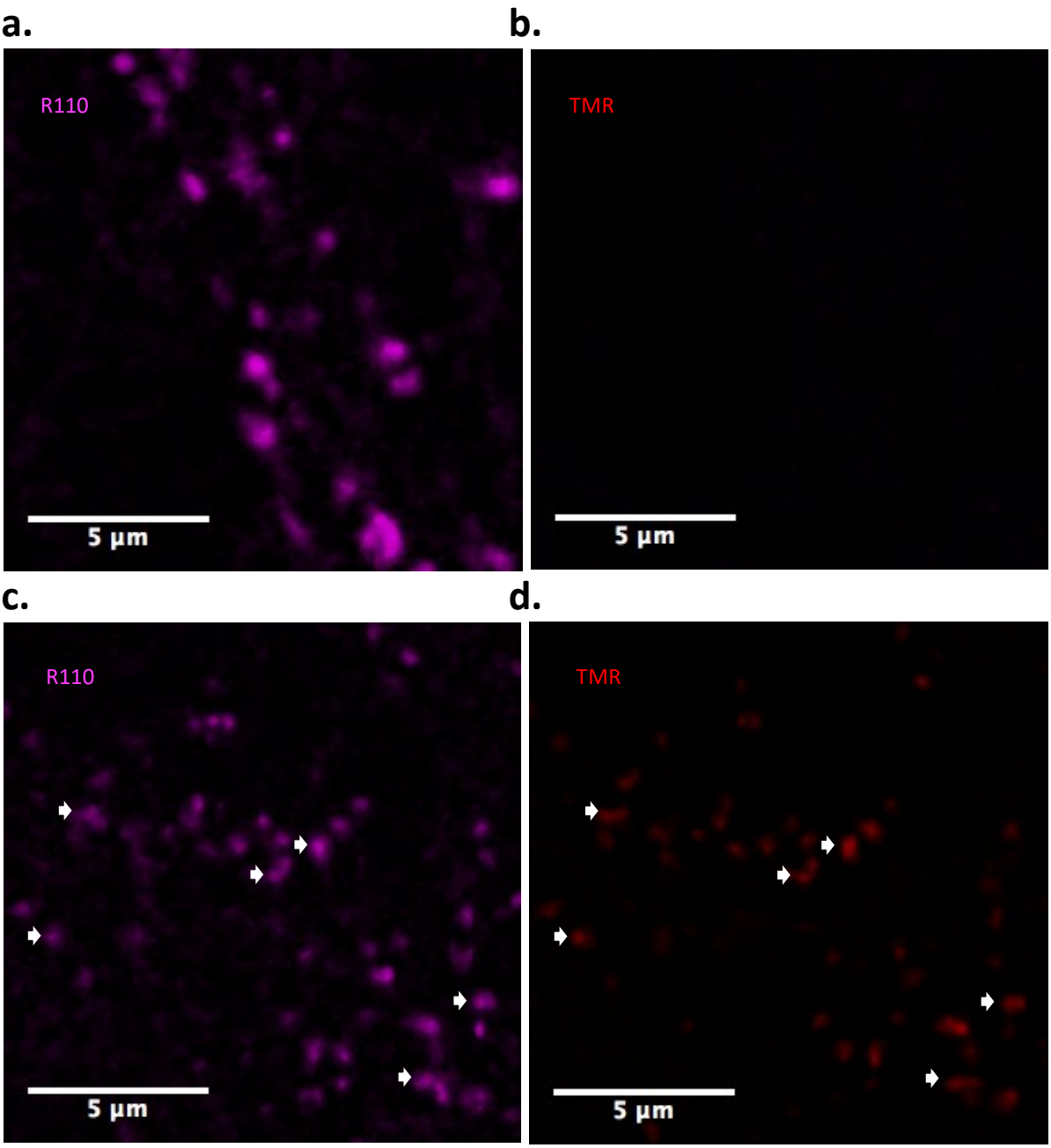

Figure 4.56. Pulse-chase labelling of mature neuronal primary cultures at DIV29+.
Example images of pulse-chase labelling in hippocampal primary cultures prepared from PSD-95$^{HaloTag/HaloTag}$ mice. Cultures were grown on glass coverslips until DIV28, when pulse ligand was added for 16 hours (R110Direct, 50nM). On DIV29, chase ligand (TMR, 500nM) was added for 1 and 24 hours. After incubation, cells were fixed in 4% PFA, imaged using the LSM510, and puncta analysed using the Imaris software. **a.** Image showing the pulse ligand (R110Direct) channel after 1 hour of chase (TMR) incubation. **b.** Image showing the chase ligand (TMR) channel after 1 hour of chase incubation. Note the lack of signal, as HaloTag binding sites are saturated by the pulse ligand, preventing chase ligand binding. **c.** Image showing the pulse ligand channel after 24 hours of chase incubation. **d.** Image showing the chase ligand channel after 24 hours of chase incubation. Note the presence of TMR-labelled puncta, as new PSD-95-HaloTag proteins have been synthesised over the 24 hours, and these have been labelled by the TMR chase ligand.

1-hour chase incubation (DIV29). As in previous experiments in immature neurons, the pulse ligand signal is very strong. In contrast, no chase ligand signal is visible at this time point at all (figure 4.56.b). 24 hours later (DIV30), pulse ligand puncta are still very clearly visible (figure 4.56.c). However, chase ligand puncta have now begun to appear as well (figure 4.56.d).

In figure 4.57 I compare the bulk APFI of cultures at DIV29-30 with the results for cultures aged between DIV15-16. From the graph in figure 4.57.a we can first observe that the APFI for the pulse ligand at the 1-hour time point is slightly higher at DIV29 (72.45 ± 3.32 AU) than at DIV15 (65.97 ± 1.69 AU), but this difference is not statistically significant (Welch's t-test, p=0.15). After 24 hours, however, we can observe a marked difference between neurons aged DIV16 and DIV30. Pulse ligand APFI at DIV30 is significantly higher at this time point (60.90 ± 4.13 AU) than at DIV16 (41.44 ± 0.85 AU). Here, the difference is statistically significant (p=0.016). What is also interesting to note is that for the older (DIV29+) neurons, the difference in APFI of the pulse ligand is not much different between DIV29 (1-hour time point) and DIV30 (24-hour time point). While APFI has gone down, the difference is not statistically significant (p=0.074).

Next, in figure 4.57.b we can see chase ligand APFI at the 24-hour time point. While the intensity is slightly higher at DIV30 (34.88 ± 2.48 AU) than at DIV16 (29.63 ± 1.42 AU), this difference is not statistically significant (p=0.12).

Looking at puncta numbers, we can first see that there are a lot more synaptic puncta at the 1-hour time point in older cultures than younger ones (figure 4.57.c, 601.77 ± 76.85 puncta per image at DIV29 compared to 406.16 ± 76.57 puncta per image at DIV15). However, due to the great variability this difference is not statistically significant (Welch's t-test, p=0.097). At the 24-hour time point, we can see that the pulse ligand puncta number has not gone down by much in older cultures (down to an average of 536.77 ± 37.34 puncta per image, p>0.05, figure 4.57.c), while it has gone down significantly for young cultures (down to an average of 189.15 ± 26.64 puncta per image, figure 4.57.c). The difference between these values is statistically highly significant (p=0.00024). The number of chase-ligand labelled puncta at the 24-hour time point (figure 4.57.d) is also significantly higher at DIV30 than DIV16 (p=0.0078).

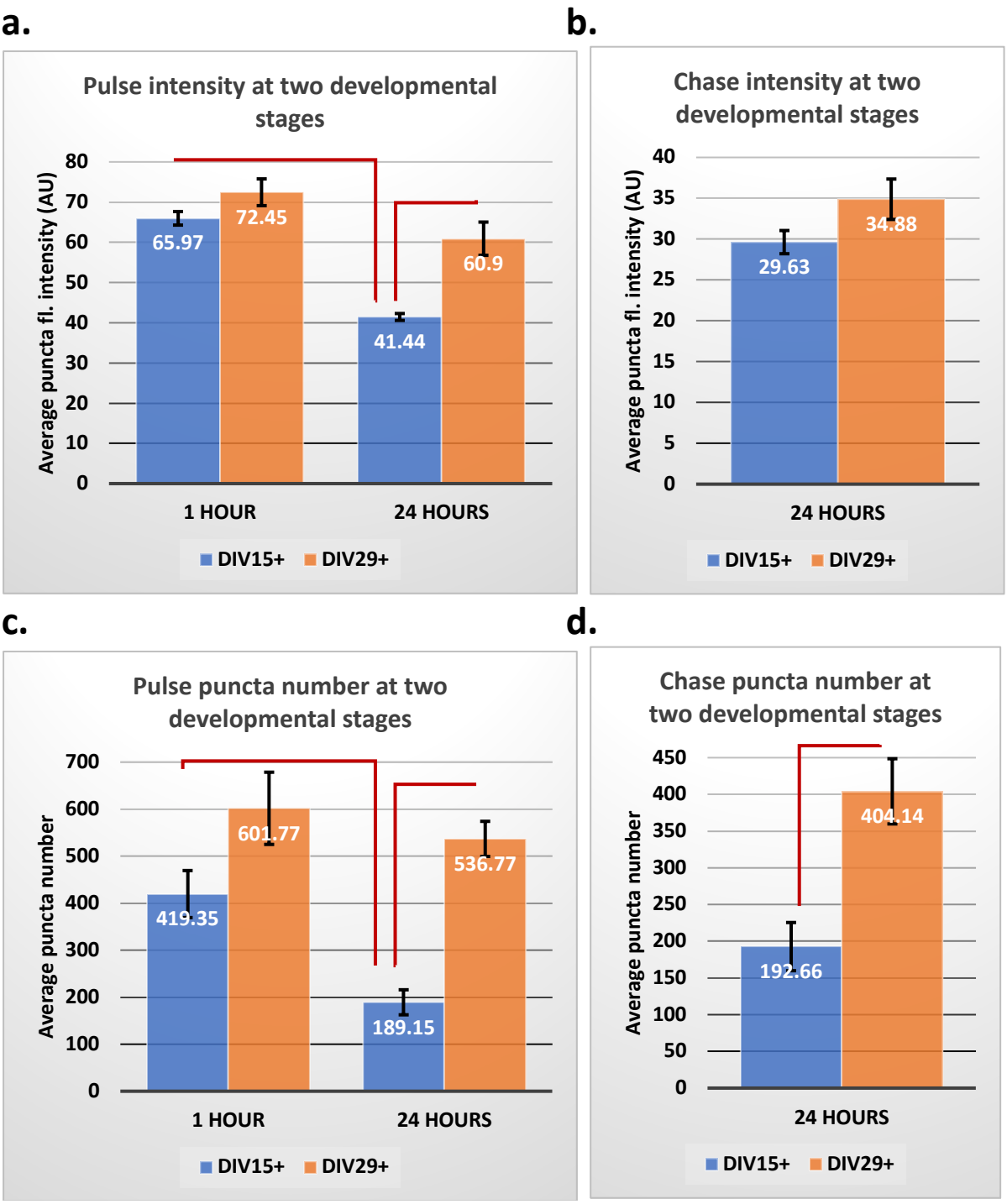

Figure 4.57. PSD-95 puncta intensities and numbers in cultures at DIV15+ and DIV29+. Hippocampal neuronal primary cultures from PSD-95$^{HaloTag/HaloTag}$ mice were grown on glass coverslips for 14 days and 28 days. At DIV14 and DIV28, cultures were incubated with the pulse ligand (R110Direct, 50nM) for 16 hours. Thereafter, cultures were incubated with the chase ligand (TMR, 500nM) for 1 hour and 24 hours. Average puncta fluorescence intensity (APFI) and number per image were then calculated. This was performed across eight different cultures (N=8) for the control group and three different cultures at DIV29+ (N=3). The graphs here present the mean values across these cultures. **a.** Graph of the R110 pulse ligand APFI. At the 1-hour time point, the difference between cultures aged DIV15 and DIV29 is not significant (Welch's t-test, p=0.15). At the 24-hour time point, the difference between

cultures aged DIV15 and DIV29 is statistically significant (p=0.016). The difference within the DIV15+ group between the 1-hour and the 24-hour time points is significant ($p=9.51x10^{-8}$). However, the difference within the DIV29+ group between the 1-hour and the 24-hour time points is not significant (p=0.074). **b.** Graph of the average TMR chase ligand APFI after 24 hours of chase incubation. APFI is not significantly different between cultures aged DIV16 and DIV30 (Welch's t-test, p=0.12). **c.** Graph of the average R110 pulse ligand puncta number. In the DIV15+ group, pulse ligand puncta number goes down significantly over the 24 hours (Welch's t-test, p=0.002). In the DIV29+ group this difference between puncta number at the 1-hour time point and the 24-hour time point is not significant (p=0.49). However, pulse ligand puncta number at the 24-hour time point differs significantly between cultures in the DIV15+ group and the DIV29+ group (p=0.00024). The two groups do not differ significantly at the 1-hour time point (p=0.097). **d.** Graph of the average TMR chase ligand puncta number after 24 hours of chase incubation. Puncta number is significantly different between cultures aged DIV16 and DIV30 (Welch's t-test, p=0.0078).

Looking at synaptic types, the overall picture that emerges is that the changes that the different synaptic types undergo between DIV29 and DIV30 in terms of the overall trend are very similar to those between DIV15 and DIV16. However, the absolute values do in some instances differ significantly between older and younger cultures. Furthermore, while the results of the younger synapses are based upon a sample size of N=8, the older cultures only have an N=3 sample size. This has the effect of making differences in values less statistically significant. For instance, there is a difference in pulse ligand APFI between type 2 (colocalised) and type 3 (non-colocalised) synapses for cultures at DIV30 (figure 4.58.c) and DIV16 (figure 4.2.b). However, this difference is not significant at DIV30 (p=0.21) while it is significant at DIV16 ($p=9.01x10^{-7}$).

Regarding average puncta fluorescence intensity (APFI), cultures at DIV30 have a higher value for both pulse and chase ligands at type 1, type 2 and type 3 synapses (i.e. in all cases; see figure 4.58). However, the difference between cultures aged DIV30 and DIV16 is not statistically significant in any of these cases (p>0.05).

Puncta number results need to be treated with caution, as there are significantly more synaptic puncta per image overall at DIV30 than DIV16. Thus, results with a greater absolute number of synaptic puncta at DIV30 than DIV16 in individual types of synapses give no valuable information. However, there is one interesting point to be made: at DIV16, the difference in chase-labelled puncta number is not significant between type 2 (colocalised) and type 1 (non-colocalised) synapses (figure 4.2.d, p=0.17). However, at DIV30 there are significantly fewer type 1 synapses than type 2

a.

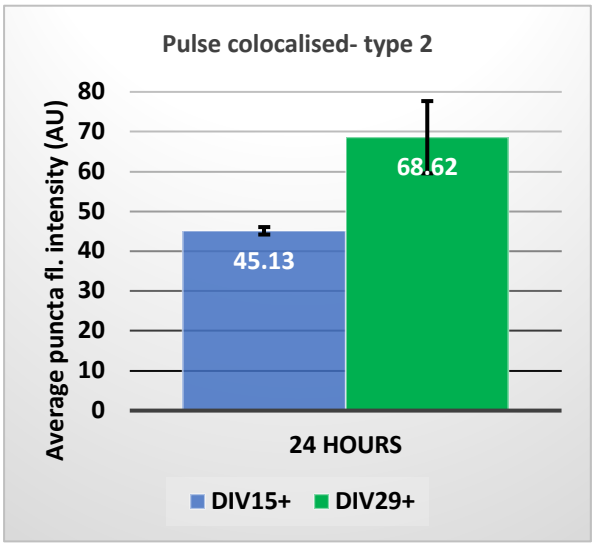
Pulse colocalised- type 2
Average puncta fl. intensity (AU)
80
70
60
50
40
30
20
10
0
45.13
68.62
24 HOURS
DIV15+
DIV29+

b.

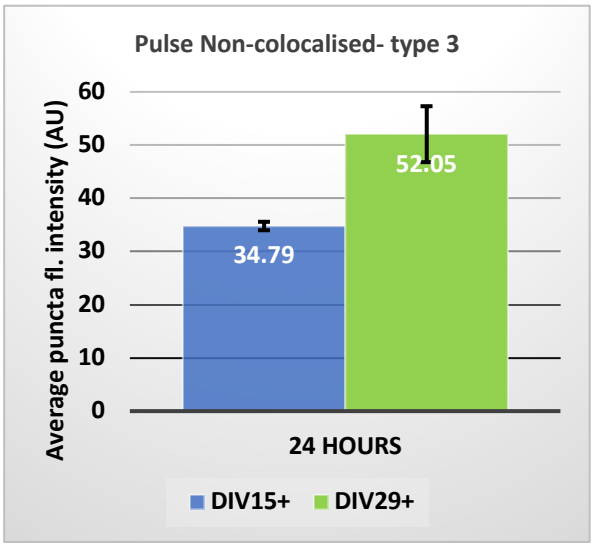
Pulse Non-colocalised- type 3
Average puncta fl. intensity (AU)
60
50
40
30
20
10
0
34.79
52.05
24 HOURS
DIV15+
DIV29+

c.

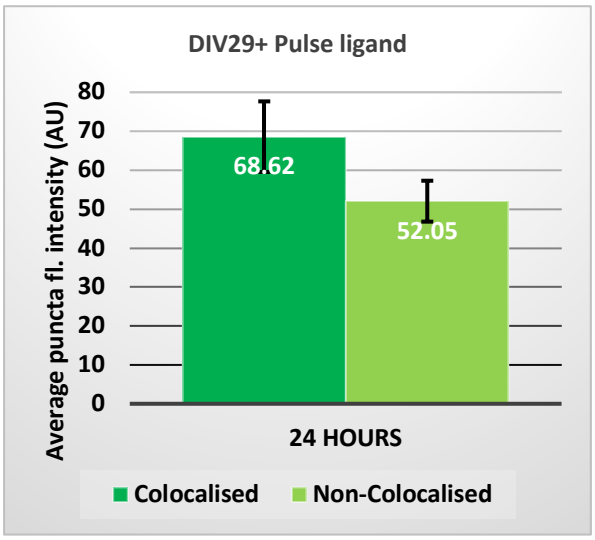
DIV29+ Pulse ligand
Average puncta fl. intensity (AU)
80
70
60
50
40
30
20
10
0
68.62
52.05
24 HOURS
Colocalised
Non-Colocalised

d.

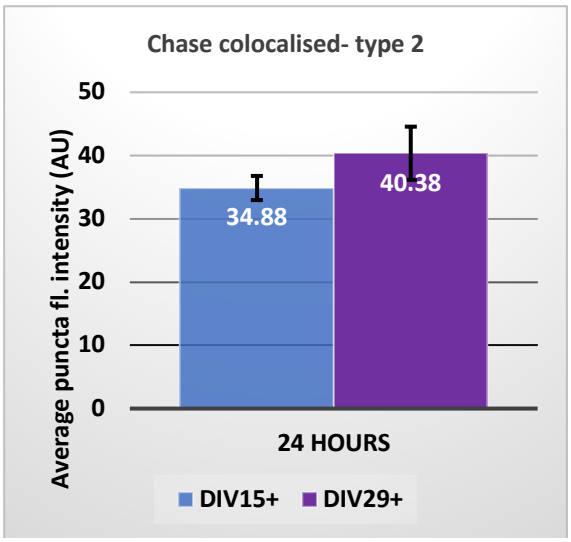
Chase colocalised- type 2
Average puncta fl. intensity (AU)
50
40
30
20
10
0
34.88
40.38
24 HOURS
DIV15+
DIV29+

e.

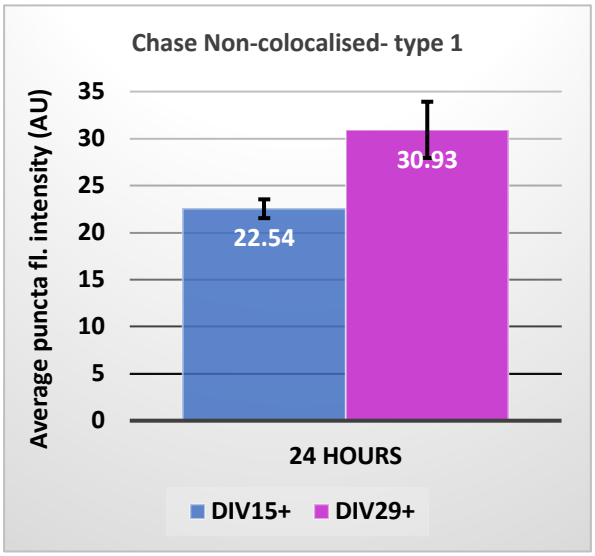
Chase Non-colocalised- type 1
Average puncta fl. intensity (AU)
35
30
25
20
15
10
5
0
22.54
30.93
24 HOURS
DIV15+
DIV29+

f.

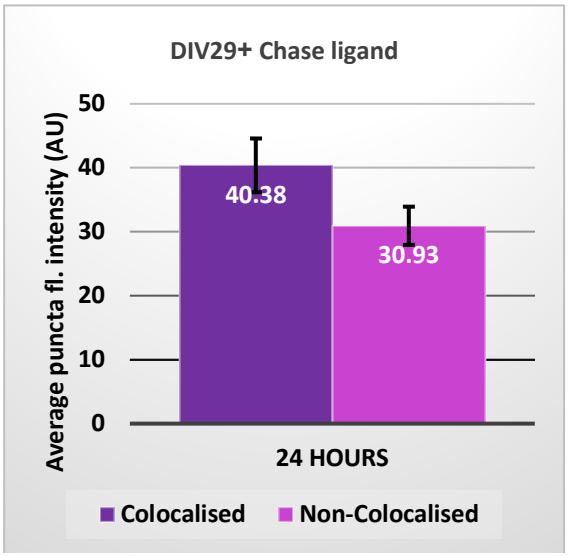
DIV29+ Chase ligand
Average puncta fl. intensity (AU)
50
40
30
20
10
0
40.38
30.93
24 HOURS
Colocalised
Non-Colocalised

Figure 4.58. The effect of age on PSD-95 average puncta intensity at different synaptic types in primary cultures.

Average puncta fluorescence intensity (APFI) per image was calculated for pulse and chase ligand labelled synaptic puncta in type 1, type 2 and type 3 synapses separately. Images were taken after 24 hours of pulse-chase treatment with 50nM R110Direct ligand (pulse) and 500nM TMR ligand (chase) in hippocampal primary cultures from PSD-95$^{HaloTag/HaloTag}$ mice. Experiments were started (pulse incubation) either at DIV14 or DIV28. This was performed across eight different cultures (N=8) for the control group and three different cultures at DIV29+ (N=3). The graphs here present the mean values across these cultures. **a.** Pulse ligand (R110Direct) APFI per image in synapses where pulse and chase ligands colocalise (type 2). The difference between cultures aged DIV16 and DIV30 is not statistically significant (Welch's t-test, p=0.12). **b.** Pulse ligand APFI per image in synapses where pulse and chase ligands do not colocalise (type 3). The difference between cultures aged DIV16 and DIV30 is not statistically significant (Welch's t-test, p=0.078).
c. Comparison of pulse ligand APFI per image in type 2 synapses and type 3 synapses in cultures aged DIV30. The difference between the two groups is not statistically significant (Welch's t-test, p=0.21). **d.** Chase ligand (TMR) APFI per image in synapses where pulse and chase ligands colocalise (type 2). The difference between cultures aged DIV16 and DIV30 is not statistically significant (Welch's t-test, p=0.32). **e.** Chase ligand APFI per image in synapses where pulse and chase ligands do not colocalise (type 1). The difference between cultures aged DIV16 and DIV30 is not statistically significant (Welch's t-test, p=0.094).
f. Comparison of chase ligand APFI per image in type 2 synapses and type 3 synapses in cultures aged DIV30. The difference between the two groups is not statistically significant (Welch's t-test, p=0.15).

synapses, even though the sample size is smaller (figure 4.59.f, p=0.027). This indicates that fewer new synapses are being formed between DIV29 and DIV30 than between DIV15 and DIV16; a result consistent with a reduced level of synaptogenesis in older neurons. This result is further supported by figure 4.60.b, where we can see that at DIV30 only 16% of synapses are chase-only type 1 synapses, while 48% are colocalised type 2 synapses and 36% are pulse-only type 3 synapses. At DIV16 (figure 4.60.a), in contrast, we see that the percentage of type 1 synapses is nearly double that of DIV30, at 29%. The conclusion from these results, therefore, must be that synaptogenesis is reduced in older cultures compared to younger ones.

Figure 4.61 shows the frequency distribution histograms over the range of average puncta fluorescence intensities for pulse-ligand puncta at the 1-hour time point. We can see from the shapes of the two graphs that cultures at DIV15 (figure 4.61.a) and DIV29 (figure 4.61.b) have very similar distributions. Both show a positive skew, with similarly steep curves. At DIV29 the peak is slightly higher (48 AU) than at DIV15

a.

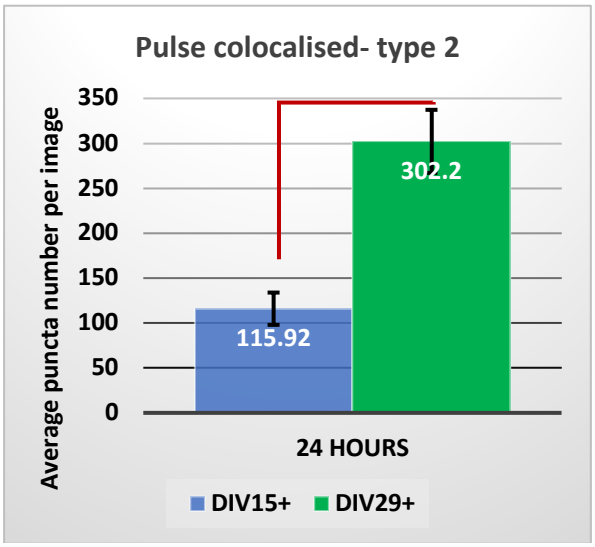
Pulse colocalised- type 2
Average puncta number per image
350
300
250
200
150
100
50
0
302.2
115.92
24 HOURS
DIV15+
DIV29+

b.

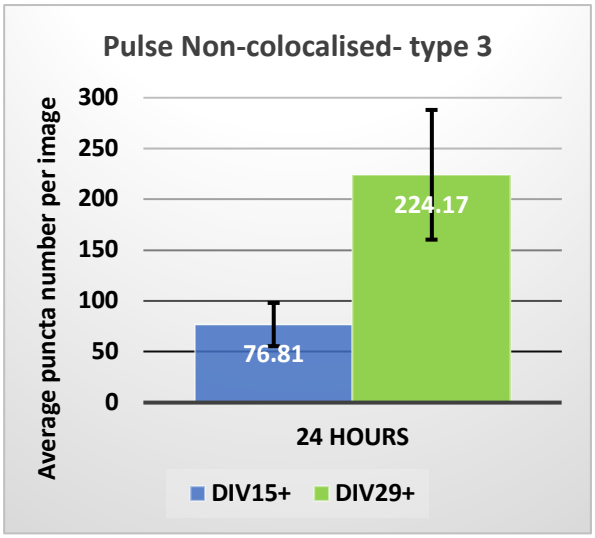
Pulse Non-colocalised- type 3
Average puncta number per image
300
250
200
150
100
50
0
224.17
76.81
24 HOURS
DIV15+
DIV29+

c.

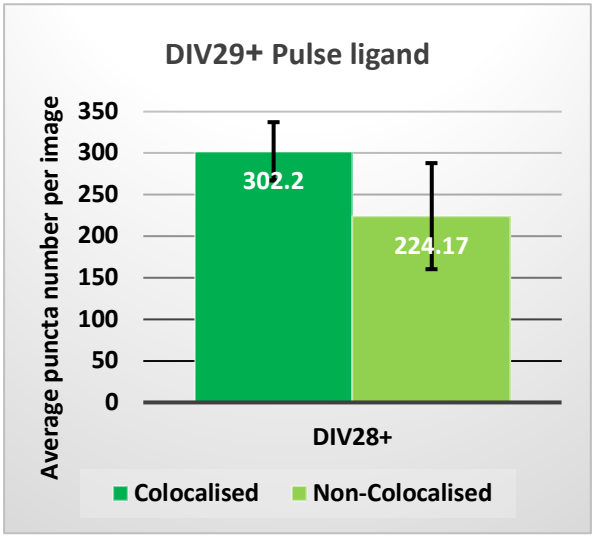
DIV29+ Pulse ligand
Average puncta number per image
350
300
250
200
150
100
50
0
302.2
224.17
DIV28+
Colocalised
Non-Colocalised

d.

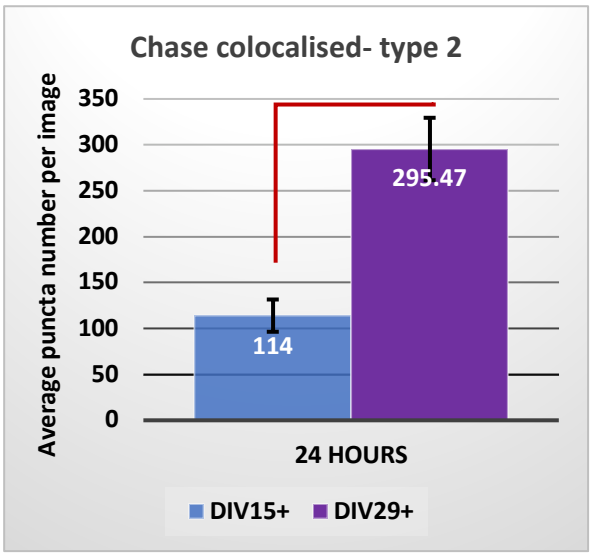
Chase colocalised- type 2
Average puncta number per image
350
300
250
200
150
100
50
0
295.47
114
24 HOURS
DIV15+
DIV29+

e.

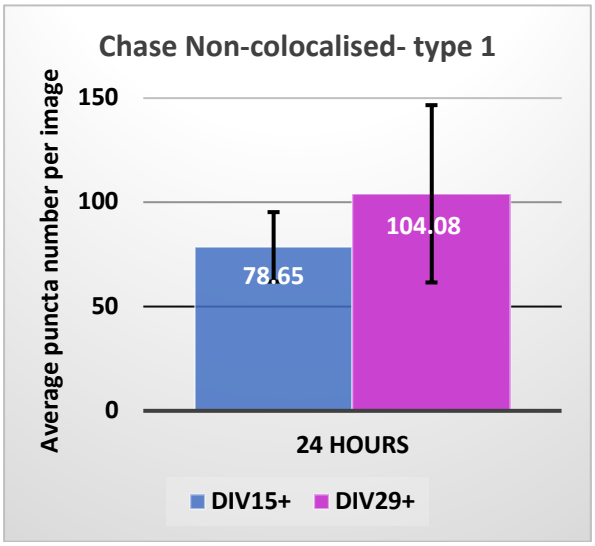
Chase Non-colocalised- type 1
Average puncta number per image
150
100
50
0
104.08
78.65
24 HOURS
DIV15+
DIV29+

f.

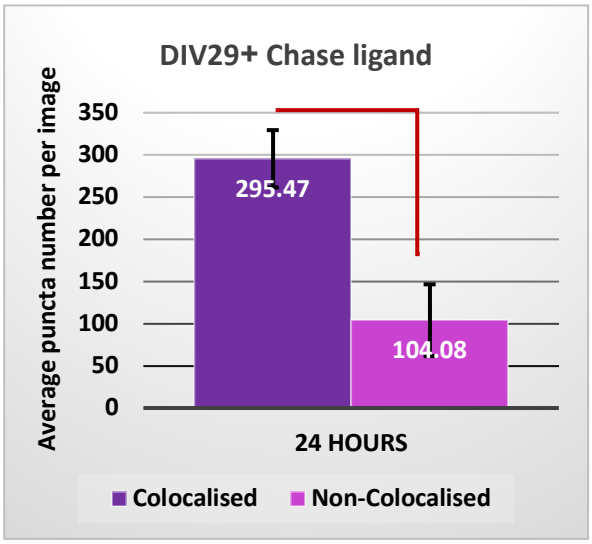
DIV29+ Chase ligand
Average puncta number per image
350
300
250
200
150
100
50
0
295.47
104.08
24 HOURS
Colocalised
Non-Colocalised

Figure 4.59. The effect of age on PSD-95 average puncta number at different synaptic types in primary cultures.

Average puncta number per image was calculated for pulse and chase ligand labelled synaptic puncta in type 1, type 2 and type 3 synapses separately. Images were taken after 24 hours of pulse-chase treatment with 50nM R110Direct ligand (pulse) and 500nM TMR ligand (chase) in hippocampal primary cultures from PSD-95$^{HaloTag/HaloTag}$ mice. Experiments were started (pulse incubation) either at DIV14 or DIV28. This was performed across eight different cultures (N=8) for the control group and three different cultures at DIV29+ (N=3). The graphs here present the mean values across these cultures. **a.** Pulse ligand (R110Direct) average puncta number per image in synapses where pulse and chase ligands colocalise (type 2). The difference between cultures aged DIV16 and DIV30 is statistically significant (Welch's t-test, p=0.016). **b.** Pulse ligand average puncta number per image in synapses where pulse and chase ligands do not colocalise (type 3). The difference between cultures aged DIV16 and DIV30 is not statistically significant (Welch's t-test, p=0.14). **c.** Comparison of pulse ligand average puncta number per image in type 2 synapses and type 3 synapses in cultures aged DIV30. The difference between the two groups is not statistically significant (Welch's t-test, p=0.36). **d.** Chase ligand (TMR) average puncta number per image in synapses where pulse and chase ligands colocalise (type 2). The difference between cultures aged DIV16 and DIV30 is statistically significant (Welch's t-test, p=0.016). **e.** Chase ligand average puncta number per image in synapses where pulse and chase ligands do not colocalise (type 1). The difference between cultures aged DIV16 and DIV30 is not statistically significant (Welch's t-test, p=0.62). **f.** Comparison of chase ligand average puncta number per image in type 2 synapses and type 3 synapses in cultures aged DIV30. The difference between the two groups is statistically significant (Welch's t-test, p=0.027).

(42 AU), which is probably due in part to the reduced amount of synaptogenesis and thus presence of fewer small, immature synapses.

The final aspect of the results section for this study looks at the ratios between pulse and chase ligands at type 2 synapses, after 24 hours. From figure 4.62.b we can see that type 2 synapses at DIV30 are slightly more heterogeneous than at DIV16 (figure 4.62.a), as the graph's slopes are even more shallow, with a gentler peak that is also lower (5.15% compared to 8.76%). The mean ratio (3.42 ± 0.028) is higher, as is the median ratio (2.89), than at DIV16 (mean: 2.55 ± 0.051; median: 2.06) (figure 4.62.c). Colocalised type 2 synapses, then, contain a greater proportion of old PSD-95 at DIV30 than at DIV16. The explanation for this is most likely that type 2 synapses at DIV16 are still less mature, and therefore recruiting more newly-synthesised PSD-95, than at DIV30.

Finally, I find that the positive correlation between pulse and chase ligand intensity, when type 2 synapses grouped by pulse ligand APFI percentile, remains strongly positive. At DIV30, R^2=0.89, compared to an R^2 value of 0.96 at DIV16 (figure 4.62.d).

a.

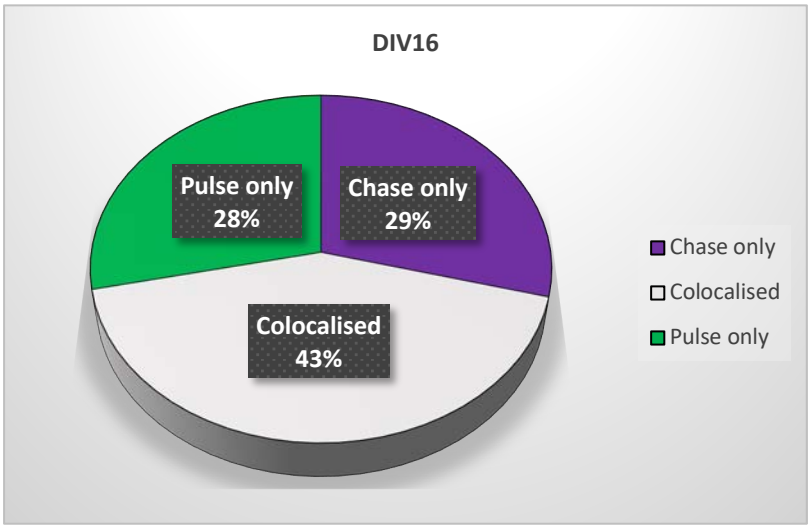

b.

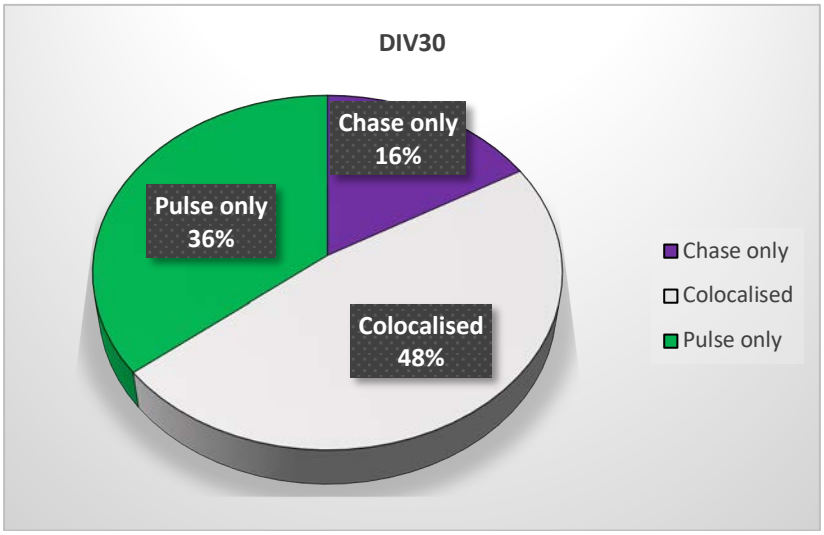

Figure 4.60. Proportional representation of synaptic population by HaloTag ligand-labelling at different developmental stages.

Synaptic puncta were categorised according to whether they colocalised with puncta labelled by the other ligand or not. This pie chart depicts the proportional representation of the three types of synaptic puncta observed.

Images were taken after 24 hours of pulse-chase treatment with 50nM R110Direct ligand (pulse) and 500nM TMR ligand (chase) in hippocampal primary cultures from PSD-95$^{HaloTag/HaloTag}$ mice. Cultures were ages DIV16 or DIV30 at the time of data collection.

a. At DIV16, 28% of puncta contain only the pulse (R110Direct) ligand (type 3), 43% of puncta contain both pulse and chase (TMR) ligands (type 2), and 29% contain only the chase ligand (type 1). **b.** At DIV30, 36% of puncta contain only the pulse (R110Direct) ligand (type 3), 48% of puncta contain both pulse and chase (TMR) ligands (type 2), and 16% contain only the chase ligand (type 1).

a. **b.**

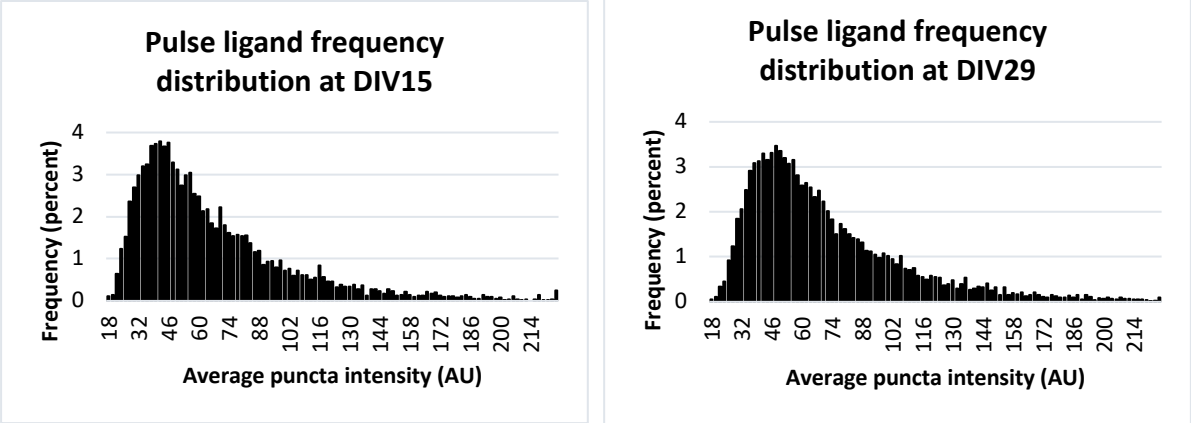

Figure 4.61. Frequency distribution histograms of synaptic puncta labelled with the pulse ligand at different developmental stages.

The histograms depict the full range of average puncta fluorescence intensities of pulse ligand puncta after 16 hours of incubation with the pulse ligand (R110Direct, 50nM), and 1 hour of incubation with the chase ligand (TMR, 500nM). **a.** At DIV15, the histograms reveals a positive skew and heterogenous synaptic population in terms of PSD-95 expression levels. Mean intensity is 65.97 ± 1.69 arbitrary units (AU), with median intensity being 54.94 AU and the mode being 42 AU (3.79% of puncta). **b.** At DIV29, the histograms also shows a positive skew and heterogenous synaptic PSD-95 population. Mean intensity is 72.45 ± 3.32 AU, with median intensity being 60.00 AU and the mode being 48 AU (3.46% of puncta).

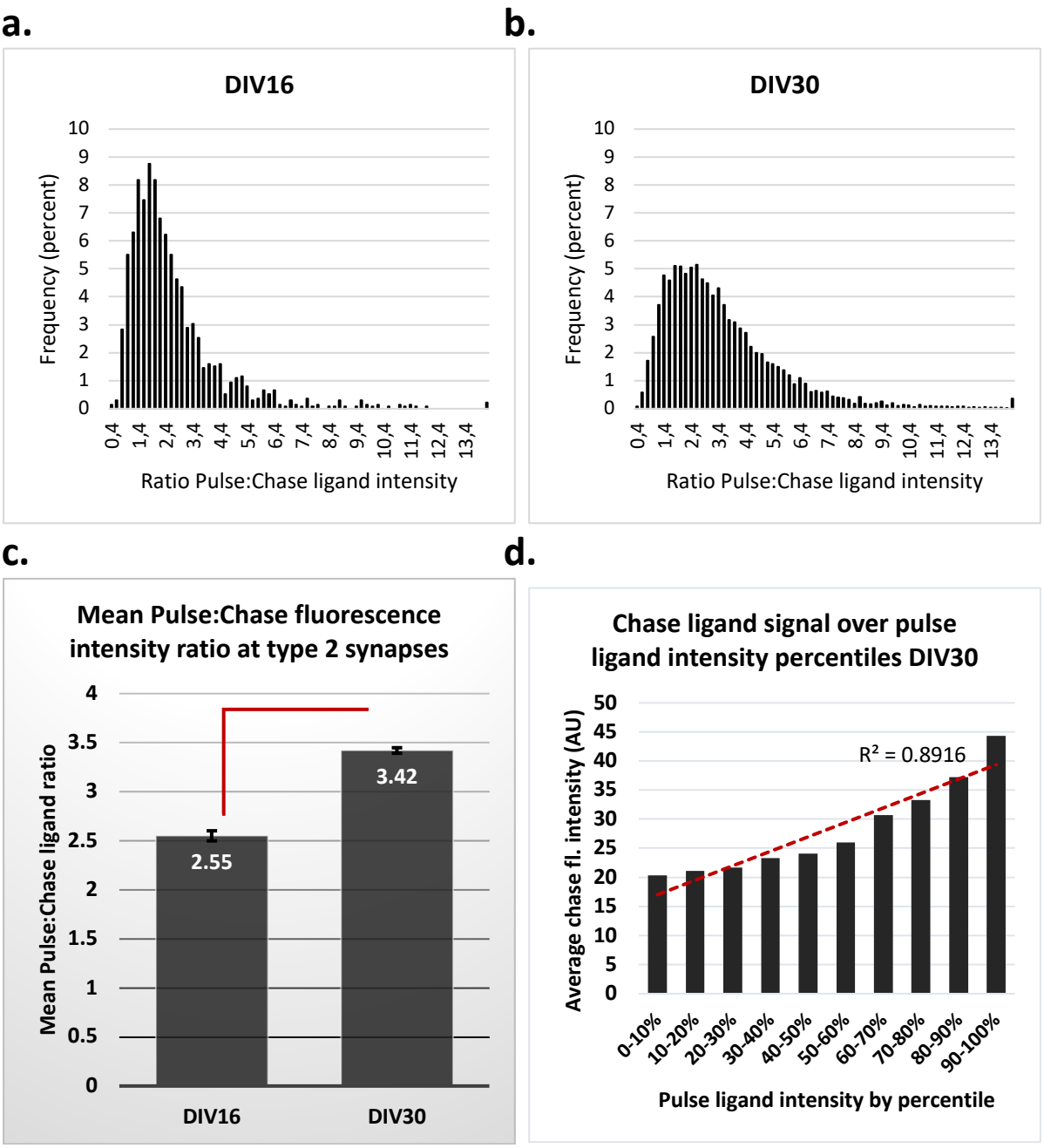

Figure 4.62. Graphs showing the ratio of pulse to chase ligands at individual type 2 synapses at different developmental stages.

In the synaptic population in which pulse and chase ligand-labelled PSD-95-HaloTag molecules were colocalised (type 2), the ratio of pulse ligand fluorescence intensity to chase ligand fluorescence intensity was calculated for each individual synapse. The frequency histograms represent the frequencies of all the pulse:chase ratios. **a.** Frequency distribution at DIV16. Mean ratio: 2.55 ± 0.051 (SEM), Median ratio: 2.06, Mode: 1.8 (8.76%). **b.** Frequency distribution at DIV30. Mean ratio: 3.42 ± 0.028 (SEM), Median ratio: 2.89, Mode: 2.6 (5.15%). **c.** Comparison of mean pulse:chase ligand ratio in cultures aged DIV16 and DIV30. The difference is statistically significant (Welch's t-test, $p=9.24x10^{-48}$). **d.** Colocalising (type 2) synapses were sorted by their pulse ligand APFI (lowest to highest). For each ten percentile steps, average chase ligand APFI was calculated. At DIV30, there is a strong positivie correlation ($R^2=0.89$).

4.5.2 Discussion of developmental study

There are a few major findings from this study that stand out particularly. The main observations are:

1. The loss of pulse ligand signal over 24 hours appears to be much smaller between DIV29 and DIV30 compared to that between DIV15 and DIV16. This effect is so pronounced that there is in fact no significant difference in the DIV29+ group between pulse ligand APFI at the 1-hour and 24-hour time points (figure 4.57.a).

2. There is a significantly reduced number of type 1 synapses at DIV30 compared to DIV16. We can observe this in two different figures: Firstly, figure 4.59.f shows us that there are significantly fewer type 1 synapses than type 2 synapses at DIV30, while at DIV16 this difference is not significant (figure 4.2.d). Secondly, figure 4.60 illustrates nicely that the proportion of synapses that belong to type 1 has shrunk dramatically at DIV30 compared to DIV16.

3. The other finding is that apart from the two points mentioned above, most other results are remarkably similar in the two experimental groups. While some absolute numbers do differ between the two groups, particularly regarding puncta numbers, these results must be seen in the context of the larger total number of synapses at DIV30 than DIV16. However, the frequency histograms are, for instance, remarkably similar between the two groups.

Working upwards, point number 3 indicates that while neuronal primary cultures may overall be more mature at around 4 weeks after plating down than around 2 weeks after plating, the general characteristics of these synaptic populations are nevertheless similar. Synapses are clearly very heterogenous in terms of their average puncta fluorescence intensity at both developmental stages, indicating that even among mature synapses, there appears to be a wide range in terms of PSD-95 expression. Most type 2 synapses at DIV16 are also very similar to type 2 synapses

at DIV30, for instance in terms of their ratio of pulse to chase ligand intensity. The main difference in these synapses appears to be the rate of PSD-95 turnover.

Point number 2 is an unsurprising and expected observation. Since it is known that synaptogenesis takes place mainly throughout the first 3 weeks after primary neurons are plated down, and slows down thereafter (Lesuisse and Martin, 2002; Cohen et al., 2013), it is to be expected that there would be a lower number of type 1 synapses that contain purely newly-synthesised PSD-95 at DIV30 than DIV16. This simply reflects reduced synaptogenesis in mature cultures. What is more surprising is that there are more type 3 synapses, i.e. synapses that contain solely old but no new PSD-95 at all. In chapter 4.3.3 it was postulated that these synapses may not be incorporating new PSD-95 as they are perhaps in the process of being pruned away, or that they are in the process of turning into 'silent' or 'quiet' synapses with a very slow rate of PSD-95 turnover. There is no biological explanation as to why there should be greater rates of synaptic pruning in 4-week old cultures than 2-week old cultures, particularly since synaptogenesis is reduced. It is also possible that these synapses are replacing degraded PSD-95 from dendritic PSD-95, diffusing between spines. However, a more likely explanation is that these synapses simply turn over PSD-95 at a very slow rate, if at all, and perhaps newly-synthesised PSD-95 in these synapses is so small in number that is falls below the detection parameters set on the Imaris software. It is, ultimately, another piece of evidence for there being a great discrepancy in PSD-95 turnover rates between individual synapses, with some synapses experiencing high and others low rates of PSD-95 turnover. Likely, this is simply linked to lower levels of activity in these synapses (Hruska et al., 2015). Nevertheless, this observation further enhances the mystery surrounding type 3 synapses, and their rate of PSD-95. Clearly, this type of synapse will require further investigation.

The final point of observation is the most interesting and perhaps surprising one. The fact that pulse ligand intensity does not significantly go down over 24 hours strongly indicates that the PSD-95 degradation rate slows down at this developmental stage. Indeed, this may be linked to the increase in type 3 synapse numbers. When calculating PSD-95 half-life using these new values, a half-life of 95.79 hours is obtained. This is of course vastly greater than the 35.78 hours obtained at DIV16. While the ~36-hour result for PSD-95 half-life at DIV16 matches that found in the

literature (>36 hours, El-Husseini et al., 2002; >24 hours, Todd et al., 2003), all of these results also used younger primary cultures, between DIV14 and DIV21. However, a study by Cohen at al. (2013) found a PSD-95 half-life value of 88 hours, significantly closer to my result of ~96 hours at mature cultures. In that study, the method used was SILAC, but with a greatly enhanced labelling period (7 days). However, a study conducted in live, 9-week old mice using stable isotope labelling of mammals (SILAM) yielded a half-life of 367 hours (Price et al., 2010). While this primarily implies a difference between protein turnover in cultures and live animals, it may also be that the developmental stage has a significant impact on the result. Indeed, a study by Mammen et al. (1997) has shown that the half-life of another synaptic protein, GluR1, differs significantly between neuronal cultures at DIV11 and younger cultures at DIV4. My results for the culture at DIV30 are restricted to three biological replicates, however, limiting the scope of interpretation of these results. Nevertheless, there appears to be a clear indication that PSD-95 experiences developmental shifts in its rate of turnover.

4.6 Chapter conclusion

In chapter 3, I introduced the PSD-95^{HaloTag} KI mouse line and presented the data to establish this mouse as a viable tool for the study of SPD-95 turnover. I then set about presenting a pulse-chase method with which I am able to measure the turnover of PSD-95 in hippocampal primary cultures, and performed a basic experiment, allowing me to work out PSD-95 half-life. In this chapter, I have taken these basic tools and used them to deepen my understanding of PSD-95 turnover from a bulk to a single-synapse level. In doing so I was able to categorise synapses into three different types, according to their PSD-95 expression profile. By splitting synapses up based on whether they express only old, only new or both old and new PSD-95, I could analyse these subgroups separately. Furthermore, I was able to calculate and plot frequency histograms of ratios of pulse to chase ligands within individual synapses that expressed both, as well as plotting frequency histograms of average puncta fluorescence intensities in different synaptic types.

From this data I was able to conclude that type 2 synapses, containing both old and new PSD-95, are most likely mature and stable synapses that continuously turn over PSD-95, experience high rates of activity, and therefore contain not only the greatest amount of PSD-95 overall, but also more old and more new PSD-95 than type 1 and type 3 synapses. This finding was consistent throughout all of my experiments, in untreated cultures, cultures treated with various chemical agents, and also in older cultures around DIV30.

Type 1 synapses are almost certainly immature synapses that have recently formed via synaptogenesis and are in the process of establishing PSDs and incorporating essential proteins such as PSD-95. The fact that they only contain new PSD-95 makes sense in this context of immaturity (Butko et al., 2012). Their intensity frequency histogram fits this explanation, as it is skewed towards lower average fluorescence intensities, and perhaps most indicative is the finding that these synapses are reduced in frequency in mature cultures around DIV30, a time known to experience lower rates of synaptogenesis than younger cultures. To probe into this further, it would perhaps be interesting to stain for presynaptic vesicle markers, and correlate these markers with synaptic types. Butko et al. (2012) found that immature synapses containing newly synthesised PSD-95 were opposed to presynaptic active zones with very few neurotransmitter vesicles. This, then, may be a further avenue of approach to clarify the identity of type 1 synapses with greater certainty.

Type 3 synapses are older synapses that exclusively contain old PSD-95 (pulse-labelled), but no new PSD-95. This type of synapses is the most difficult to interpret. They contain less old PSD-95 than do type 2 synapses, and their lack of new PSD-95 implies that PSD-95 turnover in these synapses may be drastically reduced compared to other synapses. A study by Ehrlich et al. (2007) postulates that PSD-95 is necessary for structural changes in synapses to be able to take place following LTP and LTD. They show that transient changes in PSD-95 at synapses causes a bidirectional modification of synaptic transmission and spine morphology. If changes in synaptic strength cause changes in PSD-95, it seems intuitive that a lack of change in PSD-95 levels may be an indicator of no change in strength occurring at such synapses. Furthermore, a weakening of a given synapse may lead to the loss of PSD-95, without any concomitant gain to replace lost molecules. Such synapses, then, would contain

a reduced amount of old PSD-95, but no new PSD-95. This is precisely what we seen in type 3 synapses: lower levels of old PSD-95 than in type 2 synapses, with no new PSD-95 present. We also see an increase in the number of such type 3 synapses in older cultures (DIV30), when we might expect synaptic strength to be undergoing less flux than at an earlier developmental stage, and indeed the number of synapses being strengthened (type 2 synapses, to some extent) may be closer to the number that are simultaneously being weakened than in immature neurons, where net synaptic change may tend towards a strengthening. Thus, it seems that type 3 synapses are synapses undergoing a weakening of synaptic transmission or no change at all. Indeed, they may be transitioning towards a 'silent' state, in which a synapse expresses no AMPA receptors and most likely no PSD-95 (Huang et al., 2015; Béı ̈que et al., 2006). However, since silent synapses have been associated with an immature synaptic state, this is less likely than the explanation of a simple reduction in synaptic strength.

The study involving the application of various drugs to the primary cultures during the 24-hour chase period yielded a variety of interesting results. The direct neuronal activity modulators TTX and BCC did not appear to affect PSD-95 turnover markedly, although TTX did enhance the retention of old PSD-95 at synapses. BDNF treatment raised overall synaptic PSD-95 levels, affecting both synthesis and degradation rates. Ketamine treatment appeared to retain more old PSD-95 at synapses, which is indicative of enhanced PSD-95 cycling into synapses from dendrites or reduced PSD-95 degradation.

The proteasome inhibitors lactacystin and MG132, along with the protein synthesis inhibitors anisomycin and cycloheximide, had the strongest impact upon PSD-95 turnover. Both classes of drugs affected PSD-95 synthesis and degradation to a similar degree, surprisingly, leading me to put forward a theoretical proteostatic mechanism. This mechanism postulates that protein synthesis and degradation are tightly interconnected and balanced mechanisms, at least for certain crucial synaptic proteins such as PSD-95. Synapses aim to retain PSD-95 levels within certain concentration ranges, and if PSD-95 levels are skewed in any way, for instance by a drug, the neuron responds by modulating PSD-95 synthesis or degradation in order to match synaptic demand in a homeostatic response.

Finally, it appears that PSD-95 turnover in older cultures differs significantly from turnover rates at an earlier developmental stage. In my study I find PSD-95 half-life significantly increased at DIV30 compared to DIV16, and I am also able to observe a significant reduction in synaptogenesis in older cultures.

Overall, then, the pulse-chase protocol using the HaloTag system in a PSD-95^{HaloTag} KI mouse line appears well-suited for the study of the turnover of PSD-95 at synapses. The method displays clear strengths compared to other methods used to evaluate protein turnover, such as SILAC or FRAP. It is very versatile, allowing for bulk analysis as well as single-synapse analysis and the differential labelling of 'old' and 'new' subpopulations of the same protein. This last point, particularly, lets it stand out as a technique, as not only can these two subpopulations of the same protein be analysed separately, but also in a complementary fashion when looking at ratios of both types within single synapses. Some of the weaknesses of the study, such as being unable to definitively separate protein degradation from diffusion out of individual synapses, and being unable to measure total PSD-95 levels, can be solved by modifying the experimental approach. Using a single-ligand labelling protocol to supplement the pulse-chase labelling would allow for the monitoring of changes of total PSD-95 levels at synapses. Performing western blots on some of the cultures would have given further evidence of total PSD-95 changes in cells or synapses (using synaptosome preparations). Indeed, the fact that HaloTag ligands can bind to HaloTag fusion proteins within cell lysate, withstand boiling in SDS, and are highly quantitative without requiring an antibody staining makes this another interesting method of analysing changes in PSD-95 levels. Finally, a live-cell imaging approach would allow for the visualisation of PSD-95 dynamics, including mobility, synthesis and degradation, in live cells using the HaloTag system.

Chapter 5: Conclusion

5.1 Summary of findings

5.1.1 PSD-95-HaloTag knock-in mice are phenotypically normal

The results in chapter 3.2.1 indicate by SDS PAGE that PSD-95 levels in PSD-95-HaloTag mice are not significantly different from WT mice. It is also demonstrated that PSD-95-HaloTag fusion proteins localise to 1.5MDa supercomplexes, just like WT mice (chapter 3.2.2). Chapter 3.2.3 demonstrates that PSD-95-HaloTag mice are electrophysiologically normal. Brain slices prepared from het PSD-95-HaloTag mice also show that PSD-95 expression levels display a normal patterning when stained with HaloTag ligands (chapter 3.3.2). Primary cultures from PSD-95-HaloTag mice display a clear punctate staining at dendritic synapses when immunocytochemically stained for PSD-95 (chapters 3.3.3-5). Overall, it can be concluded that PSD-95-HaloTag KI mice are phenotypically normal as they express normal levels of PSD-95 and display a normal localisation of PSD-95 in the brain, to synapses and into postsynaptic supercomplexes.

5.1.2 HaloTag ligands used in a pulse-chase paradigm to investigate PSD-95 turnover

First, in chapter 3.3, it is demonstrated that the HaloTag technology can be used to visualise PSD-95-HaloTag fusion proteins in a primary culture setting. This is done by establishing that fluorescent HaloTag ligand puncta in primary cultures colocalise with anti-PSD-95 antibody staining, are opposed by presynaptic markers, and are located along dendrites stained for MAP2, as well as being absent in WT mice. Next, it was found that the TMR and R110Direct HaloTag ligands used in my experiments are fluorescently stable over 24 hours in cells kept in cell culture incubators for 24 hours, and proven that labelling cells with one ligand saturates all HaloTag binding sites, preventing the binding of a second ligand. A pulse-chase method by which it is possible to separately label previously-present (‘old’) and newly synthesized PSD-95 with two different fluorescent ligands was then established, allowing for the separate analysis and monitoring of subpopulations of the same target protein. Thus, it is found that over 48 hours, between DIV15 and DIV17, old PSD-95 is steadily degraded and

new PSD-95 is synthesized and incorporated into synapses. PSD-95 half-life is calculated to be approximately 36 hours, in line with some previous literature (El-Husseini et al., 2002).

5.1.3 Categorising synapses according to PSD-95 turnover profiles

In chapter 4.3, PSD-95 turnover at single synapses is analysed. Synapses are castegorised into three types: type 1 synapses contain only newly synthesised PSD-95, type 2 synapses contain both new and old PSD-95, and type 3 synapses contain only old PSD-95. This means that synapses have different rates of PSD-95 turnover, which is evident when looking at the synaptic population that was present throughout the entire experiment (type 2 and type 3 synapses): type 3 synapses clearly experience no new PSD-95 synthesis, while type 2 synapses do.
It is found that at DIV16, the majority of synapses are type 2 synapses. It is further found that on average, type 2 synapses contain both more old and more new PSD-95 than either type 1 or type 2 synapses. Finally, it is found that type 2 synapses are very heterogeneous, both in terms of their total PSD-95 expression level and in terms of their ratio of old to new PSD-95 expression.

5.1.4 The effects of activity modulation on PSD-95 turnover

PSD-95 turnover in the presence of either tetrodotoxin (TTX) or bicuculline (BCC) is analysed. The results indicate that slightly but significantly more old PSD-95 is retained at synapses than in untreated controls following 24 hours of TTX treatment, while synthesis remains unchanged, indicating a slight increase in synaptic PSD-95. However, none of the other results differed significantly from untreated controls.

5.1.5 The effects of BDNF treatment on PSD-95 turnover

Following 24 hours of BDNF treatment, it is found that slightly but significantly more old PSD-95 is retained at synapses than in untreated controls. It is also found that there is a significant increase in new PSD-95 at synapses following BDNF treatment. Together, this indicates that total PSD-95 levels at synapses go up. When analysing

synaptic types, it is found that type 3 synapses retain significantly more old PSD-95 than controls, yet colocalised type 2 synapses do not. Further, BDNF treatment causes significantly more new PSD-95 to be found at type 2 synapses, but type 1 synapses do not contain more new PSD-95 than untreated controls.

5.1.6 The effects of ketamine treatment on PSD-95 turnover

Following 24 hours of ketamine treatment, it is found that similar to TTX and BDNF treatment, significantly more old PSD-95 is retained at synapses. This difference is significant both at type 2 and type 3 synapses. New PSD-95 levels at synapses are unaffected, as are puncta numbers.

5.1.6 The effects of proteasome inhibition on PSD-95 turnover

The proteasome inhibitors lactacystin and MG132 were separately added to primary cultures for 24 hours. It was found that both drugs have profound effects on PSD-95 turnover at all levels. Both drugs significantly reduced the degradation of PSD-95, and both drugs significantly reduced the synthesis of PSD-95. It was found that both type 3 and type 2 synapses have reduced PSD-95 degradation. Type 2 synapses were found to have much less new PSD-95 than untreated controls. Type 1 synapses, however, had the same amount of new PSD-95 as controls following lactacystin treatment, and only slightly (albeit significantly) less new PSD-95 than controls following MG132 treatment.

Like in untreated controls, type 2 synapses retain more old PSD-95 than type 3 synapses.

Type 1 and type 2 synapses contain equal amounts of new PSD-95, unlike untreated controls, which display significantly more new PSD-95 in type 2 synapses than type 1 synapses.

Both drugs have the effect of vastly reducing the amount of type 1 synapses present, while significantly reducing type 2 synapse numbers and greatly increasing the number of type 3 synapses.

As can be expected from these results, type 2 synapses display a marked increase in the ratio of old:new PSD-95 in colocalising type 2 synapses.

5.1.7 The effects of protein synthesis inhibition on PSD-95 turnover

The protein synthesis inhibitors anisomycin and cycloheximide were added to primary cultures for 24 hours. The results were very similar to those collected following treatment with proteasome inhibitors. Both drugs significantly reduced the degradation of PSD-95, and both drugs significantly reduced the synthesis of PSD-95. Both type 3 and type 2 synapses were found to have reduced PSD-95 degradation. Type 2 synapses were again found to have much less new PSD-95 than untreated controls. Type 1 synapses had only slightly (but significantly) less new PSD-95 than controls following anisomycin and cycloheximide treatment.

Like in untreated controls, type 2 synapses retain a lot more old PSD-95 than type 3 synapses.

Unlike in controls, type 1 and type 2 synapses contain the same amount of new PSD-95.

As with proteasome inhibitors, I find that protein synthesis inhibitors have the effect of massively reducing the amount of type 1 synapses present, while significantly reducing type 2 synapse numbers and greatly increasing the number of type 3 synapses.

Again, type 2 synapses displayed a marked increase in the ratio of old:new PSD-95 in colocalising type 2 synapses.

5.1.8 PSD-95 turnover at different developmental ages

PSD-95 turnover rates were compared between cultures aged DIV15-DIV16 and DIV29-DIV30. It was found that the average amount of PSD-95 per synapse at the start of the experiment was the same in both groups. However, at DIV29-30 synapses displayed a significantly lower rate of PSD-95 degradation, while still incorporating new PSD-95 to the same extent as synapses at DIV15-16. At the single-synapse level, none of the results differed significantly, which was most likely due to the smaller sample size of cultures at DIV29-30. However, the observed trend was that PSD-95

degradation at DIV29-30 was reduced both in type 3 and type 2 synapses to an equal extent.

As a proportion of the whole synaptic population, cultures aged DIV30 were found to contain more type 3 synapses and fewer type 1 synapses than at DIV16, while the proportion of type 2 synapses remained roughly equal. Indeed, there were significantly fewer type 1 synapses than type 2 synapses at DIV30 in absolute numbers as well. This indicates reduced synaptogenesis at older cultures.

Within type 2 synapses, the ratio of pulse:chase ligands was significantly higher at DIV30 than DIV16, in line with reduced degradation of old PSD-95.

5.2 Methodological considerations

In this project, I set out with two goals in mind: first, to establish a working method using the HaloTag technology that would allow me to monitor the turnover of PSD-95; and second, to use this method to evaluate how PSD-95 turnover is affected by various changes. In working towards these goals, I obtained many results that provided me with intriguing insights into synapse biology. In this section, I will discuss the methodological considerations that need to be taken into account when using this method, and the consequences this has for my results. I will not, at this stage, discuss the biological implications of my findings further, as I have already done so within the relevant subchapter discussions in chapter 4.

Firstly, a brief recap of the pulse-chase labelling method and the subsequent quantification will be provided. The method is based around the principle that the HaloTag pulse ligand (R110Direct) will label all existing PSD-95-HaloTag fusion proteins present in the neurons at the start of the experiment. This is important as it means that one has captured the entire population of PSD-95 proteins that are present at this time, allowing for their monitoring from this point onwards. It is also critical to this method because proteins tagged with the pulse ligand cannot be tagged with the chase (TMR) ligand, ensuring that there is a clearly defined boundary between two subpopulations of PSD-95: those present at the start of the experiment, and those synthesised thereafter. Nevertheless, pulse-labelled PSD-95 proteins are very diverse in terms of their age, and some of them will be nearing the end of their metabolic lifespan while others will only recently have been synthesised. This also sets the method apart from metabolic labelling experiments using SILAC, for instance, because in such experiments proteins are tagged as they are being synthesised, which means that the duration of the labelling period is a critical determinant of the size of the tagged protein population. This has both advantages and disadvantages: while the HaloTag method can be certain to have labelled the entire PSD-95 population present at the start of the experiment, this population is much more diverse, while when using SILAC one knows that all labelled proteins were synthesised during the labelling period and not before. However, if one wants to capture a large enough sample size, then long labelling times are needed for SILAC, which in fact creates the

same outcome- one doesn't know at what point in the labelling process proteins were synthesised. Ultimately, then, it appears to be advantageous that the HaloTag pulse-chase labelling technique captures the entire population of target proteins present at the start of the experiment. PSD-95 proteins synthesised after the chase ligand has been added, on the other hand, are a lot more homogenous: they have all been synthesised within the chase period (usually 24-hours). One of the strengths of the method, then, is the clear and distinct labelling of 'old' and 'new' target proteins.

One of the major advantages of this method over other methods is the fact that proteins can be studied at individual synapses, something that SILAC for example is unable to do. This has allowed for the measuring of PSD-95 turnover at synapses, rather than at a cell-wide level. However, it comes with a caveat that was addressed throughout the previous discussions of results in the various subsections. This is the fact that, as mentioned in chapter 1, PSD-95 is a dynamic and mobile protein known to be cycled into and out of synapses without this necessarily being due to synthesis and degradation. Indeed, this is mainly the 'turnover' rate that FRAP experiments measure, rather than the metabolic turnover rate of synthesis and degradation. This means that when looking at a single synapse, a reduction in pulse-labelled PSD-95 can mean that old proteins were degraded- or cycled out of the synapse. This means that looking at ratios of old to new PSD-95 within synapses are perhaps not very informative, since they are the combined result of turnover and mobility. Nevertheless, when mean values are calculated across a very large number of synapses, the results are a reliable indicator of PSD-95 degradation and synthesis. This is because molecules may move from one synapse to another, but they will be included in the overall calculation no matter which synapse they are at. Therefore, 'bulk' turnover rates are reliable indicators of overall PSD-95 synthesis and degradation. How, then, are these results set apart from other bulk techniques, such as SILAC? Besides the fact that only synaptic, but not cytoplasmic, PSD-95 is included, my method allows for single synapses to be categorised into three different types. This is certainly a novel insight into the turnover of PSD-95 at synapses. These categories also restrict, to some extent, the mobility of PSD-95 between synapses of different categories. While PSD-95 molecules may indeed be moving regularly between synapses within type 2 (colocalised) synapses, type 3 synapses contain solely old PSD-95, and furthermore, contain less old PSD-95 than type 2 synapses do, on average. While it is hard to pin

down the degradation rate of PSD-95 at such synapses (they could be degrading/cycling out PSD-95 faster than type 2 synapses, thus containing less old PSD-95; or they may have started off with less PSD-95 to begin with), we can conclude that they experience no influx of new PSD-95. We can therefore infer that these are synapses in a state of decline or stagnation, and can be expected to be experiencing little synaptic activity, which is correlated with PSD-95 turnover (Hruska et al., 2015). Indeed, Cane et al.'s (2014) finding that synapses tend to lose PSD-95 a significant time period before being pruned indicates that this may be the best explanation for the state of type 3 synapses.

Along the same vein, type 2 synapses contain both old and new PSD-95, indicating that PSD-95 turnover and mobility are ongoing in these synapses. As mentioned in chapter 4, these synapses appear to be very diverse in terms of their total PSD-95 content. While Butko et al. (2012) found that new PSD-95 molecules tend to localise to newly formed synapse, my analysis indicates that type 2 synapses contain more newly-synthesised PSD-95 than do type 1 synapses. This indicates that these are stable spines (as Cane et al. (2014) show that greater levels of PSD-95 in a synapse correlate with stability) and that they are also quite active, as they are experiencing ongoing PSD-95 turnover (Hruska et al., 2015). This makes sense given that this is the most numerous (43%) of the three types of synapses. Interestingly, Butko et al. (2012) also found that stimulated synapses preferentially recruit newly-synthesized PSD-95, rather than recruiting old PSD-95 from a common dendritic pool that gets replenished by synthesis. This does indicate that the presence of new PSD-95 at synapses is a marker of synaptic activity. Furthermore, Bingol and Schuman (2006) found that synaptic activity enriches synapses in proteasomes, linked to PSD-95 degradation. Colledge et al. (2003) also found that NMDAR activity induces PSD-95 ubiquitination and subsequent degradation at synapses. Taken together, the evidence points to the turnover of PSD-95 that was measured at synapses being a measurement of PSD-95 synthesis and degradation more so than protein mobility.

Finally, type 1 synapses contain only new PSD-95 and are clearly newly formed synapses, in line with Butko et al.'s (2012) finding. Since Cane et al. (2014) found that dendritic spines that failed to recruit PSD-95 were unstable and rapidly pruned away again, it seems likely that these type 1 synapses are stable, and in the process of recruiting PSD-95 to a newly forming PSD. Interestingly, the fact that new PSD-95 levels, and thus also total PSD-95 levels, are on average lower in type 1 synapses

than in type 2 synapses indicates that PSD-95 is recruited to new synapses after synaptogenesis in a gradual fashion. This is opposed to the possibility that PSDs might establish a full complement of PSD-95 in an all-or-nothing approach.
Clearly, then, this sort of analysis of subpopulations of synapses is a unique feature of this HaloTag method. It allows for a novel approach to analysing proteins and their dynamics, and allows synaptic heterogeneity to be probed in a unique fashion.

One further methodological consideration to be mentioned is that the results pertaining to puncta numbers are very variable, and only in extreme cases statistically significant. When imaging coverslips, areas containing large amounts of dendritic branches were selected and it was aimed to minimise the presence of cell bodies. Nevertheless, images varied greatly in the density of dendritic branches and hence of synaptic puncta. Thus, while puncta number results tend to mirror puncta intensity results and also often differ from controls in many cases, the results are frequently not significant due to the high variance within the results. As can be seen in the various graphs, error bars denoting the standard error of the mean tend to be very large for graphs representing puncta numbers.

5.3 Critiques and improvements

In this section, I will outline areas of my project that I believe could have been done differently or could have had additional elements that would have strengthened the results and the conclusions drawn from them.

The first point to be brought up here is one that was addressed repeatedly while discussing the results. One element that many previous studies have analysed and emphasised is the changes in total PSD-95 levels following various chemical treatments, such as activity modulation. With my technique, old and new PSD-95 proteins are labelled with two different ligands, which provides new information about these two subpopulations. However, it also loses the ability to discern whether total PSD-95 levels in cells or synapses have changed. It is still possible to infer that total PSD-95 at synapses has gone up, on average, if both more pulse ligand is being retained and more chase ligand is being incorporated, such as following BDNF treatment. Nevertheless, a more direct measure would be ideal, and would yield useful additional information. For instance, it would be very useful to find out if treatment with proteasome inhibitors or protein synthesis inhibitors affects total PSD-95 levels, or if neurons are indeed able to retain PSD-95 levels within a certain range by regulating synthesis or degradation according to the proteostatic model. This analysis would be useful at a whole-cell level, as well as at a synaptic level.
In other studies, total PSD-95 levels have been analysed by western blotting at a whole-cell levels, and by immunohistochemistry at a synaptic level. However, in this area, too, the HaloTag technology provides key advantages over some of these approaches.

Firstly, in order to get a whole-cell measurement of PSD-95 levels, one could have cultured additional wells of primary neurons, and after drug treatment, harvested these for biochemical analysis rather than imaging. At that point, a synaptosome preparation could have been performed to enrich for synaptic proteins, or else whole-cell lysate could have been analysed. As analysis methods, the first obvious choice would be to perform SDS PAGE and western blotting analysis, using antibodies against PSD-95 or the HaloTag protein. Using an antibody against the HaloTag would have the

advantage of circumventing potential false positive labelling that can arise when using an antibody against PSD-95, as MAGUK proteins are structurally quite similar, and some of the commercially available antibodies are known not to distinguish between some of these proteins due to epitope similarities. However, another approach would be to label PSD-95-HaloTag fusion proteins with a HaloTag ligand directly, as demonstrated in chapter 3.3.1. This would be highly specific and quantitative, and avoid common pitfalls of western blotting: western blots often display non-specific binding and antibody cross-reactivity, all of which would be avoided by a direct labelling with HaloTag ligands. The results would also be more quantitative, as a single ligand binds to a single protein, whereas this is not the case for antibodies. The results could then be analysed similarly to a western blot by using a denaturing gel followed by a quantification of the intensity of the bands corresponding to PSD-95-HaloTag.
To probe this more directly at a synaptic level, the single-ligand labelling presented in chapter 3.3.6 would be ideal. This works very much like a normal immunocytochemical antibody staining. By labelling synapses with a single ligand only, one tags all PSD-95 proteins present; yet, again, this technique is a lot more quantitative than antibody staining. This is because antibody staining can vary in its effectiveness and occasionally display variance between samples. When using a saturating concentration of a HaloTag ligand, on the other hand, one can be certain that one has tagged the entire population of PSD-95. In this way, changes in synaptic PSD-95 levels can easily be visualised and quantified, and compared to untreated controls. Nevertheless, conventional immunocytochemistry could also have been used, and both of these methods would have allowed to me gather data on the overall fluorescence intensity corresponding to total PSD-95 levels in different cultures. These various methods, then, would allow for the quantification of total PSD-95 expression at cells or synapses, and would be useful adjuncts to the experiments performed by me.

Another set of experiments that could have been performed in order to strengthen the validity of the results is to perform a toxicity assay for the various drugs that were used to treat the primary cultures. Such an assay would have involved treating the neurons with the chemical compounds in the same manner and at the identical concentration as during the experiments, but to evaluate their effect on neuronal viability thereafter. There are various assays that can be used to analyse whether neurons are undergoing

apoptosis and necrosis. One assay, for instance, gives an indication of cell membrane integrity by monitoring lactate dehydrogenase release (Cummings et al., 2004). The reason why this may be important is that some of the effects observed after drug treatment could conceivably be explained by a breakdown of cellular mechanisms during apoptosis or necrosis. For example, proteasome inhibitors and protein synthesis inhibitors appear to cause a marked reduction in both PSD-95 synthesis and degradation. However, if the neuron is undergoing cell death, it is possible that PSD-95 turnover is disrupted by this, rather than a direct effect of the drug. Dying cells may, thus, cease to synthesise and degrade proteins. It would, therefore, be useful to perform such an assay in order to remove this possibility as an alternative explanation for the results. However, it is worth noting that it is unlikely that cell death is an explanation for the results obtained during this study. Firstly, the health of neuronal cultures was closely monitored after the 24-hour treatment period by a visual inspection using a light microscope. Experience in working with primary cultures allowed for the visual identification of the markers of cell death in these cultures, and this led to the exclusion of ketamine treatment at a high concentration from the experimental groups due to the induction of cell death brought on by this treatment (see chapter 4.4.4.1). Secondly, concentrations used in this project matched those used widely in the literature, and indeed were occasionally below these levels (see lactacystin treatment, chapter 4.4.5.3). Nevertheless, an assay would have been ideal in order to definitively reject such alternative explanations.

Another additional point of analysis to be made that would likely have been useful and interesting is the method of synaptic puncta analysis. The Imaris software was used to identify synaptic puncta and calculate their average puncta fluorescence intensity. This provides a good indication of the concentration of PSD-95 molecules present at the synapse, since each PSD-95 molecule is tagged with a single fluorescent ligand molecule in a highly quantitative way. Average fluorescence intensity, thus, reveals a lot about the concentration of PSD-95 at a given synapse. However, this measurement does not give an indication of the total amount of PSD-95 in the synapse, since a large and a small PSD may contain the same concentration of PSD-95 but different total amounts.

Thus, integrated puncta intensity quantified by the Imaris software is a second measurement that would have been very informative when used in addition to average intensity/concentration. This measurement is the results of the sum of fluorescence units within a detected punctum structure, and would provide a measurement of the total amount of PSD-95 present in each synapse. While it would not make a good standalone measurement without taking into account PSD-95 concentration as well, it would certainly be an excellent adjunct to my current method of quantifying PSD-95 in synapses. It would, however, necessitate taking into account puncta area as well. It is conceivable, for instance, that newly formed synapses containing only new PSD-95 (i.e. type 1 synapses) might have a smaller area than mature synapses. Indeed, puncta area is another measurement that could be of interest. It might be intriguing to analyse whether any of the chemical modulations have an effect on PSD-95 puncta area, as it is conceivable that some may affect spine morphology and perhaps lead to changes in the size of spines and PSDs.

Thus, adding the measurements of integrated puncta intensity and puncta area to the results would have added further interesting perspectives to the analysis of PSD-95's expression and turnover at synapses.

5.4 Future directions

Apart from including the improvements mentioned in the above section, chapter 5.3, in future studies, there are various other experiments that could be performed. Many of the following suggestions are experiments that are fascinating in their own right, rather than contributing additional value to the experiments that were performed.

The first set of experiment that would be a logical 'next step' is to probe further into the synaptic heterogeneity observed, and attempt to understand what determines synaptic types. While it can be stated with some confidence that type 1 synapses are immature synapses recently formed through synaptogenesis, the identity of type 3 synapses, containing only old but no new PSD-95, is a lot less clear. Interpretations were put forward as to their identity, but further investigation is surely warranted. An analysis of other synaptic markers could be a first step in this analysis. This could be used to ascertain that type 1 synapses are indeed immature (for instance by labelling presynaptic neurotransmitter vesicles, which should be present in much smaller numbers at the presynaptic boutons of immature synapses (Butko et al., 2012)).

To probe whether type 3 synapses are in a silent state, it might be interesting to stain for AMPAR subunits, and observe whether type 3 synapses have lower levels of AMPAR expression. Furthermore, presynaptically silent synapses have also been described, and these can be identified by their lack of FM 1-43 dye uptake following stimulation (Yao et al., 2006). While technically challenging, it might be possible to probe for such characteristics. Other postsynaptic markers could of course also be tested for: the activity-induced protein Arc/Arg3.1 (Arc) is a good indicator of synaptic activity, for instance. It might, therefore, be of interest to stain cultures for Arc, and correlate the expression of this protein with synaptic types. While this could be used to discover whether type 3 synapses indeed do not experience much activity and are therefore stagnant in their rate of PSD-95 turnover, it could also be interesting to probe type 2 synapses further. Thus, one might be able to correlate increased Arc expression with different ratios of old to new PSD-95 at individual synapses. This is particularly interesting because our lab actually has a further knock-in mouse line, expressing Arc fused to the 'Venus' yellow fluorescent protein (YFP). By crossing this mouse line with

the PSD-95-HaloTag mice, it would be very simple to observe both these proteins and correlate synaptic activity with PSD-95 turnover and different synaptic types.

Another set of experiments that would be of great interest is live imaging. This would allow for the visualisation of PSD-95 dynamics, for instance by using two-photon microscopy similar to the study by Gray et al. (2006), but in cultures, and thereby visualising the movement of fluorescently labelled PSD-95 proteins between dendritic spines. Combining this method with the HaloTag pulse-chase labelling technique could provide interesting insights, as it could reveal differential mobility between old and new PSD-95. This could also reveal differences in PSD-95 dynamics at synapses of different types. It would most likely be necessary to remove unbound ligands from the medium as far as possible, but this should not be a massive hurdle. Clearly, this is a particularly interesting avenue to proceed along in future studies. Thus, one could combine such a live imaging approach with drug treatments such as activity modulation. This would allow for an observation of the effects of activity blockade or enhancement on PSD-95 dynamics at individual synapses in a direct and very short-term fashion, including synthesis and degradation rates at dendritic spines.

Further, spatial interactions between PSD-95 and other proteins, as well as PSD-95's cellular spatial distribution, could be looked at using the HaloTag technology. Combining Pulse-Chase labelling protocols as utilised during this project with labels and tags that allow for the identification of individual neurons could allow for an interesting analysis of PSD-95 dynamic in individual neurons, and thereby allow for the contrasting of PSD-95 turnover results between single neurons and even different dendrites of the same neuron. For example, sparse transfections using a fluorescent protein tagged to a cytoplasmic protein could allow only some few neurons to express fluorescent proteins along their dendrites, as well as dye filling of single neurons. By studying PSD-95 turnover within synapses that are associated with a labelled neuron and contrasting the results with another single labelled neuron on the same coverslip could allow for interesting insights into differences in PSD-95 turnover between cells. In this way, it would perhaps be possible to create categories of neurons that display certain PSD-95 turnover profiles rather than just categories of synapses, as was done in this project. Indeed, one could even go a step further and combine such an approach with the activation of specific individual neurons using techniques such as

calcium uncaging and channel rhodopsins to gain a better understanding of the effect of activity on PSD-95 turnover at single synapses. Such an approach would be a lot more precise than the 'bulk' targeting of whole cultures using drugs like TTX or BCC. As such, the results they could yield would be a lot more discerning in many ways.

As mentioned in the introduction, the HaloTag technology can also be used to purify proteins and their binding partners (chapter 1.3.3.). Combined with a pulse-chase labelling protocol, this could be used to isolate solely PSD-95 that has been newly synthesised. To this end, one could begin an experiment in very similar fashion to my experiments, with minor changes and a biochemical affinity capture protocol at the end. For example, a fluorescent ligand A could be used to label pre-existing old PSD-95. Instead of using a second fluorescent ligand as the chase ligand, however, one could use the commercially available biotin ligand instead (a ligand with a biotin functional group attached). If newly synthesised proteins are now labelled with the biotin ligand, then these proteins can selectively be affinity-purified by using streptavidin or avidin beads. Thus, after the 24-hour chase labelling protocol (perhaps in the presence of a chemical modulator), the cultured neurons could be harvested, lysed and snap frozen. Streptavidin beads can then be used to capture PSD-95-HaloTag fusion proteins that are labelled with the biotin chase ligand B, while not capturing old proteins tagged with the fluorescent pulse ligand A. In this way, one could purify multiprotein supercomplexes that are, perhaps, assembled only by newly synthesised PSD-95 in response to activity. Once isolated, these complexes can then be biochemically analysed and compared to the complexes captured without a chemical stimulus, or all known PSD-95 complexes. Indeed, this protocol could also be used to capture complexes containing only old PSD-95. In that case, one would use the biotin ligand as the pulse ligand, and chase with a fluorescent ligand. In that case, the affinity purification step would isolate only complexes containing old PSD-95 but not those containing new PSD-95 (although complexes containing both old and new PSD-95 would also be captured). There are surely myriads of interesting questions and manipulations one could include in such an experimental set-up, and this highlights very well just how versatile the HaloTag technology is.

A further highly interesting direction one could take is to utilise the homemade HaloTag ligands that cause the acute degradation of a tagged protein. As described in the

introduction (chapter 1.3.4) these ligands are hydrophobic and cause a tagged protein to be marked for degradation. This ligand was developed in the lab of Craig Crews, and I was in fact able to obtain a sample of these ligands. I only tested them a few times, but was able to qualitatively observe a marked reduction in PSD-95 antibody staining in primary cultures after applying this ligand (called PROTAC). While the application protocol requires refinement, it is easily possible to imagine a number of ways this ligand could be used to probe PSD-95's function further. If one could degrade old PSD-95 using this ligand as the pulse ligand, for example, then remove most of this ligand and add a second chase ligand that is fluorescent in order to outcompete the remaining PROTAC ligands (exactly like in my pulse-chase protocol), one would be able to visualise newly synthesised PSD-95 following complete removal of old PSD-95. It would be interesting to see if the cell responds by massively increasing PSD-95 synthesis in such a scenario, and if some synapses will be able to preferentially recruit this PSD-95 over other synapses. The effects on other proteins could also be explored, such as on AMPA and NMDA receptors, and how this effects the number of synaptic puncta present (perhaps synapses are lost). Equally so, new PSD-95 synthesis could effectively be prevented while retaining old PSD-95 by pulse labelling it with a fluorescent ligand first, and then following this up with the PROTAC ligand. Unlike protein synthesis inhibitors such as anisomycin, this would not affect other proteins, solely PSD-95. It would thus be absolutely fascinating to monitor whether this has the same effect as using these drugs in blocking not only PSD-95 synthesis but also degradation. If so, this experiment would provide a vital next step in support of the proteostatic model of synapses keeping PSD-95 levels within a specific range by controlling its synthesis and degradation (see chapter 4.4.7). Numerous other applications for this PROTAC ligand could surely be found.

Finally, the greatest step forward and utmost achievement would be to manage to label PSD-95-HaloTag fusion proteins in live mice. Indeed, this is something I tried on a few occasions, but was unable to accomplish. Multiple previous studies have used the HaloTag labelling system in live mice, however, the target proteins were always located within tumours xenografted into the flanks of mice, and HaloTag ligands were delivered by intraperitoneal injections. This means that ligands were injected in close proximity to the tumours, and did not have to pass additional hurdles such as the blood-brain barrier (BBB). Since the HaloTag ligands are tiny and cell membrane

permeating, they should be able to cross the BBB, and personal communications with Promega have revealed that there is a large pharmaceutical company that is currently working on creating an assay using the HaloTag technology to determine whether drugs cross the BBB or not. The difficulty in labelling fusion proteins in the brain, then, is most likely linked to dosage and clearance. Ligands need to be administered at a concentration high enough to allow them to penetrate into the brain at a concentration that is high enough to label a significant amount of proteins. Since the ligands will invariably diffuse throughout the entire animal, and thus be dilute throughout the volume of its body, they must be administered at a very high concentration indeed. My first experiment involved administration by intraperitoneal injection, and following experiments were performed with tail-vein injections. However, in no instance could a significant synaptic puncta staining be observed in slices taken from injected mice. It is possible that ligand quantity was insufficient and/or clearance was rapid. Incubation time was 24 hours, but future studies will have to attempt to establish a clearance rate. This could, for instance, be done by taking blood samples from injected mice at set intervals after injection, isolate the plasma, and analyse the fluorescence intensity of the ligands within. Other studies have also applied the ligand by tail-vein injection (Hong et al., 2011), and established that clearance of the ligands occurred rapidly through the hepatobiliary or renal pathway. Neklesa et al. (2011) also monitored ligand clearance, and found serum levels to drop by 75% over 24 hours. Ultimately, a more direct but more invasive approach might be the injection of the ligand directly into the brain. This would reduce the issues of dilution and clearance to a great extent. If the labelling of PSD-95 in the brains of live mice is indeed accomplished, this would prove to be a breakthrough, but create a whole host of new questions. If one wanted to probe the temporal aspects of PSD-95 in a similar fashion as this project has done, one would need to ascertain that proteins are saturated with one ligand before applying a second ligand. This second ligand could, however, be applied post-mortem to brain slices. If one were to be able to solve the host of technical issues (how quickly is the unbound pulse ligand cleared, to prevent it from continuing to label newly synthesised PSD-95?), one could ask truly profound questions. Learning and memory exercises could be applied to mice, and PSD-95 synthesised in response to such stimulation localised at a whole-brain as well as single-synapse level. At that point, the HaloTag technology would truly have reached the pinnacle of its potential.

References

Abdallah, C. G., Adams, T. G., Kelmendi, B., Esterlis, I., Sanacora, G., & Krystal, J. H. (2016). Ketamine's Mechanism of Action: A Path To Rapid-Acting Antidepressants. *Depression and Anxiety*, *33*(8), 689–697.

Alvarez-Castelao, B., & Schuman, E. M. (2015). The regulation of synaptic protein turnover. *Journal of Biological Chemistry*, *290*(48), 28623–28630.

Ashby, M. C., & Isaac, J. T. R. (2011). Maturation of a Recurrent Excitatory Neocortical Circuit by Experience-Dependent Unsilencing of Newly Formed Dendritic Spines. *Neuron*, *70*(3), 510–521.

Bane, V., Lehane, M., Dikshit, M., O'Riordan, A., & Furey, A. (2014). Tetrodotoxin: Chemistry, toxicity, source, distribution and detection. *Toxins*, *6*(2), 693–755.

Bayés, A., van de Lagemaat, L. N., Collins, M. O., Croning, M. D. R., Whittle, I. R., Choudhary, J. S. & Grant, S.G.N. (2011). Characterization of the proteome, diseases and evolution of the human postsynaptic density *Nature Neuroscience*, *14*(1), 19–21.

Beique, J.-C., Lin, D.-T., Kang, M.-G., Aizawa, H., Takamiya, K., & Huganir, R. L. (2006). Synapse-specific regulation of AMPA receptor function by PSD-95. *Proceedings of the National Academy of Sciences*, *103*(51), 19535–19540.

Bence, M., Arbuckle, M. I., Dickson, K. S., & Grant, S. G. N. (2005). Analyses of murine Postsynaptic Density-95 identify novel isoforms and potential translational control elements. *Molecular Brain Research*, *133*(1), 143–152.

Bianchetta, M. J., Lam, T. T., Jones, S. N., & Morabito, M. A. (2011). Cyclin-Dependent Kinase 5 Regulates PSD-95 Ubiquitination in Neurons. *Journal of Neuroscience*, *31*(33), 12029–12035.

Bingol, B., & Schuman, E. M. (2006). Activity-dependent dynamics and sequestration of proteasomes in dendritic spines. *Nature*, *441*(7097), 1144–1148.

Bingol, B., Wang, C. F., Arnott, D., Cheng, D., Peng, J., & Sheng, M. (2010). Autophosphorylated CaMKII Acts as a Scaffold to Recruit Proteasomes to Dendritic Spines. *Cell*, *140*(4), 567–578.

Boisvert, F.-M., Ahmad, Y., Gierliński, M., Charrière, F., Lamont, D., Scott, M., Lamond, A. I. (2012). A Quantitative Spatial Proteomics Analysis of Proteome Turnover in Human Cells. *Molecular & Cellular Proteomics*, *11*(3), M111.011429.

Browne, C. A., & Lucki, I. (2013). Antidepressant effects of ketamine: Mechanisms underlying fast-acting novel antidepressants. *Frontiers in Pharmacology*, *4 DEC*(December), 1–18.

Butko, M. T., Yang, J., Geng, Y., Kim, H. J., Jeon, N. L., Shu, X., Lin, M. Z. (2012). Fluorescent and photo-oxidizing TimeSTAMP tags track protein fates in light and electron microscopy. *Nature Neuroscience*, *15*(12), 1742–1751.

Cai, C., Li, H., Rivera, C., & Keinänen, K. (2006). Interaction between SAP97 and PSD-95, two Maguk proteins involved in synaptic trafficking of AMPA receptors. *Journal of Biological Chemistry*, *281*(7), 4267–4273.

Cajigas, I. J., Will, T., & Schuman, E. M. (2010). Protein homeostasis and synaptic plasticity. *The EMBO Journal*, *29*(16), 2746–2752.

Cane, M., Maco, B., Knott, G., & Holtmaat, A. (2014). The Relationship between PSD-95 Clustering and Spine Stability In Vivo. *Journal of Neuroscience*, *34*(6), 2075–2086.

Carlin, R. K., Grab, D. J., Cohen, R. S., & Siekevitz, P. (1980). Isolation and characterization of postsynaptic densities from various brain regions: Enrichment of different types of postsynaptic densities. *Journal of Cell Biology*, *86*(3), 831–843.

Catarino, T., Ribeiro, L., Santos, S. D., & Carvalho, A. L. (2013). Regulation of synapse composition by protein acetylation: the role of acetylated cortactin. *Journal of Cell Science*, *126*(Pt 1), 149–62.

Chalfie, M., Tu, Y., Euskirchen, G., Ward, W. W., & Prasher, D. C. (1994). Green Fluorescent Protein as a Marker for Gene Expression. *Science*, *263*(5148), 802–805.

Charych, E. I., Akum, B. F., Goldberg, J. S., Jornsten, R. J., Rongo, C., Zheng, J. Q., & Firestein, B. L. (2006). Activity-Independent Regulation of Dendrite Patterning by Postsynaptic Density Protein PSD-95. *Journal of Neuroscience*, *26*(40), 10164–10176.

Chen, J., & Pan, H.-L. (2017). Dissecting molecular architecture of post-synaptic density at excitatory synapses. *Journal of Neurochemistry*, 3–6.

Chen, L., Chetkovich, D. M., Petralia, R. S., Sweeney, N. T., Kawasaki, Y., Wenthold, R. J., Nicoll, R. a. (2000). Stargazin regulates synaptic targeting of AMPA receptors by two distinct mechanisms. *Nature*, *408*(6815), 936–43.

Chen, X., Nelson, C. D., Li, X., Winters, C. A., Azzam, R., Sousa, A. A., Reese, T. S. (2011). PSD-95 Is Required to Sustain the Molecular Organization of the Postsynaptic Density. *Journal of Neuroscience*, *31*(17), 6329–6338.

Chen, X., Vinade, L., Leapman, R. D., Petersen, J. D., Nakagawa, T., Phillips, T. M., Reese, T. S. (2005). Mass of the postsynaptic density and enumeration of three key molecules. *Proceedings of the National Academy of Sciences*, *102*(32), 11551–11556.

Chen, X., Levy, J. M., Hou, A., Winters, C., Azzam, R., Sousa, A. A., Reese, T. S. (2015). PSD-95 family MAGUKs are essential for anchoring AMPA and NMDA receptor complexes at the postsynaptic density. *Proceedings of the National Academy of Sciences*, *112*(50), E6983–E6992.

Chen, Z., Cornish, V. W., & Min, W. (2013). Chemical tags: Inspiration for advanced imaging techniques. *Current Opinion in Chemical Biology*, *17*(4), 637–643.

Cheng, M. C., Lu, C. L., Luu, S. U., Tsai, H. M., Hsu, S. H., Chen, T. T., & Chen, C. H. (2010). Genetic and functional analysis of the DlG4 gene encoding the post-synaptic density protein 95 in schizophrenia. *PLoS ONE*, *5*(12).

Cho, K. O., Hunt, C. A., & Kennedy, M. B. (1992). The rat brain postsynaptic density fraction contains a homolog of the drosophila discs-large tumor suppressor protein. *Neuron*, *9*(5), 929–942.

Choi, M., Lee, S. H., Wang, S. E., Ko, S. Y., Song, M., Choi, J.-S., Son, H. (2015). Ketamine produces antidepressant-like effects through phosphorylation-dependent nuclear export of histone deacetylase 5 (HDAC5) in rats. *Proceedings of the National Academy of Sciences*, *5*, 201513913.

Chung, H. J., Huang, Y. H., Lau, L.-F., & Huganir, R. L. (2004). Regulation of the NMDA Receptor Complex and Trafficking by Activity-Dependent Phosphorylation of the NR2B Subunit PDZ Ligand. *Journal of Neuroscience*, *24*(45), 10248–10259.

Cohen, L. D., Zuchman, R., Sorokina, O., Müller, A., Dieterich, D. C., Armstrong, J. D., Ziv, N. E. (2013). Metabolic Turnover of Synaptic Proteins: Kinetics, Interdependencies and Implications for Synaptic Maintenance. *PLoS ONE*, *8*(5).

Cohen, N. A., Brenman, J. E., Snyder, S. H., & Bredt, D. S. (1996). Binding of the inward rectifier K+ channel Kir 2.3 to PSD-95 is regulated by protein kinase A phosphorylation. *Neuron*, *17*(4), 759–767.

Colledge, M., Snyder, E. M., Crozier, R. A., Soderling, J. A., Jin, Y., Langeberg, L. K., Scott, J. D. (2003). Ubiquitination Regulates PSD-95 Degradation and AMPA Receptor Surface Expression. *Neuron*, *40*(November), 595–607.

Collins, M. O., Husi, H., Yu, L., Brandon, J. M., Anderson, C. N. G., Blackstock, W. P., Grant, S. G. N. (2006). Molecular characterization and comparison of the components and multiprotein complexes in the postsynaptic proteome. *Journal of Neurochemistry*, *97 Suppl 1*(m), 16–23.

Constals, A., Penn, A. C., Compans, B., Toulmé, E., Phillipat, A., Marais, S., Choquet, D. (2015). Glutamate-Induced AMPA Receptor Desensitization Increases Their Mobility and Modulates Short-Term Plasticity through Unbinding from Stargazin. *Neuron*, *85*(4), 787–803.

Craig, a M., & Boudin, H. (2001). Molecular heterogeneity of central synapses: afferent and target regulation. *Nature Neuroscience*, *4*(6), 569–578.

Cromm, P. M., & Crews, C. M. (2017). Targeted Protein Degradation: From Chemical Biology to Drug Discovery. *Cell Chemical Biology*.

Cummings, B. S., Wills, L. P., & Schnellmann, R. G. (2004). Measurement of Cell Death in Mammalian Cells. *Curr Protoc Phamacol*, *1*(Lemasters 1999), 1–30.

Dahlmann, B. (2007). Role of proteasomes in disease. *BMC Biochemistry*, *8*(Suppl 1), S3.

Daniels, D. L., Méndez, J., Mosley, A. L., Ramisetty, S. R., Murphy, N., Benink, H., Washburn, M. P. (2012). Examining the complexity of human RNA polymerase complexes using HaloTag technology coupled to label free quantitative proteomics. *Journal of Proteome Research*, *11*(2), 564–575.

Delacre, M., Lakens, D., & Leys, C. (2017). Why Psychologists Should by Default Use Welch's t-test Instead of Student's t- test. *International Review of Social Psychology*, *30*(1), 92–101.

Deng, P.-Y., & Lei, S. (2007). Long-term depression in identified stellate neurons of juvenile rat entorhinal cortex. *Journal of Neurophysiology*, *97*(1), 727–37.

Di Liegro, I., Savettieri, G., Coppolino, M., Scaturro, M., Monte, M., Nastasi, T., Cestelli, A. (1995). Expression Of Synapsin-I Gene In Primary Cultures Of Differentiating Rat Cortical-Neurons. *Neurochemical Research*, *20*(2), 239–243.

DiAntonio, A., & Hicke, L. (2004). Ubiquitin-Dependent Regulation of the Synapse. *Annual Review of Neuroscience*, *27*(1), 223–246.

Dieck, S. tom, Kochen, L., Hanus, C., Heumüller, M., Bartnik, I., Nassim-Assir, B., Schuman, E. M. (2015). Direct visualization of newly synthesized target proteins in situ. *Nature Methods*, *12*(5), 411–414.

Djakovic, S. N., Schwarz, L. A., Barylko, B., DeMartino, G. N., & Patrick, G. N. (2009). Regulation of the proteasome by neuronal activity and calcium/calmodulin-dependent protein kinase II. *Journal of Biological Chemistry*, *284*(39), 26655–26665.

Dong, C., Upadhya, S. C., Ding, L., Smith, T. K., & Hegde, A. N. (2008). Proteasome inhibition enhances the induction and impairs the maintenance of late-phase long-term potentiation. *Learning & Memory (Cold Spring Harbor, N.Y.)*, *15*(5), 335–347.

Dong, Z., Han, H., Li, H., Bai, Y., Wang, W., Tu, M., Wang, Y. T. (2015). Long-term potentiation decay and memory loss are mediated by AMPAR endocytosis. *The Journal of Clinical Investigation*, *125*(January).

Duman, R. S., & Aghajanian, G. K. (2012). Synaptic dysfunction in depression: potential therapeutic targets. *Science*, *338*(6103), 68–72.

Ehlers, M. D. (2003). Activity level controls postsynaptic composition and signaling via the ubiquitin-proteasome system. *Nature Neuroscience*, *6*(3), 231–242.

Ehrlich, I. (2004). Postsynaptic Density 95 controls AMPA Receptor Incorporation during Long-Term Potentiation and Experience-Driven Synaptic Plasticity. *Journal of Neuroscience*, *24*(4), 916–927.

Ehrlich, I., Klein, M., Rumpel, S., & Malinow, R. (2007). PSD-95 is required for activity-driven synapse stabilization. *Proceedings of the National Academy of Sciences*, *104*(10), 4176–4181.

El-Husseini, A., Schnell, E., & Chetkovich, D. (2000). PSD-95 involvement in maturation of excitatory synapses. *Science*, *290*(5495), 1364–8.

El-Husseini, A. E., Craven, S. E., Chetkovich, D. M., Firestein, B. L., Schnell, E., Aoki, C., & Bredt, D. S. (2000). Dual palmitoylation of PSD-95 mediates its vesiculotubular sorting, postsynaptic targeting, and ion channel clustering. *Journal of Cell Biology*, *148*(1), 159–171.

El-Husseini, A. E. D., Schnell, E., Dakoji, S., Sweeney, N., Zhou, Q., Prange, O., Bredt, D. S. (2002). Synaptic strength regulated by palmitate cycling on PSD-95. *Cell*, *108*(6), 849–863.

Elias, G. M., Elias, L. A. B., Apostolides, P. F., Kriegstein, A. R., & Nicoll, R. A. (2008). Differential trafficking of AMPA and NMDA receptors by SAP102 and PSD-95 underlies synapse development. *Proceedings of the National Academy of Sciences of the United States of America*, *105*(52), 20953–20958.

Elias, G. M., Funke, L., Stein, V., Grant, S. G., Bredt, D. S., & Nicoll, R. A. (2006). Synapse-Specific and Developmentally Regulated Targeting of AMPA Receptors by a Family of MAGUK Scaffolding Proteins. *Neuron*, *52*(2), 307–320.

Emes R. D., & Grant, S. G. N. (2012). Evolution of Synapse Complexity and Diversity. *Annual Review of Neuroscience*, 35:111–131

Ennis, H. L., & Lubin, M. (1964). Cycloheximide: Aspects of Inhibition of Protein Synthesis in Mammalian Cells. *Science*, *3650*(146), 1474–1476.

Ezkurdia, I., Juan, D., Rodriguez, J. M., Frankish, A., Diekhans, M., Harrow, J., Tress, M. L. (2014). Multiple evidence strands suggest that theremay be as few as 19 000 human protein-coding genes. *Human Molecular Genetics*, *23*(22), 5866–5878.

Fernández, E., Collins, M. O., Uren, R. T., Kopanitsa, M. V, Komiyama, N. H., Croning, M. D. R., Grant, S. G. N. (2009). Targeted tandem affinity purification of PSD-95 recovers core postsynaptic complexes and schizophrenia susceptibility proteins. *Molecular Systems Biology*, *5*(269).

Feyder, M., Karlsson, R.-M., Mathur, P., Lyman, M., Bock, R., Momenan, R., Holmes, A. (2010). Mouse {Dlg4 (PSD-95)} gene deletion and human {DLG4} gene variation is associated with phenotypes relevant to autism-spectrum disorders and Williams-Beuren syndrome. *American Journal of Psychiatry*, *4*(December), 1508–1517.

Feyissa, A. M., Chandran, A., Stockmeier, C. A., & Karolewicz, B. (2009). Reduced levels of NR2A and NR2B subunits of NMDA receptor and PSD-95 in the prefrontal cortex in major depression. *Progress in Neuro-Psychopharmacology and Biological Psychiatry*, *33*(1), 70–75.

Fioravante, D., & Byrne, J. H. (2011). Protein degradation and memory formation. *Brain Research Bulletin*, *85*(1–2), 14–20.

Fonseca, R., Vabulas, R. M., Hartl, F. U., Bonhoeffer, T., & Nägerl, U. V. (2006). A Balance of Protein Synthesis and Proteasome-Dependent Degradation Determines the Maintenance of LTP. *Neuron*, *52*(2), 239–245.

Fossati, G., Morini, R., Corradini, I., Antonucci, F., Trepte, P., Edry, E., Matteoli, M. (2015). Reduced SNAP-25 increases PSD-95 mobility and impairs spine morphogenesis. *Cell Death and Differentiation*, *22*(9), 1425–1436.

Frank, R. A. W., Komiyama, N. H., Ryan, T. J., Zhu, F., O'Dell, T. J., & Grant, S. G. N. (2016). NMDA receptors are selectively partitioned into complexes and supercomplexes during synapse maturation. *Nature Communications*, *7*, 11264.

Frank, R. A. W., Zhu, F., Komiyama, N. H., & Grant, S. G. N. (2017). Hierarchical organization and genetically separable subfamilies of PSD95 postsynaptic supercomplexes. *Journal of Neurochemistry*, *142*(4), 504–511.

Frank, R. A., & Grant, S. G. (2017). Supramolecular organization of NMDA receptors and the postsynaptic density. *Current Opinion in Neurobiology*, *45*, 139–147.

Frankland, P. W. (2006). Stability of recent and remote contextual fear memory. *Learning & Memory*, *13*(4), 451–457.

Fremeau, R. T. (2004). Vesicular Glutamate Transporters 1 and 2 Target to Functionally Distinct Synaptic Release Sites. *Science*, *304*(5678), 1815–1819.

Fujita, Y., Kuchimaru, T., Kadonosono, T., Tanaka, S., Hase, Y., Tomimoto, H., Takahashi, R. (2012). In Vivo Imaging of Brain Ischemia Using an Oxygen-Dependent Degradative Fusion Protein Probe. *PLoS ONE*, *7*(10), 1–8.

Fukata, Y., Dimitrov, A., Boncompain, G., Vielemeyer, O., Perez, F., & Fukata, M. (2013). Local palmitoylation cycles define activity-regulated postsynaptic subdomains. *Journal of Cell Biology*, *202*(1), 145–161.

Gardoni, F., Polli, F., Cattabeni, F., & Di Luca, M. (2006). Calcium-calmodulin-dependent protein kinase II phosphorylation modulates PSD-95 binding to NMDA receptors. *European Journal of Neuroscience*, *24*(10), 2694–2704.

Goedert, M., Crowther, R. A., & Garner, C. C. (1991). Molecular characterization of microtubule-associated proteins tau and map2. *Trends in Neurosciences*, *14*(5), 193–199.

Gould, T. D., Zanos, P., & Zarate, C. A. (2017). Ketamine Mechanism of Action: Separating the Wheat from the Chaff. *Neuropsychopharmacology*, *42*(1), 368–369.

Graf, E. R., Zhang, X., Jin, S. X., Linhoff, M. W., & Craig, A. M. (2004). Neurexins induce differentiation of GABA and glutamate postsynaptic specializations via neuroligins. *Cell*, *119*(7), 1013–1026.

Grant, S. G. N. (2013). SnapShot: Organizational Principles of the Postsynaptic Proteome. *Neuron*, *80*(2), 534e1.

Gray, N. W., Weimer, R. M., Bureau, I., & Svoboda, K. (2006). Rapid redistribution of synaptic PSD-95 in the neocortex in vivo. *PLoS Biology*, *4*(11), 2065–2075.

Grollman, A. P. (1967). Inhibitors of Protein Biosynthesis. *The Journal of Biological Chemistry*, *242*(13), 3226–3233.

Hakim, V., Cohen, L. D., Zuchman, R., Ziv, T., & Ziv, N. E. (2016). The effects of proteasomal inhibition on synaptic proteostasis. *The EMBO Journal*, *9*(6), e201593594.

Hanus, C., & Schuman, E. M. (2013). Proteostasis in complex dendrites. *Nature Reviews Neuroscience*, *14*(9), 638–648.

Harris, K. M. (1999). Structure, development, and plasticity of dendritic spines. *Current Opinion in Neurobiology*, *9*(3), 343–348.

He, Y., Xu, Y., Zhang, C., Gao, X., Dykema, K. J., Katie, R., Xu, H. E. (2013). Identification of a Lysosomal Pathway That Modulates Glucocorticoid Signaling and the Inflammatory Response. *Science Signaling*, *4*(61).

Herring, B. E., & Nicoll, R. A. (2016). Long-Term Potentiation: From CaMKII to AMPA Receptor Trafficking. *Annual Review of Physiology*, *78*(1), 351–365.

Herzog, E., Takamori, S., Jahn, R., Brose, N., & Wojcik, S. M. (2006). Synaptic and vesicular co-localization of the glutamate transporters VGLUT1 and VGLUT2 in the mouse hippocampus. *Journal of Neurochemistry*, *99*(3), 1011–1018.

Hong, H., Benink, H. A., Zhang, Y., Yang, Y., Uyeda, H. T., Engle, J. W., Cai, W. (2011). Halotag: A novel reporter gene for positron emission tomography. *American Journal of Translational Research*, *3*(4), 392–403.

Hou, L., Antion, M. D., Hu, D., Spencer, C. M., Paylor, R., & Klann, E. (2006). Dynamic Translational and Proteasomal Regulation of Fragile X Mental Retardation Protein Controls mGluR-Dependent Long-Term Depression. *Neuron*, *51*(4), 441–454.

Hruska, M., Henderson, N. T., Xia, N. L., Le Marchand, S. J., & Dalva, M. B. (2015). Anchoring and synaptic stability of PSD-95 is driven by ephrin-B3. *Nature Neuroscience*, *18*(11), 1594–1605.

Hu, X., Ballo, L., Pietila, L., Viesselmann, C., Ballweg, J., Lumbard, D., Dent, E. W. (2011). BDNF-Induced Increase of PSD-95 in Dendritic Spines Requires Dynamic Microtubule Invasions. *Journal of Neuroscience*, *31*(43), 15597–15603.

Huang, X., Stodieck, S. K., Goetze, B., Cui, L., Wong, M. H., Wenzel, C., Schlüter, O. M. (2015). Progressive maturation of silent synapses governs the duration of a critical period. *Proceedings of the National Academy of Sciences*, *112*(24), E3131–E3140.

Huber, K. M., Kayser, M. S., & Bear, M. F. (2000). Role for Rapid Dendritic Protein Synthesis in Hippocampal mGluR-Dependent Long-Term Depression. *Science*, *288*(5469), 1254–1256.

Husi, H., Ward, M. a, Choudhary, J. S., Blackstock, W. P., & Grant, S. G. (2000). Proteomic analysis of NMDA receptor-adhesion protein signaling complexes. *Nature Neuroscience*, *3*(7), 661–669.

Huttner, W. B., Schiebler, W., Greengard, P., & De Camilli, P. (1983). Synapsin I (protein I), a nerve terminal-specific phosphoprotein. III. Its association with synaptic vesicles studied in a highly purified synaptic vesicle preparation. *Journal of Cell Biology*, *96*(5), 1374–1388.

Huybrechts, S. J., Van Veldhoven, P. P., Brees, C., Mannaerts, G. P., Los, G. V., & Fransen, M. (2009). Peroxisome dynamics in cultured mammalian cells. *Traffic*, *10*(11), 1722–1733.

Ifrim, M. F., Williams, K. R., & Bassell, G. J. (2015). Single-Molecule Imaging of PSD-95 mRNA Translation in Dendrites and Its Dysregulation in a Mouse Model of Fragile X Syndrome. *Journal of Neuroscience*, *35*(18), 7116–7130.

Isaac, J. T. R., Nicoll, R. A., & Malenka, R. C. (1995). Evidence for silent synapses: Implications for the expression of LTP. *Neuron*, *15*(2), 427–434.

Kang, H., & Schuman, E. (1996). A requirement for local protein synthesis in neurotrophin-induced hippocampal synaptic plasticity. *Science (New York, N.Y.)*, *273*(5280), 1402–6.

Karpova, A., Mikhaylova, M., Thomas, U., Knöpfel, T., & Behnisch, T. (2006). Involvement of Protein Synthesis and Degradation in Long-Term Potentiation of Schaffer Collateral CA1 Synapses. *Journal of Neuroscience*, *26*(18), 4949–4955.

Kazdoba, T. M., Leach, P. T., Silverman, J. L., & Crawley, J. N. (2014). Modeling fragile X syndrome in the FMR1 knockout mouse. *Intractable & Rare Diseases Research*, *3*(4), 118–133.

Kennedy, M. B. (2000). Signal-Processing Machines at the Postsynaptic Density. *Science*, *290*(5492), 750–754.

Kim, M. J., Futai, K., Jo, J., Hayashi, Y., Cho, K., & Sheng, M. (2007). Synaptic Accumulation of PSD-95 and Synaptic Function Regulated by Phosphorylation of Serine-295 of PSD-95. *Neuron*, *56*(3), 488–502.

Kosaka, N., Ogawa, M., Choyke, P. L., Karassina, N., Corona, C., McDougall, M., Kobayashi, H. (2009). In vivo stable tumor-specific painting in various colors using dehalogenase-based protein-tag fluorescent ligands. *Bioconjugate Chemistry*, *20*(7), 1367–1374.

Kramer, G., & Krijgsveld, J. (2016). Turning Over Paradigms in Protein Decay. *Developmental Cell*, *39*(3), 284–285.

Krug, M., Lössner, B., & Ott, T. (1984). Anisomycin blocks the late phase of long-term potentiation in the dentate gyrus of freely moving rats. *Brain Research Bulletin*, *13*(1), 39–42.

Lang, C., Schulze, J., Mendel, R. R., & Hänsch, R. (2006). HaloTag™: A new versatile reporter gene system in plant cells. *Journal of Experimental Botany*, *57*(12), 2985–2992.

Lau, C. G., & Zukin, R. S. (2007). NMDA receptor trafficking in synaptic plasticity and neuropsychiatric disorders. *Nature Reviews Neuroscience*, *8*(6), 413–426.

Le Quesne, J. P., Spriggs, K. A., Bushell, M., & Willis, A. E. (2010). Dysregulation of protein synthesis and disease. *The Journal of Pathology*, *220*, 140–151.

Lee, S.-H., Choi, J.-H., Lee, N., Lee, H.-R., Kim, J.-I., Yu, N.-K., Kaang, B.-K. (2008). Synaptic Protein Degradation Underlies Destabilization of Retrieved Fear Memory. *Science*, (February), 1253–1257.

Lesuisse, C., & Martin, L. J. (2002). Long-Term Culture of Mouse Cortical Neurons as a Model for Neuronal Development, Aging and Death. *Journal of Neurobiology*.

Levy, J. M., Chen, X., Reese, T. S., & Nicoll, R. A. (2015). Synaptic Consolidation Normalizes AMPAR Quantal Size following MAGUK Loss. *Neuron*, *87*(3), 534–548.

Li, J. H., Wang, Y. H., Wolfe, B. B., Krueger, K. E., Corsi, L., Stocca, G., & Vicini, S. (1998). Developmental changes in localization of NMDA receptor subunits in primary cultures of cortical neurons. *The European Journal of Neuroscience*, *10*(January), 1704–1715.

Li, K. W., Hornshaw, M. P., Van Der Schors, R. C., Watson, R., Tate, S., Casetta, B., Smit, A. B. (2004). Proteomics analysis of rat brain postsynaptic density: Implications of the diverse protein functional groups for the integration of synaptic physiology. *Journal of Biological Chemistry*, *279*(2), 987–1002.

Li, N., Lee, B., Liu, R.-J., Banasr, M., Dwyer, J. M., Iwata, M., Duman, R. S. (2010). mTOR-Dependent Synapse Formation Underlies the Rapid Antidepressant Effects of NMDA Antagonists. *Science*, *329*(August), 959–965.

Li, T. P., Song, Y., MacGillavry, H. D., Blanpied, T. A., & Raghavachari, S. (2016). Protein Crowding within the Postsynaptic Density Can Impede the Escape of Membrane Proteins. *Journal of Neuroscience*, *36*(15), 4276–4295.

Lisman, J. E., Raghavachari, S., & Tsien, R. W. (2007). The sequence of events that underlie quantal transmission at central glutamatergic synapses. *Nature Reviews Neuroscience*, *8*(8), 597–609.

Liu, P., Jenkins, N. A., Copeland, N. G., Liu, P., Jenkins, N. A., & Copeland, N. G. (2003). A Highly Efficient Recombineering-Based Method for Generating Conditional Knockout Mutations A Highly Efficient Recombineering-Based Method for Generating Conditional Knockout Mutations, 476–484.

Lopez-salon, M., Alonso, M., Vianna, M. R. M., Viola, H., Mello, T., Izquierdo, I., Medina, J. H. (2001). The Ubiquitin-Proteasome Cascade Is Required for Mammalian Long-Term Memory Formation. *European Journal of Neuroscience*, *14*(October), 1820–1826.

Los, G. V, Encell, L. P., Mcdougall, M. G., Hartzell, D. D., Karassina, N., Zimprich, C., Wood, K. V. (2008). HaloTag: A Novel Protein Labeling Technology for Cell Imaging and Protein Analysis. *ACS Chemical Biology*, *3*(6), 373–382.

MacGillavry, H. D., Song, Y., Raghavachari, S., & Blanpied, T. A. (2013). Nanoscale scaffolding domains within the postsynaptic density concentrate synaptic ampa receptors. *Neuron*, *78*(4), 615–622.

Mammen, a L., Huganir, R. L., & O'Brien, R. J. (1997). Redistribution and stabilization of cell surface glutamate receptors during synapse formation. *The Journal of Neuroscience : The Official Journal of the Society for Neuroscience*, *17*(19), 7351–8.

Marrs, G. S., Green, S. H., & Dailey, M. E. (2001). Rapid formation and remodeling of postsynaptic densities in developing dendrites. *Nature Neuroscience*, *4*(10), 1006–1013.

Matsuzaki, M., Ellis-Davies, G. C. R., Nemoto, T., Miyashita, Y., Iino, M., & Kasai, H. (2001). Dendritic spine geometry is critical for AMPA receptor expression in hippocampal CA1 pyramidal neurons. *Nature Neuroscience*, *70*(4), 646–656.

Matsuzaki, M., Honkura, N., Ellis-Davies, G. C. R., & Kasai, H. (2004). Structural basis of long-term potentiation in single dendritic spines. *Nature*, *70*(4), 646–656.

McShane, E., Sin, C., Zauber, H., Wells, J. N., Donnelly, N., Wang, X., Selbach, M. (2016). Kinetic Analysis of Protein Stability Reveals Age-Dependent Degradation. *Cell*, *167*(3), 803–815.e21.

Melloni, R. H., & Degennaro, L. J. (1994). Temporal onset of synapsin-I gene-expression coincides with neuronal differentiation during the development of the nervous-system. *Journal Of Comparative Neurology*, *342*, 449–462.

Migaud, M., Charlesworth, P., Dempster, M., Webster, L. C., Watabe, A. M., Makhinson, M., Grant, S. G. N. (1998). Enhanced long-term potentiation and impaired learning in mice with mutant postsynaptic density-95 protein. *Nature*, 433–439.

Miyazaki, T., Fukaya, M., Shimizu, H., & Watanabe, M. (2003). Subtype switching of vesicular glutamate transporters at parallel fibre-Purkinje cell synapses in developing mouse cerebellum. *European Journal of Neuroscience*, *17*(12), 2563–2572.

Muddashetty, R. S., Kelic, S., Gross, C., Xu, M., & Bassell, G. J. (2007). Dysregulated Metabotropic Glutamate Receptor-Dependent Translation of AMPA Receptor and Postsynaptic Density-95 mRNAs at Synapses in a Mouse Model of Fragile X Syndrome. *Journal of Neuroscience*, *27*(20), 5338–5348.

Muddashetty, R. S., Nalavadi, V. C., Gross, C., Yao, X., Xing, L., Laur, O., Bassell, G. J. (2011). Reversible Inhibition of PSD-95 mRNA Translation by miR-125a, FMRP Phosphorylation, and mGluR Signaling. *Molecular Cell*, *42*(5), 673–688.

Murrough, J. W., Collins, K. A., Fields, J., DeWilde, K. E., Phillips, M. L., Mathew, S. J., Iosifescu, D. V. (2015). Regulation of neural responses to emotion perception by

ketamine in individuals with treatment-resistant major depressive disorder. *Translational Psychiatry*, *5*(2), e509.

Nabavi, S., Fox, R., Proulx, C. D., Lin, J. Y., Tsien, R. Y., & Malinow, R. (2014). Engineering a memory with LTD and LTP. *Nature*, *511*(7509), 348–352.

Nair, D., Hosy, E., Petersen, J. D., Constals, A., Giannone, G., Choquet, D., & Sibarita, J.-B. (2013). Super-Resolution Imaging Reveals That AMPA Receptors Inside Synapses Are Dynamically Organized in Nanodomains Regulated by PSD95. *Journal of Neuroscience*, *33*(32), 13204–13224.

Neklesa, T. K., Tae, H. S., Schneekloth, A. R., Stulberg, M. J., Corson, T. W., Sundberg, T. B., Crews, C. M. (2011). Small-molecule hydrophobic tagging–induced degradation of HaloTag fusion proteins. *Nature Chemical Biology*, *7*(8), 538–543.

Nelson, C. D., Kim, M. J., Hsin, H., Chen, Y., & Sheng, M. (2013). Phosphorylation of Threonine-19 of PSD-95 by GSK-3 is Required for PSD-95 Mobilization and Long-Term Depression. *Journal of Neuroscience*, *33*(29), 12122–12135.

Newman, J., Peat, T. S., Richard, R., Kan, L., Swanson, P. E., Affholter, J. A., Terwilliger, T. C. (1999). Haloalkane dehalogenases: Structure of a Rhodococcus enzyme. *Biochemistry*, *38*(49), 16105–16114.

Nicoll, R. A. (2017). A Brief History of Long-Term Potentiation. *Neuron*, *93*(2), 281–290.

Nithianantharajah, J., Komiyama, N. H., McKechanie, A., Johnstone, M., Blackwood, D. H., Clair, D. S., … Grant, S. G. N. (2013). Synaptic scaffold evolution generated components of vertebrate cognitive complexity. *Nature Neuroscience*, *16*(1), 16–24.

Noritake, J., Fukata, Y., Iwanaga, T., Hosomi, N., Tsutsumi, R., Matsuda, N., Fukata, M. (2009). Mobile DHHC palmitoylating enzyme mediates activity-sensitive synaptic targeting of PSD-95. *Journal of Cell Biology*, *186*(1), 147–160.

Okabe, S., Kim, H. D., Miwa, a, Kuriu, T., & Okado, H. (1999). Continual remodeling of postsynaptic density and its regulation by synaptic activity. *Nature Neuroscience*, *2*(9), 804–811.

Okabe, S., Urushido, T., Konno, D., Okado, H., & Sobue, K. (2001). Rapid redistribution of the postsynaptic density protein PSD-Zip45 (Homer 1c) and its differential regulation by NMDA receptors and calcium channels. *The Journal of Neuroscience*, *21*(24), 9561–9571.

Okada, H., Zhang, W., Peterhoff, C., Hwang, J. C., Nixon, R. A., Ryu, S. H., & Kim, T.-W. (2010). Proteomic identification of sorting nexin 6 as a negative regulator of BACE1-mediated APP processing. *FASEB Journal : Official Publication of the Federation of American Societies for Experimental Biology*, *24*(8), 2783–94.

Ostroff, L. E., Fiala, J. C., Allwardt, B., & Harris, K. M. (2002). Polyribosomes redistribute from dendritic shafts into spines with enlarged synapses during LTP in developing rat hippocampal slices. *Neuron*, *35*(3), 535–545.

Pak, D. T. S., Yang, S. Y., Rudolph-Correia, S., Kim, E., & Sheng, M. (2001). Regulation of dendritic spine morphology by SPAR, a PSD-95- associated RapGAP. *Neuron*, *31*(2), 289–303.

Patrick, G. N., Bingol, B., Weld, H. A., & Schuman, E. M. (2003). Ubiquitin-Mediated Proteasome Activity Is Required for Agonist-Induced Endocytosis of GluRs. *Current Biology*, *13*(23), 2073–2081.

Peça, J., & Feng, G. (2012). Cellular and synaptic network defects in autism. *Current Opinion in Neurobiology*, *22*(5), 866–872.

Penzes, P., Johnson, R. C., Sattler, R., Zhang, X., Huganir, R. L., Kambampati, V., Eipper, B. A. (2001). The neuronal Rho-GEF Kalirin-7 interacts with PDZ domain-containing proteins and regulates dendritic morphogenesis. *Neuron*, *29*(1), 229–242.

Price, J. C., Guan, S., Burlingame, A., Prusiner, S. B., & Ghaemmaghami, S. (2010). Analysis of proteome dynamics in the mouse brain. *Proceedings of the National Academy of Sciences*, *107*(32), 14508–14513.

Riccomagno, M. M., & Kolodkin, A. L. (2015). Sculpting Neural Circuits by Axon and Dendrite Pruning. *Annual Review of Cell and Developmental Biology*, *31*(1), 779–805.

Rigaut, G., Shevchenko, A., Rutz, B., Matthias, W., Mann, M., & Séraphin, B. (1999). A generic protein purification method for protein complex characterization and proteome exploration. *Nature Biotechnology*, *17*(10), 1030–1032.

Ropers, H. H. (2008). Genetics of intellectual disability. *Current Opinion in Genetics and Development*, *18*(3), 241–250.

Ross, C. A., & Poirier, M. A. (2004). Protein aggregation and neurodegenerative disease. *Nature Medicine*, *10*(7), S10–S17.

Rubinsztein, D. C. (2006). The roles of intracellular protein-degradation pathways in neurodegeneration. *Nature*, *443*(7113), 780–786.

Ruxton, G. D. (2006). The unequal variance t-test is an underused alternative to Student's t-test and the Mann-Whitney U test. *Behavioral Ecology*, *17*(4), 688–690.

Salemi, G., Ferraro, D., & Savettieri, G. (1990). Triiodothyronine accelerates the synthesis of Synapsin I in developing neurons from fetal rat brain cultured in a synthetic medium. *Neurochemical Research*, *15*(8), 827–831.

Sampedro, M. N., Bussineau, C. M., & Cotman, C. W. (1981). Postsyaptic density antigens: preparation and characterization of an antiserum to postsyaptic densities. *Journal of Cell Biology*, *90*, 675–686.

Sans, N., Petralia, R. S., Wang, Y. X., Blahos, J., Hell, J. W., & Wenthold, R. J. (2000). A developmental change in NMDA receptor-associated proteins at hippocampal synapses. *The Journal of Neuroscience : The Official Journal of the Society for Neuroscience*, *20*(3), 1260–1271.

Schägger, H. (2001). Blue-Native Gels to Isolate Protein Complexes from Mitochondria. *Methods in Cell Biology*, *65*(1), 231–244.

Schiebler, W., Jahn, R., Doucet, J. P., Rothlein, J., & Greengard, P. (1986). Characterization of synapsin I binding to small synaptic vesicles. *Journal of Biological Chemistry*, *261*(18), 8383–8396.

Schnell, E., Sizemore, M., Karimzadegan, S., Chen, L., Bredt, D. S., & Nicoll, R. A. (2002). Direct interactions between PSD-95 and stargazin control synaptic AMPA receptor number. *Proceedings of the National Academy of Sciences*, *99*(21), 13902–13907.

Spacek, J., & Harris, K. M. (1997). Three-dimensional organization of smooth endoplasmic reticulum in hippocampal CA1 dendrites and dendritic spines of the immature and mature rat. *The Journal of Neuroscience: The Official Journal of the Society for Neuroscience*, *17*(1), 190–203.

Speese, S. D., Trotta, N., Rodesch, C. K., Aravamudan, B., & Broadie, K. (2003). The Ubiquitin Proteasome System Acutely Regulates Presynaptic Protein Turnover and Synaptic Efficacy. *Current Biology*, *13*(2), 899–910.

Steiner, P., Higley, M. J., Xu, W., Czervionke, B. L., Malenka, R. C., & Sabatini, B. L. (2008). Destabilization of the Postsynaptic Density by PSD-95 Serine 73 Phosphorylation Inhibits Spine Growth and Synaptic Plasticity. *Neuron*, *60*(5), 788–802.

Steward, O., & Schuman, E. M. (2003). Compartmentalized synthesis and degradation of proteins in neurons. *Neuron*, *40*(2), 347–359. https://doi.org/10.1016/S0896-6273(03)00635-4

Strauch, R. C., Mastarone, D. J., Sukerkar, P. A., Song, Y., Ipsaro, J. J., & Meade, T. J. (2011). Reporter protein-targeted probes for magnetic resonance imaging. *Journal of the American Chemical Society*, *133*(41), 16346–16349.

Sturgill, J. F., Steiner, P., Czervionke, B. L., & Sabatini, B. L. (2009). Distinct Domains within PSD-95 Mediate Synaptic Incorporation, Stabilization, and Activity-Dependent Trafficking. *Journal of Neuroscience*, *29*(41), 12845–12854.

Südhof, T. C. (2012). The presynaptic active zone. *Neuron*, *75*(1), 11–25.

Tai, H.-C., & Schuman, E. M. (2008). Ubiquitin, the proteasome and protein degradation in neuronal function and dysfunction. *Nature Reviews Neuroscience*, *9*(11), 826–838.

Takumi, Y., Ramirez-Leon, V., Laake, P., Rinvik, E., & Ottersen, O. P. (1999). Different modes of expression of AMPA and NMDA receptors in hippocampal synapses. *Nat Neurosci*, *2*(7), 618–24.

Tanaka, J., Horiike, Y., Matsuzaki, M., Miyazaki, T., Ellis-Davies, G. C. R., & Kasai, H. (2008). Protein Synthesis and Neurotrophin-Dependent Structural Plasticity of Single Dendritic Spines. *Science*, *319*(September), 1683–1688.

Tang, G., Gudsnuk, K., Kuo, S. H., Cotrina, M. L., Rosoklija, G., Sosunov, A., Sulzer, D. (2014). Loss of mTOR-Dependent Macroautophagy Causes Autistic-like Synaptic Pruning Deficits. *Neuron*, *83*(5), 1131–1143.

Tatavarty, V., Sun, Q., & Turrigiano, G. G. (2013). How to Scale Down Postsynaptic Strength. *Journal of Neuroscience*, *33*(32), 13179–13189.

Todd, P. K., Mack, K. J., & Malter, J. S. (2003). The fragile X mental retardation protein is required for type-I metabotropic glutamate receptor-dependent translation of PSD-95. *Proceedings of the National Academy of Sciences*, *100*(24), 14374–14378.

Topinka, J. R., & Bredt, D. S. (1998). N-terminal palmitoylation of PSD-95 regulates association with cell membranes and interaction with K+ channel K(v)1.4. *Neuron*, *20*(1), 125–134.

Toro, C., & Deakin, J. F. W. (2005). NMDA receptor subunit NRI and postsynaptic protein PSD-95 in hippocampus and orbitofrontal cortex in schizophrenia and mood disorder. *Schizophrenia Research*, *80*(2–3), 323–330.

Tsai, N. P. (2014). Ubiquitin proteasome system-mediated degradation of synaptic proteins: An update from the postsynaptic side. *Biochimica et Biophysica Acta - Molecular Cell Research*, *1843*(12), 2838–2842.

Tsai, N. P., Wilkerson, J. R., Guo, W., Maksimova, M. A., Demartino, G. N., Cowan, C. W., & Huber, K. M. (2012). Multiple autism-linked genes mediate synapse elimination via proteasomal degradation of a synaptic scaffold PSD-95. *Cell*, *151*(7), 1581–1594.

Tseng, J.-C. (2012). In Vivo Fluorescent Labeling of Tumor Cells with the HaloTag® Technology. *Current Chemical Genomics*, *6*(1), 48–54.

Tsuriel, S., Geva, R., Zamorano, P., Dresbach, T., Boeckers, T., Gundelfinger, E. D., Ziv, N. E. (2006). Local sharing as a predominant determinant of synaptic matrix molecular dynamics. *PLoS Biology*, *4*(9), 1572–1587.

Urh, M., & Rosenberg, M. (2012). HaloTag, a Platform Technology for Protein Analysis. *Current Chemical Genomics*, *6*, 72–8.

Vallejo, D., Codocedo, J. F., & Inestrosa, N. C. (2016). Posttranslational Modifications Regulate the Postsynaptic Localization of PSD-95. *Molecular Neurobiology*, *54*(3), 1759–1776.

Verpelli, C., & Sala, C. (2012). Molecular and synaptic defects in intellectual disability syndromes. *Current Opinion in Neurobiology*, *22*(3), 530–536.

Wojcik, S. M., Rhee, J. S., Herzog, E., Sigler, A., Jahn, R., Takamori, S., Rosenmund, C. (2004). An essential role for vesicular glutamate transporter 1 (VGLUT1) in postnatal development and control of quantal size. *Proceedings of the National Academy of Sciences USA*, *101*, 7158–7163.

Won, S., Incontro, S., Nicoll, R. A., & Roche, K. W. (2016). PSD-95 stabilizes NMDA receptors by inducing the degradation of STEP. *Proceedings of the National Academy of Sciences*, *113*(32), E4736–E4744.

Won, S., Levy, J. M., Nicoll, R. A., & Roche, K. W. (2017). MAGUKs: multifaceted synaptic organizers. *Current Opinion in Neurobiology*, *43*, 94–101.

Yan, B. C., Park, J. H., Ahn, J. H., Lee, J. C., Won, M. H., & Kang, I. J. (2013). Postsynaptic density protein (PSD)-95 expression is markedly decreased in the hippocampal CA1 region after experimental ischemia-reperfusion injury. *Journal of the Neurological Sciences*, *330*(1–2), 111–116.

Yao, J., Qi, J., & Chen, G. (2006). Actin-Dependent Activation of Presynaptic Silent Synapses Contributes to Long-Term Synaptic Plasticity in Developing Hippocampal Neurons. *J Neurosci*, *26*(31), 8137–8147.

Yoshii, A., & Constantine-Paton, M. (2007). BDNF induces transport of PSD-95 to dendrites through PI3K-AKT signaling after NMDA receptor activation. *Nature Neuroscience*, *10*(6), 702–711.

Zeidan, A., & Ziv, N. E. (2012). Neuroligin-1 loss is associated with reduced tenacity of excitatory synapses. *PLoS ONE*, *7*(7).

Zheng, C. Y., Petralia, R. S., Wang, Y. X., Kachar, B., & Wenthold, R. J. (2010). SAP102 Is a Highly Mobile MAGUK in Spines. *Journal of Neuroscience*, *30*(13), 4757–4766.

Zheng, S., Gray, E. E., Chawla, G., Porse, B. T., O'Dell, T. J., & Black, D. L. (2012). PSD-95 is post-transcriptionally repressed during early neural development by PTBP1 and PTBP2. *Nature Neuroscience*, *15*(3), 381–388.

Ziv, N. E., & Fisher-Lavie, A. (2014). Presynaptic and Postsynaptic Scaffolds: Dynamics fast and slow. *The Neuroscientist*, *20*(5), 439–452.